orrosion Problems in Coal-Fired oiler Superheater and eheater Tubes
reside Corrosion

EPRI

EPRI CS-1653
Project 644-1
Final Report
November 1980

ywords:
High-Temperature Corrosion
Coal-Fired Boilers
ron-Based Alloys
Nickel-Based Alloys
Coatings

MASTER

pared by
ster Wheeler Development Corporation
ingston, New Jersey

LECTRIC POWER RESEARCH INSTITUTE

DISCLAIMER

This report was prepared as an account of work sponsored by an agency of the United States Government. Neither the United States Government nor any agency thereof, nor any of their employees, makes any warranty, express or implied, or assumes any legal liability or responsibility for the accuracy, completeness, or usefulness of any information, apparatus, product, or process disclosed, or represents that its use would not infringe privately owned rights. Reference herein to any specific commercial product, process, or service by trade name, trademark, manufacturer, or otherwise does not necessarily constitute or imply its endorsement, recommendation, or favoring by the United States Government or any agency thereof. The views and opinions of authors expressed herein do not necessarily state or reflect those of the United States Government or any agency thereof.

DISCLAIMER

Portions of this document may be illegible in electronic image products. Images are produced from the best available original document.

Master

Corrosion Problems in Coal-Fired Boiler Superheater and Reheater Tubes
Fireside Corrosion

CS-1653
Research Project 644-1

Final Report, November 1980
Work Completed, February 1979

Prepared by

FOSTER WHEELER DEVELOPMENT CORPORATION
12 Peach Tree Hill Road
Livingston, New Jersey 07039

Principal Investigator
I. M. Rehn

Prepared for

Electric Power Research Institute
3412 Hillview Avenue
Palo Alto, California 94304

EPRI Project Manager
J. Stringer

Fossil Plant Performance and Reliability Program
Coal Combustion Systems Division

DISTRIBUTION OF THIS DOCUMENT IS UNLIMITED

ORDERING INFORMATION

Requests for copies of this report should be directed to Research Reports Center (RRC), Box 50490, Palo Alto, CA 94303, (415) 965-4081. There is no charge for reports requested by EPRI member utilities and affiliates, contributing nonmembers, U.S. utility associations, U.S. government agencies (federal, state, and local), media, and foreign organizations with which EPRI has an information exchange agreement. On request, RRC will send a catalog of EPRI reports.

Copyright © 1986 Electric Power Research Institute, Inc.

EPRI authorizes the reproduction and distribution of all or any portion of this report and the preparation of any derivative work based on this report, in each case on the condition that any such reproduction, distribution, and preparation shall acknowledge this report and EPRI as the source.

NOTICE

This report was prepared by the organization(s) named below as an account of work sponsored by the Electric Power Research Institute, Inc. (EPRI). Neither EPRI, members of EPRI, the organization(s) named below, nor any person acting on their behalf: (a) makes any warranty or representation, express or implied, with respect to the accuracy, completeness, or usefulness of the information contained in this report, or that the use of any information, apparatus, method, or process disclosed in this report may not infringe privately owned rights; or (b) assumes any liabilities with respect to the use of, or for damages resulting from the use of, any information, apparatus, method, or process disclosed in this report.

Prepared by
Foster Wheeler Development Corporation
Livingston, New Jersey

ABSTRACT

This program was conducted to develop improved alloys for superheater and reheater tubes in direct coal-fired steam generators in order to extend the service life of the tubes, and to evaluate materials for use at higher operating temperatures than currently in use. The program consisted of a broad literature review and laboratory evaluation involving 19 commercial and semicommercial alloys, 19 custom-melted alloys and 18 types of high-temperature coatings, subjecting them to flowing flue gas and molten alkali-iron trisulfate ash at 1250 and 1450°F (675 and 790°C). The commercial and semicommercial alloys suffered severe attack and pitting under the laboratory fireside test environment at 1250°F (675°C). In the custom-melted group, the best alloy (25%Ni-20%Cr-2%Al-2.4%Si) generated a dense, adherent scale which reduced pitting by a factor of four when subjected to the molten trisulfate. The character of the pitting attack is best described as an electrochemical mechanism where the molten trisulfate provides the electrolyte and transfers away the metal consumed at the active anodic areas. Protective scales were observed only on a few alloys of higher silicon content; these alloys are believed to offer significant improvement in useful life in steam generators firing corrosive coals. The magnesium zirconate ($MgZrO_3$) coating was resistant to corrosive attack, providing a self-healing mechanism by the formation of high-melting sulfates within its pores. This pore plugging effect withstood exposure cycles which would seriously damage conventional stainless steel tubes.

Blank Page

EPRI PERSPECTIVE

PROJECT DESCRIPTION

Fireside corrosion of coal-fired boilers, particularly of the superheaters, became a significant problem in the 1950s, the increasing impact being in part attributable to the increase in superheat temperature. Research programs conducted in the late 1950s and early 1960s were able to elucidate many of the aspects of the corrosion process, in particular making clear the importance of alkali (sodium and potassium)-containing sulfates in the ash deposit on the tube surfaces. The impact of the problem diminished sharply in part as a result of a reduction of superheat temperature, in part because of improved coal selection, and in part because of improvements in furnace design and operation. In severe cases, improved materials involving corrosion-resistant claddings were used with success.

However, increasing reliance on coal, the need to burn coals that are intrinsically more corrosive, and the move toward more efficient cycles with (perhaps) increased superheat temperatures have resulted in a need for further study of this problem. Since the middle 1960s there has been considerable improvement in our understanding of corrosion by molten alkali salts, principally as a result of studies of gas turbine hot corrosion. This project was intended to develop more information on the corrosion of a range of alloys in environments similar to those experienced by superheater tubes in pulverized coal boilers.

PROJECT OBJECTIVES

RP644-1 had two objectives. One was to study superheater fireside corrosion, and the other was to study steam-side exfoliation of scale in superheaters and reheaters. This second aspect will be reported separately.

An initial task was to review the work published on fireside corrosion. This review appears in the present report.

The objectives of the remainder of this part of the project were, firstly, to determine the response of a range of alloy coatings to an environment similar to that experienced by the surface of a superheater tube in a furnace burning a corrosive coal and, secondly, to develop an understanding of the mechanism of reactions involved in the corrosion. This understanding should then help in the design of improved alloys or coating systems.

PROJECT RESULTS

It was concluded that an electrochemical mechanism was important in the corrosion. This is an interesting suggestion and certainly explains the appearance of localized deep pits on alloys normally thought to be resistant, such as IN 671. A second point of some importance relates to the decrease in corrosion as the temperature rises above 700°C or so, which has been reported in a number of earlier studies. It is suggested that this may be attributable to the isothermal laboratory experiments carried out in those studies; under these conditions, the corrosive alkali iron trisulfate is not stable. However, if the trisulfate is formed on the metal surface at a lower temperature and then heated above 700°C, severe pitting corrosion is possible.

The integrity of the oxide scale appeared to be an important factor in determining the corrosion resistance of alloys systems. The addition of small amounts of aluminum and silicon appear to be beneficial in this respect, but the investigation was too short for an optimum composition to be identified.

The most important coating material tested in this project was $MgZrO_3$, apparently because of its stability and because of its freedom from the

problems associated with porosity. Further testing of this coating will be undertaken in an extension of the present project.

John Stringer, Program Manager
Materials Support Group

Blank Page

ACKNOWLEDGMENTS

The author is indebted to Dr. Dale Peters of the Paul D. Merica Research Laboratory of INCO in Sterling Forest, New York, for his assistance in planning and preparing the custom-melted alloys used in this program and in examining the microstructures before and after exposure. He provided valuable assistance in energy dispersive x-ray analysis, x-ray diffraction, and electron microprobe evaluation of the corroded samples. He also provided background data on the oxidation and sulfidation behavior.

The author was also assisted by J. C. Spoganetz and G. J. Stanko of Foster Wheeler Development Corporation in the preparation of coupons and the performance of tests. Mr. Spoganetz provided assistance in descaling and evaluating the exposed materials, and Mr. Stanko assisted in the metallography, photography, and examination of the materials after testing.

Blank Page

TABLE OF CONTENTS

Section		Page
1	INTRODUCTION	1-1
	1.1 Need for a Wide-Ranging Materials Survey	1-1
	1.2 Test Program Objective	1-2
	1.3 Scope of the Test Program and Evaluation of Tube Materials for Conventional and Advanced Coal-Burning Utility Generators	1-3
2	EXPERIMENTAL APPROACH AND TEST PLAN	2-1
	2.1 Simulation of Fireside Corrosion	2-1
	2.1.1 Flue Gas System and Analysis	2-1
	2.1.2 Synthetic Fuel Ash	2-1
	2.2 Materials Selection	2-2
	2.3 Specimen Preparation	2-2
	2.4 Test Sequence	2-6
	2.4.1 Introduction	2-6
	2.4.2 Procedure	2-7
	2.5 Methods of Evaluating Corrosion Losses	2-7
	2.5.1 Visual and Photographic Evaluation	2-7
	2.5.2 Physical Measurements and Pitting Evaluation	2-11
	2.5.3 Microscopic Examination	2-11
	2.5.4 Analysis and Chemical Evidence	2-12
3	RESULTS OF FIRESIDE TESTS	3-1
	3.1 Phase 1 - Commercial and Semicommercial Alloy Testing	3-1
	3.1.1 Task 1.4.1 - Oxidation in Flue Gas	3-1
	3.1.2 Task 1.4.2 - Fireside Attack on Commercial Alloys	3-7
	3.1.3 Task 1.4.3 - Effects of Carbon and Chloride Additions on Fireside Corrosion	3-19
	3.1.4 Conclusions From the Evaluation of Phase 1 Alloys	3-29

Section			Page
	3.2	Phase 2 - Developmental Alloy Testing	3-30
		3.2.1 General	3-30
		3.2.2 Results of Exposure of Phase 2 Alloys	3-32
		3.2.3 Examination of Phase 2 Coupons	3-38
		3.2.4 X-Ray Diffraction Data on Deposits and Scale	3-48
		3.2.5 Effects of Adding NaCl to Simulated Ash	3-52
		3.2.6 Effects of Alloy Content on Fireside Attack	3-53
		3.2.7 Preliminary Evaluation of Alloy 4 Adherent Scale After Two Cycles of Fireside Exposure	3-54
		3.2.8 Conclusions From Phase 2 Tests	3-55
	3.3	Phase 3 - Coating Testing	3-56
		3.3.1 General	3-56
		3.3.2 Severely Corroded Materials	3-56
		3.3.3 Diffused Aluminum Surface Alloy (Alonizing)	3-60
		3.3.4 Iron-Based Plasma Spray Coatings	3-66
		3.3.5 Nickel-Chromium-Based Coatings	3-69
		3.3.6 Inert Barrier Coatings	3-75
		3.3.7 Tribaloy Coatings	3-78
		3.3.8 Metallography and Analytical Results	3-78
		3.3.9 Summary of Phase 3 Coating and Surface-Treatment Evaluations	3-116
4		STATE-OF-THE-ART DEVELOPMENTS RESULTING FROM PHASE 3 TESTS OF COATINGS AND SURFACE TREATMENTS	4-1
	4.1	The Role of Aluminum	4-1
	4.2	The Role of Chromium	4-2
	4.3	The Role of Silicon	4-4
	4.4	Development of Inert Corrosion Barrier Coatings	4-4
	4.5	Composite Silicide Coatings	4-5
	4.6	Performance of the Ni-Cr Alloy Coatings	4-5
	4.7	Test Procedure for Coatings	4-6
5		DATA OBTAINED FROM SUPPLEMENTAL TESTS	5-1
	5.1	Rate of Attack	5-1
	5.2	Changes in the Liquid-Phase Composition	5-1
	5.3	Preoxidized Specimen Test Data	5-2

Section		Page
	5.4 Reexposure of Promising Samples	5-3
	5.5 Reexposure of Coated Specimens	5-3
	5.6 Substitute Materials Used in Place of Unsuitable Coatings	5-4
6	ADVANCEMENT IN THE STATE OF THE ART	6-1
7	CONCLUSIONS AND RECOMMENDATIONS	7-1
8	REFERENCES	8-1
	APPENDICES	
	Appendix A - A Review of the Literature on Steam Generator, Superheater, and Reheater Tube Material for Coal-Fired Systems	
	Appendix B - Alloys and Coated Specimens for Fireside Testing	
	Appendix C - Experimental Design and Test Procedure	
	Appendix D - Representative Data From Phase 1 Tests	
	Appendix E - Examination of Scales and Deposits	

ILLUSTRATIONS

Figure		Page
1.1	View of First Specimen Loading in the Upper Row of Tubes of the Fireside Test Retort Assembly	1-5
2.1	Fireside Corrosion Retort	2-9
3.1	Simulated Ash Pitting as a Function of Time at 1250°F (675°C)	3-10
3.2	Differential Thermal Analysis of Corrosion Deposits Compared With That of $(Na,K)_3Fe(SO_4)_3$	3-13
3.3	Fireside Corrosion Losses as a Function of Alloy Constituents	3-17
3.4	Random Variation in Pitting of High Alloys--1.5X	3-26
3.5	Photomacrograph of Exposed Surface of IN-671 Specimen After Testing at 1250°F (675°C)--3X	3-27
3.6	Fireside Attack--Phase 2--1.5X (Alloys 1, 3, 4, and AISI 314)	3-34
3.7	Fireside Attack--Phase 2--1.5X (Alloys 5, 6, 7, and 8)	3-35
3.8	Fireside Attack--Phase 2--1.5X (Alloys 5, 6, 13, and 15)	3-37
3.9	Exposed Surface of Alloy 1 (not descaled) Showing Poorly Adherent Chromium-Sulfide Scale Under the Ash Deposits	3-39
3.10	Exposed Surface of Alloy 2 (not descaled) Showing Poorly Adherent Chromium-Sulfide Scale Containing Other Elements	3-40
3.11	Exposed Surface of Alloy 3 Showing a More Adherent Scale Which Was Retained on Cool-Down	3-42
3.12	Exposed Surface of Alloy 4 Showing a More Adherent, Dense Scale Adjacent to the Alloy	3-43
3.13	Exposed Surface of Alloy 5 Showing a Poorly Adherent Sulfide Scale	3-45
3.14	Exposed Surface of Alloy 15 Showing the Porous Deposits Over Intermittent Areas of Oxide on the Alloy Surface	3-46

Figure		Page
3.15	Exposed Surface of Alloy 12 Showing a Different Type of Deep Pit Formation and a Nonprotective Scale	3-47
3.16	Exposed Surface of Alloy 17 Showing a Scale Which Was Adherent in Some Areas	3-49
3.17	Optical Micrograph of Mechanically Alloyed 310SS (Alloy 19) After Exposure	3-50
3.18	Transverse Macrosections of Chromized Specimens After Exposure--8X	3-61
3.19	Descaled Specimens of Chromized Alloys--1.5X	3-62
3.20	Transverse Macrosections of Siliconized Alloy Coupons--8X	3-63
3.21	Transverse Macrosections of Alonized Specimen--8X	3-64
3.22	Microsection of Alonized Incoloy 800--100X	3-65
3.23	Transverse Macrosections of Kanthal and $CrSi_2$ Coatings After Test--8X	3-67
3.24	Transverse Macrosections of Kanthal and Duplex Coatings--8X	3-68
3.25	Surface of Ni-Cr-Al and Fe-Cr-Al Coated Specimens After Descaling--1.5X	3-70
3.26	Transverse Macrosections of Ni-Cr-Al Coated Specimens--8X	3-71
3.27	Ni-Cr (IN-671) Coated Specimen--8X	3-72
3.28	Transverse Macrosections of Ni-Cr-Si (IN-671 + Si) Coated Specimens--8X	3-74
3.29	Macrosections of Plasma-Coated Ni-Al (Metco 404) Specimens After Test--8X	3-76
3.30	Transverse Macrosections of Exposed Specimens--8X	3-77
3.31	Plasma-Deposited ZrO_2 Coating--8X	3-79

Figure		Page
3.32	Photomacrographs of Exposed Surfaces of Tribaloy-Coated Specimens After Descaling Showing Irregular Attack and Some Cracking of the Coatings--1.5X	3-80
3.33	Transverse Macrosections of Tribaloy-Coated Specimens--8X	3-81
3.34	Chromized HT-9 Specimens--100X	3-82
3.35	Chromized 304SS Showing Almost Total Loss of High-Chromium-Enriched Surface by Corrosion	3-84
3.36	Chromized Nitronic 40 Showing a Thin Layer of the 40% Cr Alloy Surface Deeply Penetrated by Electrochemical Pitting	3-85
3.37	Chromized Incoloy 800 Showing Electrochemical Pitting After 48-Hour Exposure to Fireside Attack--250X, Etched	3-86
3.38a	Microstructure of Chromized HT-9 Before Test--500X	3-88
3.38b	Analytical Profile of Iron and Chromium Obtained by Electron Microprobe Scan of the Chromized Alloy Steel	3-88
3.39	Chromized HT-9 After Exposure	3-89
3.40a	Microprobe of Unexposed Chromized 304SS Specimen Indicating High-Chromium Surface	3-90
3.40b	Chromized 304SS Before Exposure	3-90
3.41	Chromized 21-6-9 Before and After Exposure	3-91
3.42	Chromized Incoloy 800 After Exposure	3-93
3.43	Alonized 304SS Before and After Exposure Showing Some Loss of the Outer Surface but Reduced Pitting--100X	3-94
3.44	Microsection of Alonized Incoloy 800 Before and After Exposure--100X	3-95
3.45	Alonized Incoloy 800 After Exposure	3-96

Figure		Page
3.46	Alonized 304SS After Exposure--300X	3-97
3.47	Fe-Cr-Al Coating on HT-9	3-99
3.48	Metallized Kanthal Coating on 309SS	3-101
3.49	Duplex Coating ($CrSi_2$ over Kanthal) on 347SS--100X	3-102
3.50	Microprobe Analysis Profile of Exposed Duplex Coating--330X	3-103
3.51	Microsections of Plasma-Deposited $CrSi_2$ Coating	3-104
3.52	Microstructures of Ni-Cr-Al Coated 347SS--100X	3-106
3.53	Plasma-Deposited IN-671 on Incoloy 800 Showing Several Corrosion Effects--100X	3-107
3.54	Microprobe Analysis Profile of Coating and Substrate of IN-671 Coating Before and After Exposure	3-108
3.55	Exposure of Ni-Cr-Si Coating--100X	3-109
3.56	Ni-Al Coating (Metco 404) on 347SS	3-111
3.57	$MgZrO_3$ Coating on Stainless Steel	3-112
3.58	Exposed Tribaloy Coating	3-114
3.59	Microprobe Analyses Profiles of Tribaloy 800 Before and After Exposure	3-115
4.1	Alloy IN-671 After a 48-Hour Exposure	4-3

LIST OF TABLES

Table		Page
1.1	Chemical Composition of Phase 1 Alloys for Fireside Tests	1-7
1.2	Experimental Alloy/Cladding Design Compositions	1-8
1.3	Coatings	1-9
2.1	Alloy Compositions for Phase 2 Fireside Tests	2-3
2.2	Phase 3 Alloys With Coatings and Surface Treatments	2-4
2.3	Fireside Corrosion Test Plan	2-8
2.4	Descaling Treatments After Fireside Tests	2-10
3.1	Chemical Composition of Phase 1 Alloys for Fireside Tests	3-2
3.2	Flue Gas Exposures for Retorts 1 and 3	3-3
3.3	Flue Gas Exposures for Retort 2	3-4
3.4	Effect of Increased Temperature on Weight Gain of Base Materials Exposed to Synthetic Flue Gas for 250 Hours	3-6
3.5	Fireside Corrosion Test Results for Simulated Coal Ash Plus Flue Gas Exposures	3-8
3.6	Fireside Test--Summary of Exposures	3-15
3.7	Fireside Attack Using Carbon (Char) Added to Ash for 48-Hour Exposure at 1250°F (674°C)	3-20
3.8	Fireside Tests for Retort 12 at 1450°F (785°C) Showing Maximum Penetration Caused by Ash Containing Free Carbon	3-21
3.9	Fireside Tests for Retorts 14 and 15 Showing the Maximum Penetration Values Caused by Adding NaCl to Ash at 1250 and 1450°F (675 and 790°C) for 48-Hour Exposure	3-23
3.10	Fireside Tests for Retort 13 Showing the Effect of Surface Preoxidation on Corrosion at 1250°F (675°C)	3-24

Table		Page
3.11	Pitting of Selected Commercial Alloys Exposed to Simulated Fireside Attack, Comparing Preoxidized With Unoxidized Specimens	3-28
3.12	Alloy Compositions for Phase 2 Fireside Tests	3-31
3.13	Fireside Corrosion--Performance of Phase 2 Alloys	3-33
3.14	XRD Analyses of Outer Loose Deposits and the Scale Near the Surface of 19 Alloys Exposed to Simulated Coal Ash and Flue Gas	3-51
3.15	Phase 3 Surface Treatments and Coatings Exposed to Fireside Attack	3-57

SUMMARY

Although fireside corrosion of boiler superheater and reheater tubes in service in coal-fired boilers has been a problem for more than 30 years, no direct solution has previously been found, nor has a more corrosion-resistant material been developed.

This program was conducted to evaluate materials designed to resist the corrosion caused by these alkali-iron-trisulfate deposits resulting from coal combustion. Commercial, semicommercial, and experimental alloys were tested in laboratory-scale fireside conditions representative of severe corrosive environments found in commercial service.

The program involved a literature review and laboratory tests in which 38 alloy compositions in the Fe-Cr, Fe-Cr-Ni, and the Fe-Ni-Cr systems were tested. Some of these alloys also contained aluminum, silicon, and yttrium. Eighteen high-temperature coating systems were tested, using the same fireside test retort as used to simulate the exposure of alloys to adverse alkali-sulfate deposits in commercial steam generators.

The laboratory results indicated that all commercial and semicommercial alloys in the Fe-Cr, Fe-Cr-Ni, and the Fe-Ni-Cr systems were subject to severe pitting attack in the molten alkali-iron trisulfate at 1250°F (675°C). The matrix of alloy compositions was designed to evaluate the effects of individual metal additions. The results demonstrated beneficial effects of chromium, aluminum, columbium, silicon, and manganese additions to austenitic stainless steels and Fe-Ni-Cr alloys. A molybdenum addition of greater than 1 percent increased the corrosion in comparison to alloys without molybdenum. The nickel additions were helpful up to about 20 percent, but then resulted in increased pitting at a higher nickel content.

A limited number of tests were performed with chloride added to the sulfates, and at a higher temperature, 1450°F (790°C), with interesting results.

Several unexpected observations helped identify the mechanism and demonstrate the complex nature of the molten trisulfate attack:

- Corrosion proceeded at a rapid initial rate as soon as the sulfates became molten, resulting in losses to 304SS as high as 0.008 in. (203 μm) within the first 24 hours. During the second 24-hour period the rate was only half the initial rate, and with longer exposure times, the corrosion fell to a very low level.

- The dissolved corrosion products altered the liquid corrodent. This was noted on all but the low-alloy steels. In some cases, progressive solidification retarded attack while in others there was a greater depletion because of secondary reactions in the slag. (The laboratory tests did not simulate the deslagging and continued deposit build-up that would occur in actual coal-burning units.)

- Another unexpected observation was the detrimental effect of preoxidized alloy surfaces. Even the oxide scales that were high in Cr_2O_3 and/or Al_2O_3 were not beneficial. These effects together with the nature and distribution of the pits tended to support the electrochemical mechanism for the molten trisulfate attack rather than a general metal attack.

- Diffusion chromizing also suffered severe pitting by the fireside corrodents despite the high chromium content at the surface of the four different alloys tested. A significant increase in local corrosion penetration of the chromized surface having a high chromium content (40 to 60 percent) appears to further support the electrochemical attack mechanisms and underscore the need for greater homogeneity in the chromium content.

The most promising alloy tested contained a composition of 24%Ni-20%Cr-2%Al-2.4%Si-Bal.Fe, and generated a protective, adherent scale which was not selectively attacked. This composition may be difficult to manufacture because of its aluminum and silicon levels, but should be effective as a cladding material.

None of the compositions tested were indicated as the optimum alloy. Therefore, it is recommended that further alloy modifications to the Fe-Cr-Ni-Si system be evaluated with alloy systems containing manganese, niobium, and aluminum to enhance the scale adhesion.

Several of the coatings tested were protective in the initial exposures, but the porosity generally permitted an attack at the coating/metal interface. Further work on eliminating coating porosity may be fruitful in the case of the more resistant silicon containing coatings.

The $MgZrO_3$ coating was the most resistant coating material tested because of its stability and freedom from problems caused by porosity. The $MgZrO_3$ coupons demonstrated an efficient self-sealing surface because of the high-melting sulfates which filled the pores. This coating remained resistant to attack on repeated exposures at 1250°F (675°C) with new added corrodent.

SECTION 1
INTRODUCTION

Section 1

INTRODUCTION

This report presents the final data and evaluation of materials testing performed by Foster Wheeler Development Corporation (FWDC) under Task 1 - Fireside Corrosion, EPRI Contract No. RP-644-1, "Design of Improved Materials Systems for Coal-Fired Boiler, Superheater, and Reheater Tubes." The objective of this work was to evaluate the materials specified in the work scope using a comparative laboratory test technique to establish direct data for defining the relative performance of materials and coatings exposed to a simulated fireside attack.

1.1 NEED FOR A WIDE-RANGING MATERIALS SURVEY

Fireside corrosion has been a problem for over 30 years, but no direct solution has been found, nor has a corrosion-resistant material been developed to date. The current practice in the United States is to minimize fireside corrosion by limiting metal temperature and selecting coals with low sodium and sulfur contents. The results of excessive corrosion are tube failures, consequent shutdown for tube replacement, and costly loss of plant operating time.

An important aspect of material problems for advanced systems is the maximum temperature limit for existing ferritic or austenitic steel tubes. Based on the available corrosion data, use of existing higher alloys and nickel alloys does not ensure extended life or increased service-temperature capability. In fact, so little valid data on high-temperature alloys can be found in the literature that no long-life materials can be selected for service at temperatures above 1200°F (650°C) in a plant using other than low-alkali coals. The current economic situation and the demand for conservation of fuel resources indicate that utilization of the marginal and lower grade (more corrosive) coals may be inevitable.

A review of the available literature on fireside corrosion, summarized in Appendix A,[1*] evaluated recent developments as an aid in determining which alloy systems are more promising and in clarifying the mechanism of fireside deposit attack on steels. None of the fireside corrosion studies reviewed included a broad materials survey for fireside applications except for the tests reported by Greenert,[2] which were made under specialized conditions (high sodium chloride) for marine boilers. Most of the studies of fireside problems were directed toward the nature of deposits and the causes of corrosion of the steels normally used for superheater and reheater tube service.

Where corrosion data were reported as "rate of loss," wide variations were observed from one source to another because of the intermittent or sporadic nature of the corrosive attack. Corrosive deposits that develop from different coals vary substantially in degree of attack, so data on losses obtained for one type of steel usually cannot be compared with data for another alloy obtained elsewhere.

Thus we proposed development of the test described in Section 1.2.

1.2 TEST PROGRAM OBJECTIVE

The objective of the test program was to evaluate the commercial, semi-commercial, and experimental alloys specified in the work scope, using a laboratory fireside corrosion test designed to make a direct comparison of materials under reproducible conditions simulating a severe fireside corrosive environment. The comparative corrosion data obtained were then used to:

- Define the influence of individual alloy elements
- Indicate the differences in rate of attack for exposures up to 500 hours

*Numbers designate references in Section 8.

- Evaluate the relative losses at 1450 and 1250°F (790 and 675°C)
- Determine the effects of free carbon additions to the ash
- Compare the effects of ash containing chlorides with those of a chloride-free ash
- Make a comparative evaluation of the listed coatings and surface treatments for possible improvements to materials for steam generator tubes.

1.3 SCOPE OF THE TEST PROGRAM AND EVALUATION OF TUBE MATERIALS FOR CONVENTIONAL AND ADVANCED COAL-BURNING UTILITY BOILERS

The scope of work for Task 1 - Fireside Corrosion was defined as follows:

- Review the current literature on fireside failure modes for state-of-the-art materials in fossil fuel boilers
- Identify the corrosion processes involved in fireside corrosion of state-of-the-art materials for the three regimes:
  - Alkali sulfate-induced attack
  - Sulfate-chloride attack (chloride added to sulfate ash deposits)
  - Carburization/oxidation attack (possibly including sulfidation).

  In this study the metal temperatures were 1250 and 1450°F (675 and 790°C), the atmosphere corresponded to a flue gas with 5-percent excess oxygen, and the role of carbon in slag deposits was evaluated.
- Establish failure modes and design criteria for resistant systems, with the following research directions indicated:
  - Design of new classes of high-temperature alloys for fireside corrosion resistance, scale adherence, and strength
  - Design of coating/cladding systems for existing alloys
  - Evaluation of wrought superalloys in coal-fired boiler conditions
  - Design of alloys suitable for the external layer in composite tubes.

The following Task 1 subtasks were performed:

- Subtask 1.1 - Design and Construction of Fireside Simulation Corrosion Test Facility

  - Retort Design

    A retort assembly (Figure 1.1), consisting of a bank of tubes, intake and exit manifolds, and a mixing chamber, was designed to carry out the simulated fireside corrosion experiments. The design allowed for an incoming flue-gas mixture to contact Fe_2O_3, which precatalyzed the oxidation of SO_2 to SO_3. The flue gas then passed through a mixing chamber and was distributed into a series of tubes (5 per row, 3 per column) containing the specimens. From the exit manifold, the flue gas was piped into water-filled flasks to assure equal flow distribution--one flask for each column of tubes. The retorts were designed to fit available box-type resistance-heated furnaces.

  - Preparation of Corrodents

    A synthetic combustion gas, consisting of 10 percent H_2O, 14 percent CO_2, 3.6 percent O_2, 0.25 percent SO_2, and 72 percent N_2, was obtained by controlled mixing of gases utilizing precision rotometers and high-purity gases obtained from cylinders. The gas mixture was catalyzed to produce the desired amount of SO_3. The SO_3 content of the furnace atmosphere was 500 to 800 ppm near the catalyst. A gas velocity of 3 to 5 mm/s over the ash supplied sufficient SO_2 and SO_3 to the metal surface.

    Monitoring of SO_3 in the gas stream was accomplished by the following standard method: A sample of the gas stream was drawn off and passed through a trap at 32°F (0°C) to remove SO_3 as H_2SO_4 and then passed through a second trap at -320.8°F (-196°C) to recover the SO_2. Analysis of the SO_3 was made by the barium perchlorate method. The CO_2, O_2, and H_2O content of the gas was also analyzed to verify the flow meter calibration. During the preliminary design phase of the screening tests, alternate approaches were examined to be certain that the method proposed was the best route to take.

    The basic synthetic coal ash consisted of 37.5-mol percent Na_2SO_4, 37.5-mol percent K_2SO_4, and 25.0-mol percent Fe_2O_3. The coal ash was made from reagent-grade pure compounds. To obtain a uniform, homogeneous mixture, the weighed constituents were blended for 24 hours in a mixer and thermally treated at 750°F (400°C) for 24 hours. The thermally treated mixture was pulverized, passed through a 100-mesh screen, and applied to the surface of the specimen in a controlled manner (75 mg/cm^2) to ensure consistency from one specimen to the next.

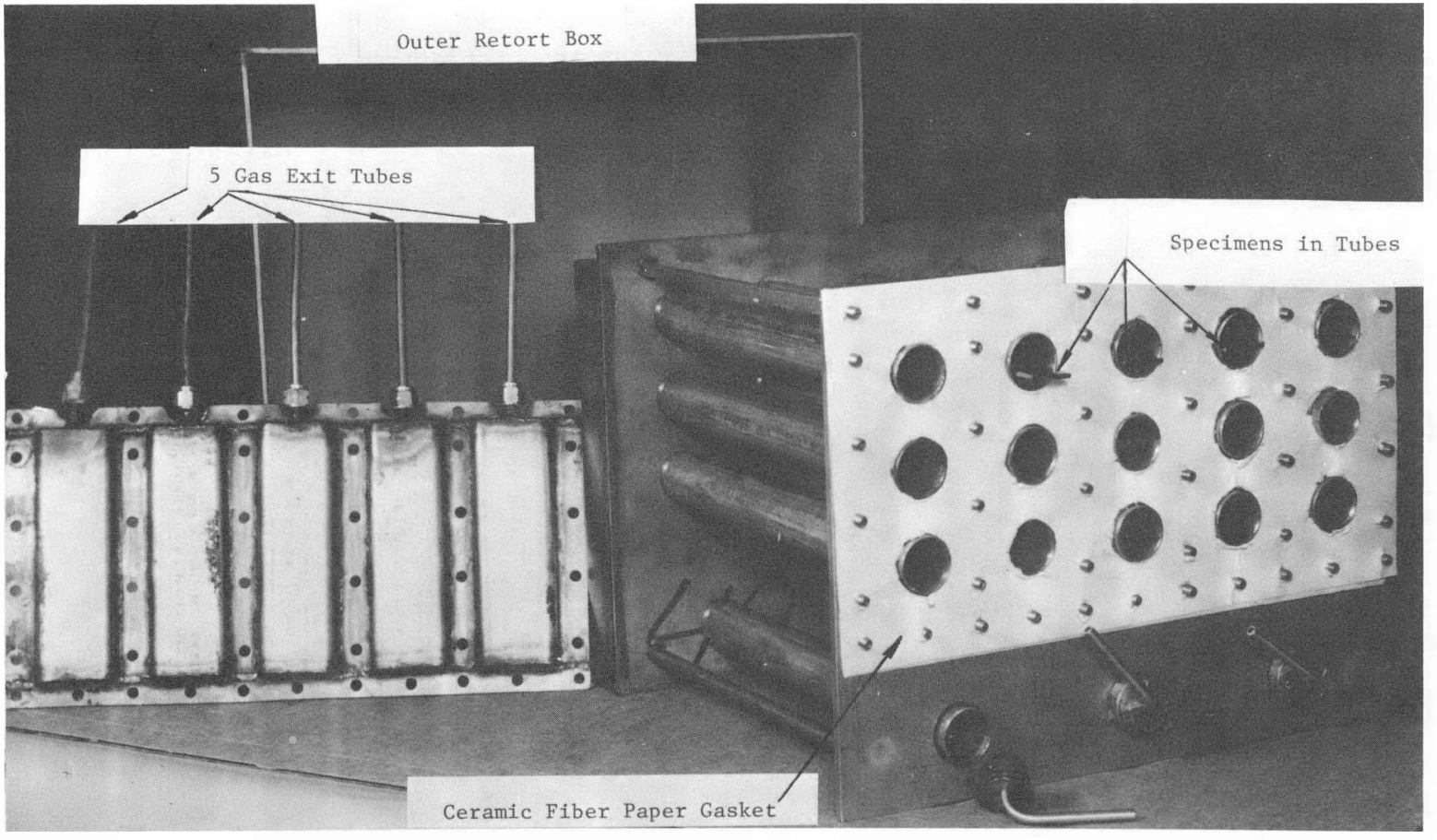

Figure 1.1 View of First Specimen Loading in the Upper Row of Tubes of the Fireside Test Retort Assembly (The gas exit manifold, shown at the left, was installed over the ends of the tubes and sealed with the ceramic fiber paper gasket. The bottom row of tubes contains Fe_2O_3--a catalyst for forming SO_3 in the incoming gas before it passes over the specimens.)

- Subtask 1.2 - Materials Tested

  - 1.2.1 - Commercial and Semicommercial Materials. The commercial and semicommercial alloys listed in Table 1.1 were tested. Commercial alloys were obtained from vendors and semicommercial alloys were supplied by the International Nickel Company (INCO).

  - 1.2.2 - Alloy Design Matrix. To expand the materials matrix, the alloys listed in Table 1.2 were prepared by induction melting at INCO's Paul D. Merica Research Laboratory. A number of the alloys were selected to evaluate the effect of increasing the chromium and nickel levels with or without a simultaneous increase in aluminum or silicon or both.

    In addition to those alloys, the 25%Cr-35%Ni alloy was prepared with 4-percent aluminum to obtain a material that would form a continuous Al_2O_3 external scale rather than the Cr_2O_3 scale expected on the other alloys. The 25%Cr-35%Ni alloy, with and without the 4-percent aluminum, was prepared with 0.1 and 0.5 percent yttrium to test the effect of this reactive element, yttrium, on scale adhesion. Further evaluation of the effect of yttrium was obtained by including a 310SS alloy in the test with 0.6-percent yttrium and with 0.5 Y_2O_3 as a dispersed oxide phase.

  - 1.2.3 - Coatings. The coatings listed in Table 1.3 were applied to specimens of the commercial steels.

    -- 1.2.3.1 - Diffusion Coatings.

    Alonizing - The Alonizing process diffuses aluminum into the material to form an aluminum-rich alloy surface with improved corrosion-resistant properties in many environments. The commercial process is performed by loading the material in a retort, surrounding it with a mixture of blended aluminum powders, and heating it to 1850 to 1900°F (1010 to 1040°C). The depth of aluminum penetration is controlled by processing time and temperature with a standard range of 0.010- to 0.030-in. (250- to 760-μm) penetration.

    Chromizing - The chromizing process diffuses chromium into material, producing an alloy that contains over 40-percent chromium at the surface and thus improving oxidation and corrosion resistance. This process is similar in many respects to gas-nitriding or carburizing; and since it is a diffusion coating, there are no disbonding problems. The depth of diffusion (generally 2 to 5 mil) varies with the time and temperature of treatment and the chemistry of the metal being treated.

    Siliconizing - In the siliconizing process, silicon is diffused into the material to form a silicon-enriched case. The process uses silicon carbide in a retort and introduces a

Table 1.1 Chemical Composition of Phase 1 Alloys for Fireside Tests (% by Weight)

Alloy	Heat or Lot No.	C	Mn	P	S	Si	Ni	Cr	Fe	Mo	Al	Ti	V	Cu	Other
Ferritic Alloys															
2-1/4%Cr-1%Mo	52816	0.12	0.55	0.020	0.023	0.29	0.15	2.34	Bal.	0.87	---	---	---	---	Co 0.13
HT-9 (Sandvik Tube)	4-52112	0.22	0.52	0.018	0.005	0.35	0.50	11.3	Bal.	0.97	---	---	0.26	---	W 0.50
Austenitic SS															
304	47832	0.055	1.71	0.022	0.025	0.55	8.40	18.34	Bal.	0.11	---	---	---	0.08	Co 0.16
347	8083689	0.059	1.58	0.03	0.015	0.67	10.30	18.50	Bal.	0.17	---	---	---	0.16	Cb 0.61
	30W2	0.055	1.72	---	---	0.81	9.8	18.1	Bal.	---	---	---	---	---	Cb 0.84
310	8084791	0.069	1.77	0.028	0.014	0.46	20.40	25.30	Bal.	---	---	---	---	---	---
	04964	0.045	0.18	---	---	0.14	22.1	22.3	Bal.	---	---	---	---	---	---
314	7401-8001	0.068	1.06	0.042	0.024	1.73	21.1	24.2	Bal.	0.01	---	---	---	0.02	---
	46W	0.056	2.03	---	---	2.09	19.4	23.3	Bal.	---	---	---	---	---	---
IN-840	---	0.041	0.13	---	---	0.77	20.6	20.3	Bal.	---	---	---	---	---	---
High-Manganese Alloy															
21-6-9 (Nitronic 40)	346087	0.021	9.2	0.016	0.003	0.67	7.21	20.1	Bal.	0.16	---	---	---	0.13	N 0.32
High-Iron Superalloys															
IN-737	---	0.032	<0.1	---	---	<0.1	37.5	17.2	Bal.	1.44	0.59	0.52	---	---	Cb 1.03
Incoloy 800H	---	0.056	0.88	---	---	0.24	31.2	20.4	Bal.	---	0.47	0.46	---	0.63	---
Incoloy 800	HH2118A	0.05	0.93	---	0.007	0.42	31.24	21.54	44.72	---	0.39	0.35	---	0.33	---
A-286	29385	0.041	1.32	0.023	0.003	0.54	25.10	15.22	Bal.	1.40	0.17	2.18	0.27	0.26	B 0.007
AL-6X	00629	0.013	1.65	---	0.005	0.33	24.41	20.0	Bal.	6.5	0.03	---	---	---	---
Nickel-Base Superalloys															
Inconel 625	---	0.019	0.13	---	---	0.19	Bal.	21.8	2.9	8.9	0.26	0.21	---	---	Cb 3.8
IN-671	---	0.059	<0.1	---	---	0.38	Bal.	45.5	---	---	0.034	0.26	---	---	---
Semicommercial Alloys															
IN-549	---	0.099	<0.1	---	---	0.28	43.7	19.5	Bal.	---	2.5	---	---	---	---
IN-809	---	0.010	<0.1	---	---	<0.1	Bal.	36.8	17.1	---	---	0.5	---	---	---
IN-811	---	0.014	0.79	---	---	0.35	34.1	20.7	Bal.	---	1.98	---	---	---	---
IN-814	---	0.10	0.62	---	---	0.21	Bal.	32.1	15.6	---	3.48	0.35	---	---	---

Table 1.2 Experimental Alloy/Cladding Design Compositions

Alloy No.	Nominal Chemistry (% by Weight, Balance Fe)*				
	Ni	Cr	Al	Si	Y
1	25	20	---	---	---
2	25	20	2	---	---
3	25	20	---	2	---
4	25	20	2	2	---
5	35	25	---	---	---
6	35	25	2	---	---
7	35	25	---	2	---
8	35	25	2	2	---
9	40	30	---	---	---
10	40	30	2	---	---
11	40	30	---	2	---
12	40	30	2	2	---
13	35	25	4	---	---
14	35	25	4	---	0.1
15	35	25	4	---	0.5
16	35	25	---	---	0.1
17	35	25	---	---	0.5
18	20	25	---	---	0.6
19	20	23	---	---	0.5 Y_2O_3 †

*Alloys contain 0.08% carbon maximum, approximately 0.2% manganese.
†Mechanical alloy.

Note: The results of chemical analysis and metallographic examination of the above alloys are presented in Appendix A.

stream of silicon tetrachloride to the retort at an elevated temperature, generally around 1850°F (1010°C). In carbon steel the high-silicon case contains about 14-percent silicon and thus has improved resistance to corrosion and oxidation.

Table 1.3 Coatings

Diffusion Coatings	Alonizing Chromizing Siliconizing
Plasma Spray Coatings:	
Iron-Based Alloy	Fe-16%Cr-10%Al
Chromium-Nickel Alloys	50%Cr-50%Ni 45%Cr-45%Ni-5%Al-5%Si
Nickel-Based Alloys	Ni_3Al 50%Ni-32%Mo-15%Cr-3%Si (Tribaloy)
Cobalt-Based Alloy	52%Co-28%Mo-17%Cr-3%Si
Others	Calcium impregnation of Ni_3Al

-- 1.2.3.2 - Plasma-Arc Spray Coatings. The iron-based coatings were selected based on their improved oxidation resistance. The coating alloy selected posseses the maximum predicted useful life when compared with pure iron, the ratio being approximately 250,000:1.

In general, high-nickel alloys have poor resistance when they come into contact with sulfidizing gases and alkali metal sulfates. Increasing the chromium content in nickel alloys results in improved resistance to some sulfur-containing contaminants. The coating selection of 50%Cr-50%Ni was based upon its excellent performance in oil-fired steam generators. The 50%Cr-50%Ni alloys are also commercially available in the form of coextruded clad tubing as INCO 671. Modifications were also made to the 50%Cr-50%Ni coating by the addition of silicon or aluminum powders to the plasma-arc spray. The selected nickel-based alloy coatings provided preliminary comparative information during screening tests.

The cobalt-based alloy coating, developed primarily as a wear-resistant coating, by the E. I. Du Pont de Nemours Company, is is reported to have excellent corrosion-resistant properties. The composition of the alloy is designed to produce a large percentage of Laves phase that is highly stable up to its melting point [2900°F (1595°C)]. The alloy is reported to form stable, adherent oxides that are effective in minimizing wear and corrosion.

-- 1.2.3.3 - Other Coatings. The other systems evaluated were novel approaches that had not been considered previously.

Since the plasma-arc sprayed coatings usually contain a finite amount of microporosity, impregnating the Ni_3Al coating with molten calcium was considered. The theory proposed was that the calcium would form a tightly adherent sulfate/oxide coating on the tube surface that would retard attack by the sodium-potassium sulfates. Because of incompatibility of the calcium with the nickel coating, CaO- and MgO-containing plasma coatings were substituted.

- Subtask 1.3 - Specimen Preparation

Specimens [1 in. x 2 in. x 0.1 in. (25 mm x 51 mm x 2.5 mm)] were prepared in duplicate after the starting sheet was metallographically examined. Attention was paid to initial grain size, inclusion levels, other dispersed phases, etc. Specimens were ground on 600 grit SiC paper and thoroughly cleaned before they were exposed to the synthetic fuel-ash environment.

- Subtask 1.4 - Test Sequence

Laboratory testing at 1250 and 1450°F (675 and 790°C) was conducted in the following order: commercial and semicommercial alloys, developmental alloys, and coatings on commercial alloys.

- 1.4.1 - The base materials listed in Table 1.1 were exposed to the synthetic combustion gas mixture for 250 and 500 hours without ash. When the ash was present on the test specimen surface, weight loss data were obtained and used in the quantification of results.

- 1.4.2 - The base materials listed in Table 1.1 were exposed to the gas-ash environment for 250 and 500 hours. Corrosion mechanisms and attack rates were determined for this alkali sulfate regime. Based on these results, an optimum test duration was selected for the remainder of the project.

- 1.4.3 - The eight selected alloys were exposed to the alkali sulfate environment with:

  -- Carbon added to the ash
  -- Carbon and sodium chloride added to the ash.

  Corrosion mechanisms and attack rates were determined for both regimes.

- 1.4.4 - The alloy compositions listed in Table 1.2 and preoxidized specimens of 25%Cr-35%Ni with and without the aluminum and yttrium additions were exposed to the gas-ash environment for the predetermined test duration. Corrosion mechanisms and attack rates were established for this alkali sulfate regime.

- 1.4.5 - A statistical sampling of compositions from the alloy design matrix was exposed to the gas-ash and gas-ash-chloride environments. Attack rates and mechanisms were determined for these regimes.

- 1.4.6 - Both the specimens prepared by the application of the coatings listed in Table 1.3 to the previously selected base materials and the standard specimens were exposed to the same 1250°F (675°C) fireside environment for ease in making a direct comparison of the corrosion data.

- Task 1.5 - Specimen Evaluation. Test specimens were evaluated in varying degrees by the following techniques:

  - Macroscopic examination
  - Metallographic examination
  - Electron-probe microanalysis
  - Weight-loss determination
  - X-ray diffraction.

  In addition, the Scanning Electron Microscope (SEM) and Scanning Auger Microprobe were used as required. Test evaluation methods were in accordance with accepted industry standards, such as ASTM or NACE, where applicable.

  - 1.5.1 - Pretest Evaluation. Alloy specimens were obtained from single heats of material with appropriate certification. Representative samples of alloy specimens were also precharacterized by microscopic inspection. The initial weight of each specimen in 1.4.1 and 1.4.2 was determined and recorded immediately before exposure. All data from these examinations were identified and maintained for use in analyzing the specimens after testing (see Appendix B). The special compositions in Table 1.2 were characterized chemically and metallographically as shown in Appendix B.

- 1.5.2 - Post-Test Evaluation. Upon completion of the tests, the specimens were examined microscopically, photographed when appropriate, descaled, and weighed to determine metal loss. A duplicate specimen with the corrosion product intact was used for the structural examination to identify the processes involved in the fireside corrosion of the selected group of materials. Cross sections of the exposed specimens with scales intact were prepared, examined by light microscopy, and photographed. Metal loss, depth of penetration, and internal oxidation measurements were made with a micrometer-stage microscope. Depth of attack was measured on the descaled coupons with a point micrometer.

  Electron-probe microanalysis was used to determine the elemental distribution in the corrosion scale, attacked surface metal, and unaltered alloy matrix. The SEM and associated energy-dispersive analyses were used to characterize surface attack on some samples, and x-ray diffraction (XRD) was used to determine the crystal structure of the corrosion product films.

SECTION 2
EXPERIMENTAL APPROACH AND TEST PLAN

Section 2

EXPERIMENTAL APPROACH AND TEST PLAN

2.1 SIMULATION OF FIRESIDE CORROSION

The experimental approach to the simulation of fireside corrosion consisted of passing a steady flow of a synthetic flue gas over a group of selected materials. The alloys tested, in the form of sheet coupons, were placed in a retort designed to provide uniform exposure to all test pieces. To simulate the fireside corrosion environment developed in a coal-fired system, a synthetic ash consisting of blended alkali sulfates and Fe_2O_3 was prepared and placed on the exposed top surfaces of the specimens prior to furnace exposure. A high temperature of 1250°F (675°C), higher than that found in conventional power plants, was used to obtain accelerated results. The composition of the synthetic ash and flue gas used was the same as that which had been used in other laboratory studies of fireside corrosion.

2.1.1 Flue Gas System and Analysis

The synthetic flue gas mixture was continuously blended from cylinder gases which were controlled and measured by flow meters. It was composed of 72 percent (by volume) N_2, 14 percent CO_2, 10 percent H_2O, 3.6 percent O_2 and 0.25 percent SO_2. Flue gas components, including water, were determined by gas analysis to verify the desired composition. The SO_3 content (500 to 800 ppm) in the test retort was higher than the bulk gas analysis in a commercial boiler flue gas; however, it was not higher than the effective SO_3 content normally found near the tube surface where corrosion occurs. The effective SO_3 content near a catalytic surface is very much higher than the bulk SO_3 (average) analysis.[3,4]

2.1.2 Synthetic Fuel Ash

As stated in Section 1.3, the synthetic fuel ash was prepared from blended powders of potassium, Na_2SO_4, and Fe_2O_3 in weighed proportions as the

precursor to $(Na,K)_3Fe(SO_4)_3$ which forms when the ash is reacted with flue gas containing SO_3. The composition of the ash in mol percent was: 37.5 percent Na_2SO_4, 37.5 percent K_2SO_4, and 25 percent Fe_2O_3. The individual effects of the addition of carbon and NaCl) to the fuel ash were evaluated using concentrations of 10 percent carbon and 3 percent NaCl. Batches of the "ash" were weighed, dried, and ball-milled for 24 hours to ensure effective mixing; screened; and stored in glass bottles.

At the time of application, the dry powder was mixed with a small amount of camphor binder in alcohol solution to ensure adherence to the test coupon during the assembly and start-up of the retort. The camphor binder evaporates from the system completely on warm-up above 200°F (95°C). The removal of the binder was verified, and no difference in the corrosion was obtained when the binder was eliminated.

2.2 MATERIALS SELECTION

Testing of materials for the program was divided into three phases:

- Phase 1 - Commercial and Semicommercial Alloys
- Phase 2 - Developmental Alloys
- Phase 3 - Coatings on Commercial Alloys.

The chemical composition of materials tested in the three phases is detailed in Table 1.1 (Section 1) and Tables 2.1 and 2.2.

2.3 SPECIMEN PREPARATION

Test specimens of all the alloys for Phases 1 and 2 (Tables 1.1 and 2.1) were prepared as 1-in. x 2-in. x 0.1- to 0.125-in. (25-mm x 51-mm x 3.5- to 3.2-mm) coupons, hand ground on the test surface with 600 grit SiC paper, and thoroughly cleaned before exposure. Thickness readings in several areas of each

Table 2.1 Alloy Compositions for Phase 2 Fireside Tests

Alloy No.	Actual Chemical Analysis (% by Weight, Balance Fe)						
	Ni	Cr	Al	Si	Y	Mn	C*
1	24.7	19.8	---	0.41	---	0.64	0.025
2	25.4	19.6	2.04	0.40	---	0.60	0.026
3	25.3	19.4	---	2.27	---	0.57	0.026
4	24.2	19.6	2.00	2.40	---	0.59	0.034
5	33.5	24.4	---	0.40	---	0.70	0.026
6	34.0	24.5	2.00	0.40	---	0.74	0.035
7	34.1	24.2	---	2.30	---	0.74	0.025
8	33.7	24.1	1.90	2.30	---	0.62	0.013
9	38.5	30.2	---	0.50	---	0.72	0.024
10	39.0	30.2	1.80	0.40	---	0.74	0.020
11	38.7	30.5	---	2.30	---	0.71	0.027
12	39.3	29.7	1.80	2.40	---	0.76	0.019
13	33.0	24.4	3.70	0.40	---	0.70	0.015
14	33.9	24.3	3.70	0.40	0.01	0.75	0.021
15	37.2	24.2	4.20	0.44	0.60	0.72	0.025
16	35.1	24.3	---	0.44	0.06	0.57	0.033
17	35.4	24.7	---	0.37	0.53	0.68	0.031
18	18.4	25.1	---	0.45	0.58	0.67	0.041
19†	20.0	23.0	0.30	---	0.65 Y_2O_3	---	0.045

*Nominal carbon analysis was 0.035 percent maximum for all alloys except 18 and 19 which had 0.045 percent maximum.
†Mechanical alloy.

Note: The metallographic characterization of the listed alloys is presented in Appendix B.

Table 2.2 Phase 3 Alloys With Coatings and Surface Treatments

Diffusion Coatings (Commercial High-Temperature Diffusion)	Alonizing Chromizing Siliconizing
Plasma Spray Coatings:	
Iron-Based Alloys	Fe-16%Cr-10%Al (elemental) Kanthal A-1 (applied by metallizing)
Chromium-Nickel Alloys	50%Cr-50%Ni (IN-671) 45%Cr-45%Ni-5%Al-5%Si (elemental) 45%Cr-48%Ni-5%Si (IN-671 + Si)
Nickel-Based Alloys	Ni_3Al 50%Ni-32%Mo-15%Cr-3%Si (Tribaloy)
Cobalt-Based Alloy	52%Co-28%Mo-17%Cr-3%Si
Nonmetallic	$CrSi_2$ $MgZrO_3$ ZrO_2

Note: Further details and characterization of the coated specimens are presented in Appendix B.

specimen were recorded along with the weight, and representative specimens were photographed (1.5X). The Phase 1 alloy sheet materials were all obtained from commercial or semicommercial heats. A few alloys were reannealed, as required.

A catalog of Phase 1 and 2 alloy microstructures (Appendix B) lists grain size measurements, hardness readings, and some electron microprobe determinations of phase compositions as a comparative index for the as-tested materials. All alloy microstructures, in hot rolled and annealed conditions are shown in Appendix B.

The first 18 Phase 2 alloys in Table 2.1 were prepared as 30-lb (13.6 kg) vacuum-induction melts at INCO's Paul D. Merica Research Laboratory. Electrolytic iron, pure nickel pellets, and vacuum-grade pure chromium were melted in an Al_2O_3 crucible; deoxidized with a carbon addition; and allowed to boil at 2645°F (1450°C). The addition of 0.4-percent silicon metal and 0.7-percent electrolytic manganese followed. Further silicon and aluminum alloying additions and an yttrium addition in six heats were made shortly before pouring at 2625°F (1440°C) into 4-in. x 4-in. (102-mm x 102-mm) cast iron molds. The cast structures were broken up by forging the billets from 2150°F (1175°C). The 3-in. (76-mm)-thick plate of each alloy was then reheated to 2150°F (1175°C) and hot rolled in about four passes to a 1/4-in. (6.35-mm)-thick strip.

During the forging operation, hot shortness was encountered in a number of the yttrium-containing alloys. The heats were remelted, and by lowering the forging and hot rolling temperatures to about 2000°F (1095°C), hot cracking was eliminated.

Metallographic examination (Appendix B), showed that the hot-rolled plates were generally recrystallized. However, most plates exhibited substantial banding, possibly as a result of segregation. Also, layers of material with differing grain sizes, and in some cases layers of unrecrystallized material, may have caused banding. To ensure that all the alloys were similar in

microstructure, pieces of the plate were annealed at 2200°F (1205°C) for 1 hour in an argon environment and water quenched to prevent precipitation of the secondary phases on cooling. This treatment, which is typical of one that would be used for commercial alloys, resulted in fully recrystallized, austenitic grain structures of intermediate grain sizes. Alloy 15, containing 4-percent aluminum and 0.5-percent yttrium, showed a substantial amount of a dark etching phase (apparently lower melting) at the grain boundaries. Microprobe examination showed this to be a high-yttrium, high-aluminum phase containing 8-percent yttrium and 19.2-percent aluminum. A globular phase in the grain interiors contained 55-percent nickel, 20.8-percent yttrium, and 9.1-percent aluminum. Alloy 17 had the same 0.5-percent yttrium metal addition but no aluminum. In this case, the higher melting, high-yttrium phase (56.5%Ni-26.9%Y) appeared as a coarse globular phase with a stringer distribution. Because of the coarseness of the yttrium-containing phases in the annealed alloy (No. 17), samples of this alloy in the hot worked condition were also exposed in the fireside corrosion test.

Alloy 19 was a mechanically alloyed material of the nominal 310SS composition, dispersion strengthened with 0.65-percent Y_2O_3. The material was made by processing appropriate powders using INCO's high-energy milling technology. The powder was consolidated by powder extrusion in a steel jacket followed by hot and cold rolling to plate. The structure is typical of many mechanically alloyed materials, which have a very elongated grain structure in the extrusion direction (Appendix B, Alloy 19).

2.4 TEST SEQUENCE

2.4.1 Introduction

The test sequence for the fireside corrosion experiments provided a reproducible, systematic method for testing materials under the required conditions. In Task 1.4.1, specimens were tested in the flue gas atmosphere without ash. This test established a baseline for comparison because it was the least

corrosive environment. In subsequent tests, Tasks 1.4.2 through 1.4.6, the effects of simulated fuel ash were evaluated alone and with separate additions of carbon and sodium chloride in a flue gas environment. The test sequence is shown in Table 2.3, Fireside Corrosion Test Plan.

2.4.2 Procedure

Specimens were loaded into the retort tube assembly (Figure 2.1). Once loaded, the exit manifold cover plate was sealed and bolted to the front of the retort. The retort was then placed in an outer retort box, which was sealed, lowered into a furnace, heated under a nitrogen purge for 18 hours at 250 to 300°F (120 to 150°C), and then heated to the test temperature. When the test temperature was reached, the flowing flue gas mixture was introduced, and flow was maintained throughout the test. Upon completion of the test, the retort was cooled under a nitrogen purge until ambient temperature was reached. The specimens were then removed. Appendix C gives further details of the procedure.

2.5 METHODS OF EVALUATING CORROSION LOSSES

After testing, specimens were evaluated by visual observations, macrophotographs, physical measurements, pitting description, microscopic examination, and electron beam analysis.

2.5.1 Visual and Photographic Evaluation

After the specimens were removed from the retort, their surfaces were examined for pitting tendency, coating behavior, and ash activity. Specimens to be examined microscopically were coated with epoxy to provide a backing surface that prevented chipping of the scale/deposit when a transverse cross section was removed. Specimens that were not cut for microscopic examination and most of the remaining portions of those that were received the descaling treatment described in Table 2.4.

In some cases photographs of the reaction surface were taken before the specimens were descaled. After descaling was completed, the reaction surfaces

Table 2.3 Fireside Corrosion Test Plan

Test Sequence	Specimens	Gas Mixture	Synthetic Coal-Ash	Retort No.	Exposure (°F, h)
Phase 1:					
1.4.1	Base materials 18 commercial alloys	Flue gas*	None	1 2 3	1250, 250 1450, 250 1250, 500
1.4.2	Base materials 18 commercial alloys	Flue gas*	Simulated ash†	4 5 6	1250, 250 1250, 500 1440, 250
1.4.2.1	Base materials 18 commercial alloys	Flue gas*	Simulated ash†	7 8	1250, 100 1250, 24
1.4.2.2	Base materials 18 commercial alloys	Air only	Prefused $(Na,K)_3Fe(SO_4)_3$	9	1250, 50
1.4.3	8 selected alloys	Flue gas*	Simulated ash† + 10% carbon	10 11 12	1250, 48 1250, 48 1450, 48
1.4.3.1	Preoxidized specimens 8 selected alloys	Flue gas*	Simulated ash	13	1250, 48
1.4.3.2	8 selected alloys	Flue gas*	Simulated ash† + 3% NaCl	14 15	1250, 48 1450, 48
Phase 2:					
1.4.4	Special alloy compositions	Flue gas*	Simulated ash†	16	1250, 48
1.4.5	Statistical sampling from alloy design sampling	Flue gas* Flue gas*	Simulated ash† Simulated ash† + 3% NaCl	17 18	1250, 48 1250, 48
Phase 3:					
1.4.6	Specimens with coatings and diffusion alloys	Flue gas* Flue gas*	Simulated ash† Simulated ash + NaCl	19 20	1250, 48 1250, 48

*72% N_2, 14% CO_2, 10% H_2O vapor, 3.6% O_2, 0.25% SO_2 (SO_3 formed in the retort).
†37.5% Na_2SO_4, 37.5% K_2SO_4, 25% Fe_2O_3 (mol %), blended and dried.

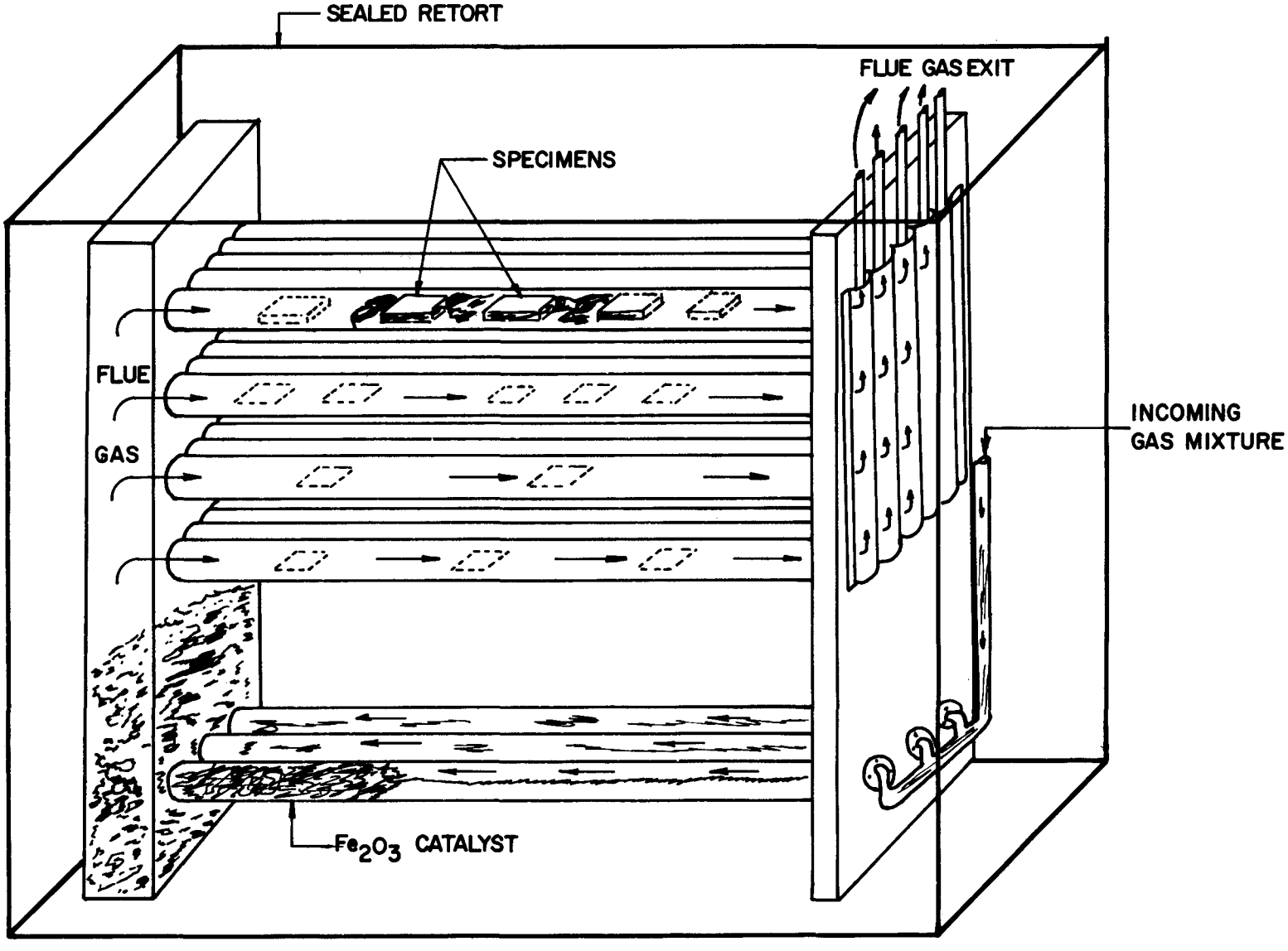

Figure 2.1 Fireside Corrosion Retort

Table 2.4 Descaling Treatments After Fireside Test

Material	Description	Immersion Time (min)
Primary Scale Loosening and Softening		
All materials except coated samples with high-aluminum or nonmetallic materials	Fused NaOH at 800°F	15 (then cold water quench)
Secondary Descaling Conditions		
304SS 310SS 347SS 21-6-9SS 737SS	Pumice scrubbed followed by immersion in 10% HNO_3 distilled water at 160°F (72°C) for varying periods of time and repumiced as required.	10 (minimum)
Carbon steel 2-1/4%Cr-1/2%Mo HT-9 Incoloy 800, 840 High-nickel alloys	Pumice scrubbed followed by immersion in 18% inhibited HCl at 140°F (60°C) for several minutes and repumiced as required.	1 to 3

of the specimens were photographed (approximately 1.5X) (see Appendix D). Photographs at 8X were also taken of the transverse cross sections of representative specimens that were cut for microscopic observation.

2.5.2 Physical Measurements and Pitting Evaluation

The descaled specimens were measured with point micrometers for thickness in five or more locations where the pretest thickness measurements were made. By comparing both measurements and compensating for the gas corrosion (see Section 3), a characterization of the average corrosive losses representative of the specimens was determined. In most cases, many round-bottomed pits with similar depths were observed. Pitting depths, observed from transverse cross sections photographed at 8X, were measured by comparing the thickness at unattacked areas with that at areas containing the deepest pits. Where pitting appeared severe, average loss and typical pit depths were recorded. In Phase 1, the weight of the specimen was recorded before and after testing as another means of determining the general corrosion behavior. The data obtained with various measurement techniques were in agreement.

2.5.3 Microscopic Examination

Microscopic examination of the specimens was carried out in three forms: metallography, secondary and backscatter electron imaging in an SEM, and electron beam analysis. The samples used for these examinations were transverse cross sections removed from the specimens before the descaling treatment. Pitting depths, scale/deposit formations, coating structures, and elemental concentration profiles were among the aspects studied and photographed.

After exposure to the fireside environment, the specimens were examined by a variety of metallographic techniques. Specimens for examination in the optical microscope, the SEM, or electron probe microanalyzer were usually coated with an epoxy to prevent spalling of the corrosion product layers during cutting and grinding. Specimens were then mounted in either bakelite or epoxy, ground on SiC papers, and polished with a diamond abrasive.

2.5.4 Analysis and Chemical Evidence

The loose outer deposits and the adherent inner scales were identified by XRD on a Siemens diffractometer using Cu-K-alpha radiation, with a graphite crystal monochromator on the diffracted beam and a proportional flow counter.

A Cambridge Stereoscan 180 SEM equipped with Princeton Gamma Tech Energy-Dispersive X-Ray (EDX) analysis equipment was used for much of the examination of cross sections of corroded specimens. Phases in the uncorroded alloy; the internal diffusion-attacked region, when present; and the corrosion product layers were identified by combining XRD information and chemical information from the EDX analysis.

An Applied Research Laboratory wave length dispersive electron probe microanalyzer was used when quantitative phase analysis was desired or when detailed information was sought on diffusion gradients and compositional changes below the corroded surface. The instrument has an analytical resolution of about 1 μm^3 of material. Raw x-ray intensity data are converted to compositions using a computerized ZAF correction procedure.

Microprobe and SEM specimens were coated by sputtering with a thin layer of carbon to improve conductivity when imaging the nonconductive regions of the specimens.

SECTION 3
RESULTS OF FIRESIDE TESTS

Section 3

RESULTS OF FIRESIDE TESTS

3.1 PHASE 1 - COMMERCIAL AND SEMICOMMERCIAL ALLOY TESTING

3.1.1 Task 1.4.1 - Oxidation in Flue Gas

The base materials listed in Table 3.1 were initially tested in the flowing synthetic flue gas before they were evaluated for their resistance to fireside attack.

3.1.1.1 Data Obtained. Oxidizing effects of the synthetic flue gas (72 percent N_2, 14 percent CO_2, 10 percent H_2O (v), 3.6 percent O_2, 0.25 percent $SO_2 + SO_3$)* were determined at 1240 and 1440°F (670 and 780°C) by weight changes and metal losses. The experimental technique and equipment worked well, but the flue gas exit tubes suffered corrosive attack because of the sulfuric acid condensate at the acid dew point. The gas exit system was revised in subsequent exposures using water-cooled Teflon downcomers.

The results of the tests at 1240 and 1440°F (670 and 780°C) comprise the data shown in Tables 3.2 and 3.3. Good oxidation resistance was demonstrated by all but the lowest alloy steel, 2-1/4%Cr-1%Mo; however, 1240°F (670°C) is about 100°F (55°C) above the normal service temperature for 2-1/4%Cr-1%Mo alloy steel, so the adverse oxidation rate of this alloy was expected. The results of a comparison of some of the higher alloy losses with the oxidation of 304SS and 347SS, however, were not as expected; that is, some of the higher alloys, such as IN-809 and IN-671, experienced greater oxidation-related changes than did the stainless steels. Nevertheless, in both alloy groups the oxide formation was still thin. However, the scale formed by flue gas alone is not an indication of the resistance to attack by the fused ash deposits.

*By volume.

Table 3.1 Chemical Composition of Phase 1 Alloys for Fireside Tests (% by Weight)

Alloy	Heat or Lot No.	C	Mn	P	S	Si	Ni	Cr	Fe	Mo	Al	Ti	V	Cu	Other
Ferritic Alloys															
2-1/4%Cr-1%Mo	52816	0.12	0.55	0.020	0.023	0.29	0.15	2.34	Bal.	0.87	---	---	---	---	Co 0.13
HT-9 (Sandvik Tube)	4-52112	0.22	0.52	0.018	0.005	0.35	0.50	11.3	Bal.	0.97	---	---	0.26	---	W 0.50
Austenitic SS															
304	47832	0.055	1.71	0.022	0.025	0.55	8.40	18.34	Bal.	0.11	---	---	---	0.08	Co 0.16
347	8083689	0.059	1.58	0.03	0.015	0.67	10.30	18.50	Bal.	0.17	---	---	---	0.16	Cb 0.61
	30W2	0.055	1.72	---	---	0.81	9.8	18.1	Bal.	---	---	---	---	---	Cb 0.84
310	8084791	0.069	1.77	0.028	0.014	0.46	20.40	25.30	Bal.	---	---	---	---	---	---
	04964	0.045	0.18	---	---	0.14	22.1	22.3	Bal.	---	---	---	---	---	---
314	7401-8001	0.068	1.06	0.042	0.024	1.73	21.1	24.2	Bal.	0.01	---	---	---	0.02	---
	46W	0.056	2.03	---	---	2.09	19.4	23.3	Bal.	---	---	---	---	---	---
IN-840	---	0.041	0.13	---	---	0.77	20.6	20.3	Bal.	---	---	---	---	---	---
High-Manganese Alloy															
21-6-9 (Nitronic 40)	346087	0.021	9.2	0.016	0.003	0.67	7.21	20.1	Bal.	0.16	---	---	---	0.13	N 0.32
High-Iron Superalloys															
IN-737	---	0.032	<0.1	---	---	<0.1	37.5	17.2	Bal.	1.44	0.59	0.52	---	---	Cb 1.03
Incoloy 800H	---	0.056	0.88	---	---	0.24	31.2	20.4	Bal.	---	0.47	0.46	---	0.63	---
Incoloy 800	HH2118A	0.05	0.93	---	0.007	0.42	31.24	21.54	44.72	---	0.39	0.35	---	0.33	---
A-286	29385	0.041	1.32	0.023	0.003	0.54	25.10	15.22	Bal.	1.40	0.17	2.18	0.27	0.26	B 0.007
AL-6X	00629	0.013	1.65	---	0.005	0.33	24.41	20.0	Bal.	6.5	0.03	---	---	---	---
Nickel-Base Superalloys															
Inconel 625	---	0.019	0.13	---	---	0.19	Bal.	21.8	2.9	8.9	0.26	0.21	---	---	Cb 3.8
IN-671	---	0.059	<0.1	---	---	0.38	Bal.	45.5	---	---	0.034	0.26	---	---	---
Semicommercial Alloys															
IN-549	---	0.099	<0.1	---	---	0.28	43.7	19.5	Bal.	---	2.5	---	---	---	---
IN-809	---	0.010	<0.1	---	---	<0.1	Bal.	36.8	17.1	---	---	0.5	---	---	---
IN-811	---	0.014	0.79	---	---	0.35	34.1	20.7	Bal.	---	1.98	---	---	---	---
IN-814	---	0.10	0.62	---	---	0.21	Bal.	32.1	15.6	---	3.48	0.35	---	---	---

Table 3.2 Flue Gas Exposures for Retorts 1 and 3

Alloy	Retort 1 [1230-1240°F (665-670°C), 250 Hours] Weight Gain (mg/cm^2)	Descaled* Wt. Loss (mg/cm^2)	Appearance and Comments	Retort 3 [1240°F (670°C), 500 Hours] Weight Gain (mg/cm^2)	Descaled* Wt. Loss (mg/cm^2)	Appearance and Comments
2-1/4%Cr-1%Mo	20.6 22.3	63.2 ---	Hard, gray Hard, black & gray	60.84	---	Loose, black
HT-9	0.235 0.300	--- 0.866	Hard, glossy brown	0.393 0.357	--- 0.95	Hard, black
304SS	0.104 0.143	--- 3.04*	Hard, black spots Partly black	0.454 0.467	1.06 ---	Hard, spotted
347SS	0.007 0.042	--- 0.68	Bronze temper color	0.233 0.127	1.03 0.783	Hard, gray, glossy
310SS	0.111 0.110	--- 0.95	Hard, black	0.250	1.48	Partly soft, gray
314SS	0.042 0.039	--- 0.65	Gray, glossy	0.208 0.220	1.05 1.17	Hard, brownish gray
21-6-9	0.708 0.710	--- 2.44†	Hard, black Black, smooth	0.555 0.311	2.6 2.2	Gray, some greenish
IN-737	0.093	---	Bright, with some tarnished spots	0.262	1.10	Hard, bright, iridescent
Incoloy 800	0.227 0.208	--- 2.24†	Partly dark gray Some gray glossy areas	2.33§	2.8	Soft, gray pits
A286	0.157 0.210	--- 2.12†	Dark gray Hard	0.380	1.47	Gray, some pits
Al-6X	0.350 0.140	--- 1.39†	Dark, dull	0.273	1.7	Loose, dark
Inconel 625	0.0702	---	Bronze glossy	0.299	0.70	Hard, dense, gray
IN-549	Nil	---	Glossy, gold	0.166	0.48	Thin, glossy
IN-809	0.043	---	Hard, black	0.276	0.81	Dark
IN-811	0.0167	---	Hard, dark	0.903	---	Bronze, spotted
IN-671	---	---	---	1.610	1.13	Hard, some green spots

*Some doubt exists about descaled data accuracy because of the uneven scale removal.
†Subject to some pitting because of the descaling acid.
§Some oxide "dusting" initiated.

Table 3.3 Flue Gas Exposures for Retort 2 [1440°F (780°C), 250 Hours]

Alloy	Weight Gain (mg/cm^2)	Descaled* Wt. Loss (mg/cm^2)	Appearance and Comments
2-1/4%Cr-1%Mo	157.0 164.0	--- 411.0	Heavy buildup, loose scale
HT-9	0.350 0.260	1.63 ---	Hard, black, adherent
304SS	0.230 0.260	--- 0.556	Hard, dark scale, semiglossy
347SS	0.072 0.075	--- 0.490	Metallic gray on polished surface
310SS	0.228 0.336	0.830 ---	Dark gray, small spots
314SS	0.150 0.116	--- 0.561†	Small black specks over metallic gray
IN-840	0.186 0.221	0.470 ---	Hard, dark gray
21-6-9	0.943 0.960	1.47 ---	Black, glossy, chipped on edge
IN-737	0.071 0.163	--- 0.807†	Hard, dark gray
Incoloy 800H	0.343 0.360	--- 0.740	Black, gray along edge
A286	0.698 0.574	--- 0.875	Hard, black, some gray spots
Al-6X	0.196 0.217	--- 0.890†	Black and gray (Gray was soft.)
Inconel 625	0.195 0.110	--- 0.440	Soft, dark, dull
IN-671	0.225 0.303	0.607 ---	Soft and gray Dark green
IN-549	0.163 0.210	0.471 ---	Hard, bronze, metallic
IN-809	0.264 0.333	--- 0.759	Soft powdery surface, green
IN-811	0.210 0.205	0.510 ---	Hard, very light Gold-bronze
IN-814	0.140 0.186	--- 0.375	Hard, light yellow Gray, glossy

*Some doubt exists about descaled data accuracy because of the uneven scale removal.
†Subject to some pitting because of the descaling acid.

The very small oxidation-related weight gains were affected by variations in surface conditions (only one side was polished). These data were reproducible but were subject to some minor weight-gain error because the scale on the coupon edges adhered to the retort tube surfaces, leading to small weight losses from some coupons. (An error of about 1 mg may have occurred in some cases, such as IN-549.)

The descaled weight loss was subject to some error because of the chemical descaling problem, which varied with the alloy. Some coupons, indicated by a dagger on Tables 3.2 and 3.3, developed spots of visible pitting during the scale-removal process. The descaling-related error increased the weight losses 1 to 2 mg/cm^2 on a few specimens.

3.1.1.2 Effect of Higher Temperature. The effect of oxidation at increased temperature is shown by a comparison of the 250-hour weight gain results listed in Table 3.4. Most alloys gained in weight--but a few, including HT-9, 347SS, IN-737, and AL-6X, were not significantly different. The 2-1/4%Cr-1%Mo specimens from Retort 2 [1440°F (780°C)] were so heavily attacked that there was an obvious increase in the external dimensions. After descaling, the average penetration of the 2-1/4%Cr-1%Mo steel was 0.034 in. (865 μm), with greater losses at the edges.

The very thin, protective oxides on the 347SS, 314SS, IN-549, IN-811, and IN-814 were distinctly different from the oxides on the other austenitic and nickel-based alloys listed in Table 3.3. Some of the alloys, such as IN-809 and IN-671, formed a soft, powdery-type oxide, which appeared to be "metal dusting." The influence of surface preparation was also very evident, as indicated by the different type of scale on the as-machined surfaces compared with that on the hand-lapped surfaces. Most of the austenitic stainless steels and the IN-549 demonstrated this influence, showing thinner, denser scales on the lapped surface.

Table 3.4 Effect of Increased Temperature on Weight Gain of Base Materials Exposed to Synthetic Flue Gas for 250 Hours

Alloy	Weight Gain (mg/cm^2)	
	Retort 1 1230 to 1240°F (665 to 670°C)	Retort 2 1440°F (780°C)
2-1/4%Cr-1%Mo	22.3	157.3
HT-9	0.235	0.255
304SS	0.104	0.230
347SS	0.007	0.072
310SS	0.111	0.228
314SS	0.042	0.150
IN-840	Not Tested	0.186
21-6-9	0.708	0.943
Incoloy 800H	0.227	0.343
A-286	0.157	0.574
AL-6X	0.350	0.196
Inconel 625	0.070	0.110
Inconel 671	Not Tested	0.303
IN-737	0.093	0.068
IN-549	Nil	0.163
IN-809	0.043	0.264
IN-811	0.017	0.205
IN-814	Not Tested	0.140

The oxides on the higher alloys were so thin that only limited checks could be made on the oxide phases. The 21-6-9 alloy, exposed at 1440°F (780°C), showed heavier scale with isolated sulfides in the metal near the interface, but other alloys did not exhibit any sulfidation as a consequence of the flue gas exposure.

The XRD and SEM evaluations of the scale obtained in Task 1.4.1 are shown in Appendix D. Also included are the electron microprobe data for the 2-1/4%Cr-1%Mo specimens used to identify the scale components resulting from the flue gas exposures.

3.1.1.3 Conclusions From Task 1.4.1. The 2-1/4%Cr-1%Mo ferritic steel was found unsatisfactory for flue gas exposures above its normal engineering limits [1050 to 1075°F (565 to 580°C)]; however, none of the other alloys would be restricted in their use at 1200 to 1250°F (650 to 675°C) based on the gas-phase metal losses alone. This does not imply compatibility with fireside deposits where corrosive ash deposits occur, since the gas phase oxidation is controlled by a different mechanism. The retort system was also demonstrated to be adequately designed for the test.

3.1.2 Task 1.4.2 - Fireside Attack on Commercial Alloys

3.1.2.1 Test Results for 250- and 500-Hour Exposures. Metal losses from exposure to 1240°F (675°C) flue gas plus the simulated coal ash forming molten alkali-iron trisulfate resulted in substantially greater attack rates than the previous exposures to flue gas only (Subsection 3.1.1.1). The resultant 250- and 500-hour surface recession and weight loss data for the listed Phase 1 commercial alloys are presented in Table 3.5. The differences in the degree of attack as affected by the alloy composition were reproducible and substantial. Extending the exposure time to 500 hours (Retort 5), however, had an unexpectedly small effect upon the metal losses. In some of the cases shown in Table 3.5, the loss was less in the 500-hour test than in the 250-hour test (Retort 4). The only apparent explanation for this unexpected inconsistency

Table 3.5 Fireside Corrosion Test Results for Simulated Coal Ash Plus Flue Gas Exposures*

Alloy	Retort 4 [1240°F (670°C), 250 Hours]			Retort 5 [1250°F (675°C), 500 Hours		
	Specimen (Serial No.)	Descaled Wt. Loss (mg/cm^2)	Metal Loss (mils) Max./Avg.†	Specimen (Serial No.)	Descaled Wt. Loss (mg/cm^2)	Metal Loss (mils) Max./Avg.†
2-1/4%Cr-1%Mo	7	---	24/20	9	243§	20/12
	8	330§	24/19			
HT-9	7	---	6/4	9	171	14/8
	8	114	5/4			
304 SS	9	---	8/6	12	194	12/8
	10	147	12/7			
347 SS	14	---	4/2	15	69	5/3
	19	29	4/1.5			
310 SS	8	---	5/4	11	102	7/5
	9	133	9/5.5			
314 SS	6	---	3/2	10	51	5/3
	8	110	6/4			
IN-840	3	---	7/4	6	72	5/4
	4	88.5	7/6			
21-6-9	7	---	5/2	9	84.5	6/3
	8	32.8	2.5/2			
IN-737	11	---	7/5	14	150	13/8
	12	110	8.5/5			
Incoloy 800H	8	---	11/8	9	149	6/5
	10	173.4	15/10			
A286	8	---	12/7	10	114	8/6
	9	222	18/12			
AL-6X	7	---	10/8	9	62	7/5
	8	175	21/11			
Inconel 625	11	---	1/---	13	13	0.2/---
	12	31.2	2/---			
IN-671	6	---	2/---	11	9	2/---
	7	34.6	5.5/---			
IN-549	6	---	6/3	8	44	4/2
	7	95.3	8/6			
IN-809	10	---	1/0.5	13	14	3/1
	12	71	3.5/---			
IN-811	10	---	6/2	12	56.9	5/3
	11	76.4	8/---			
IN-814	14	---	2/---	16	22.5	2/1
	15	28.5	5/2			

*Flue gas was - 72% N_2, 14% CO_2, 10% H_2O Vapor, 3.6% O_2, 0.25% SO_2. Simulated ash - 37.5% Na_2SO_4, 37.5% K_2SO_4, 25% Fe_2O_3 blended and dried.
†The maximum metal loss was the measured depth of pits.
§Weight losses were corrected for lower surface oxidation because of gas-metal reaction, where significant.

was that a few specimens in Retort 5 had lost part of the liquid trisulfate by run-off sometime during the test. Later detailed examination showed that solidification of the deposits was the primary reason for termination of attack during the 250- and 500-hour tests. The depth of surface penetration, or pit depth (usually the maximum loss), shown on Table 3.5 was determined to be the best gauge of materials performance.

The nature of the metal loss in most alloys was very similar: predominantly a pitting attack with generally round-bottomed pits. Apparently, the attack was not controlled by metallurgical factors, but rather resulted from localized electrochemical attack. (For the wide variety of alloy compositions tested, all suffered surprisingly similar pitting attack.)

3.1.2.2 Test Results of Corrosion Tests of Shorter Duration (Subtask 1.4.2.1). The observation that the results of the 500-hour test were little different from those of the 250-hour test suggested that the corrodent available to the sample was spent or solidified; therefore, the need for shorter-time tests was evident. The Test Plan was augmented to include Subtasks 1.4.2.1 and 1.4.2.2, which included exposures of 100, 50, and 24 hours to define the rate of attack. The tests were performed in the same manner as the 250- and 500-hour tests.

The corrosion results from these shorter tests are shown in Figure 3.1. A 48-hour exposure was determined to be a satisfactory basis for comparing the fireside losses for various alloys. The longer exposures tended to produce more oxides in the deposits and added secondary reaction products that made interpretation of the primary attack more difficult. The maximum attack rate for most alloys occurred at 24 hours or sooner. For example, 304SS had a penetration of 8 mil (203 μm) after the first 24 hours and approximately 4 mil (102 μm) additional penetration after the second 24-hour period. Detailed results from the test specimens are presented in Appendix D.

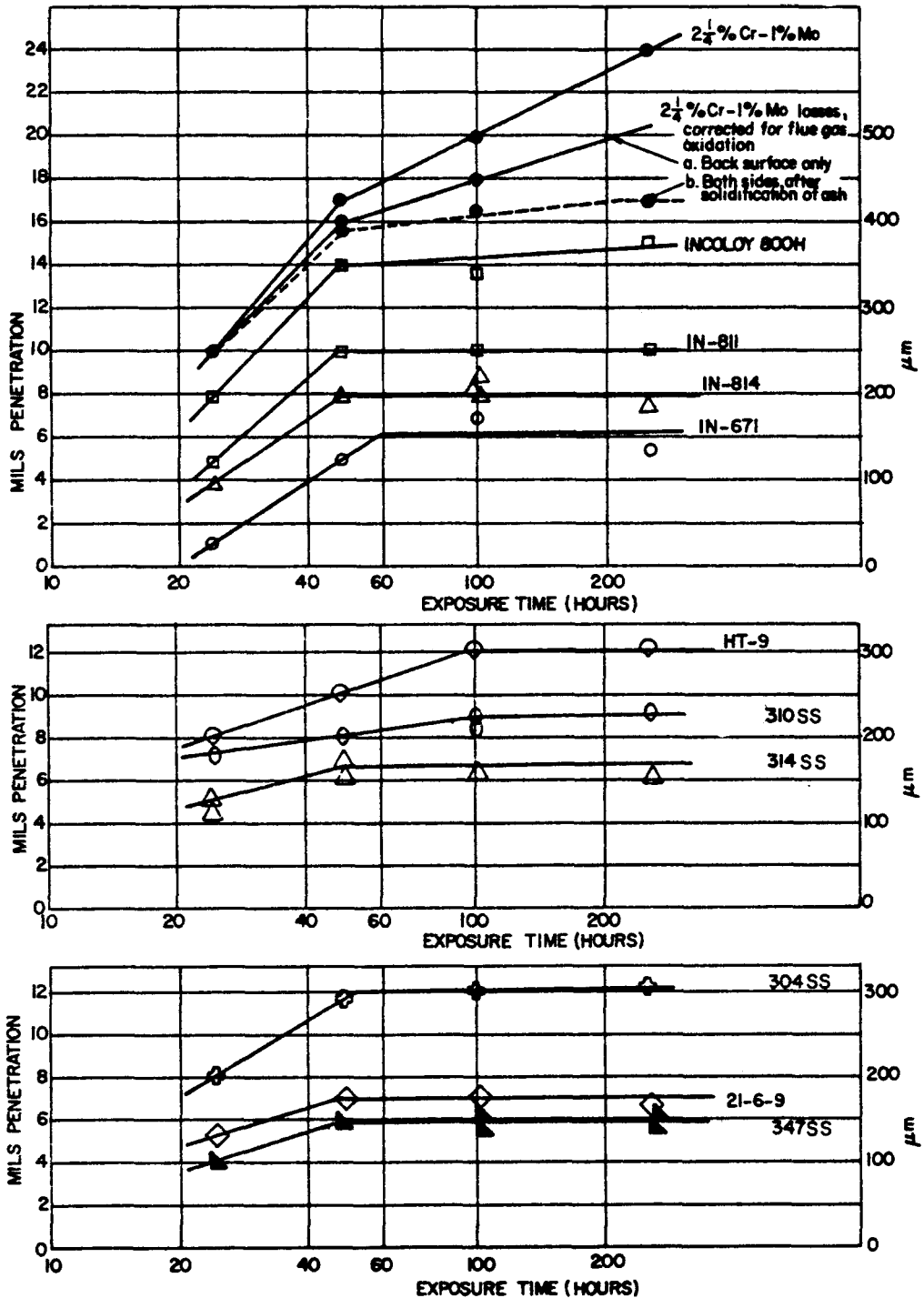

Figure 3.1 Simulated Ash Pitting as a Function of Time at 1250°F (675°C)

3.1.2.3 Mode of Formation of Corrosive Condition (Subtask 1.4.2.2). The attack rates were highest in the first 24 hours and tapered off or nearly stopped after 48 hours, as illustrated in Figure 3.1. This decreased attack rate was caused by the depletion or freezing of the molten corrodent. The straight lines for the initial attack rates (Figure 3.1) are arbitrary; more data from exposures of 10 to 40 hours are needed to establish the rate curves. The leveling off to a horizontal line appears to be the result of solidification or depletion of the liquid phase. Based on the 24- to 48-hour data, no indication of a slow start or initial resistance to the liquid-phase attack was observed.

Since sufficient "ash" was present from the start, the rate of formation of the liquid alkali-iron trisulfate depended on the transfer of SO_3 from the flue gas to the solid surfaces. The original estimate of 10 to 12 hours to form the liquid was based on the absorption of gas-phase SO_3 only; however, it has since been pointed out that the more abundant SO_2 absorbed on the Fe_2O_3 surfaces may be catalytically oxidized in situ, so that the required trisulfate can be produced in less than an hour. Even in a utility boiler flue gas with only 30 to 50 ppm by volume SO_3 in the bulk volume of the gas, the effective SO_3 at the corroding surface is much higher--equivalent to the equilibrium value for the SO_2 oxidation, which may be 1500 or 2000 ppm by volume, as shown by Krause, Levy, and Reid.[4]

The actual rate of the initial reaction should depend on numerous factors: the passive surface, the nature of the electrochemical potentials, the formation or stimulation of cathodic surfaces, and the formation of the liquid-phase corrodent. The present data show that a rapid start is likely once a liquid phase is present. Since all the low alloy steels, 304SS, and Incoloy 800 show the greatest loss rates in the first 24 hours, it is obvious that thin oxide scales are not a barrier to the liquid phase. After 24 hours the liquid phase is altered substantially from the initial melt composition because of the mass of metal in the corrosion product. Such differences in the sulfate melts,

which do not greatly change the short-time rate of attack (comparing high- and low-alloy steels), are evidence of the electrochemical mechanism of corrosion. If the high electrical conductivity is retained in the corrodent and the continuing supply of oxidant is available, the electrochemical cell will function with high or low alloys. The corrosion current may be controlled by the ion mobility of the metal, which will be greatly reduced as the complex sulfate salts freeze because of depletion, dilution with corrosion products, decomposition, or cooling of the melt.

Some supplemental effort was made to determine whether the changes in the melting point alone or the disappearance of the alkali-iron trisulfate would correlate with the decrease in the corrosion rates between 48 and 100 hours (under controlled laboratory conditions). While most alloys noticeably altered the melting-point characteristics of the slag (compare Curves B and C with Curve A) after 100 hours or more, some alloys (such as 21-6-9) effected a partial melting at a lower temperature (Curve D on Figure 3.2). After a 250-hour exposure in the retort, the ash from 304SS exhibited a higher melting point--from 1026 to 1265°F (535 to 685°C)--with only about 15 percent of the mixture in a molten state, as indicated by Curve E. Alloys containing molybdenum and manganese generated the most rapid changes in melting point, notably after 24 and 48 hours of exposure (curves not included on Figure 3.2). The 100-hour corrosion products for Al-6X were fully solidified before 100 hours had passed (as represented by Curve G). On the other hand, 347SS had significantly lower corrosion rates than 304SS (Figure 3.1) and displayed the lowest decomposition or depletion rates of the alkali-iron trisulfates (Curve B) because of the smaller amounts of alloy taken into the melt.

Because the corrosion rate in 347SS was reduced without depletion of the trisulfate in the melt, we concluded that the corrosion rate was limited by a passivity phenomenon on the surface or by altered cathode surfaces. The manganese-containing Nitronic 40 (21-6-9) alloy, on the contrary, terminated the rapid attack by raising the melting point and by altering the nature of

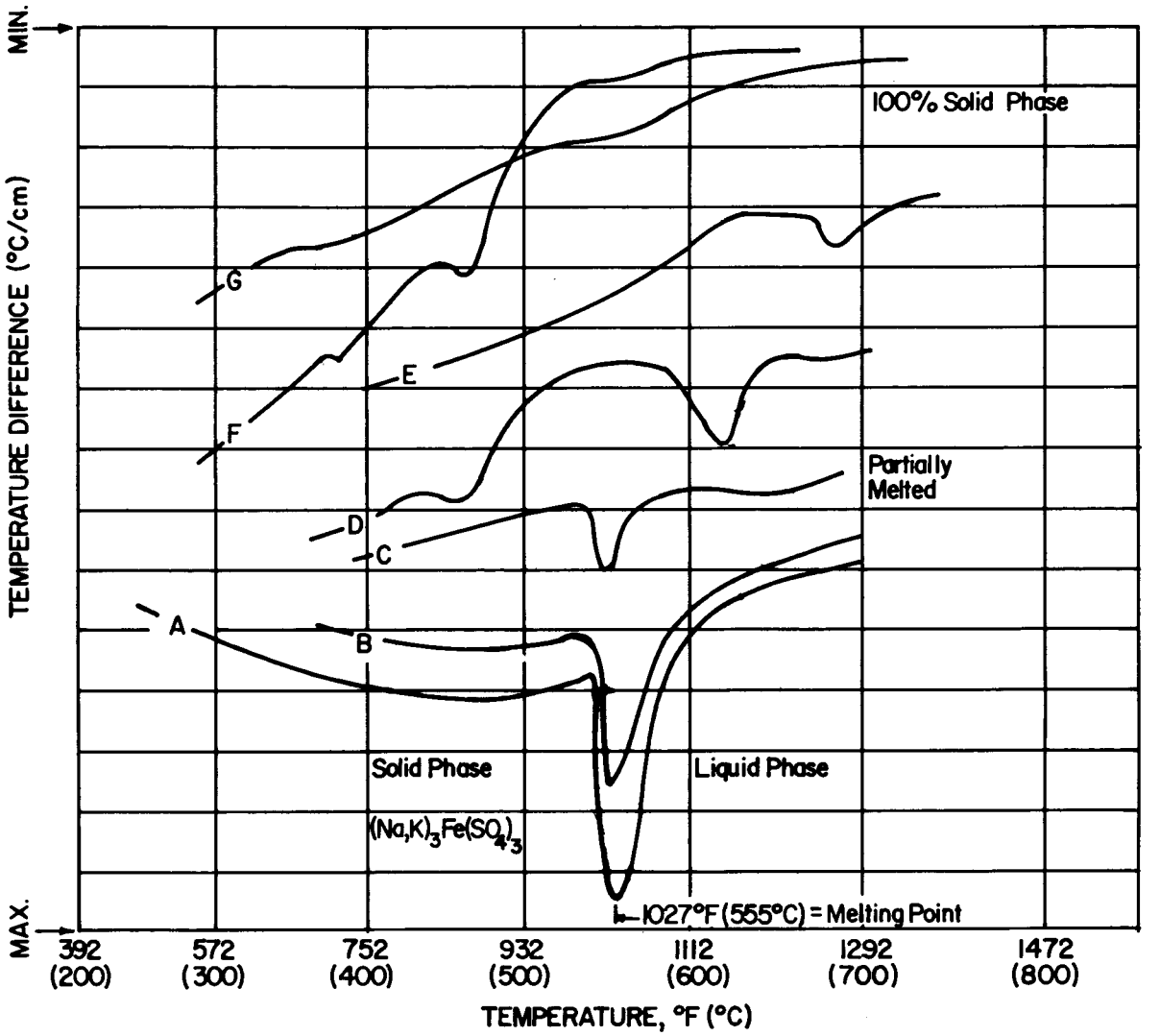

Note: Curves B through G transposed from seperate charts for location and extent of melting and raised for clarity.

LEGEND:

A. Unexposed $(Na,K)_3Fe(SO_4)_3$ thermal arrest as a result of melting at 1027°F (555°C)
B. Deposits from 347SS specimen, exposed 100 hour
C. Deposits from 304SS specimen, exposed 100 hour
D. Deposits from 21-6-9 specimen, exposed 100 hour
E. Deposits from 304 SS specimen, exposed 250 hour
F. Deposits from HT-9 specimen, exposed 100 hour
G. Deposits from Al-6X specimen, exposed 100 hour

Figure 3.2 Differential Thermal Analysis of Corrosion Deposits Compared With That of $(Na,K)_3Fe(SO_4)_3$

the sulfate mixture. In a separate Differential Thermal Analysis (DTA) run with 10 percent $MnSO_4$ added to synthetic $(Na,K)_3Fe(SO_4)_3$, the melting point increased in less than 2 hours of heating above the 1026°F (535°C) initial melting point. We assumed that the Fe^{+3} is reduced by the Mn^{+2} ion, that cyclic oxidation-reduction of Fe^{+2}/Fe^{+3} occurs in the presence of SO_3, and that manganese may reduce the catalytic oxidation rates within the ash. No detailed study of the chemistry of the molten sulfate salts was made. The acid-base and the oxidation-reduction reactions are both affected by the SO_2/SO_3 environment in the flue gas. We concluded from the DTA studies that the variation in corrosion rates from alloy to alloy among the high alloys was significantly affected by the nature of the metal-ion corrosion products--not solely by passive surfaces, etc. A somewhat passive film, however, may be formed on a few alloys, such as 347SS. Further evaluation of this analytical method may prove fruitful.

Added examination of the ash deposits and corrosion products was performed by x-ray diffraction, SEM, and by electron probe microanalysis. The data are shown in Appendix D.

3.1.2.4 Results of Commercial Alloy Evaluation. The objective of this evaluation was not to duplicate all coal-fired boiler conditions, but rather to simulate the worst condition occurring with high-alkali coals (such as Midwestern) that form the liquid sodium-potassium-iron trisulfate. Test performance results for Retorts 4 through 10 are summarized in Table 3.6 and Figures 3.1 and 3.3. The influences of the alloy constituents were reproducible, as shown by the results of Retorts 4, 7, and 10. These retorts were exposed for 250, 100, and 48 hours respectively at 1240 to 1250°F (670 to 675°C).

The indicated effects of alloy composition within the restraints of the alloys tested present a useful set of relationships of corrosion metal losses as a function of alloy constituents (Figure 3.3). The results were also plotted against the individual element composition to determine whether the 48- and 100-hour test results were consistent with those obtained from the 250-hour tests. The trends were very similar, but the curves for aluminum and chromium

Table 3.6 Fireside Test--Summary of Exposures

Retort No.	Objective	Time (h)	Temp. °F (°C)	Gas Atmosphere	Corrodent Ash	Comment
Phase 1 Materials Test:						
1	Determine flue-gas oxidation penetration.	250	1240 (670)	Flue gas	None	Oxide scale.
2	Determine flue-gas oxidation penetration.	500	1240 (670)	Flue gas	None	Oxide scale.
3	Determine flue-gas oxidation penetration.	250	1440 (780)	Flue gas	None	Oxide scale and sulfidation on some alloys.
4	Determine fireside attack by trisulfate.	250	1240 (670)	Flue gas	Simulated ash*	Severe attack and pitting.
5	Determine fireside attack by trisulfate for longer time.	500	1240 (670)	Flue gas	Simulated ash	No increase over Retort 4.
6	Determine high-temperature fireside attack.	250	1440 (780)	Flue gas	Simulated ash	Severe pitting; less general attack.
7	Determine fireside attack for shorter time.	100	1250 (675)	Flue gas	Simulated ash	Results similar to Retort 4.
8	Determine start-up of attack.	24	1250 (675)	Flue gas	Simulated ash	Attack similar to Retort 4.
					Synthetic trisulfate†	Reduced pit depth.
9	Compare trisulfate attack with gas oxidation of alloy in contact with sulfates.	50	1250 (675)	Air only	Simulated ash	No sign of pitting attack; light scale only.
					Synthetic trisulfate	Attack in air similar to Retort 7.
10	Evaluate effect of carbon.	48	1250 (675)	Flue gas	Simulated ash + carbon	Results similar to Retort 4.
11	Determine effect of active free carbon in ash.	48	1250 (675)	Flue gas§	Simulated ash* + carbon	Very little effect caused by carbon.
12	Determine high-temperature fireside attack.	48	1450 (790)	Flue gas§	Simulated ash* + carbon	Fused and pitted with carbon added. No pitting without carbon.

*"Simulated ash" was 37.5% Na_2SO_4, 37.5% K_2SO_4, 25% Fe_2O_3 (mol %) blended and dried.
†Synthetic $(Na,K)_3Fe(SO_4)_3$ was formulated, fused, and ground in the lab.
§Simulated high sulfur gas was 72% N_2, 14% CO_2, 10% H_2O vapor, 3.6% O_2, 0.25% SO_2 + SO_3.

Table 3.6 Fireside Test--Summary of Exposures (Cont)

Retort No.	Objective	Time (h)	Temp. °F (°C)	Gas Atmosphere	Corrodent Ash	Comment
13	Evaluate preoxidized alloys.	48	1250 (675)	Flue gas	Simulated ash	Reduced number but deeper pits.
14	Determine combined corrodent attack.	48	1250 (675)	Flue gas	Simulated ash + 3% NaCl	Severe pitting by fused ash + NaCl.
15	High-temperature combined attack.	48	1450 (790)	Flue gas	Simulated ash + 3% NaCl	Without NaCl no attack; some pitting with NaCl.
Phase 2 Materials Test:						
16	Determine variation of fireside attack on high alloys.	48	1250 (675)	Flue Gas	Simulated ash*	Benefit of silicon content verified.
17	Determine variation of fireside attack on high alloys.	48	1250 (675)	Flue gas	Simulated ash (3% NaCl on some)	Synergistic effects and high Al effects noted.
18	Determine variation of fireside attack on high alloys.	48	1250 (675)	Flue gas	Simulated ash + 35% NaCl	Verificaiton of previous results.

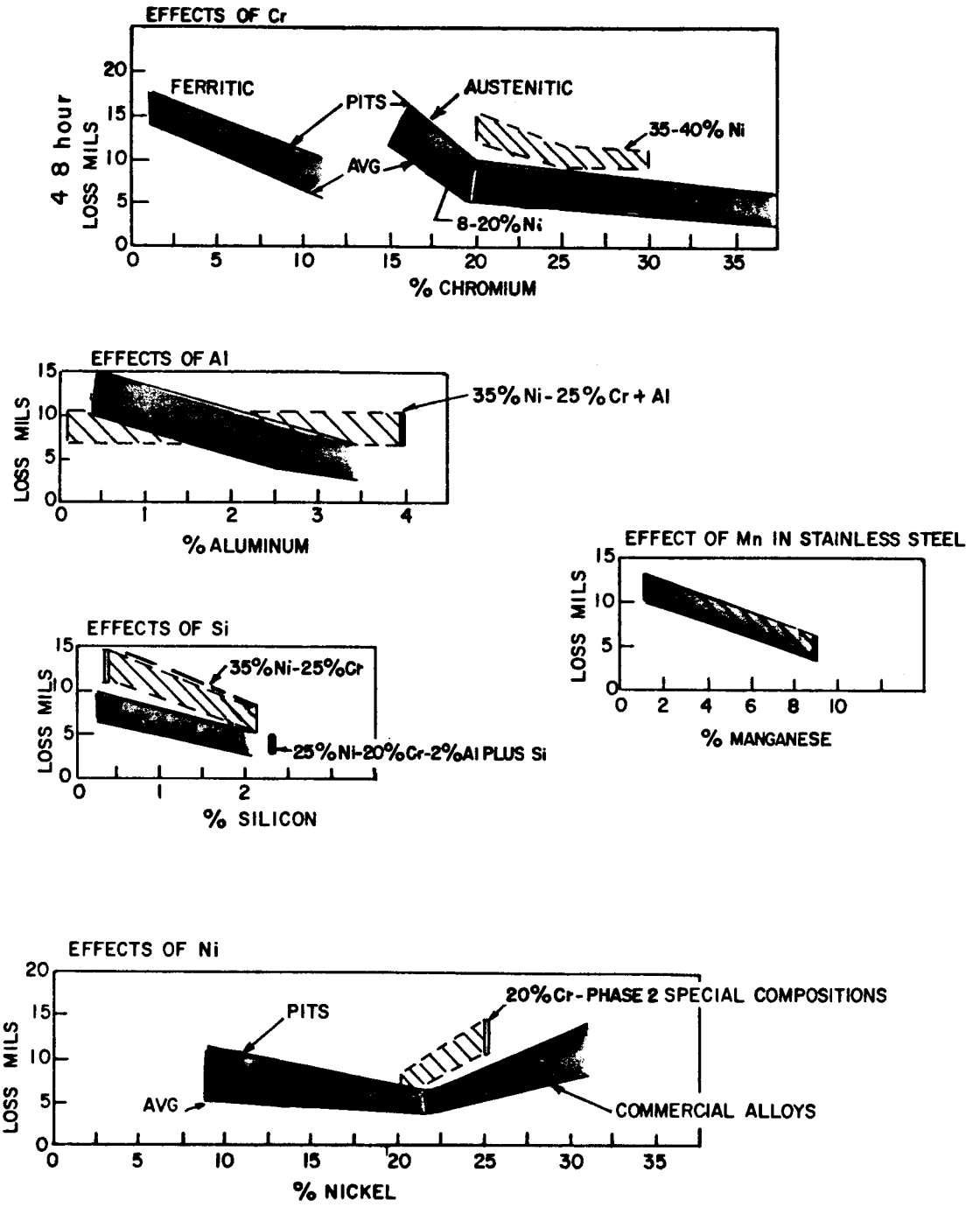

Figure 3.3 Fireside Corrosion Losses as a Function of Alloy Constituents (The 1250°F (675°C) alloy losses are plotted against the elemental variations. Solid bars = Commercial alloys based on data from Phase 1;[6] Cross-hatched bars = Phase 2 special alloy compositions.)

were not as steep as previously indicated in the Retort 4 data.[5] There was a change in the curve for ferritic steel because of the correction for oxidation of the back surface of the coupon (also explained in Figure 3.1 for 2-1/4%Cr-1%Mo). The back surface is used as a reference for measuring pit depth and average corrosion, but only the 2-1/4%Cr-1%Mo steel suffered significant oxidation scaling loss and had the scale subsequently removed by the descaling procedure.

Five elements--chromium, aluminum, silicon, manganese, and niobium--appear beneficial to corrosion resistance, but the question of their combined effects is not easy to answer based on the 19 alloys tested (Table 3.1). A curve showing the influence of chromium was plotted mainly from alloys with varying amounts of iron, chromium, and nickel (except for the 15-percent chromium point representing the data from A286). The effect of aluminum was shown by plotting the data from Incoloy 800, IN-549, and IN-814. Silicon influence was shown by comparing the data for 310SS with that for 314SS. The 6-percent molybdenum in AL-6X appeared to be significantly detrimental, compared with IN-840 or 310SS; however, the 9-percent molybdenum in Inconel 625 was not detrimental at 1250°F (675°C) in the low-iron higher alloy matrix (Ni-Cr-Nb). The effect of adding manganese was indicated by the tests on 21%Cr-6%Ni-9%Mn (Nitronic 40). Compared with 304SS, the 9-percent manganese was beneficial at 1250°F (675°C). These results appear to agree with Greenert,[2] who found that a 14%Cr-14%Mn had good resistance but that 202SS with 8-percent manganese was about the same as 347SS. At the higher temperature of 1450°F (790°C), however, high-manganese alloys are subject to excessive oxidation and sulfidation. Niobium was only evaluated up to 0.8 percent (347SS) but was consistently beneficial throughout the test duration, as shown in Figure 3.1 (bottom chart).

The influence of nickel additions was obtained from 304SS, IN-840, and Incoloy 800H, indicating a minimum loss at about 20-percent nickel followed by increasing attack at 31-percent nickel. Although these data are preliminary, the trends appear reproducible, and other alloys in the test were consistent with the trend shown in Figure 3.3.

The inability to isolate one elemental change at a time is an inherent problem in tests of this type using commercial alloys. Some effects of Fe:Cr and Fe:Ni ratios are inevitable when comparing alloys with different chromium contents; for example, the Fe:Cr ratio, not constant in most cases, would alter the apparent effect of nickel additions. More detailed data on the effects of alloy constituents were added by the Phase 2 results.

3.1.3 Task 1.4.3 - Effects of Carbon and Chloride Additions on Fireside Corrosion

3.1.3.1 Effect of Carbon on Fireside Corrosion. The effect of carbon additions was evaluated in the Retort 10 test, using 9-percent by weight char (from Indiana No. 5 coal) blended in the synthetic ash. The exposure was run for 48 hours at 1250°F (675°C) to minimize side effects, as shown in Table 3.7. Because of the oxidizing nature of the flue gas, the carbon particles appeared to be largely oxidized. Adding 9-percent carbon to the ash using an oxidizing gas environment produced no significant change. These results were checked using a higher carbon content in the ash--15-percent carbon in Retort 11 (Table 3.7). The appearance of descaled specimens after testing was not noticeably different from samples tested without carbon addition (Retort 11 specimens in Appendix D).

Test results at 1450°F (790°C) were different, as demonstrated by the Retort 12 data in Table 3.8; since carbon-free ash apparently does not form molten alkali-iron trisulfate at that temperature, no significant attack occurred. The effect of carbon in the ash, however, was pronounced, causing severe pitting. Thus adding carbon char to the simulated ash extended the range of the high corrosion rates to higher temperatures (Table 3.8). Further research on the effect of carbon at higher temperatures was beyond the scope of this test.

Table 3.7 Fireside Attack Using Carbon (Char) Added to Ash for 48-Hour Exposure at 1250°F (675°C)

Alloy	Retort 10--9%C		Retort 11--15%C		Effects of Carbon Compared With Previous Tests†
	General Attack (in.)	Pitting* (in.)	General Attack (in.)	Pitting* (in.)	
HT-9	0.005	0.010	0.006	0.010	None
304SS	0.005	0.010	0.005	0.010	None
310SS	0.003	0.008	0.004	0.008	None
314SS	0.002	0.006	0.0025	0.007	Slight
347SS	0.003	0.005	0.004	0.006	Slight
21-6-9	0.003	0.005	0.004	0.010	Slightly worse
IN-800H	0.006	0.012	0.006	0.013	None
IN-811	0.005	0.011	---	---	None
IN-671	0.001	0.004	---	---	None

*Maximum (total) penetration at pit (measured after descaling).
†Losses without carbon are shown in Table 3.5 and Figure 3.1.

Table 3.8 Fireside Tests for Retort 12 at 1450°F (785°C) Showing Maximum Penetration Caused by Ash Containing Free Carbon

Alloy	No Carbon (mil)	15% Carbon Added (mil)
304SS	No attack*	18†
310SS	No attack	12
347SS	No attack	Edge pitted
21-6-9	No pits	10†
IN-800H	No attack	18†
IN-811	No attack	21†
IN-671	No attack	---

*Ash not fused; molten alkali-iron trisulfate apparently not formed.
†Fused ash visible on all specimens showing attack, largely pitting.

3.1.3.2 Fireside Corrosion by Ash Deposits Containing Chloride at 1250°F (675°C). Although NaCl additions to the simulated ash deposits may not be representative of the majority of American coals, some sizable Midwestern coal deposits contain sufficient chloride to induce chloride-accelerated attack on materials more sensitive to such attack. Using an assumed concentration factor of 10 to 1 for coal combustion, we added 3-percent NaCl to the simulated ash for comparison.

The results of the Retort 14 test at 1250°F (675°C), shown in Table 3.9, indicate the following:

- Initially, the steels appeared to suffer somewhat greater attack with the NaCl added. Closer examination revealed increased general corrosive attack (Figures D.5 and D.6 in Appendix D) but less pronounced pitting attack.

- The slightly higher alloys, such as 310SS and Incoloy 800H, were not significantly affected by the NaCl addition.
- The IN-811 and IN-671 had deeper pits with the NaCl addition. Data for IN-671 (Table 3.9) are not conclusive because the alloy occasionally appears to have full corrosion resistance on isolated samples and pitting on others.

Some further indication of the effects of chloride was obtained from Phase 2 alloy tests, discussed in Section 3.2. It should not be assumed that the 48-hour test resulted in a complete end to the attack, because longer term tests were not performed with the chloride-containing ash. The purpose of this test was mainly to explore the relative importance of the chloride content to fireside attack.

3.1.3.3 Fireside Corrosion by Ash Deposits Containing Chloride at 1450°F (790°C). Results from the addition of NaCl to the ash used in the fireside test at 1450°F (790°C) were substantially more decisive than those for the tests at 1250°F (675°C). The type of corrosion observed from the chloride-modified high-temperature test was a pronounced pitting attack with a reduced general corrosion rate. Thus the effects of chloride on the mode of attack at 1450°F (790°C) were more notable than those at 1250°F (675°C), as indicated in Table 3.10.

The test was performed by bringing the ash-loaded specimens to the test temperature under nitrogen gas to prevent the formation of the alkali-iron trisulfate at lower temperatures. The flue gas was then introduced.

Upon removal of specimens from the retort after a 48-hour exposure, the ash on specimens without NaCl added was not fused and still retained the α-hematite (rust) color. The ash on specimens with 3-percent NaCl added was fused and black because of the corrosion deposits. Apparently, the presence of chloride extended the temperature range for attack by alkali sulfates or by

Table 3.9 Fireside Tests for Retorts 14 and 15 Showing the Maximum Penetration Values Caused by Adding NaCl to Ash at 1250 and 1450°F (675 and 790°C) for 48-Hour Exposure

Alloy	Retort 14 [1250°F (675°C)]		Retort 15 [1450°F (790°C)]	
	No NaCl (mil)	3% NaCl Added (mil)	No NaCl (mil)	3% NaCl Added (mil)
HT-9	12	15	---	---
304SS	8	10	No attack*	8†
347SS	6	11	No attack*	20§
310SS	10	12	No attack*	12§
21-6-9	9	9	---	---
IN-800H	12	12	No attack*	21§
IN-811	11	15	No attack*	>10 (estimated)
IN-671	None	8¶	No attack*	Edge attack about 8

*Ash not fused; molten alkali-iron trisulfate apparently not formed.
†Fused ash visible on all specimens showing attack, largely pitting.
§No general attack, excluding the thin oxide scale, but a few large pits were observed; ash fused.
¶Few pits and much less attack elsewhere.

some other means produced a liquid-phase attack at 1450°F (790°C). Without the NaCl addition, no liquid phase was formed and no pitting occurred.

The measurements made on the descaled specimens, shown in Table 3.9 (Retort 15), indicate that all the high-temperature alloys exposed to chloride-containing sulfates were pitted, but practically no general attack was evident. (Examples of the corrosion attack are shown in Figures C.7 and C.8 in Appendix C.) Strangely, Incoloy 811 and 310SS displayed small, deep pits, while Incoloy 800 and 304SS suffered broad round-bottom pits. Specimens on the left of both figures were exposed to the same conditions without NaCl added to the ash.

Table 3.10 Fireside Tests for Retort 13 Showing the Effect of Surface Preoxidation on Corrosion at 1250°F (675°C)

Alloy	Pitting Loss After Test	
	Polished Surface (mil)	Preoxidized Surface (mil)
HT-9	14	13
304SS	12	12
347SS	8	8
314SS	10	16*
21-6-9	8	12
IN-800H	10	14†
IN-811	14	18†
IN-671	4	17†

*Heat treatment for preoxidation apparently produced silicon loss at the surface, and some chromium depletion was assumed.
†Few pits and much less attack elsewhere.

3.1.3.4 Fireside Attack on Preoxidized Alloy Surfaces. Testing of preoxidized surfaces was added to the Test Plan (Table 2.4, Test Sequence 1.4.3.1) for several reasons:

- The assumed resistance of high-temperature oxide scales (oxides high in Cr_2O_3, spinel, or Al_2O_3) to fireside attack was not previously evaluated.
- The variations in rapid initial attack rates were assumed to be sensitive to the surface condition.
- An apparent variation in the wetting of the surface by the molten trisulfate corrodent was observed, as shown in Figures 3.4 and 3.5.
- Some alloys, such as IN-671 (49%Ni-49%Cr), appeared to be corrosion-resistant over a large percentage of the area but severely pitted in local areas (Figure 3.5), suggesting variations in the oxide films.

The local failure may be the result of an inferior oxide film covering in the areas of significant pitting. The tests were performed at 1250°F (675°C) under the standard test environment (Table 3.7, Retort 13).

The results of the test using specimens with preformed surface scales, presented in Table 3.10, indicate that no benefit was derived from the oxide scales. The preformed scales evaluated in the test (Retort 13) were designed to give a dense, well-formed Cr_2O_3 on some alloys, compared with other alloys with Fe-Ni-Cr spinel surfaces. Some of the alloys produced Al_2O_3 in the scale. The procedure used to form the scales is described in Appendix B. Table 3.11 presents additional data on the scale identification and the results for specimens not included in Table 3.10. The pitting data included in Table 3.11 were for one location only; however, the pit measurements listed in Table 3.10 are representative data collected by the normal procedure on descaled coupons.

The iron-based alloys produced very little change as a result of preoxidation, indicating that the molten trisulfate attack is nearly the same for

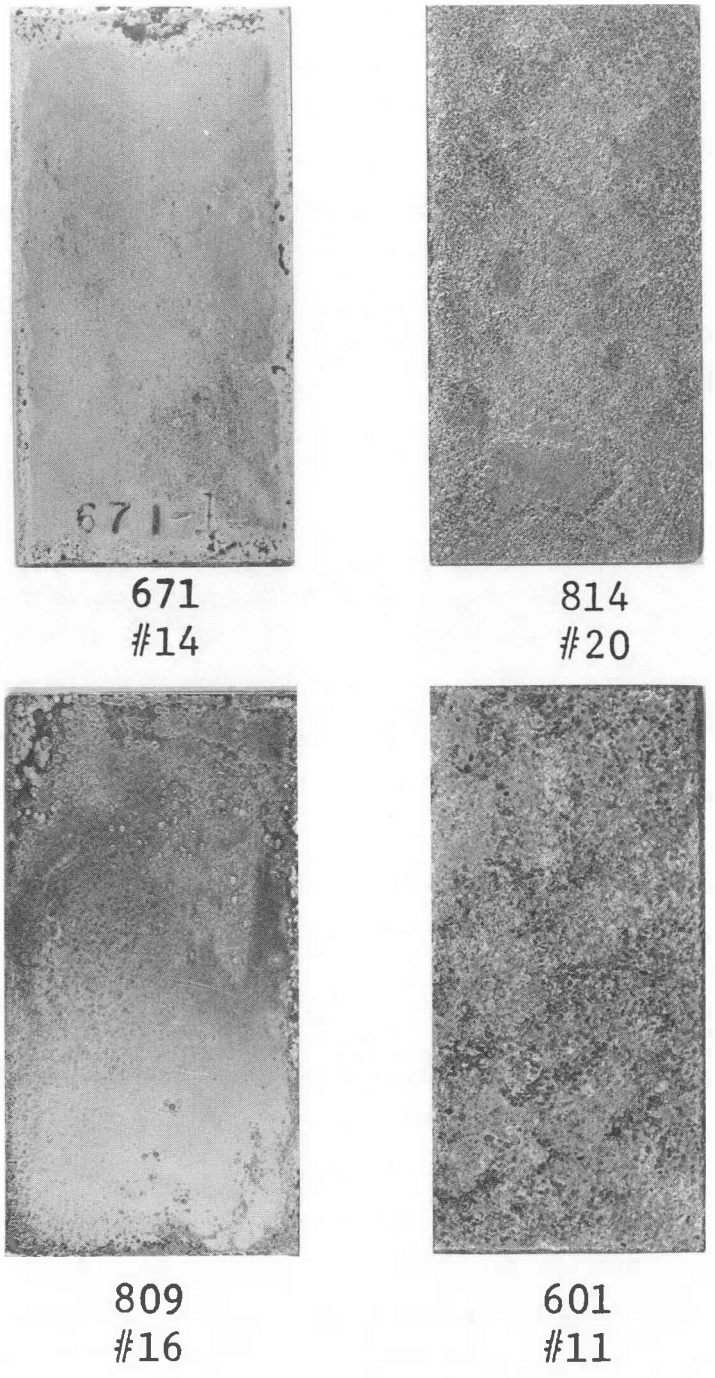

Figure 3.4 Random Variation in Pitting of High Alloys--1.5X (Fireside attack on high-nickel alloys showed little general corrosion, but a few deep pits and a tendency to heavier attack near the edges were observed. Aluminum additions increased the general attack and produced smaller pits.)

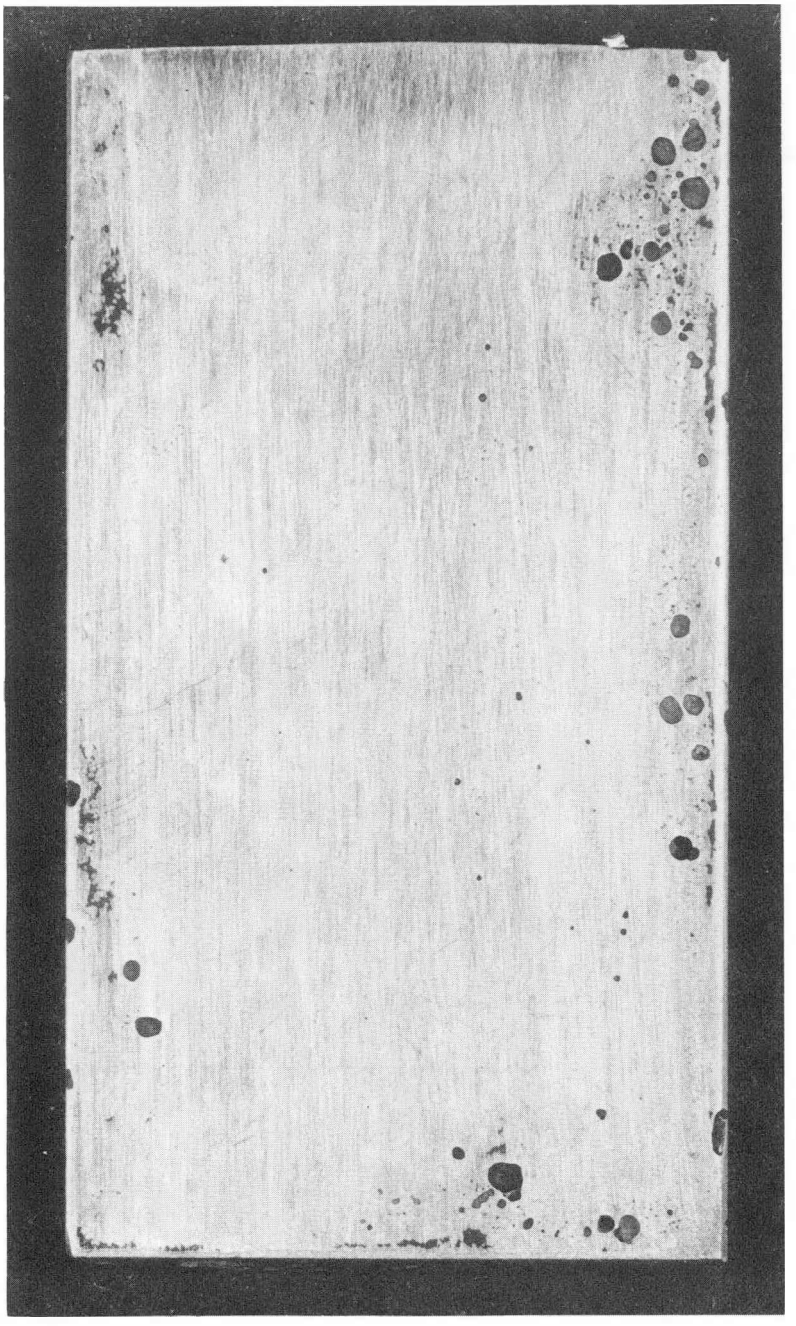

Figure 3.5 Photomacrograph of Exposed Surface of IN-671 Specimen After Testing at 1250°F (675°C)--3X
(Random pitting but no general corrosion.)

Table 3.11 Pitting of Selected Commercial Alloys Exposed to Simulated Fireside Attack, Comparing Preoxidized With Unoxidized Specimens*

Alloy Specimen	Temperature of 24-Hour Air Oxidation Treatment (°F/°C)	XRD Scale Identification	% of Surface Attacked (1 Section)	Pit Depth Taken at 1 Location (mil)
800-34	---	---	50	5
800-32	1832/1000	Cr_2O_3(m), Spinel(m)	100	11
811-26	---	---	100	12
811-21	2012/1100	Spinel(m), Cr_2O_3(w) α-Al_2O_3(vw)	100	14
21-6-9	---	---	100	8
21-6-9	1652/900	$MnCr_2O_3$(s)	100	9
314-20	---	---	>95	8
314-17	2192/1200†	Cr_2O_3(m), Spinel(mw)	100	10
671	---	---	<5	2 to 16§
671	2012/1100	Cr_2O_3(s), Spinel(w)	1 pit	0.5 to 16§

*Measurements taken from low-magnification micrographs (one section); Retort 13--48 hours at 1250°F (675°C).
†In cracked NH_3 (flowing gas) over NiO.
§View of specimen surface shows a low density of rather deep pits, up to 16 mil. These particular cross sections did not happen to intersect these large pits.

the oxides as for the polished alloy. Some of the higher alloys exhibited fewer but deeper pits that were sometimes oddly distributed, as shown in Figures 3.4 and 3.5.

The first evaluation of the preoxidized 314SS was not considered satisfactory because of the high-temperature oxidation treatment [2192°F (1100°C)] that caused the loss of silicon from the scale. Later tests indicated much lower attack rates when the silicon was retained in the scale, presumably as silicates.

The oxide scale remaining on IN-671 was examined after testing and found to be Cr_2O_3 on the flat surfaces between the pits--very similar to the original scale before testing. While the scale adherence to the base metal was good, defects or compositional variables leading to the localized initiation of pitting may be unavoidable. Once the oxide is permeated, the electrochemical attack may be assisted by the larger cathodic surface area provided by the oxide surface. Thus deeper pits were formed on the preoxidized specimen than were formed on the polished samples of the same alloy.

The effect of Al_2O_3 in the scale was also not beneficial, as indicated by the test results on IN-811. The test results agree with other observations, indicating that the molten alkali-iron trisulfate effectively wets and dissolves Al_2O_3 at 1250°F (675°C). The aluminum sulfate combines with the corrosive liquid and remains in the deposits. An XRD study of the exposed alloy scales did not find Al_2O_3 in the scale layers after testing. The attack on alumina may also explain why IN-811 was no better and sometimes suffered deeper pits than Incoloy 800.

3.1.4 Conclusions From the Evaluation of Phase 1 Alloys

A simple solution to the problem of fireside corrosion in steam generators burning high-alkali iron-containing coals cannot be found using established

commercial alloys. On the other hand, when more information about the passivity behavior and the factors controlling electrochemical attack is developed, some substantial extension of the useful steam generator tube life will be feasible.

We concluded that oxides formed by preoxidizing the steels and Fe-Cr-Ni and Ni-based alloys were of no advantage; in the case of the higher alloys, the oxides may have contributed to greater loss rates. There is a strong indication that surface chromium depletion caused by oxidation may weaken the passivity that limits the electrochemical attack. Fluxing by the molten alkali-iron trisulfate may eliminate any protection the heat-treatment-formed oxides may offer.

The effects of NaCl and carbon additions were not significant at 1250°F (675°C) but were notable at 1450°F (790°C). The range of rapid high-temperature attack was extended to 1450°F (790°C).

The influence of alloy modifications on the reduction of attack has not been fully defined. Further improvements may be achieved through understanding of the combined or synergistic effects of several elements. Since the tests indicated that some elements, such as niobium, improve the alloy surface passivity, and other elements, such as manganese, appear to alter the fused trisulfate, there may be better ways of combining the effects of several elements.

3.2 PHASE 2 - DEVELOPMENTAL ALLOY TESTING

3.2.1 General

The Phase 2 alloys, produced in conformance with Subtasks 1.4.4 and 1.4.5, used custom-melted and rolled alloys to provide a clear comparison of the effects of alloy additions of aluminum, silicon and yttrium individually and in pairs (Table 3.12). Three alloy matrix types were used for the study: 25%Ni-20%Cr, 35%Ni-25%Cr, and 40%Ni-30%Cr. These types were selected to provide as much solid solubility and ductility as feasible for the composition and, where possible, to provide a good high-temperature material for mechanical and

Table 3.12 Alloy Compositions for Phase 2 Fireside Tests

Alloy No.	Chemical Analysis (% by Weight, Balance Fe)*†					
	Ni	Cr	Al	Si	Y	Mn
1	24.7	19.8	---	0.41	---	0.64
2	25.4	19.6	2.04	0.40	---	0.60
3	25.3	19.4	---	2.27	---	0.57
4	24.2	19.6	2.0	2.40	---	0.59
5	33.5	24.4	---	0.40	---	0.70
6	34.0	24.5	2.0	0.40	---	0.74
7	34.1	24.2	---	2.30	---	0.74
8	33.7	24.1	1.9	2.30	---	0.62
9	38.5	30.2	---	0.50	---	0.72
10	39.0	30.2	1.8	0.40	---	0.74
11	38.7	30.5	---	2.30	---	0.71
12	39.3	29.7	1.8	2.40	---	0.76
13	33.0	24.4	3.7	0.40	---	0.70
14	33.9	24.3	3.7	0.40	0.01	0.75
15	37.2	24.2	4.2	0.44	0.60	0.72
16	35.1	24.3	---	0.44	0.06	0.57
17	35.4	24.7	---	0.37	0.53	0.68
18	18.4	25.1	---	0.45	0.58	0.67
19§	20.0	23.0	0.3	---	0.65 Y_2O_3	---

*Carbon analysis was 0.035% maximum for all alloys except 18 and 19, which had 0.045% maximum.
†A full analysis of the alloys is shown in Table 2.1.
§Mechanical alloy.

creep requirements. The preparation, rolling, and evaluation of the heats are described in Section 2.2 and Appendix B.

The alloys contained more nickel than was considered optimum; but at the time they were designed, the relationship of alloy constituents to corrosion (as presented in Figure 3.3) was unknown. To verify the effect of a lower nickel content, a few samples of commercial alloys were run in parallel with the custom alloys. By identifying the effects of such selected elements as aluminum and silicon and their synergistic effects on resistance to attack, further alloy improvements to lower the corrosion attack below that for the listed alloys are possible.

3.2.2 Results of Exposure of Phase 2 Alloys

Samples in Retorts 16, 17, and 18 were exposed at 1250°F (675°C) for 48 hours, as shown in Table 3.6. The resultant attack of individual alloys is compiled in Table 3.13, which shows the maximum penetration that was judged representative based on repeatable pitting or metal loss from two or three coupons. As expected, individual coupons produced some scatter, similar to previous experience. The degree of scatter is shown by the comparison of the results of individual alloys for Retorts 16, 17, and 18 in Table 3.13.

The most significant trends, shown in Figures 3.6 and 3.7, reveal that the more severe pitting attack of the Fe-Ni-Cr based material decreased with the addition of 2 percent silicon. Adding aluminum with the silicon provided some further benefit. The addition of aluminum without silicon was not as beneficial as previously indicated in Phase 1. Comparison of the descaled coupons of Alloys 5 and 6 (Figure 3.7) reveals that, although pit size was decreased, general attack was increased.

The data on maximum penetration corroborate those trends previously observed in Phase 1 (i.e., the effect of individual alloy constituents in general) except for the effect of aluminum addition shown in Figure 3.3. It is also

Table 3.13 Fireside Corrosion--Performance of Phase 2 Alloys
[48 Hours at 1250°F (675°C)]

Alloy No.	Nominal Composition					Retort 16			Retort 17			Retort 18	
									Standard Ash		Ash + 3% NaCl	Standard Ash	Ash + 3% NaCl
	Ni	Cr	Al	Si	Y	General Attack (mil)	Maximum Penetration (mil)	Type of Pits*	General Attack (mil)	Maximum Penetration (mil)	Maximum Penetration (mil)	Maximum Penetration (mil)	Maximum Penetration (mil)
1	25	20	---	---	---	†	15	L	†	14	18	13	15
2	25	20	2	---	---	†	13	L	†	10	13	11	§
3	25	20	---	2	---	4	8	S	3	5	§	10	§
4	25	20	2	2	---	2.5	4.5	S	2	3	2	5	4
5	35	25	---	---	---	†	8.5	L	†	10	17	5	13
6	35	25	2	---	---	5	8	S	5	10	§	12	15
7	35	25	---	2	---	4	6	S	4	7	§	10	§
8	35	25	2	2	---	3	4	S	4	4	9	5	9
9	40	30	---	---	---	†	11	L	†	11	14	11	12
10	40	30	2	---	---	†	8	M	†	9	§	8	13
11	40	30	---	2	---	3	6	S	4	5	§	3	5
12	40	30	2	2	---	3	4	S	3	4	4	3.5	6
13	35	25	4	---	---	5	10	B	---	8	8	6	12
14	35	25	4	---	0.1	4	6	---	---	12	8	10	12
15	35	25	4	---	0.5	5	8	S	---	5	5	9	6
16	35	25	---	---	0.1	5	9.5	M	---	12	§	7	10
17	35	25	---	---	0.5	5	15	---	---	11(B)	§	10	7
18	20	25	---	---	0.6	4	8.5	---	---	8	§	9	5
19	20	23	---	---	0.5 Y_2O_3	---	10	B	---	6	§	12	§

*L = Large pits; S = small pits; M = Moderate or shallow pits; B = Broad, shallow pits.
†Pitted primarily, but some areas unattacked.
§Not tested.

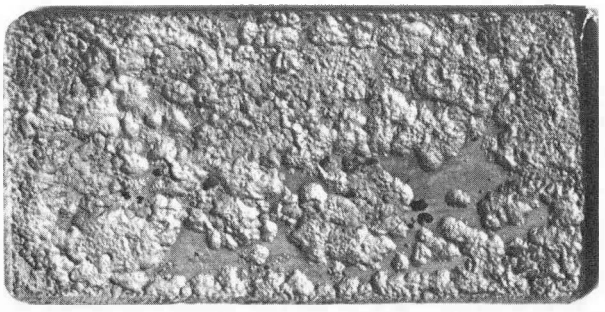

ALLOY 1 #1

25%Ni-20%Cr-0.45%Si

Loss (largely pitting) - 15 mil

ALLOY 3 #2

25%Ni-20%Cr-2.3%Si

General attack - 3 to 4 mil plus 4-mil pits

Max. penetration - 7 to 8 mil

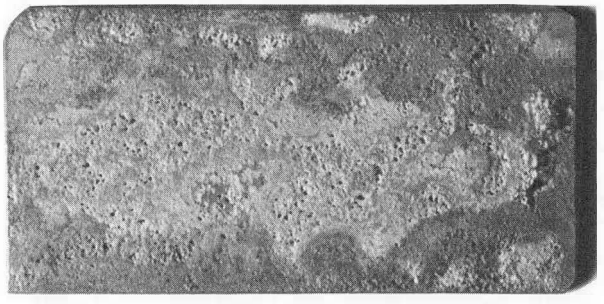

ALLOY 4 #1

25%Ni-20%Cr-2%Al-2.4%Si

General attack - 2 to 3 mil plus 2-mil pits

Max. penetration - 4 to 5 mil

AISI 314 #16

21%Ni-24%Cr-2%Si*(shot-peened)

Total penetration - 2 to 2-1/2 mil

*Commercial Type 314SS.

Figure 3.6 Fireside Attack--Phase 2--1.5X
(Alloys 1, 3, 4, and AISI 314)

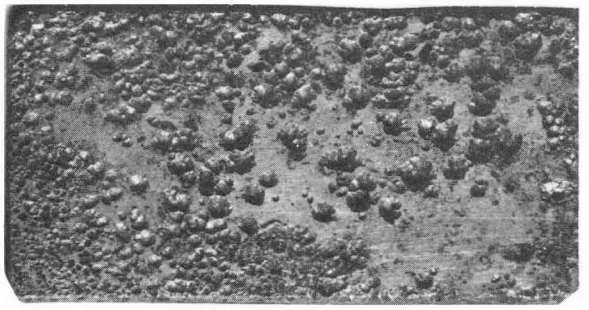

ALLOY 5 #3

35%Ni-25%Cr-0.4%Si

Chloride added (shown) - 17-mil pitting
(without chloride - 8 mil pitting)

ALLOY 6 #4

35%Ni-25%Cr-2%Al-0.4%Si

General attack plus pitting - 10 mil
(no chloride added)

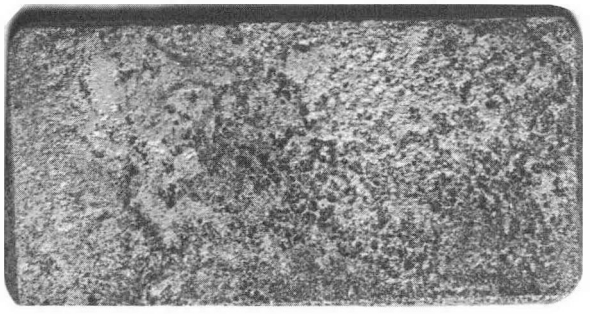

ALLOY 7 #4

35%Ni-25%Cr-2.3%Si

General attack plus pitting - 7.0 mil

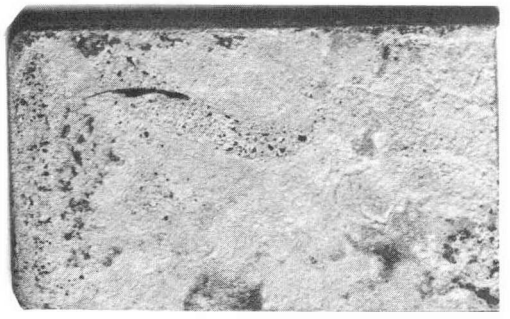

ALLOY 8 #4

35%Ni-25%Cr-2%Al-1.29%Si*

General attack - 5 mil

*Surface depletion of Si and Cr suspected from preparation of specimen.

Figure 3.7 Fireside Attack--Phase 2--1.5X
(Alloys 5, 6, 7, and 8)

evident that the nickel content of the Phase 2 alloys was above the optimum level, indicated to be between 20- and 22-percent nickel. Evidence for the latter conclusion was obtained by including some 310SS and 314SS coupons in Retorts 16, 17, and 18 as controls. The most resistant sample coupon appeared to be 314SS, which was ground and shot-peened lightly with glass beads before testing to remove depleted surface layers, as shown in Figure 3.6 (bottom). Fine grain size is also considered desirable.

The previously indicated trend of smaller pits observed for commercial alloy IN-811 with 2-percent aluminum compared with Incoloy 800 is more clearly shown by comparing the descaled coupons of Alloys 5, 6, and 13 presented in Figure 3.8. Alloy 13 with 4-percent aluminum displayed fine pits despite the high general corrosion loss; Alloy 5 with no aluminum displayed large pits with very little general attack.

The limited effects of yttrium on the 35%Ni-25%Cr-4%Al alloy are revealed by comparing Alloy 15 (0.5 percent yttrium) with Alloy 13 (no yttrium), shown in Figure 3.8 (lower two coupons). (See also Table 3.13.) The improvement, if any, may be affected by scatter because of scale variations. Silicon additions combined with yttrium were not investigated in Phase 2 but may be more helpful than the aluminum-plus-yttrium modification. None of the alloys with low silicon were consistently as good as Alloys 3 or 4 with 2-percent silicon added.

The addition of yttrium without aluminum to the 35%Ni-25%Cr matrix can be evaluated by comparing Alloys 16 and 17 with Alloy 5 (Table 3.13). The measured losses or pitting on descaled coupons indicates that no significant improvement was obtained, while the values from Retort 16 losses show a progressive deterioration with increased additions of yttrium, perhaps the result of scatter in the depth of pits. The appearance of other alloys not shown in Figures 3.6 through 3.8 are included in Appendix D.

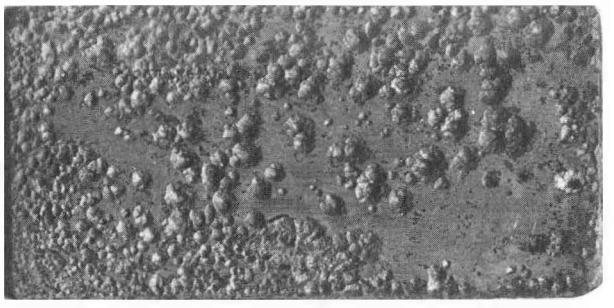

ALLOY 5

35%Ni-25%Cr

Max. penetration - 10 mil

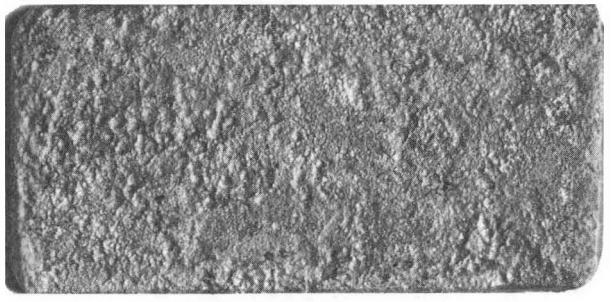

ALLOY 6

35%Ni-25%Cr-2%Al

Max. penetration - 10 mil

ALLOY 13

35%Ni-25%Cr-4%Al

Max. penetration - 8 mil

ALLOY 15

35%Ni-25%Cr-4%Al-0.5%Y

Max. penetration - 5 mil

Figure 3.8 Fireside Attack--Phase 2--1.5X
(Alloys 5, 6, 13, and 15)

3.2.3 Examination of Phase 2 Coupons

The changes in the degree of pitting and the observed mode of attack were previously described in Section 3.2.2.

Alloys in the previous tests (Phase 1) did not develop a reliable, adherent scale formation, partly because of the solubility and fluxing of the corrosion products by the liquid trisulfate corrodent and partly because of the electrochemical pitting attack through or below the surface films. The metallography of many alloys generally indicates that the nondescaled specimens may form an adherent scale in spots and none in adjacent areas, which may be related to the pitting variations. Because conventional cutting and grinding of specimens after exposure frequently fracture and dislodge the outer deposits and scale, special care was required to prepare specimens. Scale loss also occurred during cool-down on some alloys, but not on others.

Examination of Alloys 1 through 4 provides a more definite comparison of the behavior of the corrosion products as influenced by the alloy composition. The visible scale layer on some samples (not descaled) was usually a very poorly bonded mixture of oxides and sulfides as shown in Figure 3.9 (Alloy 1). The EDX check at Point 4 on the first layer (Figure 3.9), which was poorly adherent to Alloy 1, indicated that the chromium-rich oxide-sulfide was formed adjacent to the alloy surface. (Note that oxygen is not detected by EDX.) The scale layer in the lower view was removed, but the surface was similar to the surface of Fe-Cr-Ni and Fe-Ni-Cr alloys previously affected by attack. Rapid surface recession was evident, but no internal oxidation or sulfidation was seen.

Alloy 2 with 2-percent aluminum was not significantly better in retaining the oxide-sulfide scale, as shown in Figure 3.10. It is important to note that the oxide-sulfide scale does not retain aluminum as it would in an oxidizing gas-formed scale. A similar observation was made in the case of IN-814, which retained no aluminum in the scales observed despite the 3-1/2 percent aluminum in the alloy. A simple explanation for this is: The aluminum easily

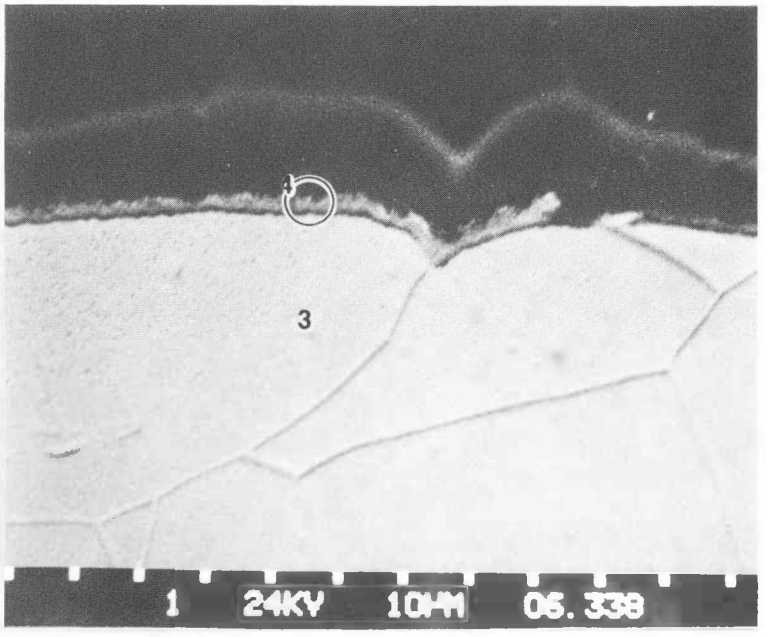

SEM: 1000X

PHASE COMPOSITION

3 - Base Alloy: Fe, Ni, Cr

4 - Scale: Cr(s), S(s), Si(w), Fe(w)

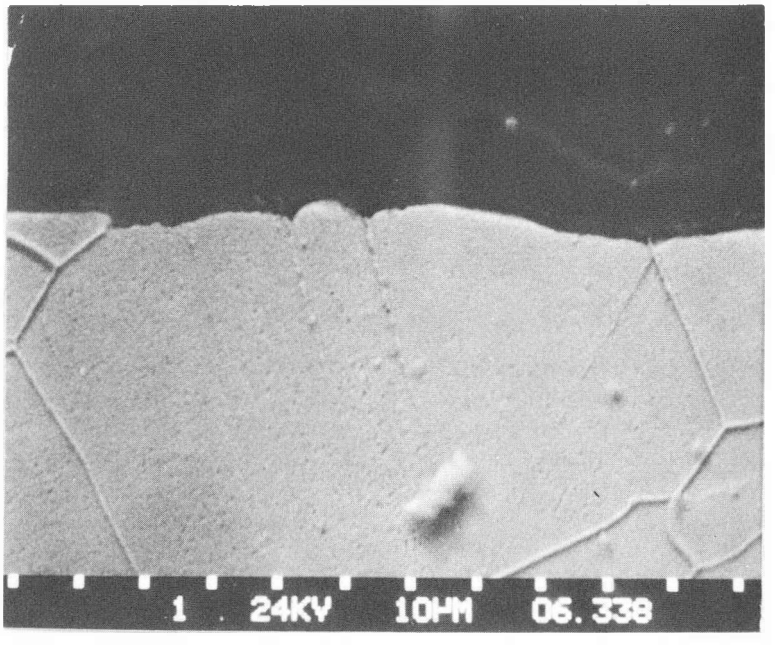

SEM: 1000X

Figure 3.9 Exposed Surface of Alloy 1 (not descaled) Showing Poorly Adherent Chromium-Sulfide Scale Under the Ash Deposits

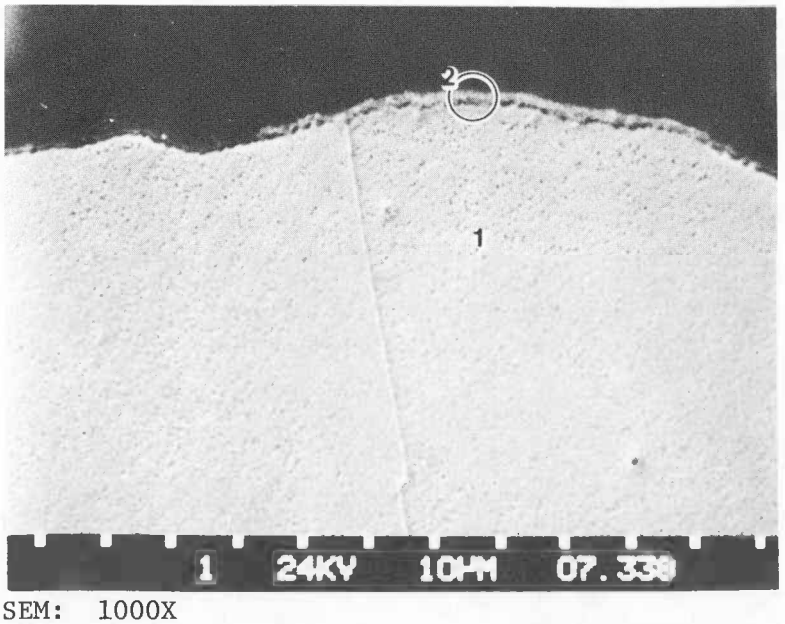

SEM: 1000X

PHASE COMPOSITION

1 - Base Metal: Fe, Ni, Cr, Al

2 - Scale: Cr(s), S(s), Fe(m), Ni(w), Si(vw), Al(vw)

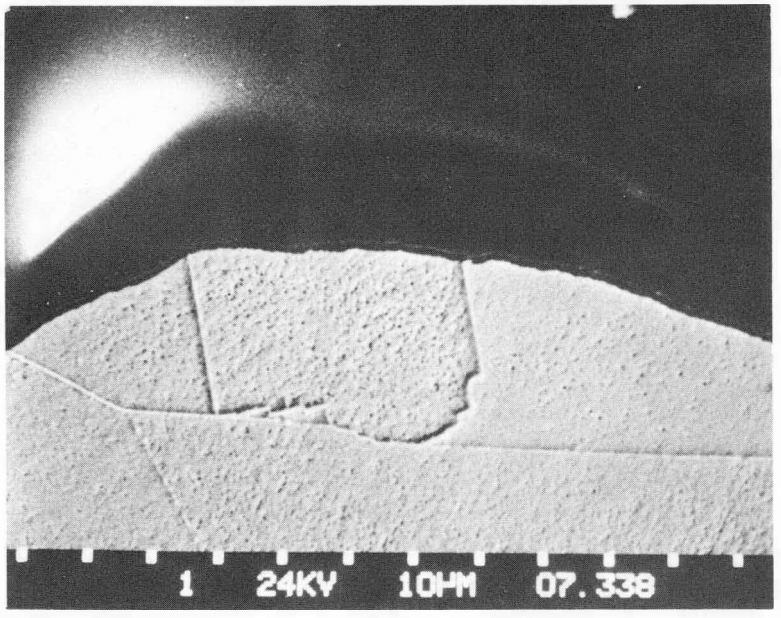

SEM: 1000X

Figure 3.10 Exposed Surface of Alloy 2 (not descaled) Showing Poorly Adherent Chromium-Sulfide Scale Containing Other Elements

combines with the trisulfate melt and becomes part of the problem corrosive phase, as indicated by the increased general attack. The chemical attack of pure, high-density Al_2O_3 by the alkali-iron trisulfate was also discussed in the "Fifth Quarterly Progress Report.[6]

The silicon-containing alloys demonstrated an increased stability and adherence of the scale below the outer deposits, first noted by the difference in the macroscopic behavior of coupons. Silicon tended to produce a better-bonded scale that was not easily removed by scraping or by heating and cooling. Alloy 3 with 2.3-percent silicon is shown in Figure 3.11.

The corrosive attack resulted in "deposit" layers outside the denser scale, identified in Figure 3.11 by Points 1 and 2 in the upper view and by Point 7 in the lower view. The denser scale (Points 2 and 7) is considered to be formed as a solid at the surface, which retained silicon--possibly as silicates in addition to the chromium-rich sulfide phase. Much of the outer deposit material appears to be progressively solidified as the alkali-iron trisulfate is consumed by the corrosion reaction. The outer surface (Point 4) in the upper view is a mixed oxide that is formed atop the liquid, corrosive deposits.

Examination of Alloy 4 revealed a more distinct phase separation between the scale and the corrosive ash deposits and greater structural contrast between the dense scale and the residue of the ash (Figure 3.12). We do not know whether the adherent, oxide-sulfide scale causes the reduced attack by separating the alloy from the corrodent, but this influence appears likely. No special effort was made to analyze for silicon, which may be present in the scale as silicates.

Another important aspect in the retention of the scale in commercial steam generators is the repeat-cycle attack after the ash deposits have been removed. If the removal of the heavy deposits also rips off the scale, as seen in many previous tests and shown in Figures 3.9 and 3.10, the second attack cycle will be as severe as the first and corrosion will proceed. With Alloy 4, however, the dense layer may well be retained, limiting the attack by separating

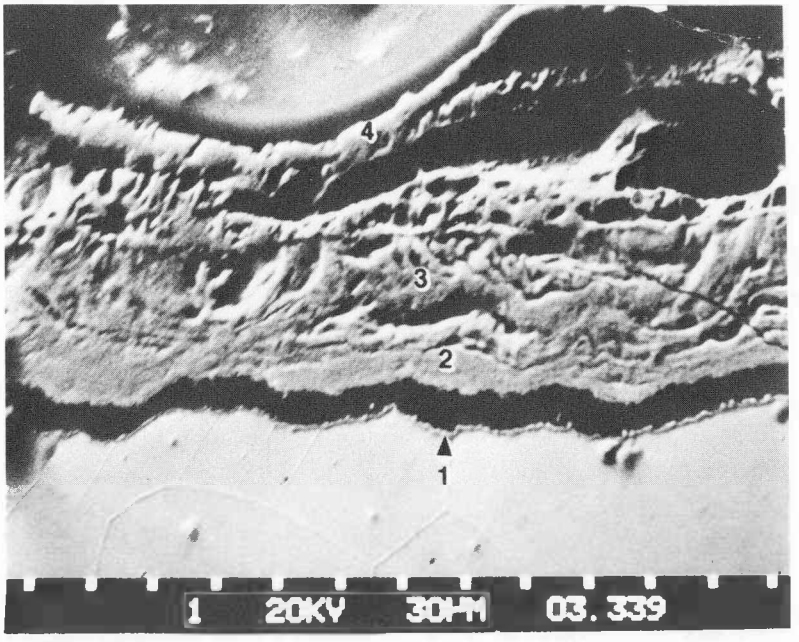

SEM: 300X

PHASE COMPOSITION

Scale and Deposits

1 - Cr, Ni, Fe all(m), Si, S(w)

2,3 - Cr(s), Si(m), K(m), S(w)

4 - Fe(s), Ni(w)

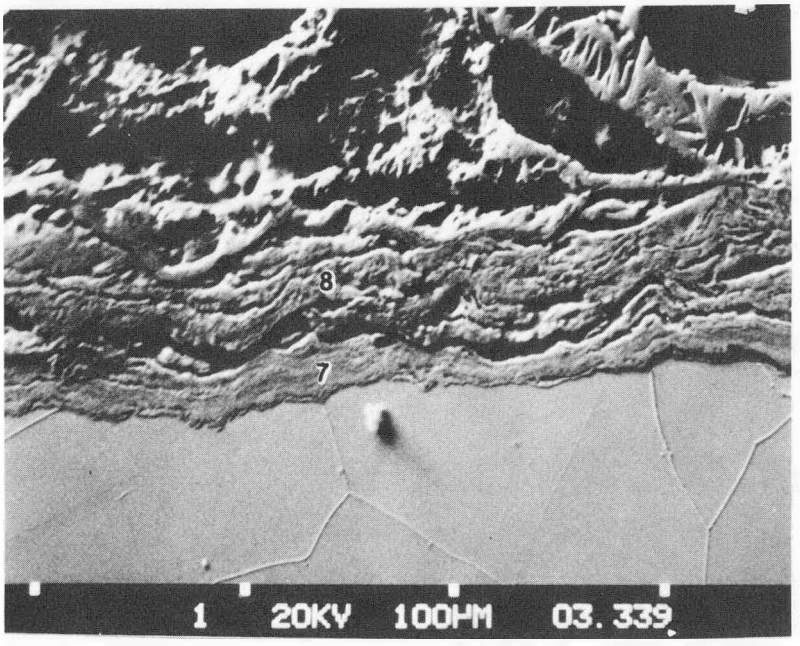

SEM: 300X

7 - Cr(s), Fe(w), Ni(m), Si(m), S(m)

8 - Same as 7 except S(vw)

Figure 3.11 Exposed Surface of Alloy 3 Showing a More Adherent Scale Which Was Retained on Cool-Down

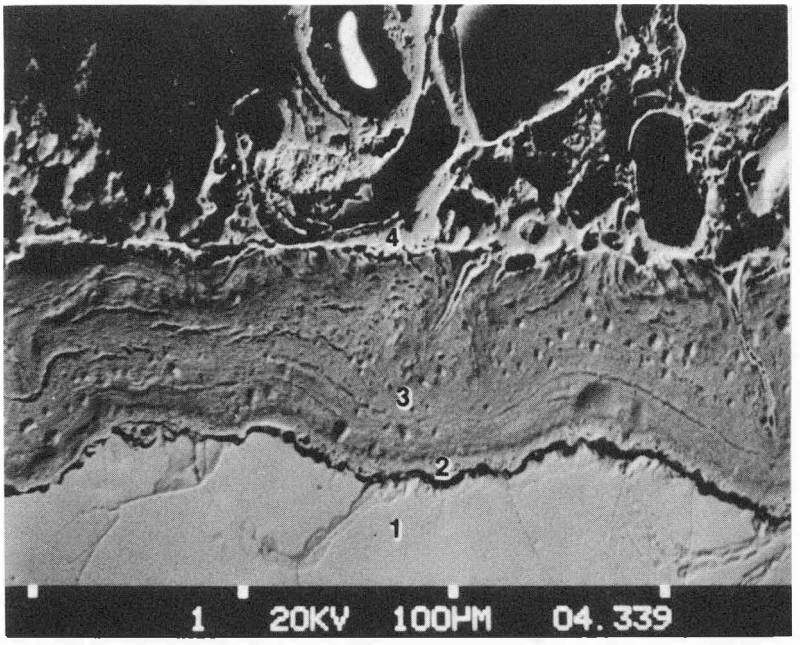

SEM: 300X

PHASE COMPOSITION

1 - Base Metal: Fe, Ni, Cr

2 - Cr(s), Fe(w), Ni(w), Al(vw), Si(vw), S(s)

3 - Same with S(w) and K(w)

4 - Cr(s), Fe(m), Ni(vw) (oxide)

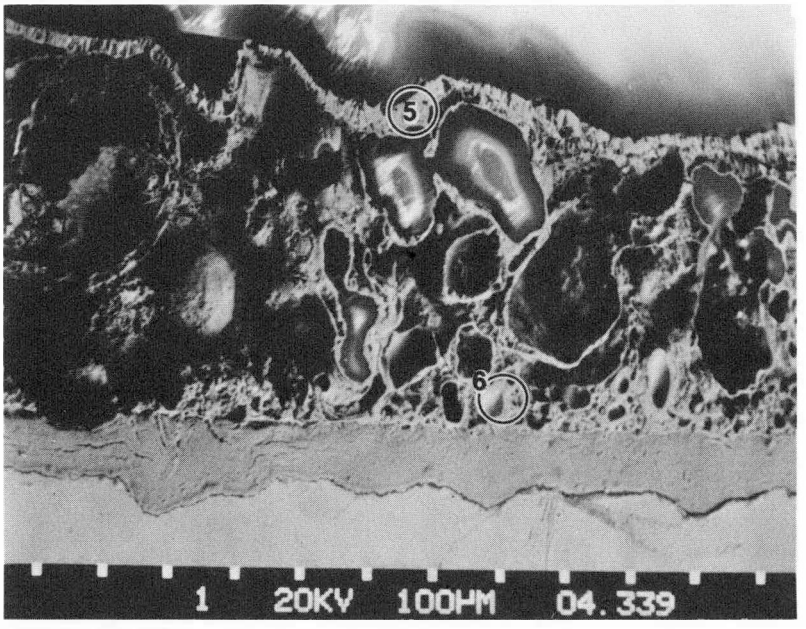

SEM: 100X

5 - Fe(s), Ni, Cr(vw), K(vw)

6 - Fe(s), Cr(m), Al(w), Ni(w), K(vw)

Figure 3.12 Exposed Surface of Alloy 4 Showing a More Adherent, Dense Scale Adjacent to the Alloy

the liquid phase from the metal surface. In the latter case, the repeat formation of the liquid corrodent will result in much less metal loss than in the first cycle. The denser scale, assuming a higher melting point, will also limit the corrosion rate by reducing the Fe ion mobility in the solid more than in the liquid sulfates. One reexposed specimen of Alloy 4 demonstrated that the scale was indeed protective.

The higher alloy matrix of 35%Ni-25%Cr, Alloys 5 through 8, was not significantly better than the 25%Ni-20%Cr Alloys, 1 through 4. This conclusion was drawn from a comparison of the condition of the descaled surfaces shown in Figures 3.6 and 3.7 and was also evident in the microsection of Alloy 5 shown in Figure 3.13. The oxide-sulfide scale formed on Alloy 5 was not significantly better than those on Alloys 1 and 2, which also had low silicon. The Alloy 5 scale apparently was composed of more sulfide than oxide. Note that the silicon indication in this scale may have come from the SiC paper used for grinding the specimen.

The 35%Ni-25%Cr alloy (Alloy 15), which contained 4 percent aluminum and 0.5 percent yttrium--mentioned previously in relation to Figure 3.8--was among those in which large or deep pits were not formed but in which general surface attack was prominent. A good indication of the shallow pitting characteristic is evident in Figure 3.14, which shows the microsection of a pitted area [0.0012-in. (30-μm) deep] selected at random. Alloy 15 produced a Cr_2O_3-type scale within the pit area and along the alloy surface. The shallow attack may also be the result of reduced ion mobility caused by the scale. Yttrium was sought but was not within the range of the EDX measurement. The analysis indicated a Cr_2O_3-type scale low in metal sulfides (less than 1 percent). The sulfide print test on the scaled surface (with loose deposits removed) showed that weak, isolated spots of sulfides were formed. Other alloys examined had a higher sulfide content in the mixed sulfide-oxide scale. Shallow pitting was not the case in most other alloys, as illustrated by Alloy 12 (Figure 3.15).

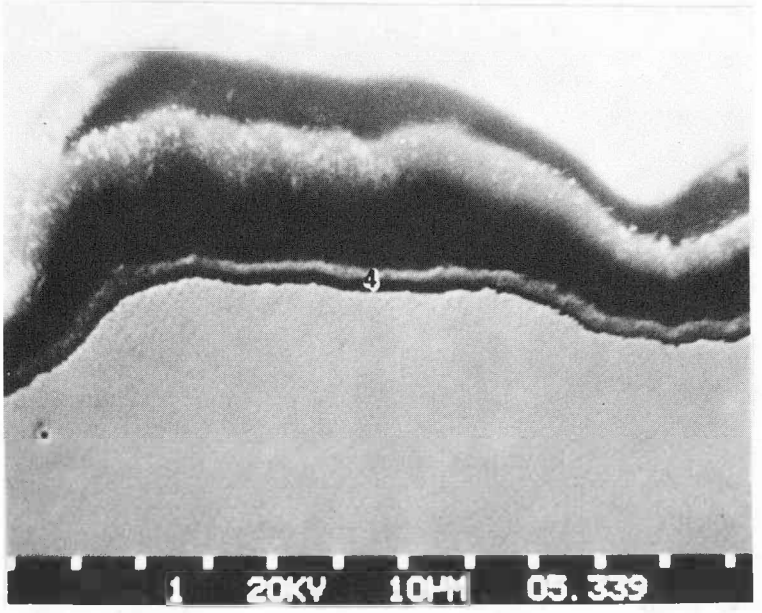

SEM: 1000X

PHASE COMPOSITION

4 - Cr(s), Fe, Ni(m), Si(m), S(s)

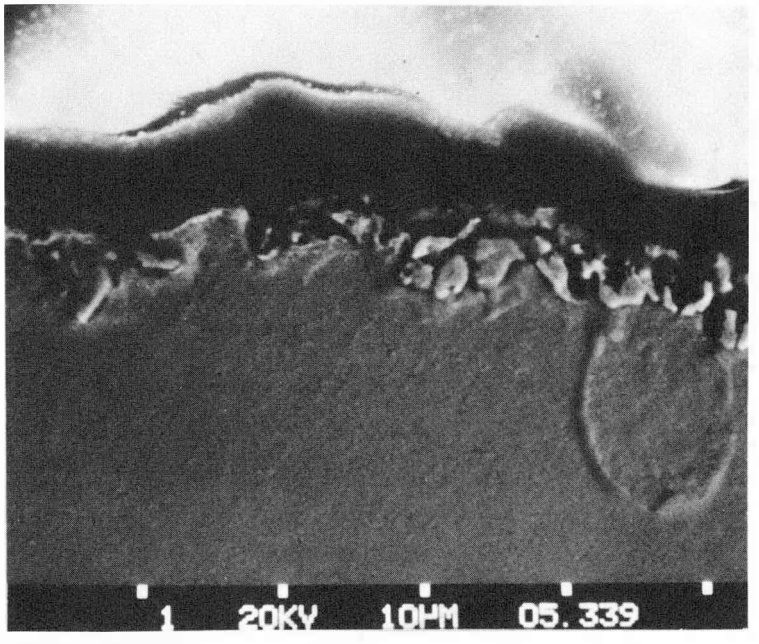

SEM: 2000X

Figure 3.13 Exposed Surface of Alloy 5 Showing a Poorly Adherent Sulfide Scale (somewhat different from those containing silicon)

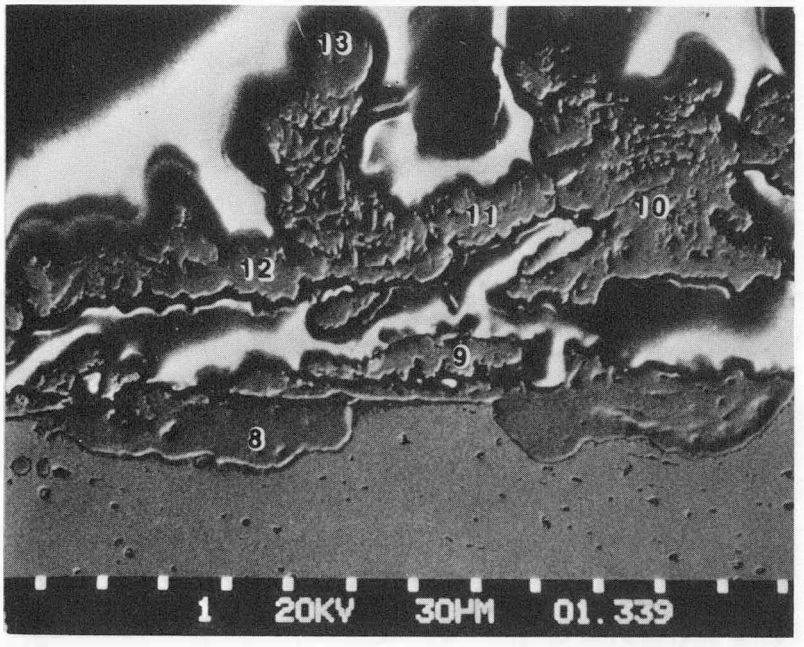

PHASE COMPOSITION

Oxide Scale

8 - Cr(s)

Scale and Deposits

9-13 - Fe(s), Ni(s), Al, S, K(w)

SEM: 300X

Figure 3.14 Exposed Surface of Alloy 15 Showing the Porous Deposits Over Intermittent Areas of Oxide on the Alloy Surface (Shallow pitting was noted.)

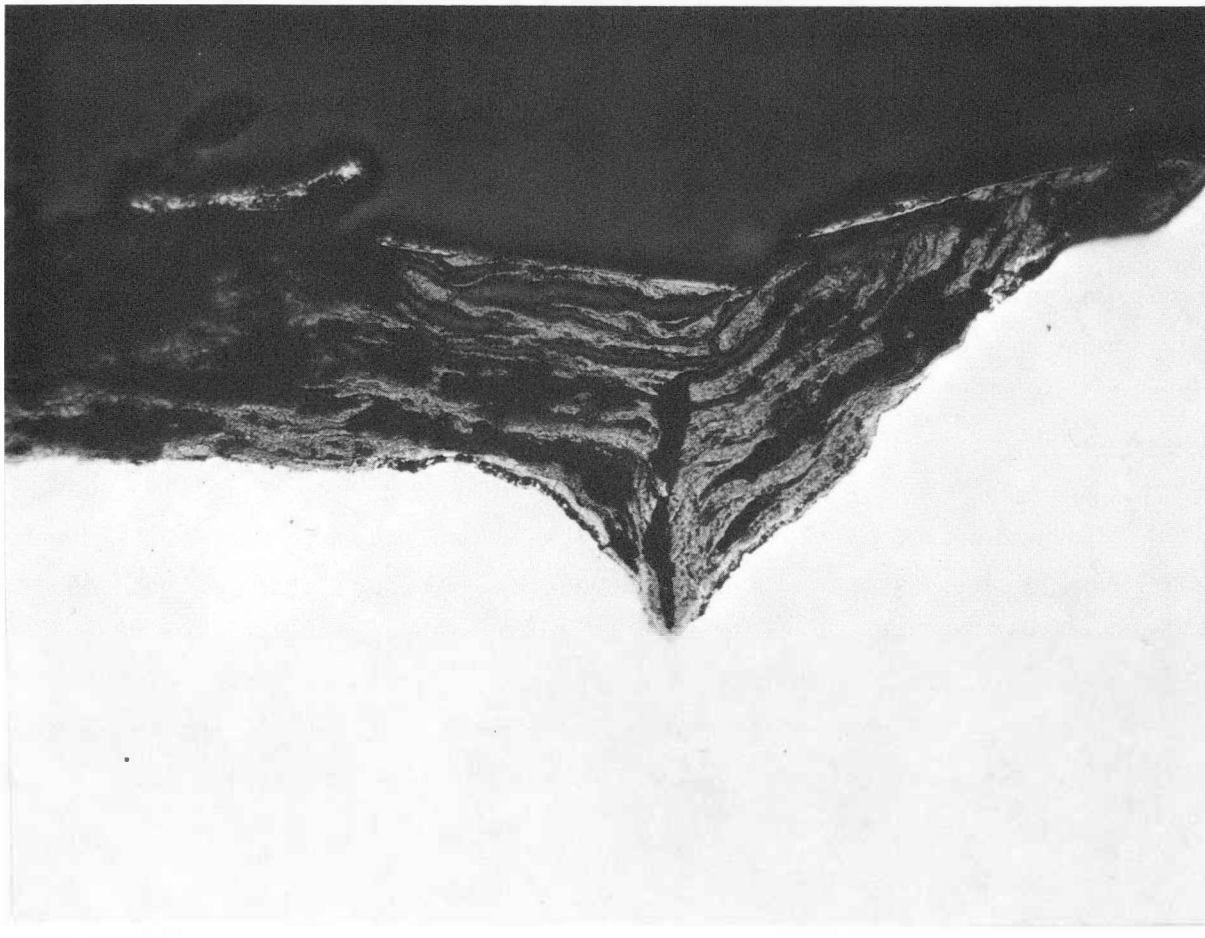

SEM: 250X

Figure 3.15 Exposed Surface of Alloy 12 Showing a Different Type of Deep Pit Formation and a Nonprotective Scale

Alloy 17 was designed to evaluate the effects of yttrium on the 35%Ni-25%Cr alloy without aluminum, as shown in Figure 3.16. The results of all three retort tests showed no significant difference from Alloy 5; that is, severe pitting similar to Alloy 1 (Figure 3.6) predominated. Little visible benefit can be attributed to the 0.5-percent yttrium in Fe-Ni-Cr-0.5%Y or to the 0.1-percent yttrium in Alloy 16. While aluminum plus yttrium resulted in reduced pitting, the general attack was still severe. None of the alloys in Phase 2 that were low in silicon seemed very promising.

Alloy 18 was designed to evaluate the addition of yttrium to 310SS. The results showed a small reduction in pitting compared with Alloys 16 and 17; but when compared with the previous tests of commercial 310SS, no significant effect was noted. The pitted surface of Alloy 18 is indistinguishable from that of commercial 310SS.

The last alloy in Table 3.13, Alloy 19, was mechanically alloyed using Y_2O_3 powder blended with powdered 310SS and was pressed, sintered, and hot-rolled into strip. The tests of this alloy also show no indication of a beneficial effect of Y_2O_3, as indicated by the gas oxidation behavior of this modified alloy. The deeply pitted surface seen in Figure 3.17 showed no significant influence of the Y_2O_3 on the alloy surface or scale behavior.

3.2.4 X-Ray Diffraction Data on Deposits and Scale

The XRD analyses of the exposed specimens were conducted after all the residue from the ash deposits was removed and after the outer, loose deposits were removed from the exposed samples to obtain the scale compositions shown in Table 3.14. While several sulfides should presumably be present, only FeS was formed well enough to give an XRD pattern. We looked for other oxides such as Al_2O_3, NiO, and SiO_2 but did not find them. Al_2O_3 is apparently extracted by the trisulfate melt, the residue of which has not been analyzed in detail.

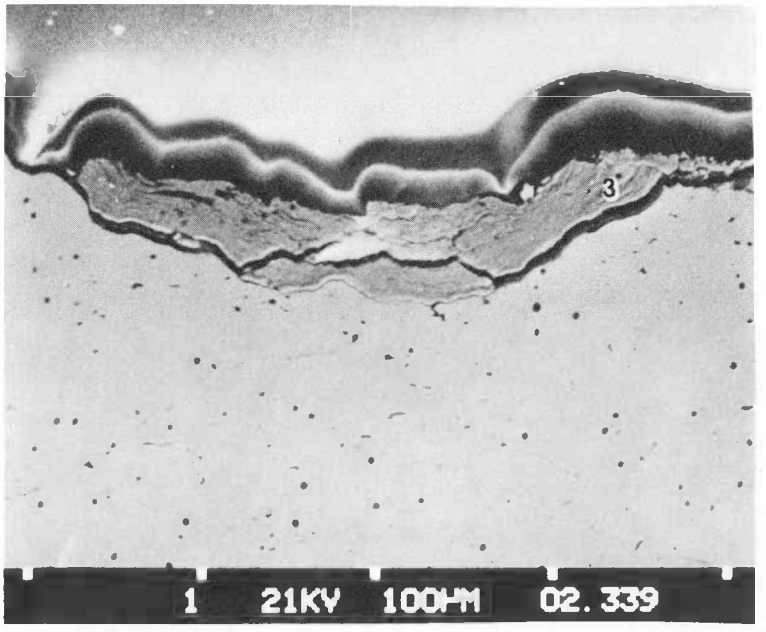

PHASE COMPOSITION

3 - Cr(s), Fe, Ni(vw), Si, K(m), S(s)

SEM: 265X

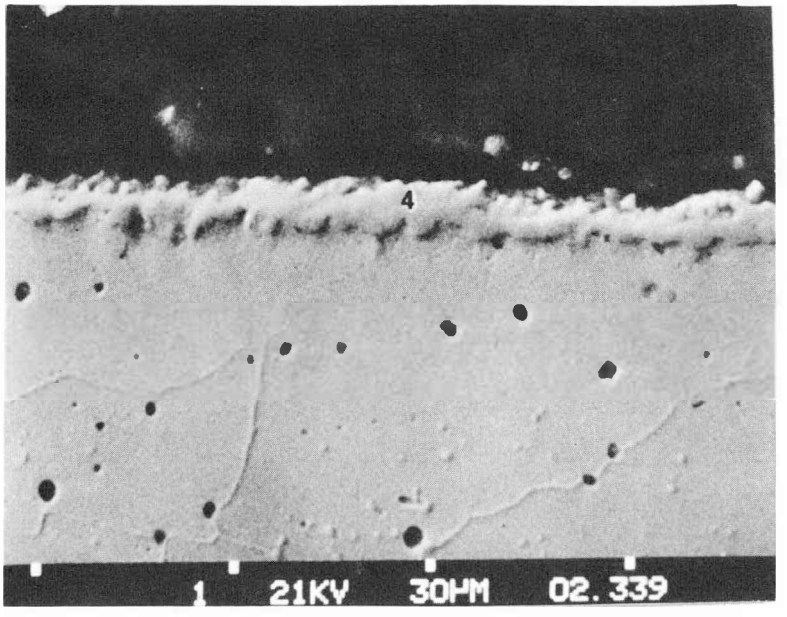

4 - Cr(s), Fe, Ni(vw)

SEM: 1000X

Figure 3.16 Exposed Surface of Alloy 17 Showing a Scale Which Was Adherent in Some Areas

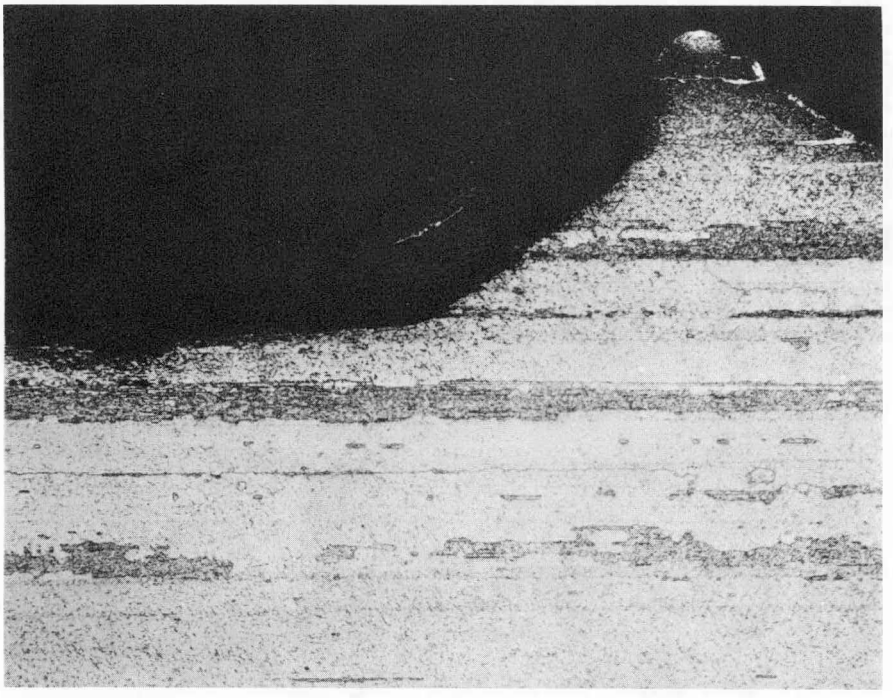

SEM: 200X

Figure 3.17 Optical Micrograph of Mechanically Alloyed 310SS (Alloy 19) After Exposure

Table 3.14 XRD Analyses of Outer Loose Deposits and the Scale Near the Surface of 19 Alloys Exposed to Simulated Coal Ash and Flue Gas [Coupons from Retort 17--48-hour cyclic exposure at 1250°F (675°C)]

Alloy No.	Nominal Composition* Ni	Cr	Al	Si	Y	Deposit or Scale†	Scale Component (XRD) γ-Fe_2O_3	α-Fe_2O_3	Cr_2O_3	Fe_2SiO_4	$Fe(AlCr)_2O_4$	FeS	$KNaSO_4$
1	25	20	-	-	-	SS	← none →						
						Dep	s§		vw§			vw	m§
2	25	20	2	-	-	SS	← none →						
						Dep	s		vw			w	m
3	25	20	-	2	-	SS	s		w			w	
						Dep	s	m	vw			m	w
4	25	20	2	2	-	SS	m	m					
						Dep	s					m	w
5	35	25	-	-	-	SS	w						
						Dep	s		m			m	m
6	35	25	2	-	-	SS	vw						
						Dep	s		w			m	w
7	35	25	-	2	-	SS	w		w				
						Dep	s	m	m			m	
8	35	25	2	2	-	SS	w		s				
						Dep	m		m			w	w
9	40	30	-	-	-	SS	s		w				
						Dep	s	m	m			w	w
10	40	30	2	-	-	SS	m						
						Dep	s		w			m	w
11	40	30	-	2	-	SS	m		m			w	
						Dep	w	s	w			w	w
12	40	30	2	2	-	SS	w		s	s			
						Dep	m		m	m			w
13	35	25	4	-	-	SS			w				
						Dep	s	m	w			w	w
14	35	25	4	-	0.1	SS	s		s				w
						Dep	s		w			w	w
15	35	25	4	-	0.5	SS	s		w		m	w	
						Dep	s	w	w		m	w	
16	35	25	-	-	0.1	SS	m						
						Dep	s		m			m	m
17	35	25	-	-	0.5	SS	m		m				
						Dep	s	w	m			w	m
18	20	25	-	-	0.6	SS	m		m				
						Dep	s		s			w	m
19	20	23	-	-	0.5 Y_2O_3	SS	← none →						
						Dep	s	m	m			w	w
310	20	25	-	-	-	SS	s						
						Dep	← none →						

*Balance Fe.
†SS = Scale retained on the metal surface; Dep = Outer loose deposit or scale/deposit mixture.
§Nomenclature: s = Strong, m = Medium, w = Weak, vw = Very weak.

The indicated differences in compositions obtained by EDX (shown in Figures 3.9 through 3.14) when compared with the XRD data presented in Table 3.14 result from differences in chemical sensitivity of the two methods and the difference in area between the small spot evaluated by EDX and the larger surface area covered by XRD. Whereas the EDX data show a strong sulfur line (Figure 3.10, Point 2, and Figure 3.11, Point 7), the XRD scales show Cr_2O_3 types that also contain sulfides at those locations. Oxygen content was not determined but was present in all the scales and deposits. The XRD analysis corresponding to the EDX data for Alloy 3 (Figure 3.11) indicated that Cr_2O_3 and FeS were weak but that γ-Fe_2O_3 was strong. Thus the XRD data include several compounds or phases, but the EDX method records the elements only. Since many thin scale layers were present, as seen in Figure 3.11, no conflict exists in these data. The x-ray line for FeS may represent a mixed metal sulfide, and the indicated oxides also may contain other metals. Only one alloy produced an aluminum compound in the scale and deposits--Alloy 15 (see Table 3.14). Nickel compounds were also not significant as separate compounds, as shown by XRD; however, the EDX analysis shows that nickel was present in most of the deposits and scale formations.

One result indicated by the XRD analysis, which may be significant, was that alloys with better resistance to attack (Alloys 4, 8, and 12) did not have as much γ-Fe_2O_3 in the scale as the more vigorously pitted alloys. The higher chromium alloys (Alloys 8 and 12) had a greater percentage of Cr_2O_3-type scale.

3.2.5 Effects of Adding NaCl to Simulated Ash

The effects of a 3-percent NaCl addition were evaluated at 1250°F (675°C), as indicated in Table 3.13. The effects of NaCl were not very great; however, its addition resulted in deeper pitting on alloys with a tendency toward pitting (such as Alloys 1, 5, and 9). This result is not the same as seen in commercial alloys with more silicon and manganese (see Section 3.1.4.5). However, some of the alloys containing aluminum plus silicon, such as Alloy 4, were apparently

not significantly affected by the NaCl. No explanation of why Alloy 8 was inferior to Alloys 4 and 12 was apparent, but only a few specimens were tested in this fashion.

The tests seem to indicate that corrosion of the 4-percent aluminum plus yttrium (Alloy 15) was unchanged by the 3-percent NaCl addition; but as before, the aluminum and yttrium were not retained in the scale in amounts high enough for analysis. The mechanism dictating their behavior is not clear. If the addition of NaCl was very important, some further tests on these alloys and an aluminum plus silicon plus yttrium modified Fe-based alloy would be very interesting.

In summary, indications are that the alloys that seem to form an adherent dense scale were not seriously altered by the NaCl addition. However, alloys higher in nickel suffered deeper pitting when NaCl was added.

3.2.6 Effects of Alloy Content on Fireside Attack

The influences of alloy constituents on fireside attack as found for the commercial alloys (Phase 1) was described in the Section 3.1.4.4 and shown in Figure 3.3. Results indicated that the rapid pitting attack was reduced by the addition of chromium, silicon, and niobium to stainless steels and Fe-Ni-Cr alloys; however, not one of the commercial alloys was resistant to attack.

The Phase 2 results were consistent with the trends for commercial alloys, except for the effects of adding aluminum to alloys low in silicon. Figure 3.3 shows the alloy trends obtained from the Phase 2 data superimposed on the figures with the results for commercial alloys.

The curve illustrates that the effects of chromium (top) may be altered because of the variations of nickel, which was a limitation of the original

alloy selection. The effects of nickel are likewise affected by the alloy selection, as indicated in the curve for nickel (bottom). Phase 2 maximum penetrations on chromium additions are above the Phase 1 values because of the higher nickel content, as shown in this figure.

The emphasis of the Phase 2 test plan was to show the effects of adding aluminum, silicon, and aluminum plus silicon (Figure 3.3). Adding aluminum with low silicon was not beneficial in the Phase 2 alloys except for altering the mode of attack from severe pitting to a more general attack. The addition of silicon and aluminum plus silicon was significantly beneficial, as shown in the figure. The effect of the combined aluminum plus silicon might have been more conspicuous if all the samples had been exposed to repeated cycles of attack, since the silicon-containing alloys, such as Alloys 4 and 8, formed an adherent scale that was retained. A preliminary evaluation of the repeated exposure of a few selected alloys is given in Section 3.2.7.

The effects of nickel are suggested in the lower graph (Figure 3.3). Although the apparent minimum attack seen for the commercial alloys may be correct, both chromium and nickel were varied. Thus the curve should be considered as an indication only, because the optimum alloy was outside the range of selected alloys.

The effects of niobium were not supplemented in the Phase 2 study, but were reported previously[6] using data from 347SS and comparing them with 304SS.

3.2.7 Preliminary Evaluation of Alloy 4 Adherent Scale After Two Cycles of Fireside Exposure

Specimens of Alloys 4, 5, and 8 were taken from Retort 18 and reexposed without chemical descaling. The outer surface of the ash deposit was mechanically removed, and a fresh application of synthetic ash was coated on the sample for inclusion in Retort 19.

The twice-exposed samples were measured and examined as before with the following results: Alloy 4 was not greatly changed in the second exposure except for the attack on the lower surface. This attack was caused by the wetting and flow of the fused alkali-iron trisulfate to that surface, which was not contacted in the original exposure. Alloys 5 and 8, however, were both subject to added losses in the second cycle that were nearly the same as in the first cycle.

The combined losses from the two exposures were as follows (correcting for losses on the lower surface):

Alloy	Loss [in. (μm)] (max. penetration)
4	0.004 (102)
5	0.017 (432)
8	0.012-0.014 (305-356)

The scale retention on Alloy 4 is the only apparent reason for prevention of the further attack seen on the other alloys after repeated exposure.

3.2.8 Conclusions From Phase 2 Tests

Silicon and silicon plus aluminum in Alloy 4 were of significant advantage in producing a surface scale that retards or limits corrosion rates. The fact that the scale may be retained through repeated exposures, as shown with Alloy 4, is apparently a good indication of the longer term promise for the combined aluminum plus silicon alloys. Since the 25%Ni-20%Cr-2%Al-2%Si (Alloy 4) was superior to the 35%Ni-25%Cr-2%Al-2%Si (Alloy 8), the effect of reduced nickel content on the scale stability and adherence should be evaluated further, using repeated exposures.

Additional analyses of the scale composition of Alloy 4 may be desirable to determine the role of silicon and aluminum in its composition. Other

elements capable of stabilizing silicates within the scale may be added for further enhancement of the scale retention and for bulky protective effects.

3.3 PHASE 3 - COATING TESTING

3.3.1 General

In Phase 3 the same fireside evaluations of coated and diffused alloy surface treatments used in Phases 1 and 2 were performed. In meeting the requirements of Subtask 1.4.6, some special considerations were given to coated materials. Specimen preparation, for example, did not include the abrasive rubbing used on the alloy sheet specimens. Tests were performed on the as-coated surfaces only, without polishing.

The test exposures were performed with the same synthetic ash mixtures and the same flue gas used in Phases 1 and 2. To ensure an accurate comparison with the noncoated materials, control specimens of polished 310SS were included in each retort. The results of simulated fireside tests on the coated specimens are presented in Table 3.15. The control specimens demonstrated good reproducibility in every test retort exposure.

3.3.2 Severely Corroded Materials

A number of the coating systems exhibited interesting and unexpected performance, the most notable of which was the severe penetration of the diffusion-chromized specimens. For each of these 40- to 60-percent chromized alloy steels--HT-9, 304SS, 21-6-9 (Nitronic 40)--the pitting was deeper than that expected for the parent metal without the high-chromium surface, which was not assumed to be easily corroded. Other similar failures of chromized steels when exposed to slag have been reported elsewhere; however, in oxidizing gas, the chromized alloys are usually very satisfactory.

The failure of chromized Incoloy 800 was not quite as serious as that of the austenitic steels, as shown in the photomacrographs of the section coupons

Table 3.15 Phase 3 Surface Treatments and Coatings Exposed to Fireside Attack

Coating	Specimen No.	Loss or Maximum Penetration in. (μm)	Coating Stability	Pitting Below Coating	Comments
DIFFUSION:					
Alonized:					
Incoloy 800	Al-1	0.002 (51)	Good	None	No pitting; surface loss from outer layer only.
Incoloy 800 (exposed twice)	Al-2	0.003-0.004 (76-102)	Very good	None	No pitting; intermetallic layer not penetrated.
304SS	Al-1	0.003 (76)	Good	None	Attack limited to outer layer of coating.
304SS	Al-2	0.004 (102)	Good	None	Same as above.
Chromized:					
HT-9	16	0.015 (381)	Fair*	Serious	Local, severe pitting through coating and diffused substructure.
HT-9	18	0.016 (406)	Fair*	Serious	Same as above.
304SS	Cr-3	0.012 (305)	Fair*	Serious	Deep, localized, round pits.
304SS	Cr-2	0.012 (305)	Fair*	Serious	Deep, localized, round pits.
21-6-9	37	0.016 (406)	Questionable	Serious	Attack much deeper than uncoated substrate.
Incoloy 800	Cr-2	0.010 (254)	Fair*	Serious	Coating not protective.
Siliconized:					
2-1/4%Cr-1%Mo	28	0.010 (254)	Lost	None	General attack; not pitted.
304SS	55	0.008 (203)	Lost	Serious	Similar to noncoated 304SS.
347SS	39	0.002-0.005 (51-127)	Largely failed	30% of surface	Coating too thin, but may be beneficial.
Alloy 2	6	0.005-0.008 (127-203)	Largely failed	80% of area	Coating failed; general attack.
Alloy 13	9	0.003 (76)	Mostly lost	Serious	General attack reduced.
PLASMA SPRAY AND METALLIZED:					
Fe-Cr-Al (Elemental) on HT-9	FCA	0.002 (51)	Fair	Local areas	Pitting only in porous areas.
Fe-Cr-Al (Elemental, heat treated) on HT-9	FCAl	0.002 (51)	Good to fair	Minor	Generally satisfactory in short exposures.
Metallized Kanthal (Fe-25%Cr-5%Al) on 309SS	KD-5	0.005 (127)	Good to fair	Moderate	Coating as prepared was too thin and porous.
Metallized Kanthal (Fe-25%Cr-5%Al) on 309SS	KD-9	0.002-0.008 (51-203)	Good	Local	Porosity penetration, but good where not so porous.
"Duplex"-$CrSi_2$ over Kanthal on 347SS	63	0.002-0.003 (51-76)	Good	Nil	Shows promise; not free of porosity.

NOTE: Coatings are described in Table 1.3.

*Chromized surfaces were mechanically and metallurgically stable but were unstable relative to corrosion in the molten salt.

Table 3.15 Phase 3 Surface Treatments and Coatings Exposed to Fireside Attack (Cont)

Coating	Specimen No.	Loss or Maximum Penetration in. (μm)	Coating Stability	Pitting Below Coating	Comments
"Duplex"-$CrSi_2$ over Kanthal on 347SS	61	0.002 (51)	Good	Minor	Pitting associated with porosity.
"Duplex"-$CrSi_2$ over Kanthal on 347SS	62	0.005* (127)	Good	Minor	Pitting associated with porosity.
"Duplex"-$CrSi_2$ over Kanthal on 347SS	64	0.006* (152)	Good	Minor	Pitting associated with porosity.
$CrSi_2$† on 430SS	7	0.002-0.003 (51-76)	Good	0.001-0.002 in. (25-51 μm)	Some porosity penetration.
$CrSi_2$ on 430SS	8	0.005 (127)	Good	0.003 in. (76 μm)	Penetration of porosity without apparent change of coating microstructure.
Ni-Cr-Al (Elemental) on 347SS	X	0.001-0.002 (25-51)	Changed§	Nil	Coating remained intact as a barrier despite internal oxidation.
Ni-Cr-Al (Elemental) on 347SS	Y	0.004 (102)	Changed§	Minor	Similar to 347-X, but edge chipped.
Ni-Cr-Al on 347SS (Second Exposure)	NCA-10	0.003 (76)	Internal oxidation	0.002 in. (51 μm)	Retained mechanical stability despite internal oxidation.
Ni-Cr Prealloyed (IN-671) on Incoloy 800	44	None	Minor internal oxidation	Nil	Coating remained intact as a barrier despite internal oxidation.
Ni-Cr Prealloyed (IN-671) on Incoloy 800	45	None	Minor internal oxidation	None	Same as above; some edge chipping.
Ni-Cr (IN-671) (Second Exposure)	45	0.002-0.004 (51-102)	Internal oxidation	Minor	Coating chemically changed; mechanically sound.
Ni-Cr-Si on 309SS (IN-671 + Si)	A	0.002-0.003 (51-76) Local spots	Fair to good	0.001	Good except for small coating defects and pores.
Ni-Cr-Si on 309SS (IN-671 + Si)	B	0.001 (25)	Fair to good	Trace	Less internal oxidation than IN-671. Substrate protected.
Ni-Cr-Si on 309SS (IN-671 + Si)	D	0.015-0.003 (38-76)	Fair to good	Trace	Minor corrosion at porous spots.
Ni-Cr-Si on 309SS (IN-671 + SI)	J	0.003 (76)	Fair to good	Nil	Less porosity-related attack.
Ni-Cr-Al-Si (Elemental)	CrAlSi	None	Changed§	None	Complex heterogeneous microstructure.
Ni-Cr-Al-Si (Elemental)	$AlSi_2$	Chipped	Localized areas oxidized	None	Problem as a result of coating segregation.
Ni-Cr-Al (Commercial) (Metco 443)	L	0.005-0.010 (127-254)	Questionable	Some	Local failures resulting from porosity and attack at base.
Ni-Cr-Al (Commercial) (Metco 443)	M	0.008-0.010 (203-254)	Some oxidation	Local pitting	Weakness resulting from poor coating density (not inherent in material).
Ni-Al (Metco 404) on 347SS (Second Exposure)	404	Coating lost	Failed second test	Serious	Penetrated on second exposure despite "good" first result.

*Penetration indicated was largely the result of attack during the descaling procedure using hot caustic.
†Metco XP-1137 powder applied by plasma spray.
§Microstructural changes resulting from internal oxidation from exposure.

Table 3.15 Phase 3 Surface Treatments and Coatings Exposed to Fireside Attack (Cont)

Coating	Specimen No.	Loss or Maximum Penetration in. (μm)	Coating Stability	Pitting Below Coating	Comments
Ni-Al (Metco 404)(heat treated)	347-11	Thickness increased	Changed*	Very minor	Prevented significant attack despite internal oxidation.
Ni-Al (Metco 404)(as sprayed)	347-50	0.001-0.005 (25-127)	Poor	Edge attack	Edge coating loss on cool-down contained sulfide and oxides after exposure.
Ni-Al (Metco 404)(as sprayed)	347-53	Variable	Poor	Edge attack	Edge coating loss on cool-down contained sulfide and oxides after exposure.
Ni-Al (Metco 404)(as sprayed)	347-59	Variable	Poor	Edge attack	Edge coating loss on cool-down contained sulfide and oxides after exposure.
$MgZrO_3$† on 304SS (Metco 210)	(M-210)	0.001 (25) (surface)	Excellent	None	Self-healing porosity as a result of formation of $MgSO_4$.
$MgZrO_3$† on 304SS (Metco 210)	(M-210)	Slight increase	Excellent	None	No loss, no penetration.
$MgZrO_3$† on 304SS (Metco 210)	(304-8)	Slight increase	Excellent	None	No loss, no penetration.
$MgZrO_3$† on 304SS (Metco 210)	(304-9)	Slight increase	Excellent	None	No loss, no penetration.
$MgZrO_3$† on 304SS (Metco 210) (exposed twice)	(304-9)	Slight increase	Excellent	None	(Not descaled.)
ZrO_2 on 2-1/4%Cr-1%Mo (Metco 201)	201	0.002§ (51)	Good¶	None	Bond failed after cool-down; coating removed intact.
ZrO_2 on 2-1/4%Cr-1%Mo (Metco 201)	CrMo	0.002§ (51)	Good¶	None	Probably oxidized below coat same as above.
ZrO_2 on 347SS	71	0.001§ (25)	Good¶	None	Coating lost during descaling (no bond coating).
Tribaloy 700 (Ni-Mo-Cr-Si) on 310	T-71	0.008-0.009 (203-229)	Top surface corroded	0.001	Residual coating adhered.
Tribaloy 700 (Ni-Mo-Cr-Si) on 310	T-72	0.010** (254)	Composition changed	0.002	Residual coating adhered.
Tribaloy 800 (Co-Mo-Cr-Si) on 310	T-82	0.008 (203)	Composition altered	0.001	Part of coating retained.
Tribaloy 800 (Co-Mo-Cr-Si) on 310	T-83	0.008 (203)	Composition	0.001	Part of coating retained.

*Microstructural changes resulting from internal oxidation from exposure.
†Bond coating on Ni-Al applied on the stainless substrate to assure good bonding.
§P.M. - Parent metal.
¶Bond lost as a result of lack of bonding coat but appeared to be chemically stable.
**Maximum loss at pitted area.

(Figure 3.18). To verify that the alloy surface was as high in chromium as we presumed, samples of unexposed chromized steel were examined by the microprobe method discussed in Section 3.4.2. Figure 3.18 shows the 48-hour metal losses at the round-bottom pits with the distinctive appearance of anodic areas subjected to sizable current densities. A second run in Retort 20 demonstrated that the severe attack was also repeatable (see coupons in Figure 3.19). The high chromium content is probably not in totally solid solution but may contain complex carbides, nitrides, or chromium gradients that assist in the early breakdown of the passive films.

The siliconized specimens were not as deeply pitted as the chromized specimens and the silicon-rich layer perhaps functioned as a weakly protective coating--but too thin to retard the attack except in a small area. The siliconized 2-1/4%Cr-1%Mo specimen in Table 3.15 was attacked by general, uniform corrosion, but none of the coating remained. Several of the siliconized specimens suffered smaller corrosion losses in the 48-hour exposure tests than comparable base alloy specimens presumably would have, but there was no indication that the lower rate would be sustained in further exposure cycles (see Figure 3.20). The 4-percent aluminum Alloy 13 may possibly have developed a protective thick scale in repeat cycles, but the complex alloy plus the special coating suggests a very high cost. The anticipated prospect of generating a more protective silicate scale at the start of the exposures was not realized, and the very thin silicon-enriched surface corroded away too rapidly for this purpose.

3.3.3 Diffused Aluminum Surface Alloy (Alonizing)

The Alonized specimens were obtained by the Alon process applied to coupons of 304SS and Incoloy 800 (from the same raw material tested in Phase 1). The results were more favorable than those for most of the other coatings in that they indicated that the high-aluminum surface composition had suppressed the tendency toward pitting. The inner layer of intermetallic compounds was not penetrated by the fireside attack (see Figures 3.21 and 3.22).

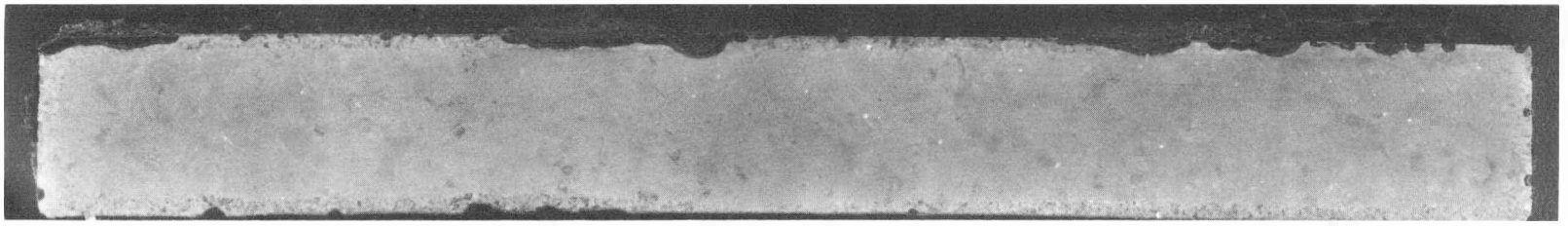

Chromized HT-9

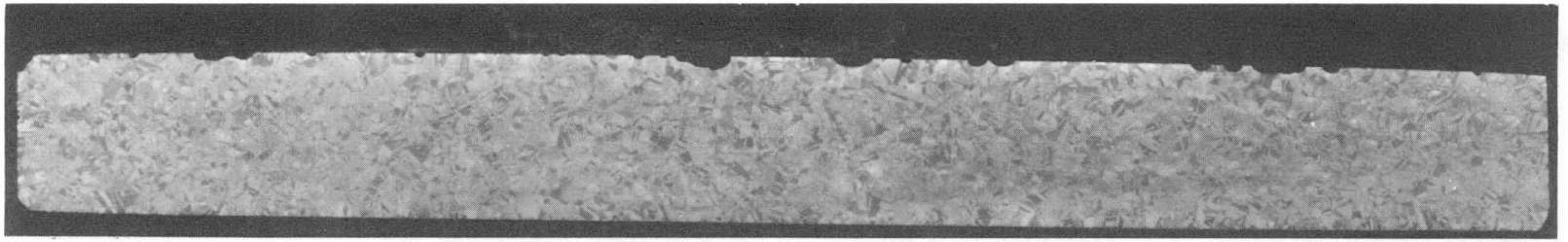

Chromized 304

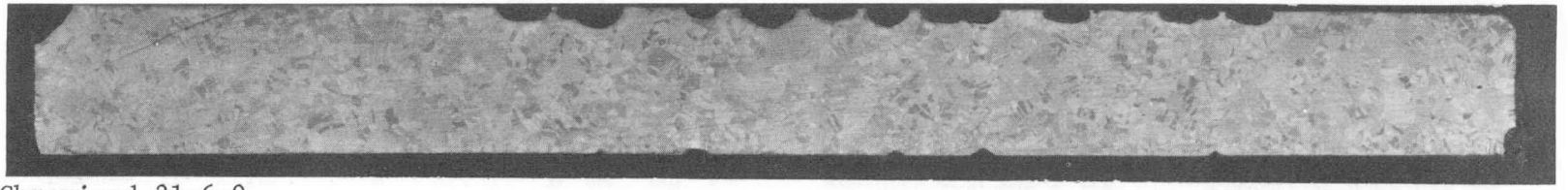

Chromized 21-6-9

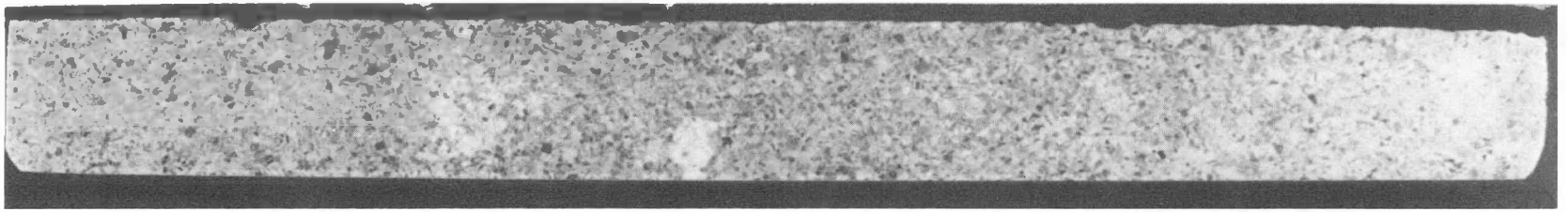

Incoloy 800

Figure 3.18 Transverse Macrosections of Chromized Specimens After Exposure--8X (All specimens with high-chromium surface compositions suffered a severe pitting attack. The pit depth was greater than normal for a 10 percent chromium wrought alloy steel.)

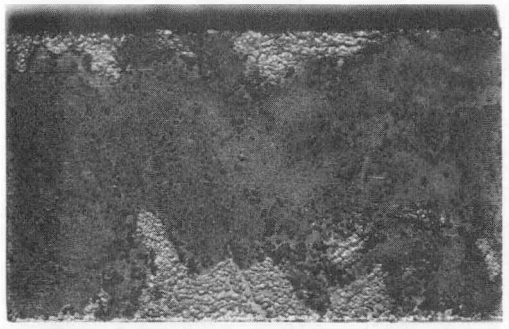

Chromized 304

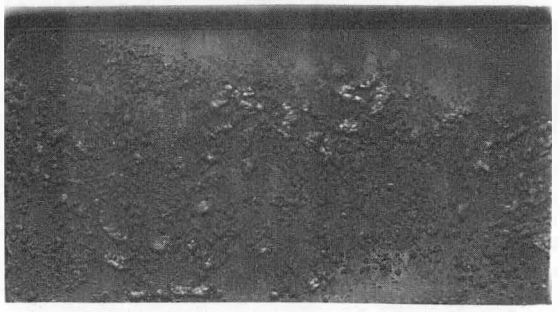

Chromized 21-6-9

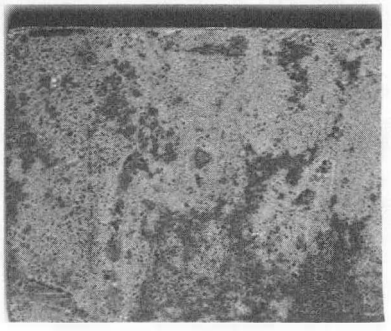

Chromized
Incoloy 800

Figure 3.19 Descaled Specimens of Chromized Alloys--1.5X

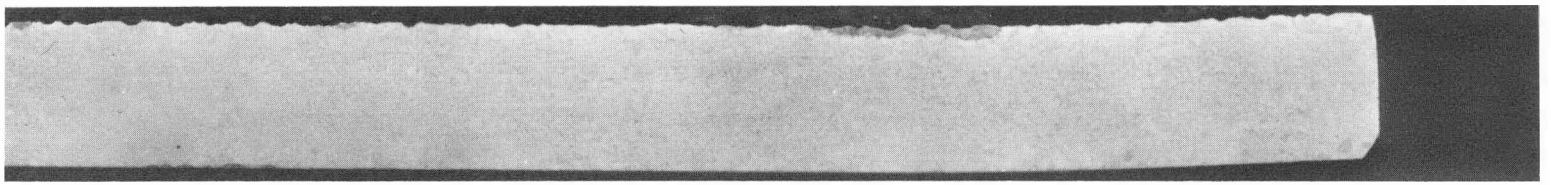

304-55: Siliconized Type 304.

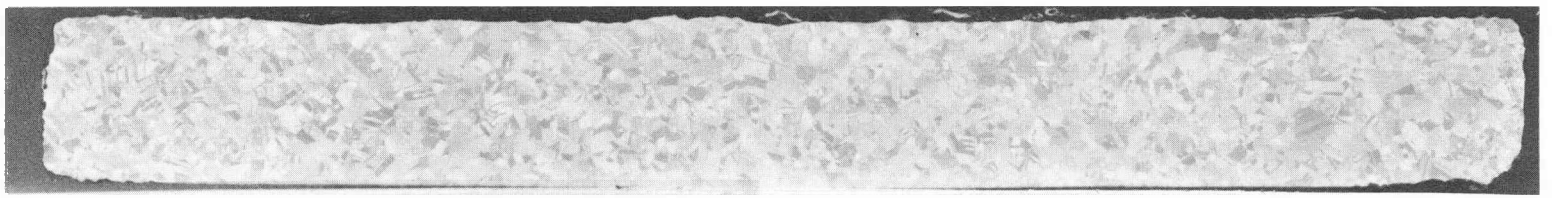

2-6: Siliconized Alloy 2 (25%Ni-20%Cr-2%Al).

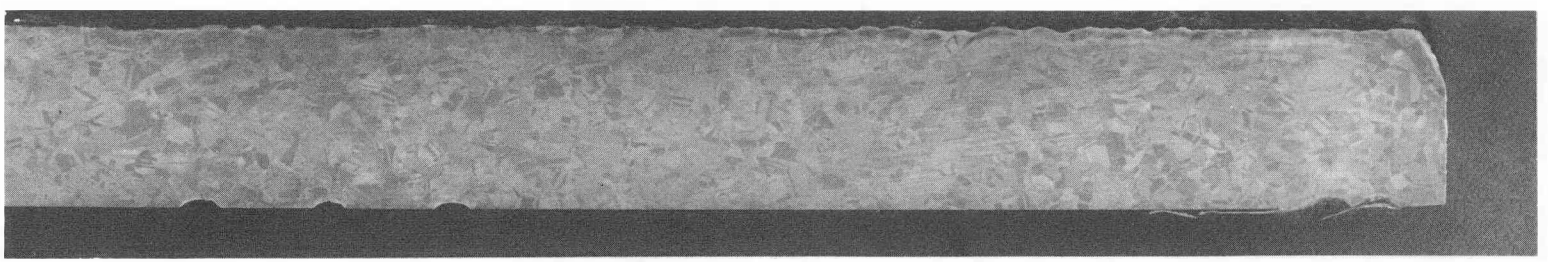

13-9: Siliconized Alloy 13 (35%Ni-25%Cr-4%Al).

Figure 3.20 Transverse Macrosections of Siliconized Alloy Coupons--8X [The siliconized surface was too thin to provide lasting protection (compare pitting on untreated surface in bottom photomacrograph with pitting in top photomacrograph)].

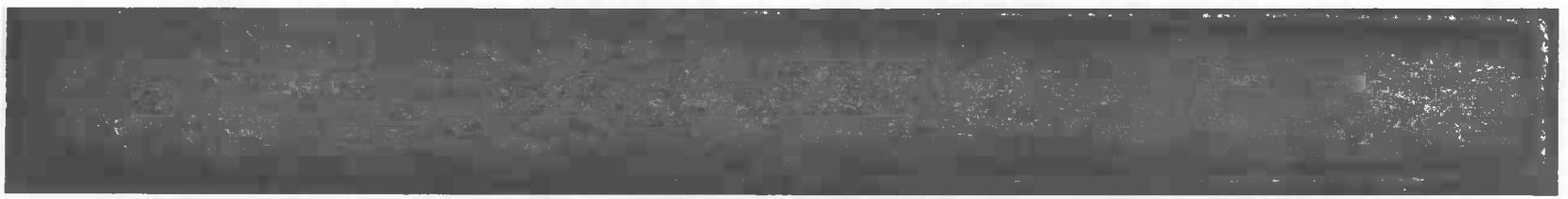

Incoloy 800, A1-2.

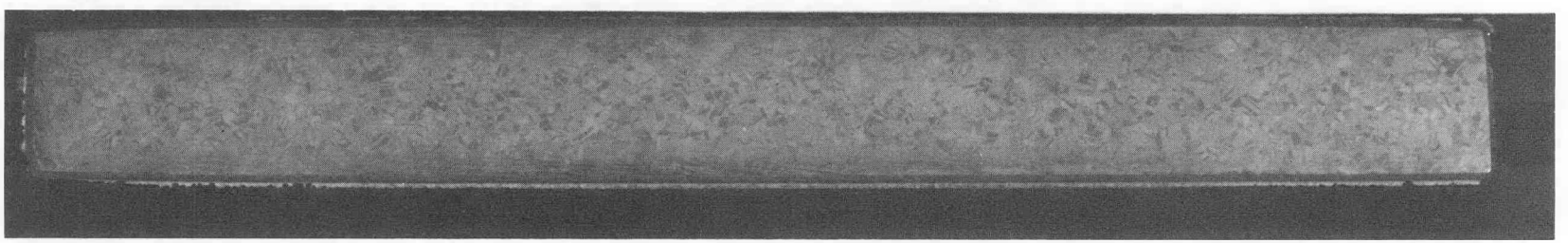

304SS, A1-1.

Figure 3.21 Transverse Macrosections of Alonized Specimen--8X (No severe pitting noted on any of the specimens containing the aluminides formed by diffusing aluminum. Specimens were descaled causing some loss of outer surface phase.)

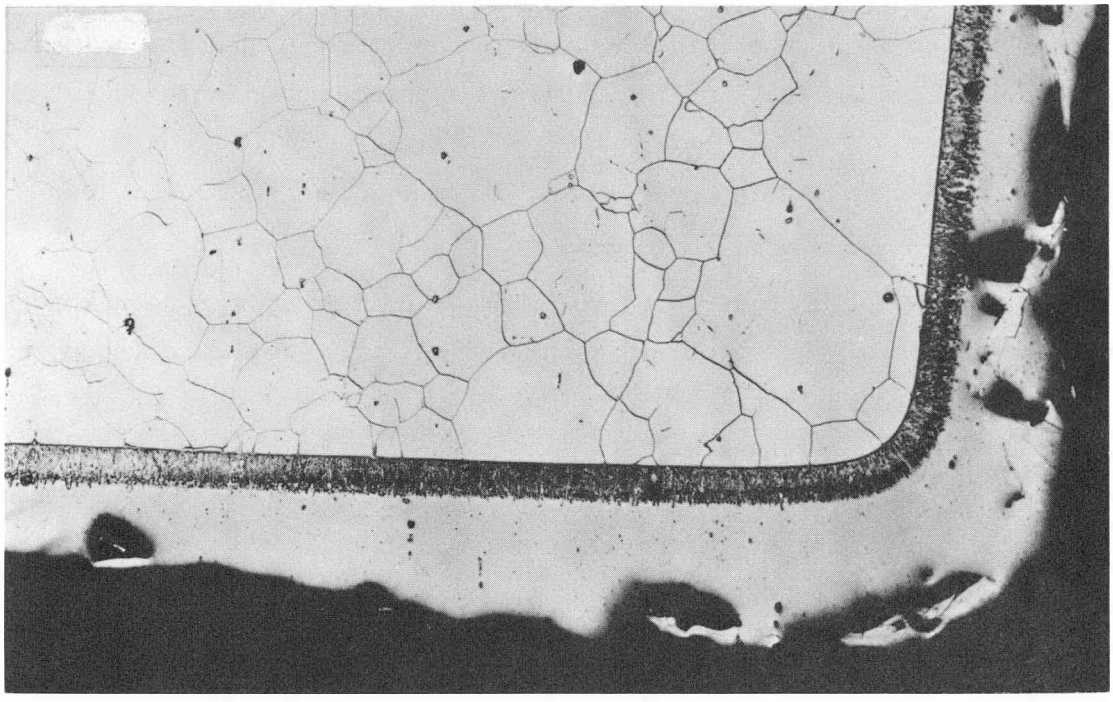

Figure 3.22 Microsection of Alonized Incoloy 800--100X (Surface alloy and diffused layer were resistant to severe fireside corrosion, apparently as a result of cathodic protection. Cutting and grinding of the specimen after testing caused some chipping of the outer phase.)

As indicated in Table 3.15, one of the Alonized Incoloy 800 specimens was exposed twice, simulating repeated corrosion cycles. The data listed for losses are believed to include some surface loss from chemical descaling after both exposures. Some of the outer high-aluminum phase was lost trying to descale the coupons after the exposure. The sections cut for mounting were not cut prior to descaling in this case, so the measured loss data may be high. The test exposures should be repeated for several cycles on coupons that are not chemically descaled to obtain longer-term performance. Additional data, microstructures, and analysis of the Alonized specimens are included in Section 3.4.2.

3.3.4 Iron-Based Plasma Spray Coatings

Indications of good performance by Fe-Cr-Al alloys have been reported by Greenert,[2] and others,[7] but problems when fabricating and welding these Fe-Cr-Al alloys have discouraged their use. As coatings, they are easy to apply and may perform as well as the wrought alloys. The high-aluminum Fe-Cr-Al was applied as an elemental powder blend, partially alloyed during the plasma deposition. While this was one of the best-adhering coatings, the distributed fine porosity allowed some small micro areas of attack at the base of the coating.

Prealloyed Kanthal (Fe-25%Cr-5%Al) was applied by a metallizing method using Kanthal A-1 wire. This method provided good alloy control, but the coating still retained significant porosity. Even though the coating used in the test was too thin (single-pass) and porous, the material was considered promising. Improved coatings and methods of sealing porosity are known, but further development of the coatings was outside the scope of this test.

The use of $CrSi_2$ plasma deposited over the Kanthal coating was chosen to produce a low porosity coating that reduced surface attack. The silicide compound itself is very resistant to the molten sulfate, but a little more improvement of the coating appears necessary to eliminate porosity. Photomacrographs showing sections through the duplex-coated specimen compared with the single-pass Kanthal surface are shown in Figures 3.23 and 3.24.

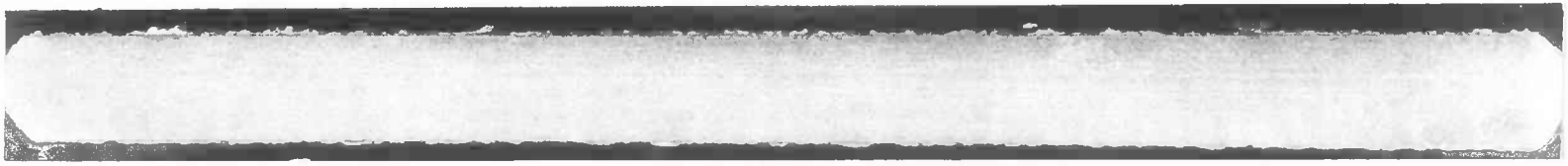

KD-5: Single metallized coating of Kanthal--very thin before the test but prevented pitting.

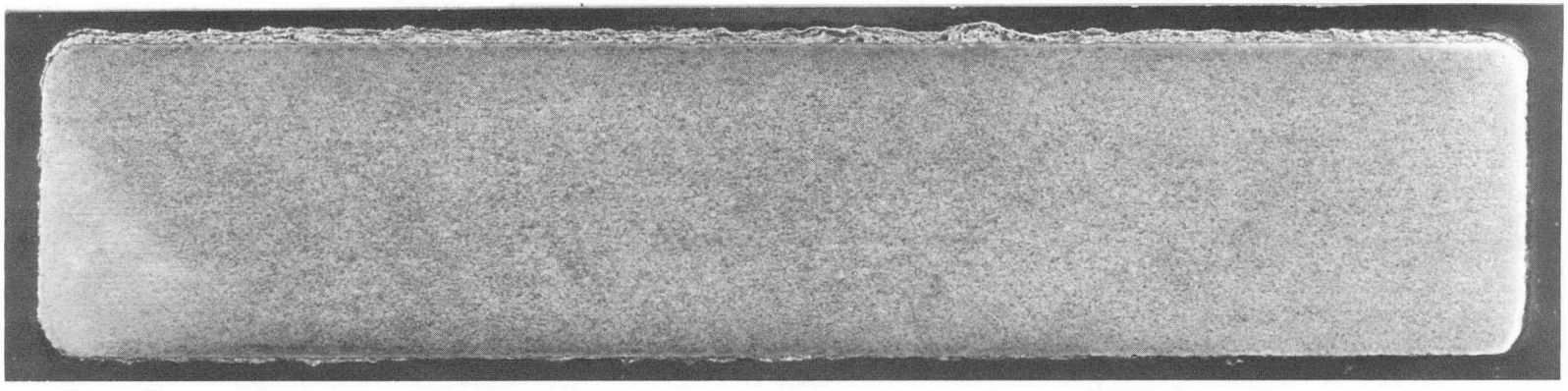

347-63: "Duplex" coating.

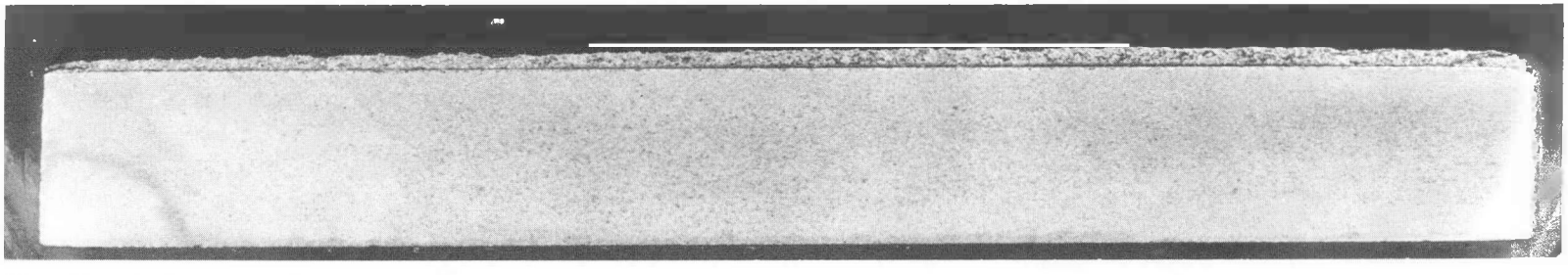

430-7: $CrSi_2$ coating.

Figure 3.23 Transverse Macrosections of Kanthal and $CrSi_2$ Coatings After Test--8X
(Some minor attack caused by porosity was noted on all three specimens.)

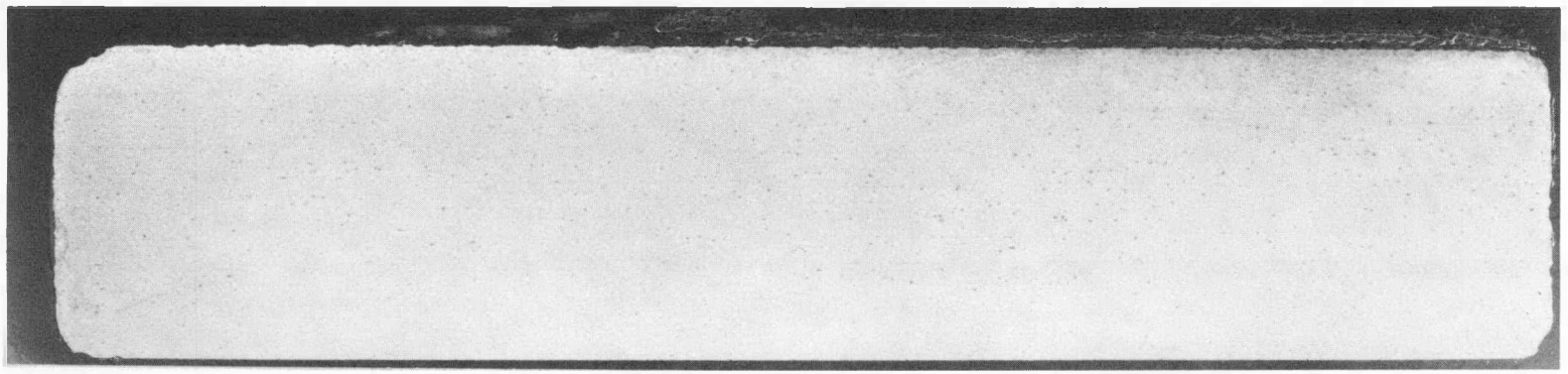

347-63: Coated with $CrSi_2$ over Kanthal ("Duplex" coating). Not significantly attacked but porous.

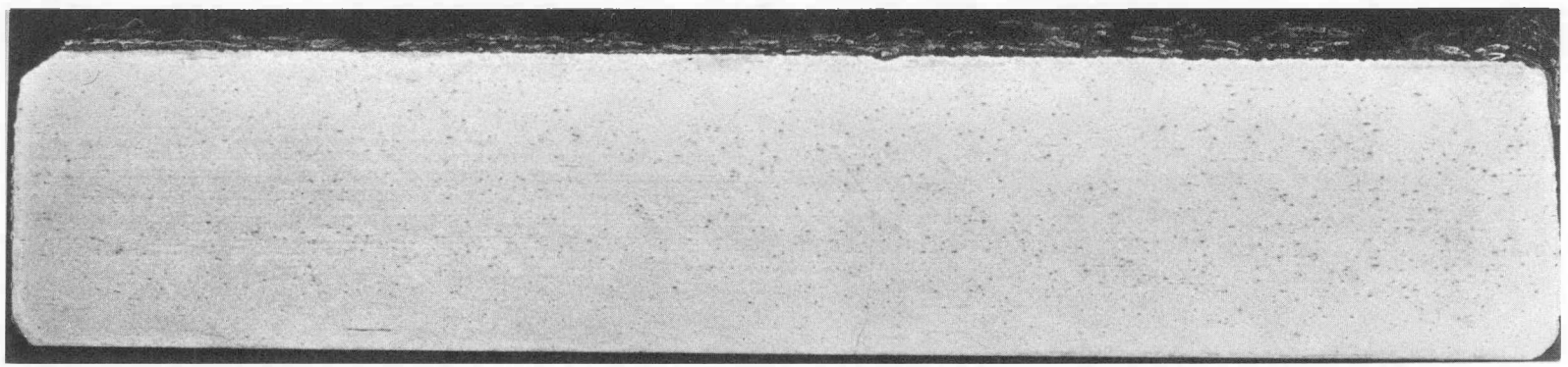

347-62: Coated with $CrSi_2$ over Kanthal ("Duplex" coating). Not significantly attacked but porous.

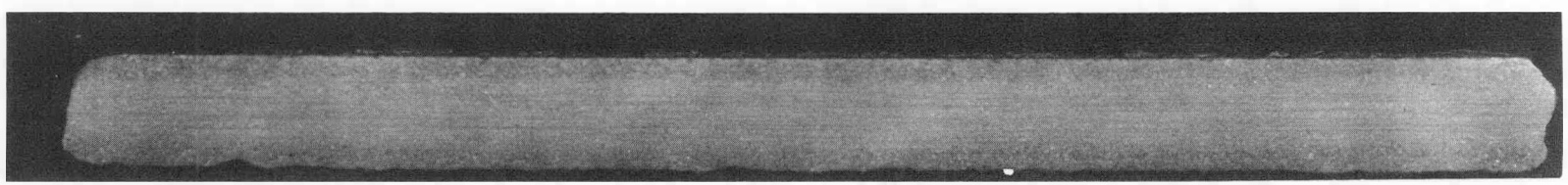

KD-9: Kanthal only. Prevented serious pitting but also porous. Thicker coating may be desirable. Uncoated bottom surface was pitted.

Figure 3.24 Transverse Macrosections of Kanthal and Duplex Coatings--8X

Also included in Figure 3.23 is a specimen of the $CrSi_2$ coating directly applied to a ferritic chromium steel. The performance data for this coating are listed in Table 3.15. If porosity could be reduced, losses for the silicide coating would presumably be very small.

3.3.5 Nickel-Chromium-Based Coatings

The evaluation of plasma-deposited Ni-Cr-Al coatings was designed to test modifications of the IN-671 composition as coatings, because not only can it be tested more cheaply than a wrought alloy, but in some cases, it is the only form that can be obtained for test purposes. Coatings produced from elemental and from prealloyed powders were both included.

The fireside performance of the elemental 45%Ni-45%Cr-10%Al compositions was superficially very good, showing resistance to pitting. The coating surfaces, however, were roughened like the Kanthal coating, possibly because of fine pits in the outer surface of the coating (Figure 3.25).

The changes in the microstructure indicated in Table 3.15 resulted from oxidation and possibly some sulfide formation in the coating matrix. Despite those chemical changes, the Ni-Cr-Al coatings remained mechanically stable and resisted serious attack on the second exposure cycle, as indicated by the macrosections shown in Figure 3.26.

The Ni-Cr (IN-671) coated specimen in Table 3.15 (Specimen 45) that was exposed to two cycles also retained most of the coating, as shown in Figure 3.27. The several specimens tested with plasma-deposited IN-671 coatings were free of the widely separated deep pitting observed in the wrought IN-671 alloy sheet evaluated in the Phase 1 tests (Figure 3.5). The coatings, which have a very uniform chromium distribution, appeared to have a resistance to electrochemical pitting, at least reducing the size and depth of pits. Short-term screening tests, however, do not provide a measure of the total life expectancy of either the coating or the wrought alloy; they only indicate trends.

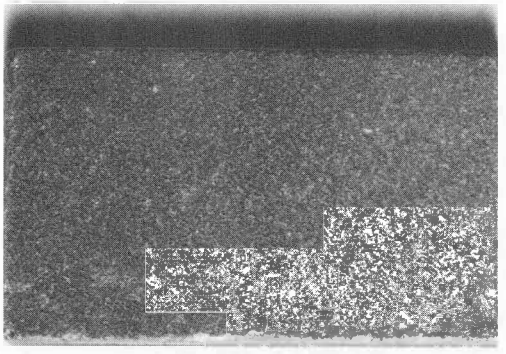

Fe-Cr-Al (Kanthal + $CrSi_2$)
Coating on 347

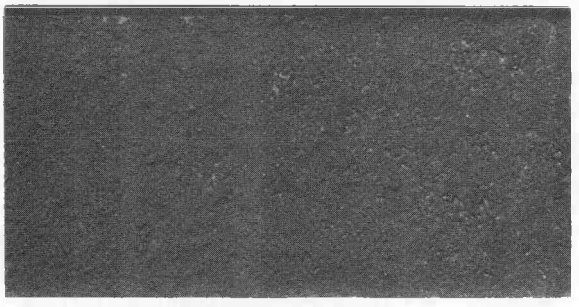

Ni-Cr-Al (elemental)
Plasma Spray on 347

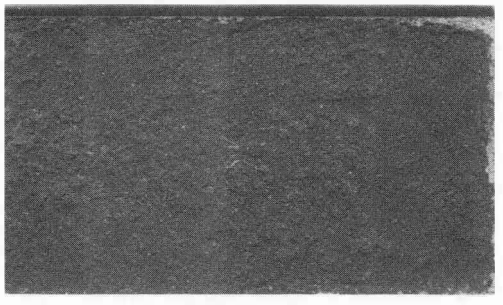

Ni-Cr-Al (elemental)
Plasma Spray 347

Figure 3.25 Surface of Ni-Cr-Al and Fe-Cr-Al Coated Specimens After Descaling--1.5X (Elemental and prealloyed specimens were generally promising, but edge chipping was noted.)

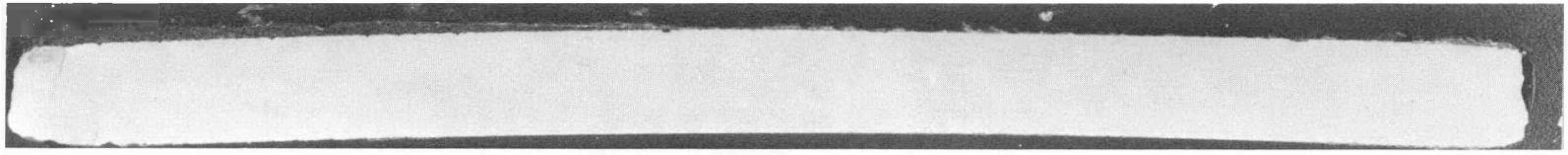

NCA-10: Exposed surface was the lower surface shown in the print.

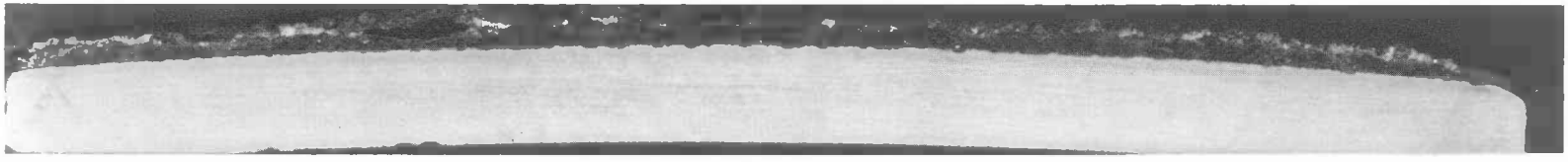

NCA-10 (second exposure): Coating retained but brittle.

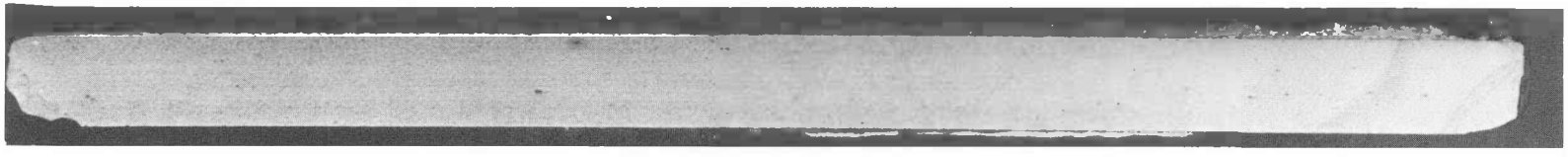

347-X: First exposure to fireside test resulted in no penetration of substrate.

Figure 3.26 Transverse Macrosections of Ni-Cr-Al Coated Specimens--8X (Nickel-based coatings on 347SS.)

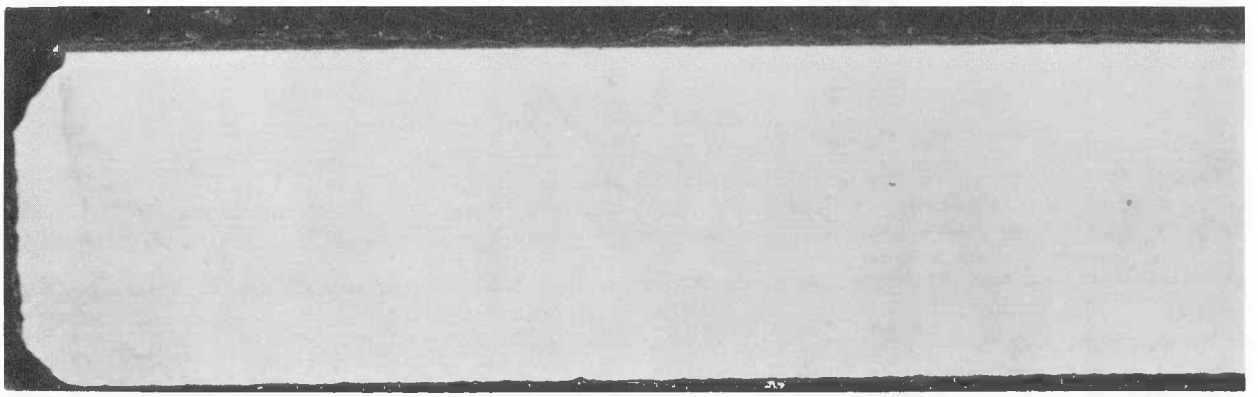

IN-671: First exposure.

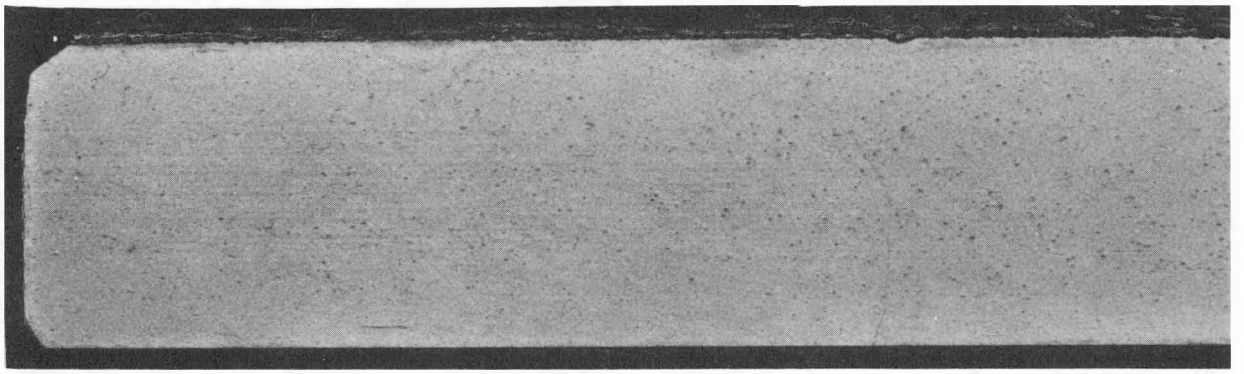

IN-671: Second exposure.

Figure 3.27 Ni-Cr (IN-671) Coated Specimen--8X

Two other modifications of the 50%Cr-50%Ni alloy coatings were evaluated: Ni-Cr-Si and Ni-Cr-Al-Si. The silicon addition to the alloy powder was intended to reduce porosity and to help control internal oxidation. From the standpoint of coating integrity, Ni-Cr-Si gave favorable results, as shown by the macro-sections presented in Figure 3.28. The upper two samples shown in that figure (309-A and 309-B) were preannealed in argon at 1850°F (1010°C). Preannealing is now deemed unnecessary because the unannealed specimen 309-J (Ni-Cr-Si) had the least attack resulting from porosity penetration of any specimen in the Ni-Cr-Si or Ni-Cr-Al groups. Also, no evidence of brittle fracture or chipping was seen in the unannealed specimen.

The Ni-Cr-Al-Si elemental blend (made from 80%Ni-20%Cr alloy powder plus elemental Cr plus Al plus Si) was plasma-sprayed in the same fashion as the preliminary elemental powders and was screened for corrosion stability. Despite the general resistance to attack, the lack of homogeneity in the microstructure gave cause for attempting to heat-treat this composite material. The heat treatment, however, produced serious chipping and delamination of the coating during subsequent tests on two specimens, so further testing was not attempted.

Evaluation of the commercial Ni-Cr-Al coating (Metco 443) was included for comparison with the 50%Ni-50%Cr materials. Metco 443, with a composition of about 71%Ni-20%Cr-6%Al (plus minor elements), is often used as a first coating or "bonding coat" under a hard surface carbide or ceramic coating. The aluminum helps to bond to the substrate material and provides improved (gas phase) oxidation resistance at the interface. The test of the Metco 443 coating did not show any advantage over the elemental Ni-Cr-Al or the IN-671 coatings in fireside exposure. Attack on the Metco 443 consisted of both exposed surface attack and penetration of the coating porosity. The test results did not indicate a problem with the use of Metco 443 as a first layer or bonding coat under another material but did when using it as the top surface coating.

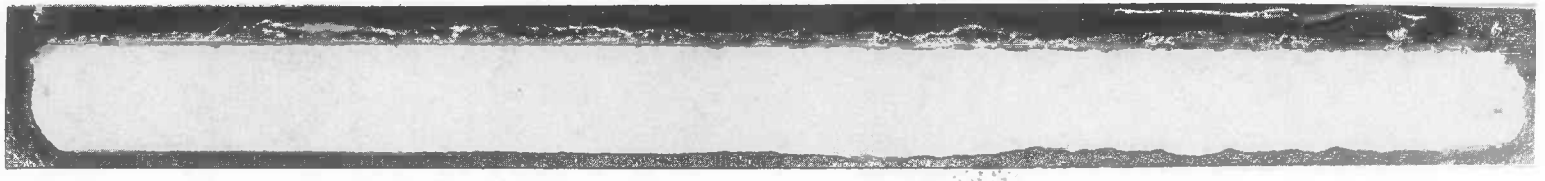

309-A: Received a pretest heat treatment.

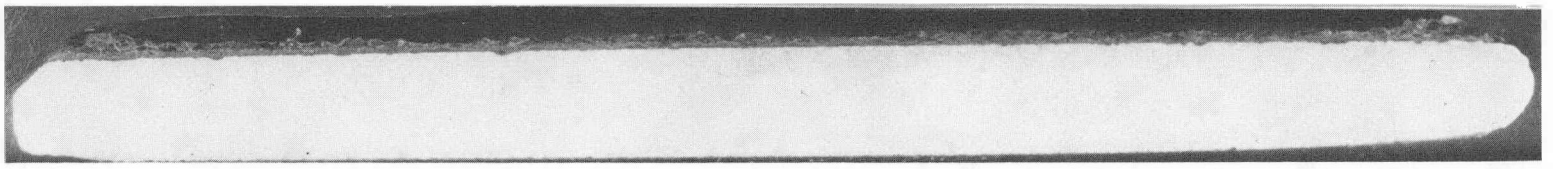

309-B: Received a pretest heat treatment.

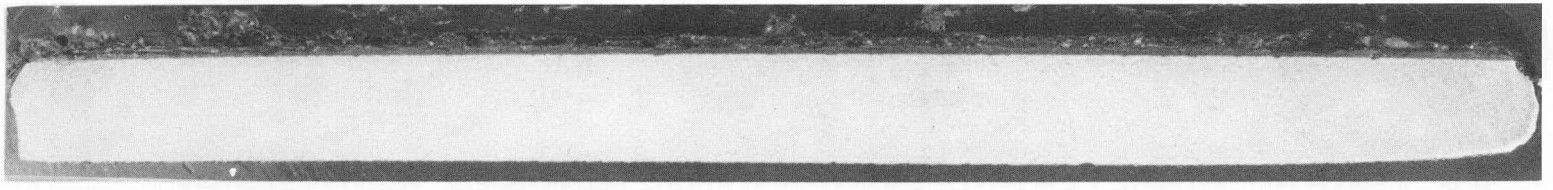

309-D: Received a pretest heat treatment.

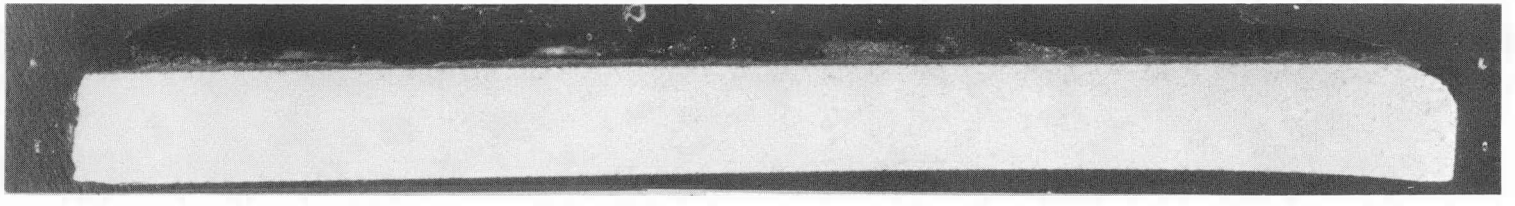

309-J: Not heat treated. Most resistant.

Figure 3.28 Transverse Macrosections of Ni-Cr-Si (IN-671 + Si) Coated Specimens--8X
(Some penetration and internal oxidation were apparent after test.)

Evaluation of the nickel aluminide-type coatings resulted in a variety of different effects, indicating that the effectiveness of material was greatly dependent on the technique and quality of the application. Some of the first samples which were preannealed were resistant and adherent, despite internal changes.

The heat-treated Ni-Al coatings gave protection on one test exposure; however, the second exposure produced a loss of coating (loss of bond) and attack of the substrate, as indicated in Table 3.15 for Specimen 347-404. The Ni-Al coatings on some specimens were not as seriously affected, as shown in the upper two samples in Figure 3.29; but all Ni-Al samples suffered internal oxidation and sulfidation, so presumably the mechanical properties were also affected. Thus the test would have been misleading if only one exposure cycle had been used.

3.3.6 Inert Barrier Coatings

The magnesium-zirconate ($MgZrO_3$) coatings test was a supplemental test added as a result of data collected from European and United Kingdom experiences on the merits and weaknesses of MgO coatings. The $MgZrO_3$ coating is an improved MgO type developed for the protection of flame-holders and combustion chambers; it retains the advantages of MgO without the weaknesses previously observed. (MgO was affected by moisture and was too porous and weak.) The test results demonstrated that relatively inert characteristics of the surface were combined with a strong, adherent coating material. Figure 3.30 (bottom) presents the 8X macrosection, after exposure, for Specimen 304-8; additional results using $MgZrO_3$ are presented in Section 3.3.8.8. A further indication of this inert barrier characteristic was the fact that the residual ash after the test was free of corrosion products, such as nickel and chromium oxides. All other samples of exposed coatings contained some corrosion products after testing.

The ZrO_2 coating was also screened to see whether its chemically inert behavior would be retained in the fireside corrosion environment. The results

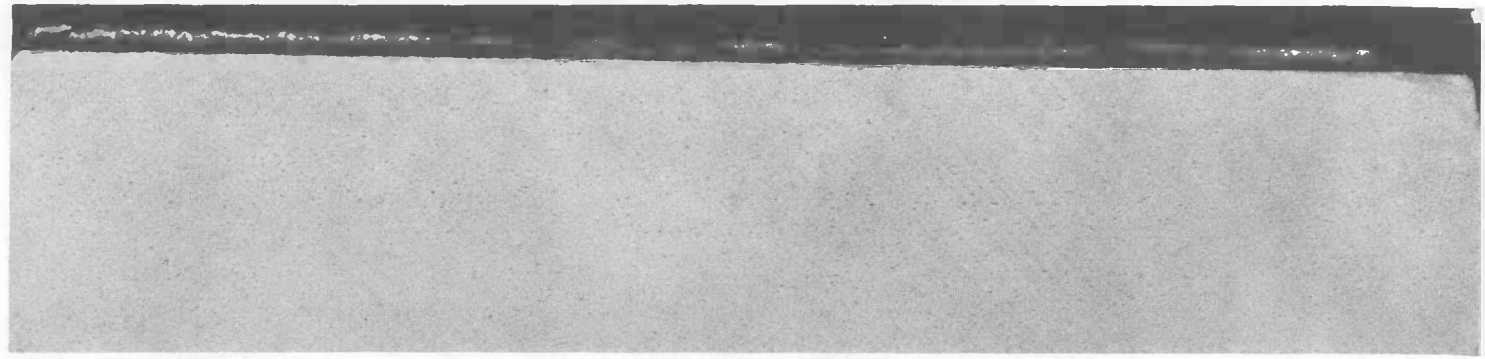

347-50

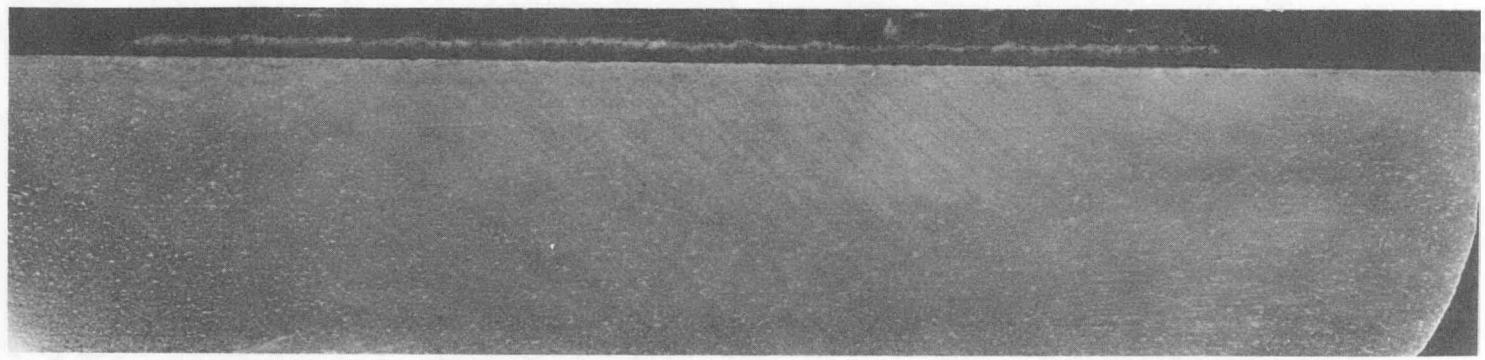

347-53

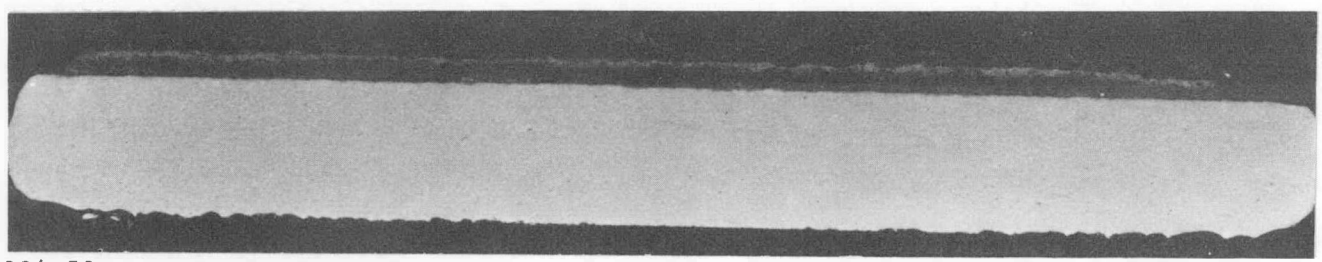

304-59

Figure 3.29 Macrosections of Plasma-Coated Ni-Al (Metco 404) Specimens (347-50 and 347-53) After Test--8X [These coatings, without abrasive blast pretreatment, were not bonded as well as the previous Ni-Al coatings, (304-59). Coating fractures occurred during post-test cutting--not during testing.]

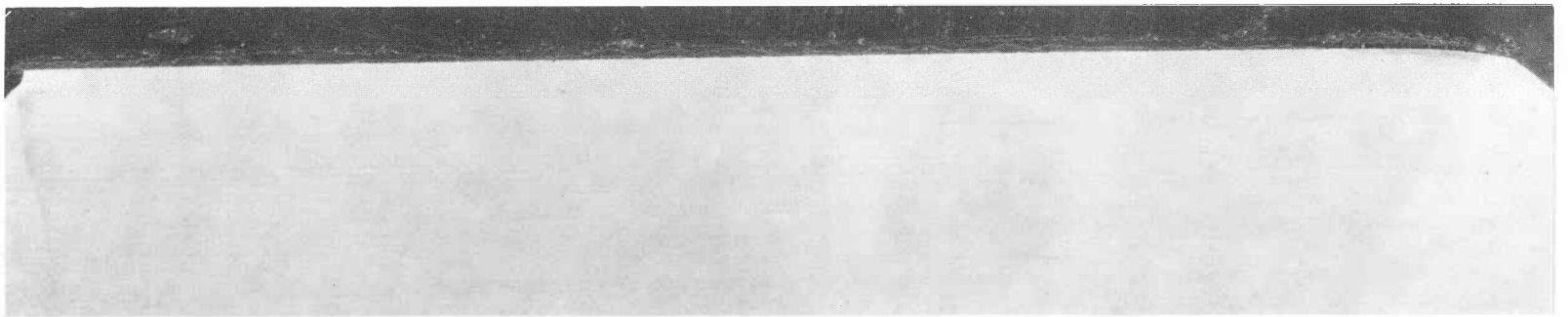

800-44: No penetration of coating (Ni-Cr on Incoloy 800) after one test.

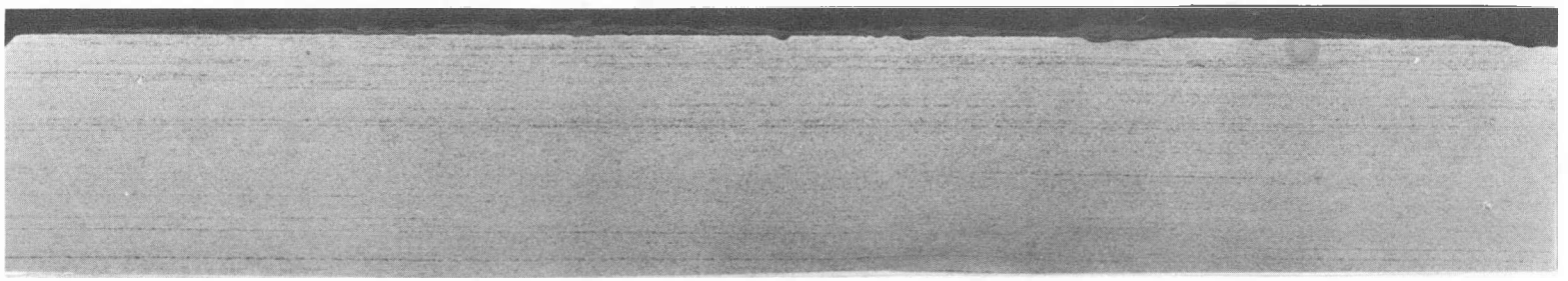

800-45: The same Ni-Cr coating developed a few pits below the coating after two cycles of testing.

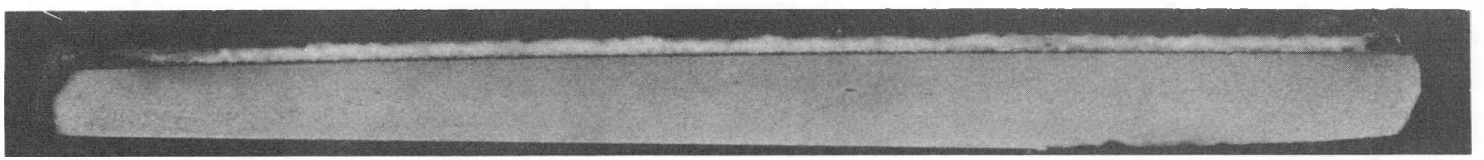

304-8: $MgZrO_3$ coating that appeared highly resistant. (Edge chipped during cutting operation.)

Figure 3.30 Transverse Macrosections of Exposed Specimens--8X

suggest that the oxide may well resist attack by the molten sulfate but that a better bond to the substrate is required. The oxide penetration at the substrate served to loosen the entire coating, as shown in Figure 3.31. It should be noted, however, that the 2-1/4%Cr-1%Mo was not pitted, nor was it visibly corroded under the coating, indicating that the loss of bond occurred after cool-down. The same result was observed on two specimens of ZrO_2 on 347SS and two of 2-1/4%Cr-1%Mo tested in different retorts. Because of a poor application technique, the coating provided good protection for one cycle only.

3.3.7 Tribaloy Coatings

The Tribaloy coatings tested (Table 3.15) had been recommended for combustion environments, but fireside corrosion resistance was not reported. The substantial buildup of nickel salts atop Tribaloy T-700 indicated that a reaction had occurred. After testing, cobalt-based Tribaloy T-800 was covered with violet cobalt salts, and the descaled surfaces retained some of the coatings, as shown in Figure 3.32. The residual coating was only slightly permeated and showed good adherence, as demonstrated in the macrosections in Figure 3.33. The base metal was protected for the first cycle, but repeated testing is required to verify whether attack will occur during repeated cycling.

3.3.8 Metallography and Analytical Results

Representative samples of the corroded, coated specimens were examined metallographically and in some cases analyzed by means of EDX and XRD techniques.

3.3.8.1 Examination of Chromized Alloy and Stainless Steels. The microstructures of all four chromized materials displayed pronounced evidence of electrochemical pitting after 48-hour exposure to simulated fireside attack. The increased chromium content at the surface was not beneficial. Figure 3.34 shows the microstructure of the post-test chromized HT-9, which was more severely pitted than untreated HT-9, in spite of over 62-percent chromium on the exposed alloy surface. Also evident in that figure is that the electrochemical-type pitting progressed through the high-chromium surface and penetrated the

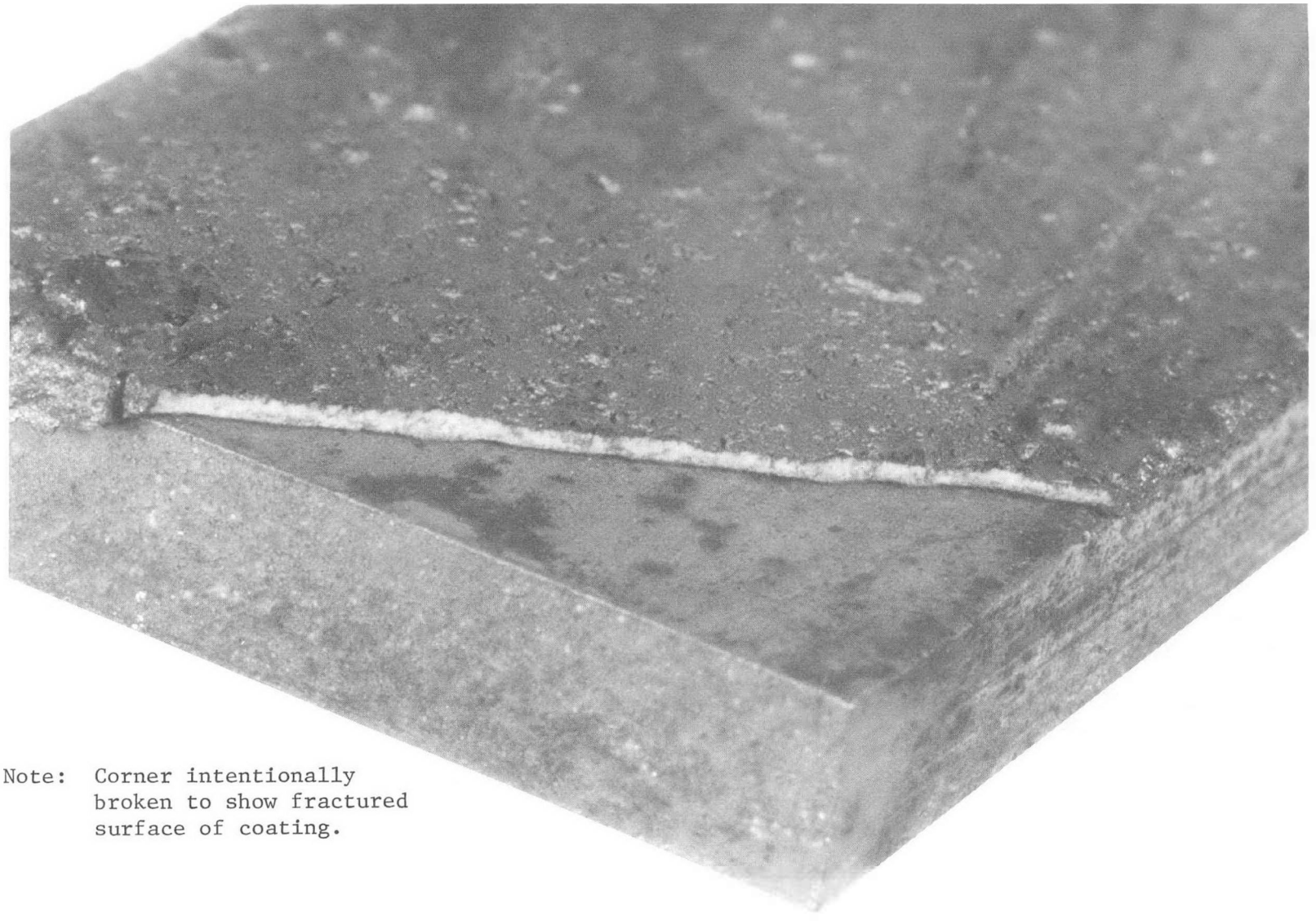

Note: Corner intentionally broken to show fractured surface of coating.

Figure 3.31 Plasma-Deposited ZrO_2 Coating--8X (Coating bond on 2-1/4%Cr-1%Mo failed on post-test cool-down. Although resistant to liquid-phase attack, coating allowed oxygen penetration to steel surface, resulting in loosening of the entire coating, but no pitting.)

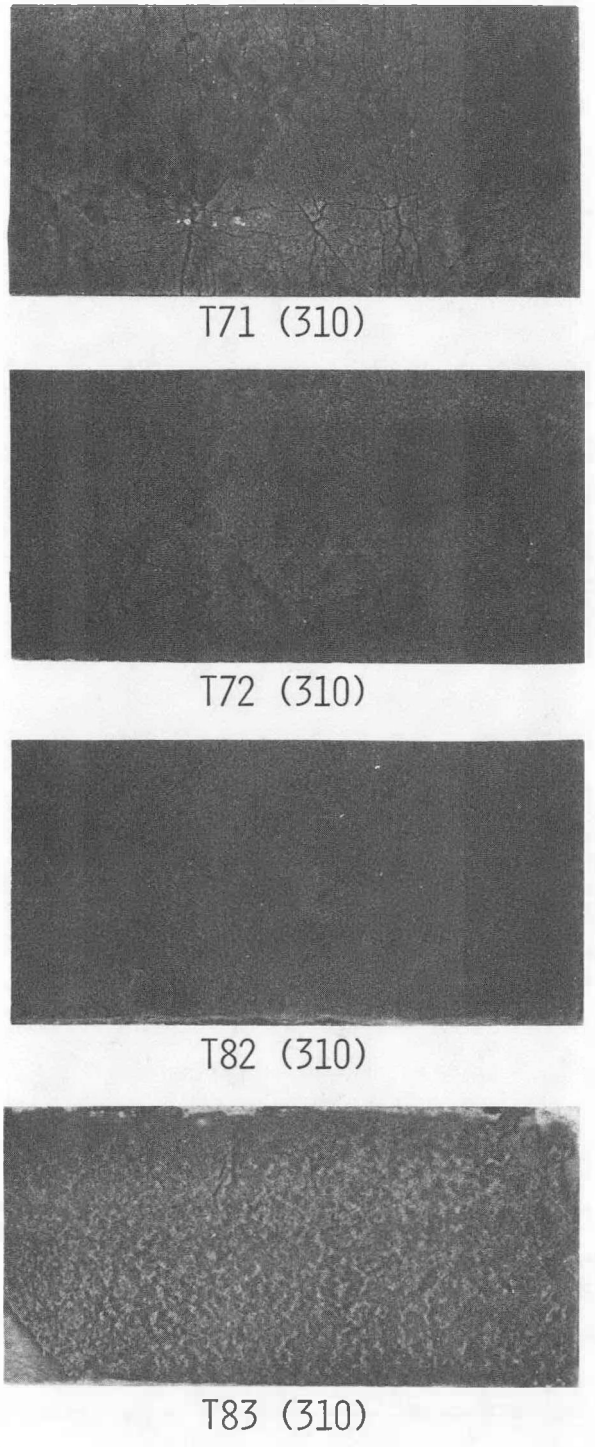

Figure 3.32 Photomacrographs of Exposed Surfaces of Tribaloy-Coated Specimens After Descaling Showing Irregular Attack and Some Cracking of the Coatings--1.5X

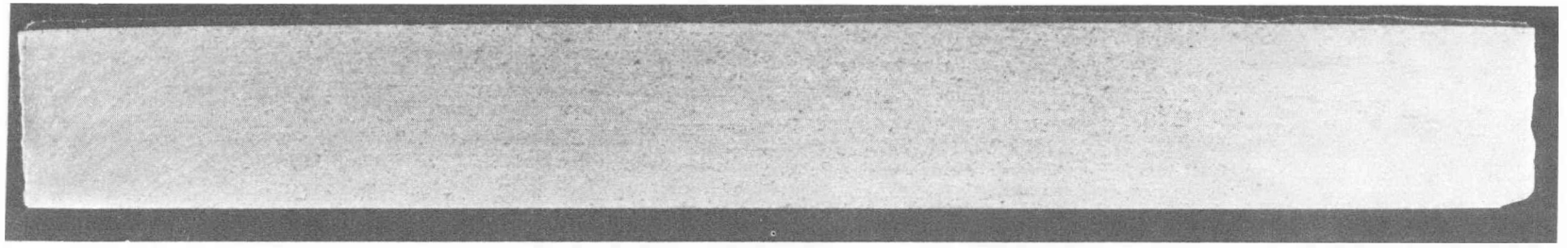

T-72: Ni-Mo-Cr-Al

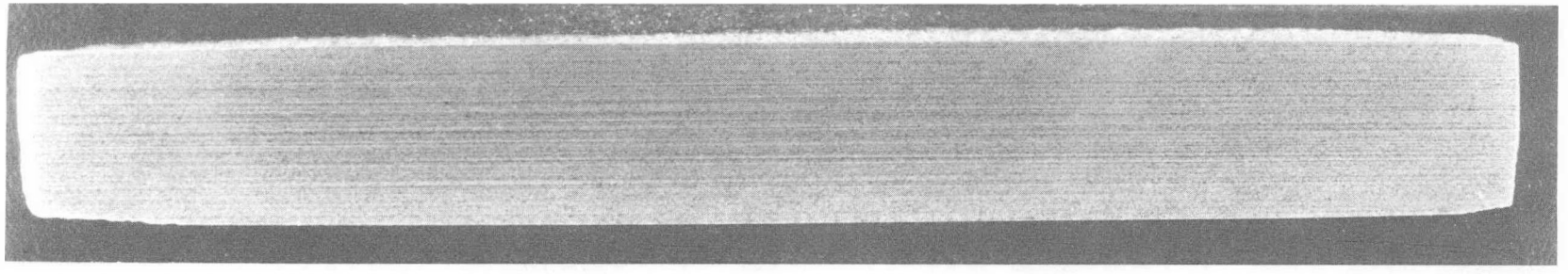

T-82: Co-Mo-Cr-Al

Figure 3.33 Transverse Macrosections of Tribaloy-Coated Specimens--8X (Neither of the heavy Tribaloy coatings appeared resistant, but they did protect the substrate for the 48-hour exposure.)

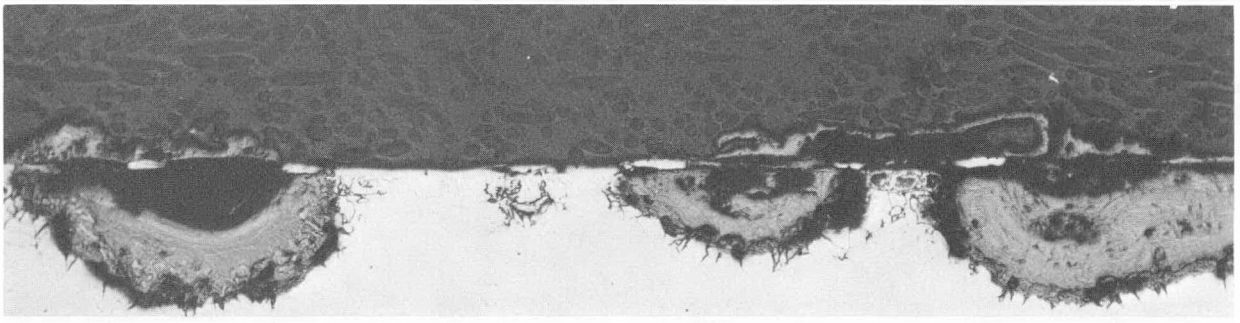

HT-9-16: Unetched.

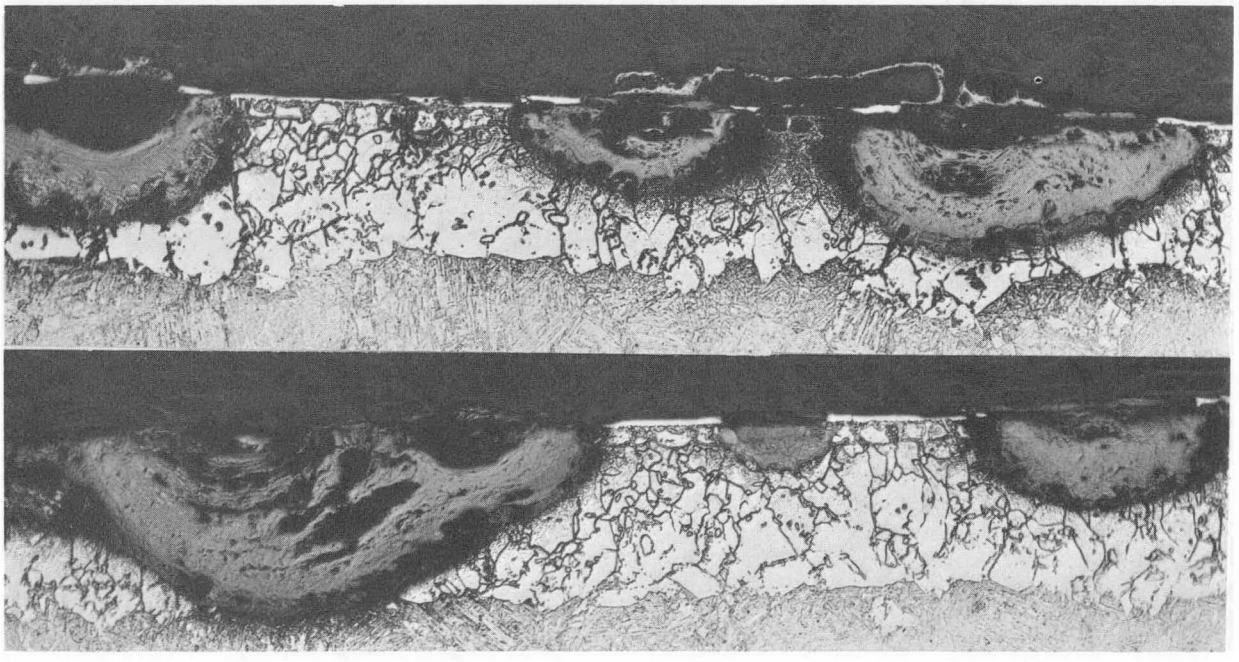

$FeCl_3$ + HCl: Chromium-diffused area revealed.

Figure 3.34 Chromized HT-9 Specimens--100X (Electrochemical pits penetrated the thin high-chromium band and progressed through the high-chromium ferritic case. Other pits continued deeply into the martensitic parent metal structure.)

ferritic phase (increased in chromium by diffusion) down to the martensitic base metal (after the rapid cool-dowm). Note that small areas of the high-chromium surface remained at the original surface and were, in some cases, undermined by the progress of pit growth. Other pits, not shown, continued deeply into the martensitic structure.

The chromized 304SS suffered accelerated electrochemical attack of the 45-percent chromium-enriched case; little of the high-chromium surface was retained. Figure 3.35 shows the typical pitting of 304SS in which the electrochemical attack appeared independent of the steel microstructure of the substrate. The grain boundary attack in 304SS was less pronounced than observed for the ferritic-martensitic HT-9. The source of the initial corrosion potentials may be the chromium gradients across the surface rather than those within the microstructure.

The chromized Nitronic 40 (21-6-9) alloy, which in Phase 1 had shown improved corrosion resistance compared with 304SS, was more severely affected after chromizing. While the 21-percent chromium in Nitronic 40 compared with the 18-percent chromium in 304SS, was assumed to be beneficial, an increase in the chromium between 40 and 45 percent by chromizing was actually degrading to fireside corrosion resistance. Figure 3.36 shows the etched microstructure after a 48-hour attack by the molten alkali-iron trisulfate at 1250°F (675°C). The measured pitting depth (listed in Table 3.15) was 0.016 in. (405 μm) or about twice the penetration depth observed for the uncoated 21-6-9 in the Phase 1 tests.

Electrochemical pitting attack was also observed in the chromized Incoloy 800, and no apparent benefit was achieved by the high-chromium-diffused surface. Figure 3.37 shows the structure of etched microsections, which also indicated the retention of a complex multilayer scale in the pitted areas. With chromized Incoloy 800, however, the area of deep pitting covered less than 10 percent of the exposed surface, while the lower alloys all suffered greater

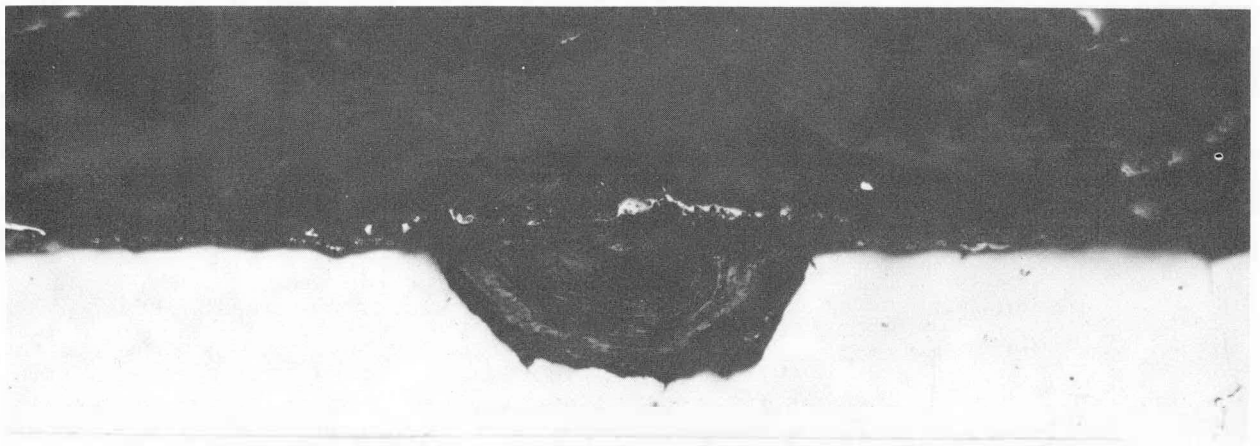

304-Cr-2: 250X. Note some remaining high-chromium fragments on the surface.

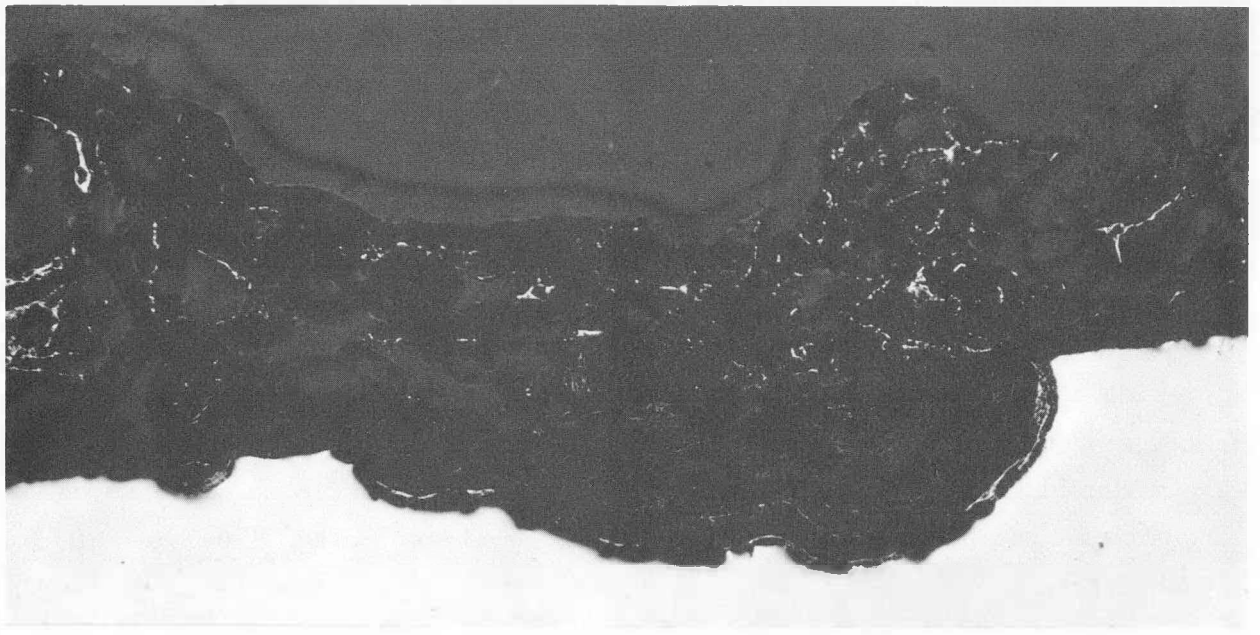

304-Cr-2: 100X. Note pit grew far beyond the high-chromium enriched area.

Figure 3.35 Chromized 304SS Showing Almost Total Loss of High-Chromium-Enriched Surface by Corrosion [Fragments of high-alloy case remain in scale formation (black).]

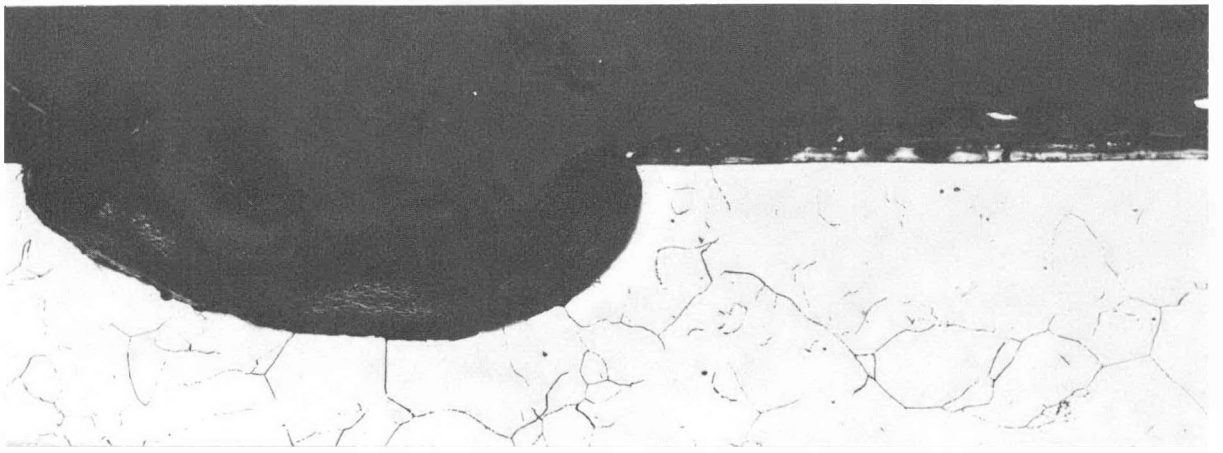

21-6-9: 100X, etched.

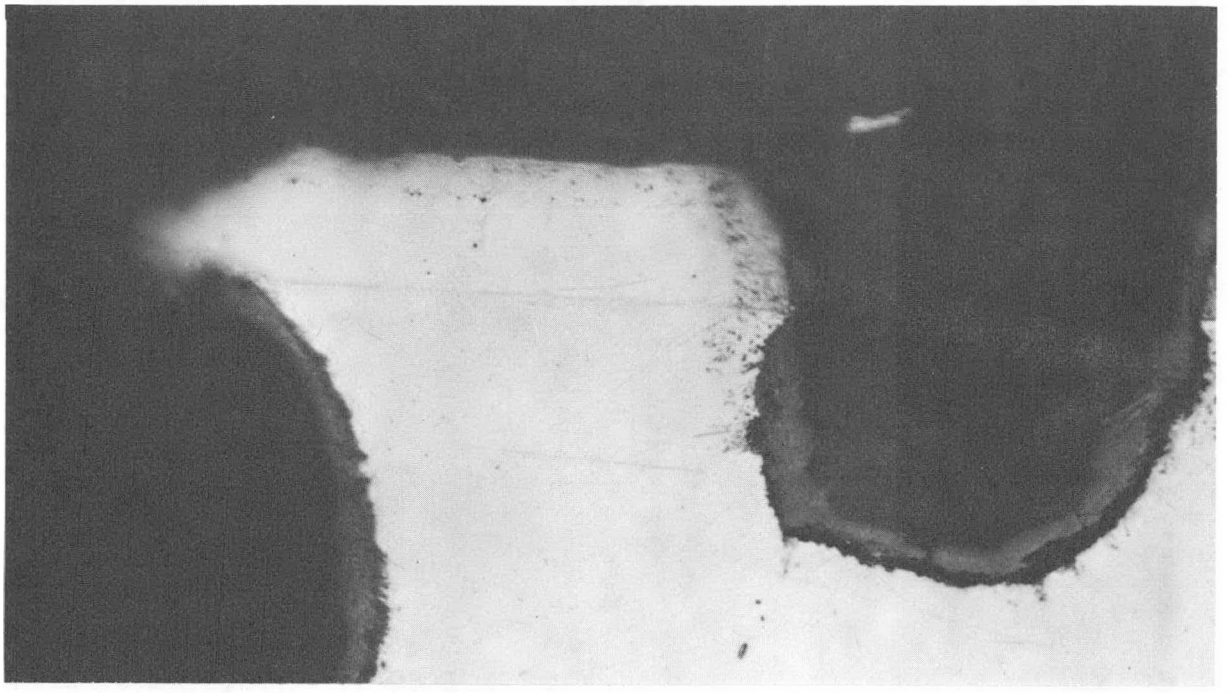

Cr-37: 500X, unetched. The anodic pit surface retained three-layer-type scale.

Figure 3.36 Chromized Nitronic 40 Showing a Thin Layer of the 40% Cr Alloy Surface Deeply Penetrated by Electrochemical Pitting

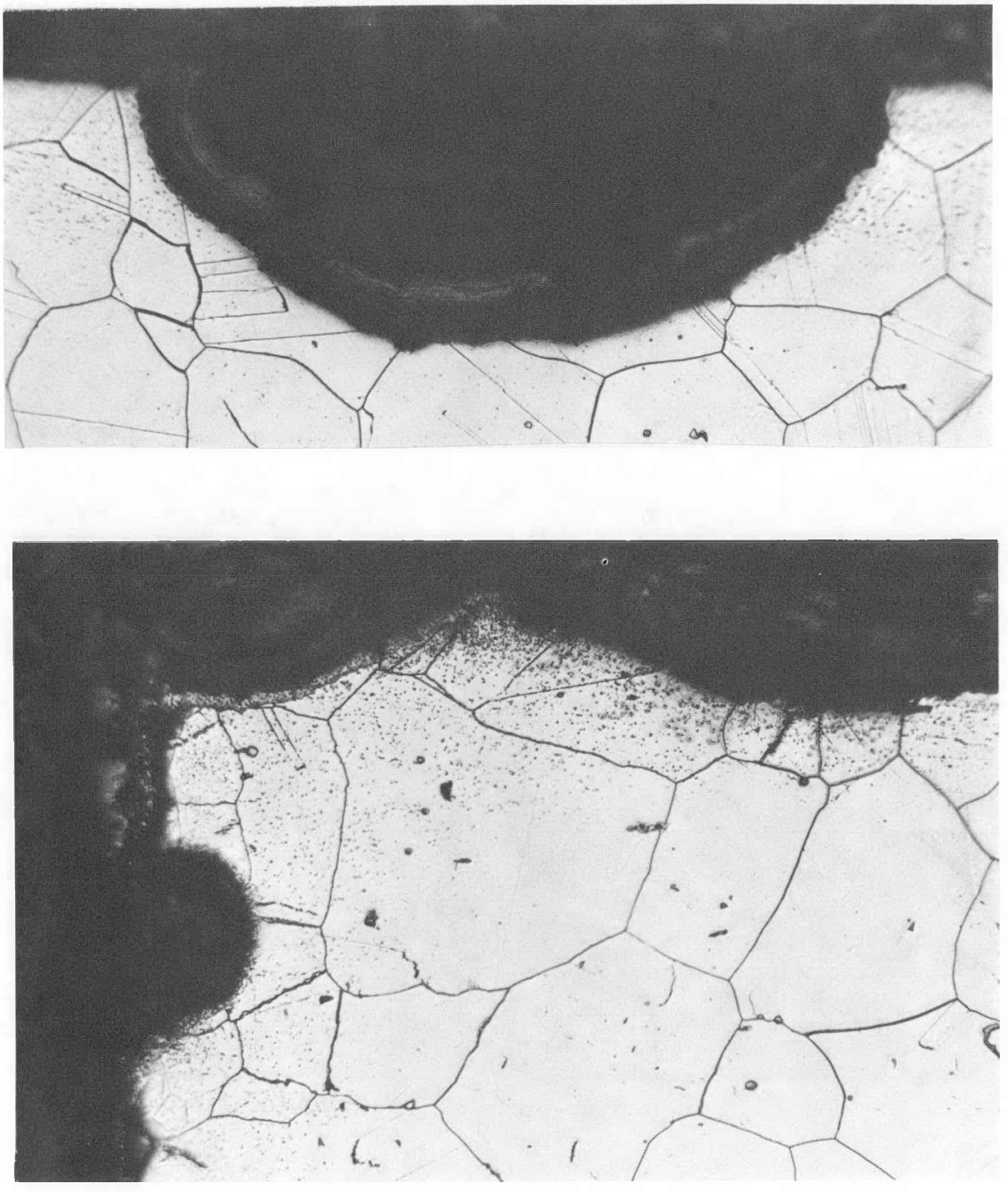

Figure 3.37 Chromized Incoloy 800 Showing Electrochemical Pitting After 48-Hour Exposure to Fireside Attack--250X, Etched (Only traces of the remaining high-chromium surface were found near the left lower corner.)

areas of surface penetration. The few specimens used in these tests illustrate the problem encountered with nonhomogenous materials, but the depth of pitting will vary with the geometry and other factors as well.

3.3.8.2 Electron Microprobe Analysis of Chromized Specimens. The additional microprobe analysis of the chromized materials before the fireside testing (Figure 3.38a) was considered necessary to ensure that the material used in these tests was a representative chromized material and not some accidental substitution. The analysis after exposure is also helpful to learn more about the changes occurring during the fireside test. The analytical profile data for unexposed chromized HT-9 are presented in Figure 3.38b, which indicates that the highly enriched chromium surface contained over 60-percent chromium to a depth of about 17 μm, dropping rapidly to between 13- and 25-percent chromium in the enriched ferritic band. The exposed chromized HT-9 was also evaluated (Figure 3.39) and showed little change except in the corrosion pit that contained oxides and sulfides.

The microprobe data for the unexposed chromized 304SS specimen demonstrated a somewhat simpler profile (Figure 3.40a). The comparable Fe-Cr profile for chromized 304SS after fireside exposure, shown in Figure 3.40b, again gave no change except at the corroded areas. The pitted areas go beyond the enriched chromium depth with no evidence that the high-chromium content would improve the resistance to pitting.

Chromized Nitronic 40 (21-6-9) was produced with a somewhat deeper case of enriched chromium (Figure 3.41). The manganese was lowered in the outer 0.0014 in. (35-40 μm) case where the chromium was enriched, but the nickel was unaffected. The profile analysis after the test is also shown in Figure 3.41. No significant benefit was observed from the deeper zone of high chromium, since the worst pitting extended to more than 0.015 in. (380 μm) deep, or nearly 10 times the depth of the high chromium. Based on the analysis (Figure 3.36), the corrosion products within the pits contained both oxides and sulfides.

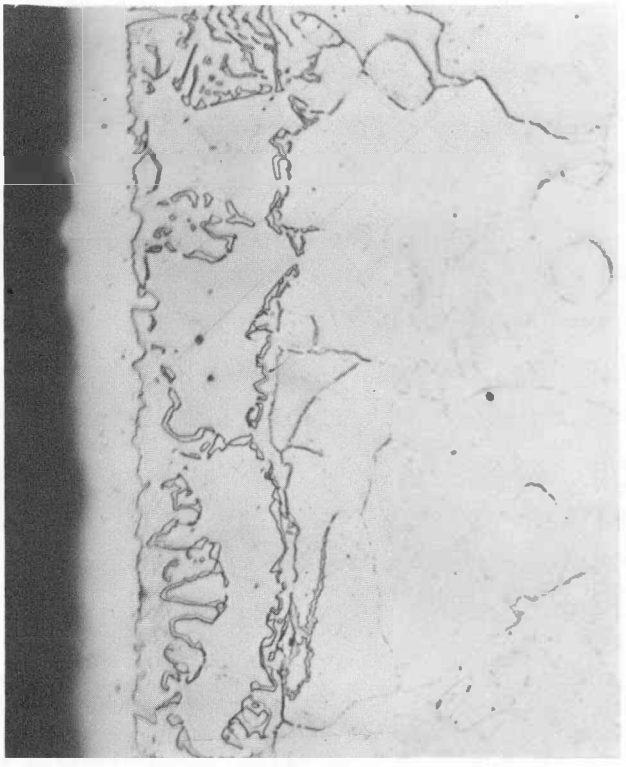

Figure 3.38a Microstructure of Chromized HT-9 Before Test--500X

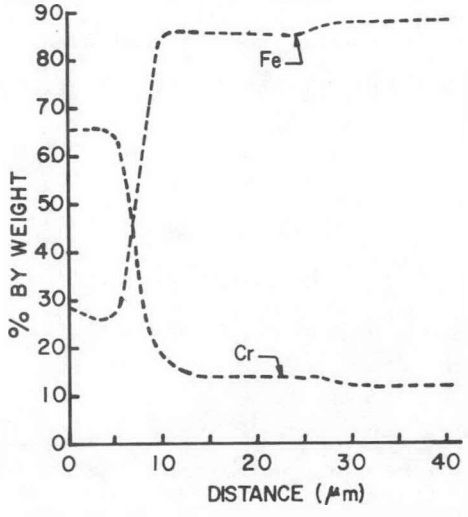

Figure 3.38b Analytical Profile of Iron and Chromium Obtained by Electron Microprobe Scan of the Chromized Alloy Steel Shown Above

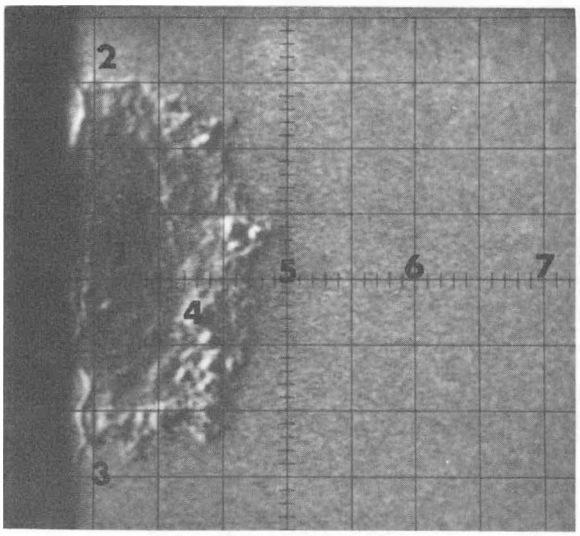

100X, exposed.

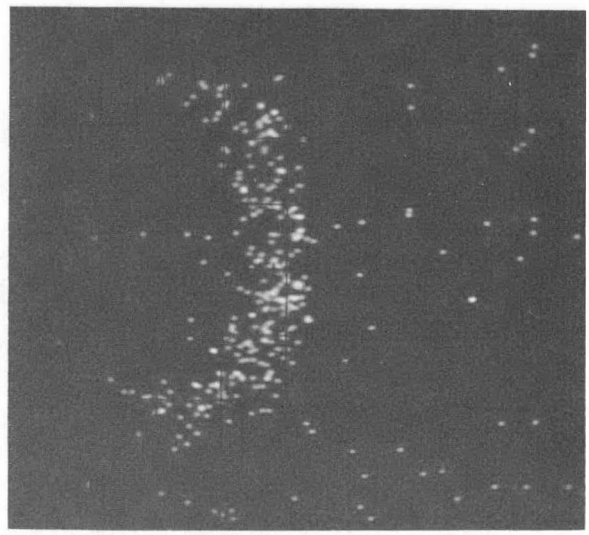

100X, exposed. Indicates sulfur dep sition in the scale.

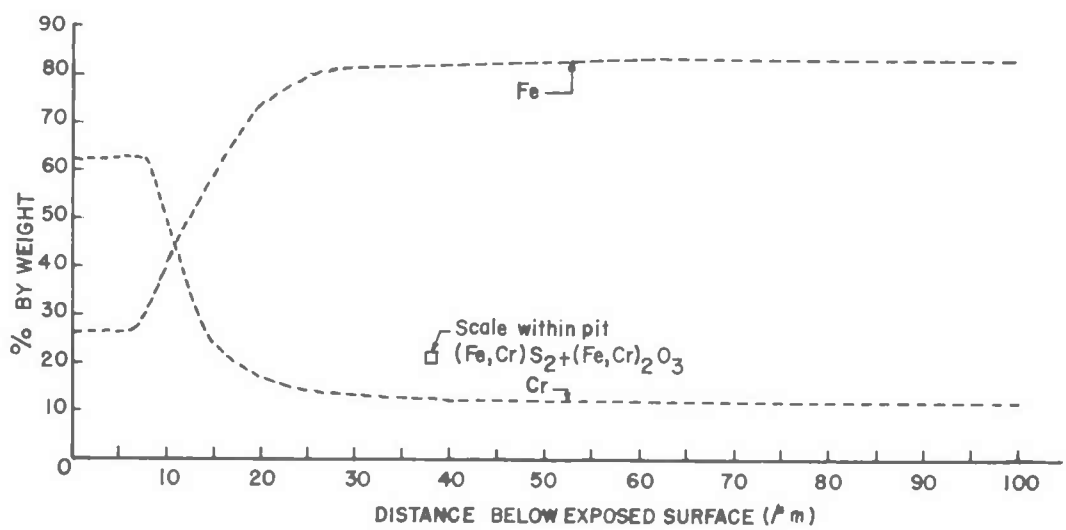

Figure 3.39 Chromized HT-9 After Exposure (Pitted area penetrates deeply below the chromium-enriched core. Sulfides and oxides found within the crater.)

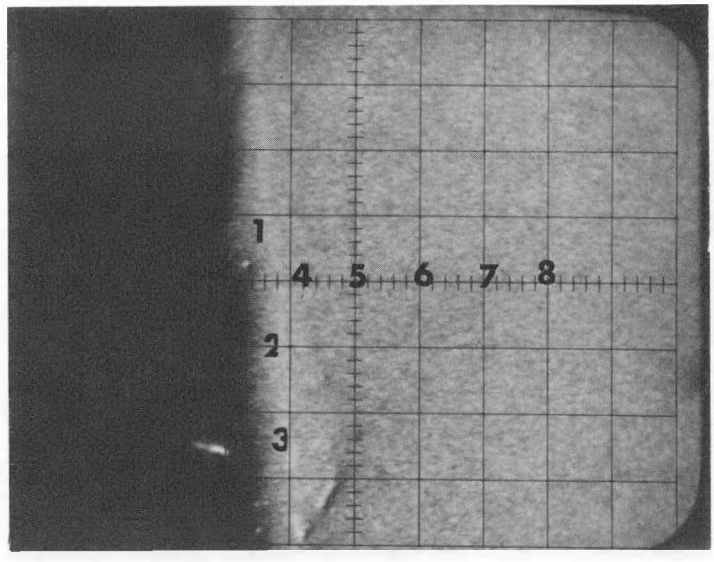

Figure 3.40a Microprobe of Unexposed Chromized 304SS Specimen Indicating High-Chromium Surface

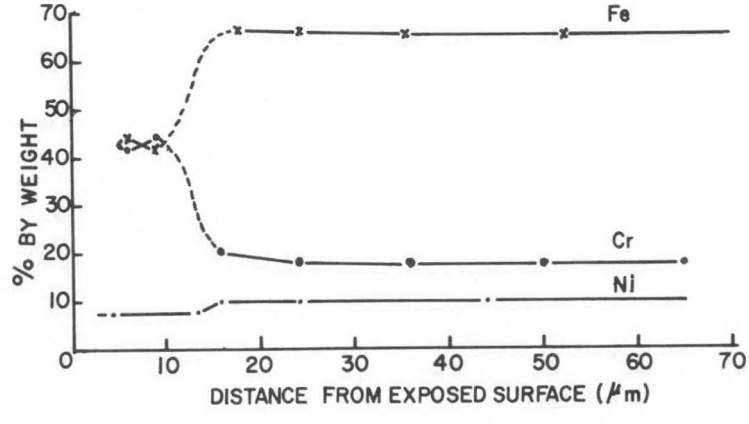

Figure 3.40b Chromized 304SS Before Exposure (Only pitted areas were changed after exposure.)

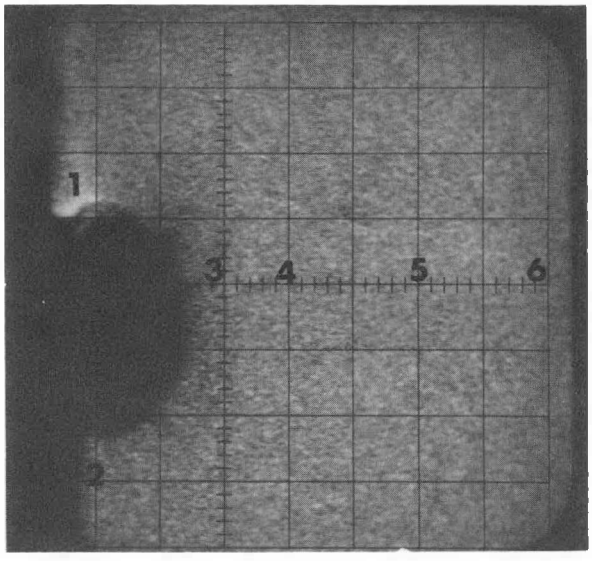

100X, exposed.

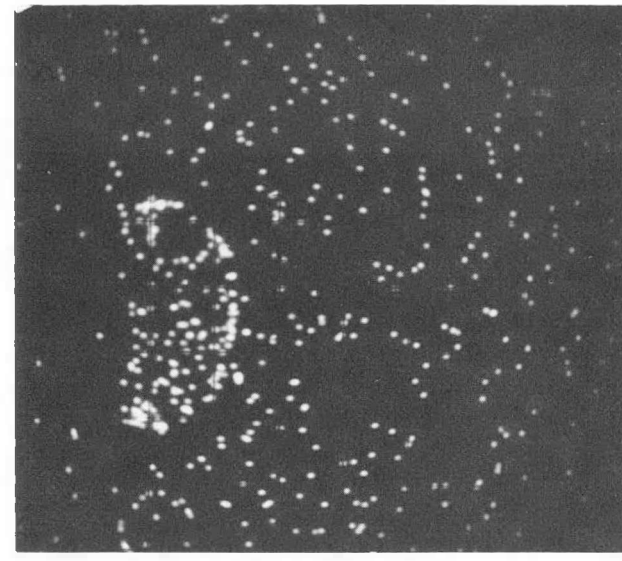

100X, exposed. Indicates sulfur deposition in the scale.

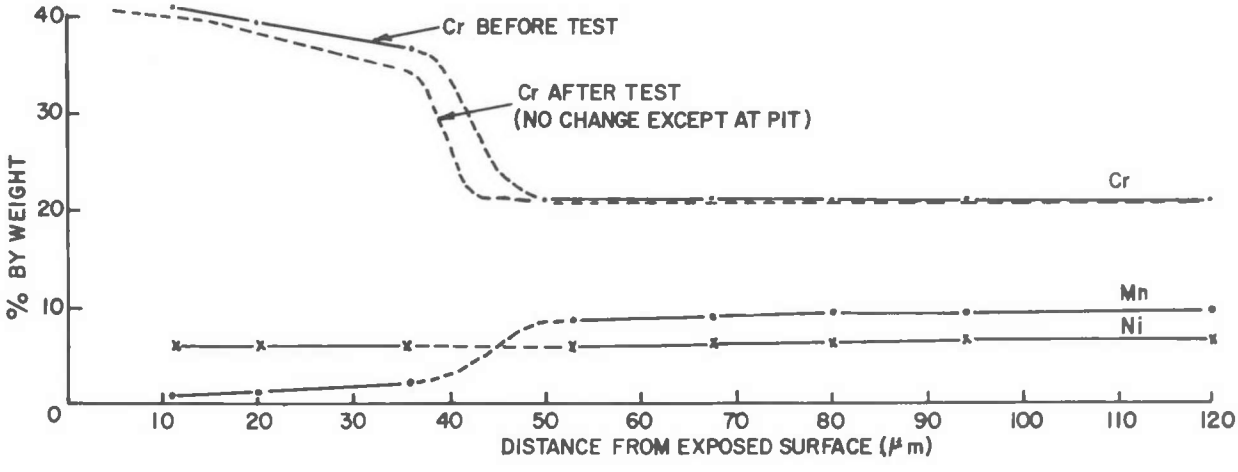

Figure 3.41 Chromized 21-6-9 Before and After Exposure (No significant change except for loss at pits. Note sulfides in pit corrosion products.)

The electron microprobe analysis for the chromized Incoloy 800 after exposure is shown in Figure 3.42. The post-test changes observed in the analysis show that the high-chromium layer was largely converted to oxides, such as Cr_2O_3, but isolated sulfides distributed throughout the scaled surface were also evident. It is interesting to note that the highest sulfide concentration was in the area of the original surface within the corrosion-produced scale. Thus we can conclude that high-chromium compositions form sulfides as easily as low-chromium alloys.

3.3.8.3 Examination of Alonized Specimens. The "Alonized" diffused-aluminum-surface alloys produced by the Alon process were evaluated as coatings on 304SS and Incoloy 800. Both aluminum-diffusion treated materials appeared to be more resistant to the deep pitting common to most other materials. Alonized 304SS suffered some loss* of the outer high-aluminum phase, but the gray-etching diffused layer of precipitated intermetallic compounds remained intact, as shown in Figure 3.43. The diffused aluminum surface apparently limited the attack--at least the Alonized 304SS specimen was not subjected to aggressive electrochemical pitting while the high-aluminum phase was present.

A similar behavior was noted for Alonized Incoloy 800. The metallographic examination of the exposed Incoloy 800 showed that the outer high-aluminum phase suffered some surface loss but that the intermetallic precipitate band was not penetrated (Figure 3.44). The inner diffused layer was also mechanically sound and essentially unaltered by the exposure. Effects of fireside exposure on the Alonized samples were checked by electron microprobe analysis to determine changes in the alloy profiles. The results indicate good stability of the surface alloy and no internal attack (Figures 3.45 and 3.46).

*Some loss of the outer layer occurred during chemical descaling after the test.

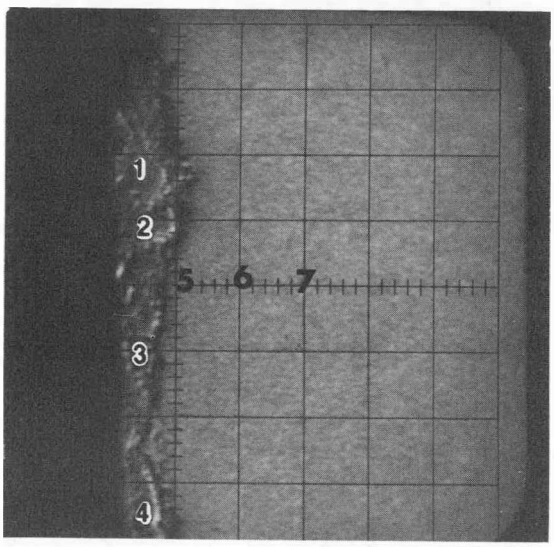

500X, exposed.

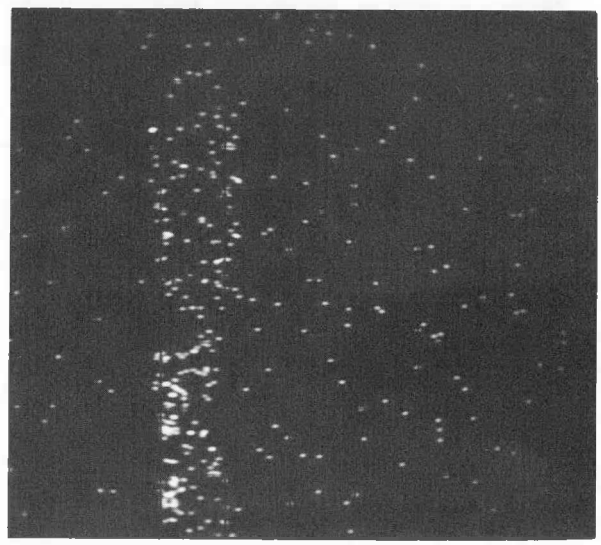

500X, exposed. Indicates sulfur deposition in the scale.

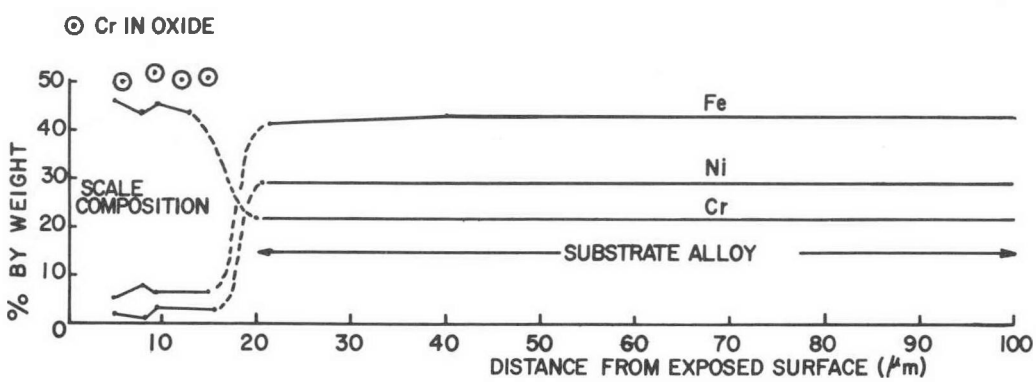

Figure 3.42 Chromized Incoloy 800 After Exposure (Adherent Cr_2O_3-type scale containing sulfur was observed as were other metals in minor amounts. Unpitted surface areas appeared unchanged from the original chromized microstructure.)

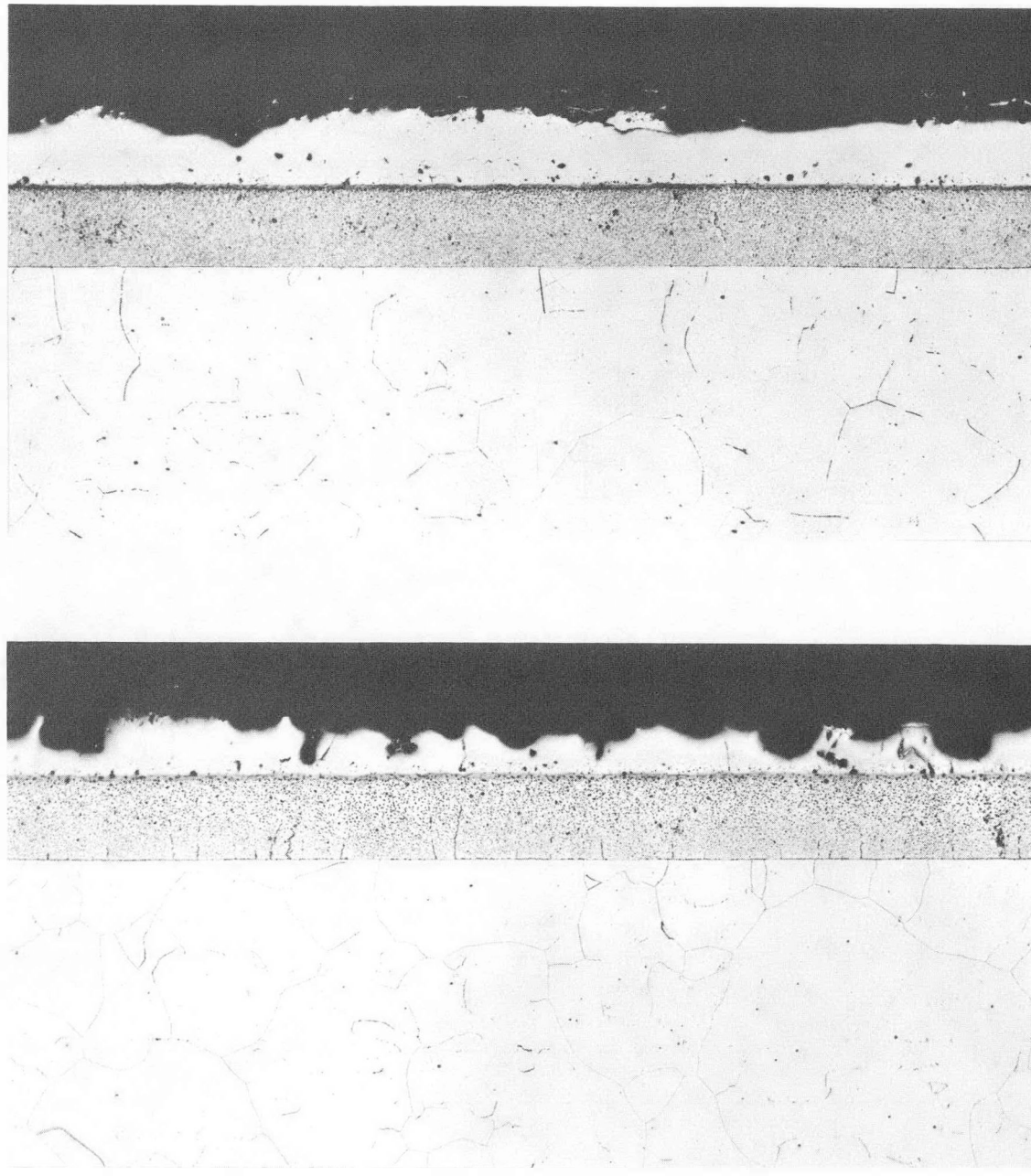

Figure 3.43 Alonized 304SS Before (Top) and After (Bottom) Exposure Showing Some Loss of the Outer Surface but Reduced Pitting--100X (Some of the outer coating was lost in the chemical descaling.)

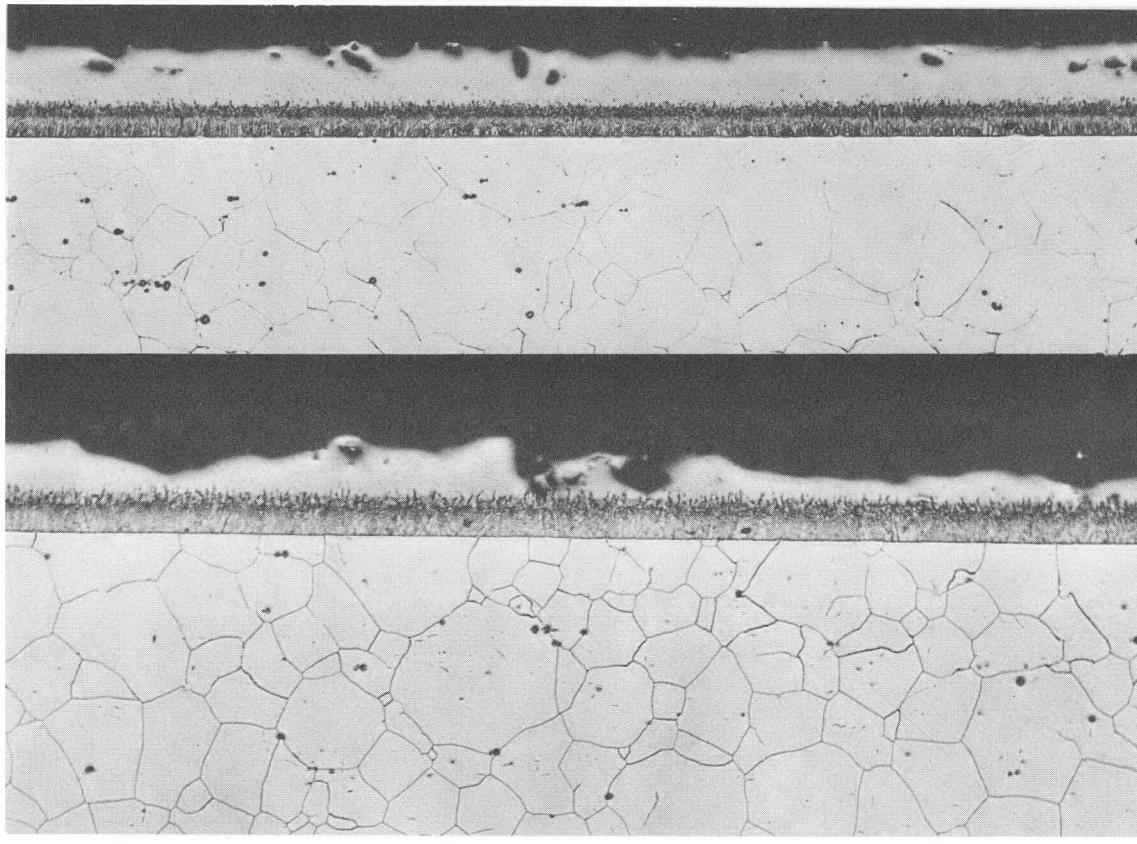

Figure 3.44 Microsection of Alonized Incoloy 800 Before (Top) and After (Bottom) Exposure--100X [Resistance to fireside attack suggests cathodic protection provided by the high-aluminum phase(s). Some of the outer coating layer was lost upon cutting and some may have been removed by the acid descaling treatment after fireside exposure. No penetration of the intermetallic layer (gray phase) was found.]

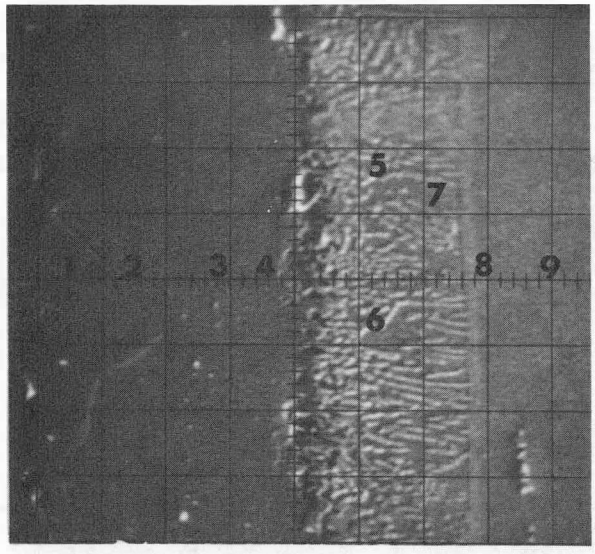

500X, exposed.

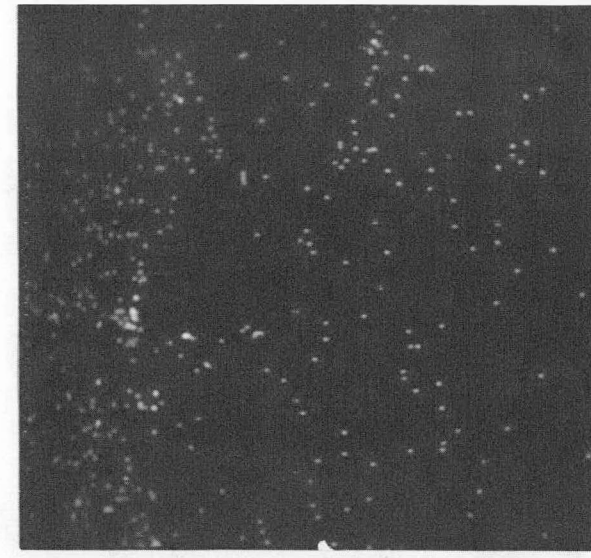

500X, exposed. Indicates sulfur deposition in the scale.

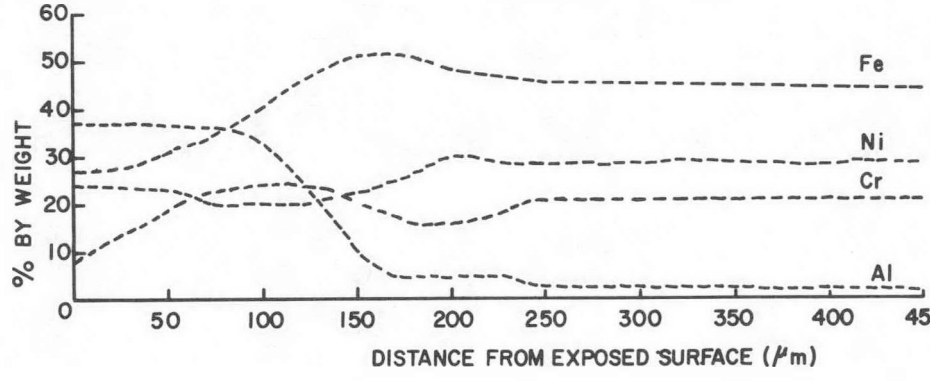

Figure 3.45 Alonized Incoloy 800 After Exposure (Analysis profile shows no significant changes other than some surface recession and a very low level of sulfides in the corrosion deposits.)

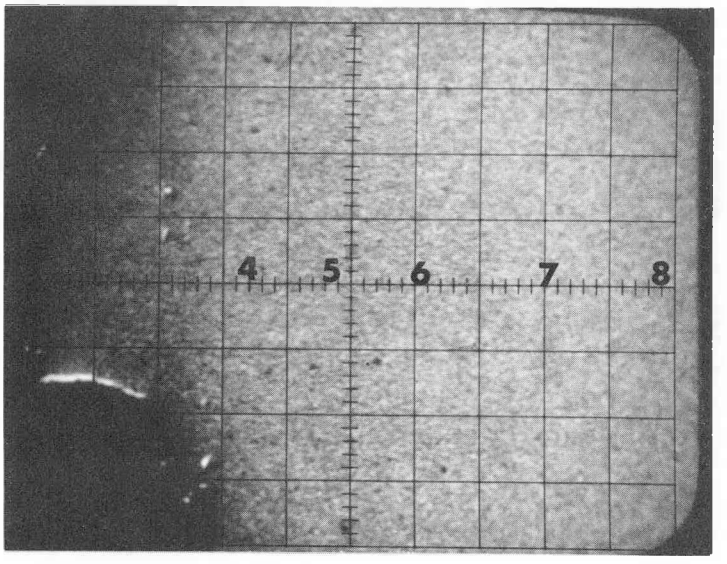

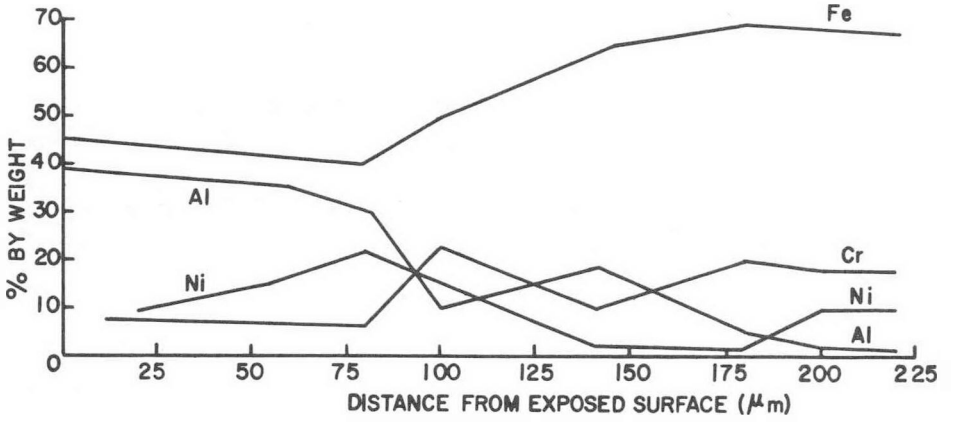

Figure 3.46 Alonized 304SS After Exposure--300X (Analysis profiles were obtained by microprobe. No sulfides were observed.)

An additional test was performed to determine whether the Alonzied surface on stainless steel would provide it with some cathodic protection. The aluminized coating was ground down at one end to expose a strip of the substrate prior to the fireside test. The limited attack on the exposed material contrasted with the test results of the Ni-Cr-based coatings in which exposed edges led to metal loss, undermining the edge of the coating. The lack of resistance of Al_2O_3 to the sulfate may also limit the life of surface films.

While the diffused-aluminum surface is apparently a step forward, this material must be tested for several cycles (without chemical descaling) to obtain a better assessment of the service life of Alonized alloys.

3.3.8.4 Evaluation of Siliconized Specimens. A metallographic examination of the siliconized specimens was conducted to determine the effectiveness of silicon surface enrichment. The samples retained little, if any, of the silicon-enriched surface--the thin layers of increased silicon were corroded away. The only significant improvement was observed for 2-1/4%Cr-1%Mo steel, which did not suffer any significant pitting but only general corrosion. Alloy 13 (from Phase 2) was siliconized to see whether the 4-percent aluminum in the alloy plus silicon would produce a protective scale. Unfortunately, the siliconizing treatment produced only a thin film (2 to 4 μm) of siliconized surface, which was helpful but did not sufficiently stabilize the surface scale for long-life service. The depth of pitting for siliconized Alloy 13 was 0.003 in. (76 μm), compared with about 0.008 to 0.010 in. (203 to 254 μm) obtained for the as-polished material in Phase 2 (Task 1.4.4).

3.3.8.5 Examination of Plasma-Deposited and Metallized Iron-Based Coatings. Evaluation of the Fe-Cr-Al coatings produced from elemental powders indicated that they were a promising class of materials; but because of their complex, heterogeneous microstructure, we decided to evaluate a more controllable coating composition, such as prealloyed Kanthal. The preliminary tests of the elemental Fe-Cr-Al coatings produced the microstructures shown in Figure 3.47.

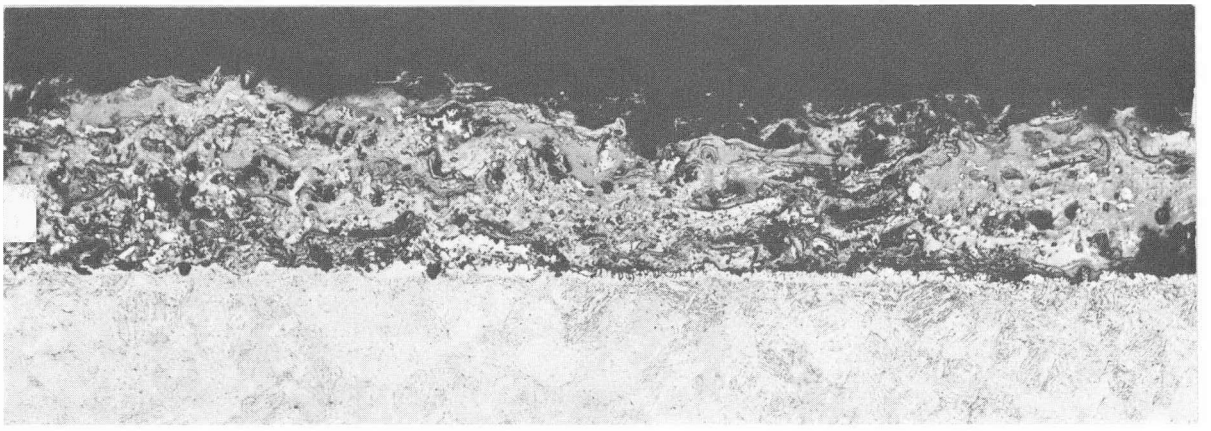

100X

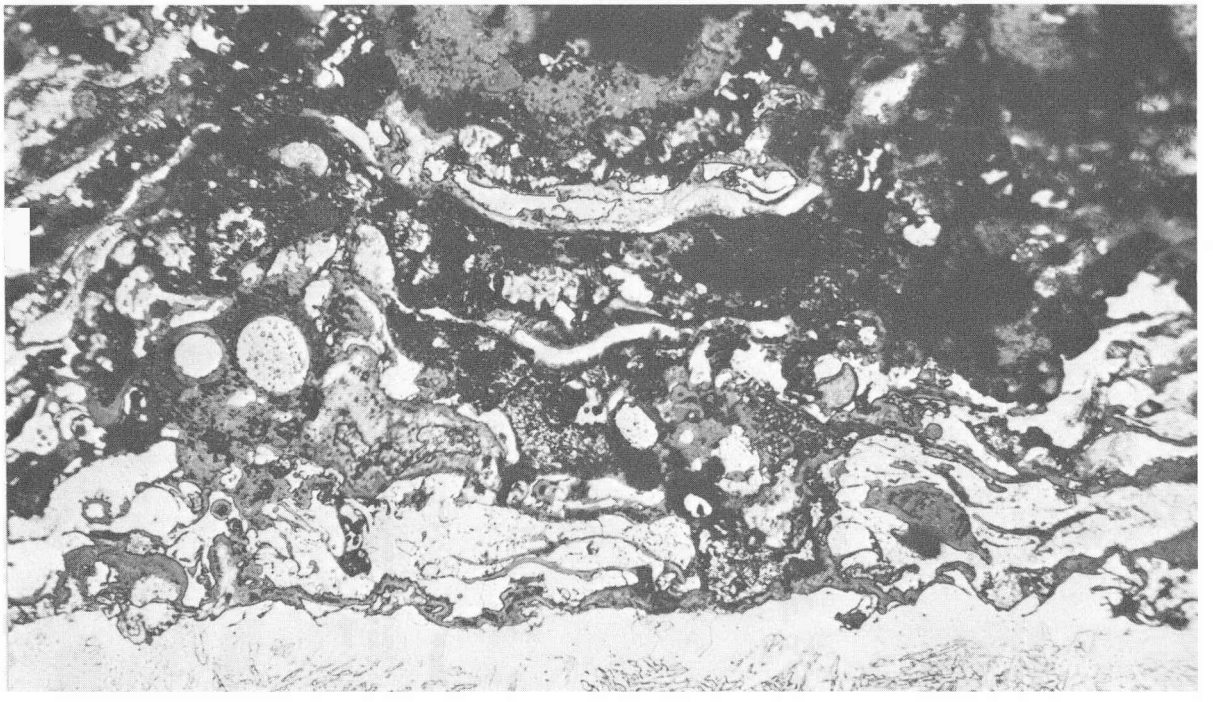

500X

Figure 3.47 Fe-Cr-Al Coating on HT-9 (This exposed coating from elemental powders was apparently resistant to the fireside attack. Some corrosion products were found within the pores such as the black and gray area at the right near the center of the coating. No cracks or separations were produced in the test.)

The Kanthal-coated specimens displayed good stability and were not subject to serious internal attack, as indicated in Figure 3.48. Some refinements of the metallizing technique, or the use of a plasma spray deposition, is suggested from these initial tests. The coating supplied was too thin [0.002 in. (51 μm) minimum] and somewhat porous, but it did bond well to the stainless steel substrate. Probably a heavier application and a suitably impregnated sealer would be a candidate for a long-life protective system.

The survey of available coating systems compatible with the fireside environment introduced several materials that offer greater chemical resistance than the alloy coatings listed; one of these is chromium disilicide ($CrSi_2$). Application of this material over the Kanthal coating was labelled as a "duplex" coating system.

The test behavior of the duplex coating was very good, but the group of specimens obtained was more porous than desirable; however, a low-porosity silicide coating can be achieved. Typical microstructures of the duplex coatings after testing are shown in Figure 3.49. Some internal corrosion resulting from porosity was visible, but the substrate was not pitted. The silicide phase was not altered based on the microstructure and on the electron microprobe analysis; however, some corrosion products were seen in pores of the Kanthal (Figure 3.50). Additional tests may indicate whether the filled pores will be able to terminate the corrosion attack.

The microstructure of the directly applied $CrSi_2$ coating clearly exhibits the weakness of a porous coating in permitting access by the molten salt (Figure 3.51). Where porosity is excessive, it is evident that, in time, the corrosion process will undermine large areas, presumably leading to coating loss. Sealing pores by means of a fused $CrSi_2$ coating or by means of surface impregnation is feasible, but such techniques were beyond the scope of this survey.

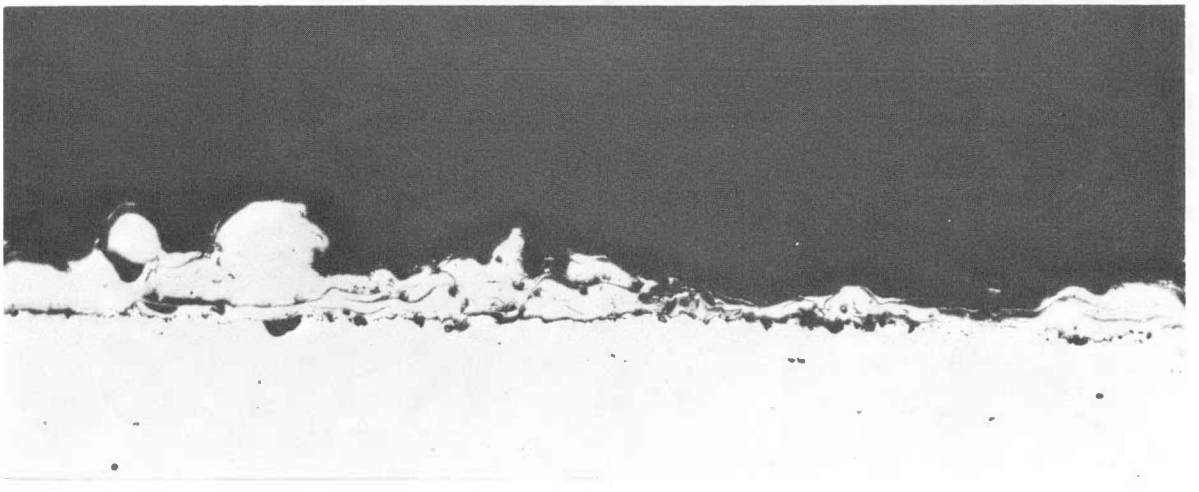

100X

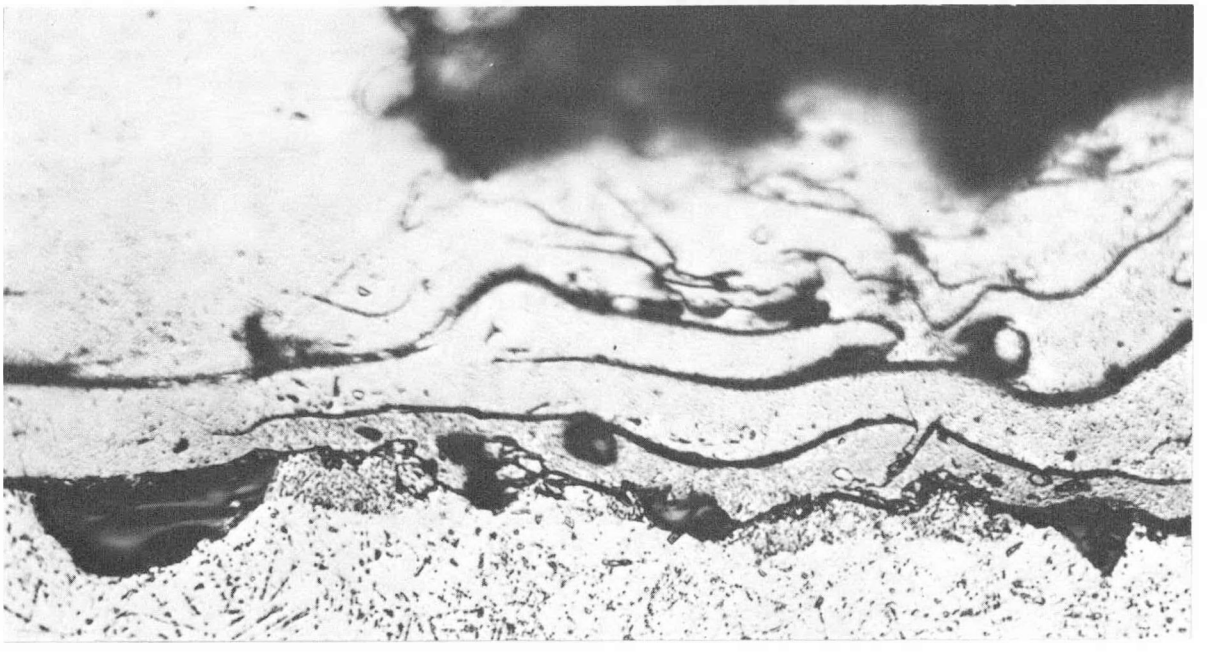

500X

Figure 3.48 Metallized Kanthal Coating on 309SS (Microstructure of Kanthal coating after exposure indicated very little change other than some loss from the surface, which was too irregular for accurate measurement. However, substrate attack caused by porosity was observed.)

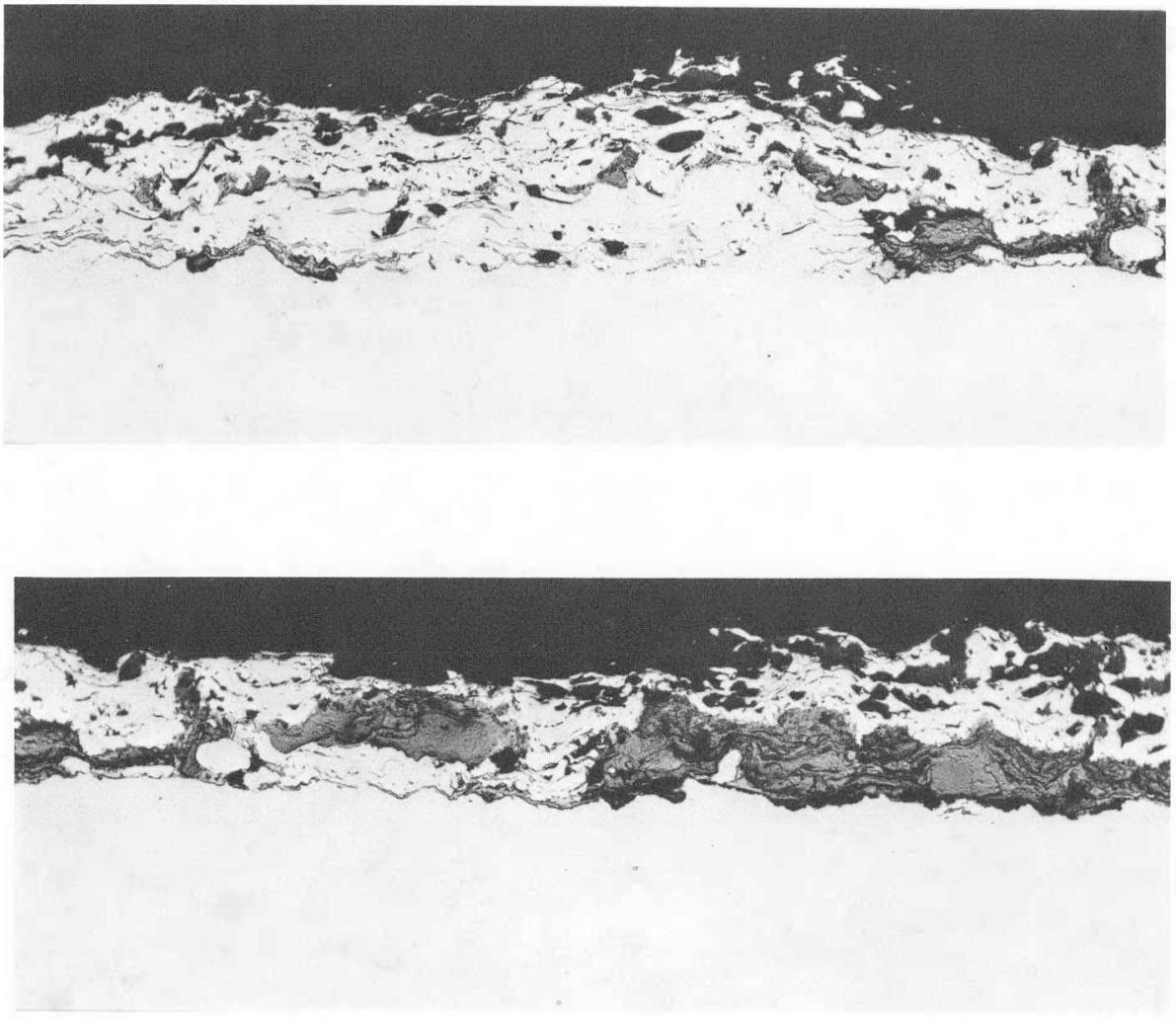

Figure 3.49 Duplex Coating ($CrSi_2$ over Kanthal) on 347SS--100X (Structure of specimens after exposure show good retention of the coating and very limited internal attack. The lower view shows the most affected location of several specimens.)

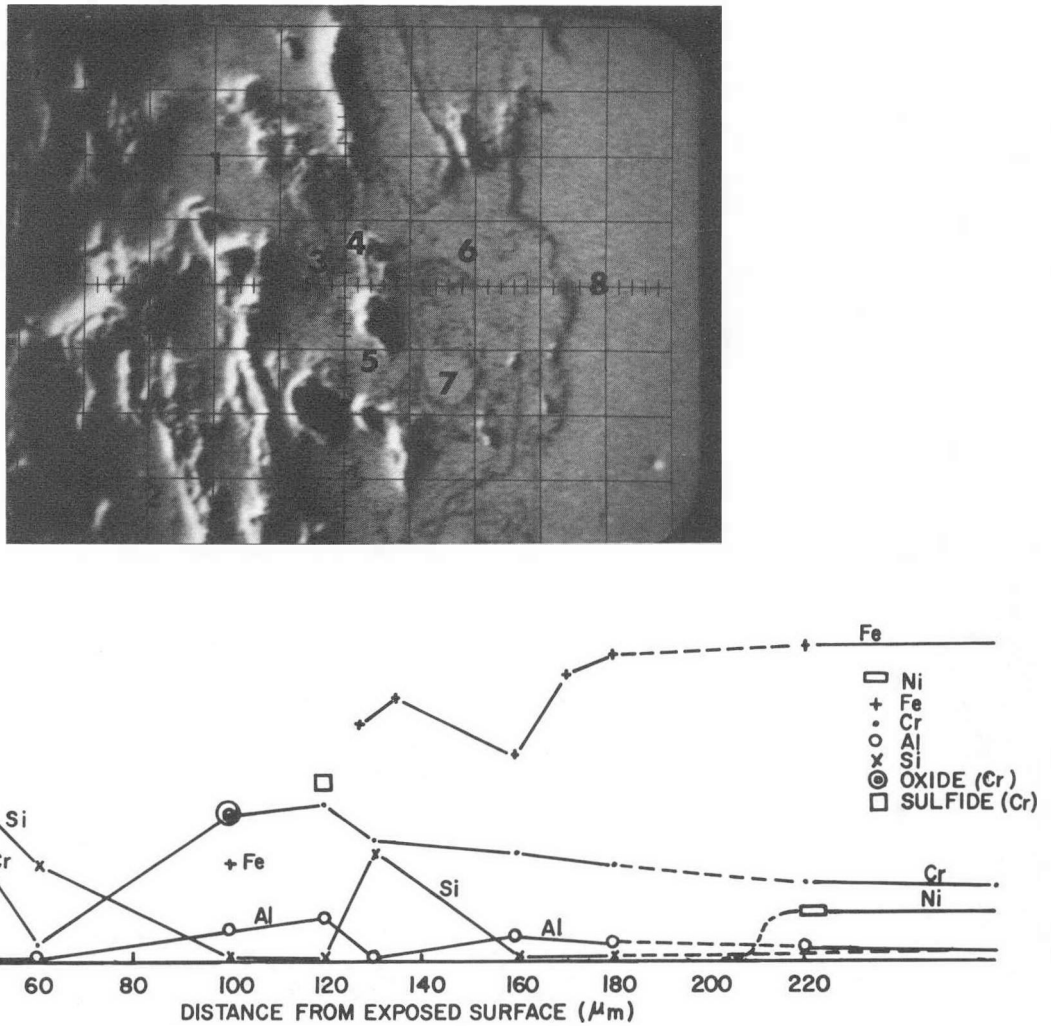

Figure 3.50 Microprobe Analysis Profile of Exposed Duplex Coating--330X (Isolated corrosion products are shown within the pores in the Kanthal. Otherwise, there is little change.)

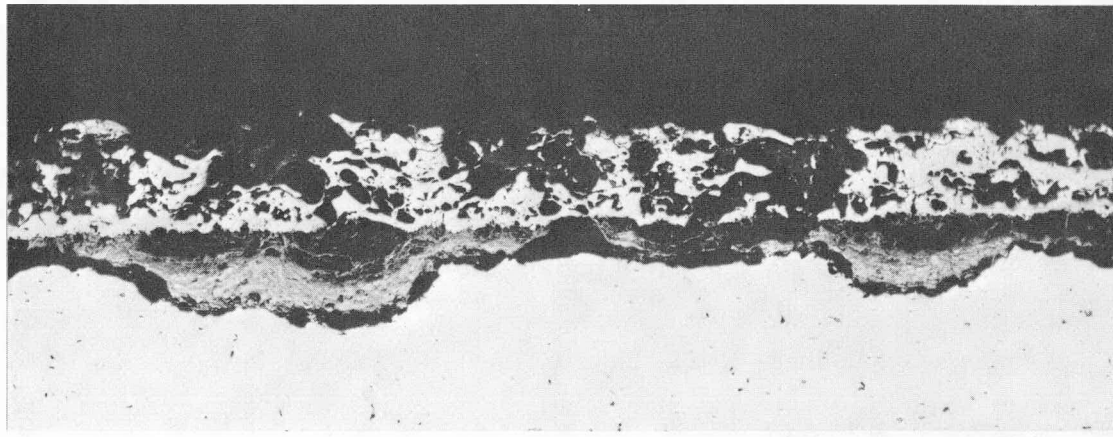

100X

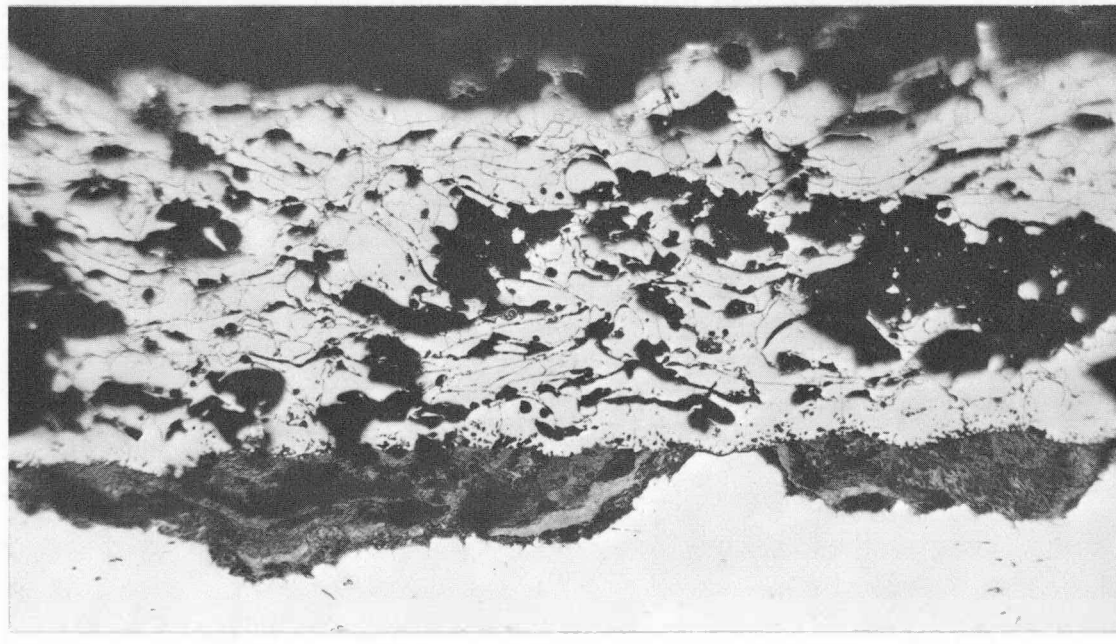

250X

Figure 3.51 Microsections of Plasma-Deposited $CrSi_2$ Coating (Coating was resistant to fireside attack but allowed some molten trisulfate corrodent to penetrate the pores and attack the stainless steel substrate.)

3.3.8.6 Examination of Plasma-Deposited Ni-Cr Based Coatings. Initial tests of the Ni-Cr-Al coatings based on mixtures of elemental powders indicated that these coatings were well-bonded but had some of the same problems of heterogeneity as the Fe-Cr-Al coatings. (Compare Figure 3.52 with Figure 3.48). In addition, there was more pronounced internal oxidation during exposure, so further effort was directed toward prealloyed powder-type coatings.

The microstructures of the exposed Ni-Cr coatings using plasma deposition of prealloyed IN-671 powder are shown in Figure 3.53. The IN-671 coating in the top view was undermined at the edge, indicating that Incoloy 800 was anodic to the coating and thus limited the attack on the coating at the expense of the substrate--an undesirable combination. The gray phase and oxide content in the exposed coating was increased substantially, as indicated by the microprobe analysis shown in Figure 3.54. Results of the second test exposure are shown in the lower view in Figure 3.53. The progressive loss of the coating by corrosion allowed serious pitting of the substrate.

The microstructure of the Ni-Cr-Si coating was examined to evaluate the effect of silicon added to IN-671. The coating obtained by adding 5 percent silicon to the IN-671 powder prior to plasma spray displayed small areas of improved stability and other areas of rapid deterioration, suggesting that although the silicon was not well blended, it may have been beneficial in areas of enrichment above some minimum value. The microstructures shown in Figure 3.55 illustrate the variable composition, which may be a problem because of insufficient silicon or else simply inadequate quality-control methods. Some of the specimens suffered a smaller loss than others; however, all had some internal attack at porous areas.

The 45%Ni-45%Cr-5%Al-5%Si coating listed in Table 3.15, given a preliminary test, exhibited the same problem of nonhomogeneity that accelerates internal corrosion and oxidation. Since the Ni-Cr-Al-Si coating exhibited no advantage over the Fe-Cr-Al or Ni-based coatings, no further tests were attempted.

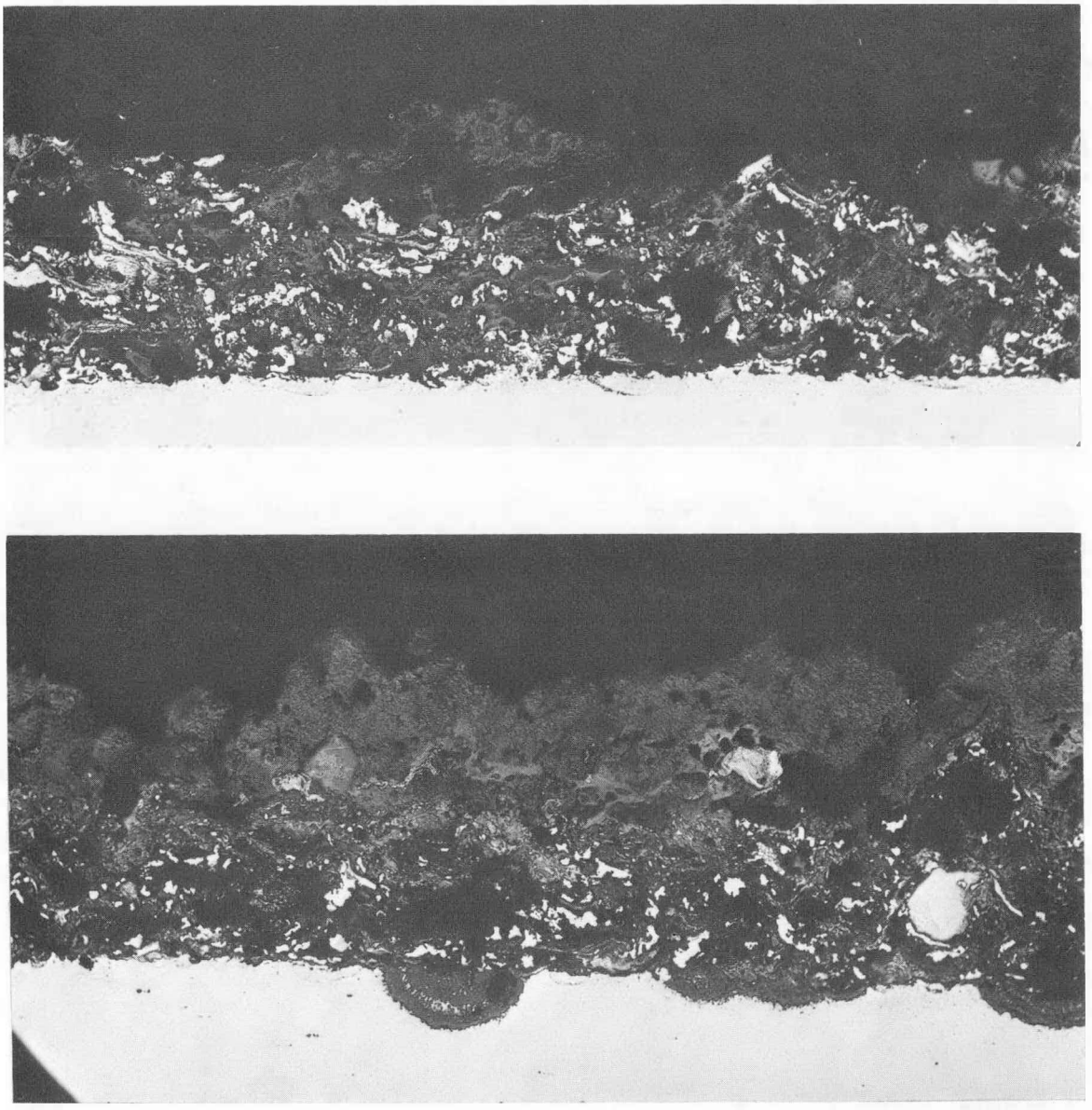

Figure 3.52 Microstructures of Ni-Cr-Al Coated 347SS--100X [The first exposure (top) displayed good protection of the substrate. The second exposure (bottom), however, showed extensive internal oxidation of coating and attack at the substrate pit.]

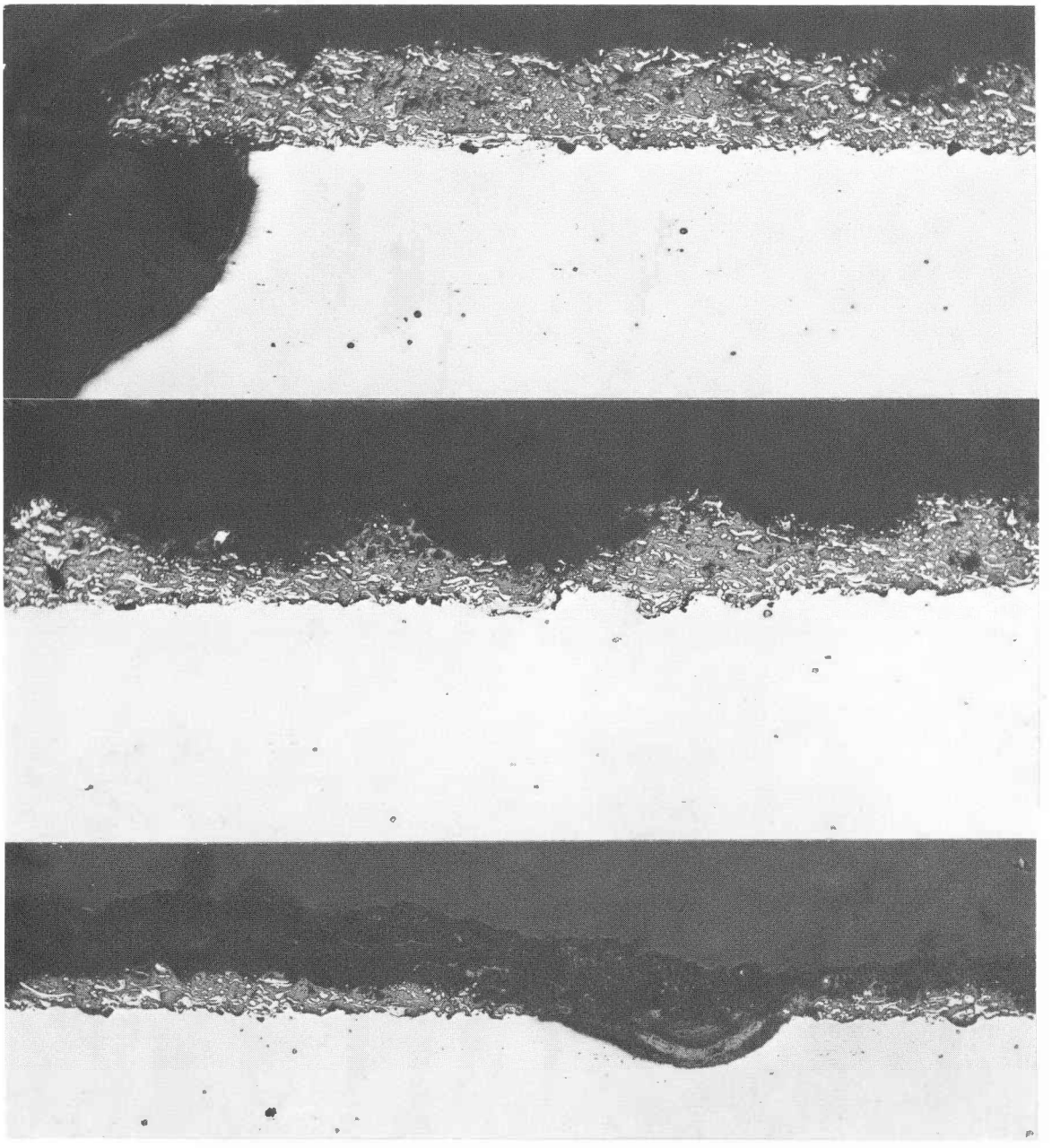

Figure 3.53 Plasma-Deposited IN-671 on Incoloy 800 Showing Several Corrosion Effects--100X [Edge attack (top two views) suggests that the substrate was anodic to the coating. Failure of coating during second exposure is shown in bottom view.]

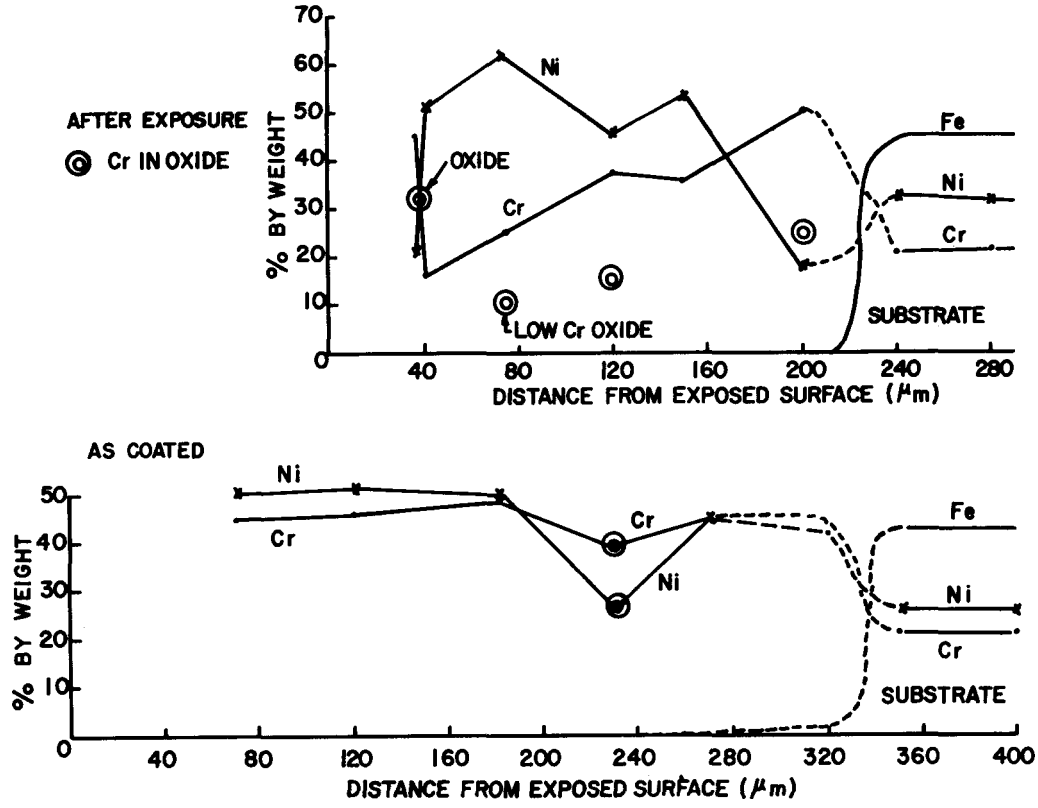

Figure 3.54 Microprobe Analysis Profile of Coating and Substrate of IN-671 Coating Before and After Exposure (Some oxides were formed during coating. The changes during exposure include chromium depletion and oxide formation.)

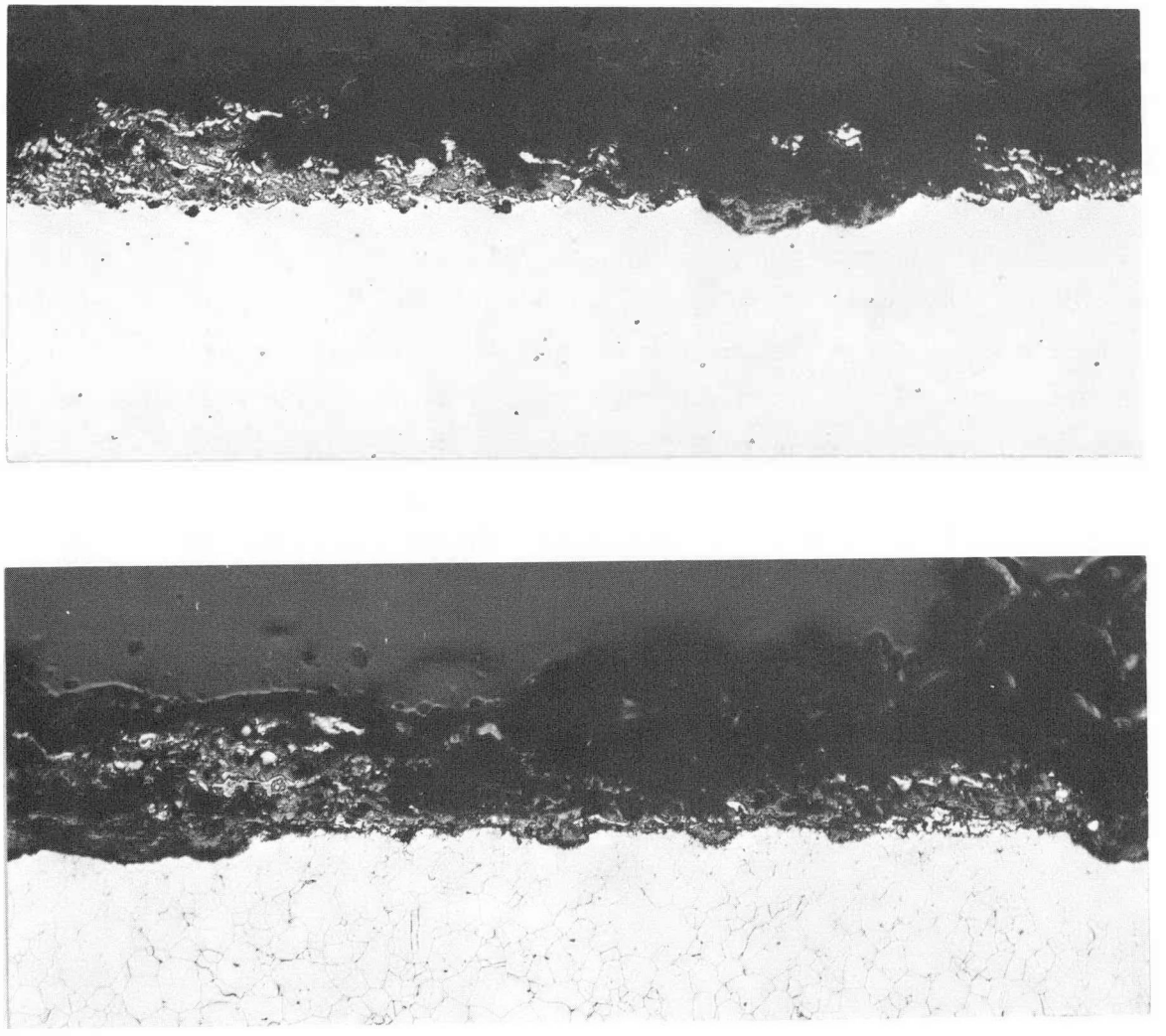

Figure 3.55 Exposure of Ni-Cr-Si Coating--100X [This coating (5% Si), produced by adding silicon to IN-671, was not homogeneous--some areas were much more resistant than others. Some of the problems appeared to be caused by insufficient silicon (top) and some by lack of fusion (bottom). Both coating defects can be eliminated by higher silicon in the starting mix.]

A commercial 72%Ni-20%Cr-6%Al coating (Metco 443) was also given a preliminary test to determine its behavior. The coating was not as dense as expected because of the choice of parameters used in plasma spraying. The results showed rapid internal attack and oxidation (Table 3.15) as well as surface recession. The porous Metco 443 coating exhibited no advantage over the 50%Ni-50%Cr and other coatings.

3.3.8.7 Examination of Ni-Al Coatings. A commercial Ni-Al-type coating was evaluated and compared with the Ni-Cr-Al coatings. Initial coating performance was superficially better than that of some previous nickel-based coatings but showed instability of the microstructure because of internal oxidation. Figure 3.56 shows that some penetration of the Ni-Al coating did occur and that the attack contributed to loss of bond on other specimens where porosity was excessive. A microprobe analysis of the exposed Ni-Al coating indicated that sulfides were formed at or very near the metal-coating interface.

Since the Ni-Al coating was promising based on its external appearance, one sample--Specimen 347-404 (Table 3.15)--was exposed to a second cycle. The results showed that the in situ "oxidized" coating was not promising as an adherent, protective scale. The second exposure resulted in complete coating failure.

3.3.8.8 Examination of Nonmetallic Corrosion Barrier Coatings. The test of the commercial $MgZrO_3$ coating (Metco 210) was the first to provide isolation of synthetic ash from the metal substrate. The first two specimens, (labeled M-210 on Table 3.15), were examined since the test results indicated that there was a different type of protection developed from that offered by other coatings. The microstructures indicated that the molten trisulfate did not penetrate more than the outer surface (Figure 3.57). The original coating was less than 90 percent dense with small pores (approximately 1 to 4 μm) in the as-deposited $MgZrO_3$. We concluded that a reaction product, presumably a high-melting sulfate such as $MgSO_4$, at the exposed surface was providing a self-healing mechanism, forming a seal at the surface. A thin Ni-Al bonding

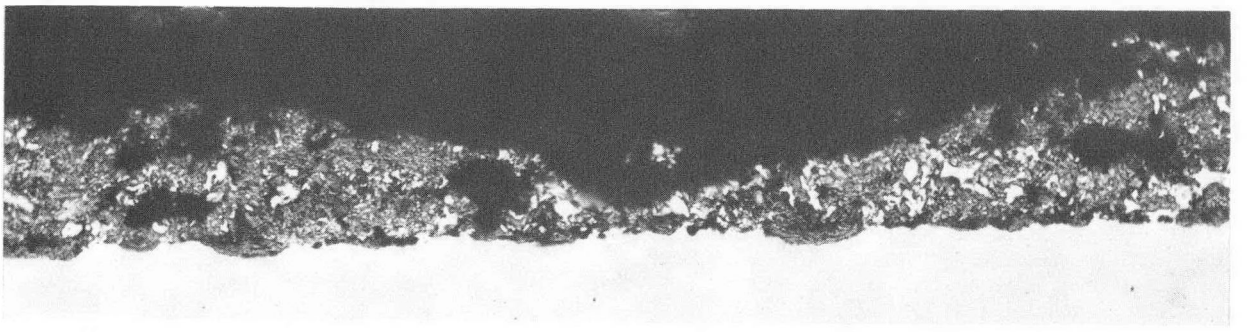

100X

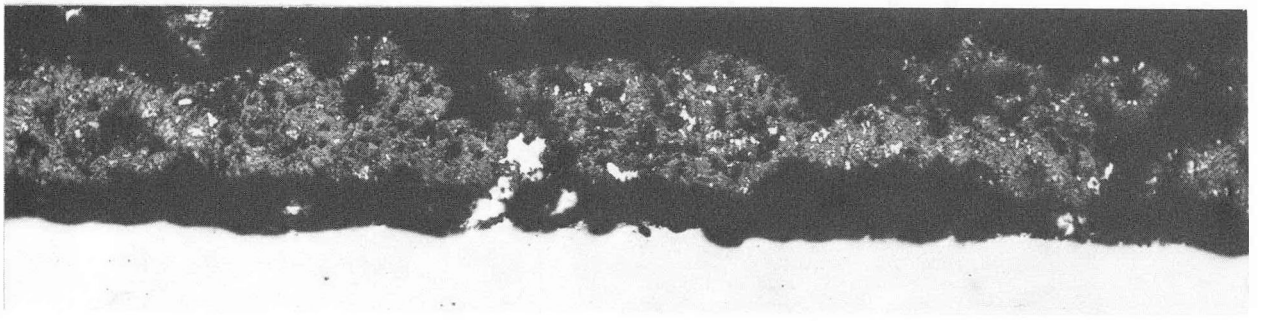

100X

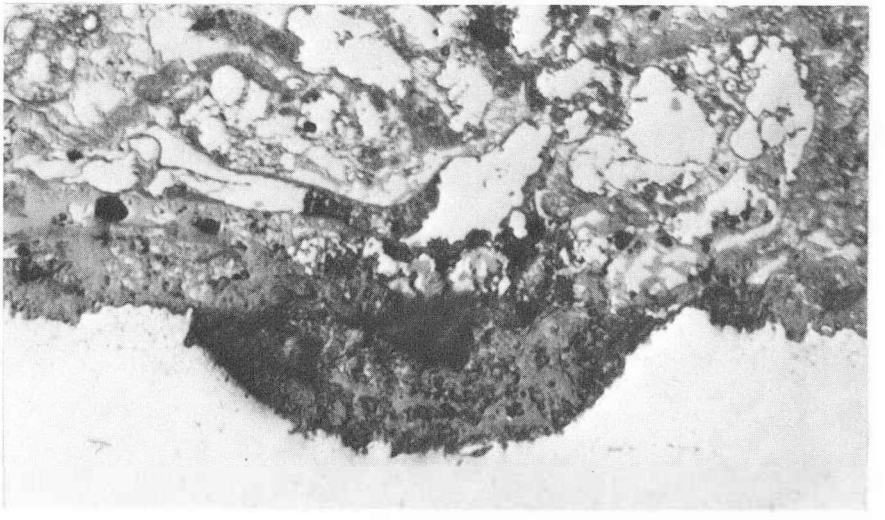

500X

Figure 3.56 Ni-Al Coating (Metco 404) on 347SS [The corrosive molten salt penetrated the coating pores resulting in attack below the coating (bottom). In some cases the bond was lost (center).]

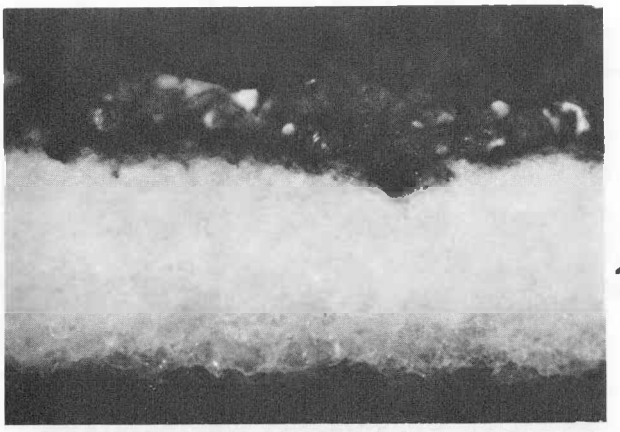

$MgZrO_3$ Coating After Exposure

Polarized Light--100X
No penetration by sulfates.

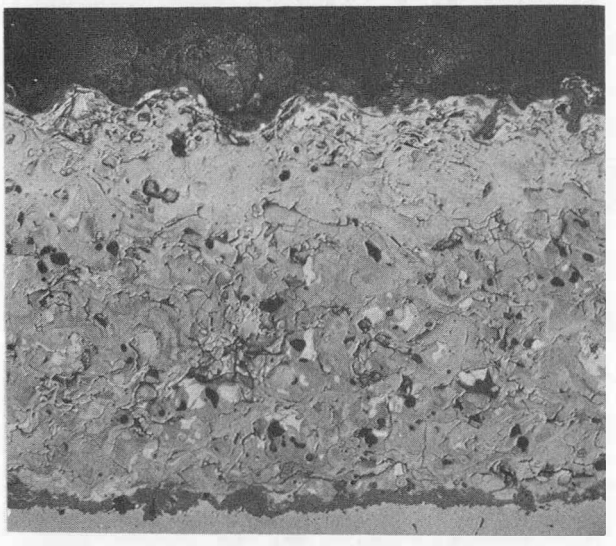

$MgZrO_3$ Coating After Exposure

SEM (Backscatter Technique)--180X
Structure of full coating thickness was unaffected by exposure.

Fireside Ash Deposits

Gray Sulfate Layer

SEM--750X
Self-plugging of pores was evident.

Figure 3.57 $MgZrO_3$ Coating on Stainless Steel (The coating exhibited self-plugging of pores by developing a high-melting sulfate, and it withstood repeated exposure.)

coat applied under the $MgZrO_3$ of the coating was unaffected by the exposure (Any good bonding coating, such as Kanthal, can be used to provide good mechanical attachment to the surface.) This magnesium zirconate coating was the only material seen to date that prevented molten sulfate penetration of the pores.

These $MgZrO_3$ tests were reproduced in later tests with similar results--no microstructural change occurred during exposure. Specimen 304-9 was returned for a second simulated fireside exposure with no evident change. No chromium was present in the ash deposits, and isolation of the alkali-iron trisulfate from the stainless steel substrate was complete.

The other nonmetallic coating tested was ZrO_2, applied by plasma spray directly to the steel (and stainless steel) coupons without the recommended Ni-Al bonding coat. The coating protected the substrate, but oxidation of the bonding loosened the coating on cool-down (refer to Figure 3.31), thus underscoring the need for proper surface preparation and coating application procedures in fireside environments. The ZrO_2 did not appear to be altered--only the metal substrate was oxidized, weakening the bond.

3.3.8.9 Examination of Tribaloy. Specimens of Tribaloy T-700 and T-800 coatings were tested as indicated in Table 3.15 and were found to react with the ash, forming sizable amounts of corrosion products. The microstructures of the nickel-based T-700 and the cobalt-based T-800 are shown in Figure 3.58. Surface attack was evident from the thickness loss, but only minor amounts of internal oxidation were seen in the remaining coating. The microprobe analysis profiles of the T-800 coating before and after exposure are shown in Figure 3.59. Some depletion of chromium, as well as added oxides, was observed in the microstructure, but surface recession was the most notable change.

An interesting question is why the molybdenum content on a nickel- or cobalt-based material does not lead to the catastrophic oxidation or accelerated fireside attack experienced with all the iron-based molybdenum alloys. However,

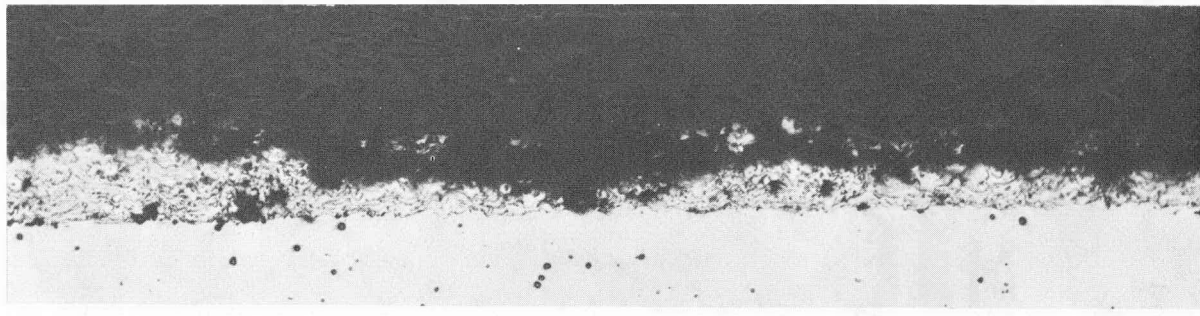

100X

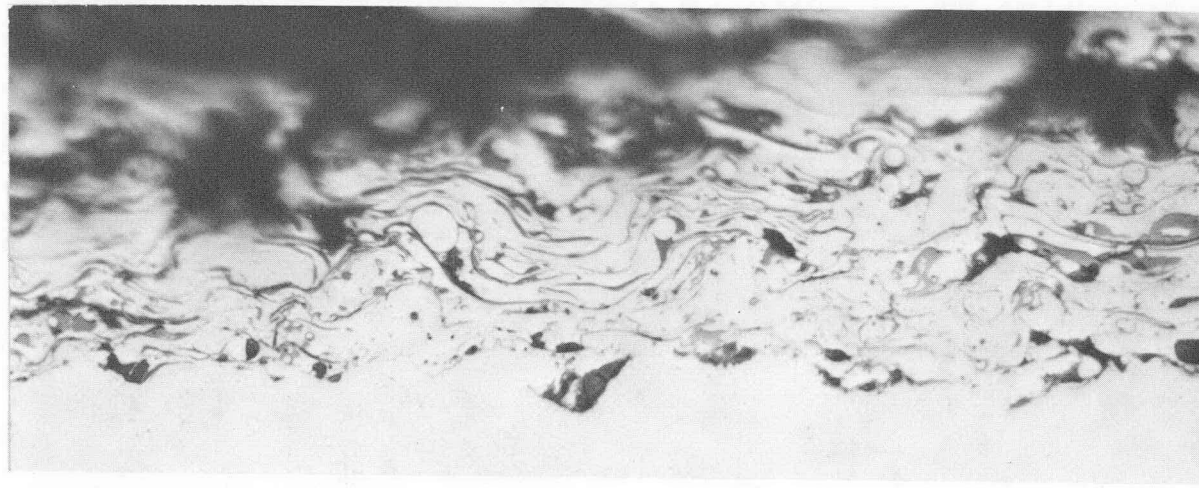

500X

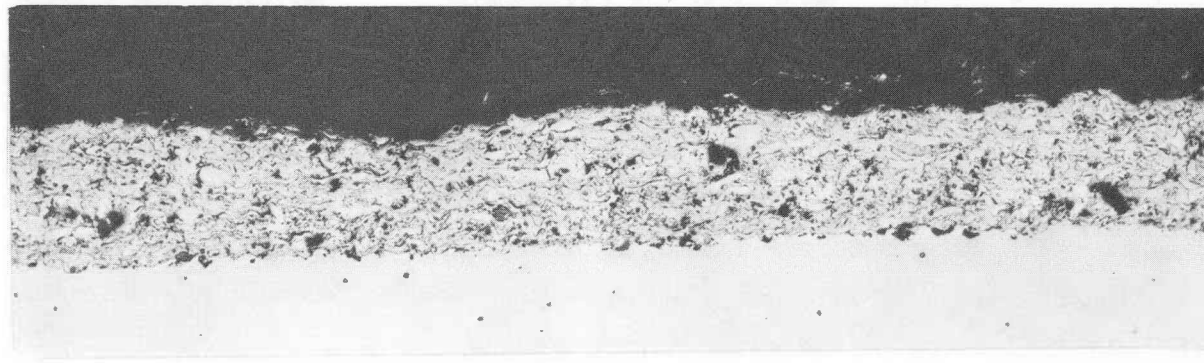

100X

Figure 3.58 Exposed Tribaloy Coating (The nickel-based coating lost metal from the exposed surface and suffered some internal oxidation. The cobalt-based coating suffered similar changes but, apparently, slower loss rates.)

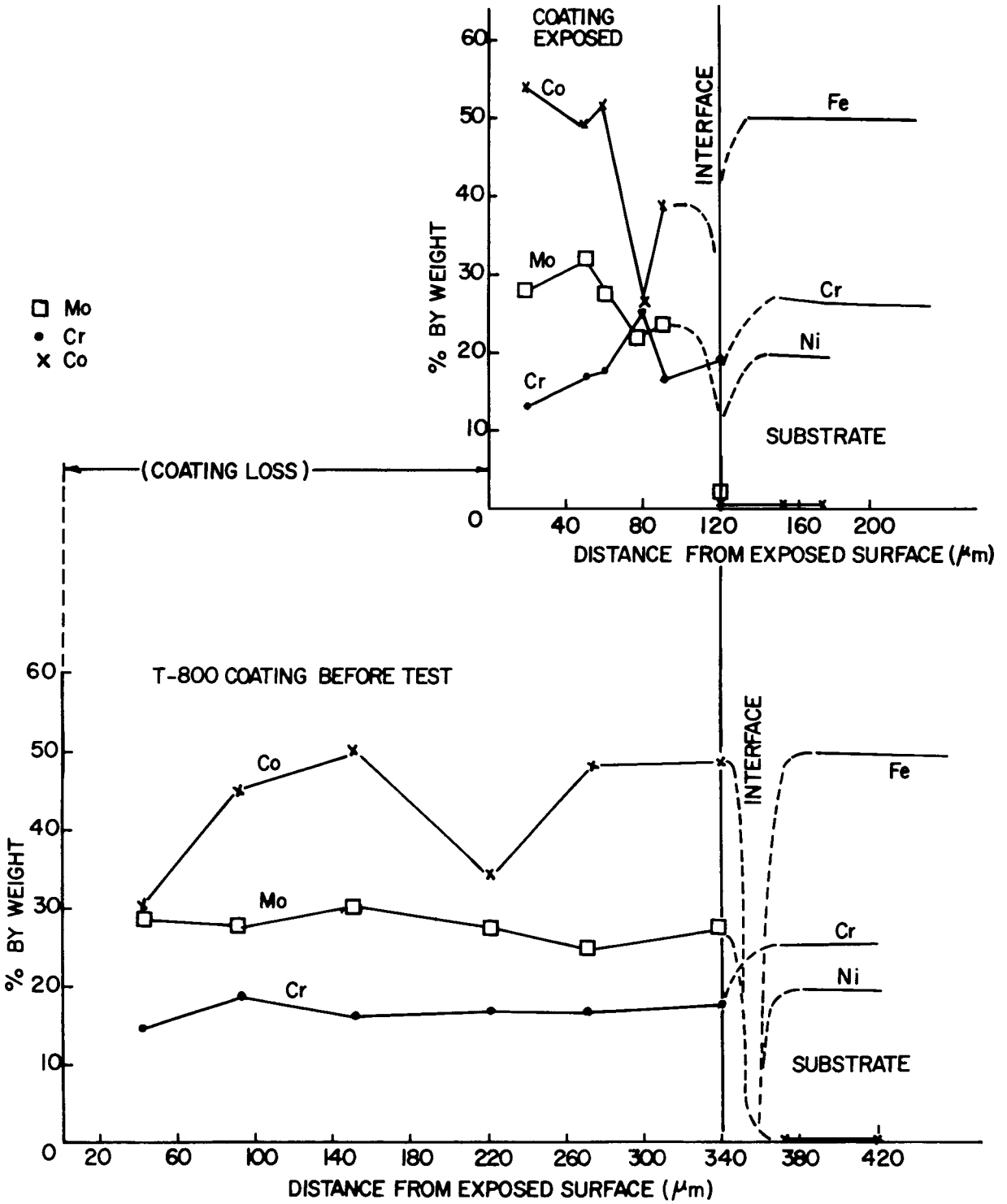

Figure 3.59 Microprobe Analyses Profiles of Tribaloy 800 Before and After Exposure (Small internal oxides were formed, and some loss of chromium near the surface was noted.)

such results may possibly occur with the Tribaloy coatings at higher temperatures.

3.3.9 Summary of Phase 3 Coating and Surface-Treatment Evaluations

The macroscopic and external examinations of most high-temperature alloys (Phases 1 and 2) and coatings (Phase 3) exposed to the simulated fireside test reveal the rapid attack and metal losses occurring in the first 48 hours of exposure. Several promising material improvements are immediately apparent when examining the Phase 3 coated materials systems not previously investigated.

Since the fabrication limitations of structural alloys prevent any significant inclusion of intermetallic compounds (such as $CrSi_2$, FeAl, NiAl, and Ni_3Al in wrought alloys), only coatings or surface diffusion treatments can be employed for such materials. From an engineering point of view, none of the structural alloy systems covered in Phase 1 exhibited stable passivity in thin films or adequate compatibility with the corrodent. The Phase 3 results indicate that several of the coating constituents may offer these advantages.

The striking contrast of the resistance of Alonized alloys compared with that of the chromized alloys appears to underscore the electrochemical nature of the attack. The high-aluminum phase, outer surface remained intact; and no deep, penetrating pitting was seen. The chromized alloys, on the other hand, showed accelerated attack through the high-chromium alloy surface with no benefit from the very high chromium content. The attack of the chromized materials is described as electrochemical pitting with an adverse cathode-to-anode surface area ratio.

The resistance to attack by coatings of $CrSi_2$, ZrO_2, and $MgZrO_3$ (largely magnesium meta-zirconate) is a good indication that inert corrosion barriers are not too difficult to develop. Compared with other materials, the self-healing pores and stability of the magnesium zirconate coating were excellent, and it appears to have long-life potential.

Limiting corrosion by the use of cathodic protective mechanisms is considered a new and attractive possibility. The first indication of this was seen in the Alonized, high-aluminum diffused materials introduced in Phase 3. Precipitates containing Fe-Al and Ni-Al compounds were present and appear to be stable. The intermetallic compounds of aluminum with iron, nickel, and chromium were formed in the diffused layers and apparently protected the substrate alloy. In one specimen where one end of the aluminum-diffused surface was deliberately removed, there was no pitting of the parent metal close to the aluminum-enriched case, suggesting that the cathodic protection had been in effect. This protective mechanism seems to demonstrate the principle; however, it is not proposed as a permanent cathodic barrier because of the high solubility of aluminum sulfates in the molten ash.

SECTION 4

STATE-OF-THE-ART DEVELOPMENTS RESULTING FROM PHASE 3 TESTS OF COATINGS AND SURFACE TREATMENTS

Section 4

STATE-OF-THE-ART DEVELOPMENTS RESULTING FROM PHASE 3 TESTS OF COATINGS AND SURFACE TREATMENTS

4.1 THE ROLE OF ALUMINUM

Previous Phases 1 and 2 tests of aluminum additions demonstrated that the aluminum was of little benefit. The exception was in those alloys with 2-percent silicon plus 2-percent aluminum, such as Alloy 4, which generated a protective adherent scale. In that case aluminum may have served as a silicate stabilizer in the scale.

While alloy additions of aluminum up to 4 percent were not effective in eliminating corrosion, higher concentrations of aluminum within the surface layers appeared to be much more effective. Aluminum in solid solution in steel did little to eliminate corrosion; however, as a compound or phase higher in concentration, it prevented severe surface pitting. This observation seems to strengthen the case for the electrochemical mechanism of attack as the primary corrosion mechanism.

If aluminum is to provide cathodic protection, it is needed in rather high concentrations, such as those found in the aluminides, to produce a sufficient electrode potential.

Substitutes for aluminum, including a number of highly anodic elements such as titanium, zirconium, niobium, tantalum, and possibly rare earths, which form stable intermetallic compounds, will probably be more effective or longer lasting than aluminum. Another technique to minimize alloy development is to apply a surface compound or coating to the tube that will endure despite a more anodic potential.

4.2 THE ROLE OF CHROMIUM

While both nickel- and iron-based alloys benefit from chromium alloy additions up to about 30 percent, the higher chromium applied by the chromizing process aggravates pitting. There was no improvement in fireside performance from high chromium so diffused into the surface of the alloy. High-chromium surfaces are reported to be microstructurally nonuniform,[7,8] containing nodules and exhibiting variations in concentration of chromium because of microstructural variations and grain-boundary effects on iron diffusion into the chromium-enriched surface. In addition, the outer chromized structure surface contains very fine precipitates of complex carbides[8,9] and, presumably, nitrides that may serve to provide active cathodic surface areas within the chromized layer.

In the wrought alloys, variations in the chromium concentration at the surface stimulate corrosion, as suggested by the irregular but limited area under attack in the wrought IN-671 alloy (48-percent chromium). Over much of the surface, the passivity of the IN-671 was good, but local irregularities in chromium may produce cathodic surfaces and initiate an electrochemical cell at that location (Figure 4.1). The chromium gradients seem to be a more probable cause of corrosion in the IN-671 than the carbide precipitate, since the carbides are very fine and widely distributed within each grain in the alloy.

The observation that uniformly electrodeposited chromium prevents corrosion as long as the coating lasts[10] indicates that uniformly distributed chromium is much better electrochemically than the chromized surface distribution. The gas oxidation experience, however, is just the reverse.

Given a homogeneous distribution of chromium (in a stainless steel, for example) the surface chromium activity will be far from truly uniform after conventional anneal and pickle treatments because of chromium depletion. A 304SS (new tube) from the mill normally has a surface chromium content ranging from 8 to 12 percent because of chromium depletion by oxidation and removal of the oxide.

IN-671: 3X Pitted specimen showing large uncorroded areas and a few severe pits.

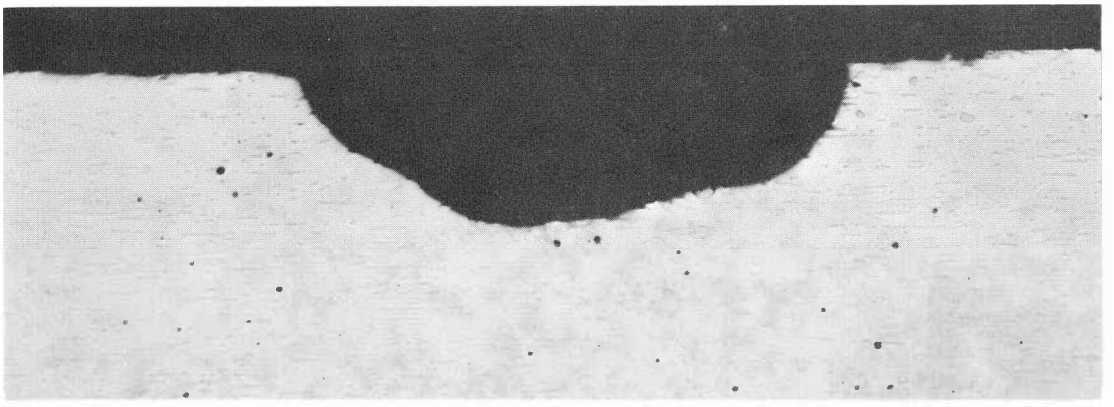

IN-671: 100X. Typical pit after descaling, illustrating local anodic metal loss in wrought alloy sheet (The coating of the same composition did not suffer this type of pitting.)

Figure 4.1 Alloy IN-671 After a 48-Hour Exposure

The conclusion indicated by comparing corrosion data from various chromized alloys was that the nominal or average chromium concentration at the surface did not correlate with pit depths. For example, the 60- to 65-percent chromium layer on chromized HT-9 was no more resistant to fireside corrosion than the 11-percent chromium in the untreated HT-9. Chromized 304SS and 21-6-9 alloys were essentially as deeply pitted as chromized HT-9. Increased chromium levels in the base alloy did not help. On the other hand, without chromizing, the more uniformly distributed chromium in solid solution in wrought alloys indicated that higher chromium was beneficial to corrosion resistance. For example, 310SS was always better than 304SS. Chromium carbide or nitride precipitates at or near the chromized surfaces may also provide a corrosion potential.

4.3 THE ROLE OF SILICON

The results of silicon additions in the Phases 1 and 2 material tests indicated that silicon is one of the elements that benefits the corrosion resistance of stainless steels and higher alloys. The thin (12 to 14 μm) siliconized surfaces with 4- to 5-percent silicon did not live up to expectation, possibly because the general corrosion rate was too high or a passive surface film was not established. On the other hand, the chromium disilicide ($CrSi_2$) coating was very resistant to corrosion, indicating that the chemical stability of the compound contributes greatly to its corrosion resistance, as compared with the poor corrosion resistance exhibited by metallic chromium or silicon as alloy constituents. The same enhancement of corrosion resistance by compound formation is indicated by the formation of AlNi and associated aluminides, which are more corrosion resistant than either nickel or aluminum separately in solid solution.

4.4 DEVELOPMENT OF INERT CORROSION BARRIER COATINGS

The performance of the $MgZrO_3$ coating proved it to be the most resistant coating material because of its stability and its resolution of the porosity and defect problems. Most other coatings suffered from penetration by the corrodent into the pores, which could in time lead to local failure of the

bond. The $MgZrO_3$ coupons demonstrated an efficient self-sealing surface because of the precipitated $MgSO_4$ (or some more complex, high-melting sulfate), so that only the outer 10 percent or less of the coating was actually exposed to the corrosive alkali-iron trisulfate. Extensive coating development is not required to utilize the $MgZrO_3$ coatings. It has been used for a number of years in aircraft applications, on furnace brazing fixtures, and for a number of nonferrous foundry applications. The bond and adherence of the $MgZrO_3$ coating are very good when not subjected to heavy impact loading.

These observations suggest that the $MgZrO_3$ coating will outlast the other tested nonmetallic materials, such as the Al_2O_3-SiO_2, SiO_2, and MgO.[11]

4.5 COMPOSITE SILICIDE COATINGS

The primary advantage of the $CrSi_2$ coating is its resistance to reaction with molten sulfates. Other advantages are its generally metallic properties at high temperatures and its apparently good bonding to the metals. With some additional work to solve the porosity problem, it may be as good as the $MgZrO_3$ coating.

By making a two-part, or composite, coating with the Kanthal sublayer, there is a good prospect that a long-life coating system can be developed, but some long-term testing is needed to verify this.

4.6 PERFORMANCE OF THE Ni-Cr ALLOY COATINGS

Plasma-deposited Ni-Cr (IN-671) was resistant to pitting; the wrought alloy of the same composition was not. Neither the 48%Cr-50%Ni (IN-671) plasma-deposited coating nor the Ni-Cr-Al coatings performed in a manner that would have been predicted from the performance of the corresponding wrought alloys. Internal attack and oxidation rather than pitting of the coating clearly limit its useful life. The higher surface area, porosity, and oxygen content of the original coatings apparently accelerate internal penetration or transport of

oxygen and sulfur into the microstructure. All coatings were spray applied by commercial firms using their normal coating techniques, and no attempt was made to produce special low-oxide-content deposits. (A fused surface layer method, at some additional expense, would be one method to produce a special, low-oxide coating.)

The plasma coated IN-671 specimens were free from the large, random pits seen in the wrought alloy (Figure 4.1) perhaps the result of the improved uniformity of the chromium in the coating or the change in the anode-cathode surface area relationship caused by the texture and oxygen content of the surface coating. Modifications of the Ni-Cr coating system by the addition of silicon may produce a long-life coating, but further development is required.

4.7 TEST PROCEDURE FOR COATINGS

The retort method of testing, using small amounts of ash replenished after approximately 100 hours, is good for comparing materials. This replenishing can be done by cooling down and mechanically removing the spent ash and applying new, synthetic or "natural" ash to the surface of the coupon. These repeated exposures will provide the needed, longer time, exposure effects. By repeated heating and cooling in the fireside retort, an accelerated test representing years of exposure can be performed in a few months. In the coal-burning superheater, for example, many months can pass with very little or no accumulated ash deposits. Laboratory tests, however, can be performed to effect a 10-to-1 acceleration of corrosion.

SECTION 5
DATA OBTAINED FROM SUPPLEMENTAL TESTS

Section 5

DATA OBTAINED FROM SUPPLEMENTAL TESTS

As indicated in Section 3.1, a number of questions arose from the early test results; thus supplemental testing was required so that decisions on the conduct of the subsequent tests could be made.

5.1 RATE OF ATTACK

The first unexpected observation was that the 500-hour losses resulting from fireside attack were almost the same as those reported for the first 250-hour exposure. Supplemental tests were performed to clarify the duration of attack and to acquire more information on the nonregenerative behavior of the fixed supply of synthetic ash. The results, shown in Figure 3.1, define the rapid attack for the first 48 hours and the subsequent decline in rate of attack, which approached zero.

This test series showed that when the alkali-iron trisulfate was consumed or diluted significantly with the corrosion products, the attack was essentially stopped. It was also apparent that no mechanism for continuing the regeneration of a liquid phase was functioning in a closed system (except for flowing gas). These observations tend to support the cyclic, repetitive-attack theory applied to commercial boilers, which is based on deslagging and acquisition of a fresh supply of corrodent from time to time for a continuation of the corrosive attack.

5.2 CHANGES IN THE LIQUID-PHASE COMPOSITION

A series of tests on the ash residue after exposures of 48, 100, and 250 hours was made using differential thermal analysis (DTA) and differential calorimetric analysis (DCA) to determine the changes in the ash resulting from corrosion. The test results are discussed in Section 3.1.2.3 and depicted in

Figure 3.2. The results indicated that the improved corrosion resistance provided by some elements of the alloy, such as niobium in 347SS, is clearly different from the resistance provided by other elements, such as manganese, chromium, and silicon, although these may be responsible for some reduction in stainless steel penetration. Niobium appeared to improve the surface passivity somewhat--less of the $(Na,K)_3Fe(SO_4)_3$ was consumed during exposure. Manganese was different--it promoted decomposition within the liquid phase.

Several other detailed observations were noted that seem to support the electrochemical mechanism of corrosion:

- The hemispherical shape and the distribution of pits were not related to any known metallurgical parameters.
- The pitted surface was frequently polished, as expected for an electrochemical attack.
- There was a lack of significant change in the mode of attack over a wide range of alloy compositions, suggesting that the limiting parameter in most cases is the corrosion current rather than the surface-reaction films.
- The electrical conductivities of the alkali sulfates rise dramatically in the same temperature range as the increasing corrosion rates shown in the frequently reported bell-shaped curve.[1,10]

5.3 PREOXIDIZED SPECIMEN TEST DATA

During the early phases of the test program, we observed that the pitting losses were erratic and often not linked to definable variables in the microstructure. The theory that oxide films on the steel and nickel alloys were responsible for this behavior and that "better" oxide scales enhance alloy protection was considered. Tests were performed on specially prepared, oxidized specimens that were precharacterized (see Section 3.1.3.4). The results of these tests were not as expected, since no corrosion benefit was found for the oxidized surfaces. In fact, in the case of the higher alloys, the pitting depth was greater (see Tables 3.10 and 3.11).

We concluded that the preformed oxides were readily dissolved by the molten complex sulfates and that chromium depletion at the surface may lead to deeper pitting. In general, these test data supported the concept of the electrochemical mode of attack.

5.4 REEXPOSURE OF PROMISING SAMPLES

Since the 48-hour exposure test was not intended to simulate long-life effects and since long exposures in the existing retorts were of no value, the concept of repeat testing of individual specimens of a few promising materials was adopted. The results of these reexposures were significant in a number of instances, especially for determining the value of the protective scale formed on Alloy 4, as described in Section 3.2.3 (Figure 3.12). This test, though preliminary, was considered significant because the addition of 2%Al-2%Si formed a stabilized scale that did not occur on other alloys. Further reexposures to establish whether the scale remains stabilized and protective appear warranted.

5.5 REEXPOSURE OF COATED SPECIMENS

In Phase 3, several of the coated materials--Ni-Cr-Al, Ni-Al, and Ni-Cr-Si--were apparently successful, although internal changes, such as oxidation and sulfidation, were evident. The reexposure testing of these coatings (two exposures of the same coupon) is necessary to verify that the altered compositions show any further benefit.

From these repeat tests, we concluded that:

- Porosity in the coating could lead to early failure.
- Only a few of the coating materials were sufficiently corrosion resistant to endure long exposures in service.
- The Ni-Cr-based alloy systems applied by plasma spray would, in time, lose their integrity because of internal oxidation.

- The $MgZrO_3$-type coating (Metco 210) retained adherence, was capable of self-sealing of the pores, and thus appeared to have no porosity corrosion problem.

- Porosity in the $CrSi_2$ coating would lead to coating loss unless the coating was impregnated. The silicide material was apparently stable.

5.6 SUBSTITUTE MATERIALS USED IN PLACE OF UNSUITABLE COATINGS

Use of the calcium-impregnated Ni-Al coatings called for in the work scope was not feasible because of the calcium side-reactions. The $MgZrO_3$ and ZrO_2 coatings were substituted for the impregnated material. If impregnating the pores using a lower temperature technique or a plasma spray were developed, the use of impregnated Fe-Cr-Al coatings would be recommended.

SECTION 6
ADVANCEMENT IN THE STATE OF THE ART

Section 6

ADVANCEMENT IN THE STATE OF THE ART

The results obtained in all three phases of the fireside test program should aid in eliminating a number of candidate materials that are not significantly better than the older, established stainless steels. Molybdenum steel alloys, for example, with more than 1- or 2-percent molybdenum should be avoided. In nickel and cobalt alloys containing molybdenum, the threshold for accelerated attack is at a higher temperature--above 1250°F (675°C). The high-temperature "superalloys," in general, offer no advantage over the 300 series stainless steels. In addition, test results showed that preoxidized surfaces and other conditions that produced chromium depletion of the alloy surface clearly intensified the pitting problem.

Commercial pack chromizing with its inherent nonuniform chromium distribution was also not helpful in reducing corrosion, even where the chromium analysis was 60 percent at the surface. The absolute value of the chromium in the alloy surface was not as important in reducing corrosion as its uniformity of distribution, based on a comparison between the chromized and nonchromized surfaces in four alloy systems. The presence of carbides and nitrides in the high-chromium alloy may also initiate electrochemical pitting. Other referenced experience[10] indicates that a uniformly applied chromium electroplate is not subject to pitting for the duration of the coating life.

Control measures to eliminate electrochemical pitting by the molten trisulfates required a different alloy design approach than those used for gaseous oxidation resistance. One of the promising approaches is suppression of the electrochemical attack by cathodic protective measures. Another approach is stabilization of the silicate-containing scales to generate an in situ corrosion barrier other than the usual oxide scales.

High aluminum content in the Alonized surface-diffused layers is believed to effect a type of cathodic protection. Further testing is required

to determine the effective life of the Alonized case, but the initial exposures were promising because of the conspicuous control of the pitting mechanism.

The Phase 3 tests indicated that at least two classes of coatings--$MgZrO_3$ and Fe-Cr-Al--show promise and that one or both will prove to have long-life potential. The development that showed the most promise was the $MgZrO_3$ coating, which was stable and without a porosity problem under fireside conditions. The corrosion barrier produced by the $MgZrO_3$ eliminated the weakness and short-life problems of the older MgO coating. Additional work on the Fe-Cr-Al-type coating covered with chromium disilicide or other silicide coatings to stop the porosity attack may also provide a long-life protective coating.

The combined influences of aluminum and silicon on the corrosion resistance of Alloy 4 suggest that more stable silicates in the corrosion products will retard corrosion and promote the scale adherence that was previously lacking. We believe the optimization of this alloy modification will strengthen the future potential for the bimetallic or clad-tube approach.

The influence of carbon and chloride additions to the ash was not very significant at 1250°F (675°C), but these additions promoted a severe fireside attack at higher temperatures. Thus carbon and chloride additions are effective in extending the range of severe fireside attack to higher temperatures. In short, with 3-percent NaCl added to the ash, the "bell-shaped" corrosion curve no longer would look like a bell on the high-temperature side.

The available literature gives no indication of the corrosion rate once the liquid-phase complex sulfates are formed; however, the data obtained in this program indicate that corrosion is rapid once started. The 24-hour test produced penetration losses of about 0.008 in. (203 μm) on such alloys as 304SS and Incoloy 800 at 1250°F (675°C).

Thus the state of the art for fireside corrosion has been advanced but, as stated earlier, more work is needed to verify some of the postulations.

SECTION 7
CONCLUSIONS AND RECOMMENDATIONS

Section 7

CONCLUSIONS AND RECOMMENDATIONS

The tests, encompassing a wide range of alloy compositions, have led to the conclusion that none of the present-day alloys available for steam generator tubing have good resistance to aggressive fireside corrosion. The alloy compositions available will be corrosion-limited in service life when exposed to corrosive deposits and complex sulfate attack.

The observed characteristics of fireside attack can best be ascribed to the electrochemical mechanism that is relatively nonselective of alloy compositions and surface conditions. The hemispherical-type electropolished pits indicate that metal was removed in a pattern not correlated with microstructural characteristics.

The absence of pitting attack on stainless steels and other alloys at 1450°F (790°C) may be a "laboratory curiosity" that prevented the formation of the alkali-iron trisulfate. Under realistic conditions, where molten trisulfates were formed at lower temperatures and raised to 1450°F (790°C), severe pitting occurred. Thus the high-temperature side of the bell curve represents only isothermal exposures to simulated fireside conditions. Better definition of the shape on the high-temperature side can only be obtained with further testing at various temperatures.

The presence of aluminum in high concentration, such as in the Alonized 304SS and Incoloy 800 alloys, provided some cathodic protection to the surface of the steel. Assuming a primary corrosion produced by electrochemical corrosion currents, several candidates for cathodic protective metals on the surface--aluminum, niobium, titanium, zirconium, and tantalum--should be effective. All of these can be considered more anodic than chromium and may be applied in the form of stable intermetallic compounds.

FWDC recommends verifying the cathodic protection characteristics indicated by several alternate metals, such as niobium, zirconium, and titanium (applied as metallic compounds), and comparing them with the Alonized aluminum. Further testing to determine the life of the aluminum case on stainless steel and Incoloy 800 is also recommended.

The significant increase in penetration of a surface with a very high chromium content (40 to 60 percent), apparently induced by a nonuniform chromium content on the surface, appears to support the theory of electrochemical attack and underscore the need for greater homogeneity in the chromium content. A direct demonstration of the effect of chromium gradients is therefore recommended.

The potential advantage of cladding alloys with compositions similar to Alloy 4 (25%Ni-20%Cr-2%Al-2.4%Si), which generated a protective adherent scale with a greater ability to withstand deslagging operations, is that they may extend the life of the presently available materials. Evaluating the influence of individual alloy constituents on corrosion resistance has demonstrated that an important factor is the variation in scale stability in contact with the corrosive media. None of the compositions tested approached the optimum alloy. We recommend that further alloy modifications to the Fe-Cr-Ni-Si system be evaluated with metals such as manganese, niobium, and aluminum.

The unexpected failure of metallic oxides (including Al_2O_3, Cr_2O_3, and spinel scales) to resist the molten alkali-iron trisulfate attack suggests that an acid fluxing mechanism must occur. The screening of other nonmetallic materials, however, revealed that some (e.g., SiO_2, mullite (Al_2O_3-SiO_2), ZrO_2, $ZrSiO_4$, and $MgZrO_3$) were resistant to the same attack. Relating these materials to a protective scale mechanism supports the concept of forming silicates to improve resistance. FWDC recommends that future alloy modifications be directed to additions that will increase the silicate in the corrosion scale.

The $MgZrO_3$ coating was the most resistant coating material tested because of its stability and its freedom from problems caused by porosity. Most other coatings suffer from penetration of the pores, which may in time lead to local failure of the bond. The $MgZrO_3$ coupons demonstrated an efficient self-sealing surface because of the precipitated sulfates in the pores. Extensive coating development is not required to utilize the $MgZrO_3$ coatings, since they have been used for a number of years in high-temperature applications. Further testing of coated tubes and coupons using this $MgZrO_3$ coating is strongly recommended.

SECTION 8
REFERENCES

Section 8

REFERENCES

1. Foster Wheeler Development Corporation, "Fireside Corrosion: A Review of the Literature on Steam Generator Superheater and Reheater Tube Materials for Coal-Fired Systems," I. M. Rehn, prepared under EPRI Contract RP-644-1, July 1978. (Also Appendix A of this report.)

2. W. J. Greenert, "High Temperature Slag Corrosion of Metallic Materials," Corrosion, Vol. 18, 1962, pp. 91t-102t.

3. W. T. Reid, H. H. Krause, and R. E. Barrett, "Project Review and Fourth Summary Report on Formation of Alkali Iron Sulfates and Other Compounds Causing Corrosion in Boilers and Gas Turbines," prepared for the ASME Committee on Corrosion and Deposits From Combustion Gases by Battelle Memorial Institute, July 1, 1966 to June 30, 1968.

4. H. H. Krause, A. Levy, and W. T. Reid, "Sulfur Oxide Reactions: Radioactive Sulfur and Microprobe Studies of Corrosion and Deposits," Transactions of the ASME, Journal of Engineering for Power, Vol. 90, Series A, No. 1, January 1968, pp. 38-44.

5. Foster Wheeler Development Corporation, "Fourth Quarterly Progress Report--Design of Improved Materials Systems for Coal-Fired Boiler Superheater and Reheater Tubes," prepared under EPRI Contract RP-644-1, March 1977.

6. Foster Wheeler Development Corporation, "Fifth Quarterly Progress Report--Design of Improved Materials Systems for Coal-Fired Boiler Superheater and Reheater Tubes," prepared under EPRI Contract RP-644-1, July 1977.

7. N. R. Chapman, et al., "The Oxidation of a Number of Chromized and Chrome-Aluminized Alloys in Flowing Air and Flue-Gas Atmospheres - I," Anti-Corrosion Methods and Materials, Vol. 17, No. 12, December 1970, pp. 10-26.

8. Private Communications, November 16 and 23, 1976, from William Hudson of Alloy Surfaces Company, Wilmington, Delaware, to I. M. Rehn of Foster Wheeler Development Corporation.

9. V. D. Osintsev, et al., "Effect of the Condition of Diffusion Chromizing and Heat Treatment on the Corrosion Resistance of Chromized Steel in Hot Sulphur-Containing Gases," Fiziko-Khimicheskaia Mekhanika Materialov, Vol. 9, No. 2, 1973, pp. 17-19.

10. A. L. Plumley, W. R. Sylvester, and R. W. Borio, "Interactions of Materials Leading to Metal Wastage in Steam Generators," presented at the International Conference on Ash Deposits and Corrosion From Impurities in Combustion Gases, Engineering Foundation Conferences, New England College, Henniker, New Hampshire, June 26 to July 1, 1977.

11. R. Rasch, "Flue Gas Side Corrosions Description of Typical Damage, Corrosion Mechanism and Measures for Prevention," Technische Mitteilungen, Vol. 65, No. 2, February 1972, p. 82.

APPENDIX A

FIRESIDE CORROSION: A REVIEW OF THE LITERATURE ON STEAM GENERATOR SUPERHEATER AND REHEATER TUBE MATERIALS FOR COAL-FIRED SYSTEMS

CONTRACT NO. RP-644-1

PREPARED FOR

ELECTRIC POWER RESEARCH INSTITUTE
PALO ALTO, CALIFORNIA 94303

BY

IRWIN M. REHN, PROJECT ENGINEER

JULY 1978

LEGAL NOTICE

"This report was prepared by Foster Wheeler Development Corporation (FWDC) as an account of work sponsored by the Electric Power Research Institute (EPRI). Neither EPRI, members of EPRI, FWDC, nor any person acting on behalf of either;

"a. Makes any warranty or representation, express or implied, with respect to the accuracy, completeness, or usefulness of the information contained in this report, or that the use of any information, apparatus, method, or process disclosed in this report may not infringe privately owned rights; or

"b. Assumes any liabilities with respect to the use of, or for damages resulting from the use of, any information, apparatus, method, or process disclosed in this report."

This report prepared by:

Irwin M. Rehn
Project Engineer

The contents of this report have been reviewed and approved by:

William R. Abbett, Jr.
Chief Metallurgist

Jeffrey L. Blough
Manager, Materials Technology Department

TABLE OF CONTENTS

Section		Page
1	INTRODUCTION AND SCOPE	1-1
2	HISTORICAL BACKGROUND/PLANT EXPERIENCE	2-1
3	TEST PROBES AND SUBSCALE FURNACE TESTS	3-1
4	LABORATORY CORROSION DATA	4-1
	4.1 General	4-1
	4.2 Sulfur Oxidation Chemistry and Thermodynamics	4-2
	4.3 Adsorption and Chemisorption on Fly-Ash Surfaces	4-9
	4.4 Formation and Deposition of Alkali Salts on Tube-Wall Surfaces	4-11
5	INFLUENCE OF ALLOY MODIFICATIONS ON FIRESIDE CORROSION	5-1
	5.1 General	5-1
	5.2 Corrosion of Ferritic Alloys	5-2
	5.3 Corrosion of Austenitic Alloys	5-4
	5.4 High Nickel and Experimental Alloys	5-10
	5.5 Conclusions	5-11
6	CORROSION AND SULFIDATION MECHANISMS RELATED TO FIRESIDE CORROSION	6-1
	6.1 Introduction	6-1
	6.2 Liquid-Phase Chemical Attack	6-2
	6.3 Electrochemical Mechanisms of Corrosion by Fireside Deposits	6-4
	6.3.1 Prerequisites for Electrochemical Attack	6-5
	6.3.2 Electrode Potentials and Electrode Reactions	6-6
	6.3.3 Gas Atmosphere Tests and Their Effect on Electrochemical Attack	6-8
	6.3.4 Electrochemical Corrosion Meter	6-11
	6.3.5 Polarization Effects	6-12
	6.3.6 Electrochemical Cell Initiation	6-15
	6.4 Effect of Chloride Additions on Corrosion Mechanisms	6-17

Section		Page
7	SURFACE TREATMENTS AND COATINGS FOR FIRESIDE APPLICATION	7-1
	7.1 Metal Shields	7-1
	7.2 Alloy Cladding of Tubes	7-2
	7.3 Diffusion Alloy Surfaces	7-3
	7.4 Protective Coatings	7-5
8	CONCLUSIONS AND STATE OF THE ART	8-1
9	REFERENCES	9-1
10	SUPPLEMENTARY BIBLIOGRAPHY	10-

LIST OF ILLUSTRATIONS

Figure		Page
2.1	Noncorroded and Corroded 18-8, Type 321 Tubes From Short Superheater Platen	2-4
4.1	Catalytic Formation of SO_3 Producing High Concentrations Near Surface in Flowing Gas Mixture of $N_2 + SO_2 + O_2$ at 1100°F (593°C) in 5.8 Percent SO_2	4-6
4.2	Sulfur in Ash After Exposure to Synthetic Flue Gas at Various Temperatures	4-10
4.3	Melting Points in the Sodium- and Potassium-Iron Trisulfate	4-13
5.1	Effect of Alloying Constituents on Corrosion Rate	5-3
5.2	Corrosion of 18-8, Type 321 and 25-20, Type 310 by White Layer in Synthetic Flue Gas	5-5
6.1	Liquid-Phase Corrosion Indicated by Rapid Metal-Loss Rates During 5-day Exposures to Simulated Fireside Corrosion	6-2
6.2	Ferritic Reheater Tube With Deposit	6-5
6.3	Potential Time Curves of Three Alloys in Fused Sulfate in Air	6-9
6.4	Effect of SO_3 Partial Pressure on the Corrosion Current on an 18%Cr-8%Ni Electrode at 1112°F (600°C)	6-14
6.5	Schematic of Cathode Stimulation Penetrating the Passive Film	6-16

Blank Page

LIST OF TABLES

Table		Page
5.1	Corrosion Rates for Different Salt Mixtures at Various Temperatures	5-4
5.2	Test Materials	5-7
5.3	Corrosion Data for Material Exposed to Various Combustion Atmospheres	5-8
5.4	Percentage Composition by Weight of Tube Alloys Tested	5-9

SECTION 1
INTRODUCTION AND SCOPE

Section 1

INTRODUCTION AND SCOPE

The significance of the attack on fireside surfaces (also called fouling corrosion or corrosive slagging) of boiler and superheater tubes first became evident in 1942 in pulverized coal-burning power plants. Since that time substantial discussion, study, and testing, have been initiated, but no practical resolution of the basic problem nor any highly resistant alloy for steam generator tubes has been reported.

Current practice in the United States has been to minimize the fireside corrosion by limiting the steam temperature, by improving the boiler design, or by selecting coals lower in alkali and sulfur content. The emphasis of this survey is on updating the recent developments following the Marchwood Conference of 1963 and on supplementing the detailed review and summary presented by Reid.[1]*

The fireside corrosion of boiler, superheater, and reheater surfaces referenced in this report includes the elevated-temperature metal wastage from steam generating but does not include the lower-temperature sulfuric acid-dewpoint attack on flue-gas exit surfaces. While this study was specifically directed toward the conditions relevant to the coal-burning utilities, some references to corrosion by deposits from oil-burning systems are included to

*Numbers designate references in Section 9.

delineate the differences between corrosion by oil and coal-derived ash deposits. A few references were taken from the literature on "hot-corrosion" problems resulting from gas turbine conditions; however, the corrosion mechanisms above 1470°F (800°C) are clearly different from the fireside attack of primary interest, which is normally limited to about 900 to 1330°F (480 to 720°C).

The open literature and widely distributed project reports surveyed indicate that the main effort has been directed toward understanding the origin and nature of the corrosion problem, the formation of deposits, and the combustion gases and sulfur chemistry contributing to the attack. However, the evaluation of materials subject to corrosion and the testing of methods to prevent or control fireside attack have received substantially less attention, as indicated by the volume of reported data.

Some of the apparent reasons for limited success in this area may be due to oversimplification of the complex chemical mode of attack and to neglect of some of the important contributing conditions, phases, or elements. Several common misconceptions are:

- Assuming the corrosion to be caused by a salt-activated oxidation mechanism
- Assuming that molten deposits or slag is simply a corrosive flux, dissolving the oxides
- Attributing the corrosion primarily to the high sulfur content of coal
- Describing the chemical reactions in terms of molecular compounds, thereby neglecting the ionic nature of the corrodents and products.

In short, the combined effects of the gases, ash deposits, and condensed phases, as well as the tube surfaces, are all significant parameters in the metal-loss syndrome.

While the number of investigations and the array of tests in progress have diminished in recent years, the emerging, definitive developments now reported are expected to reveal a significant progress in the near future. The major incentives for continued work on fireside corrosion and corrosion-resistant materials should be the increased thermal efficiency in new plants designed for higher steam temperatures, the utilization of abundant midwestern coals somewhat high in alkali, and the elimination of many unscheduled shutdowns caused by tube failures.

SECTION 2
HISTORICAL BACKGROUND/PLANT EXPERIENCE

Section 2

HISTORICAL BACKGROUND/PLANT EXPERIENCE

While isolated occurrences of severe metal loss were reported previously, the major outburst of widespread problems occurred in 1942, as related by Reid, Corey, and Cross:[2]

> Since 1942, many large central-station boiler furnaces burning pulverized coal and removing the ash as molten slag have experienced external corrosion of furnace-wall tubes. In a few cases the loss of metal was so severe as to cause failure of tubes during operation, in others, seriously thinned tubes had to be replaced to prevent unexpected interruption of service. Because the rate of corrosion under certain conditions may be so high as seriously to weaken the tubes between normally scheduled inspections, operators charged with the continuous production of power under wartime emergency conditions have been greatly concerned over prevention of further corrosion.

The corrosive attack on the boiler wall tubes was alleviated by changes in the furnace design. Similar attack was observed later on the steam-generating surfaces as the operating temperatures were increased.

The wall-tube attack was in low-temperature areas--below 900°F (482°C)--which was unexpected because of the established compatibility of alloy grates with coal-ash slag as high as 2200°F (1204°C), as demonstrated by the older spreader stokers. Mackowsky[3] reviewed the fouling and corrosion of boiler and superheater surfaces and identified the mineral constituents of coal as the cause of these problems.

Wyatt and Evans[4] described the occurrence of failures in England for the period from 1950 to 1963 as follows:

> There were 88 outages caused by external corrosion of ferritic alloys, with 24 failures occurring in one station alone. Austenitic alloys led to 2 outages by external corrosion complicated by a creep problem. During the same period, 13 outages occurred in reheater sections, with 10 of these at one station. Corrosion was most severe about 60 deg on either side of the center line of the tube facing the oncoming gas stream, and most failures occurred in the active length of tubes, not at bends or attachment points. These authors concluded that the maximum steam temperature consistent with a reasonable life would be 1050F [565°C] when burning "aggressive" coals. With the best fuels, the steam temperature might be as high as 1200F [649°C].

There is obviously a difference between the mode of attack in the superheaters and reheaters that suffer maximum losses above 1050°F (565°C) and that occurring in lower-temperature furnace-wall tubes.

The circumstantial explanation for the apparent discrepancy in temperature ranges was offered by Nelson and Cain, Jr.,[5] who suggested a three-peaked curve of metal wastage as a function of temperature. The low-temperature (wall-tube losses) peak loss occurs at about 700°F (371°C); the intermediate region, described as molten-complex-trisulfate attack, ranges from 1025 to 1300°F (551 to 704°C); and a high-temperature sulfate attack occurs above 1500°F (816°C).

The assignment of rapid metal losses to mixed sulfate and trisulfate corrodents was challenged by Crossley,[6] who stressed the importance of the high SO_3 content of the flue gases which may contribute to the formation of alkali

pyrosulfates. Earlier work of Kirsch[7] had suggested that the pyrosulfate corrodents were involved but not proven.

The severity of the superheater corrosion problems increased in the space of a few years after the introduction of higher steam output temperatures, as described by Sedor, Diehl, and Barnhart:[8]

> The additional heat for the higher steam temperatures and reheat was obtained, for the most part, by placing part of the superheater or reheater in the higher gas-temperature zones of the secondary furnace. The increased metal temperatures have required the more extensive use of austenitic materials.
>
> ...The second and far more serious of the two problems was the accelerated corrosion of the 18-8, Type 321, tubes in the short superheater platens caused by the components in the ash deposits. The severity of this corrosion is illustrated in Figure 4,* where a cross section of a corroded tube is compared to that of a noncorroded one. While metal was lost all around the periphery of the tube, the metal loss was greatest on the side subjected to the blast of the soot-blower nozzles. After only 18 months of service, one tube failed because of thinning of the wall, and many other tubes were also badly corroded. Most of the tubes in the corroded area were replaced to prevent a series of service interruptions from similar failures.

Since the fireside problems were widespread and complex, involving different coals and various furnace designs, a number of different theories were

*Figure 2.1 in this report.

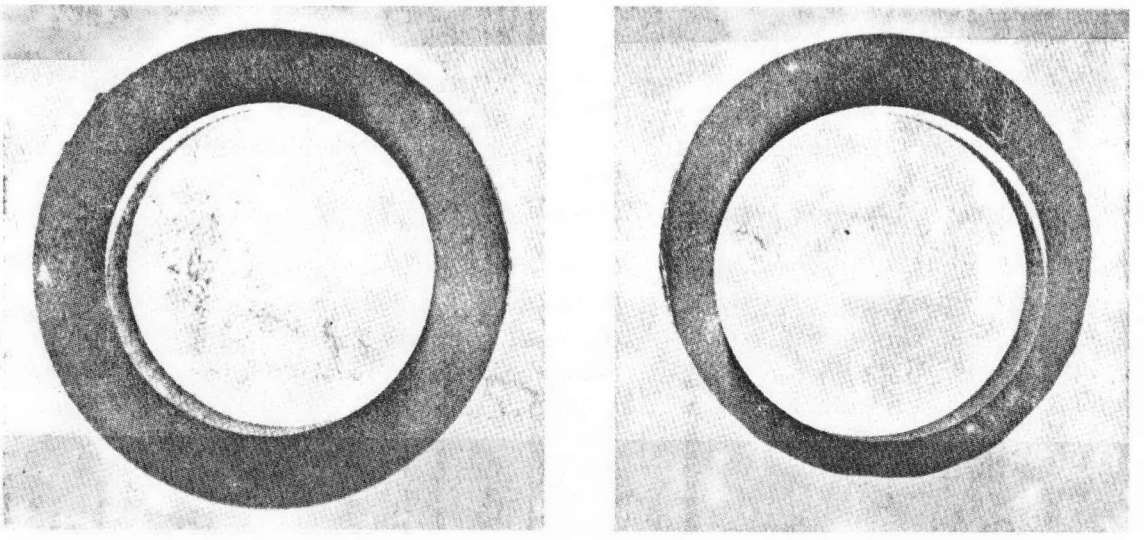

Noncorroded Corroded

Figure 2.1 Noncorroded and Corroded 18-8, Type 321 Tubes From Short Superheater Platen[8]
[The wall thickness was reduced from 0.380 to 0.130 in. (965 to 330 μm) by fireside attack in 18 months of service.]

developed in Europe, England, and the United States. Several of these theories were discussed by Bishop[9] as follows:

> (i) that alkali vapours condense upon the tubes to form a sticky matrix ('fly-paper') which collects impinging particles of fly-ash,
>
> (ii) that the initial deposit consists of powdery fly-ash; sulphur oxides diffuse 'down' the temperature gradient towards the tube surface and eventually form an 'inner layer',
>
> (iii) that the initial deposit consists of molten and partially-molten particles of fly ash,

(iv) that alkali-metal and/or alkaline-earth oxides (Na_2O, CaO) are deposited upon the tubes and are then converted to sulphates and pyrosulphates by sulphur oxides in the gas stream,

(v) that alkali chloride vapours (NaCl), from high chlorine coals, and alkali hydroxide vapours (NaOH), from low-chlorine coals, condense upon tubes and are subsequently converted to sulphates,

(vi) that silicon compounds (SiS, SiS_2, SiO) are evolved from silicate minerals during combustion and condense on tubes as sub-micron particles which are rapidly oxidized to form silica.

In view of the general and qualitative character of these theories, it is appropriate to comment briefly upon the present knowledge of the mechanisms by which vapours and particles reach the tube surfaces and upon some of the conditions that are likely to favour the retention of deposited matter.

Superheater tubes are inefficient collectors of ash. Nevertheless, in circumstances where fouling is favoured, deposits form rapidly and, in extreme cases, can enforce the shut-down of a boiler after as little as 100 h operation. The formation of a deposit necessitates that particles and vapours should penetrate the boundary layers which exist at the surface of the tube.

Bishop[9] also analyzed the conditions contributing to fouling, such as:

(i) the presence of sticky molten matter on (a) fly-ash particles, due to water-soluble alkalis and/or (b) the tube surface,

(ii) the presence of very fine particles and/or water-soluble alkalis which encourage sintering in masses of fly-ash, particularly during the early stages of sintering,

(iii) the presence of acicular crystals of oxide which project from an oxidized tube surface, trap ash particles and encourage the build-up of deposits,

(iv) an irregular surface texture which is likely to influence collection during the first three hours of deposition,

(v) the development of an epitaxial relationship between potassium aluminum sulfate, $K\,Al(SO_4)_2$, in the deposited matter and ferric oxide in the scale layer on the tube.

The origin, analysis, and mechanics of fouling were not sufficient to explain why the rapid metal wastage occurred, which was most serious under the deposits. The only "corrodents" that were sufficiently verified by analysis were the alkali sulfates, such as $K_3Fe(SO_4)_3$, Na_2SO_4, K_2SO_4, and $NaAl(SO_4)_2$, as reported by Adams and Raask.[10] Pyrosulfates were not found by any of the investigators, so there was no proof that they were involved.

In the United States, Nelson and Cain[5] demonstrated that only a liquid-phase attack could approach the high rates of metal loss and that losses resulting from gas-metal attack were orders of magnitude too low on metals such as stainless steel. The melting points of $Na_3Fe(SO_4)_3$ and $K_3Fe(SO_4)_3$ and their eutectics corresponded to the temperature range in which the greatest attack on superheaters had been observed.

Nelson and Cain[5] performed a series of laboratory tests to demonstrate that the high rates of loss could be caused by the complex liquid sulfates:

> The present work has shown that molten complex iron and/or aluminum alkali sulfates formed in fireside deposits of boilers having steam temperatures above about 950°F [510°C] are responsible for corrosion of superheater and reheater tubes. This corrosion is a chemical reaction in which tube metal reacts with molten sulfates to give iron oxide and sulfide.

> It starts at temperatures below the oxidation (scaling) temperature limit for alloys used in these sections of a boiler. Gas-phase scaling-temperature limits, therefore cannot be used to judge the suitability of a given alloy for service in an area subject to liquid-phase corrosion by complex sulfates of an ash deposit. For instance, the 321 stainless steel alloy encounters rapid liquid-phase attack at about 1025°F [551°C], whereas its resistance to corrosion by flue gas alone is satisfactory at higher than 1450°F [788°C]. Liquid-phase corrosion is bracketed between melting and maximum synthesis temperatures of the complex sulfates present on tube surface under the deposits.

The majority of investigators were in agreement that the complex sulfate mixtures and trisulfates were responsible for the metal losses but admitted doubts about how the alkali salts were concentrated at the tube walls and what actual corrosion mechanisms were involved. Based on these and other questions, a number of probe tests and laboratory tests were generated to obtain answers and to support methods of preventing the losses.

While most of the listed cases of corrosion in the United States have come from plants burning Midwestern coals with greater slagging and fouling tendencies, the problem is by no means isolated to those coals. Serious problems have also been reported with such other coals as lignite and brown coals,[11] bituminous coals of England and Europe, and even some anthracite coals.[12,13] A survey of corrosion in Russian and East European power plants was published in Teploenergetika.[14]

The alternative and conflicting theories for the causes of metal loss have apparently stimulated interest and developments in many related areas, such

as analytical methods, gas chemistry and physical chemistry of the condensed phases, and corrosion and metallurgy of materials used in boilers and superheaters.

SECTION 3
TEST PROBES AND SUBSCALE FURNACE TESTS

Section 3

TEST PROBES AND SUBSCALE FURNACE TESTS

Since realistic test planning casts considerable doubt on the possibility of duplicating commercial boiler environments in laboratory furnaces, several methods were pursued to obtain controlled experimental data within the full-scale boilers. Koopman, et al.,[15] reported on a successful test probe design for evaluating corrosion rates at the Joppa Station, Joppa, Illinois. The temperature-controlled rings were inserted over the probe and installed in the secondary superheater through an access door. Regulation of the air flow to the probe controlled the temperature of the specimens. By locating specimens properly, the temperature gradient along the length of the probe permitted a given alloy to be tested at several temperatures during a single test. Three alloys--Types T-11 and T-22 low alloy ferritic steels and Type 321 stainless steel--were tested under various conditions. Variables having the greatest effect on corrosion rate, namely, temperature of metal, time of exposure, and composition of coal, were studied. In addition, the effect of gas temperature and coal fineness on deposit formation and related chemical corrosion was investigated.

The results of Koopman, et al.,[15] confirmed the "bell-shaped" curve with maximum losses about 1200°F (649°C), and also demonstrated that the attack was not a simple function of time. After long periods of time with no losses, the attack accelerated and substantial losses were generated in a couple of hundred hours. Once the attack started, the stainless steel as well as the ferritic

alloys were subject to damaging losses at normal operating conditions. Variations in coal types were also clearly demonstrated, although the chemical analysis data were not the conspicuous explanation.

Additional data from the Joppa test probe were reported by Reese, Jonakin, and Koopman,[16] and showed more clearly the correlation of corrosion with coal composition. Coals with high, extractable, alkali content were always more aggressive and had a greater tendency to foul. Test probes have also been used to evaluate deposits and secondary reactions, such as the absorption of sulfur (SO_2, SO_3) by fly ash.[17]

A more extensive evaluation of major coal types from various mines was reported by Borio, et al.,[18,19] using a test furnace instead of the probe method. While the test furnace does not duplicate all the conditions of a utility boiler, such as temperature gradients and particle velocities, the small-scale furnace can create a standardized test facility in which to compare and evaluate materials, coals, and some combustion parameters.

The results of testing numerous coals[18,19] have provided reference data on relative fireside corrosion rates correlated with the analysis of each coal. The results were consistent with others showing the major influence of extractable alkali content as an index of relative corrosiveness. Borio, however, disagreed with Reese, et al.,[16] on the method of extracting the alkali content of raw coals. The older method used a water-extraction method, but Borio found that acid extraction provided a better correlation. The Borio results were reduced to a formula of relative corrosion index:

$$\text{Corrosion} = 5.96 + 5.07\left(\frac{Na_2O}{K_2O}\right) - 0.42(CaO + MgO)$$

The NaO and K_2O were expressed as parts per million of the dry coal and the MgO and CaO as percent by weight of the ash.

Borio, et al.,[19] concluded that the corrosion rate was apparently related to the acid-soluble sodium:potassium ratio, within the limits established by the test coals; that the corrosive effect of the alkalies in the coal could be reduced by adding calcium and/or magnesium as carbonates or oxides; and that the addition of enough calcium or dolomitic lime to control air pollution would in most cases reduce corrosion caused by complex alkali-iron sulfate attack to an acceptable level.

In 1967 Jackson[20] reviewed the methods of research used in England to determine the effect of plant operating parameters, as well as the more basic aspects of deposition and corrosion. He reported that examination of deposits from boilers yielded information only on the end products of the processes occurring during operation. In 1955 a technique was developed that essentially determined the rate of mass transfer of deposit constituents from the flue gas to the surface of a metal tube at a wide range of known temperatures. With this technique a 1-in. (25.4-mm)-O.D. heat-resisting steel probe was internally air-cooled, and the temperature gradient along the 8 ft (2.44 m) length inserted into the boiler flue gas was recorded by thermocouples embedded in the tube wall. These thermocouples accurately indicated the metal temperatures, which were automatically controlled. Observations using the technique in coal-fired boilers demonstrated the presence of volatile potassium compounds, formed probably by the postulated exchange reactions.

Paralleling the development of the deposition probe, Jackson[20] further reported, was the design of apparatus to study the reactions of pure compounds and simple mixtures in otherwise "clean" hydrocarbon flames of closely controlled composition. This concept was not fully developed until 1959 to 1961, and apparatus to study deposition under closely controlled conditions were used at the Central Electricity Research Laboratory (CERL). Results showed that at metal temperatures above 1202 to 1400°F (650 to 760°C)--depending on the concentration of sodium compounds in the flue gas--corrosion by deposited chlorides was unlikely and that on metals above 1472 to 1832°F (800 to 1000°C)--such as superheater supports--even sodium sulphate was not deposited. These results confirmed deductions obtained from deposition probe work. Jackson concluded that more comparative work of this kind should permit determination of the fuel and flue gas compositions and residence times corresponding to various proportions of sulphates and chlorides in the deposited material. [Other research sponsored by the Central Electricity Generating Board (CEGB) is discussed in Section 6 of this report.]

Tyul'pin, et al.,[21] utilized test probes and laboratory-scale furnaces to determine the performance of five types of superheater tube alloys in long-term tests in coals, oils, and gas fuels. Data are presented for the corrosion of superheater tubes of Cr-Mo-V (12Kh1MF), Cr-Mo-V-Si-B (12Kh2MFSR), Cr-Mo-V-Nb (12Kh2MFB-EI 531), Cr-W-Mo-V (1Kh12V2MF-EI 756), and 18%Cr-12%Ni-Ti (1Kh18N12T) steels up to 10^5-hour operation at 932 to 1292°F (500 to 700°C) in an atmosphere consisting of the combustion products of various solid, liquid, and gaseous fuels (anthracite, lignite, heavy fuel oil, natural gas, etc.) evaluated separately.

Another set of laboratory and industrial-scale corrosion tests were reported (in Russian) by Ots, et al.[22] The results of these tests show that the severity of high-temperature corrosion of boiler tubes depends not only on the temperature of the metal, time, type of steel, and other parameters, but also on the chemical and mineral composition of the fuel. The chlorine, sulfur, calcium, and alkali metals in Baltic shale are accelerators of high-temperature corrosion in steel. Laboratory and industrial corrosion tests were performed on Cr-Mo-V (12Kh1MF), Cr-Mo-V-Si-B (12Kh2MFSR), EI 531, EI 756, 18%Cr-12%Ni-Ti (1Kh18N12T), and 18%Cr-9%Ni-Ti (1Kh18N9T) steels, and the results were tabulated in relation to an equation involving activation energy.

SECTION 4
LABORATORY CORROSION DATA

Section 4

LABORATORY CORROSION DATA

4.1 GENERAL

The accumulated power plant experience with fireside corrosion expanded by the data obtained from the test probes and subscale furnace tests has established limitations for a workable design for the efficient utilization of coal. These limitations include the selection of coals with moderate or lower alkali levels (or coals that are acceptable based on the formula derived by Borio, et al.[19]). Another limitation is the maximum steam temperature of 1050°F (565°C) for "good" coals and of 1005°F (538°C) for fouling, marginal coals. The selection of alloys is important but does not eliminate the problem. Where cost or availability of good coals prohibits their use, some application of MgO or other fuel additives may be justified.

A substantial economic need for solving the problem of fireside corrosion has been evident for many years and has provided incentives for a number of independent laboratory research and development approaches. Some of the main areas of research have been:

- Sulfur oxidation chemistry, kinetics, and thermodynamics
- Absorption and solid-gas reactions with fly ash
- Formation and deposition of alkali salts on the surface of tube walls
- Thermochemistry and formation of alkali-iron trisulfates and other complex sulfate salts
- Corrosion reactions of the alkali-iron trisulfates and other low-melting sulfate salts

- Material evaluations of various alloys and coatings exposed to the various sulfate salts
- Electrochemical corrosion mechanisms in high-temperature salt media.

The first three areas of research listed above are included in this section. The latter four areas are discussed in Sections 5 through 7.

4.2 SULFUR OXIDATION CHEMISTRY AND THERMODYNAMICS

Studies of sulfur oxides are important in several areas, including the control of flue gas and stack gas acid problems and fireside corrosion problems. Early studies of the thermochemistry of flue gas were made by Boll and Patel,[23] who computed the equilibrium concentrations of 29 gases and five condensed phases for high and low fuel:air ratios. The data presented confirm previous observations that equilibrium concentrations of SO_3 are not produced in the hot flue gas; however, solid surfaces, such as steels, scale, and ash surfaces, catalyze the formation of SO_3 locally at the surface. Various discrepancies of computed gas concentrations compared with measured values indicated the need for more work in this area.

Hedley[24] reviewed the thermodynamics and the reaction kinetics related to the SO_3 formation in combustion flames. His laboratory tests on reaction rates indicated the presence of a homogeneous catalyst within the burner flame. Hedley suggested the possibility that the oxides of nitrogen were involved in a series of reactions like those used in the liquid-phase, lead-chamber process for sulfuric acid manufacture. One serious problem with that concept was the requirement for very high flame temperatures, 3690°F (2300 K), to initiate nitrogen fixation. Direct additions of NO or NO_2 to the flame produced a negative effect.

The catalytic effect of H_2O vapor was not considered, despite the evidence in Hedley's[24] reaction rates for that kind of a catalyst. The active species was thought to be atomic oxygen.

The SO_3 content of the gas was considered very significant because both the formation and stability of the alkali-iron trisulfate depends on higher SO_3 content than is normally found. Extensive work on sulfur oxidation was performed by Reid, Levy, and Barrett,[25-31] showing the importance of catalytic reactions. They found that catalysis alone within the flame is not responsible for the major part of the SO_3 that causes trouble, and therefore catalytic actions beyond the flame boundaries (such as solid surfaces) need investigation.

In addition, Reid, et al.,[29] suggested that the situation is complicated still further by reactions between the catalytically active surface material and the base material to which the catalyst is applied. For example, hematite (Fe_2O_3) pasted onto steel foil acts more rapidly in forming SO_3 than when the Fe_2O_3 is put on a bronze or a glass support. Hence, the oxidized or rusty surface of a superheater tube is not just Fe_2O_3 as far as the formation of SO_3 is concerned, but rather it is a complex mixture of Fe_2O_3, magnetite (Fe_3O_4), Fe, and perhaps FeO, as well as chromium and its oxides and other alloying metals.[29]

In their report Reid, et al.,[30] define "catalysis" as:

> ...the case where SO_2 and O_2 are adsorbed or chemisorbed on a surface, react there to form SO_3, and are then transferred from that surface by desorption of SO_3 into the flue gas. Another situation

> also can exist where a compound such as iron oxide may be converted into ferrous or ferric sulfate in the presence of SO_2 and O_2, and where the sulfate subsequently decomposes to release SO_3, thereby regenerating the iron oxide. Such reactions may be called "chemical reactivity", although in the total sense they are also catalytic processes because the reactant is regenerated and is used over and over again without being consumed.

According to Reid, et al.,[30] such cases of chemical reactivity have been the main subject of studies where the thermochemical reactions were investigated between SO_2, O_2, and SO_3 with Fe, Fe_3O_4, and Fe_2O_3 and with alkali in some later tests. These studies followed logically from earlier work in this area where it was found that:

- Neither SO_2 nor SO_3 reacts with Fe_2O_3 alone, but they do react with Fe_2O_3 on an iron support.
- When such reactions occur, both sulfides and sulfates are formed.
- The reactivity of Fe_2O_3 with sulfur oxides depends on the nature of the surface on which the Fe_2O_3 is supported.

Reid, et al.,[30] also discussed the major differences shown in the way Fe_3O_4 and Fe_2O_3 react with sulfur-containing flue gas. They determined that the lower oxide, Fe_3O_4--which may exist as mill scale and which is the intermediate stable oxidation product formed on an iron surface when it is heated--reacts more readily with sulfur oxides than does Fe_2O_3, while the higher oxide, Fe_2O_3, is more catalytically active than Fe_3O_4. They therefore concluded that as an iron surface is progressively oxidized, the intermediate oxide Fe_3O_4 first is chemically reactive, while the eventual oxidation product, Fe_2O_3, is catalytically active. Both processes may lead to SO_3 in the flue gas, through Fe_3O_4 by

the formation and decomposition of an iron sulfate (although this step is still not completely proved) and through Fe_2O_3 by the catalytic reaction of SO_2 and O_2. Another interesting point made by Reid, et al., was that although SO_3 is more likely to form sulfates than SO_2 even when O_2 is present, potentially SO_2 may be even more productive of sulfates because flue gas contains about 100 times more SO_2 than SO_3.

The following general conclusions were drawn by Reid, et al.,[31] from their evaluation of catalysts:

- Coatings of Fe_2O_3 applied to a steel surface or to an inert Vycor glass support serve as active catalysts in the formation of SO_3 from SO_2 and O_2.
- Coatings of Fe_2O_3 on an inert surface such as Vycor do not react with any oxides of sulfur in the gas stream.
- A complex iron-sulfur-oxygen compound is formed when Fe_2O_3 is coated on a steel substrate, through conversion of the Fe_2O_3 to the more reactive Fe_3O_4. The amount of this complex formed decreases as more SO_3 is found in the downstream gases, and as the temperature increases from 1000 F to 1200 F [538°C to 649°C].

Thus Reid, et al.,[31] concluded that the substrate bearing the Fe_2O_3 radically affects the nature of the surface coating. Although the sequence of Fe-FeO-Fe_3O_4-Fe_2O_3 on oxidized iron surfaces has been recognized for many years, it is not generally known that this same gradient in oxygen level from an iron surface to the outer oxidized layer also affects the characteristics of that surface in its reactions with sulfur oxides in flue gases.

Later work on catalytic surfaces reported by Krause, Levy, and Reid[32] utilized a micro sampling device called a microprobe for gas compositions near the surface. The test method also used radioactive sulfur (S-35) to allow detection of small amounts of sulfur and to trace specific reactants in a flowing gas mixture of SO_2 and SO_3. With a slowly flowing flue gas over a catalytic surface such as Fe_2O_3, the SO_3 concentration rose as high as 2000 ppm by volume near the surface and tapered off with increased distance from the surface, as shown in Figure 4.1.

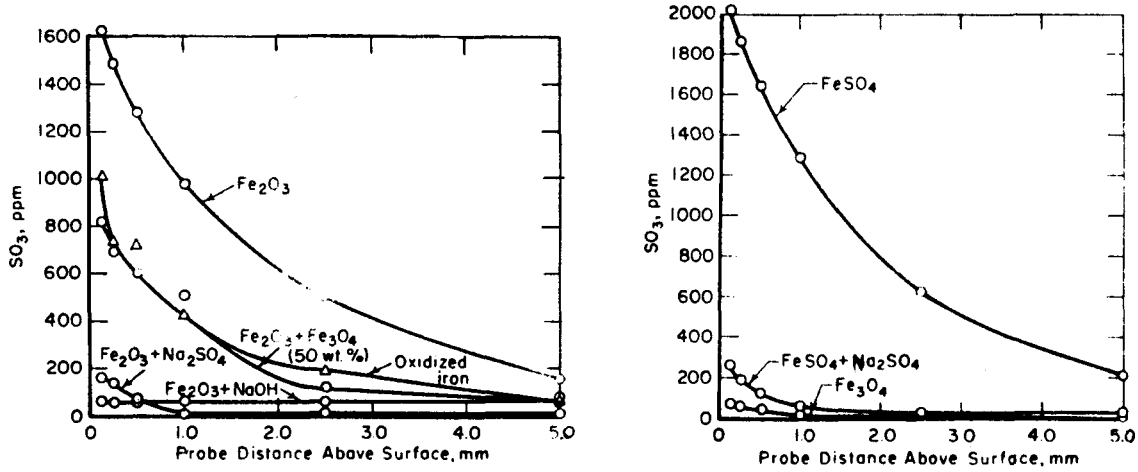

SO_3 profiles above mixtures containing Fe_2O_3

SO_3 profiles above iron oxide and sulfate surfaces

Figure 4.1 Catalytic Formation of SO_3 Producing High Concentrations Near Surface in Flowing Gas Mixture of $N_2 + SO_2 + O_2$ at 1100°F (593°C) in 5.8 Percent SO_2[32]

The radioactive sulfur (S-35) also indicated that the SO_3 was 30,000 times more reactive than $SO_2 + O_2$ in forming the complex sulfates starting with the gas mixture passing over mixed sodium sulfate and iron oxide. Later, continued work with radioactive S-35 tracer reported by Krause, et al.,[33] showed a

somewhat lower ratio for SO_3/SO_2 reactivity caused by the effect of differing oxygen levels and different surfaces. A gamma (γ) Fe_2O_3 was more reactive than an alpha (α) Fe_2O_3 (the most common form), but the gamma is only formed at lower temperatures--700 to 750°F (371 to 399°C)--by oxidation of Fe_3O_4 and is converted to the alpha at higher temperatures.

The lower-temperature studies also indicated that sodium pyrosulfate could be formed by the catalytic oxidation on surfaces below 900°F (482°C), using coatings of $Na_2SO_4 + Fe_2O_3$, despite the limited SO_3 content of the flowing gas, which is too low to stabilize the pyrosulfate.

The problem, widely recognized by those reporting research on the gas-phase and solid-gas reactions of sulfur, is that the laboratory tests oversimplify the case as it happens in actual boilers. The reported laboratory work has not obtained reaction rates that actually occur, nor has it addressed all the reactions in the gas phase or on the surface that evidently are significant. Several reactive species in the combustion flame and in the flue gas are omitted, such as SO, H_2O, SiO, KOH, and NaOH vapor. For over 30 years the alkalies (Na or K salts) have been observed to concentrate on the cooled surfaces, but the surface deposits are on the acid side (pH 3). Nevertheless, acid-base reactions in the gas phase have been generally neglected, as has the influence of acid species on the oxidation reactions.

Rasch,[34] in reviewing the work in Germany regarding fireside attack, reported some of the SO_2 oxidation studies. The heterogeneous reaction data were viewed as catalysis assisted by chemisorption of SO_2 on the surfaces. The

catalysts considered most significant--Fe_2O_3, vanadium pentoxide (V_2O_5), and vanadyl sulfate--were studied where high vanadium coals are used.

Another contribution to the SO_2 oxidation rate is H_2O vapor, as illustrated by Martin, Manning, and Reed.[35] The presence of H_2O in flue gas was shown to increase the gas-phase oxidation rate of $SO_2 + (O) \rightarrow SO_3$.

Recently, a new investigation of gas-phase species involved in coal-fired systems was begun by Milne and Beachey[36] by means of a molecular beam mass spectrometer. This program will help to identify more of the reacting species, such as SO, alkali oxide vapors, and alkali metal salts--including sodium sulfate (Na_2SO_4) and sodium sulfite (Na_2SO_3) vapors. The Na_2SO_3 also might be important intermediate species in the sequence of oxidation.

These recent developments suggest that the reactions in the gas are more complex than originally contemplated, but the equilibrium data and observations of reaction kinetics, both in the laboratory and in coal-burning facilities, are still very useful.

The observation that the effective SO_3 concentration is significantly higher than the measurable values in the flue gas has now been clarified by the catalytic studies.[32,33] However, many aspects of the problem still remain unexplained--a problem that increases in complexity, as more and more data become available, involving more and more reactions.[31] Most investigations have oversimplified the problem (unintentionally) because the experimental approach attempts to isolate individual reactions from among a maze of numerous reacting species.

4.3 ADSORPTION AND CHEMISORPTION ON FLY-ASH SURFACES

The general subject of surface reactions and absorption goes beyond the scope of this study; however, Weintraub, Goldberg, and Orning[17] performed some important chemisorption studies relating to the concentrations of reactive species entering into fireside corrosion. Samples of fly ash taken from pulverized coal-fired plants were used to examine the influence of temperature gradients on the oxides of sulfur absorbed (or chemisorbed) on the fly-ash surfaces. The study was designed to evaluate how the thick deposits of ash on tube surfaces affect the concentration of the corrosive species. The results showed that the fly-ash samples exposed to flue gas tended to concentrate sulfate or SO_3 progressively higher toward the coldest region, adjacent to the cooled surface. The high-temperature, exposed, outer deposits were depleted somewhat because of migration, but the increased SO_3 concentration in the cold layers of ash (greater than a factor of 2) proved to be that absorbed from the flue gas.

Evaluation of isothermal exposures of fly ash in the flue gas demonstrated a peak increase in sulfur compounds from the gas for exposures around 1100°F (593°C), falling off at 1400°F (760°C) and higher temperatures, as shown in Figure 4.2. The test results of the fly-ash samples from different types of coal confirmed the degree of corrosion expected from each type, as shown by the ash samples marked B-1, B-2, and C-1 in Figure 4.2. That is, the high-sodium ash (from Illinois No. 6 coal), marked M-1, produced higher concentrations of sulfates than other types of fly ash known to be less corrosive. Weintraub, et al.,[17] also noted that some alkali metal salt migrated toward the cold surface but not in proportion to the sulfate concentration.

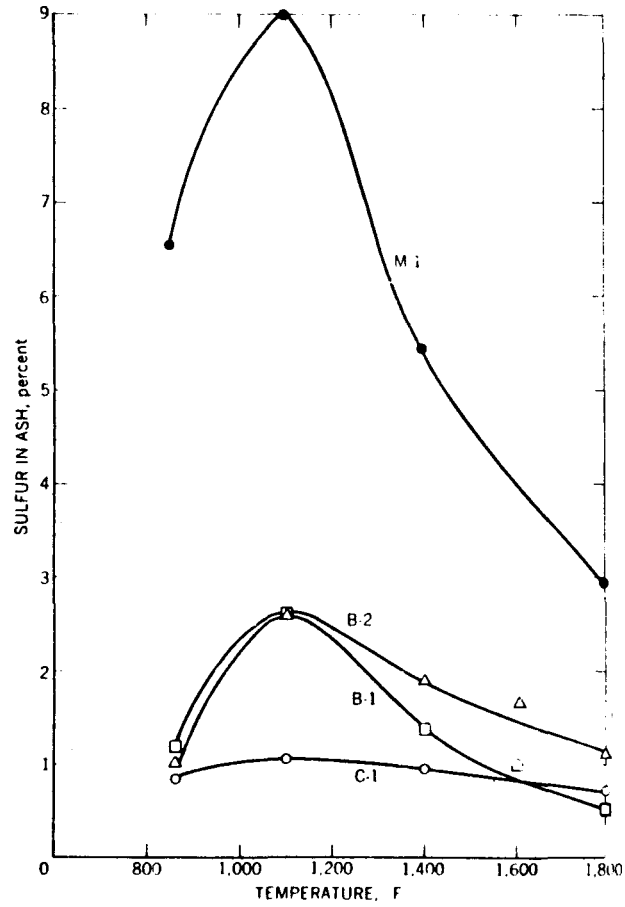

Figure 4.2 Sulfur in Ash After Exposure to Synthetic Flue Gas at Various Temperatures[17]

Rasch[34] studied the adhesion of fly-ash-produced deposits and how it varied depending on the temperatures of the gas near the substrate. Both the bonded, sintered deposits and the loose, porous deposits contributed to the formation of corrosive, molten, eutectic phases. The composition gradients within the deposits were unexplained.

Anderson and Goddard[37] determined the SO_3 pressure as a function of temperature gradients within layers of the ash deposits. They indicated that

the high concentrations of condensed-phase SO_3 were not primarily derived by selective adsorption, but rather by the catalytic activity of the SO_2 chemisorbed on the ash. The melting range of the "white layers" beneath the ash deposits (the corrosive phase) was indicated by a lower SO_3 partial pressure than occurs in the solid phase before melting (i.e., melting reduced the apparent dissociation pressure).

4.4 FORMATION AND DEPOSITION OF ALKALI SALTS ON TUBE-WALL SURFACES

The presence of increased concentrations of alkali metal compounds on tube surfaces compared with their concentrations in the ash has long been known.[1,2] The apparent mechanism for the formation of alkali salts has been the subject of much discussion and study.[38-40]

Despite significant differences in the coal analysis[39,18,20] from various areas, the corrosive deposits always contain a substantial enrichment of the alkali metal salts, including sodium and potassium sulfates and complex trisulfates comprising sodium, iron, aluminum, and other metals. The occurrence of salts on the tube surfaces has been explained in several ways, including:

- Vapor deposition on the cooled surfaces
- Liquid-phase migration through the ash deposits
- Catalytic formation by gas-solid reaction
- Particle impingement.

Bishop[9] studied the early stages of alkali deposition by means of an experimental combustor. He found that the long-term buildup in utility boilers

would be complicated by physical and chemical changes in the deposits not occurring in short, laboratory-simulation tests. The target temperature had a very significant effect on the aggregation of the deposits and on the adhesion of the deposit particles, with the greatest rate of deposit formation at 1112 ± 90°F (600 ± 50°C). The cementing matrix around deposited fly ash was described as a matrix of alkali compounds. Sodium analysis of primary layer deposits ranged from 19 to 22 percent by weight when the ash contained 6 to 7 percent by weight sodium.

Bishop[9] concluded that for chloride containing coals:

> (1) The chemical and physical character of the initial deposit depends to a significant extent upon the temperature of the collecting surface. In particular, sodium sulphate and sodium chloride do not appear in deposits formed at surface temperatures greater than certain limiting values, thereby indicating that alkali condensation is a dominant process during the early stages of deposition.
>
> (2) At surface temperatures from [932 to 1292°F] 500° to 700°C sodium sulphate and sodium chloride may co-deposit in substantial amounts and form a fused layer by eutectic reaction; this range of temperature is also found to be associated with the maximum rates of deposit collection.
>
> (3) Enrichment of initial deposits, relative to the composition of laboratory-prepared ash, is confined to the elements sodium, potassium, sulphur and chlorine. The sodium:potassium ratio of a coal is not necessarily reflected in the ratio for enriched deposits; for the coal used in these studies, potassium is deposited preferentially to sodium at surface temperatures below approximately [1184°F] 640°C.

Horn and Street[41] evaluated the chemical changes in ash minerals for samples taken at 1112 to 1652°F (600 to 900°C) from an experimental superheater. The analysis of alkali metal oxides varied significantly among the deposits from different regions. Ash deposits on higher-temperature sample probes retained lower amounts of sodium because of vaporization loss within the flames. The potassium was less sensitive to temperature because the stability of the mineral compounds allowed a portion of the potassium to be retained.

When deposits resulting from low-chloride coals are analyzed, the alkali sulfates and complex alkali-iron trisulfates are found, but not to the exclusion of other elements.[1,40] Emphasis has been on the mixed sodium- and potassium-iron trisulfate, because it has been positively identified in corrosive deposits from several sources[23,38,39] and because of its low melting points (see Figure 4.3). The low melting range of the mixed trisulfates coincides with the temperature range in which corrosion is rapidly increased and in which the chemisorption of SO_2/SO_3 is enhanced on the surfaces.

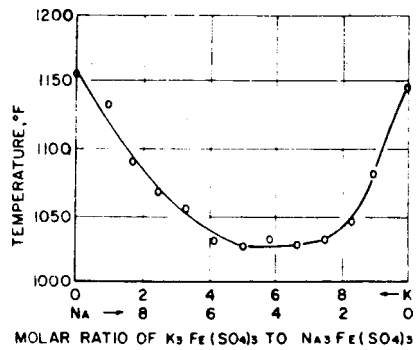

Figure 4.3 Melting Points in the Sodium- and Potassium-Iron Trisulfate[39]

The two alkali-aluminum trisulfates melt at somewhat higher temperatures--between 1200 and 1210°F (649 and 654°C)--but in the mixed alkali-iron trisulfates the melting may begin as low as 1000 to 1020°F (538 to 549°C). Lithium sulfate also lowers the eutectic melting range. The low-melting salts may be the only substance that can migrate progressively toward the tube in thick-deposit buildup areas. Some liquid flow is undoubtedly involved, as observed by the flow of fused deposits to the lower end of pendant tubes. Capillary attraction also assists the migration of fused salts toward the tube wall.

The simultaneous formation of the complex trisulfate salts with the catalytic oxidation of SO_2 on the surface of Fe_2O_3 in contact with Na_2SO_4 may be feasible (or may be accomplished in rapid sequence), since the necessary solid reactants are also catalysts for the SO_3 formation. The simultaneous reaction and catalytic oxidation of SO_2 are plausible because the conditions for both are the same, and tests by Reid, Levy, and Barrett[30,31] show that the trisulfate is formed easily in the laboratory. Further testing without SO_2 showed that although 50 ppm by weight SO_3 was retained in the gas, no catalytic oxidation occurred and no trisulfate was formed because SO_2 was absent. Therefore, it is evident that the high concentrations of SO_3 required for the formation of the trisulfate are generated on the surface of the reactants by the catalytic oxidation, rather than incrementally adsorbed from the flue gas.

The thermal migration of the liquid alkali-iron trisulfate was demonstrated by Nelson and Cain[5] using fly ash containing trisulfates distributed horizontally and heated with a temperature gradient within a silica glass tube in a synthetic flue-gas atmosphere. After 7 days, the trisulfate content in the

fly-ash samples from the lower temperature ends--900 to 1050°F (482 to 565°C)--was increased, while the trisulfate content in the fly-ash samples from the higher temperature end--1150°F (621°C) was decreased. This test was interpreted as proving that without the help of gravity, the liquid phase migrates away from the high-temperature surfaces. (Dissociation and recombination also may contribute.)

The conclusion drawn from the above several mechanisms for increasing the alkali-salt content at the tube surface is that no single process is sufficient, but rather several sources of enrichment in alkali are functioning.

When high-sodium coals are burned, some surface condensate of NaOH, KOH, Na_2SO_3, K_2SO_3, and/or Na_2SO_4 will rapidly begin on the cooled surfaces, since the boiler tubes are like condenser surfaces. The caustic deposits, if they reach the surface, would be rapidly neutralized by the acid-reacting gas. While the sulfites have been ignored, they may serve as active, intermediate compounds that are easily oxidized to the sulfates. The question of the nonequilibrium alkali containing condensable vapor compositions will be addressed more clearly by Milne and Beachey[36] as direct-sampling, molecular-beam, mass-spectra data are obtained. Milne and Beachey indicated that both NaOH and gaseous Na_2SO_4 may exist in the flame. It should be noted that extensive work on the thermochemistry of these and other compounds has been done in support of gas turbine developments which are not covered in this work.

The locations of corrosion in the superheater and reheater sections suggest that the reactive alkali is largely deposited on the impingement-exposed

tube surfaces and that heavy metal loss is normally associated with heavy ash-deposit buildup. However, isolated examples of the complex alkali-iron trisulfate away from the impingement-exposed tube surface have also been recorded.[30]

In conclusion, the enrichment of alkali salts and their migration to the tube surface may occur by two or three mechanisms, the most significant of which depends on several factors, such as location, exposure, and history of the system (boiler, superheater, and reheater).

SECTION 5
INFLUENCE OF ALLOY MODIFICATIONS ON FIRESIDE CORROSION

Section 5

INFLUENCE OF ALLOY MODIFICATIONS ON FIRESIDE CORROSION

5.1 GENERAL

When serious losses became evident on the external surfaces of superheaters, it was apparent that the problem could not be alleviated as easily as with the earlier wall-tube attack; therefore, testing of some alternate steel alloys was begun. Early results indicated that the ash deposits from the worst slagging coals attack most, if not all, tube materials to varying degrees, so little hope of solving the corrosion problems by using new materials was expressed.[1] The greatest effort in the first 25 years has been directed toward determining the cause of corrosion, classifying the types of coal, and analyzing various aspects of the flue gas and deposits; however, some material tests have been conducted.

Since the actual corrosion losses are not linear with time and the degree of attack varies from one coal to another (not to mention other variables), corrosion losses are only comparable when taken from the same test conditions and the same fuel. Borio, et al.,[19] reported peak loss rates of 0.012 to 0.013 in/yr (0.33 mm/yr) (average losses for stainless steel) and took no issue with Nelson and Cain's[5] test data showing a corrosion rate of over 1.0 in/yr (25.4 mm/yr) for Type 321SS at the same temperature. The possibility exists that both were correct based on different test periods (the latter, high rate was based on 1-week exposures); however, annual rate expressions are misleading. It is apparent that precise comparisons cannot be made between corrosion data

from one source and those from other sources; however, when internal comparisons of various materials are made under the same conditions, the relative losses may agree with other loss data when alloys are compared with their own reference material.

5.2 CORROSION OF FERRITIC ALLOYS

The early comparisons of ferritic alloys from samples of exposed superheater tubes indicated only small advantages to alloy modifications. Koopman's[15] test probe experiments were performed in the Joppa station, where corrosion troubles had been serious. Temperature-controlled rings of several alloys were inserted to produce comparable loss data as a function of temperature and material. The 1-1/4%Cr-1%Mo and 2-1/4%Cr-1%Mo losses were low, leading to the conclusion that largely gas-phase attack was being observed. Very little change was seen for the first 750 hours, after which the rate of loss rose.

Cain and Nelson[39] observed by laboratory simulation of the alkali-iron trisulfate corrosion that the advantage of going from 2-1/4%Cr to 9%Cr alloys was slight; however, some further improvement was obtained from Type 321SS, as shown in Figure 5.1. Cain and Nelson also pointed out that in all alloys tested sulfides were present in the corroded areas exposed to the liquid trisulfates. Type 321SS exhibited intergranular sulfide penetration, but only for the liquid-attacked surfaces.

Nelson and Cain[5] had previously proven that the fireside losses were not gas-phase attack but rather liquid-phase attack. The gas-phase scaling loss by Type 321SS in flue gas, for example, was less than 1 percent of the short time loss caused by the liquid alkali-iron trisulfate at 1200°F (649°C).

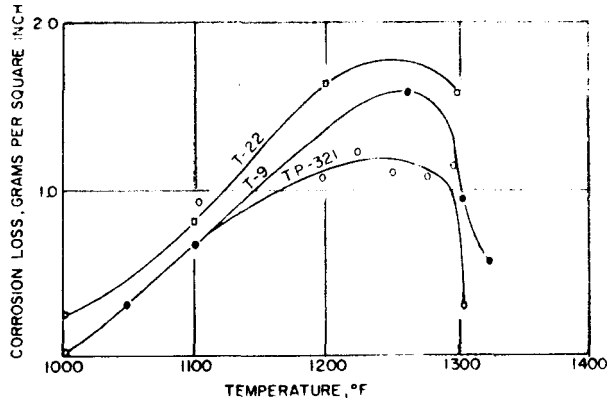

Figure 5.1 Effect of Alloying Constituents on Corrosion Rate[39]

Krause, Vaughan, and Boyd[42] evaluated seven steels, including two coated materials, for application in refuse-combustion installations utilizing coal plus refuse. The majority of data reported were for lower-temperature exposures and were not applicable to more conventional coal-burning applications. One unexpected result, however, was that additions of 0.75 percent by weight sulfur to the refuse substantially reduced the corrosion loss. The explanation for this phenomenon was that high-chloride surface deposits were prevented, or substituted, by the sulfate deposits on the surfaces below the melting points.

The laboratory data supporting the test program provide some typical comparisons of corrosion losses at varying temperatures and for several corrosive media. As shown in Table 5.1, the alkali-sulfate mixture with 1 percent by weight NaCl added was much more corrosive in the presence of SO_2 in the gas at 1000°F (538°C).

Table 5.1 Corrosion Rates for Different Salt Mixtures at Various Temperatures*[42]

Alloy	Corrosion Rate (mil/month)†					
	600°F (315°C)		800°F (427°C)		1000°F (538°C)	
	$KHSO_4$	$K_2S_2O_7$	75%K_2SO_4 25%Na_2SO_4	75%K_2SO_4 20%Na_2SO_4 5%NaCl	No SO_2 78%K_2SO_4 21%Na_2SO_4 1%NaCl	250 ppm SO_2 78%K_2SO_4 21%Na_2SO_4 1%NaCl
A106	7	24	1	18	18	73
T11	8	31	1	15	9	52
T321	18	26	0	0.5	1	16

*Synthetic flue gas: 80% air, 10% CO_2, 10% H_2O, 250 ppm SO_2.
†Mil/month x 25.4 = μm/month.

5.3 CORROSION OF AUSTENITIC ALLOYS

Sedor, Diehl, and Barnhart[8] compared Type 321SS with Type 310SS, indicating that the corrosion resistance of the higher alloy was significantly better and warranted further study. The 100-hour weight losses are shown in Figure 5.2.

The results of Sedor, et al., also indicated a peak corrosion rate at 1300°F (704°C), thus illustrating the problem of comparing data taken from different sources. The results of Cain and Nelson[39] indicated that a peak attack occurred at 1200 to 1240°F (649 to 671°C) and that the corrosion rate was much lower at 1300°F (704°C). (Compare Figure 5.1 with Figure 5.2.) The data of most investigators quantitatively affirm that the corrosion rate falls off rapidly after the peak losses. Reports[1,39] showing the lower temperature peak

and lower corrosion rates at 1300°F (704°C) were based on laboratory-simulated corrosion with a liquid phase of alkali-iron trisulfate and simulated flue gas without moisture.

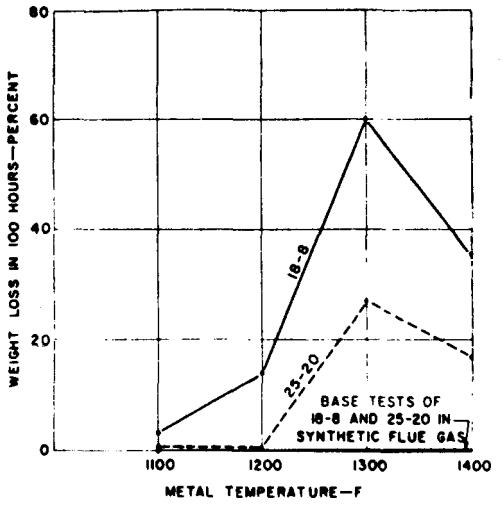

Figure 5.2 Corrosion of 18-8, Type 321 and 25-20, Type 310 by White Layer in Synthetic Flue Gas[8]

The peak corrosion at 1300°F (704°C) represents data for superheater deposits containing other metal sulfates and exposed to flue gas with moisture. The higher attack rates at 1300°F (704°C) are more realistic and result from the higher SO_3 activity in the flue gas and the superheater-generated molten sulfate deposits at that temperature, rather than from laboratory simulation. This point may be important to higher-temperature applications, i.e., corrosion probes in superheater or reheater environments are probably the most valid data, however difficult they may be to obtain. In addition, all data must be related to the specific type of fly-ash and gas environment involved.

Blank, Hall, and Jackson[43] evaluated 11 austenitic and 2 nickel-base alloys for higher-temperature superheater applications, up to 1350°F (732°C), based on 10 field test installations employing different fuels. The alloys tested are listed in Table 5.2. The various test stations were oil-, gas-, coke-, or coal-fired. However, only those stations firing oil, gas, or coke were successful in obtaining data, so coal-ash data were not included in the tabulated results. Some valid, general observations were noted, such as the catastrophic oxidation of high molybdenum and the sulfidation of nickel-base alloys. The oil-fired stations using oils with high alkali and vanadium residues demonstrated a significant corrosion attack on all materials and a severe attack on many. Types 310, 314, and 309 stainless steels were more resistant than other 300 series stainless steels and Inconel. Higher-quality fuels resulted in a much less severe attack. A partial listing of the comparative results are presented in Table 5.3. The data show that Types 310 and 314 stainless steels were better than others tested and that the molybdenum-containing steels suffered the greatest losses.

Jackson[20] reported on a number of ferritic and austenitic steels that were evaluated under simulated fireside attack using high and low chloride-containing coals. Results showed that all steels were significantly attacked and that no material selection was considered as a solution. The basic reference material was 18%Cr-12%Ni-1%Nb steel (similar to Type 347SS). While some higher alloys were marginally better, the advantages did not seem to offset other problems, such as cost. Also tested were some coatings and surface treatments, including aluminized steel, which too provided unattractive solutions.

Table 5.2 Test Materials (Composition in Percent)[43]

Material	Ni	Cr	C	Mn	Si	Mo	Other Elements
16-25-6	24.8	16.3	0.08	1.7	0.34	5.95	0.146 N_2
AISI 309S	13.8	23.7	0.09	1.4	0.58	0.03	0.132 N_2
AISI 310	20.3	25.2	0.08	1.7	0.75	0.02	---
AISI 347	11.1	17.2	0.06	1.6	0.58	0.02	0.73 Cb
AISI 308	10.0	20.8	0.06	2.0	0.38	0.24	---
AISI 309	14.54	23.12	0.13	2.0	0.40	0.15	---
AISI 314	21.45	24.56	0.09	1.3	2.20	0.13	---
AISI 321	10.36	17.72	0.07	1.4	0.47	0.15	0.45 Ti
AISI 304	8-11	18-20	0.08*	2.0*	1.0*	---	---
AISI 316	10-14	16-18	0.10*	2.0*	1.0*	2.0 -3.0	---
17%Cu-14%Mo	13-15	15.5-17.5	0.151	1.0	1.0	1.75-3.0	0.15-0.45 Ti 0.35-0.65 Cb 2.5 -4.0 Cu
Inconel	70†	11-15	0.15*	1.0*	0.5*	---	10 Fe*
Illium G	58	22	---	1.2	0.4	6.0	6.0 Cu 6 Fe
Aluminized§ mild steel	---	---	---	---	---	---	---

*Maximum.
†Minimum.
§Aluminum-coated samples of cold-rolled steel.

Table 5.3 Corrosion Data for Material Exposed to Various Combustion Atmospheres[43]

Alloy	High-Sulfur, High-Vanadium Fuel Oil*			High-Alkali Coke and Blast-Furnace Gas†		
	Weight Loss (g/in^2/month)	Decrease in Diameter (in/month)	Maximum Depth Subsurface Attack (in.)	Weight Loss (g/in^2/month)	Decrease in Diameter (in/month)	Maximum Depth Subsurface Attack (in.)
Aluminized steel	1.451	§	None	2.535	§	0.008
Illium G¶	0.835	0.0062	0.002	1.290	0.0093	0.036
Inconel	0.455	0.0032	0.009	1.762	0.0134	0.035
17%Cu-14%Mo	**	**	**	1.808	0.0139	0.010
AISI 316	2.029	0.0156	0.006	0.785	0.0061	0.008
AISI 308	0.543	0.0042	0.001	0.618	0.0048	0.001
AISI 321	3.452	0.0266	0.002	0.945	0.0075	0.005
AISI 314	0.867	0.0068	None	0.078††	0.0006	None
AISI 309	0.681	0.0052	None	0.493	0.0038	0.002
AISI 304	1.439	0.0110	None	0.783	0.0061	0.005
AISI 347	1.492	0.0114	0.001	0.643	0.0049	0.003
AISI 310	0.310	0.0023	None	0.048††	0.0004	0.005
AISI 309S	0.183	0.0013	None	0.210††	0.0016	0.001
16-25-6	**	**	**	0.810	0.0062	0.008

*Sewaren Station, 1300°F (704°C).
†Penwood Station, 1250°F (677°C).
§Because of uncertainty of density figure required in calculation, conversion to inches of radius lost per month could not be accomplished.
¶No specimens available for 4 of 6 stations.
**Specimens completely corroded away.
††Slight pitting occurred.

Without a definition of the mechanism(s) of attack, there have been no attractive leads as to what kind of material developments should be pursued for the solution to the corrosion problem.

Horn and Street[44] evaluated two austenitic alloys in comparison with one nickel-base alloy in a coal-fired experimental superheater designed to investigate problems associated with heating steam to 1400°F (760°C). The alloys tested are shown in Table 5.4.

Table 5.4 Percentage Composition by Weight of Tube Alloys Tested

	Material									
Alloy	Cr	Ni	Mo	Co	Nb	W	Ti	Al	C	Fe
G19	19	13	2	10	3	15	---	---	0.4	bal.
Nimonic 90	20	bal.	---	18	---	---	2.3	1.4	0.08	3
AISI Type 347SS	18	12	---	---	1	---	---	---	0.07	bal.

A series of tests was performed with the experimental coal-fired superheater consisting of parallel loops of the three different alloys in each test run and employing four different coals at different times. Conclusions based on metal wastage from 1022 to 1560°F (550 to 850°C) after only 100-hour exposures were:

- None of the three alloys were resistant to fireside corrosion when "aggressive" coals were used.
- All three alloys were attacked less when low-alkali coal was used.

- The bell-shaped curve (such as that shown by Cain and Nelson[39] does not drop off sharply at 1300°F (704°C) and above, as laboratory results suggest. For actual coal-fired systems, the attack at 1400°F (760°C) was still serious; however, it was reduced to low values at 1560°F (850°C).

- In the higher-temperature test comparisons, the Nimonic 90 alloy suffered less attack than the others and the G19 alloy had slightly lower losses than Type 347SS.

- In the higher-temperature area of 1450 to 1472°F (789 to 800°C), less general attack was observed but a few severe pits 0.014 to 0.016 in. (0.35 to 0.40 mm) deep occurred.

Parker, Rosborough, and Virr[45] reported 10,000-hour corrosion data obtained from test probes at the Marchwood Power Station. The oil-derived deposits and the flue-gas attack are not suggested as representative of the conditions produced by coal-derived deposits, but the results are of general interest in cases where high sulfur is present and low excess oxygen is employed. The high-chromium ferritic alloys were the best-performing alloys in oil ash, while the austenitic stainless steels suffered three to four times greater losses at 1112 to 1202°F (600 to 650°C) because of scaling and spalling of the scale. The ferritic alloys did not exfoliate excessively.

5.4 HIGH NICKEL AND EXPERIMENTAL ALLOYS

Lewis[46] and Lewis and Smith[47] reported on the relative corrosion resistance of a number of high-chromium alloys subjected to fuel-ash-corrosion conditions, with the main emphasis on higher-temperature-oil applications. Their crucible-type test provided differences in resistance which were very dependent on the V_2O_5, NaCl, and other variations in the fused salt media. The results favored such alloys as 50%Cr-50%Ni and 60%Cr-40%Ni, based on 300-hour immersion

losses. Corrosion resistance could not be correlated with chromium content alone, and many high-chromium alloys were seriously attacked.

W. J. Greenert[48] reviewed the history of failures in marine boiler service, largely relating to fuel-oil deposits. While testing of materials in a mixed alkali sulfate-chloride slag is of interest, most data apply to higher vanadium-accelerated attack, which is not within the scope of this study. In the laboratory evaluation using Na_2SO_4-10%NaCl, several materials of interest were shown to offer improved resistance, including 50%Cr-50%Ni, 100%Cr, and 25%Cr-5%Al-balance Fe. Tests were in molten slags at 1600°F (871°C) for a few hours in oxygen. Two high-manganese alloys (one of which was 14%Cr-14%Mn-balance Fe) showed better corrosion resistance than the stainless steels.

Rahoi[49] has evaluated the application of 50%Cr-50%Ni alloys for cladding on Incoloy 800, based on the results of Lewis[46] and others contributing to the corrosion data. (Typical losses for fireside corrosion were given as 1.3 to 1.9 mil/yr (0.0033 to 0.0048 mm/yr).[49] The successful cladding of Incoloy 800 with IN-671 makes the composite tube appear promising from an engineering feasibility viewpoint. The composite tube is not regarded as impervious to coal-ash corrosion resulting from "aggressive" coals but will extend the tube life under those conditions and perhaps be satisfactory with some coals that seriously attack Type 304SS. More data for corrosion rates under those conditions are needed.

5.5 CONCLUSIONS

The problem of interpreting the behavior of individual alloy elements is caused by the complex electrochemical relationships between the corrodent

and the alloy surface. Most of the major alloy elements, such as iron, nickel, manganese, chromium, and aluminum, form sulfates when corroded and thus alter somewhat the properties of the fused alkali-iron trisulfate. The loss observed when thin layers of deposits are present will not be the same as the loss observed when a large amount of alkali-iron trisulfate is present because of the potentially significant chemical changes within the fused salts. Also, although the new metal surface may show some reasonable polarization because of the passive film, after some exposure the properties are not the same. Some beneficial effects of manganese and silicon in austenitic steels have been observed but have not been studied sufficiently to make their application practical.

Another observed problem related to surface condition is that annealed stainless steels or oxidized surfaces are subject to greater losses than machined or abraded surfaces. This condition suggests that micro-heterogeneities on the surface, such as minor chromium depletion caused by heat treatment, will assist in initiating the electrochemical mode of attack.

The problems of the surface condition have not been accurately defined, but such a study may be very helpful.

SECTION 6
CORROSION AND SULFIDATION MECHANISMS RELATED TO FIRESIDE CORROSION

Section 6

CORROSION AND SULFIDATION MECHANISMS RELATED TO FIRESIDE CORROSION

6.1 INTRODUCTION

The pursuit of understanding the controlling and functioning corrosion mechanisms has continued sporadically for over 30 years. A correct understanding of such mechanisms may be the best hope of effectively combating the serious metal wastage and the costly temperature and fuel restrictions. However, the trial-and-error approach is also occasionally successful.

A popular approach has been to analyze the simplest mechanisms and use some better-established models (such as oxidation of iron) to serve as a guide. This approach easily eliminates the gaseous oxidation concept as the primary reaction, since the loss rates of fireside attack are about one order or two orders of magnitude too high and the differences between low alloys and stainless steels may be very small. The conclusion of this comparison with gas-solid oxidation, as cited by Nelson and Cain,[5] leads to liquid-phase attack (see Figure 6.1).

This discussion of mechanisms will be limited to those involving a liquid phase, although obviously secondary oxidation and sulfidation will also occur and solid-phase reactions and diffusional changes in the alloy tubes are also functional and may contribute to the overall loss. In spite of general agreement that a complex molten salt attack was indicated by the numerous examinations and test data, the conceptual reactions involving simple chemical

solution of the oxide or oxidation and solution of the metal by the liquid salts was not possible to convincingly substantiate.

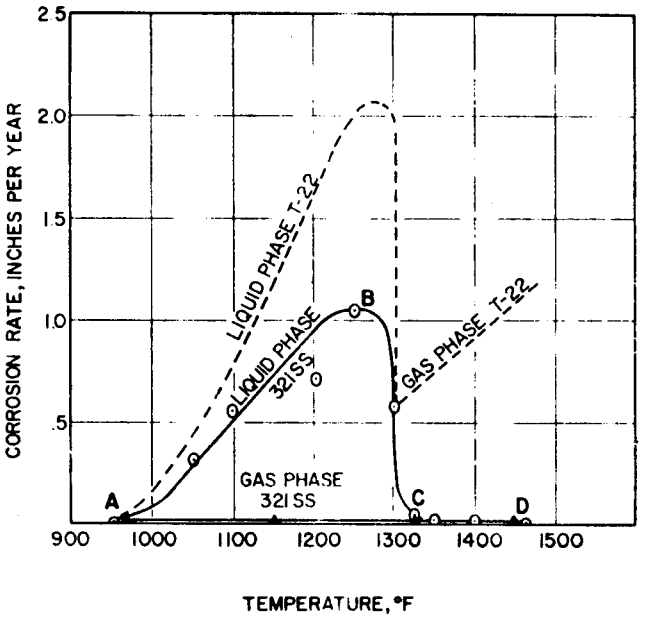

Figure 6.1 Liquid-Phase Corrosion Indicated by Rapid Metal-Loss Rates During 5-day Exposures to Simulated Fireside Corrosion[5]

6.2 LIQUID-PHASE CHEMICAL ATTACK

Two different fused-salt reaction mechanisms are widely discussed in the literature. One of these mechanisms includes the concept of Corey, Cross, and Reid,[1] who suggested that a rapid oxidation film forms which is destroyed by the reactions forming the alkali-iron trisulfates, namely:

$$3K_2SO_4 + Fe_2O_3 + 3SO_3 \rightarrow 2K_3Fe(SO_4)_3$$

and

$$3Na_2SO_4 + Fe_2O_3 + 3SO_3 \rightarrow 2Na_3Fe(SO_4)_3.$$

Thus the iron oxide is consumed by the formation of the alkali-iron trisulfate. Since none of the reactants are liquid in the exposure range in which these reactions presumably occur, the initial start-up of these reactions is difficult, requiring either a 3-component solid-solid-gas reaction or a liquid salt derived from some other means.

Nelson and Cain,[5] on the other hand, proposed that the trisulfates supply reactive sulfate ions that attack the metal directly, namely:

$$3Fe + SO_4^{--} \rightarrow Fe_3O_4 + S^{--}.$$

The dissociation of the trisulfate generates K_2SO_4 or Na_2SO_4, which will later recycle.

One major constituent of the liquid-salt phase is $KAl(SO_4)_2$, which is presumably derived from the ash constituents and may serve to stabilize the molten sulfates, since no Al_2O_3 or other Al by-products are found. In the case of corrosive attack on stainless steels, nickel is often found in the complex sulfate layer, but chromium is normally present as Cr_2O_3 in the corrosion products. Both of these concepts have some inadequacies, such as explaining why the attack is frequently severe in one or two isolated areas but much less severe at a location that is a short distance away yet covered with the same deposits. Also, the oxidation-solution sequence seems inadequate to explain why alloying the steel has so little effect on the loss. The initial oxidation rates for high-chromium alloys, stainless steels, and nickel-chromium alloys are about a factor of 10 lower than low-alloy steels, but the liquid-phase fireside-attack loss rates were only about a factor of 2 lower for the high alloys.

Adams and Raask[10] suggested that the loss of protective Cr_2O_3 films may have occurred by the SO_3 oxidation forming a volatile CrO_3 that is dissipated; however, since the local deposits of sulfides at the metal surface are the result of low oxygen activity, it is very doubtful that CrO_3 could have been formed. In addition, the vapor pressure of CrO_3 is too low below 1560°F (850°C) for significant vaporization.

Rasch[34] added the alternative suggestion that sulfides were formed in such concentrations that a low-melting sulfide-containing eutectic was formed and later decomposed. The deep, rounded pits observed were described as "melted-out craters" containing some sulfide residues. The available information on metal-sulfide melting points tends to discredit any possibility of fused sulfides (except for alloys of 70%Ni or higher) at the boiler or superheater temperatures.

While several alternative concepts of direct chemical attack have been suggested and may be plausible based on indirect evidence, they are not supportable on the basis of more direct testing.

6.3 ELECTROCHEMICAL MECHANISMS OF CORROSION BY FIRESIDE DEPOSITS

One clue to the mechanisms of attack that was overlooked for a long time was the nonuniform distribution of metal losses and pitting. Among the numerous observations of corrosion on the tubular surfaces of boilers, superheaters, and reheaters, not one case of uniform attack has been reported. A common example of the maldistribution of attack was shown by Nelson and Cain,[5] as illustrated in Figure 6.2. The greatest losses, represented by the black areas at points C

and D, were not in contact with the heavy deposits, above point A. Point B may have only an oxide scale. If a simple liquid-salt solution attack occurred, the losses would be more uniform or would increase under the heavy deposits.

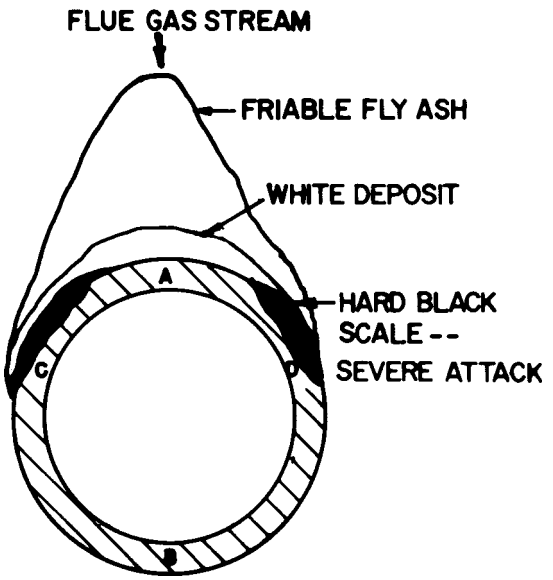

Figure 6.2 Ferritic Reheater Tube With Deposit

6.3.1 Prerequisites for Electrochemical Attack

The prerequisites for electrochemical attack can be expressed as:

- A conductive fluid in contact with the metal (The fused salt meets that requirement.)
- A source or sources of potential differences caused by surface conditions or materials differing from the basic alloy (Oxides, sulfides, or solid deposits may provide potential differences.)
- Ion mobility or convection to move corrosion products. (The molten sulfate is assumed to provide such a requirement.)

There is no fundamental reason preventing significant corrosion currents from passing within small cell areas.

6.3.2 Electrode Potentials and Electrode Reactions

The necessary potentials that are the primary source of electrochemical corrosion currents are easy to predict from the electrode reactions but not so easy to measure. The potentials for individual electrodes are normally measured against a standard reference electrode operating at the same temperature and environment.

Hills[50] indicated that the fused sulfate salts provide a medium for relatively fast reactions at high temperature, including the electrochemical oxidation at the solid-liquid interface. This anode oxidation reaction is reversible:

$$Fe \rightleftarrows Fe^{++} + 2e^{-}.$$

However, an irreversible reaction is also competing at the surface:

$$4Fe^{*} + SO_4^{--} \rightarrow 4Fe^{++} + 4O^{--} + S^{--}$$

with secondary reactions

$$Fe^{++} + S^{--} \rightarrow FeS$$

and

$$Fe^{++} + O^{--} \rightarrow FeO + O \rightarrow (\text{etc.}).$$

Another secondary reaction is possible:

$$Fe^{*++} + SO_4^{--} \rightarrow FeO + SO_3.$$

*Or other metals.

Cathode reactions are:

$$SO_4^{--} \rightleftarrows SO_3 + O^{--}$$

and

$$O^{--} \rightarrow (O) + 2e^-.$$

The cathode reactions are influenced by

$$SO_{3(gas)} \rightleftarrows SO_{3(liquid)} \text{ and } O_{2(gas)} = O_{2(liquid)}.$$

Other anions in the fused salt, such as PO_4^{---}, $Cr_2O_7^{--}$, and MoO_4^{--}, also affect the electrode potentials.

Hills[50] pointed out that the pure metals used in most structural materials (Al, Ni, Fe, Cr, etc.) all reduce sulfate ion and thus do not exist in equilibrium with fused sulfate salts. Since potentiometric measurements are thus limited, voltametric, nonequilibrium measurements are favored. The pulse methods of polarography using pulses from seconds to microseconds were investigated.

Burrows and Hills[51] obtained some electrode potentials in molten Li_2SO_4/K_2SO_4 at 1158°F (625°C) using an Ag/Ag_2SO_4 reference electrode. The measurement attempted with iron was uncertain and not reproducible because of the side reactions with the melt, but the estimated potential for iron was 0.93 V. The data also indicate that the cathodic reduction of sulfate underlies the corrosion processes found in service, namely:

$$SO_4^{--} \rightleftarrows SO_3 + O^{--}$$

and

$$O^{--} \rightarrow (O) + 2e^{-}.$$

This sulfate reduction, although not rapid, occurred in small concentrations of dissolved SO_3, as indicated by voltametric techniques.

All the data relating to sulfate systems emphasize the role of dissolved sulfur trioxide in the corrosion of metals. Burrows and Hills[51] indicated that the reduction of SO_3 to SO_2 and O^{--} has been well established and that the molten sulfates would be much more corrosive if the dissociation rate of SO_4^{--} were faster. According to Burrows and Hills:[51]

> A crucial role is played by uncharged species which are both oxidizing and acidic and which in the case of sulphates are almost certainly dissolved SO_3 and possibly also SO_2.

6.3.3 Gas Atmosphere Tests and Their Effect on Electrochemical Attack

The difference in flue-gas exposures resulting from variations in ash coverage are among the obvious physical effects that may alter the chemical attack. In a discussion of Burrows and Hills work, Fountain[51] contributed data obtained for the CEGB. When three different alloys were exposed to fused sulfates (Li_2SO_4/K_2SO_4) at 1112°F (600°C) under air atmosphere, a characteristic potential time curve was observed that clearly indicated the formation of passive films on austenitic stainless steels but not on ferritic steels, as shown in Figure 6.3. To evaluate differential aeration, a second series of tests was performed in which some steel samples were completely immersed in fused sulfate

while some were only partially immersed. After about 100 hours at 1112°F (600°C), the completely immersed samples of austenitic steel were comparatively bright and uncorroded, whereas the partially immersed specimens were badly pitted for about 2 in. (51 mm) above the melt surface. That region was covered with a black paste of oxide and fused sulfate. The part of the specimen below the melt was in most cases not too badly corroded apart from some tapering of the tip.[51]

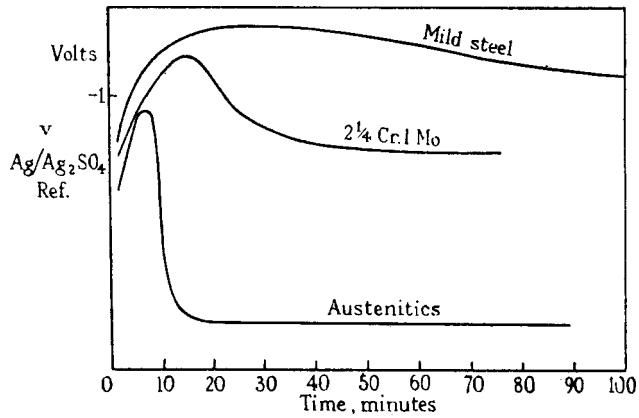

Figure 6.3 Potential Time Curves of Three Alloys in Fused Sulfate in Air[51]

A similar test that added 10 percent $K_2Fe(SO_4)_3$ resulted in catastrophic corrosion of all specimens when SO_3 was liberated and destroyed the apparent protective mechanism. We can therefore conclude that differential SO_2 and SO_3 aeration undoubtedly plays a significant role in fireside corrosion.

Reid, Krause, and Barrett[52,53] tested several types of electrochemical cells under fireside corrosion conditions in a laboratory combustion chamber to

determine the measurable anode potentials associated with alkali-sulfate corrosion. The tests showed sharp increases in anode potential when the temperatures approached the expected corrosion temperature, but the peak voltages (0.82 V) dissipated rapidly as corrosion proceeded (or as the irreversible reaction forming oxide + sulfide proceeded). The same test was repeated using a preoxidized steel electrode and similar results were obtained.

The anode potential using a preoxidized steel anode also demonstrated[52] a sharp increase in potential at about 1030°F (554°C), at which temperature the sodium-potassium-iron trisulfate forms and melts. Stable potentials were not possible, however, since the voltage decay was significant in 1 hour. (The possibility of a nonrepresentative cathode reaction involving iron, FeO, etc., plating-out on the platinum reference electrode was not determined.) The behavior of the test cells was typical of aqueous electrochemical systems with slight or marginal polarization tendencies.

Earlier tests by Reid, Krause, and Barrett[54] employed a nickel oxide cathode and a carbon steel anode covered with a mixture of alkali sulfates and Fe_2O_3. This electrochemical cell in the presence of a flue gas at 1000 to 1200°F (538 to 649°C) would clearly show when the trisulfate was being formed. In other words, a sulfur-free flue gas produced no potential; however, when combustion produced SO_2 and SO_3, a corrosion potential was measured. After repeated firings the NiO/Ni electrode was eliminated because of a reverse polarity condition. Since small currents had been passed through the cell, some plating of Fe or FeO on the cathode may have occurred.

Another significant observation made by Reid, Krause, and Barrett,[54] which was also suggested by Nelson and Cain,[5] was that while fireside corrosion required the liquid phase for start-up, corrosion did not stop at the freezing point on cooldown. After the trisulfates were formed on the surfaces bridging the anode and cathode, some residual corrosion continued on cooldown through the freezing point. This indicates that the ion mobility and diffusion of SO_3 were sufficient for continued attack below the freezing point, like a "dry cell" formed by freezing a fused salt cell. The easiest way to terminate the corrosion after it was started was to eliminate SO_2 or SO_3 from the flue gas.

6.3.4 Electrochemical Corrosion Meter

One application of the direct-reading electrochemical cell was the development[54] of an experimental corrosion meter that could be inserted into a coal-fired boiler or superheater area to identify whether fireside corrosion conditions exist, and possibly how severe. The same problem of electrode stability was observed, and fresh metal surfaces gave clear indications of corrosion, but after a few hours the potential decay caused by electrode changes made the validity of the readings questionable. Since the anode must be representative of steels exposed to the corrosion, it most likely will not last a long time under corrosive conditions. The cathode was also affected, since platinum is affected by iron and iron compounds at the elevated temperatures.

If a longer life-corrosion gage were to be developed, it would probably require a protected reference electrode and a renewable wire anode pulled in from a reserve spool so that a fresh alloy surface could be exposed.

6.3.5 Polarization Effects

The effects of electrochemical polarization are suggested by the variable and unpredictable nature of the attack. Frequently, the case histories in boilers indicate that a long period of no serious loss is terminated by rapid corrosion losses where none of the known operating parameters are changed. While this behavior may easily be dismissed as a slow buildup of deposits prior to formation of the aggressive trisulfates, it is also possible that the initial polarized condition was overcome by higher corrosion potential (in effect, penetrating a marginal, protective film) and that corrosion was accelerated. It is apparent that polarization is less conspicuous than most of the other corrosion parameters, but it may be very significant.

The corrosion potentials indicated by the experimental cells of Reid, Krause, and Barrett[52,54] demonstrated a decay rate that may have been caused by more than one process. While the changes at, or plating-out on, the cathode were probable, some tendency toward polarization at the anode would also be expected. Others, including Burrows and Hills[51] and Rahmel and Tatar-Moisescu,[55] have isolated the anode reactions and found some polarization that may be from porous surface films. Concentration-gradient effects may also be significant based on the sensitivity to gas-atmosphere changes observed by Reid, et al.[51,54] The crucial role of the dissolved SO_3 has been frequently pointed out and may well be depleted because of corrosion. Cutler, et al.,[56] observed that the electrochemical corrosion rates rose sharply with increased SO_3 in a fused alkali sulfate electrolyte and a stainless steel anode. He also described the low corrosion current with low SO_3 as surface protected by a passive oxide on the anode.

The investigations reported by Cutler and Grant[57] using a purely alkali sulfate eutectic melt (Li, K, Na) show that the polarization phenomenon followed by a breakaway corrosion rate is a general case that presumably applies to most structural materials. The model used describes the passive condition as an oxide film that may be dissolved by the liquid phase or possibly penetrated by the sulfide formation at the alloy-scale interface. Sulfidation was described as caused by the depressed oxygen activity under the scale because of limited diffusion rates in solid and liquid phases, not necessarily suggesting the electrochemical reduction of SO_2. The evidence for the electrochemical attack of the alloy as a general corrosion mechanism in fused sulfates was substantial.

The sulfidation mechanism of Cutler, et al.,[56] elaborates on the thermodynamic approach discussed by Rahmel,[58] Gulbransen and Jansson,[59] and Seybolt.[60] The thermodynamic treatment is not an alternative view from electrochemical treatment of the corrosion mechanism, but rather supplements and qualifies the proposed equilibrium reactions.

Cutler's[56] measurements of the anode and cathode properties of the unpolarized alloy surface allowed computation of the corrosion current and the corrosion rate. The measured corrosion currents of a stainless steel responded to increases in SO_3 partial pressure, as presented in Figure 6.4.

A series of electrochemical investigations by Jäkel and Schwenk,[61] Rahmel and Tatar-Moisescu,[55] and Rahmel[62,63] defined the regions of polarization on the corrosion potential-anodic current density curves. In the case of all the common, heat-resistant alloys a passive region at negative potentials was reported,

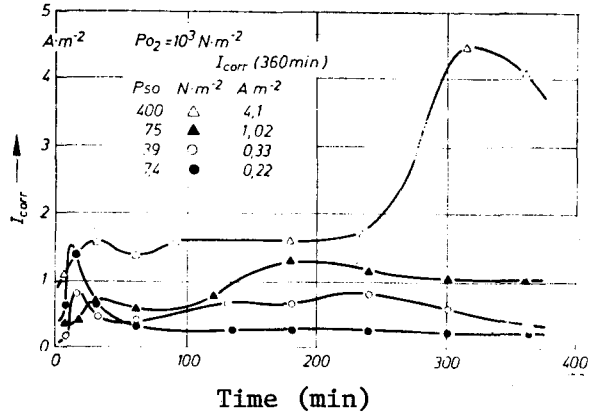

Figure 6.4 Effect of SO_3 Partial Pressure on the Corrosion Current on an 18%Cr-8%Ni Electrode at 1112°F (600°C)[56]

showing very low corrosion rates. Above a critical potential, however, a breakthrough occurs which is described as a "transpassive region." In this region of rising potential, the metal surface is covered by a porous film and corrosion currents increase.

The normally passive condition can be upset by cathode stimulation, which may trigger a breakthrough potential at the anode. Among the several significant cathode stimulants are the acid-acting species: SO_3, V_2O_5, and MoO_3. Since the SO_3 is already present, cathode stimulation is interpreted as a minor increase concentration of SO_3 on cathodic surfaces which is sufficient to generate sizable, potential changes that may be destructive to a passive film condition. Rahmel[63] suggested that molybdenum as a corrosion product of Mo-containing alloys and vanadium from some coals may be oxidized to MoO_3 and V_2O_5 within the deposits and also stimulate the cathode potential.

6.3.6 Electrochemical Cell Initiation

The questions of what starts the whole process, what condition or material starts the cell process, and whether the anode or cathode reaction is the prime mover must be addressed.

The data from Rahmel[62] indicate that the cathode stimulation mechanism may be the process initiator. If the anodic surface developed first, the metal removal, functioning like electropolishing, might turn it off. The cathode, on the other hand, would initiate a potential by simply providing electrons to an acceptor, such as SO_3, with the chemisorbed oxygen bond serving as a bridge to the metal surface.

Normally the "passive" film on the surface may be the adsorbed oxygen or the oxide film, making nearly all the alloy surface equally repulsive to the ions of the fluid. The surface oxides may not be a well-developed oxide lattice, since the metal lattice epitaxy causes defects. Such acids as SO_3, MoO_3, and V_2O_5 are electrically neutral, but normally in very low concentration.

The SO_3 finds the alloy surface at defects in the passive film and by picking up electrons from the alloy creates the site for a new cathode, as illustrated in Figure 6.5. Cathode stimulation penetrates passive films by electron transfer to acid (SO_3) that can accept electrons. The anode surface will release metal ions and supply electrons to the cathode. Completed cathode reactions may be:

$$SO_3 + 2e^- \rightarrow O^{--} + SO_2$$

or in areas of low oxygen activity:

$$SO_3 + 4e^- \rightarrow S^{--} + O^{--} + O_2.$$

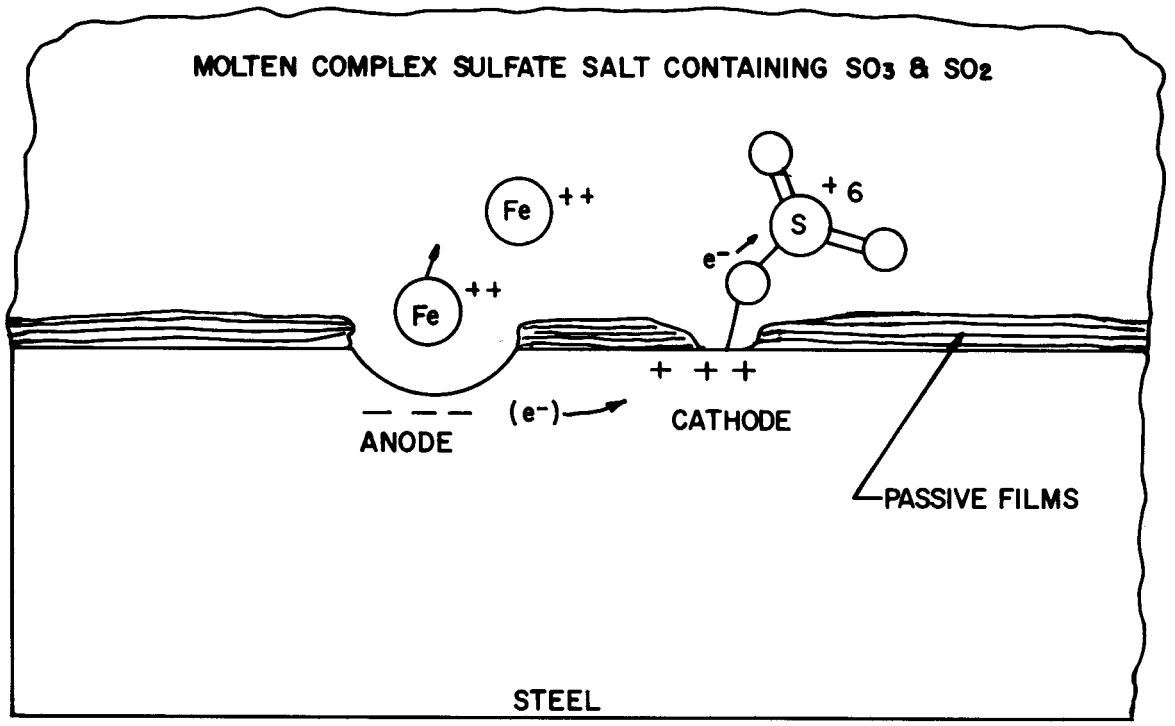

Figure 6.5 Schematic of Cathode Stimulation Penetrating the Passive Film

The fused alkali sulfate provides the following environment and materials for the corrosion current to continue:

- Supplies SO_2 and SO_3 to the cathode surface
- Makes electrical circuit complete
- Provides a matrix for metal ions to be picked up from the anode, thereby allowing ion mobility
- May serve as a depolarizing medium to prevent static charge buildup.

In short, the fused complex alkali sulfates are corrosive because they supply the surface environment with the potentially high SO_3 concentration necessary to penetrate the passive films. While the sulfate ions greatly outnumber the aggressive, oxidizing acids, they do not react spontaneously with the metal.

The once-stimulated cathode-anode current may result in a reduction of sulfate and may also plate-out some ions or metals that are in solution at the cathode. The secondary reactions in the matrix near the cathode may oxidize the metals and form oxide and sulfide by-products.

Possibly the fused sulfate melt by its equilibrium dissociation continues to supply SO_3 to the cathode surface while elsewhere a catalytic surface is generating more SO_3 from SO_2 and dissolving into the melt. The detailed chemistry of the formation and equilibria in the complex sulfate melt is still rather speculative.

6.4 EFFECT OF CHLORIDE ADDITIONS ON CORROSION MECHANISMS

While the chloride content of most coals is low enough to be considered insignificant, several studies of its effect have been conducted because British and European coals do contain measurable chloride.

During the start-up of a new system, the volatile KCl and NaCl from high-chloride coal combustion condenses out on the tubes together with the initial sulfate salt deposits. The chloride may be reduced in volume before the liquid-phase salts are formed and thus is not high in the fused sulfate corrodent unless the chloride in the coal is greater than the sulfur content.

The effects of chloride additions on sulfate attack were evaluated by Halstead and Hart[64] in relation to moderate and high-chloride-containing coals. The case histories of chloride deposits vary widely from minor to measurable chlorides in the residual deposits after long service. The reason for the elusive behavior of chlorides as a function of time of service was suggested to be the formation of a volatile species, such as $AlCl_3$. When reducing or nonoxidizing gas conditions exist, the chloride content and its effect on metals was much greater than for systems with excess oxygen in the flue gas.

In the case of coal-burning plants generating alkali-sulfate deposits (forming liquid alkali-iron trisulfates), the contribution of chloride to the already high metal losses will be small. However, in the cases of limited sulfate attack, the chloride effect may be significant. The severe cases of metal wastage studied by Halstead and Hart[64] were either quite high in chloride or were subject to oxygen-deficient flue gases--sometimes fluctuating between oxygen excess and oxygen deficiency.

In the electrochemical mechanism studies conducted by Rahmel,[62] the alkali-sulfate melts at 1160°F (627°C) with 10 percent (mol %) Cl^- so that an increased corrosion current was observed, but at 1 percent Cl^- the difference was marginal. Some cathodic reduction of SO_4^{--} ions was suggested as a possibility. Cutler, et al.,[56] also reported an initial corrosion rate increase at 1112 to 1202°F (600 to 650°C), but the effect fell off rapidly with the formation of an oxide layer.

At higher temperatures the effects of chloride may add other significant modes of attack. However, work performed for the hot corrosion studies for aircraft gas-turbine applications is outside the scope of our present task.

SECTION 7
SURFACE TREATMENTS AND COATINGS FOR FIRESIDE APPLICATION

Section 7

SURFACE TREATMENTS AND COATINGS FOR FIRESIDE APPLICATION

The experimental approaches for remedial measures to prevent excess fireside losses include:

- Installation of metal shields over superheater surfaces to catch the deposits
- Alloy cladding of tubes before fabrication
- Use of diffusion alloy surfaces, including chromizing and aluminizing
- Use of various coatings to protect or isolate the surface from corrosive liquid-sulfate deposits.

7.1 METAL SHIELDS

The first apparently successful method of attacking the fireside corrosion problem was to install shields over some of the reheater tubes to separate the deposits from the heat-transfer surfaces, as reported by Nelson and Cain.[5] Since the shields were separated by a gap, the shield surface temperature was allowed to rise--from 1400 to 1500°F (760 to 816°C)--thus providing low rates of attack on the shields and making heat-transfer dependent on radiation. To avoid their welding to the reheater tube, the shields were mechanically attached with a strap. The report[5] shows that the tube surfaces below the shields were in excellent condition after 10 months and that the shields were still intact.

Problems with shields, however, do exist. Because of changes in the heat transfer and the spacing of tubes, some increased volume is required for the reheater and must be compensated for in the design. In addition, there

appears to be a problem of deslagging when heavy ash deposits accumulate, and the possibility of damaging or losing the thin shields is obvious. The shields must also compensate for the difference of expansion, since they will operate about 400°F (222°C) above the coil temperature. Only limited use of this technique has been reported in the United States because of cost and servicing problems. Greater use of shields is reported in the United Kingdom.

7.2 ALLOY CLADDING OF TUBES

Application of a metal cladding over the superheater or reheater tubes is another remedial concept that is similar to the installation of metal shields but that eliminates the design and servicing problems associated with these shields. The metal cladding, however, will not allow the use of the higher surface temperature. The basis for cladding is simply the use of a special alloy--not feasible to fabricate as a single, monolithic tube--designed to clad over the external surface of a standard tube.

The main drawback to the concept of clad tubes is the lack of a truly resistant alloy. A few of the very high Ni-Cr alloys exhibit lower attack rates but are, nevertheless, corroded. The high-chromium alloys indicated by Lewis[45] have received some attention. Parry, et al.,[65] reported on the use of 50%Cr-50%Ni material as a promising approach for high-temperature flue gases and other corrosive gases. A more detailed account of the development and testing of the clad tubing is described by Rahoi.[48]

While the clad tube-material cost would be above that of conventional tubing, the cost of fabrication and installation is not significantly greater than for other tubes. The corrosion rate--1.9 mil/yr (0.048 mm/yr)--may not

represent the most severe exposure, so as previously discussed (see Section 5), corrosion rates reported for one specific coal are not necessarily applicable to another type. The actual service life of the composite tubes would be good as long as the high-alkali, "aggressive" coals were not used. When better alloys are available, the cladding concept will be given greater consideration. In the United Kingdom "Incoclad"--IN671 clad over Incoloy 800--has been successfully employed in boilers using some coals with slagging tendencies.

7.3 DIFFUSION ALLOY SURFACES

The use of diffusion alloy surfaces or diffused coatings provides an intermediate concept between cladding and surface coatings. Jackson[20] described several tests of surface-diffused alloys subjected to some laboratory evaluations and test probes. The CEGB also evaluated aluminized steels and siliconized and chromized tubes. Such materials are prepared by high-temperature processes that diffuse a vapor-deposited metal, such as aluminum or chromium, into the surface generally above 1830°F (1000°C). Jackson[20] did not give a full report on the test results but indicated that the chromizing had been found to be of no benefit in boiler trials, implying that the high-chromium alloy surface was rapidly destroyed. The aluminized materials had been under study in the laboratory but were not very different from higher alloys. Alloys that were siliconized also did not offer any special advantages, and their use was not repeated at that time.

Chromizing and aluminizing have been used more widely for high-temperature gas environments, and both are noted for substantial reductions of scaling losses in various types of furnaces. Chapman, et al.,[66,67] have presented a detailed report of the metallurgy and performance of chromized and

chrome-aluminized alloys in flue-gas atmospheres. Oxidation rates are reported but no data relative to liquid salt or fireside deposit resistance are given. The complex carbides present at the chromized surfaces are described. The multiphase structure of the chromized steels comprising carbides and α-Cr phases is a possible source of trouble for electrochemical attack.

Widespread use of chromized steels has also been reported in the Russian literature. Osintsev, et al.,[68] describe some of the problems involved in chromized steels. When these steels were used in systems burning sulfur-containing gas, subsurface corrosion attack and interfacial sulfidation were observed.

Krause, Vaughan, and Boyd[42] evaluated Chromized A106 (carbon steel) in comparison with ferritic chromium steels for coal-refuse fuel mixtures. They found that untreated wrought alloys were less deeply attacked and less prone to spalling.

Aluminized or diffused aluminum coatings may be helpful in some applications but are of no significant value in others. Their good performance in hot-gas service is the result of the good adherence and stability of the oxide scales containing Al_2O_3, but in the molten trisulfate medium, the oxide is rapidly dissolved and combines with the sulfates.

One attractive prospect of aluminized surfaces is that stable, bonded, intermetallic compounds, such as Ni-Al, may be produced. These compounds should be evaluated. The objective of trying to obtain a more stable, passive surface to prevent the rapid breakaway attack leads to the consideration of the intermetallic compounds.

It is apparent that many of the past trial-and-error type of tests were based on the performance of these coatings in oxidizing gases rather than in liquid-phase attack. The high-chromium surfaces produced by chromizing were not so corrosion-resistant as the high-chromium ferritic steels, which is rather obvious if the electrochemical mechanism is considered. Local alloy heterogeneity on the surface and dissimilar phases, such as carbides, would be expected to offer sites for cathode-anode cells. In their electrochemical study, Rahmel and Tartar-Moisescu[55] showed chromium to be beneficial in steel, up to a limit; for example, 24%Cr steel was very similar to 100% pure Cr.

7.4 PROTECTIVE COATINGS

Frequently over the years, the concept of applying coatings to limit or prevent fireside losses has been discussed. Coatings of both nonmetallic and metallic materials have been favored, but only limited testing has been reported. Rasch[34] discussed studies of various coatings leading to the selection of some nonmetallic materials for further study, including some Al_2O_3-SiO_2 compositions and MgO coatings. The Al_2O_3-SiO_2 coatings were in some cases self-healing in service because of the formation of complex silicates on the surface. Since the MgO was known to be beneficial as a fuel additive, it was of interest as a coating. The results of the MgO coatings mentioned by Rasch[34] were unavailable.

Laboratory tests of MgO and other nonmetallic coatings were conducted to evaluate both the suppression of the catalytic oxidation of SO_2 and the protection of the base metal.[31] The MgO coating formed a sulfate; however, the attack of the base metal was increased rather than reduced. In the same test a

kaolin coating was beneficial to the base metal (carbon steel), and the coating also reduced the catalytic oxidation at the surface.

Rahmel[69] in testing MgO coatings on an austenitic stainless steel observed a much higher metal loss than for the uncoated metal. The indication was that an excessive penetration into the alloy occurred, similar to that occurring in the oxygen-deficient gas-corrosion attack.

Metal coatings have received some attention; however, very little detailed reporting can be cited. The application[70] of metallized deposits of Hastelloy C was applied to the previously corroded superheater tubes at the Meramec plant of the Union Electric Company. The selection was made on the basis of a screening test that evaluated numerous metallized alloy deposits of stainless steel, nickel-base alloys, chromium, titanium, cobalt, and tantalum. The laboratory fireside corrosion rate of the Hastelloy C was indicated as 3 mil/yr (76 μm/yr), compared with 47 mil/yr (1194 μm/yr) for the original tube material (T11). The renewable application of the coating of 0.030 in. (0.76 mm) Hastelloy C was considered successful in preventing tube failures. Subsequent modification and a reduction of thickness to 0.015 in. (0.38 mm) using Hastelloy C-276 has improved the coating and eliminated spalling.

The unexplained observation that the high molybdenum content in a nickel-base alloy was satisfactory while iron-base alloys high in molybdenum corrode rapidly, sometimes catastrophically, needs further study. How molybdenum reacts in the liquid-phase complex sulfate is also not well known. The maximum temperature limit of the alloy surface may be very critical.

Numerous coatings and advanced surface treatments not included in this review have been developed for higher-temperature applications. While many of those developed for aircraft gas-turbine applications have been valuable in controlling the metal losses from turbine blades subjected to high-temperature attack above 1472°F (800°C), no data were available to indicate how the recent gas-turbine materials will perform under the liquid-phase attack from coal-ash deposits.

Coating developments considered from the viewpoint of the electrochemical mechanisms should be designed somewhat differently from those reported to date. One approach should be directed toward enhancing the passivity of the surface and another toward providing cathodic protection.

SECTION 8
CONCLUSIONS AND STATE OF THE ART

Section 8

CONCLUSIONS AND STATE OF THE ART

The identification of a liquid-phase trisulfate corrodent under the slag deposits was constructive in explaining the nature of the disease, but it has not as yet made the cure any easier. Nevertheless, the ability to blacklist the coals most likely to lead to excessive metal attack is presumably a help in the planning and operating of power boilers. While the properly chosen materials of fabrication did not lead to a long-term solution, the corrosion losses suffered by some alternate oxidation-resistant alloys would be two or three times greater in a given period of time. Alloys of over 2 percent molybdenum should not be used for superheater or reheaters fired by coals with fireside corrosion tendencies.

Increasing the operating temperatures in alkali-rich coal-fired steam generators will not reduce the severity of the fireside problem, unless the temperature is raised above 1400°F (760°C). Laboratory data showing low attack rates at 1300°F (704°C) based on simulated alkali-iron trisulfate conditions have not been confirmed by superheater or reheater tests and field observations. Data based on such laboratory trisulfate tests may be adequate for utilization in the range of 1050 to 1250°F (565 to 677°C). Further study is indicated for metal temperatures at 1300°F (704°C) or above.

The more basic study of the mechanism of attack by fused sulfate salts has led to renewed progress toward a correct understanding of the corrosion process. The electrochemical models have provided the only reasonable explanation

for the irregular, side-by-side distribution of attacked and unattacked surfaces. The slowness of acceptance of the electrochemical mode of attack may have been due to the obscure source of potential differences and the difficulty in obtaining direct measurements without distorting or altering the surface voltages. Rahmel[63] recently stated that the attack by molten salts in general involves electrochemical mechanisms, a belief that is widely accepted. Inman and Wrench[71] previously indicated that the molten salts including sulfates corrode metals predominantly by electrochemical mechanisms. The electrochemical concept is consistent with the observed attack on alloys with wide variations in alloy content and adapts to the conditions of assorted ash-content variables, as long as a conductive liquid phase is formed.

An interesting application of the electrochemical concept which has not been reported is the development of a system of cathodic or anodic protection to eliminate deep, aggressive pitting and metal wastage. Cathodic protection will require a metal with a more negative potential than chromium, such as aluminum, beryllium, niobium, zirconium, titanium, or rare earth, applied to the surface or bonded as an intermetallic compound to suppress corrosion currents.

Some advantage is seen in the higher alloys, as long as excessive "cathode stimulation" is avoided. Many alloys offer a somewhat better range of passive behavior than carbon steel, but after stimulation under corrosive conditions there is less advantage. The electrochemical attack may occur in either micro or macro cells.

The sulfidation reaction has been shown to occur with the electrochemical attack in the "transpassive region"--with the metal sulfide a by-product

rather than the cause of the reaction. Rahmel[63] indicated that no sulfides were found for exposures in the passive region before the accelerated attack. Sulfidation may also result from dissociation of SO_2 in low oxygen-activity areas.

Proving the vulnerability of metals to losses from externally imposed currents in fused salts appears easy; however, proving that self-generated destructive currents can occur is more difficult in fused salts. The polarization studies of Rahmel[63] and Cutler, et al.,[57,72] provided the necessary explanation for the maldistribution of corrosion attack, but they have not as yet supplied an answer needed by engineers: how to prevent depolarization or breakthrough corrosion currents.

Additional work is required to develop a means of preventing the cathode-stimulation effect or the acid fluxing of the initial passive layers. The fact that the addition of more and more chromium has little beneficial effect has been evident for a long time, but exactly what role the chromium plays in the corrosion attack sequence or whether CrO_4^{--} ions or other chromium species contribute to the attack is not clear.

One promising area of development that does not appear in the literature is the formation of more stable, passive films that are not so vulnerable to cathode stimulation or fluxing. A few elements, such as chromium, molybdenum, and vanadium, are obviously eliminated as major constituents of the surface. It has likewise been clearly shown that simple oxide scales of iron, nickel, chromium, molybdenum, vanadium, etc., are probably more harmful than beneficial. However, the possibilities of other surface materials that are not so soluble in

fused sulfates are far from exhausted. Development of a more stable, adherent scale that would not easily be converted to cathodic areas or that would limit the corrosion current and resist stimulation may be feasible.

It is highly possible that a bonded coating or surface treatment based on the above concepts will prove better than the previously tested coatings, which permit excessive attack below the coating. Hopefully such a coating, or cladding, will be developed soon so that the life of commercial alloy tubes can be extended.

SECTION 9
REFERENCES

Section 9

REFERENCES

1. W. T. Reid, External Corrosion and Deposits: Boilers and Gas Turbines, American Elsevier, New York, 1971.

2. W. T. Reid, R. C. Corey, and B. J. Cross, "External Corrosion of Furnace-Wall Tubes--I History of Occurrence," Transactions of the ASME, Vol. 67, 1945, pp. 279-288.

3. M-Th. Mackowsky, "The Mineral Constitution of Coal as the Causative Agent of the Fouling of Heating Surfaces with Particular Reference to Pulverized Fuel Firing with Liquid Slag Removal," Proceedings of the Marchwood Conference, Mechanism of Corrosion by Fuel Impurities, Johnson and Littler (ed.), Butterworths, London, 1963.

4. L. M. Wyatt and G. J. Evans, "Operational and Experimental Observations on the Fireside Corrosion of Superheater and Reheater Tubes," Proceedings of the Marchwood Conference, Mechanism of Corrosion by Fuel Impurities, Johnson and Littler (ed.), Butterworths, London, 1963.

5. W. Nelson and C. Cain, Jr., "Corrosion of Superheaters and Reheaters of Pulverized-Coal-Fired Boilers," Transactions of the ASME, Journal of Engineering for Power, Vol. 82, Series A, July 1960, pp. 194-204.

6. H. E. Crossley, "External Fouling and Corrosion of Boiler Plant: A Commentary," Journal of the Institute of Fuel, Vol. 40, 1967, pp. 342-347.

7. H. Kirsch, "Corrosion of Combustion Chambers by Slag Attack and Flue Gases of Varying Composition," Proceedings of the Marchwood Conference, Mechanism of Corrosion by Fuel Impurities, Johnson and Littler (ed.), Butterworths, London, 1963.

8. P. Sedor, E. K. Diehl, and D. H. Barnhart, "External Corrosion of Superheaters in Boilers Firing High-Alkali Coals," Transactions of the ASME, Vol. 82, Series A, 1960, pp. 181-193.

9. R. J. Bishop, "The Formation of Alkali-Rich Deposits by a High-Chlorine Coal," Journal of the Institute of Fuel, Vol. 41, 1968, pp. 51-65.

10. A. M. Adams and E. Raask, "Complex Sulphates in Coal-Fired Boiler Deposits," Proceedings of the Marchwood Conference, Mechanism of Corrosion by Fuel Impurities, Johnson and Littler (ed.), Butterworths, London, 1963, pp. 496-507.

11. G. Bonafede and L. T. Kiss, "Study of Ash Deposits from Brown Coal Fired Boilers with the Aid of Scanning and Transmission Electron Microscopy," ASME Paper No. 73-WA/CD-7, March 1973, p. 13.

12. I. P. Ivanova, et al., "High-Temperature Corrosion of Supercritical Boiler Tubes when Burning [Pulverized Fuel] Type Ash [Anthracite]," Teploenergetika, Vol. 1, January 1972, pp. 16-18.

13. I. P. Ivanova and Yu. L. Marshak, "The High Temperature Corrosion of Furnace Wall Tubes During the Combustion of Anthracite Slack," Teploenergetika, Vol. 2, February 1975, pp. 15-18.

14. "List of References on Corrosion in Thermal Power Plant, Published 1969-71," Teploenergetika, Vol. 1, January 1972, pp. 93-95.

15. J. G. Koopman, et al., "Development and Use of a Probe for Studying Corrosion in Superheaters and Reheaters," Proceedings of the American Power Conference, Vol. 21, 1959, pp. 236-245.

16. J. T. Reese, J. Jonakin, J. G. Koopman, "How Coal Properties Relate to Corrosion of High-Temperature Boiler Surfaces," Proceedings of the American Power Conference, Vol. 23, 1961, pp. 391-399.

17. M. Weintraub, S. Goldberg, and A. A. Orning, "A Study of Sulfur Reactions in Furnace Deposits," Transactions of the ASME, Journal of Engineering for Power, Vol. 83, Series A, October 1961, pp. 444-450.

18. R. W. Borio, et al., "The Control of High Temperature Fire Side Corrosion in Utility Coal Fired Boilers," U.S. Office of Coal Research R&D No. 41, Final Report, April 1969.

19. R. W. Borio, et al., "Study of Means for Eliminating Corrosiveness of Coal to High Temperature Surfaces of Steam Generating Units--II," Combustion, Vol. 39, February 1968, pp. 12-20.

20. P. J. Jackson, "Researches in the C.E.G.B. Into Fireside Fouling and Corrosion of Boiler Plant," Journal of the Institute of Fuel, Vol. 40, 1967, pp. 335-341.

21. K. K. Tyul'pin, et al., "Corrosion Resistance of Boiler Steels in the Combustion Products of Solid, Liquid and Gaseous Fuels," Teploenergetika, Vol. 8, August 1971, pp. 6-9.

22. A. A. Ots, et al., "Effect of Initial Ash Deposits on the High-Temperature Corrosion of Boiler Steel," Teploenergetika, Vol. 1, January 1972, pp. 22-25.

23. R. H. Boll and H. C. Patel, "The Role of Chemical Thermodynamics in Analyzing Gas-Side Problems in Boilers," Transactions of the ASME, Journal of Engineering for Power, Vol. 83, Series A, October 1961, pp. 451-467.

24. A. B. Hedley, "Factors Affecting the Formation of Sulphur Trioxide in Flame Gases," Journal of the Institute of Fuel, Vol. 40, 1967, pp. 142-151.

25. W. T. Reid, A. Levy, and R. E. Barrett, "First Summary Report on Thermochemical Reactions Influencing Corrosion and Deposits From Combustion Gases in Boilers and Gas Turbines," prepared for ASME Research Committee on Corrosion and Deposits From Combustion Gases by Battelle Memorial Institute, October 31, 1962.

26. W. T. Reid, A. Levy, and R. E. Barrett, "Second Summary Report on Thermochemical Reactions Influencing Corrosion and Deposits From Combustion Gases in Boilers and Gas Turbines," prepared for ASME Research Committee on Corrosion and Deposits From Combustion Gases by Battelle Memorial Institute, October 31, 1963.

27. W. T. Reid, A. Levy, and R. E. Barrett, "Third Summary Report on Thermochemical Reactions Influencing Corrosion and Deposits From Combustion Gases in Boilers and Gas Turbines," prepared for ASME Research Committee on Corrosion and Deposits From Combustion Gases by Battelle Memorial Institute, November 1, 1963-April 30, 1964.

28. W. T. Reid, A. Levy, and R. E. Barrett, "Fourth Summary Report on Thermochemical Reactions Influencing Corrosion and Deposits From Combustion Gases in Boilers and Gas Turbines," prepared for ASME Research Committee on Corrosion and Deposits From Combustion Gases by Battelle Memorial Institute, May 1, 1964-October 31, 1964.

29. W. T. Reid, A. Levy, and R. E. Barrett, "Fifth Summary Report on Thermochemical Reactions Influencing Corrosion and Deposits From Combustion Gases in Boilers and Gas Turbines," prepared for ASME Research Committee on Corrosion and Deposits From Combustion Gases by Battelle Memorial Institute, November 1, 1964-April 30, 1965.

30. W. T. Reid, A. Levy, and R. E. Barrett, "Sixth Summary Report on Thermochemical Reactions Influencing Corrosion and Deposits From Combustion Gases in Boilers and Gas Turbines," prepared for ASME Research Committee on Corrosion and Deposits From Combustion Gases by Battelle Memorial Institute, May 1, 1965-October 31, 1965.

31. W. T. Reid, A. Levy, and R. E. Barrett, "Project Review and Seventh Summary Report of Thermochemical Reactions Influencing Corrosion and Deposits From Combustion Gases in Boilers and Gas Turbines," prepared for ASME Research Committee on Corrosion and Deposits From Combustion Gases by Battelle Memorial Institute, May 1, 1962-April 30, 1966.

32. H. H. Krause, A. Levy, and W. T. Reid, "Sulfur Oxide Reactions: Radioactive Sulfur and Microprobe Studies of Corrosion and Deposits," Transactions of the ASME, Journal of Engineering for Power, Vol. 90, Series A, No. 1, January 1968, pp. 38-44.

33. H. H. Krause, A. Levy, and W. T. Reid, "Radioactive Sulfur Oxide Studies of External Corrosion Reactions on Surfaces," Transactions of the ASME, Journal of Engineering for Power, Vol. 91, Series A, July 1969, pp. 216-222.

34. R. Rasch, "Flue Gas Side Corrosions Description of Typical Damage, Corrosion Mechanism and Measures for Prevention," Technische Mitteilungen, Vol. 65, No. 2, February 1972, p. 82.

35. R. R. Martin, F. S. Manning, and E. D. Reed, "Watch for Elevated Dew Points in SO_3-Bearing Stack Gases," Hydrocarbon Processing, Vol. 53, 1974.

36. T. A. Milne and J. E. Beachey, "Direct Sampling and Characterization of Gaseous Species Responsible for Fireside Corrosion in Fossil Fuel-Fired Systems," Second Quarterly Progress Report, July 1-September 31, 1976, prepared for Energy Research and Development Administration by Midwest Research Institute, Contract No. E(49-18)-2288, Report No. FE-2288-8, November 15, 1976.

37. C. H. Anderson and C. W. Goddard, "Equilibrium SO_3 Pressures of Inner Layers of Fireside Deposits From Coal-Fired Boilers," Journal of the Institute of Fuel, Vol. 41, 1968, pp. 357-364.

38. A. Rahmel, "Influence of Calcium Sulphate and Magnesium Sulphate on the High Temperature Oxidation of Austenitic Chrome-Nickel Steels in the Presence of Alkali Sulphates Containing Deposits on the Surface and Traces of Sulphur Trioxide in the Atmosphere," Proceedings of the Marchwood Conference, Mechanism of Corrosion by Fuel Impurities, Johnson and Littler (ed.), Butterworths, London, 1963.

39. C. Cain, Jr., and W. Nelson, "Corrosion of Superheaters and Reheaters of Pulverized-Coal-Fired Boilers, II," Transactions of the ASME, Vol. 83, Series A, October 1961, pp. 468-474.

40. W. T. Reid, "Basic Problems in the Formation of Sulfates in Boiler Furnaces," Transactions of the ASME, Journal of Engineering for Power, Vol. 89, Series A, No. 2, April 1967, pp. 283-287.

41. G. Horn and P. J. Street, "Experiments With a Pilot Plant Designed to Superheat Steam to 760°C: Part 2. Flame and Deposition Studies," Journal of the Institute of Fuel, Vol. 41, 1968, pp. 219-232.

42. H. H. Krause, D. A. Vaughan, and W. K. Boyd, "Corrosion and Deposits From Combustion of Solid Waste, Part III: Effects of Sulfur on Boiler Tube Metals," Transactions of the ASME, Journal of Engineering for Power, Vol. 92, Series A, July 1975, pp. 448-452.

43. H. A. Blank, A. M. Hall, and J. H. Jackson, "Behavior of Superheater Tubing Materials in Contact With Combustion Atmospheres at 1350 F," Transactions of the ASME, Vol. 74, July 1952, pp. 813-824.

44. G. Horn and P. J. Street, "Experiments With a Pilot Plant Designed to Superheat Steam to 760°C: Part 3. Behaviour of Three High-Temperature Alloys," Journal of the Institute of Fuel, Vol. 41, 1968, pp. 258-264.

45. J. C. Parker, D. F. Rosborough, and M. J. Virr, "High Temperature Corrosion Trials at Marchwood Power Station--10,000 Hour Corrosion Probe Trials," Journal of the Institute of Fuel, Vol. 45, February 1972, pp. 95-104.

46. H. Lewis, "Nickel-Chromium Alloys With 30 to 60 per cent Chromium in Relation to Their Resistance to Corrosion by Fuel-Ash Deposits, Part 1: Corrosion-Resistance," Journal of the Institute of Fuel, Vol. 39, January 1966, pp. 8-13.

47. H. Lewis and R. A. Smith, "Corrosion of High Temperature Nickel-Base Alloys by Sulfate-Chloride Mixtures," Proceedings First International Congress on Metallic Corrosion, London, 1961, Butterworths, 1962.

48. W. J. Greenert, "High Temperature Slag Corrosion of Metallic Materials," Corrosion, Vol. 18, 1962, pp. 91t-102t.

49. D. W. Rahoi, "Controlling Fuel-Ash Corrosion With Nickel Alloys," Metals Engineering Quarterly, Vol. 14, No. 1, February 1974, pp. 44-51.

50. G. J. Hills, "Corrosion of Metals by Molten Salts," Proceedings of the Marchwood Conference, Mechanism of Corrosion by Fuel Impurities, Johnson and Littler (ed.), Butterworths, London, 1963.

51. B. W. Burrows and G. J. Hills, "The Electrochemistry of Deposits of Inorganic Constituents of Fuels at High Temperature," Journal of the Institute of Fuel, Vol. 39, 1966, pp. 168-180.

52. W. T. Reid, H. H. Krause, and R. E. Barrett, "Third Summary Report on Formation of Alkali Iron Sulfates and Other Compounds Causing Corrosion in Boilers and Gas Turbines," prepared for ASME Research Committee on Corrosion and Deposits From Combustion Gases by Battelle Memorial Institute, July 1, 1967-December 31, 1967.

53. W. T. Reid, H. H. Krause, and R. E. Barrett, "Project Review and Fourth Summary Report on Formation of Alkali Iron Sulfates and Other Compounds Causing Corrosion in Boilers and Gas Turbines," prepared for ASME Research Committee on Corrosion and Deposits From Combustion Gases by Battelle Memorial Institute, July 1, 1966-June 30, 1968.

54. W. T. Reid, H. H. Krause, and R. E. Barrett, "Second Summary Report on Formation of Alkali Iron Sulfates and Other Compounds Causing Corrosion in Boilers and Gas Turbines," prepared for ASME Research Committee on Corrosion and Deposits From Combustion Gases by Battelle Memorial Institute, January 1, 1967-June 30, 1967.

55. A. Rahmel and E. Tatar-Moisescu, "Electrochemical Investigations on the High Temperature Corrosion of High Alloy Materials (Metals) in Alkali Sulphate Melts," Werkstoffe und Korrosion, Vol. 26, No. 7, July 1975, pp. 513-520.

56. A. J. B. Cutler, et al., "Recent Research by the CEGB (Central Electricity Generating Board) into Solving Current Problems Caused by Fireside Corrosion," VGB Kraftwerkstechnik, Vol. 54, No. 9, September 1974, pp. 611-619.

57. A. J. B. Cutler and C. J. Grant, "Corrosion of Iron and Nickel Base Alloys in Alkali Sulphate Melts," Metal-Slag-Gas Reactions and Processes, Electrochemical Society, Princeton, 1975, pp. 591-607.

58. A. Rahmel, "The Scaling of Iron in Oxygen- and Sulfur-Containing Gases," Oxidation of Metals, Vol. 9, No. 5, pp. 401-408.

59. E. A. Gulbransen and S. A. Jansson, "General Concepts of Oxidation and Sulfidation Reactions: A Thermochemical Approach," High-Temperature Metallic Corrosion of Sulfur and Its Compounds, Electrochemical Society, Princeton, 1970, pp. 3-51.

60. A. U. Seybolt, "Present Status of Research on the Mechanism of Sulfidation-Oxidation (Hot Corrosion)," High-Temperature Metallic Corrosion of Sulfur and Its Compounds, Electrochemical Society, Princeton, 1970, pp. 159-169.

61. U. Jäkel and W. Schwenk, "Electrochemical Investigations on the High Temperature Corrosion of Chromium Steels in Alkali Sulphate Melts," Werkstoffe und Korrosion, Vol. 26, No. 7, July 1975, pp. 521-529.

62. A. Rahmel, "Electrochemical Investigation of the Stimulation of the Cathode Partial Reaction and the Free Corrosion of Silver and Chromium Steels in Fused Alkali Sulfates," Werkstoffe und Korrosion, Vol. 23, No. 5, May 1977, pp. 299-308.

63. A. Rahmel, "The Influence of Electrode Potential on Corrosion and Creep Behaviour of Heat Resistant Alloys in Alkali Sulphate Melts," presented at

the International Conference on Ash Deposits and Corrosion From Impurities in Combustion Gases, New England College, Henniker, New Hampshire, June 26-July 1, 1977.

64. W. D. Halstead and A. B. Hart, "The Role of Chloride in Corrosion by Flue Gas Deposits," report of the meeting held on 26-27 November 1969 at Sudbury House, CEGB Report No. RD/L/M 272.

65. P. J. Parry, et al., "Wrought Nickel-50% Chromium Alloy for Use in High-Temperature Corrosive Gases," Journal of the Institute of Fuel, Vol. 47, June 1974, pp. 117-123.

66. N. R. Chapman, et al., "The Oxidation of a Number of Chromized and Chrome-Aluminized Alloys in Flowing Air and Flue-Gas Atmospheres-II," Anti-Corrosion Methods and Materials, Vol. 18, No. 1, January 1971, pp. 12-20.

67. N. R. Chapman, et al., "The Oxidation of a Number of Chromized and Chrome-Aluminized Alloys in Flowing Air and Flue-Gas Atmospheres-I," Anti-Corrosion Methods and Materials, Vol. 17, No. 12, December 1970, pp. 10-26.

68. V. D. Osintsev, et al., "Effect of the Condition of Diffusion Chromizing and Heat Treatment on the Corrosion Resistance of Chromized Steel in Hot Sulphur-Containing Gases," Fiziko-Khimicheskaia Mekhanika Materialov, Vol. 9, No. 2, 1973, pp. 17-19.

69. A. Rahmel, "Influence of Calcium Sulphate and Magnesium Sulphate on the High Temperature Oxidation of Austenitic Chrome-Nickel Steels in the Presence of Alkali Sulphates Containing Deposits on the Surface and Traces of Sulphur Trioxide in the Atmosphere," Proceedings of the Marchwood Conference, Mechanism of Corrosion by Fuel Impurities, Johnson and Littler (ed.), Butterworths, London, 1963.

70. Cabot Corporation, "Spray Metallizing Controls Liquid Phase Corrosion in Coal-Fired Boilers," Stellite Digest, Vol. 24, No. 1, August 1973.

71. D. Inman and N. S. Wrench, "Corrosion in Fused Salts," British Corrosion Journal, Vol. 1, 1966, pp. 246-250.

72. A. J. B. Cutler, et al., "Recent Research by the CEGB into Solving Current Problems Caused by Fireside Corrosion," VGB Kraftwerkstechnik, Vol. 54, No. 9, September 1974, pp. 611-619.

SECTION 10
SUPPLEMENTARY BIBLIOGRAPHY

Section 10

SUPPLEMENTARY BIBLIOGRAPHY

Alexander, P. A., "Laboratory Studies of the Effects of Sulphates and Chlorides on the Oxidation of Superheater Alloys," Proceedings of the Marchwood Conference, Mechanism of Corrosion by Fuel Impurities, Johnson and Littler (ed.), Butterworths, London, 1963.

Antill, J. E., "Influence of Minor Alloying Elements on the High Temperature Oxidation Behaviour of a 20%Cr-25%Ni-Nb Steel," Werkstoffe und Korrosion, Vol. 22, No. 6, June 1971, pp. 513-517.

Attig, R. C. and D. H. Barnhart, "A Laboratory Method of Evaluating Factors Affecting Tube Bank Fouling in Coal-Fired Boilers," Proceedings of the Marchwood Conference, Mechanism of Corrosion by Fuel Impurities, Johnson and Littler (ed.), Butterworths, London, 1963.

Babushkin, V. N. and A. I. Borisenko, "Diffusion of Iron, Chromium and Nickel in Heat-Resistant Coatings," Protection Metals, Vol. 4, No. 3, May-June 1968, pp. 278-280.

Barrett, R. E., "High-Temperature Corrosion Studies in an Oil-Fired Laboratory Combustor," Transactions of the ASME, Journal of Engineering for Power, Vol. 89, Series A, No. 2, April 1967, pp. 288-296.

Barrett, R. E., J. D. Hummell, and W. T. Reid, "Formation of SO_3 in a Noncatalytic Combustor," Transactions of the ASME, Journal of Engineering for Power, Vol. 88, Series A, No. 2, April 1966, pp. 165-172.

Bastow, B. D. and G. C. Wood, "Multilayer Scale Formation During the Sulfidation of Nickel," Oxidation of Metals, Vol. 9, No. 6, 1975, pp. 473-496.

Baudo, G., et al., "An Electrochemical Investigation of Corrosion of Ferritic Steels in Molten Sulfates," Corrosion, Vol. 26, No. 7, July 1970, pp. 193-199.

Baumann, K., "Corrosion and Protection Against Corrosion on the Flue-Gas Side of Steam Generators," VGB Kraftwerkstechnik, Vol. 55, No. 3, March 1975, pp. 174-180.

Bergman, P. A., "Review of the Practical Aspects of Hot Corrosion Problems in Gas Turbines," High-Temperature Metallic Corrosion of Sulfur and Its Compounds, Electrochemical Society, Princeton, 1970, p. 224.

Bhide, V. S., D. J. Young, and W. W. Smeltzer, "The Sulfidation Properties of Nickel-Aluminum Alloys at 700°C," Metal-Slag-Gas Reactions and Processes, Electrochemical Society, Princeton, 1975, pp. 511-521.

Birchenall, C. E., "Diffusion in Oxides and Sulfides," Diffusion, American Society of Metals, 1973, pp. 309-332.

Bishop, R. J. and J. A. C. Samms, "Pilot Scale Investigations of the Formation of Bonded Deposits," Proceedings of the Marchwood Conference, Mechanism of Corrosion by Fuel Impurities, Johnson and Littler (ed.), Butterworths, London, 1963.

Blaise, B., et al., "The Effects of the Crystal Orientation of the Metal [Iron] and of the Partial Pressure of the Gas on the Formation of Iron Sulphide Nuclei," Comptes Rendus de l'Athenée Louisianois, Vol. 276, No. 15, April 1973, pp. 1227-1230.

Boow, J. and P. R. Goard, "Fireside Deposits and Their Effect on Heat Transfer in a Pulverized-Fuel-Fired Boiler: Part III. The Influence of the Physical Characteristics," Journal of the Institute of Fuel, Vol. 42, 1969, pp. 412-415.

Borisov, V. T., et al., "Determination of Diffusion Coefficients of Carbon in Iron with Allowance for the Kinetics of the Reaction on the Metal/Gas Interface," [All-Union Scientific Conference on] Diffusion Processes in Metals, Kiev, 1964, 1970, pp. 24-28.

Bornstein, N. S. and M. A. DeCrescente, "The Role of Sodium in the Accelerated Oxidation Phenomenon Termed Sulfidation," Metallurgical Transactions, Vol. 2, No. 10, October 1971, pp. 2875-2883.

Bourhis, Y. and C. St. John, "Na_2SO_4 and NaCl-Induced Hot Corrosion of Six Nickel-Base Superalloys," Oxidation of Metals, Vol. 9, No. 6, 1975, pp. 507-528.

Brown, H. R., et al., "Factors Influencing the Formation of Fireside Deposits During the Combustion of Morwell Brown Coal," Proceedings of the Marchwood Conference, Mechanism of Corrosion by Fuel Impurities, Johnson and Littler (ed.), Butterworths, London, 1963.

Burrows, B. W., et al., "The Electrochemistry of Deposits of Inorganic Constituents of Fuels at High Temperature," Journal of the Institute of Fuel, Vol. 39, 1966, pp. 168-180.

Calderbank, P. H., "The Mechanism of the Catalytic Oxidation of Sulphur Dioxide With a Commercial Vanadium Catalyst: A Kinetic Study," Journal of Applied Chemistry, Vol. 2, August 1952, pp. 482-492.

Cameron, C. B. and D. P. Ferriss, "Tribaloy Intermetallic Materials: New Wear- and Corrosion-Resistant Alloys," Anti-Corrosion Methods and Materials, Vol. 22, No. 4, 1975, pp. 5-8.

Coats, A. W., D. J. Dear, and D. Penfold, "Phase Studies on the Systems Na_2SO_4-SO_3, K_2SO_4-SO_3 and Na_2SO_4-K_2SO_4-SO_3," Journal of the Institute of Fuel, Vol. 41, 1968, pp. 129-132.

Condit, R. H., et al., "Self-Diffusion of Iron and Sulfur in Ferrous Sulfide," Oxidation of Metals, Vol. 8, No. 6, 1974, pp. 409-453.

"Controlled Shot Peening Eliminates Corrosion," Iron Age, Vol. 216, No. 5, August 4, 1975, pp. 64-65.

Darras, R., et al., "The Effect of Low Silicon Content and Some Surface Treatments on the Oxidation of Carbon Steels in Carbon Dioxide Atmospheres at Medium Temperatures," Werkstoffe und Korrosion, Vol. 22, No. 5, May 1971, pp. 389-402.

Davidson, D. C., et al., "Discussion on Phase Studies on the Systems Na_2SO_4-SO_3; K_2SO_4-SO_3 and Na_2-K_2SO_4-SO_3," Journal of the Institute of Fuel, Vol. 42, 1969, pp. 457-460.

Davin, A., et al., "Hot Corrosion of Cobalt-Base Alloys in the Presence of SO_2, NaCl, Na_2SO_4 and V_2O_5," Metal-Slag-Gas Reactions and Processes, Electrochemical Society, Princeton, 1975, pp. 678-692.

DeCrescente, M. A. and N. S. Bornstein, "Formation and Reactivity Thermodynamics of Sodium Sulfate with Gas Turbine Alloys," Corrosion, Vol. 24, No. 5, May 1968, pp. 127-133.

"Diffusion in Solid Metals and Alloys," Diffusion Data, Vol. 3, No. 1, April 1969 (Diffusion Information Center, Columbus, Ohio), pp. 11-35.

Duncan, J. R. and D. J. Spedding, "Initial Reactions of Sulphur Dioxide After Adsorption onto Metals," Corrosion Science, Vol. 13, No. 11, November 1973, pp. 881-889.

Dunderdale, J., et al., "Studies Relating to the Behavior of Sodium During the Combustion of Solid Fuels," Proceedings of the Marchwood Conference, Mechanism of Corrosion by Fuel Impurities, Johnson and Littler (ed.), Butterworths, London, 1963.

El-Dahshan, M. E., D. P. Whittle, and J. Stringer, "The Effect of Carbon on the Sulphidation of Cobalt-Chromium Alloys," Cobalt, No. 2, 1973, pp. 45-52.

Elliott, P., et al., "The Mechanism of Vanadium Slag Attack of Fe 23 Cr in Air in the Range 540° to 820°C," Journal of the Institute of Fuel, Vol. 46, No. 383, February 1973, pp. 77-87.

Elliott, P. and T. K. Ross, "Some Aspects of the Performance of Rare-Earth-Modified Nickel-Base Alloys in Hot Corrosion Conditions," Werkstoffe und Korrosion, Vol. 22, No. 6, June 1971, pp. 531-540.

Enke, C. G., "Corrosion and Fouling-Up from Flue Gases in Thermal Power Stations," Bander-Bleche-Rohre, Vol. 14, No. 1, January 1973, pp. 28-30.

Enyakin, Yu. P., et al., "Study of the Corrosion Effect in Boilers in Power Stations Fired with Gas of a High-Sulphur Content," Thermal Engineering, Vol. 19, No. 1, January 1972, pp. 19-23.

Faulkner, R. G. and P. J. Bridges, "Composite Tubes with High Corrosion Resistance at High Temperatures," Werkstoffe und Korrosion, Vol. 26, No. 1, January 1975, pp. 32-36.

Fontaine, P. I. and E. G. Richards, "Hot Corrosion of Nickel-Iron-Chromium Cobalt Alloys by Sulfate-Chloride and Sulfate Vanadate Simulated Fuel Ashes," Hot Corrosion Problems Associated with Gas Turbines, 1967, pp. 246-269.

Fruehan, R. J. and L. J. Martonik, "The Rate of Decarburization of Austenite in $CO-CO_2$," High Temperature Science, Vol. 3, No. 3, May 1971, pp. 224-256.

Gadda, E., et al., "Characterization by the Electron Microprobe of the Scales on Low Alloy Steels Exposed to Combustion Gases," Werkstoffe und Korrosion, Vol. 23, No. 10, October 1972, pp. 893-901.

Galmiche, P., "Corrosion of Refractory Superalloys Exposed to High-Temperature Flue Gases," Trattamenti Dei Metalli, November-December 1973, pp. 27-35.

Goebel, J. A. and F. S. Pettit, "Alloy-Molten Slag Reactions Associated With Hot Corrosion of Alloys," Metal-Slag-Gas Reactions and Processes, Electrochemical Society, Princeton, 1975, pp. 693-710.

Goebel, J. A. and F. S. Pettit, "The Influence of Sulfides on the Oxidation Behavior of Nickel-Base Alloys," Metallurgical Transactions, Vol. 1, December 1970, pp. 3421-3429.

Golub, S. and D. G. Fedak, "The Interaction of Sulphur Dioxide with Tungsten," Surface Science, Vol. 45, No. 1, September 1974, pp. 213-226.

Goodstine, S. L. and J. J. Kurpen, "Corrosion and Corrosion Product Control in the Utility Boiler Turbine Cycle," Materials Performance, Vol. 13, No. 1, January 1974, pp. 31-40.

Graham, L. D., J. D. Gadd, and R. J. Quigg, "Hot Corrosion Behavior of Coated and Uncoated Superalloys," Hot Corrosion Problems Associated With Gas Turbines, 1967, pp. 105-122.

Grantham, L. F., et al., "Corrosion of Metals in Molten Mixtures of Alkali Metal Carbonates Containing Sulfur Compounds," High-Temperature Metallic Corrosion of Sulfur and Its Compounds, Electrochemical Society, Princeton, 1970, pp. 253-269.

Gulbransen, E. A. and S. A. Jansson, "Thermochemistry of Gas-Metal Reactions," Oxidation of Metals and Alloys, American Society for Metals, 1971, pp. 63-86.

Harada, Y., "Studies on Chromium Diffusion-Coating of Nickel Superalloys: VI. Application to Oil-Fired Gas-Turbine Blades," Journal of the Metal Finishing Society, Japan, Vol. 23, No. 9, September 1972, pp. 509-514.

Hedley, A. B., "A Kinetic Study of Sulphur Trioxide Formation in a Pilot Scale Furnace," Proceedings of the Marchwood Conference, Mechanism of Corrosion by Fuel Impurities, Johnson and Littler (ed.), Butterworths, London, 1963.

Horn, G. and P. J. Street, "Experiments With a Pilot Plant Designed to Superheat Steam to 760°C: Part 1. Development and Instrumentation for Corrosion Studies," Journal of the Institute of Fuel, Vol. 41, 1968, pp. 152-161.

Hosegood, E. A., "Reactions of Sodium Compounds with the Surface of Aluminium Silicate Particles During the Combustion of Pulverised Fuel," Proceedings of the Marchwood Conference, Mechanism of Corrosion by Fuel Impurities, Johnson and Littler (ed.), Butterworths, London, 1963.

Ishibashi, E., et al., "High-Temperature Corrosion of Materials for Gas Turbines by Residual-Oil Combustion Gas," Bulletin of Japan Society of Mechanical Engineers, Vol. 13, No. 66, December 1970, pp. 1494-1503.

Ivanova, I. P. and L. A. Svistunova, "Corrosion of Steel 12Kh1MF and Various Anti-Corrosion Coatings in Flue Gas When Burning Anthracite," Teploenergetika, Vol. 1, January 1971, pp. 60-63.

Jackson, P. J. and H. C. Duffin, "Laboratory Studies of the Deposition of Alkali-Metal Salts from Flue Gas," Proceedings of the Marchwood Conference, Mechanism of Corrosion by Fuel Impurities, Johnson and Littler (ed.), Butterworths, London, 1963.

Jackson, P. J., W. E. Langdon, and P. J. Reynolds, "Automatic Continuous Measurement of Sulphur Trioxide in Flue Gases," Journal of the Institute of Fuel, Vol. 43, 1970, pp. 10-17.

Jenkinson, J. R., "Sulphur Oxide Reactions," Proceedings of the Marchwood Conference, Mechanism of Corrosion by Fuel Impurities, Johnson and Littler (ed.), Butterworths, London, 1963.

Johnson, K. E., "Electrochemical Approaches to Corrosion by Molten Salts," Metal-Slag-Gas Reactions and Processes, Electrochemical Society, Princeton, 1975, pp. 581-590.

Jones, R. L., "Some Observations on the Failure of Gas Turbine Blade Coatings in the Presence of Sodium Chloride," Metal-Slag-Gas Reactions and Processes, Electrochemical Society, Princeton, 1975, p. 762.

Kautz, K. and J. Tichatschke, "Relationship Between Flue Gas Conditions, Boiler Charge, and Corrosion in a Communal Waste Incinerator," Mitteilungen der VGB, Vol. 52, No. 3, June 1972, pp. 249-258.

Kenney, C. N. and R. F. Taylor, "Mass-Transfer in Gas/Liquid Reaction Systems," High-Temperature Chemical-Reaction Engineering Solids Conversion Processes, Institute of Chemical Engineers, 1971, pp. 110-114.

Kinoshita, K., et al., "Oxidation of Stainless Steel Tubings in High-Temperature Steam," Transactions of the Japan Institute of Metals, Vol. 15, No. 6, 1975, pp. 334-340.

Kirkaldy, J. S. "Ternary Diffusion and Its Relationship to Oxidation and Sulfidation," Oxidation of Metals and Alloys, American Society for Metals, 1971, pp. 101-114.

Konev, V. N., et al., "Oxidation of Nickel in an Atmosphere with Various Sulfur Dioxide Contents," Protection of Metals, Vol. 6, No. 4, July-August 1970, pp. 409-410.

Ladner, W. R. and K. S. Pankhurst, "The Formation of Sulphur Trioxide: The Application of Infra-red Spectrometry to Fundamental Studies," Proceedings of the Marchwood Conference, Mechanism of Corrosion by Fuel Impurities, Johnson and Littler (ed.), Butterworths, London, 1963.

Laxton, J. W., "The Influences of Excess Oxygen and Metallic Additives on the Formation and Deposition of Sulphur Oxides in Flue Gas," Proceedings of the Marchwood Conference, Mechanism of Corrosion by Fuel Impurities, Johnson and Littler (ed.), Butterworths, London, 1963.

Lees, B. and D. H. Mustoe, "Effect of Magnesium-Based Additives on High Temperature Corrosion in Oil-Fired Boilers," Journal of the Institute of Fuel, Vol. 45, July 1972, pp. 397-406.

Levy, A. and E. L. Merryman, "A Progress Report--Fundamentals of Thermochemical Corrosion Reactions," Transactions of the ASME, Journal of Engineering for Power, Vol. 87, Series A, No. 1, January 1965, pp. 116-122.

Levy, A. and E. L. Merryman, "Interactions in Sulphur Oxide-Iron Oxide Systems," Transactions of the ASME, Journal of Engineering for Power, Vol. 89, Series A, No. 2, April 1967, pp. 297-303.

Levy, A. and E. L. Merryman, "SO_3 Formation in H_2S Flames," Transactions of the ASME, Journal of Engineering for Power, Vol. 87, Series A, No. 3, October 1965, pp. 374-378.

Levy, A. and E. L. Merryman, "Sulfur Chemistry and Its Role in Corrosion and Deposits," Transactions of the ASME, Journal of Engineering for Power, Vol. 85, Series A, No. 4, July 1963, pp. 229-234.

Llewelyn, G., "Protection of Nickel-Base Alloys Against Sulfur Corrosion by Pack Aluminizing," Hot Corrosion Problems Associated With Gas Turbines, 1967, pp. 3-20.

Long, R. H., M. C. Sze, and H. Unger, "Aluminum-Rare Earth Coating Counters Corrosion Failures," Metals Progress, Vol. 107, No. 2, February 1975, pp. 52-53.

Macfarlane, J. J., "The Relationship Between Combustion Conditions and the Corrosion of Metal Surfaces by Fuel Oil Ash Deposits," Proceedings of the Marchwood Conference, Mechanism of Corrosion by Fuel Impurities, Johnson and Littler (ed.), Butterworths, London, 1963.

May, W. R., et al., "High-Temperature Corrosion in Gas Turbines and Steam Boilers by Fuel Impurities: II. The Sodium Sulfate-Magnesium Sulfate-Vanadium Pentoxide System," Industrial Engineering and Chemistry Product Research and Development, Vol. 12, No. 2, June 1973, pp. 140-145.

May, W. R., et al., "High-Temperature Corrosion in Gas Turbines and Steam Boilers by Fuel Impurities: III. Evaluation of Magnesium as a Corrosion Inhibitor," Industrial Engineering and Chemistry Product Research and Development, Vol. 12, No. 2, June 1973, pp. 145-149.

May, W. R., et al., "High-Temperature Corrosion in Gas Turbines and Steam Boilers by Fuel Impurities: IV. Evaluation of Silicon and Magnesium-Silicon as Corrosion Inhibitors," ASME No. 73-WA/CD-1, p. 5.

McKee, D. W. and G. Romeo, "Effect of Methane on Sulfur Dioxide and Sodium Sulfate-Induced Corrosion of Nickel-Base Alloys," Metallurgical Transactions, Vol. 5, May 1974, p. 1127-1139.

Morrow, III, H., "The Effects of Molybdenum and Aluminum on the Hot Corrosion (Sulfidation) Behavior of Experimental Nickel-Base Superalloys," Metallurgical Transactions, Vol. 5, No. 3, March 1974, pp. 673-683.

Mrowec, S., "Mechanism of High Temperature Metallic Corrosion by Sulfur Vapor," High-Temperature Metallic Corrosion of Sulfur and Its Compounds, Electrochemical Society, Princeton, 1970, pp. 55-109.

Mrowec, S., et al., "Problems of Gas Corrosion of Metals by the Products of Dry Distillation of Coal," Ochrona Przed Korozja, Vol. 16, No. 7, July 1973, pp. 195-199.

Mrowec, S. and A. Stoklosa, "Calculations of Parabolic Rate Constants for Metal Oxidation," Oxidation of Metals, Vol. 8, No. 6, 1974.

Narita, T. and K. Nishida, "The Effect of Sulphur Pressure on the Iron Sulphide Scale Growth at Elevated Temperatures," Transactions of the Japan Institute of Metals, Vol. 14, No. 6, November 1973, pp. 439-446.

Nelson, H. W., et al., "Report on Corrosion and Deposits in Coal- and Oil-Fired Boilers and Gas Turbines," prepared for ASME Research Committee on Corrosion and Deposits from Combustion Gases by Battelle Memorial Institute, 1959.

Niles, W. D. and C. W. Siegmund, "Reaction Between Fuel Ash Components and Additive Combinations," Proceedings of the Marchwood Conference, Mechanism of Corrosion by Fuel Impurities, Johnson and Littler (ed.), Butterworths, London, 1963.

Opik, I., "[Determining the] Corrosion Resistance of Superheater Steels from their Associated Ash Deposits," VGB Kraftwerkstechnik, Vol. 53, No. 8, August 1973, pp. 539-542.

"Overcoming Corrosion by Sulphur Compounds," The British Sulphur Corporation Ltd., November-December 1972.

Pesat, V., "Protection of Furnace Components Against Oxidation and Wear Occurring During Metallurgical Operations," Hutnik (Prague), Vol. 22, No. 10, 1972, pp. 389-393.

Pichoir, R., and J. Poulignier, "Corrosion by Combustion Gases in Turbines and Protective Techniques," Mecanique Materiaux Electricité, No. 291, March 1974, pp. 41-44.

Podhorodecki, J., et al., "Study of the Processes and Kinetics of Corrosion of Nickel-23 Wt.-% Chromium and Nickel-20 Wt.-% Chromium-1/2 Wt.-% Manganese Alloys by Sulfur and Its Compounds," Metal-Slag-Gas Reactions and Processes, Electrochemical Society, Princeton, 1975, pp. 437-447.

Podhorodecki, J. and M. Wedrychowska, "Corrosion Resistance of Aluminum Coated ST35 Steel in SO_2 Atmospheres," Ochrona Przed Korozja, Vol. 15, No. 8, August 1972, pp. 197-201.

Postelnicescu, M. and C. Neaga, "Protection of Boilers from Corrosion," Buletinul Institutal Politehnic Bucuresti, Vol. 30, No. 3/4, May-August 1968, pp. 187-205.

Raask, E., "Reactions of Coal Impurities During Combustion and Deposition of Ash Constituents on Cooled Surfaces," Proceedings of the Marchwood Conference, Mechanism of Corrosion by Fuel Impurities, Johnson and Littler (ed.), Butterworths, London, 1963.

Rahmel, A., "Kinetic Conditions for the Simultaneous Formation of Oxide and Sulfide in Reactions of Iron and Gases Containing Sulfur and Oxygen or Their Compounds," Proceedings Fifth International Congress on Metallic Corrosion, 1972, Tokyo, 1974, pp. 706-711.

Rahmel, A., "Oxidation of Iron in Oxygen-Sulphur Dioxide-Inert Gas Mixtures at 900°C," Werkstoffe und Korrosion, Vol. 23, No. 4, April 1972, pp. 272-278.

Rahmel, A. and J. A. Gonzalez, "Corrosion of Iron at 700-900°C in Gases Containing Oxygen and Sulphur, Revista de Metalurgia, Vol. 8, No. 1, January-February 1972, pp. 3-14.

Rahmel, A. and J. A. Gonzalez, "Metallographic Investigations into the Structure of the Scale after Oxidation of Iron Between 700 and 900°C in $CO-CO_2$ Mixtures with Minor Additions of COS, H_2S, or SO_2," Werkstoffe und Korrosion, Vol. 22, No. 4, April 1971, pp. 283-289.

Reid, W. T., "Basic Problems in the Formation of Sulfates in Boiler Furnaces," Transactions of the ASME, Vol. 89, Series A, April 1967, pp. 283-287.

Reid, W. T. and A. Levy, "Recent Data on the Formation of SO_3 in Flames," Proceedings of the Combustion Symposium, Institute of Combustion and Fuel Technology of Canada, Quebec Branch, Section II, March 30, 1965, pp. 1-11.

Reising, R. F., "Effects of Chromium, Molybdenum, and Tungsten on Sodium Sulfate-Induced High Temperature Corrosion of Nickel," Corrosion, Vol. 31, No. 5, May 1975.

Reising, R. F., "Molten Sodium Sulfate-Induced Corrosion of Nickel Alloys," Metal-Slag-Gas Reactions and Processes, Electrochemical Society, Princeton, 1975, pp. 747-761.

Reising, R. F. and D. P. Krause, "Corrosion Product Characterization of a Nickel-Sodium Sulfate-Air System After Exposure to Temperatures Near 1000°C," Corrosion, Vol. 30, No. 4, April 1974, pp. 131-138.

Reynaud, P., "Use of Additives to Neutralize the [Sulphur Trioxide] Fumes [in the Gases] from Combustion of Fuel [Oil] for Steam Generation at the Montereau Power Station," Revue Generale de Thermique, Vol. 13, No. 147, March 1974, pp. 235-244.

Richards, M. N. and J. Stringer, "Some Aspects of the Hot Corrosion of Cobalt-Base Alloys," British Corrosion Journal, Vol. 3, No. 4, July 1973, pp. 167-172.

Rickert, H. and K. H. Tostmann, "Influence of Phase-Boundary Reactions During Metal Oxidation: Investigations on the Sulphidation of Silver in Sulphur Vapour," Werkstoffe und Korrosion, Vol. 21, No. 11, November 1970, pp. 965-973.

Romeo, G. and W. W. Smeltzer, "The High Temperature Sulfidation Properties of Nickel-Chromium Alloys," Journal of Electrochemical Society, Vol. 119, September 1972, pp. 1267-1269.

Romeo, G., et al., "Mechanism of Sulfidation of Nickel-Chromium Alloys at 700°C as Inferred From Inert and Radioactive Marker Techniques," Journal of Electrochemical Society, Vol. 118, No. 9, August 1971, pp. 1336-1339, "Discussion," pp. 1339-1340.

Romeo, G., W. W. Smeltzer, and J. S. Kirkaldy, "Sulphidation Properties of a Nickel-20 Wt.-% Chromium Alloy at 700°C, Chimica e l'Industria, Vol. 54, No. 1, January 1972, pp. 28-34.

Sano, M. and K. Mori, "Effect of Surface Movement (Gas-Velocity) on the Rate of Gas-Metal Reactions," Journal of Iron Steel Institute (Japan), Vol. 60, No. 10, September 1974, pp. 1432-1442.

Schliesing, H., "Corrosion Protection and Coating in Power Stations: Requirements and Choice of Coating Materials," VGB Kraftwerkstechnik, Vol. 55, No. 5, May 1975, pp. 318-320.

Schonbauer, G. and H. Trenkler, "The Effect of Copper, Nickel, Sulphur, and Manganese Content on the Scaling of Steel," Radex Rundschau, Vol. 5, December 1971, pp. 577-590.

Schot, J. and P. Rollmann, "Prevention of Flue-Gas Corrosion on the Heating Surfaces of Boiler Economiser Tubes by Means of Protective Materials; and the Effect of Such Materials on Heat Transfer and Pressure Drop," Mitteilungen der VGB, Vol. 53, No. 3, March 1973, pp. 199-203.

Seybolt, A. U., "Role of Rare-Earth Additions in the Phenomenon of Hot Corrosion," Corrosion Science, Vol. 11, No. 10, October 1971, pp. 751-761.

Shirley, H. T., "Effects of Sulfate-Chloride Mixtures on Fuel Ash Corrosion of Steel and High Ni Alloys," Journal of the Iron and Steel Institute, Vol. 182, 1956, p. 144.

Shirley, H. T. "Sulphate-Chloride Attack on High Alloy Steels and Nickel Alloys," Proceedings of the Marchwood Conference, Mechanism of Corrosion by Fuel Impurities, Johnson and Littler (ed.), Butterworths, London, 1963.

Shreiber, G. K., et al., "The Exfoliation of an Aluminum Coating on Steel," Korroziya i Zashchita, Vol. 11, 1974, pp. 21-22.

Simkovich, G., "The Effect of Auxiliary Gas Solubilities in Scales Upon Parabolic Oxidation Kinetics," Werkstoffe und Korrosion, Vol. 21, No. 1, November 1970, pp. 973-977.

Spyra, W., "High-Temperature Corrosion of Iron, Nickel, Chromium, Nickel-Chromium, Iron-Chromium, and Nickel-Iron-20% Chromium Alloys by Vanadium Pentoxide and Hydrogen Sulphide, " DEW Technische Berichte, Vol. 8, No. 2, June 1968, pp. 52-58.

Steel, J. S. and E. A. Brandes, "Growth and Adhesion of Oxides in Furnace Deposits and Their Influence on Subsequent Deposition of Ash Particles as Combustion Products," Proceedings of the Marchwood Conference, Mechanism of Corrosion by Fuel Impurities, Johnson and Littler (ed.), Butterworths, London, 1963.

Stonner, A., "Effect of Reducing-Flue-Gases on Furnace-Tube Corrosion," Mitteilungen der VGB, Vol. 49, No. 3, June 1969, pp. 180-182.

Strafford, K. N. and J. M. Harrison, "The Sulphidation of Nickel-Based Alloys Containing Refractory Sulphide-Forming Elements," Metal-Slag-Gas Reactions and Processes, Electrochemical Society, Princeton, 1975, pp. 464-479.

Stringer, J. and D. P. Whittle, "High-Temperature Corrosion and Coating of Superalloys," [Symposium on] High-Temperature Materials in Gas Turbines, Baden, March 1973, 1974, pp. 283-312; "Discussion," pp. 312-314.

Stringer, J. and D. P. Whittle, "The Hot Corrosion of Nickel-Base Superalloys-The Effect of Molten Salt Chemistry," Metal-Slag-Gas Reactions and Processes, Electrochemical Society, Princeton, 1975, pp. 665-677.

Stringer, J., M. E. El-Dahshan, and I. G. Wright, "Sulfidation and Sulfidation-Oxidation of Nickel- and Cobalt-Base Alloys Containing Dispersions of Stable Oxides," Oxidation of Metals, Vol. 8, No. 6, 1974, pp. 361-377.

Thilakan, H. R., et al., "Studies on the Resistance of Alloy Steels Against Oil-Ash Corrosion-II," National Metallurgical Laboratory Technical Journal (India), Vol. 11, No. 1, February 1969, pp. 12-16.

Toft, L. H. and R. A. Marsden, "Metallurgical Aspects of the Fireside Corrosion of Superheater Tube Materials," Proceedings of the Marchwood Conference, Mechanism of Corrosion by Fuel Impurities, Johnson and Littler (ed.), Butterworths, London, 1963.

Tyul'pin, K. K., et al., "The Oxidation Resistance of Industrial Steels in the Combustion Products of Solid, Liquid, and Gaseous Fuels Used in Steam Generation in Power Stations," Vliyanie Fiz.-Khim.Sredy na Zharoprochnost' Metal. Materialov, Russian Collection, Published 'Nauka' Moscow, 1974, pp. 72-76.

Verma, S. K., D. P. Whittle, and J. Stringer, "Sulphidation of Cobalt-Based Alloys," Corrosion Science, Vol. 12, No. 7, July 1972, pp. 545-554.

Wagner, C., "Attack of Metals by Gases," Werkstoffe und Korrosion, Vol. 21, No. 11, November 1970, pp. 886-894.

Watson, M. H., "High-Temperature Corrosion of Hot-Dipped Aluminized Steel Heat Exchangers in Domestic Gas-Fired Equipment," Journal of the Institute of Fuel, Vol. 39, 1966, pp. 253-256.

Whelan, E. P. and J. M. Trenouth, "Sodium Sulphate Induced Rapid Oxidation of a Chromium Titanium-Silicon Coating on Niobium Alloy B-66," Journal of Less Common Metals, Vol. 33, No. 1, October 1973, pp. 153-170.

Yakhshiev, V. S., "The Effectiveness of Calorized Coatings on Steel in Reducing Corrosion by Hydrogen Sulphide," Korroziya i Zashchita, Vol. 9, 1971, pp. 16-18.

Young, W. E. and A. E. Hershey, "A Thermochemical Study of Some Additives to Reduce Residual Fuel Ash Corrosion," Corrosion, Vol. 13, November 1957, pp. 725t-732t.

Zelanko, P. D. and G. Simkovich, "High-Temperature Sulfidation Behavior of Iron-Based Alloys in Hydrogen Sulfide-Hydrogen Gas Mixtures," Oxidation of Metals, Vol. 8, No. 5, 1974, pp. 343-360.

Zelouf, S. and G. Simkovich, "The Kinetics of Sulfidation of Binary and Ternary Iron Alloys in H_2S/H_2 Gas Mixtures," High-Temperature Metallic Corrosion of Sulfur and Its Compounds, Electrochemical Society, Princeton, 1970, pp. 119-131.

Zusman, V. M. and V. V. Tikhonova, "Selection Formation of Ash Deposits on [Superheater] Tubes of 12% Chromium Steel," Teploenergetika, Vol. 11, November 1970, pp. 57-61.

APPENDIX B

ALLOYS AND COATED SPECIMENS FOR FIRESIDE TESTING

MATERIAL ANALYSIS AND CHARACTERIZATION OF ALLOYS

The alloys included in the Phase 1 tests were analyzed as shown in Table B.1. The detailed analysis of the Phase 2 (customer melted) alloys is shown in Table B.2. International Nickel Company's (INCO's) Paul D. Merica Research Laboratory prepared the customer-melted alloys. The following metallography hardness data and the heat treatment of each individual alloy are presented so that there is sufficient detail on all materials for any or all tests to be repeated with the same result. Complete chemical analyses together with nominal compositions, microstructures of the conditions or heat treatments of interest, hardness, grain size, and analysis of microstructural phases by electron probe microanalysis are included. Each of the 38 alloys is shown on a separate page.

PREPARATION OF PREOXIDIZED SPECIMENS FOR SUBTASK 1.4.3.1

Whether the alkali-iron trisulfate corrosion attacks the metal or the oxide of the metal or both was questionable. On low-alloy steel, the evidence indicated that both are attacked. A study of the corrosion of well-characterized, preoxidized specimens was designed to provide needed information. A dense, adherent scale was produced as the starting material surface.

In preparation, the 10 selected alloys from the base material group were oxidized in flowing air or in a cracked-ammonia atmosphere, with oxygen supplied by NiO at temperatures that would form an adherent and continuous oxide scale. The scale was identified by x-ray diffraction. The results of the oxidation are shown in Table B.3. For the most part, Cr_2O_3 is the dominant species, but Al_2O_3 layers were found on two alloys--IN-811 and IN-814.

Table B.1 Chemical Composition of Phase 1 Alloys for Fireside Tests (% by weight)

Alloy	Heat or Lot No.	C	Mn	P	S	Si	Ni	Cr	Fe	Mo	Al	Ti	V	Cu	Other
Ferritic Alloys															
2-1/4%Cr-1%Mo	52816	0.12	0.55	0.020	0.023	0.29	0.15	2.34	Bal.	0.87	---	---	---	---	Co 0.13
HT-9 (Sandvik Tube)	4-52112	0.22	0.52	0.018	0.005	0.35	0.50	11.3	Bal.	0.97	---	---	0.26	---	W 0.50
Austenitic SS															
304	47832	0.055	1.71	0.022	0.025	0.55	8.40	18.34	Bal.	0.11	---	---	---	0.08	Co 0.16
347	8083689	0.059	1.58	0.03	0.015	0.67	10.30	18.50	Bal.	0.17	---	---	---	0.16	Cb 0.61
	30W2	0.055	1.72	---	---	0.81	9.8	18.1	Bal.	---	---	---	---	---	Cb 0.84
310	8084791	0.069	1.77	0.028	0.014	0.46	20.40	25.30	Bal.	---	---	---	---	---	---
	04964	0.045	0.18	---	---	0.14	22.1	22.3	Bal.	---	---	---	---	---	---
314	7401-8001	0.068	1.06	0.042	0.024	1.73	21.1	24.2	Bal.	0.01	---	---	---	0.02	---
	46W	0.056	2.03	---	---	2.09	19.4	23.3	Bal.	---	---	---	---	---	---
IN-840	---	0.041	0.13	---	---	0.77	20.6	20.3	Bal.	---	---	---	---	---	---
High-Manganese Alloy															
21-6-9 (Nitronic 40)	346087	0.021	9.2	0.016	0.003	0.67	7.21	20.1	Bal.	0.16	---	---	---	0.13	N 0.32
High-Iron Superalloys															
IN-737	---	0.032	<0.1	---	---	<0.1	37.5	17.2	Bal.	1.44	0.59	0.52	---	---	Cb 1.03
Incoloy 800H	---	0.056	0.88	---	---	0.24	31.2	20.4	Bal.	---	0.47	0.46	---	0.63	---
Incoloy 800	HH2118A	0.05	0.93	---	0.007	0.42	31.24	21.54	44.72	---	0.39	0.35	---	0.33	---
A-286	29385	0.041	1.32	0.023	0.003	0.54	25.10	15.22	Bal.	1.40	0.17	2.18	0.27	0.26	B 0.007
AL-6X	00629	0.013	1.65	---	0.005	0.33	24.41	20.0	Bal.	6.5	0.03	---	---	---	---
Nickel-Base Superalloys															
Inconel 625	---	0.019	0.13	---	---	0.19	Bal.	21.8	2.9	8.9	0.26	0.21	---	---	Cb 3.8
IN-671	---	0.059	<0.1	---	---	0.38	Bal.	45.5	---	---	0.034	0.26	---	---	---
Semicommercial Alloys															
IN-549	---	0.099	<0.1	---	---	0.28	43.7	19.5	Bal.	---	2.5	---	---	---	---
IN-809	---	0.010	<0.1	---	---	<0.1	Bal.	36.8	17.1	---	---	0.5	---	---	---
IN-811	---	0.014	0.79	---	---	0.35	34.1	20.7	Bal.	---	1.98	---	---	---	---
IN-814	---	0.10	0.62	---	---	0.21	Bal.	32.1	15.6	---	3.48	0.35	---	---	---

Table B.2 Alloy Compositions for Phase 2 Fireside Tests

Alloy No.	Actual Chemical Analysis (% by Weight, Balance Fe)						
	Ni	Cr	Al	Si	Y	Mn	C*
1	24.7	19.8	---	0.41	---	0.64	0.025
2	25.4	19.6	2.04	0.40	---	0.60	0.026
3	25.3	19.4	---	2.27	---	0.57	0.026
4	24.2	19.6	2.00	2.40	---	0.59	0.034
5	33.5	24.4	---	0.40	---	0.70	0.026
6	34.0	24.5	2.00	0.40	---	0.74	0.035
7	34.1	24.2	---	2.30	---	0.74	0.025
8	33.7	24.1	1.90	2.30	---	0.62	0.013
9	38.5	30.2	---	0.50	---	0.72	0.024
10	39.0	30.2	1.80	0.40	---	0.74	0.020
11	38.7	30.5	---	2.30	---	0.71	0.027
12	39.3	29.7	1.80	2.40	---	0.76	0.019
13	33.0	24.4	3.70	0.40	---	0.70	0.015
14	33.9	24.3	3.70	0.40	0.01	0.75	0.021
15	37.2	24.2	4.20	0.44	0.60	0.72	0.025
16	35.1	24.3	---	0.44	0.06	0.57	0.033
17	35.4	24.7	---	0.37	0.53	0.68	0.031
18	18.4	25.1	---	0.45	0.58	0.67	0.041
19†	20.0	23.0	0.30	---	0.65 Y_2O_3	---	0.045

*Nominal carbon analysis was 0.035 percent maximum for all alloys except 18 and 19 which had 0.045 percent maximum.
†Mechanical alloy.

Note: The metallographic characterization of the listed alloys is presented in Appendix B.

Table B.3 Oxide Scales Present on 10 Alloys Before Exposure to the Trisulfate Corrosion of Preoxidized Materials

Alloy	Oxidation Treatment* at °F (°C)	Composition of the Dense Adherent Scale†
HT-9	1292 (700) in air	Cr_2O_3 (w)
310	2192 (1200) cracked NH_3 with NiO	Cr_2O_3 (mw), spinel (m)
314K	2192 (1200) cracked NH_3 with NiO	Cr_2O_3 (m), spinel (mw)
347	2192 (1200) cracked NH_3 with NiO	Cr_2O_3 (mw), spinel (mw)
21-6-9	1652 (900) in air	$MnCr_2O_3$ (s)
625	1832 (1000) in air	Cr_2O_3 (s), spinel (m)
800	1832 (1000) in air	Cr_2O_3 (m), spinel (m)
811	2012 (1100) in air	αAl_2O_3 (vw), Cr_2O_3 (w), spinel (m)
814	2012 (1100) in air	αAl_2O_3 (mw), Cr_2O_3 present as loose powder will be brushed off
671	2012 (1100) in air	Cr_2O_3 (s), spinel (w)

*This oxidation treatment was performed by the Paul A. Merica Research Laboratory of INCO, Sterling Forest, New York. Treatment time was 24 hours.
†X-ray diffraction code:
w = weak mw = moderately weak m = moderate
s = strong vw = very weak.
§Silicon was lost by vaporization from the surface.

PREPARATION OF COATED SPECIMENS (SUBTASK 1.4.6)

The coated specimens tested in Phase 3 of the program were evaluated prior to their exposure to establish their quality, microstructure, and other important properties. The purpose of this test was to clarify any changes in properties, or microstructure which may have occurred during the fireside exposure. It was also necessary, in order to ensure future development, that the coating be completely identified. The results and the identification of materials are shown in Table B.4. The corresponding test results in the fireside environment are shown in Table 3.1.5 in the main volume of this report. Figures B.38 through B.54 in this appendix show the coated specimens prior to exposure.

Table B.4 Description and Evaluation of Coated Specimens Before Exposure*

Coating and Substrate	Initial Thickness in. (μm)	Thermal Treatment	Description
Alonized†		None after coating	Two distinct layers--the outer, which exhibited minor porosity and cracks, was high aluminum, 0.004 to 0.005 (101 to 127 μm) thick, the inner was two-phase structure containing an aluminide compound precipitated within the alloy matrix. The diffusion zone was twice as wide in the 304 as it was in the 800.
800	152-203 (0.006-0.008)		
304	203-254 (0.008-0.010)		
Chromized†		None after coating	Layers-a high-chromium layer on the surface approximately 0.0008 in. (20 μm) thick and a dissuasion zone 0.0016 in. (40 μm).
HT-9*	0.008-0.0010 (20-25)		
21-6-9	0.0016 (40)		
304	0.0016 (15)		
800	0.006 (15)		
2-1/4%Cr-1%Mo	---		
Siliconized§		Diffused 1 hour	Layer of silicon-enriched area on surface (no porosity)
347	0.004 (10)	1850°F (1010°C) in He + H_2 gas	
304	0.006 (15)		
2-1/4%Cr-1%Mo	0.001 (25)		
Alloy 2	0.0005 (13)		
Alloy 13	0.0005 (13)		
Fe-Cr-Al¶		None after coating	Porous from elemental powders
Kanthal†		1800°F (980°C) KD-5, KD-16	Low porosity, 0.062 wire feed
309	50.8-203 (0.002-0.008)		

*Treatments to the Alonized, chromized, and siliconized specimens were applied by the diffusion process. The Kanthal specimens were metallized, and the "duplex" specimens were CrSi2-Plasma sprayed and Kanthal-metallized. All others were plasma sprayed.
†Established commercial process.
§Foster Wheeler Development Corporation coatings.
¶Developmental procedure by vendor.

Table B.4 Description and Evaluation of Coated Specimens Before Exposure* (Cont)

Coating and Substrate	Initial Thickness	Thermal Treatment in. (μm)	Description
"Duplex"-$CrSi_2$ over Kanthal>		1800°F (980°C) Nos. 60, 61, 62, and 63	Porosity in outer layer
347	0.52-254 (0.006-0.010)		
CrSi2*		1800°F (980°C)	Porosity scattered throughout coating Metco material used
430	127-203 (0.005-0.008)		
HT-9	---		
304	---	No. 56	
Ni-Cr-Al*		None after coating	Metco 443
347	203 (0.008)		
Ni-Cr§		None after coating	IN-671 spheroidized powder, 48% Cr, 98%Ni, 1%Ti (prepared by INCO)
800	127-254 (0.005-0.010)		
737	178-304 (0.007-0.012)		
Ni-Cr-Si§		1800°F (980°C) A, B, C, and D	IN-671 and 5% Si not fullly homogeneous, some porosity
309	102-127 (0.004-0.005)		
Ni-Cr-Al*		1800°F (980°C) L and M	Metco 443
309	127 (0.005)		
Ni-Al*			Metco 404, not full density
304	229-254 (0.009-0010)		
347	229-254 (0.009-0.010)		
$MgZrO_4$		None after coating	Metco 210
304	229-254 (0.009-0010)		

Table B.4 Description and Evaluation of Coated Specimens Before Exposure* (Cont)

Coating and Substrate	Initial Thickness	Thermal Treatment in. (μm)	Description
ZrO_2*			Metco 201, stabilized (cubic) ZrO2 plasma spray without bonding coat
2-1/4%Cr-1%Mo	203-508 (0.008-0.020)		
347	203-508 (0.008-0.20)		
Triboloy 700*		None after coating	Low porosity
310	254 (0.010)		
Triboloy 800*		None after coating	Low porosity
310	203 (0.008)		

Chemical Analysis (% by Wt.):

	Cr	Ni	Fe	C	Mn	Si	Mo	Other
Nominal	2.25	---	Bal	0.15	0.45	0.5	1.0	---
52816	2.34	0.15	Bal	0.12	0.55	0.29	0.87	0.13 Co 0.020 P 0.023 S

PN 1-55978 (250X)--Normalized and Tempered

Etchant: V_2A
Annealed Hardness: R_B 93
Annealed Grain Size: ASTM 5

Figure B.1 Characterization of Alloys Before Test
(2-1/4%Cr-1%Mo Steel)

Chemical Analysis (% by Wt.):

	Cr	Ni	Fe	C	Mn	Si	Mo	V	Other
Nominal	12	0.5	Bal	0.20	0.55	0.30	1.0	0.3	---
4-52112	11.3	0.5	Bal	0.22	0.52	0.35	0.97	0.26	0.018 P 0.005 S 0.5 W

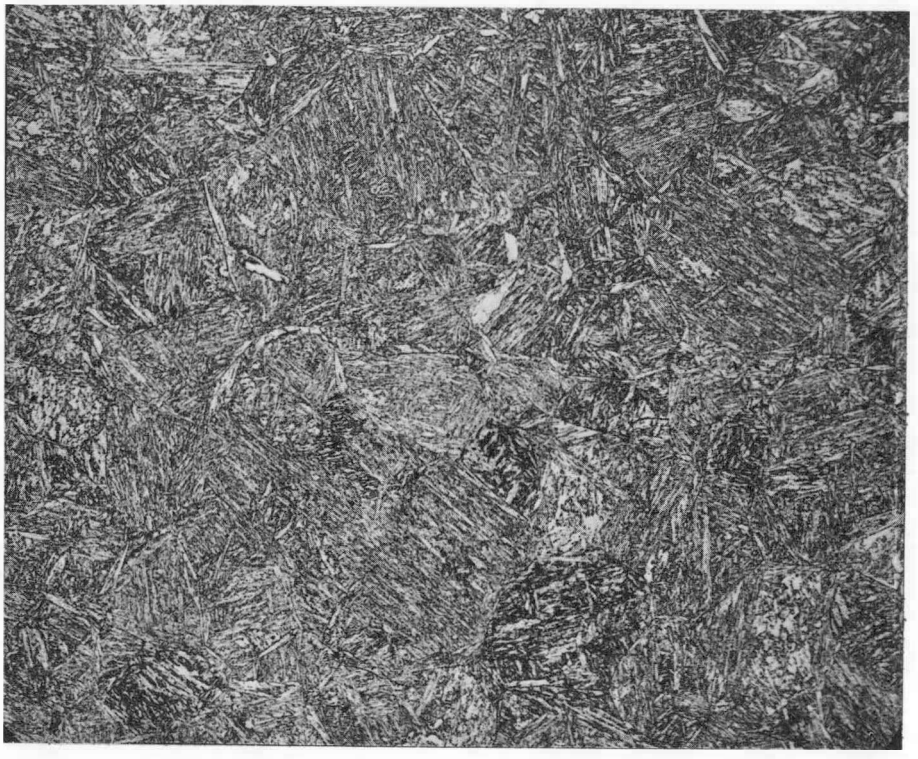

PN 1-55981 (250X)--Mill Annealed

Etchant: V_2A
Annealed Hardness: R_B 99
Annealed Grain Size: ASTM 6

Figure B.2 Characterization of Alloys Before Test
[HT-9 (Sandvik Tube)]

Chemical Analysis (% by Wt.):

	Cr	Ni	Fe	C	Mn	Si	Mo	Other
Nominal	18.5	9.5	Bal	0.05	1.0	0.5	---	---
47832	18.34	8.40	Bal	0.055	1.71	0.025	0.11	0.08 Cu 0.16 Co

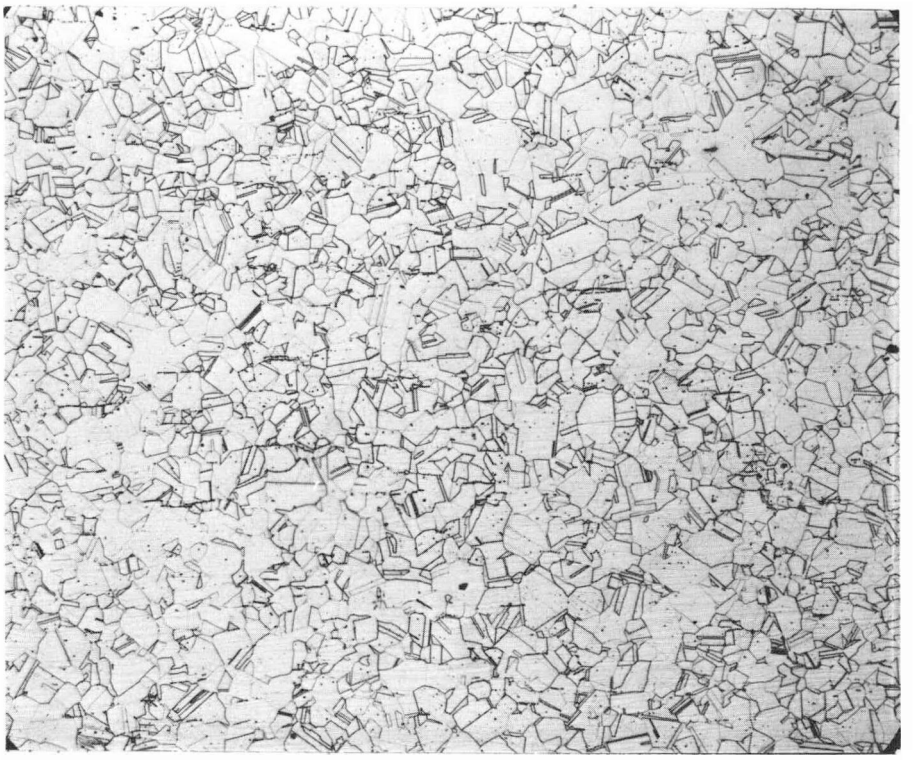

PN 1-55977 (100X)--1 h/2200°F/WQ

Etchant: V_2A
Annealed Hardness: R_B 81
Annealed Grain Size: ASTM 7

Figure B.3 Characterization of Alloys Before Test
(Type 304 Stainless Steel)

Chemical Analysis (% by Wt.):

	Cr	Ni	Fe	C	Mn	Si	Mo	Cb	Other
Nominal	18.0	11.0	Bal	0.06	1.0	0.5	---	0.6	---
30W2	18.1	9.8	Bal	0.055	1.72	0.81	---	0.84	---
8083689	18.50	10.30	Bal	0.059	1.58	0.67	0.17	0.61	0.03 P 0.015 S 0.16 Cu

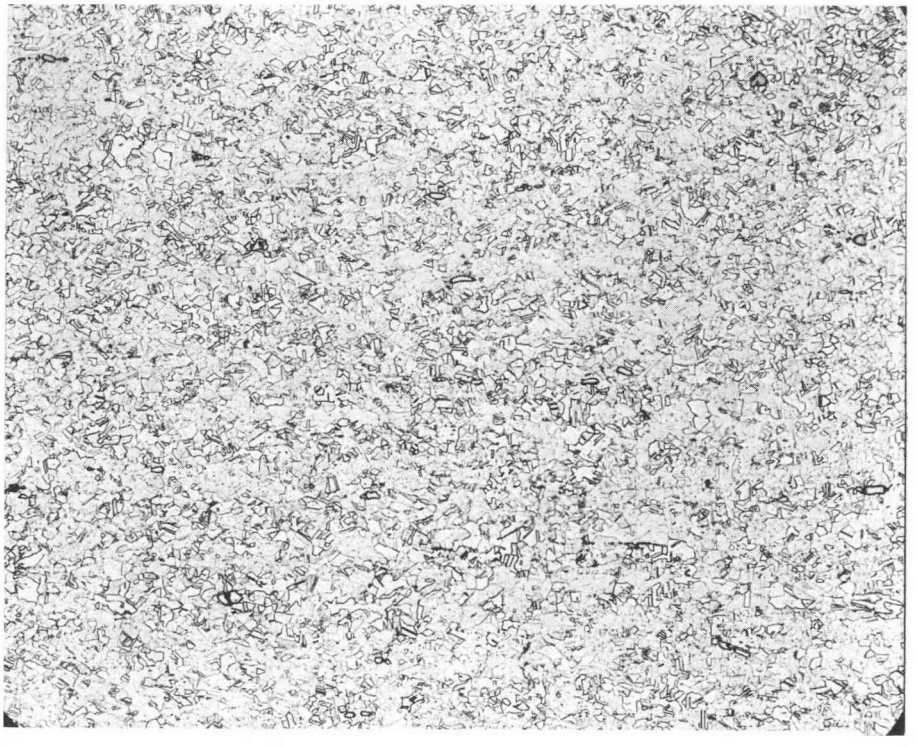

PN 1-55252 (250X)--4 h/1800°F/AC

Etchant: V_2A
Annealed Hardness: R_B 85
Annealed Grain Size: ASTM 8

Figure B.4 Characterization of Alloys Before Test
(Type 347 Stainless Steel)

Chemical Analysis (% by Wt.):

	Cr	Ni	Fe	C	Mn	Si	Other
Nominal	25	20	Bal	0.1	1.5	0.6	
04964	22.3	22.1	Bal	0.045	0.18	0.14	
8084791	25.30	20.40	Bal	0.069	1.77	0.46	0.028 P 0.014 S

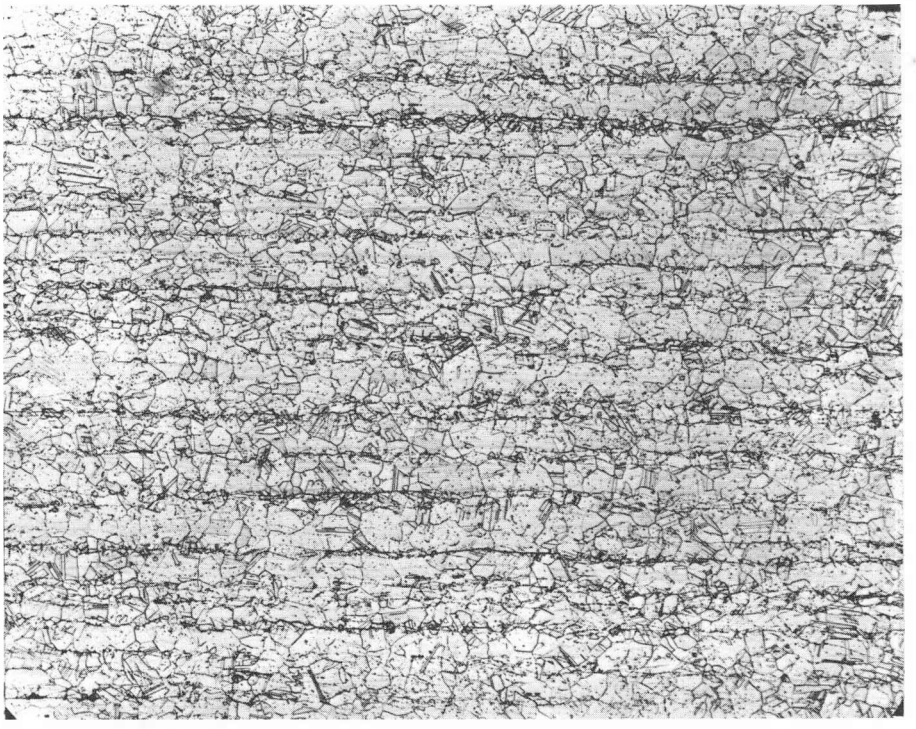

PN 1-57479 (100X)--Hot Rolled

Etchant: 60% HNO_3 in Water
Annealed Hardness: R_B 71
Annealed Grain Size: ASTM 7

Figure B.5 Characterization of Alloys Before Test
(Type 310 Stainless Steel)

Chemical Analysis (% by Wt.):

	Cr	Ni	Fe	C	Mn	Si	Mo	Other
Nominal	25	20	Bal	0.04	1.5	2.0	---	---
46W	23.3	19.4	Bal	0.056	2.03	2.09	---	---
7401-8001	24.2	21.1	Bal	0.068	1.06	1.73	0.01	0.042 P 0.024 S 0.02 Cu

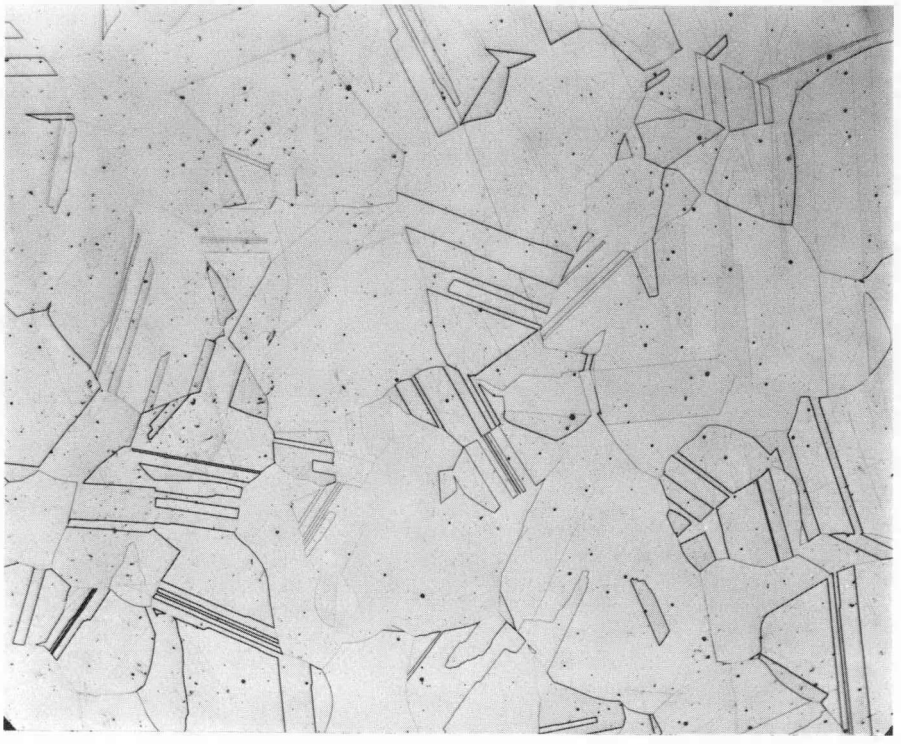

PN 1-54178 (100X)--1 h/2200°F/WQ

Etchant: V_2A
Annealed Hardness: R_B 88
Annealed Grain Size: ASTM 1

Figure B.6 Characterization of Alloys Before Test
(Type 314 Stainless Steel)

Chemical Analysis (% by Wt.):

	Cr	Ni	Fe	C	Mn	Si	Cu	S
Nominal	20	20	Bal	---	---	---	---	---
HH 8188P	20.1	21.50	56.67	0.05	0.22	0.89	0.57	0.002

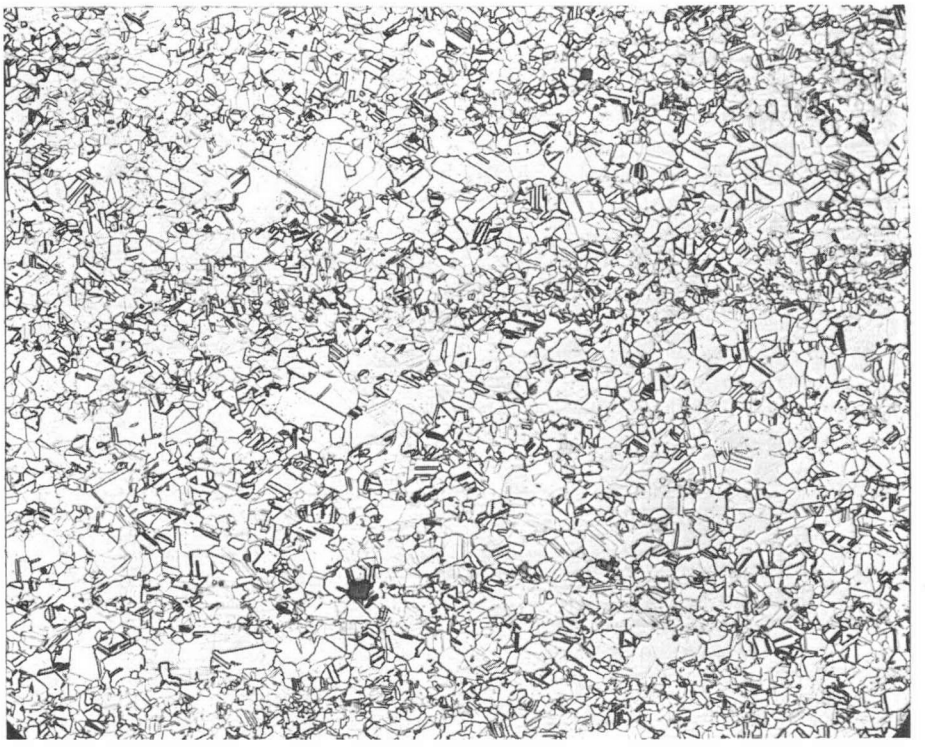

PN 1-55247 (250X)--1/4 h/1900°F/AC

Etchant: V_2A
Annealed Hardness: R_B 75
Annealed Grain Size: ASTM 8

Figure B.7 Characterization of Alloys Before Test
(Incoloy Alloy 840)

Chemical Analysis (% by Wt.):

	Cr	Ni	Fe	C	Mn	Si	Mo	N	Other
Nominal	21	6	Bal	0.04	9	0.25	---	0.27	---
346087	20.1	7.21	Bal	0.021	9.2	0.67	0.16	0.32	0.13 Cu 0.003 S 0.016 P

PN 1-55985 (100X)--Mill Annealed

Etchant: V_2A
Annealed Hardness: R_B 98
Annealed Grain Size: ASTM 5

Figure B.8 Characterization of Alloys Before Test
[21-6-9 (Nitronic 40)]

Chemical Analysis (% by Wt.):

	Cr	Ni	Fe	C	Mo	Al	Ti	Cb	B
Nominal	18	38	Bal	0	1.7	0.6	0.5	0.1	0.015
78250	17.2	37.5	Bal	0.032	1.44	0.59	0.52	1.03	<0.002

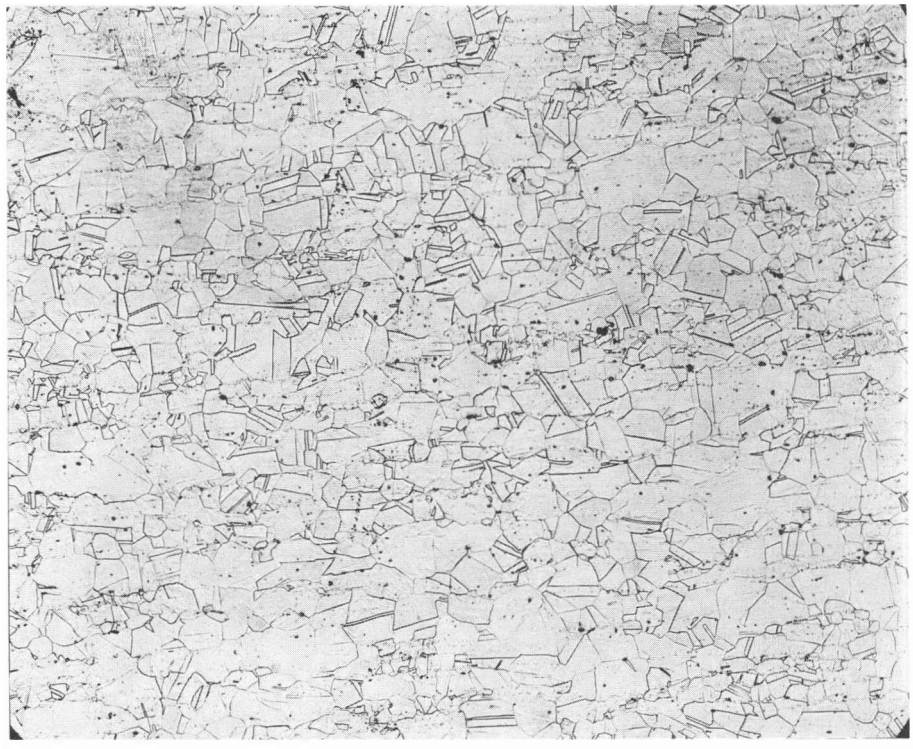

PN 1-55242 (100X)--1/2 h/1900°F/AC

Etchant: V_2A
Annealed Hardness: R_B 72
Annealed Grain Size: ASTM 6

Figure B.9 Characterization of Alloys Before Test (IN-737)

Chemical Analysis (% by Wt.):

	Cr	Ni	Fe	C	Mn	Si	Cu	Al	Ti	S
Nominal	21.0	32.5	46.0	0.05	0.75	0.50	0.38	0.38	0.38	0.008
HH-8074A (800H)	20.22	31.24	45.74	0.06	0.89	0.22	0.61	0.52	0.50	0.002
HH-2118A	21.54	31.24	44.72	0.05	0.93	0.42	0.33	0.39	0.35	---

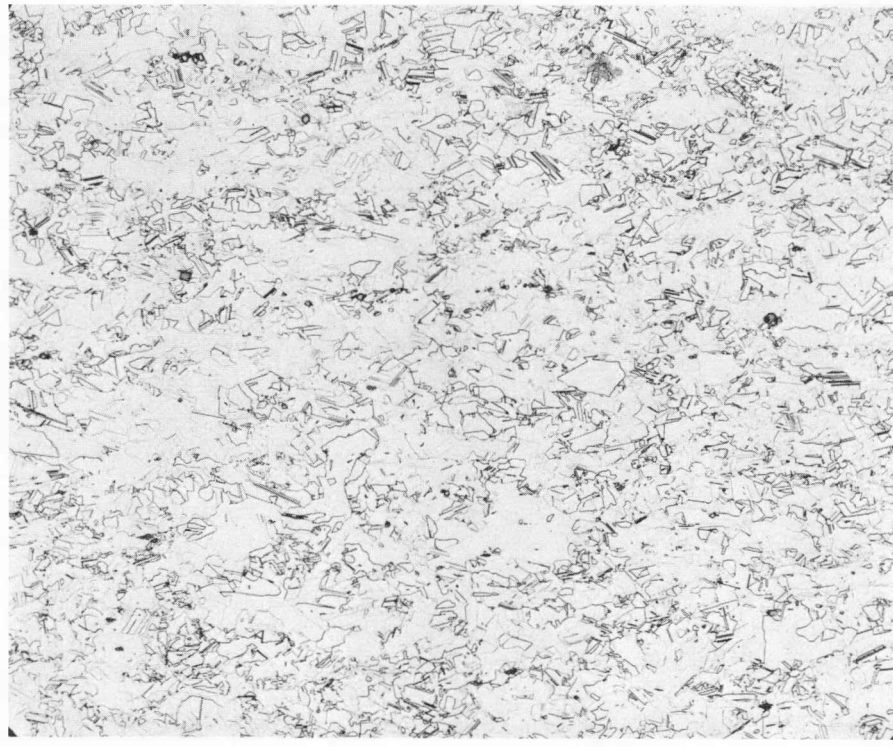

PN 1-55244 (100X)--1/4 h/1900°F/AC

Etchant: V_2A
Annealed Hardness: R_B 82
Annealed Grain Size: ASTM 8

Figure B.10 Characterization of Alloys Before Test
(Incoloy Alloy 800H)

Chemical Analysis (% by Wt.):

	Cr	Ni	Fe	C	Mn	Si	Mo	Al	Ti	Other
Nominal	15	26	Bal	---	---	---	1.3	0.2	2.0	---
29385	15.22	25.10	Bal	0.041	1.32	0.54	1.40	0.17	2.18	0.007 B 0.023 P 0.003 S 0.26 Cu

PN 1-55991 (100X)--Mill Annealed

Etchant: V_2A
Annealed Hardness: R_B 100
Annealed Grain Size: ASTM 7

Figure B.11 Characterization of Alloys Before Test (A-286)

Chemical Analysis (% by Wt.):

	Cr	Ni	Fe	C	Mn	Si	Mo	Al	S
Nominal	20	24	Bal	---	---	---	6	---	---
00629	20.0	24.41	Bal	0.13	1.65	0.33	6.5	0.03	0.005

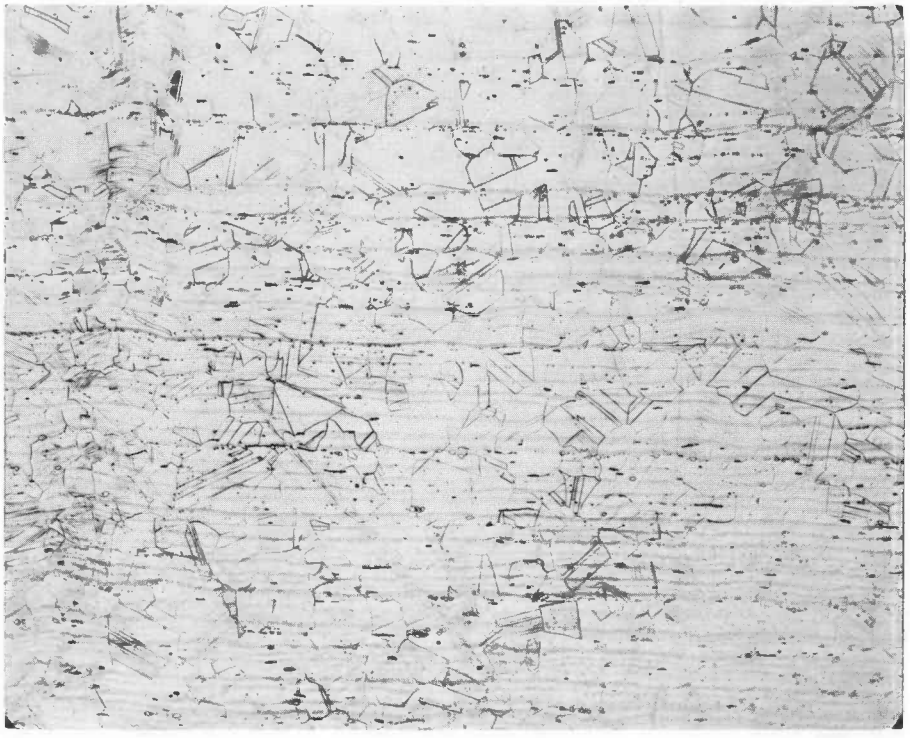

PN 1-55983 (100X)--Annealed

Etchant: V_2A
Annealed Hardness: R_C 21
Annealed Grain Size: ASTM 6

Figure B.12 Characterization of Alloys Before Test
(Allegheny Ludlum 6X)

Chemical Analysis (% by Wt.):

	Cr	Ni	Fe	C	Mn	Si	Mo	Al	Ti	Cb	Co
Nominal	21.5	61.0	2.5	0.05	0.25	0.25	9	0.2	0.2	3.65	0.5
NX-7613A	21.8	Bal	2.9	0.019	0.13	0.19	8.9	0.26	0.21	3.8	<0.1

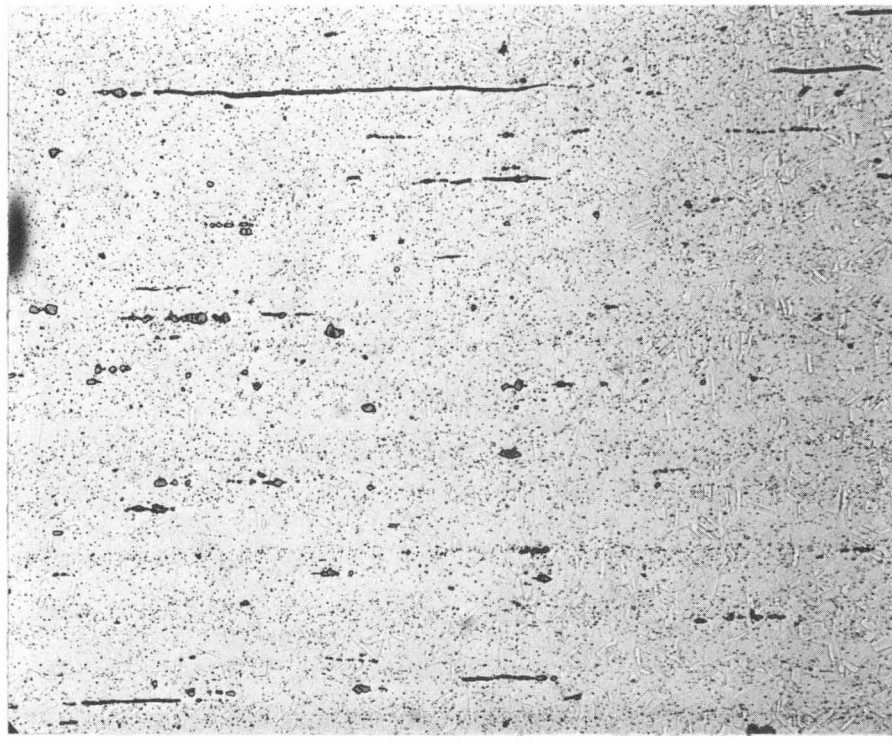

PN 1-55325 (250X)--1/2 h/1900°F/AC

Etchant: 5% Nital Electrolytic
Annealed Hardness: R_B 93
Annealed Grain Size: ASTM 8

Figure B.13 Characterization of Alloys Before Test
(Inconel Alloy 625)

Chemical Analysis (% by Wt.):

	Cr	Ni	Fe	C	Mn	Si	Al	Ti
Nominal	48	Bal	---	0.05	---	---	0.1	0.35
NX-18COES	47.4	51.2	0.89	0.06	0.08	0.34	0.034	0.26

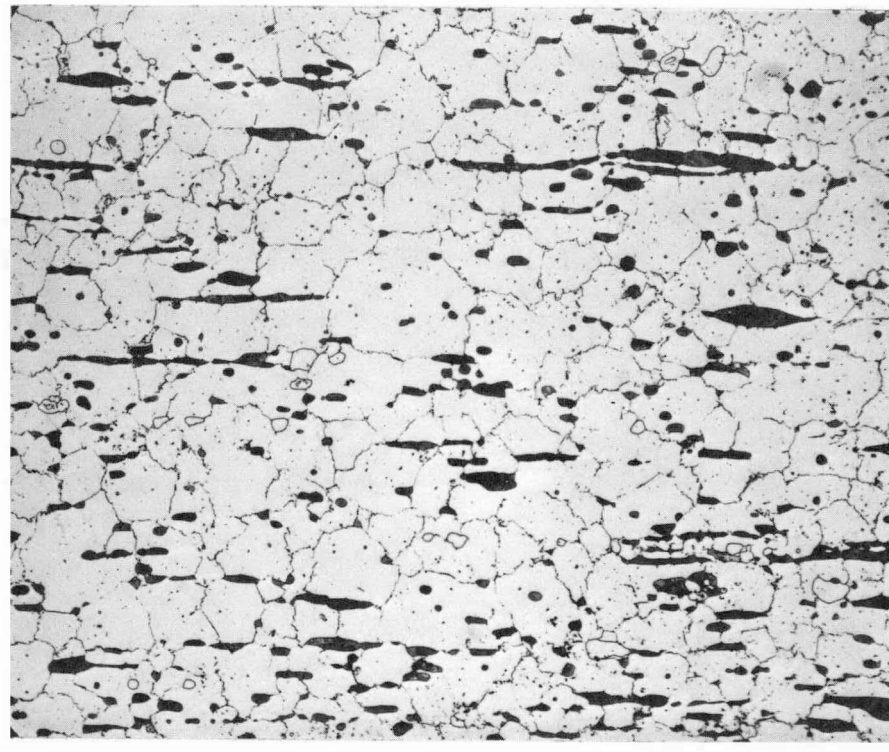

PN 1-55249 (250X)--Mill Annealed

Etchant: V_2A
Annealed Hardness: R_A 62
Annealed Grain Size: ASTM 6

Phase Analysis by Electron Probe:

	Cr	Ni
Dark Phase	74.3	23.9
Light Delineated Phase	95.0	5.0

Figure B.14 Characterization of Alloys Before Test
(Inconel Alloy 671)

Chemical Analysis (%by Wt.):

	Cr	Ni	Fe	C	Si	Al	Ti
Nominal	21	40	Bal	0.01	---	2.5	---
A-499	19.5	43.7	Bal	0.099	0.28	2.5	0.32

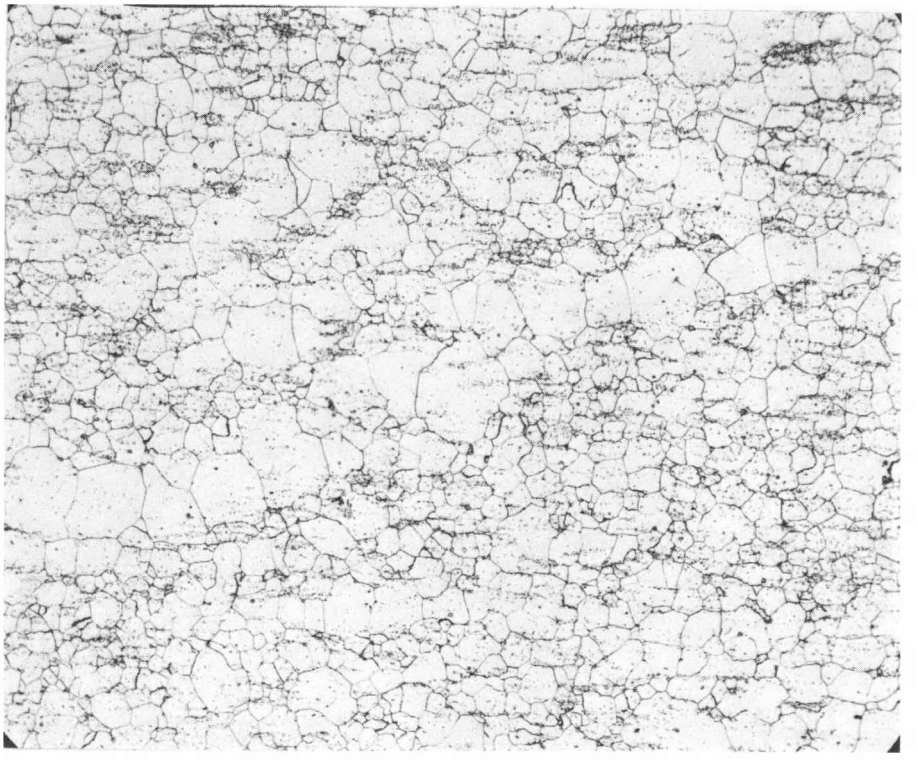

PN 1-59247 (100X)--1 h/2200°F/WQ

Etchant: 60% HNO_3
Annealed Hardness: R_B 80
Annealed Grain Size: ASTM 5

Figure B.15 Characterization of Alloys Before Test (IN-549)

Chemical Analysis (% by Wt.):

	Cr	Ni	Fe	C	Ti
Nominal	37	44	18	---	0.5
Actual	36.8	Bal	17.1	0.01	0.5

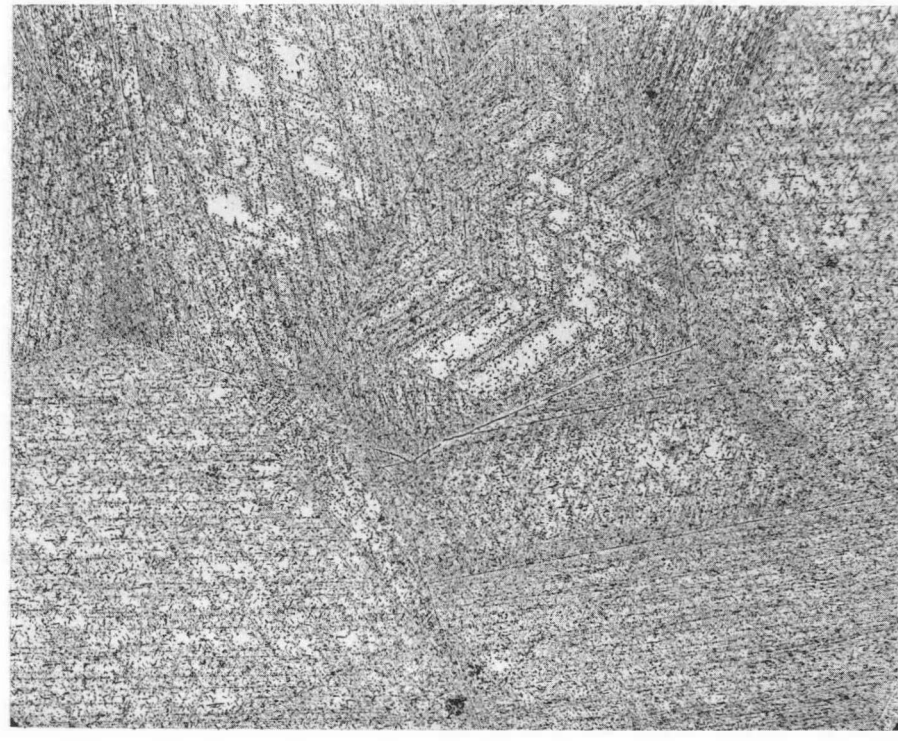

PN 1-55067 (250X)--1 h/2300°F/WQ + 2 h/1800°F/AC

Etchant: 50% Phosphoric Acid
Annealed Hardness: R_A 61
Annealed Grain Size: ASTM 4

Phase Analysis by Electron Probe:

	Cr	Ni	Fe	Al
Fine Dark Phase	52	28.3	17.8	1.0

Figure B.16 Characterization of Alloys Before Test
(Incoloy Alloy 809)

Chemical Analysis (% by Wt.):

	Cr	Ni	Fe	C	Al
Nominal	20	30	Bal	---	2.0
HH-8161K	20.7	34.1	Bal	0.014	1.98

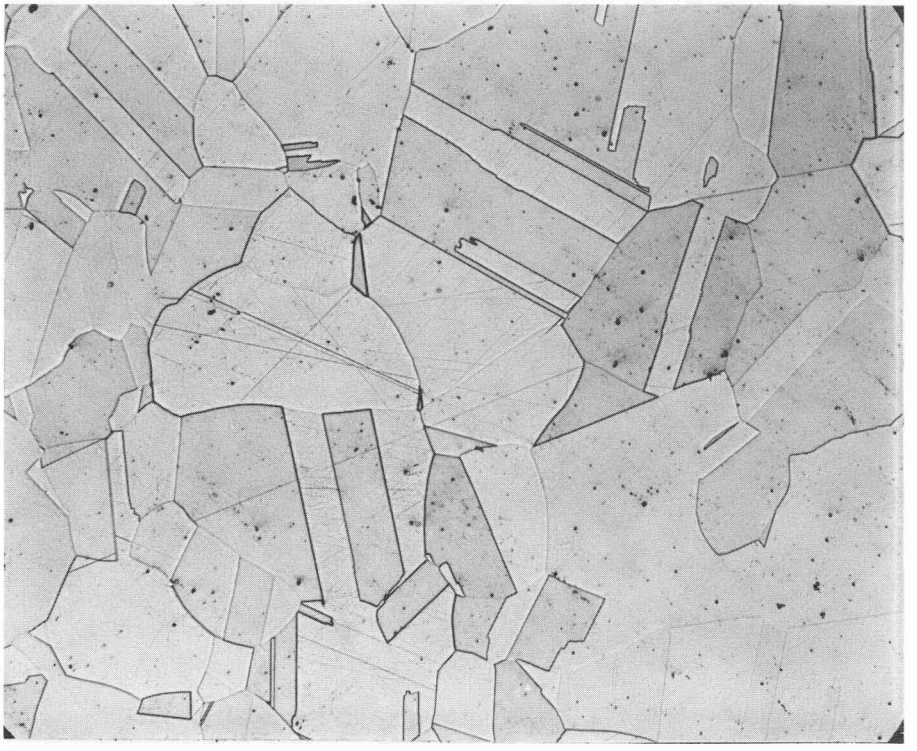

PN 1-55243 (100X)--2 h/2300°F/WQ

Etchant: V_2A
Annealed Hardness: R_B 62
Annealed Grain Size: ASTM 2

Figure B.17 Characterization of Alloys Before Test (IN-811)

Chemical Analysis (% by Wt.):

	Cr	Ni	Fe	C	Al	Ti
Nominal	32.2	Bal	16.6	---	3.4	0.35
75155	32.1	Bal	15.2	0.10	3.48	0.35

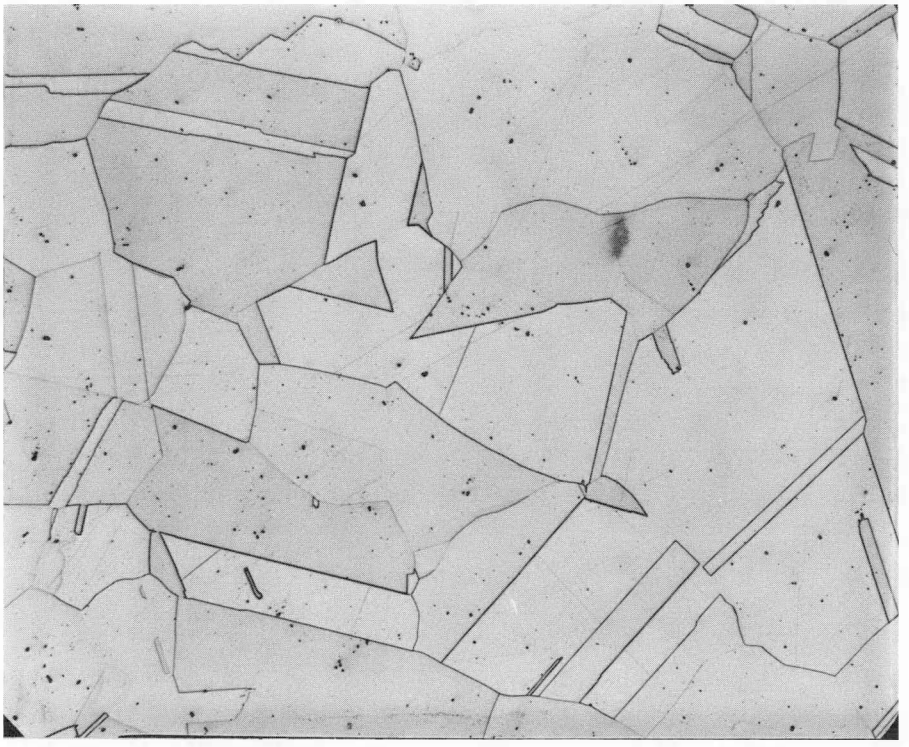

PN 1-55073 (100X)--1 h/2300°F/WQ

Etchant: V_2A
Annealed Hardness: R_B 82
Annealed Grain Size: ASTM 1

Figure B.18 Characterization of Alloys Before Test (IN-814)

Chemical Analysis (% by Wt.):

	Cr	Ni	Fe	C	Mn	Si
Nominal	20	25	Bal	0.04	0.7	0.4
Actual	19.8	24.7	Bal	0.025	0.64	0.41

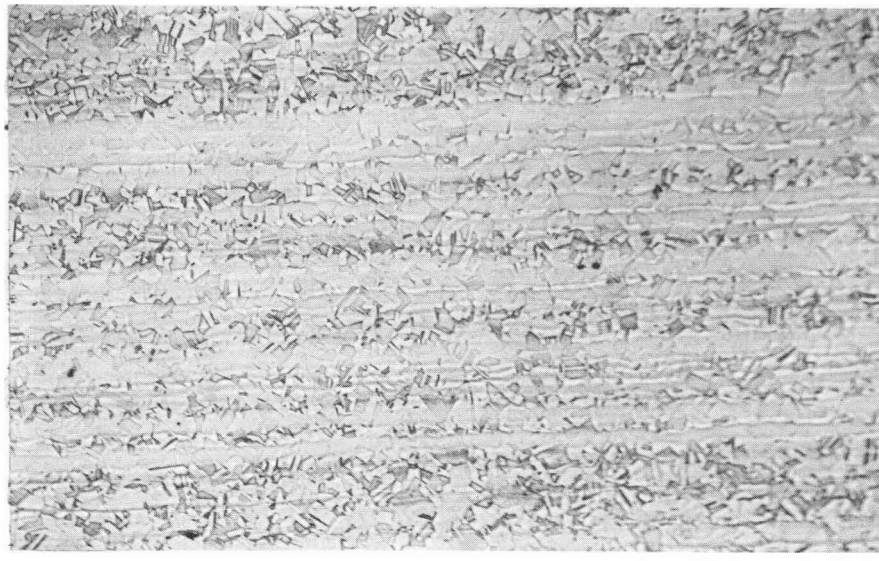

PN 1-57120 (200X)--Hot Rolled Etchant: 10% Chromic Acid

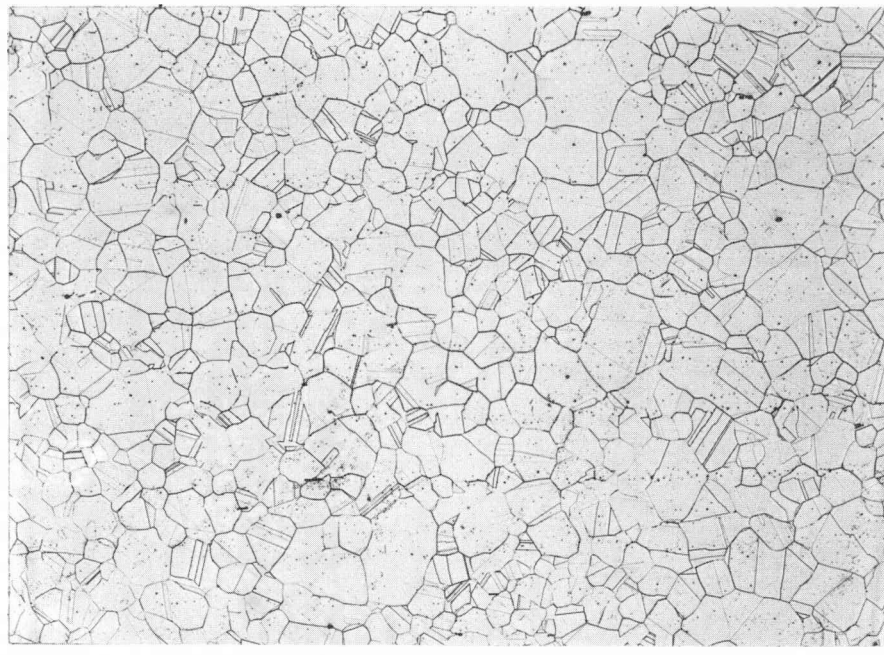

PN 1-57667 (100X)--1 h/2200°F/WQ Etchant: 10% Oxalic Acid

Annealed Hardness: R_B 55
Annealed Grain Size: ASTM 5

Figure B.19 Characterization of Alloys Before Test
[Alloy No. 1 (Heat No. 78770)]

Chemical Analysis (% by Wt.):

	Cr	Ni	Fe	C	Mn	Si	Al
Nominal	20	25	Bal	0.04	0.7	0.4	2.0
Actual	19.6	25.4	Bal	0.026	0.60	0.40	2.04

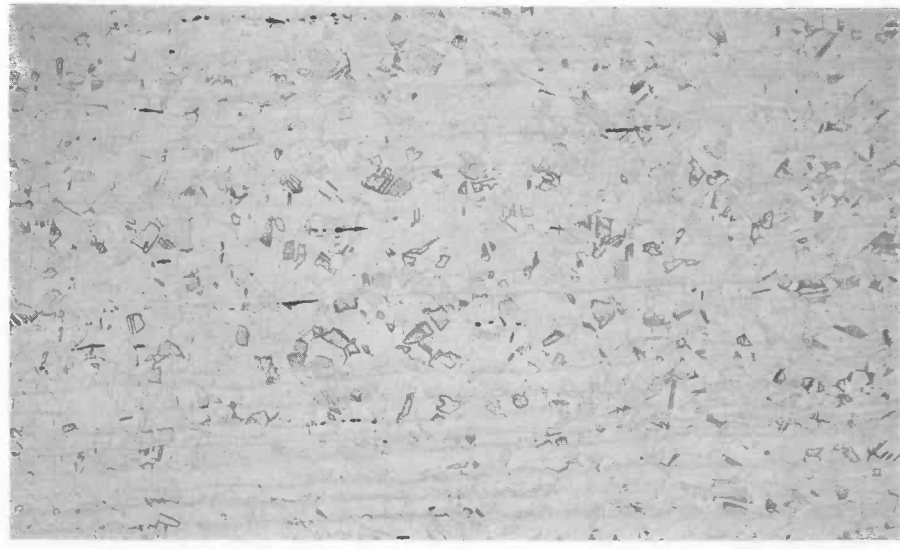

PN 1-57121 (200X)--Hot Rolled Etchant: 10% Chromic Acid

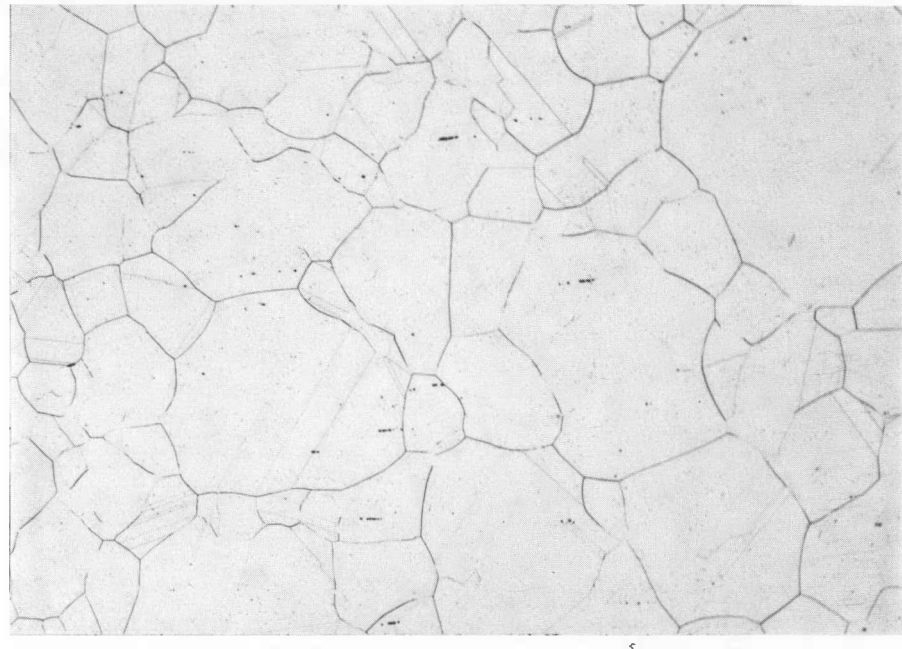

PN 1-57663 (100X)--1 h/2200°F/WQ. Etchant: 10% Oxalic Acid

Annealed Hardness: R_B 55
Annealed Grain Size: ASTM 2

Figure B.20 Characterization of Alloys Before Test [Alloy No. 2 (Heat No. 78771)]

Chemical Analysis (% by Wt.):

	Cr	Ni	Fe	C	Mn	Si
Nominal	20	25	Bal	0.04	0.7	2.4
Actual	19.4	25.3	Bal	0.026	0.57	2.27

PN 1-57122 (200X)--Hot Rolled Etchant: 10% Chromic Acid

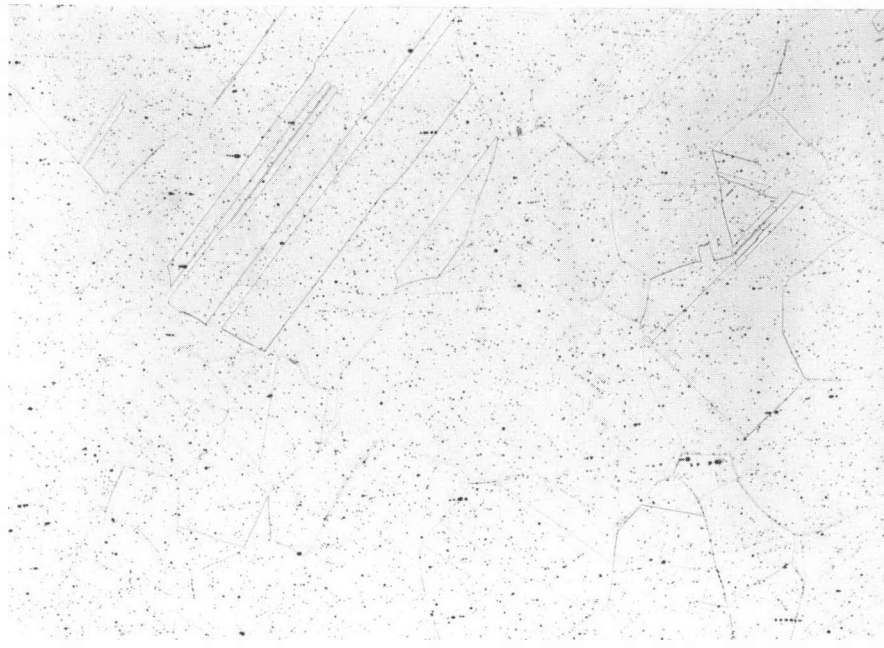

PN 1-57670 (250X)--1 h/2200°F/WQ Etchant: 10% Oxalic Acid

Annealed Hardness: R_B 57
Annealed Grain Size: ASTM 7

Figure B.21 Characterization of Alloys Before Test [Alloy No. 3 (Heat No. 78772)]

Chemical Analysis (% by Wt.):

	Cr	Ni	Fe	C	Mn	Si	Al
Nominal	20	25	Bal	0.04	0.7	2.4	2.0
Actual	19.6	24.2	Bal	0.034	0.59	2.4	2.0

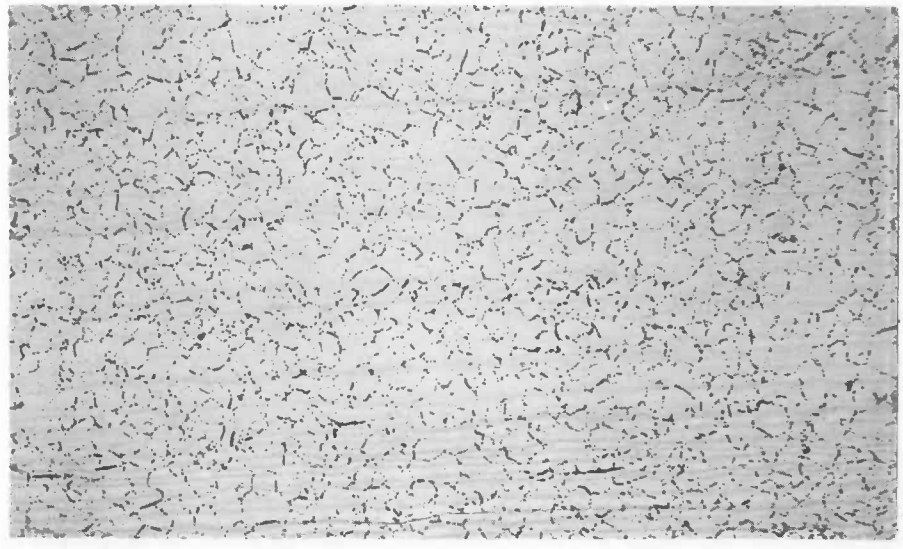

PN 1-57123 (200X)--Hot Rolled Etchant: 10% Chromic Acid

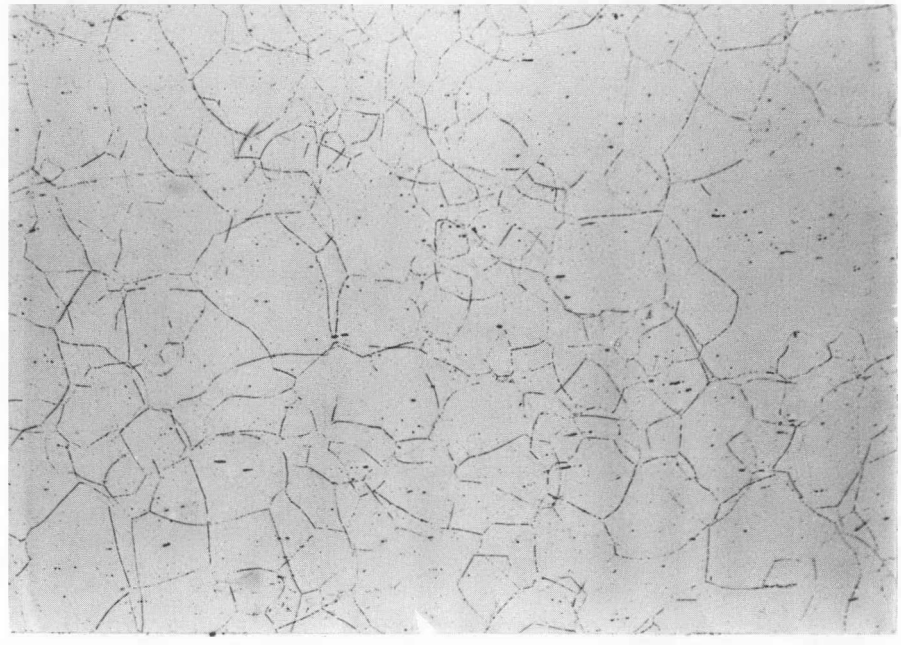

PN 1-57636 (100X)--1 h/2200°F/WQ Etchant: 10% Oxalic Acid

Annealed Hardness: R_B 62
Annealed Grain Size: ASTM 3

Figure B.22 Characterization of Alloys Before Test
[Alloy No. 4 (Heat No. 78773)]

Chemical Analysis (% by Wt.):

	Cr	Ni	Fe	C	Mn	Si
Nominal	25	35	Bal	0.04	0.7	0.4
Actual	24.4	33.5	Bal	0.026	0.70	0.4

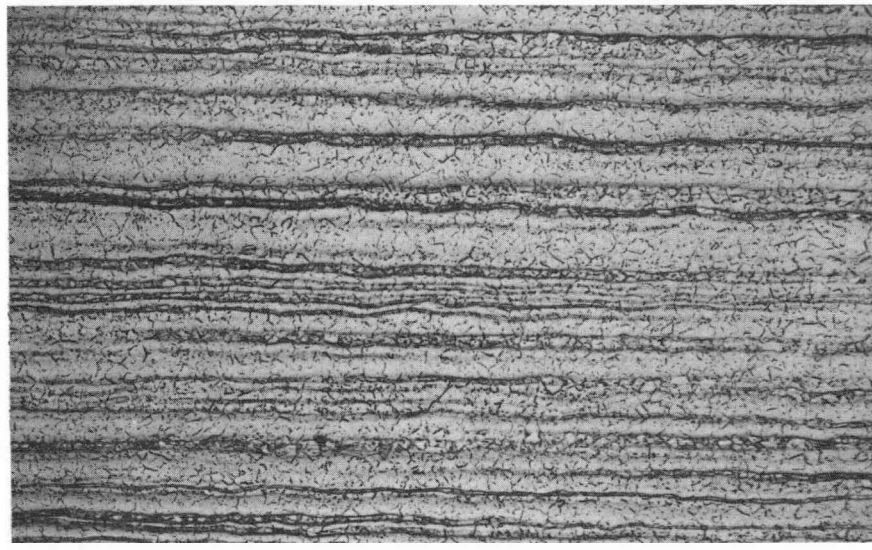

PN 1-57124 (200X)--Hot Rolled Etchant: 10% Chromic Acid

PN 1-57649 (250X)--1 h/2200°F/WQ Etchant: 10% Oxalic Acid

Annealed Hardness: R_B 56
Annealed Grain Size: ASTM 2

Figure B.23 Characterization of Alloys Before Test
[Alloy No. 5 (Heat No. 78774)]

Chemical Analysis (% by Wt.):

	Cr	Ni	Fe	C	Mn	Si	Al
Nominal	25	35	Bal	0.04	0.7	0.4	2.0
Actual	24.5	34.0	Bal	0.035	0.74	0.4	2.0

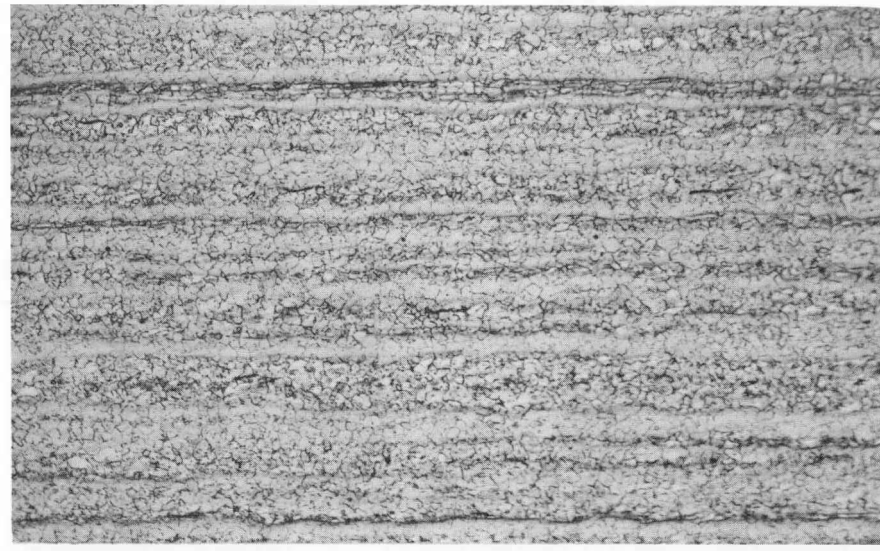

PN 1-57029 (200X)--Hot Rolled Etchant: 10% Chromic Acid

PN 1-57665 (100X)--1 h/2200°F/WQ Etchant: 10% Oxalic Acid

Annealed Hardness: R_B 65
Annealed Grain Size: ASTM 2

Figure B.24 Characterization of Alloys Before Test
[Alloy No. 6 (Heat No. 78778)]

Chemical Analysis (% by Wt.):

	Cr	Ni	Fe	C	Mn	Si
Nominal	25	35	Bal	0.04	0.7	2.4
Actual	24.2	34.1	Bal	0.025	0.74	2.3

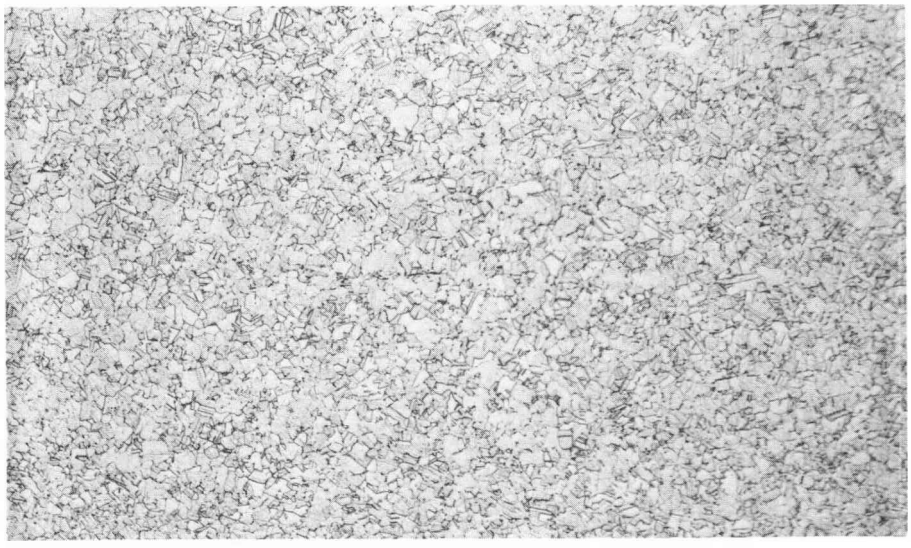

PN 1-62194 (200X)--Hot Rolled Etchant: 67% HCl, 16.5% HNO_3, 16.5% Acetone, Electrolytic

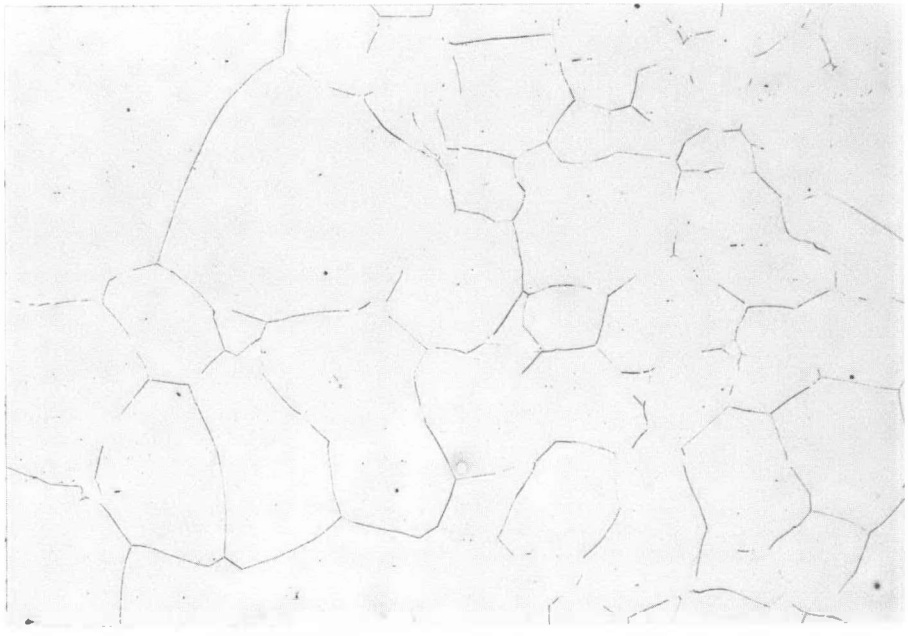

PN 1-57634 (100X)--1 h/2200°F/WQ Etchant: 10% Oxalic Acid

Annealed Hardness: R_B 61
Annealed Grain Size: ASTM 2

Figure B.25 Characterization of Alloys Before Test [Alloy No. 7 (Heat No. 78779)]

Chemical Analysis (% by Wt.):

	Cr	Ni	Fe	C	Mn	Si	Al
Nominal	25	35	Bal	0.04	0.7	2.4	2.0
Actual	24.1	33.7	Bal	0.013	0.62	2.3	1.9

PN 1-57031 (200X)--Hot Rolled Etchant: 10% Chromic Acid

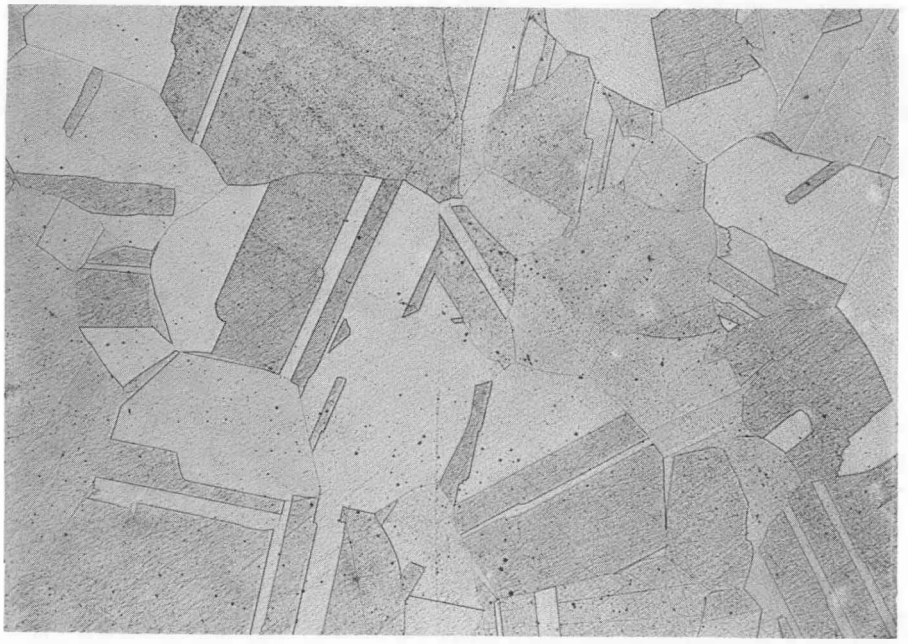

PN 1-62195 (100X)--1 h/2200°F/WQ Etchant: 67% HCl, 16.5% HNO_3, 16.5% Acetone, Electrolytic

Annealed Hardness: R_B 64
Annealed Grain Size: ASTM 6

Figure B.26 Characterization of Alloys Before Test
[Alloy No. 8 (Heat No. 78780)]

Chemical Analysis (% by Wt.):

	Cr	Ni	Fe	C	Mn	Si
Nominal	30	40	Bal	0.04	0.7	0.4
Actual	30.2	38.5	Bal	0.024	0.72	0.5

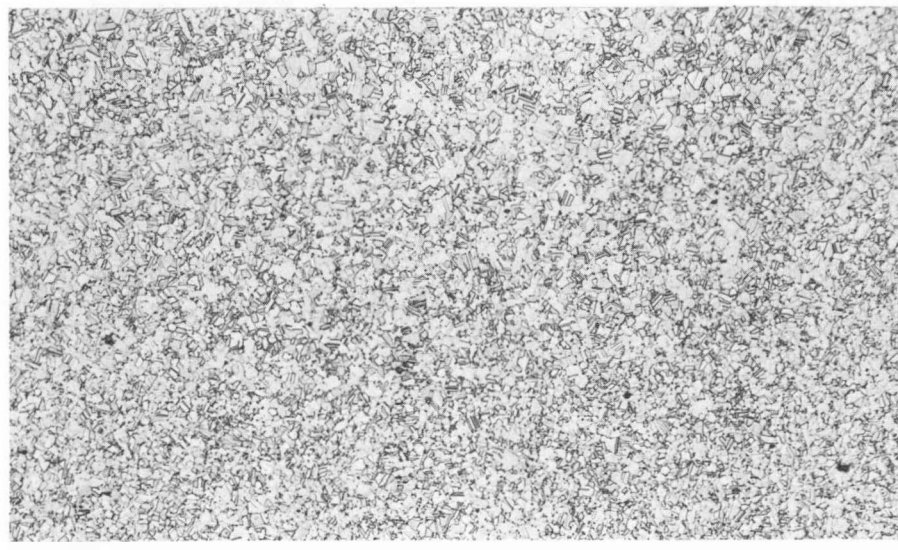

PN 1-59242 (200X)--Hot Rolled Etchant: Aqua Regia

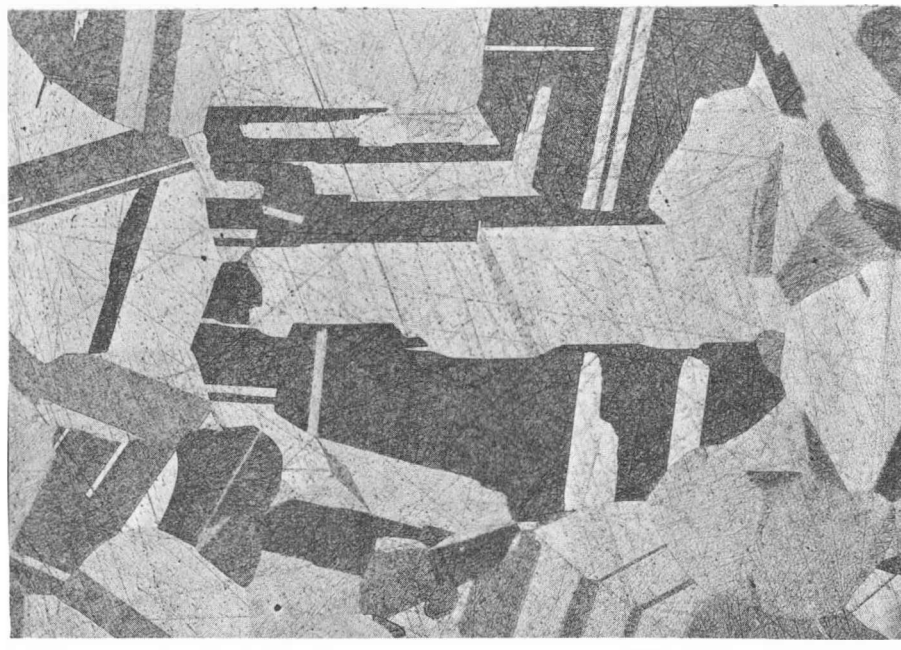

PN 1-62197 (100X)--1 h/2200°F/WQ Etchant: 67% HCl, 16.5% HNO_3, 16.5% Acetone, Electrolytic

Annealed Hardness: R_B 63
Annealed Grain Size: ASTM 3

Figure B.27 Characterization of Alloys Before Test [Alloy No. 9 (Heat No. 78781)]

Chemical Analysis (% by Wt.):

	Cr	Ni	Fe	C	Mn	Si	Al
Nominal	30	40	Bal	0.04	0.7	0.4	2.0
Actual	30.2	39.0	Bal	0.020	0.74	0.4	1.8

PN 1-57033 (200X)--Hot Rolled Etchant: 10% Chromic Acid

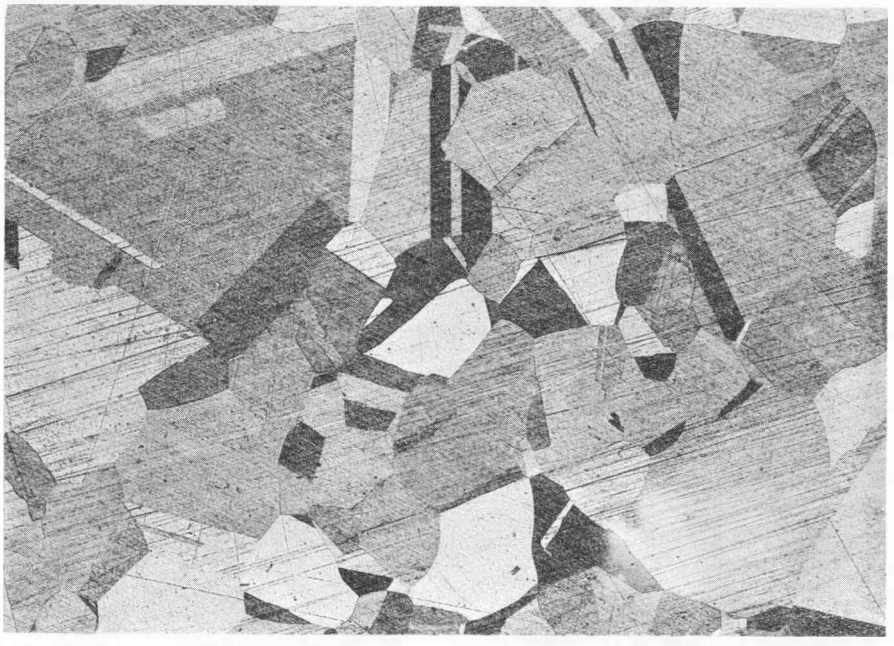

PN 1-62198 (100X)--1 h/2200°F/WQ Etchant: 67% HCl, 16.5% HNO_3, 16.5% Acetone, Electrolytic

Annealed Hardness: R_B 65
Annealed Grain Size: ASTM 3

Figure B.28 Characterization of Alloys Before Test [Alloy No. 10 (Heat No. 78782)]

Chemical Analysis (% by Wt.):

	Cr	Ni	Fe	C	Mn	Si
Nominal	30	40	Bal	0.04	0.7	2.4
Actual	30.5	38.7	Bal	0.027	0.71	2.3

PN 1-57125 (200X)--Hot Rolled Etchant: 10% Chromic Acid

PN 1-57656-A (100X)--1 h/2200°F/WQ Etchant: 10% Oxalic Acid

Annealed Hardness: R_B 65
Annealed Grain Size: ASTM 3

Figure B.29 Characterization of Alloys Before Test
[Alloy No. 11 (Heat No. 78783)]

Chemical Analysis (% by Wt.):

	Cr	Ni	Fe	C	Mn	Si	Al
Nominal	30	40	Bal	0.04	0.7	2.4	2.0
Actual	29.7	39.3	Bal	0.019	0.76	2.4	1.8

PN 1-57126 (200X)--Hot Rolled Etchant: 10% Chromic Acid

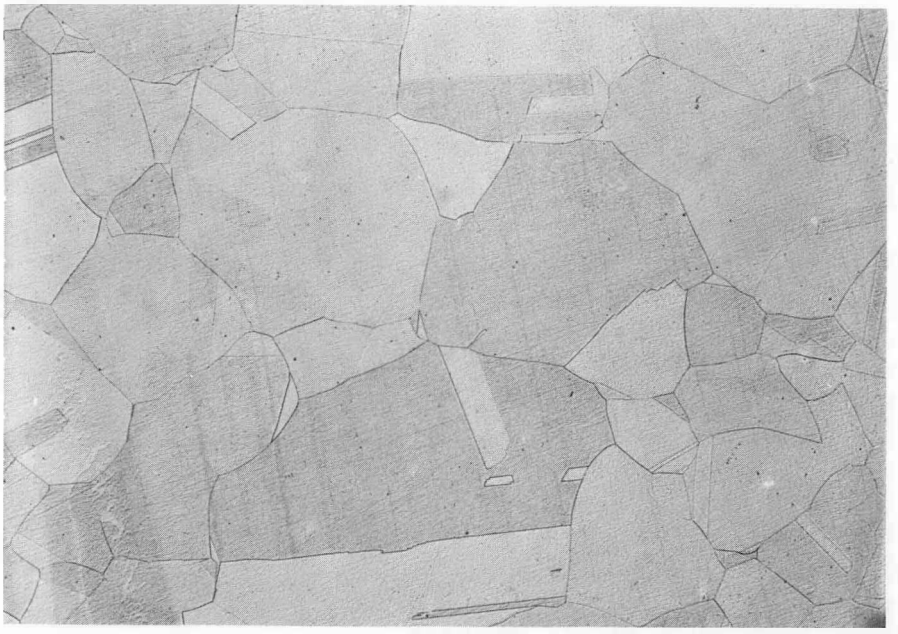

PN 1-62196 (100X)--1 h/2200°F/WQ Etchant: 67% HCl, 16.5% HNO_3, 16.5% Acetone, Electrolytic

Annealed Hardness: R_B 67
Annealed Grain Size: ASTM 1

Figure B.30 Characterization of Alloys Before Test [Alloy No. 12 (Heat No. 78784)]

Chemical Analysis (% by Wt.):

	Cr	Ni	Fe	C	Mn	Si	Al
Nominal	25	35	Bal	0.04	0.7	0.4	4.0
Actual	24.4	33.0	Bal	0.015	0.70	0.4	3.7

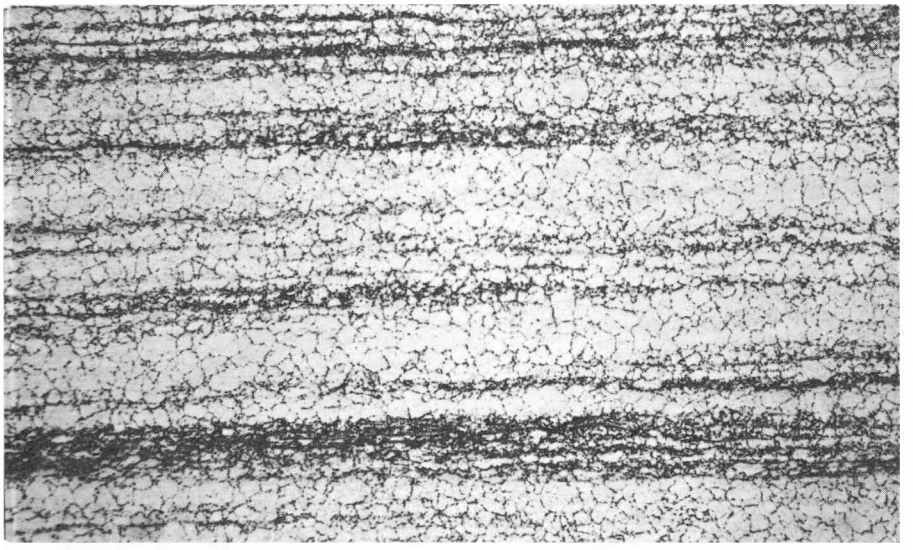

PN 1-57127 (200X)--Hot Rolled Etchant: 10% Chromic Acid

PN 1-57662 (250X)--1 h/2200°F/WQ Etchant: 10% Oxalic Acid

Annealed Hardness: R_B 69
Annealed Grain Size: ASTM 5

Figure B.31 Characterization of Alloys Before Test [Alloy No. 13 (Heat No. 78775)]

Chemical Analysis (% by Wt.):

	Cr	Ni	Fe	C	Mn	Si	Al	Y
Nominal	25	35	Bal	0.04	0.7	0.4	4.0	0.1
Actual	24.3	33.9	Bal	0.021	0.75	0.4	3.7	0.01

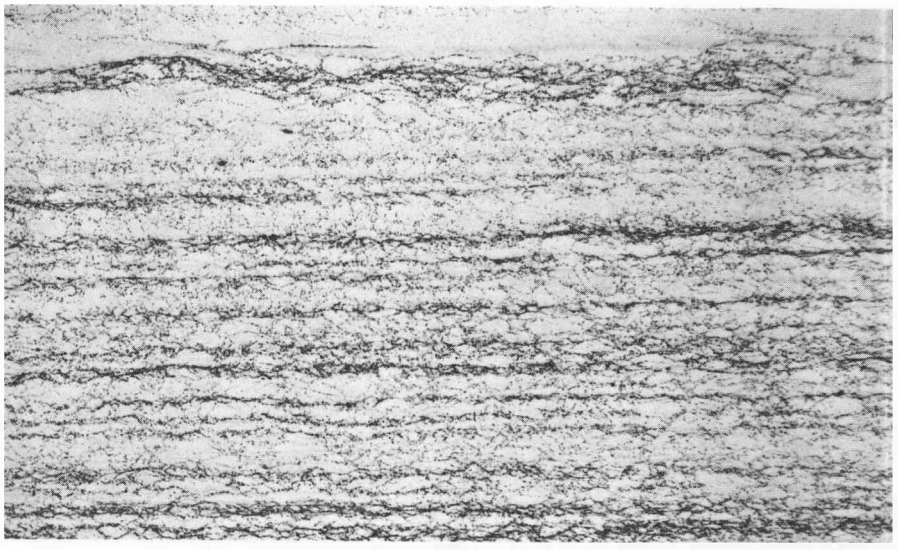

PN 1-57128 (200X)--Hot Rolled Etchant: 10% Chromic Acid

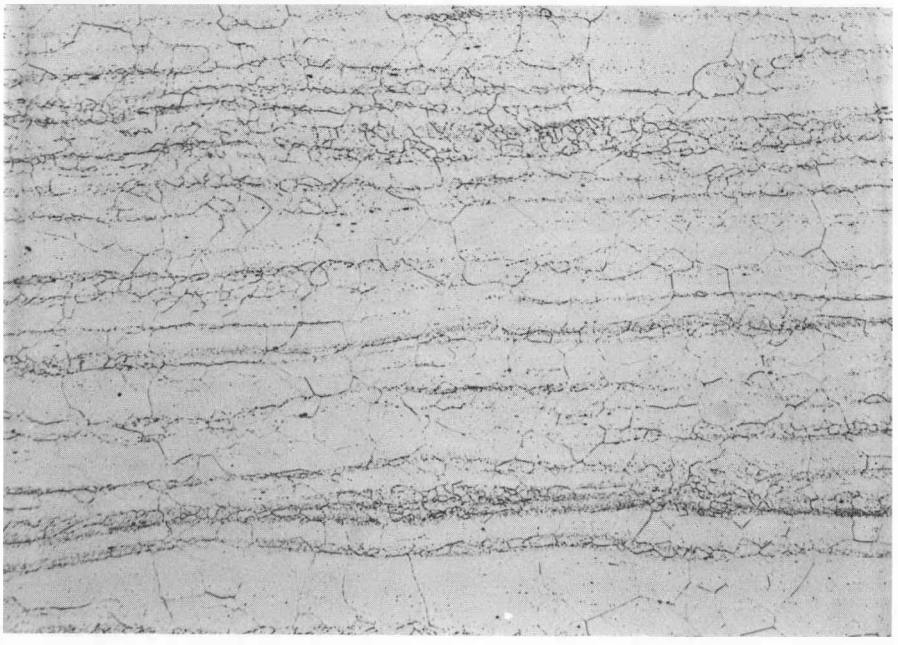

PN 1-57654 (100X)--1 h/2200°F/WQ Etchant: 10% Oxalic Acid

Annealed Hardness: R_B 67
Annealed Grain Size: ASTM 4

Figure B.32 Characterization of Alloys Before Test
[Alloy No. 14 (Heat No. 78777)]

Chemical Analysis (% by Wt.):

	Cr	Ni	Fe	C	Mn	Si	Al	Y
Nominal	25	35	Bal	0.04	0.7	0.4	4.0	0.5
Actual	24.2	37.2	Bal	0.025	0.72	0.44	4.2	0.6

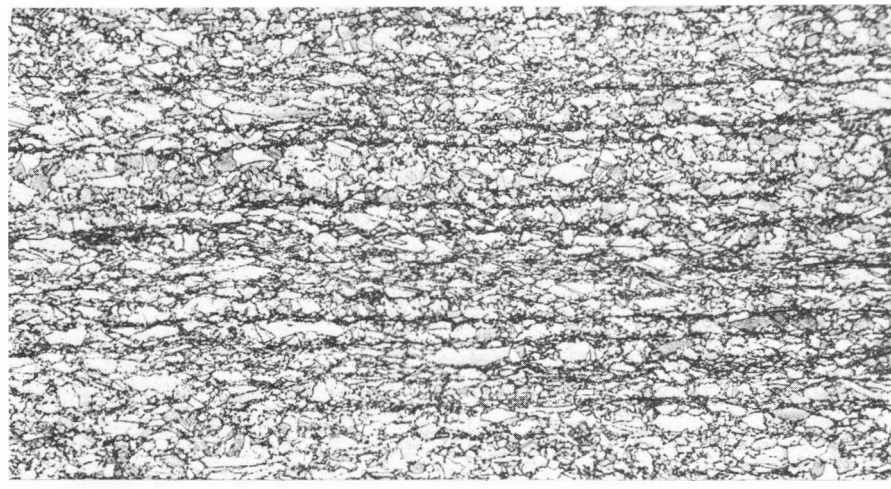

PN 1-59243 (200X)--1 h/2200°F/WQ Etchant: Aqua Regia

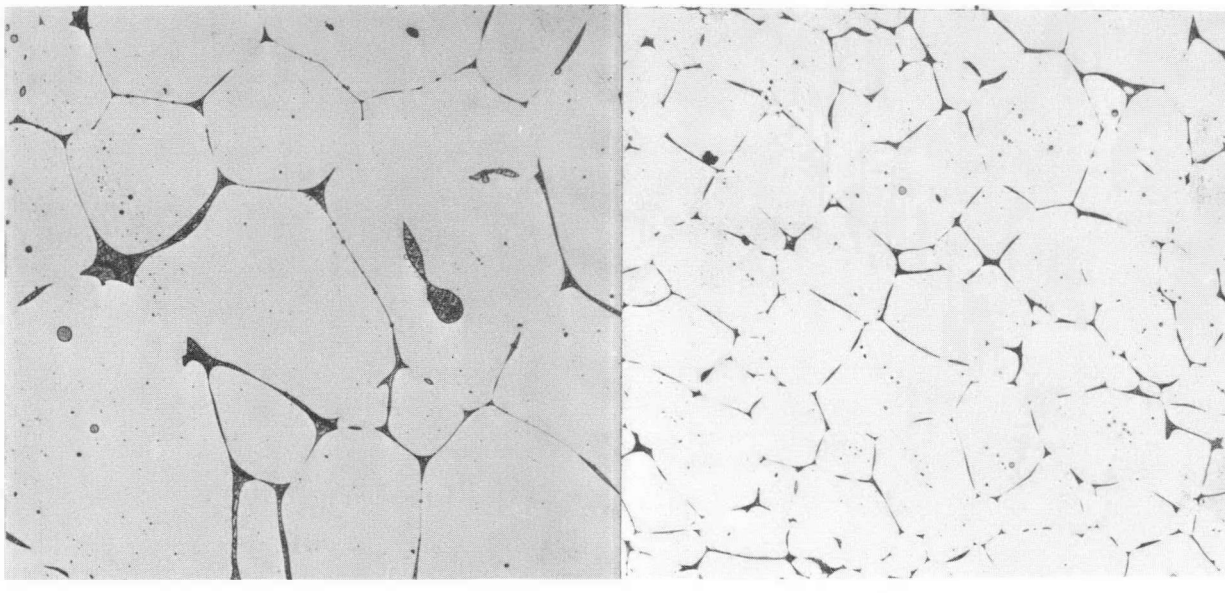

PN 1 57641 (250X)--1 h/2200°F/WQ

Etchant: 10% Oxalic Acid
Annealed Hardness: R_B 70
Annealed Grain Size: ASTM 3

PN 1-57640 (100X)--1 h/2200°F/WQ

Phase Analysis by Electron Probe:

	Fe	Cr	Ni	Y	Al
Grain Boundary	11.4	6.3	55.4	8.0	19.2
Globular	7.4	4.4	52.3	30.8	9.1

Figure B.33 Characterization of Alloys Before Test
[Alloy No. 15 (Heat No. 79287)]

Chemical Analysis (% by Wt.):

	Cr	Ni	Fe	C	Mn	Si	Y
Nominal	25	35	Bal	0.04	0.7	0.4	0.1
Actual	24.3	35.1	Bal	0.033	0.57	0.44	0.06

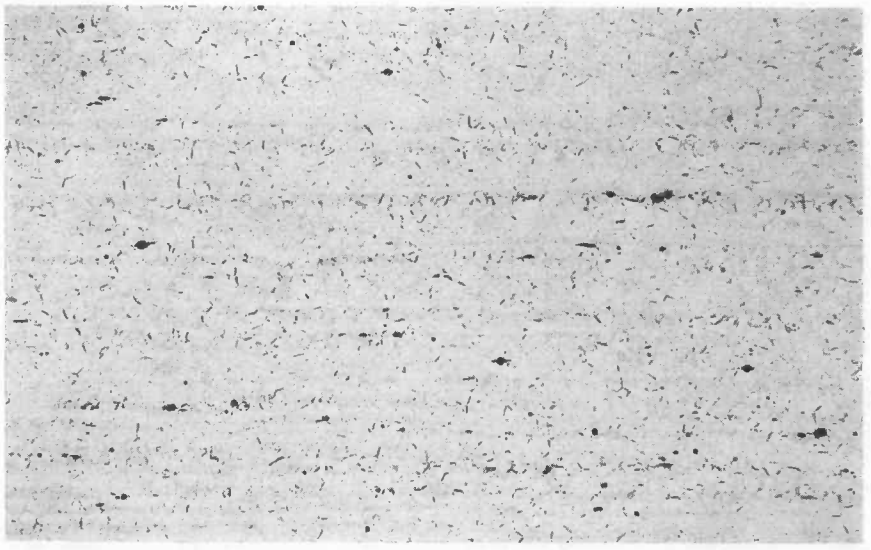

PN 1-57117 (200X)--Hot Rolled Etchant: 10% Chromic Acid

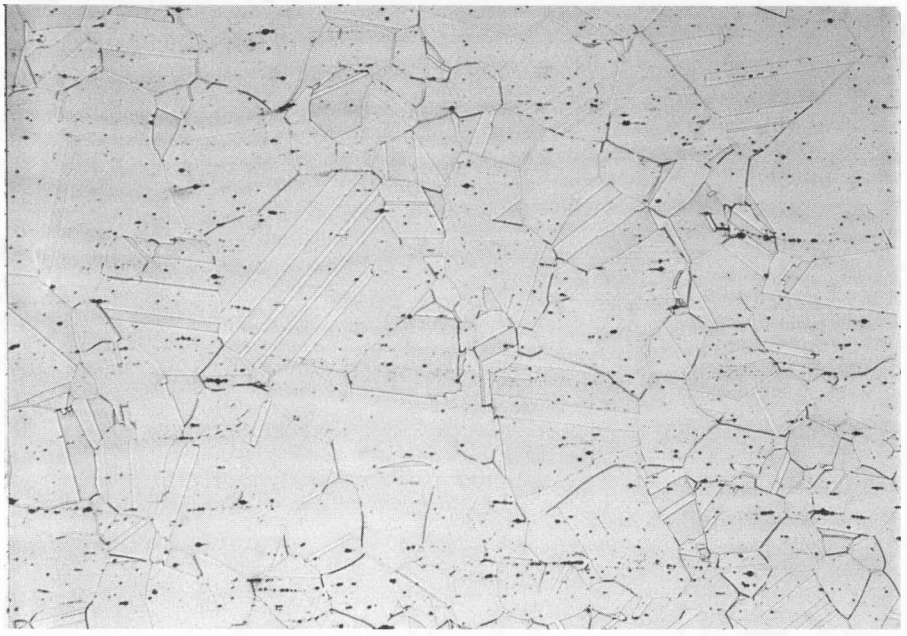

PN 1-57659 (100X)--1 h/2200°F/WQ Etchant: 10% Oxalic Acid

Annealed Hardness: R_B 64
Annealed Grain Size: ASTM 2

Figure B.34 Characterization of Alloys Before Test
[Alloy No. 16 (Heat No. 78955)]

Chemical Analysis (% by Wt.):

	Cr	Ni	Fe	C	Mn	Si	Y
Nominal	25	35	Bal	0.4	0.7	0.4	0.5
Actual	24.7	35.4	Bal	0.031	0.68	0.37	0.53

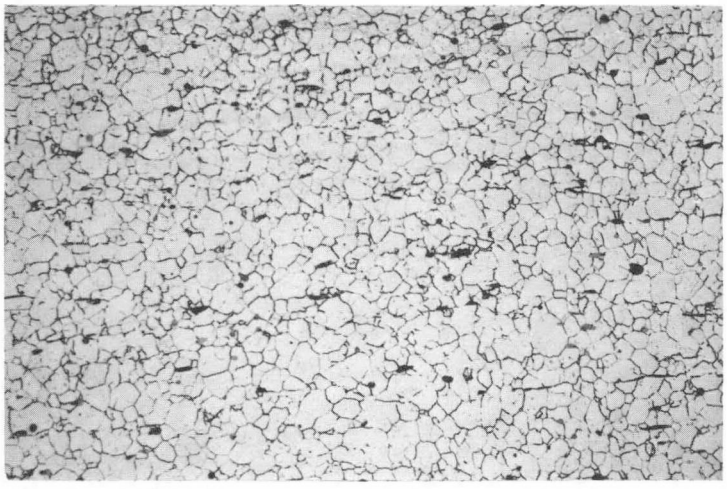

PN 1-57118 (200X)--Hot Rolled Etchant: 10% Chromic Acid

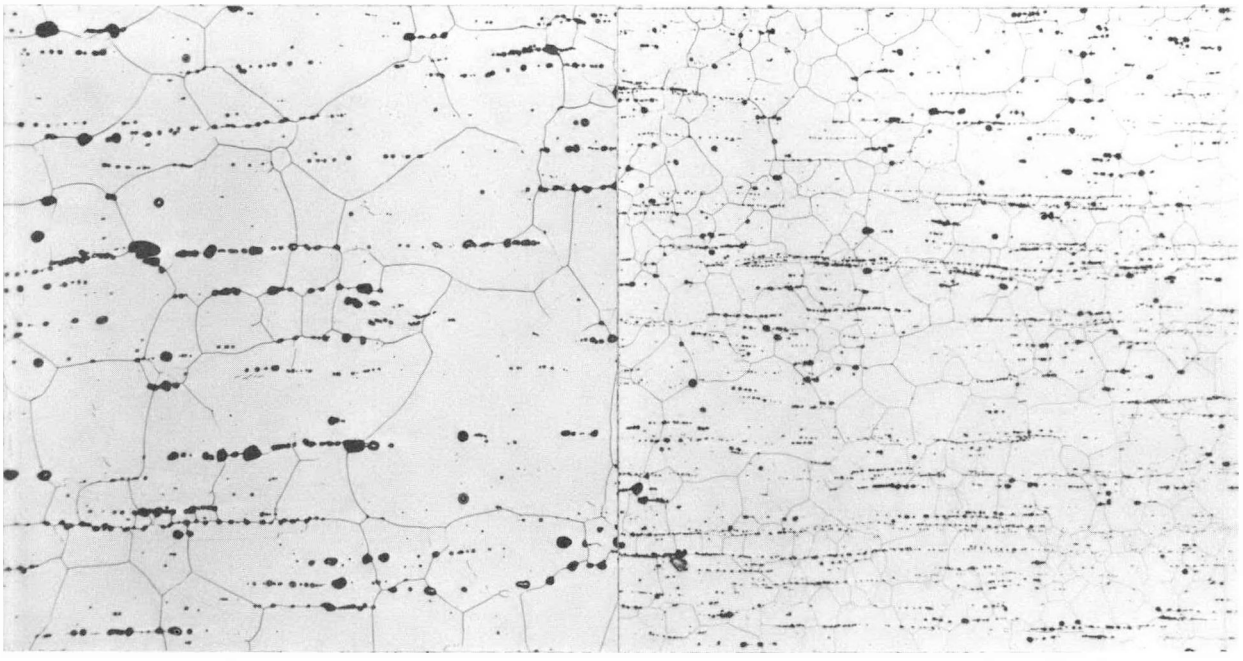

PN 1-57643 (250X)--1 h/2200°F/WQ

Etchant: 10% Oxalic Acid
Annealed Hardness: R_B 67
Annealed Grain Size: ASTM 4

PN 1-57642 (100X)--1 h/2200°F/WQ

Globular Stringer Phase Analysis by Electron Probe:

Fe	Cr	Ni	Y
13.2	6.1	56.5	26.9

Figure B.35 Characterization of Alloys Before Test
[Alloy No. 17 (Heat No. 79284)]

Chemical Analysis (% by Wt.):

	Cr	Ni	Fe	C	Mn	Si	Y
Nominal	25	20	Bal	0.1	0.7	0.4	0.5
Actual	25.1	18.4	Bal	0.041	0.67	0.45	0.58

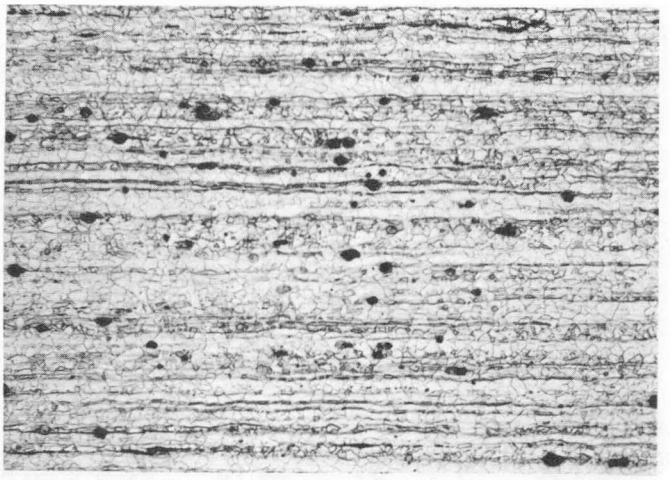

PN 1-57119 (200X)--Hot Rolled Etchant: 10% Chromic Acid

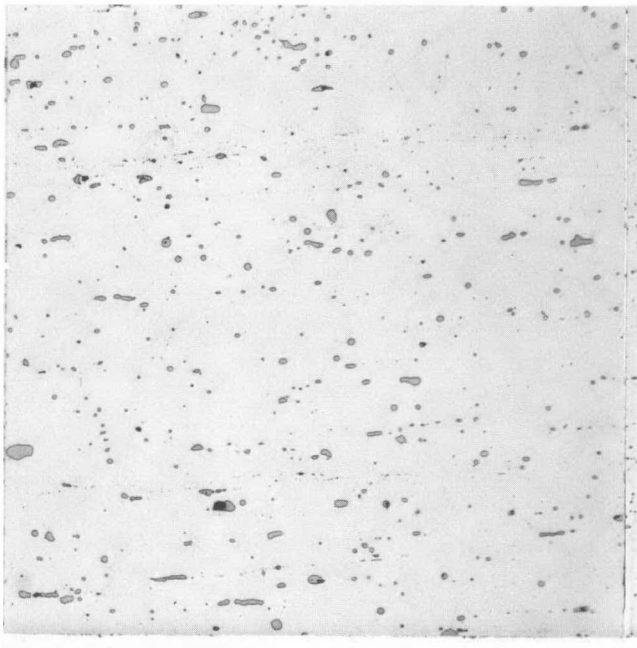

PN 1-57639 (250X)--1 h/2200°F/WQ

Etchant: 10% Oxalic Acid
Annealed Hardness: R_B 66
Annealed Grain Size: ASTM 4

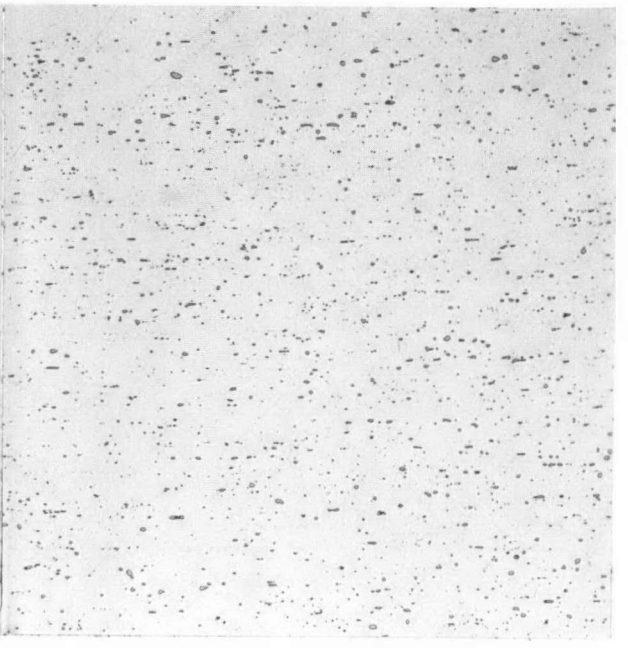

PN 1-57638 (100X)--1 h/2200°F/WQ

Globular Phase Analysis by Electron Probe:

Fe	Cr	Ni	Y
23.5	6.7	45.1	25.6

Figure B.36 Characterization of Alloys Before Test
[Alloy No. 18 (Heat No. 79288)]

Chemical Analysis (% by Wt.):

	Cr	Ni	Fe	C	Al	Y_2O_3	O_2	N
Nominal	23	20	Bal	---	---	0.5	---	---
Actual	23.0	20.0	Bal	0.045	0.3	0.65	0.41	0.12

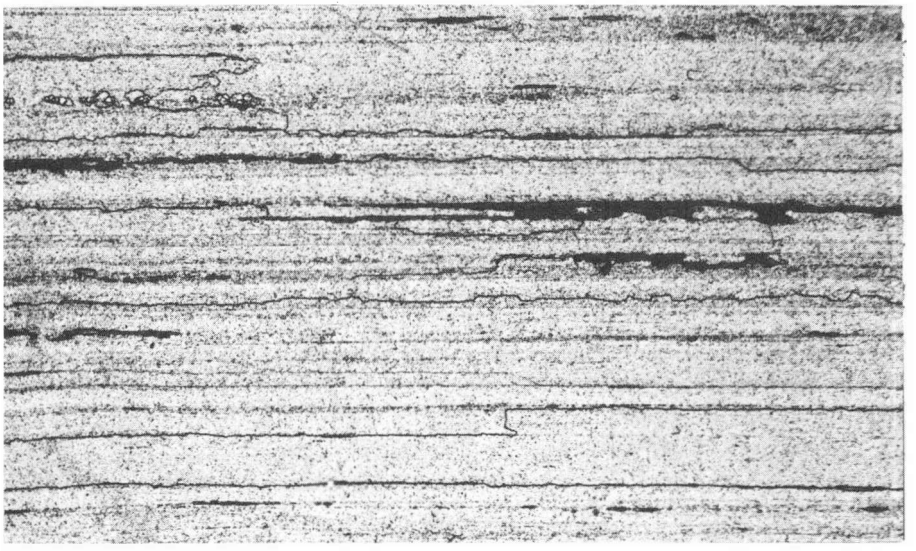

PN 1-59244 (200X)--1/2 h/2450°F/AC Etchant: 60% HNO_3

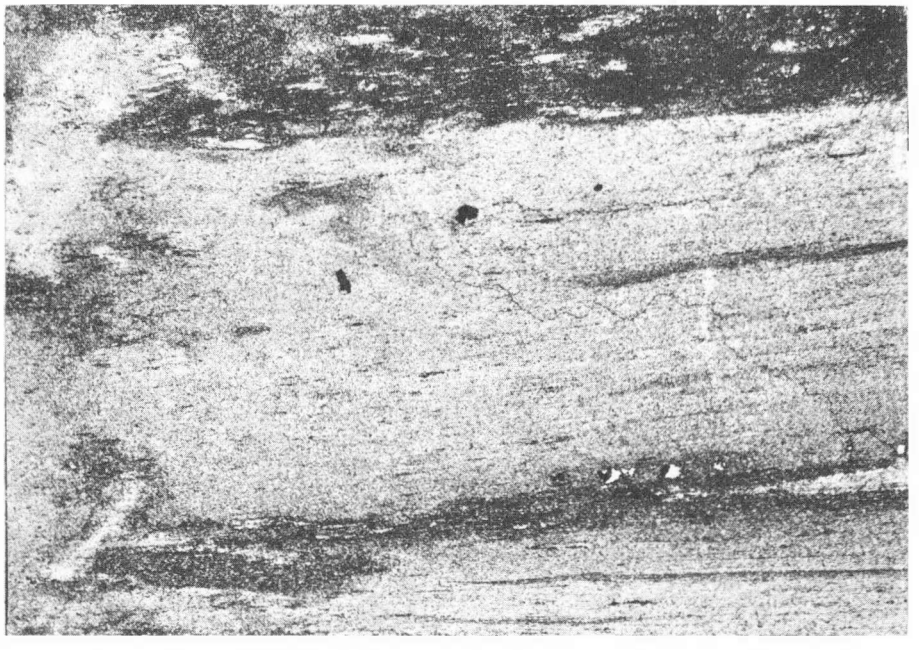

PN 1-57646 (100X)--1/2 h/2450°F/WQ Etchant: 10% Oxalic Acid

Annealed Hardness: R_B 98
Annealed Grain Size: ---

Figure B.37 Characterization of Alloys Before Test [Alloy No. 19 (Heat No. 75179 - Mechanically Alloyed)]

Alonized 800

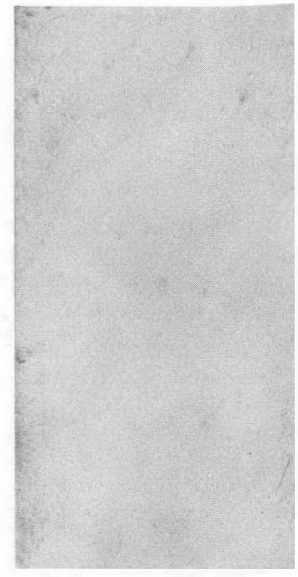

Chromized
HT 9

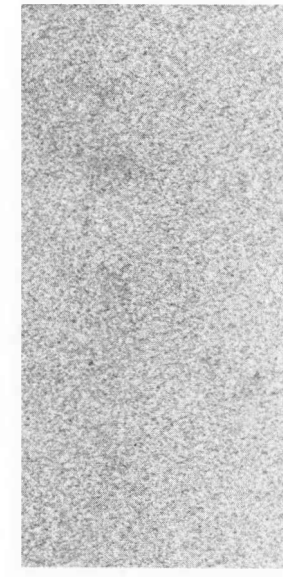

Ni-Cr-Al
on 347

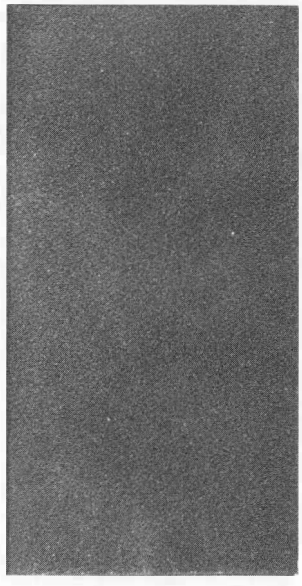

Plasma Spray
671 on 304

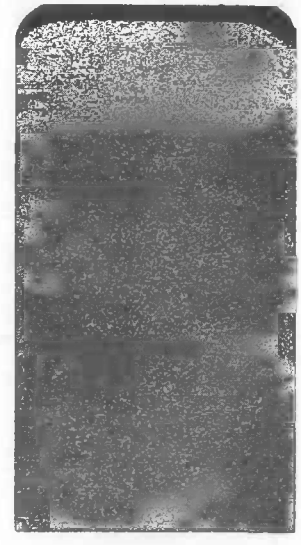

Ni-Cr-Si
on 309

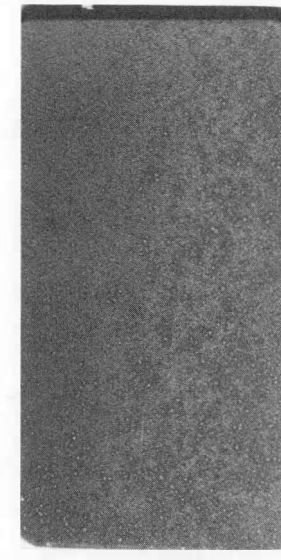

Ni-Cr-Si
on 309

Figure B.38 Photomacrographs of Coated Specimens Prior to Testing--1.5X

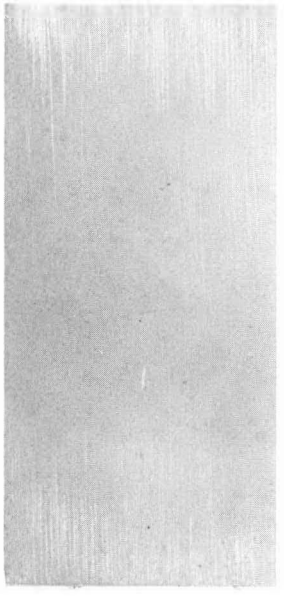

Chromized 304
(Cr 3)

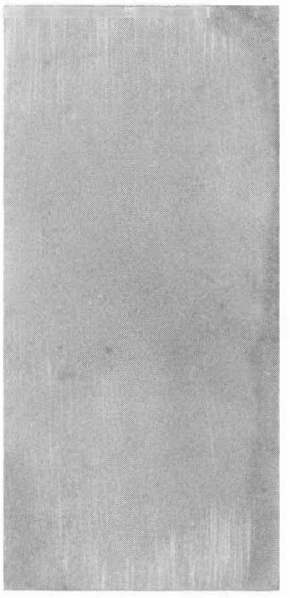

Chromized 800
(Cr 2)

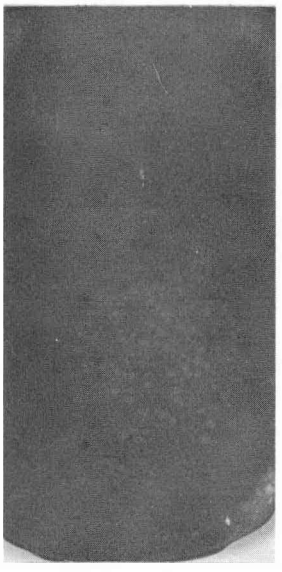

Siliconized 347
(39)

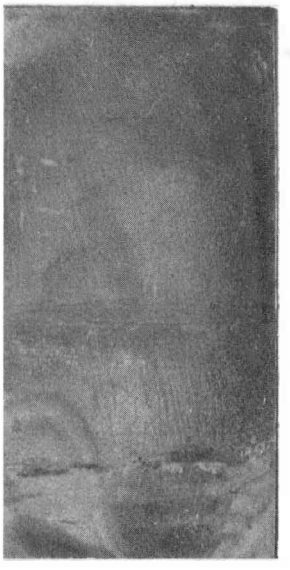

Siliconized 2-1/4Cr-1%Mo
(28)

Figure B.39 Photomacrographs of Coated Specimens Prior to Testing--1.5X

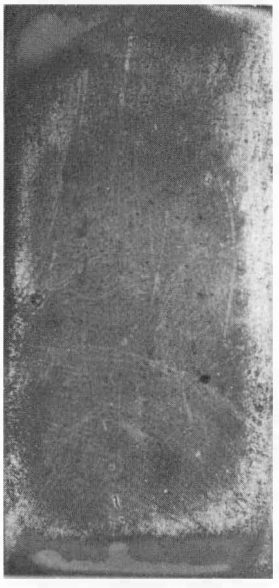

Siliconized 2
(6)

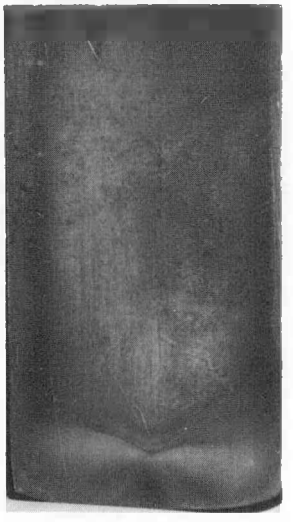

Siliconized 13
(9)

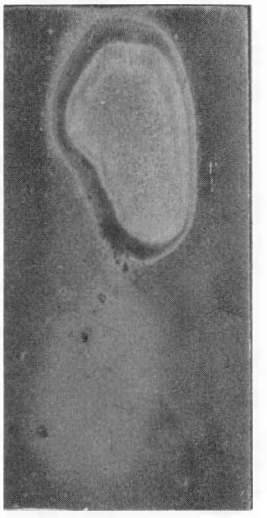

Siliconized 304
(55)

Figure B.40 Photomacrographs of Coated Specimens Prior to Testing--1.5X

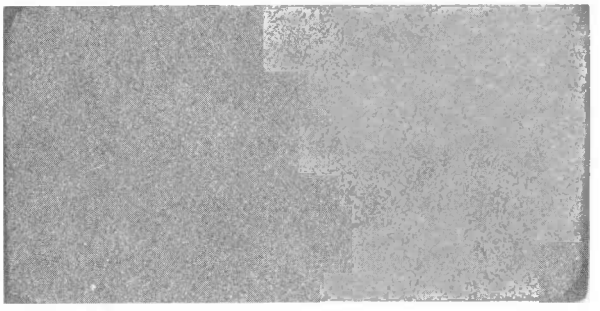

Duplex Coating
(64)

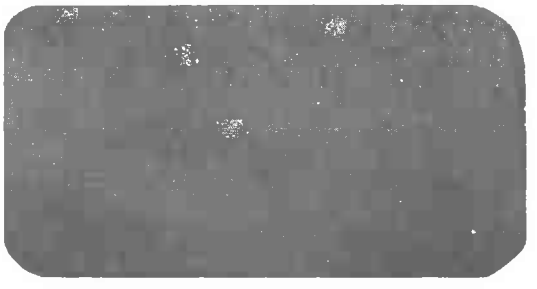

Ni-Cr-Si
on 309

Figure B.41 Photomacrographs of Coated Specimens Prior to Testing--1.5X

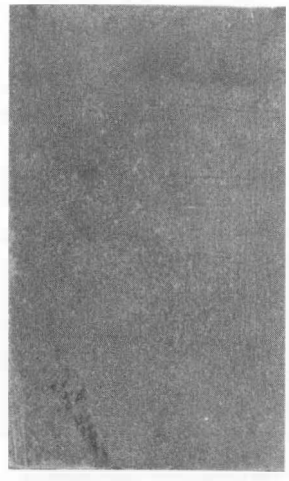

Alonized 304
(A1-1)

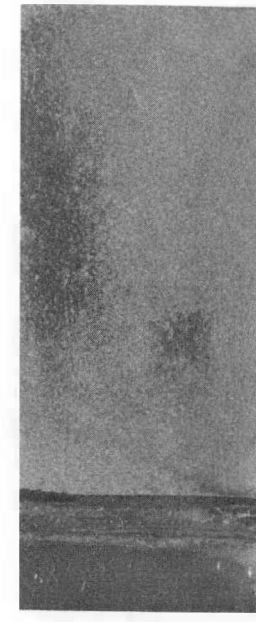

Alonized 304
(A1-2)

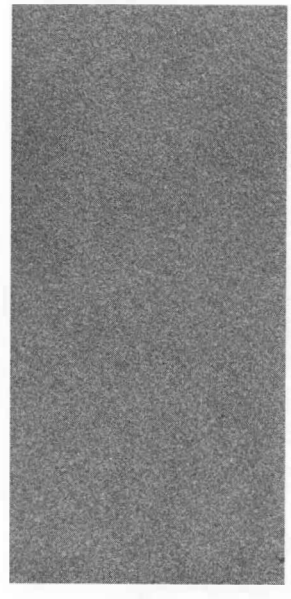

Ni-Cr-Al
on 347

Metco 210
on 304 (9)

Figure B.42 Photomacrographs of Coated Specimens Prior to Testing--1.5X

Triballoy 700

Triballoy 800

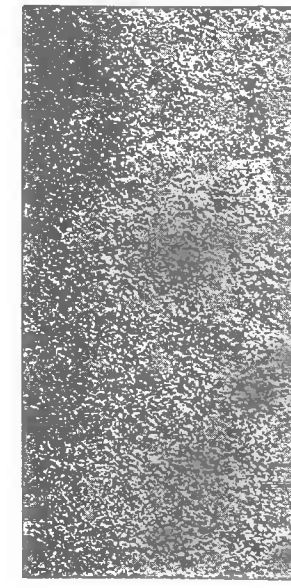

$CrSi_2$ on 430

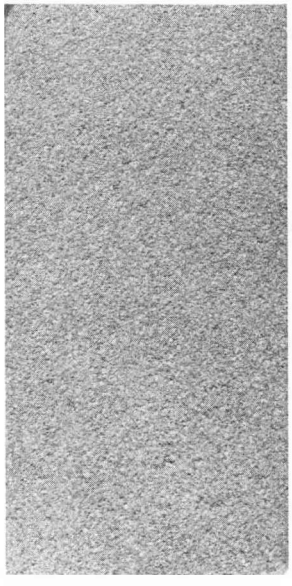

Kanthal

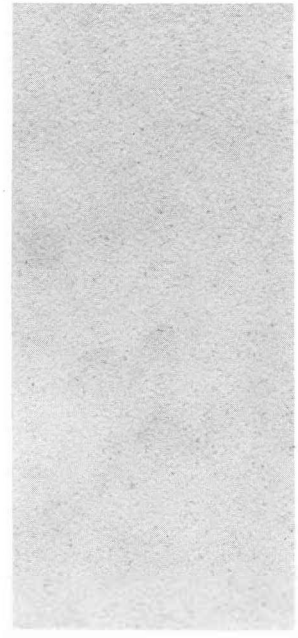

$ZrSiO_4$ on
2-1/4%Cr-1%Mo

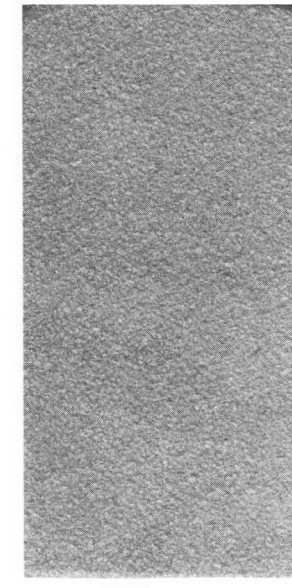

$CrSi_2$ Over Kanthal
(Duplex Coating)

Figure B.43 Photomacrographs of Coated Specimens Prior to Testing--1.5X

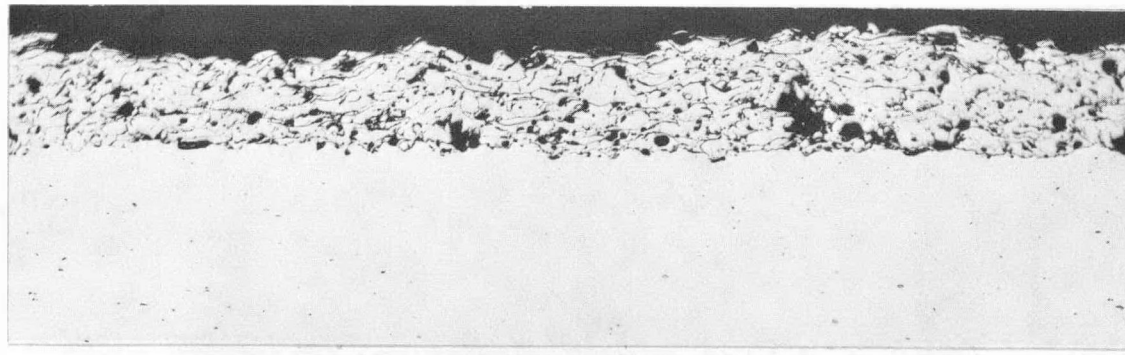

100X

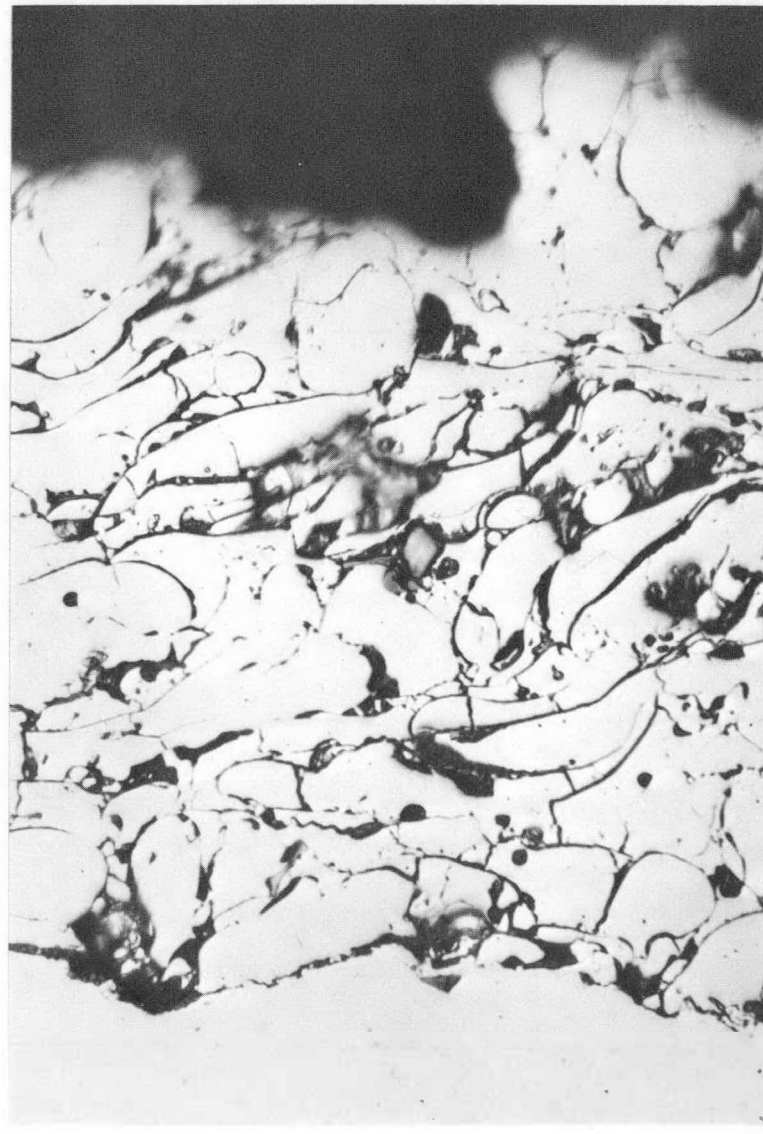

500X

Figure B.44 Microstructure of $CrSi_2$ Plasma Deposited on Ferritic Steel Before Test--Unetched (The coating was well bonded but porous.)

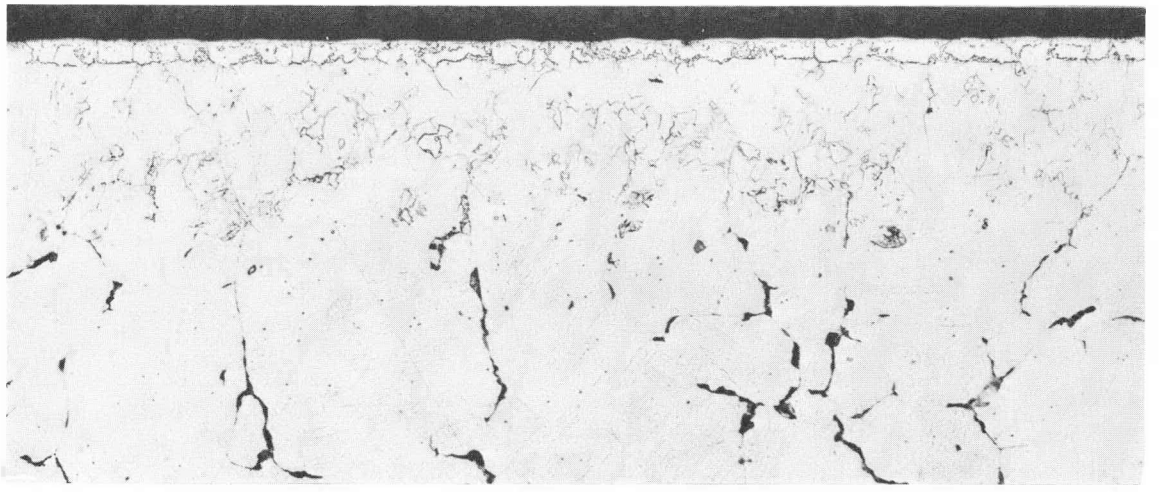

100X

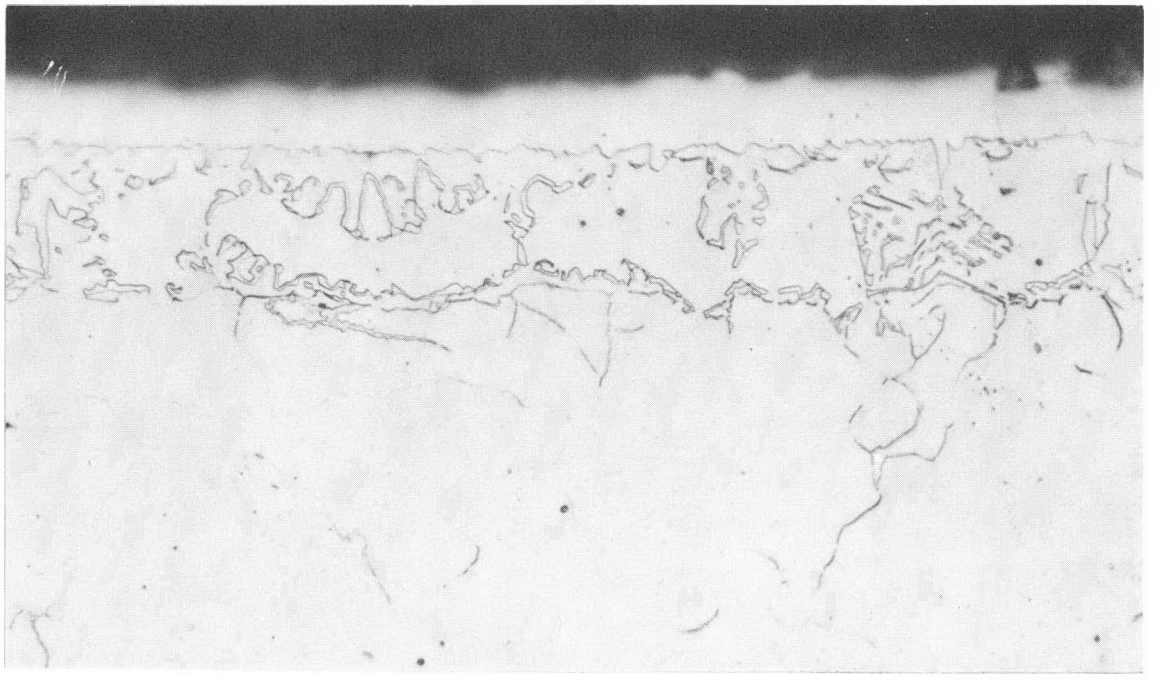

500X

Figure B.45 Microstructure of Chromized HT-9 Before Test--Etched [The outer white layer was very high in chromium. The diffusion layer, with measurable chromium enrichment, was approximately 0.003 in. (76 μm) thick.]

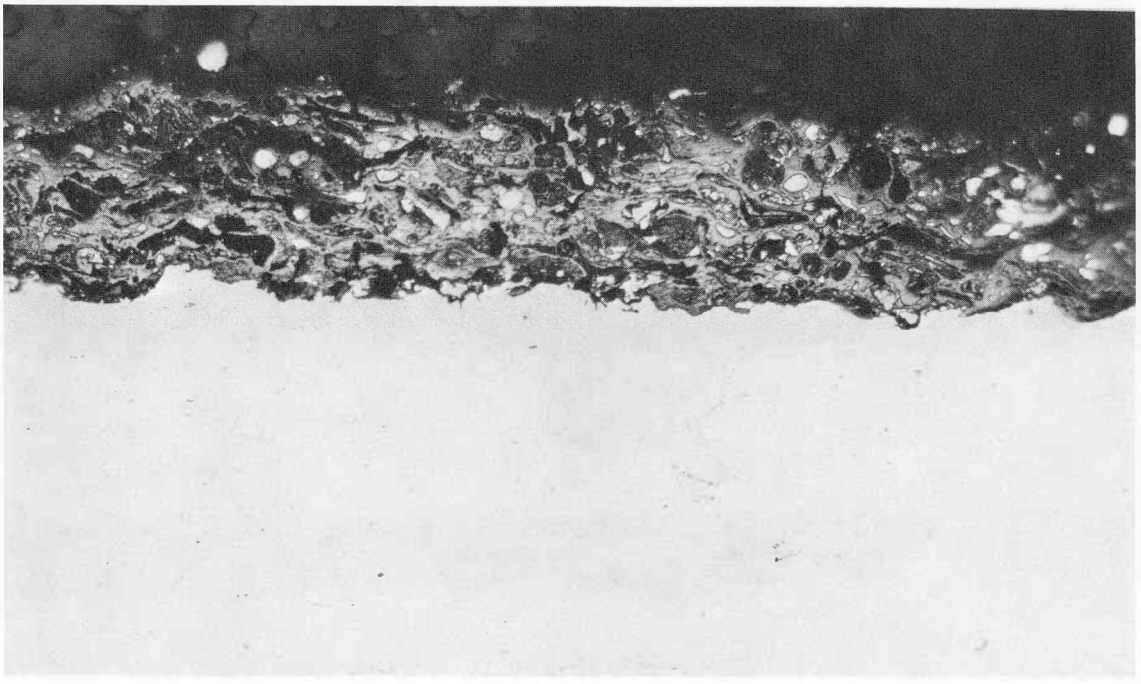

Figure B.46 Microstructure of As-Received Ni-Cr-Si Coating Applied by Plasma Spray--250X Unetched (The coating was prepared by blending pre-alloyed IN-671 powder with silicon powder added. White spheroids show some unreacted silicon particles caused by inadequate fusion. This problem could easily be alleviated by use of increased heat to fuse the coating.)

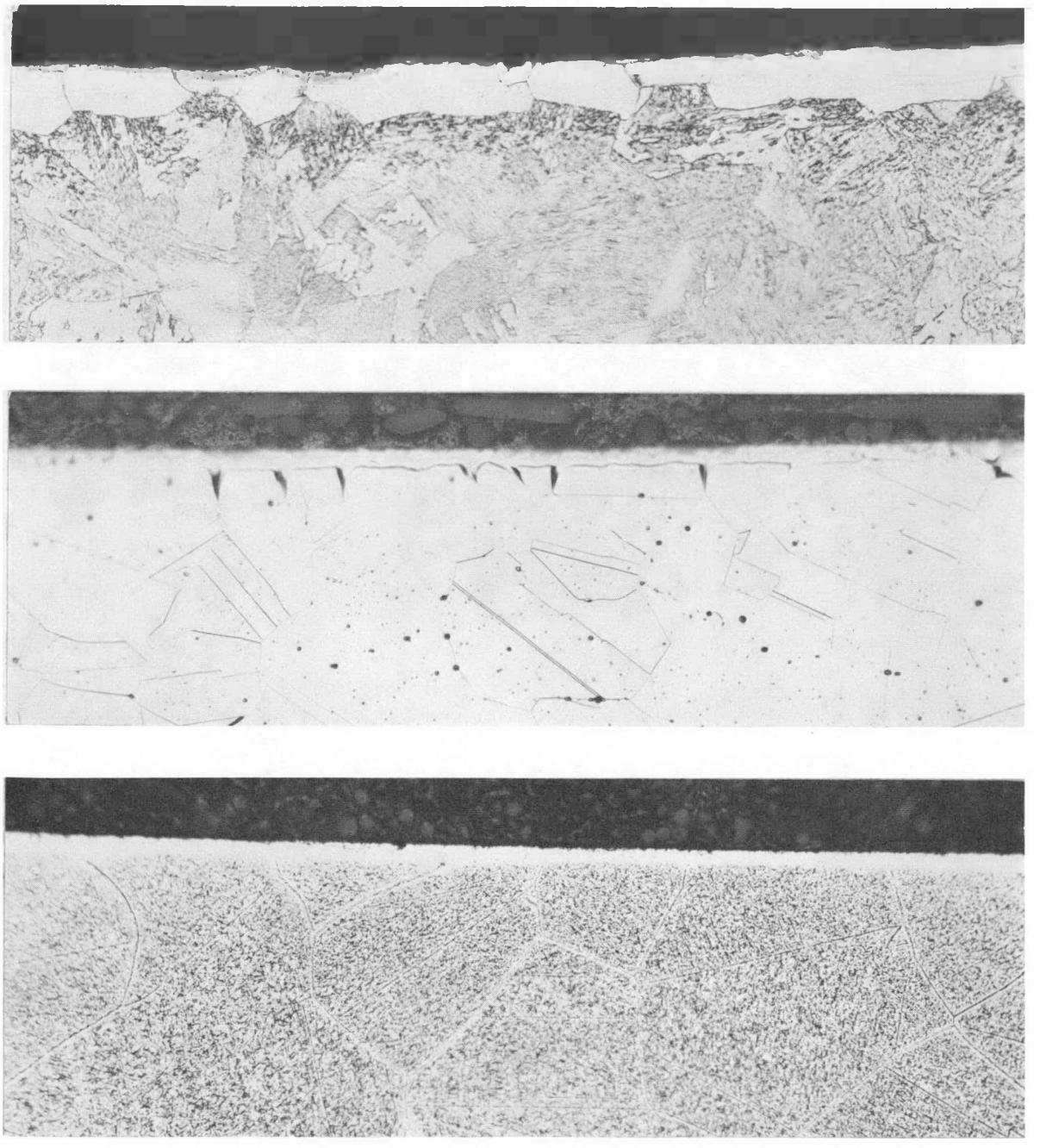

Figure B.47 Microstructure of Siliconized Surface Produced by Vapor Deposition and Diffusion at 1850°F (1010°C) in a Flowing Gas Mixture of Helium Carrier Plus Hydrogen--250X Etched [The upper figure shows a silicon-rich layer on 2-1/4%Cr-1%Mo steel. The center figure shows a thin silicon-rich layer on Type 304 stainless steel, and the lower microstructure shows a silicon-rich layer on Alloy 13 (35%Ni-25%Cr-4%Al).]

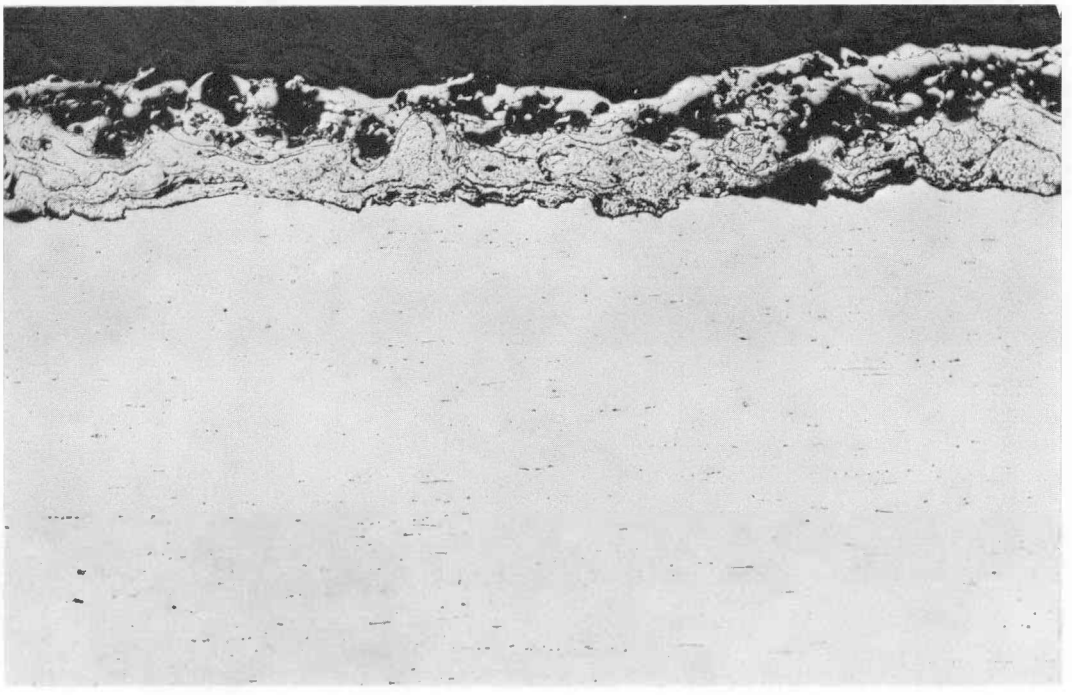

Figure B.48 Microstructure of As-Received Duplex Coating on Type 347 Stainless Steel--100X Unetched [The top surface was coated with $CrSi_2$ (Metco XP-1137) which appears as the thin white phase (very porous). The lower coating was metallized Kanthal A-1. This coating was applied with a wire gun and was well bonded but porous.]

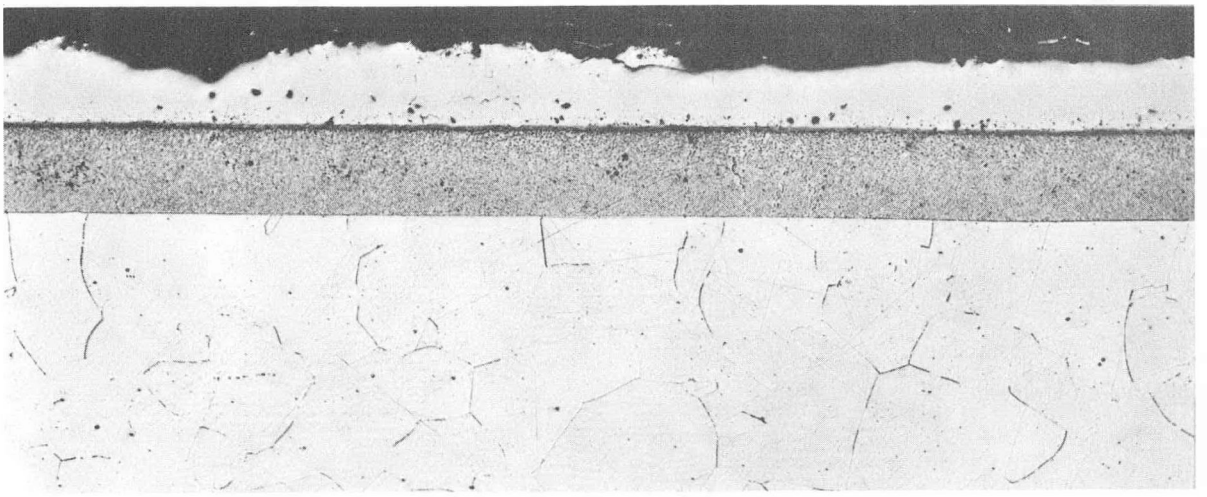

100X

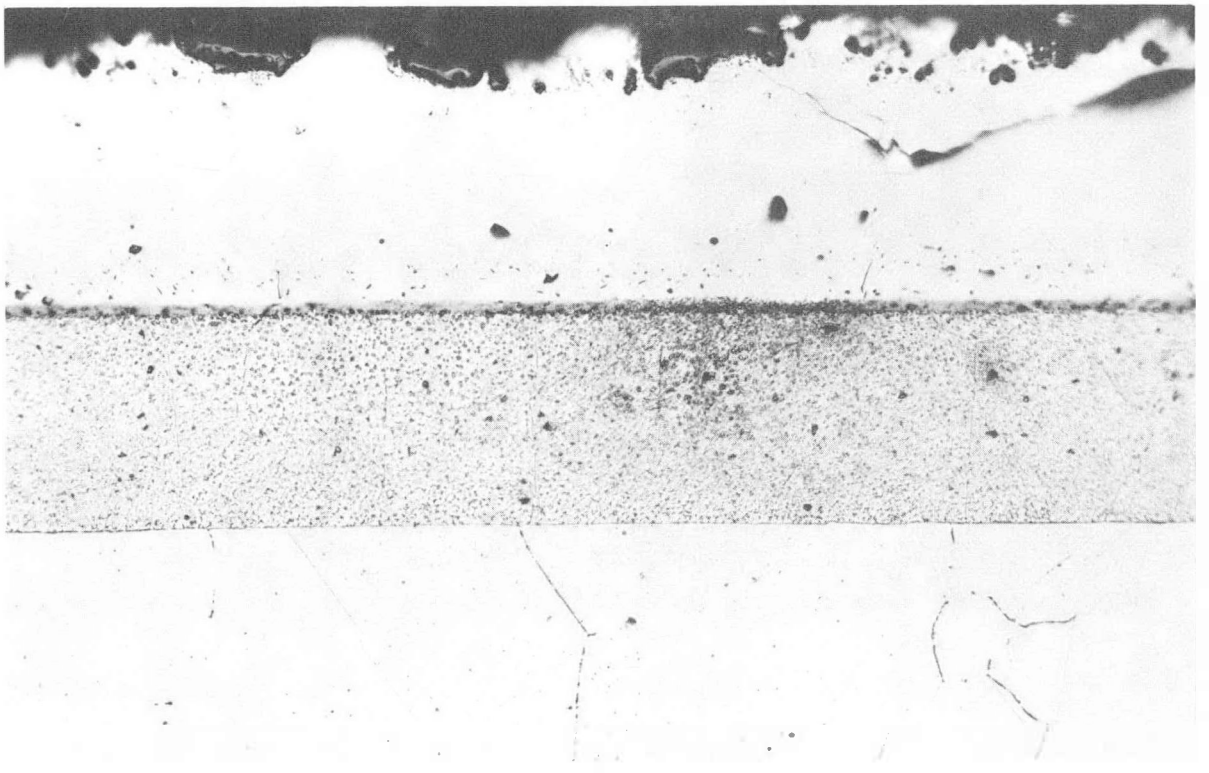

250X

Figure B.49 Microstructure of Alonized Type 304 Stainless Steel (Specimen Al-2) Before Test--Etched [The outer, exposed layer was an aluminum-rich phase, while the diffused, gray area appeared to be Ni-Al and Fe-Al compounds which precipitated during the coating process.]

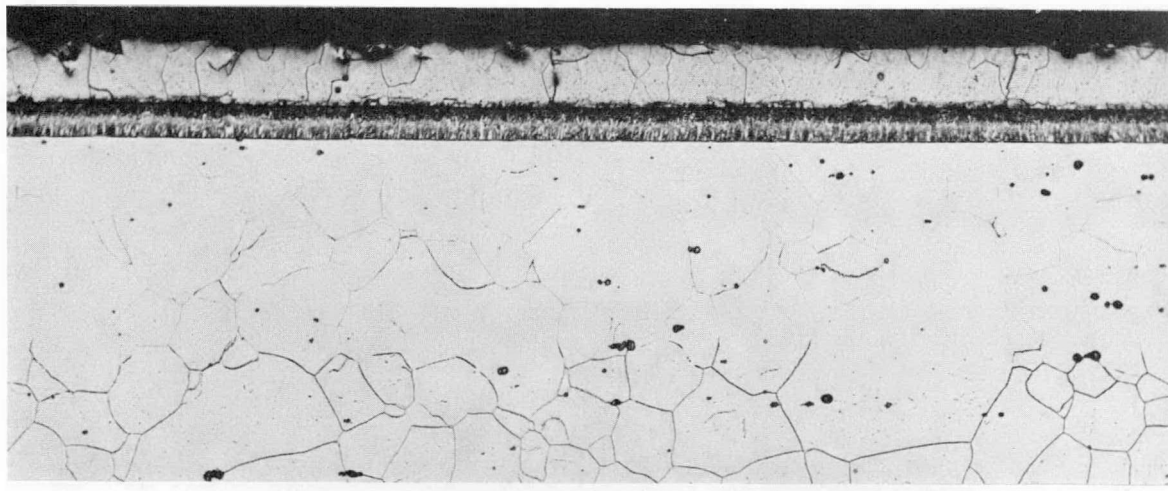

100X

500X

Figure B.50 Microstructure of Alonized IN-800 (Specimen A1-3) Before Test--Etched [The diffused aluminum-rich case was similar to Alonized stainless steel except the gray, diffused band was not as thick, and an acicular precipitate had formed (Ni-Al and Fe-Al compounds).]

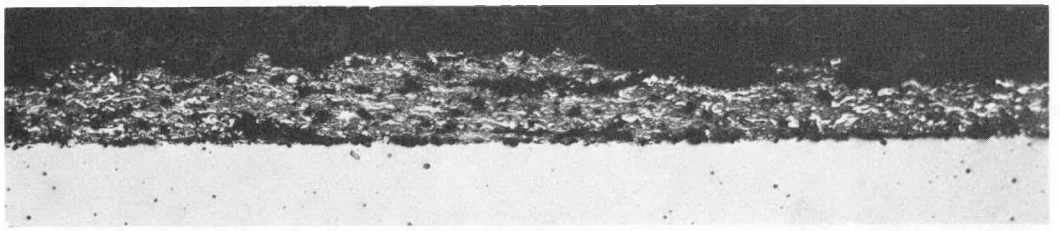

50X

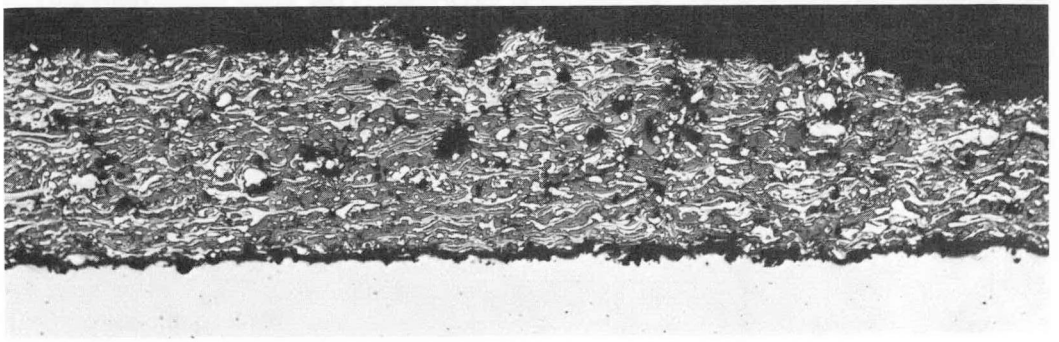

100X

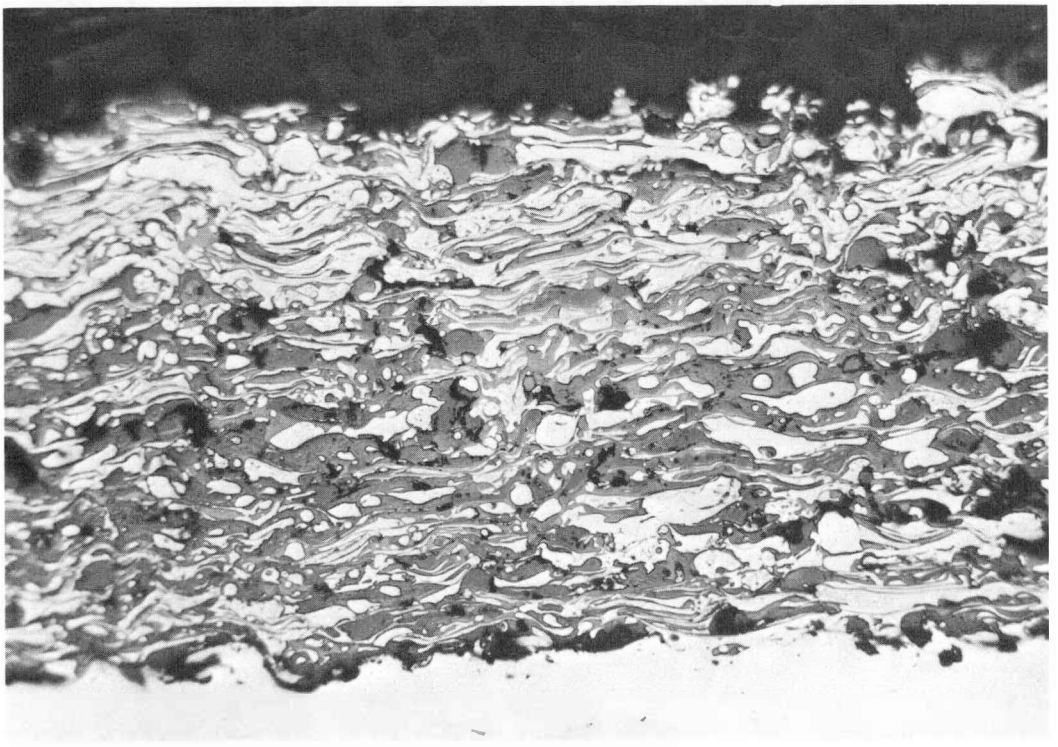

250X

Figure B.51 Microstructure of a Plasma-Deposited IN-671 (50%Cr-50%Ni) Coating on Stainless Steel (The porosity and bond to the substrate could be improved by further development of this coating system.)

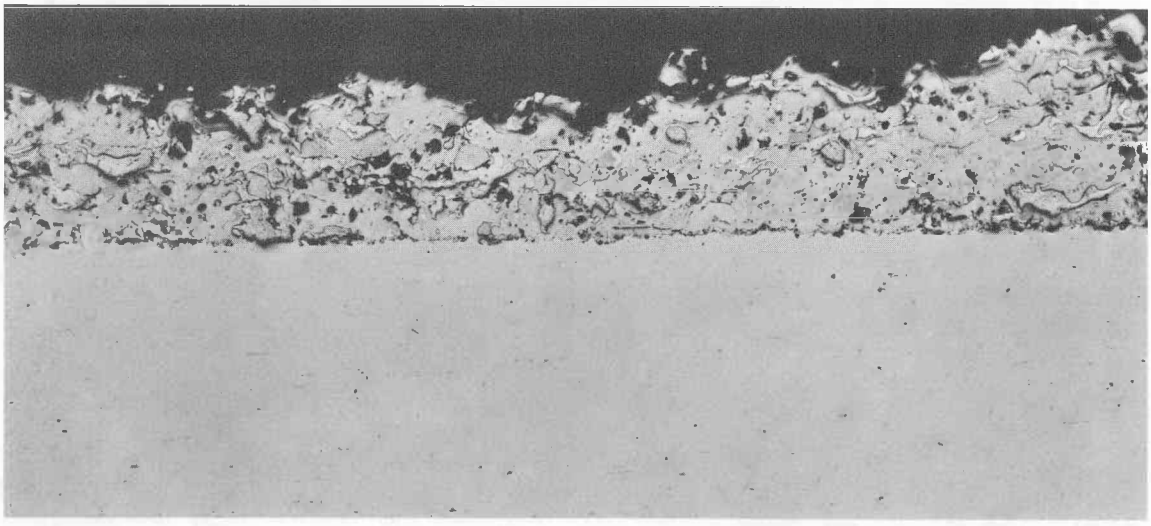

100X

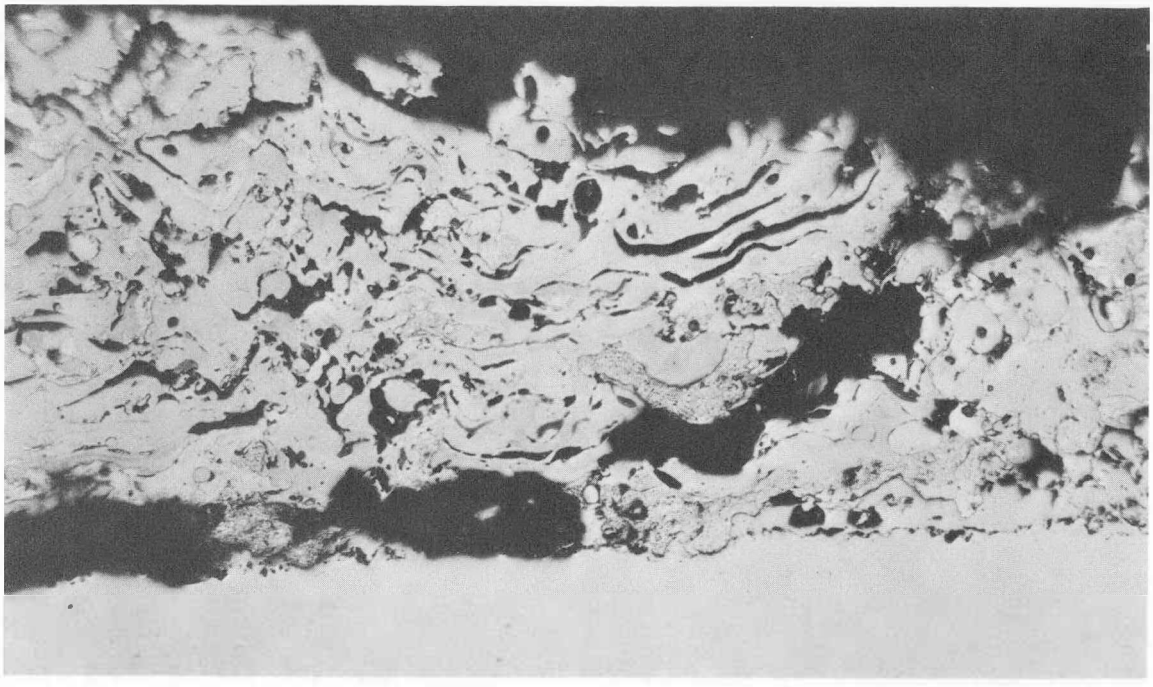

250X

Figure B.52 Microstructure of Ni-Al (Metco 404, approximately 6% Al) Plasma Deposited on Stainless Steel Before Test--Unetched (The nickel aluminide coating did not have good surface preparation prior to coating.)

APPENDIX C

EXPERIMENTAL DESIGN AND TEST PROCEDURE

RETORT DESIGN

A sketch of the retort assembly is shown in Figure C.1. The Fe_2O_3 catalyst, in the form of oxidized Armco iron turnings, was loaded into the lower three retort tubes. The incoming gas mixture interacted with the Fe_2O_3, thereby helping to promote the oxidation of SO_2 to SO_3. The gas then flowed into the back of the retort, which was filled with ceramic beads and stainless steel turnings (serving as a diffuser). The interface between gas and diffuser allowed for a thorough mixing of the gas before it entered the tubes containing the specimens. After passing over the specimens, gas exited from the retort through five stainless steel tubes that extend from the manifold cover. The tubes are connected to water-filled flasks. The bubbling of the flue gas in all the flasks indicated that gas was flowing through all of the retort tubes and that the flow was uniform. Condensate corrosion caused by sulfuric-acid was eliminated by using water-cooled Teflon tubes to carry the gas in the temperature range from 500°F (260°C) down to room temperature.

FLUE GAS MAKEUP

The synthetic flue gas mixture was composed of 72 percent N_2, 14 percent CO_2, 10 percent H_2O, 3.6 percent O_2, and 0.25 percent SO_2. (The CO_2 and SO_2 were introduced as purified dry gases.) All of the contents except the water vapor were introduced from gas cylinder tanks controlled by pressure regulators and calibrated rotometers (see Figure C.2). When the flue gas mixture was needed in the system, the proper levels of air, CO_2, and N_2 were mixed. This mixture was then passed through a heated water vaporizer column at a controlled temperature to get 10 percent water vapor (by volume). The gas exited from the vaporizer and was blended with SO_2 that had been injected downstream through a capillary tube. At this point the flue gas mixture was completed and delivered to the system.

SYNTHETIC ASH

The synthetic coal ash was a mixture of potassium sulfate, sodium sulfate, and ferric oxide in the following proportions (expressed in mol percents): 37.5 percent Na_2SO_4, 37.5 percent K_2SO_4, and 25 percent Fe_2O_3. The correct amounts of the sulfated salts needed to yield the desired ash composition were weighed and mixed. The mixture was placed in a furnace set at 500°F (260°C) and allowed to dry overnight. The proper amount of Fe_2O_3 was then added to complete the mixture, which was then ball-milled to achieve a thorough blend.

The synthetic coal ash was applied to the specimens in the form of a slurry. The coal ash blend was first mixed with a solution of camphor dissolved in alcohol to form the slurry. The mixture was then spread in an even layer across the coupon surface about to be exposed to the flue gas. When the alcohol evaporated during warm-up, the remaining camphor served as a binder to keep the ash in contact with the specimen surface.

SPECIMEN PREPARATION

Specimens of the various alloys to be tested were lapped by hand on 600 grit SiC paper and thoroughly cleaned before exposure. Three thickness measurements, made in the center of each coupon--approximately 1/4 in. (7 mm) apart--were recorded along with the weight. The specimens were loaded into the exposure tube assembly (three per tube), which allowed for up to 45 specimens to be exposed during one test period. Specimens can be tested in several surface conditions: as-ground, preoxidized, and coated. The standard treatments are the hand-ground and lapped.

TEST PROCEDURES

The tube assembly, containing the specimens, was placed in an outer retort box. Once the specimens were prepared and loaded, the retort box was sealed and placed in the furnace. The sealing process involved bolting the manifold cover onto the front end of the retort box and then sealing the cover with strips of fiberglas tape covered with ceramic cement (Sauereisen). The tape served as a sealant to

eliminate gas leaks. As a further precaution against gas leakage, the retort cover was also sealed by filling the space between the lid and cover box with commercial high-temperature mineral fiber-graphite packing, and then sealing the cover-box with Sauereisen cement (cast in situ).

The retort assembly was carefully lowered into the furnace. The exit tubes were attached to Teflon downcomers that carried the gas to the water-filled flasks. Water jackets had been fabricated to surround the Teflon and prevent overheating. (This assembly is shown in Figure C.3.) Kaowool blanket insulation was placed between the cover box and furnace lid to eliminate heat loss during the test. A thermocouple, used to monitor the test temperature, was then inserted into a thermocouple-well in the furnace lid. The retort mean-temperature could then be read on a digital output computer.

Preliminary temperature calibration indicated that the gradients among specimens were not over 5°F (3°C). The temperature of the retort was then slowly increased, held overnight at 250 to 300°F (120 to 150°C), the nitrogen was purged through the system to eliminate any pretest oxidation. The temperature was then increased between 200 and 250°F (110 and 140°C) per hour until the test temperature of 500°F (260°C) was reached. At this point the flue gas mixture was introduced. The flue gas was carried to the retort through a heated and insulated tube that maintained the gas at 150 to 170°F (65 to 77°C) and prevented condensation. In many tests the warm-up procedure was performed under N_2 or Argon gas until the test temperature was obtained.

The temperature was held constant throughout the test period and the gas flows and temperatures were recorded periodically. The first appearance of SO_3 (as fog) in the exit flue gas normally occurred within 15 minutes of the start of the SO_2 flow.

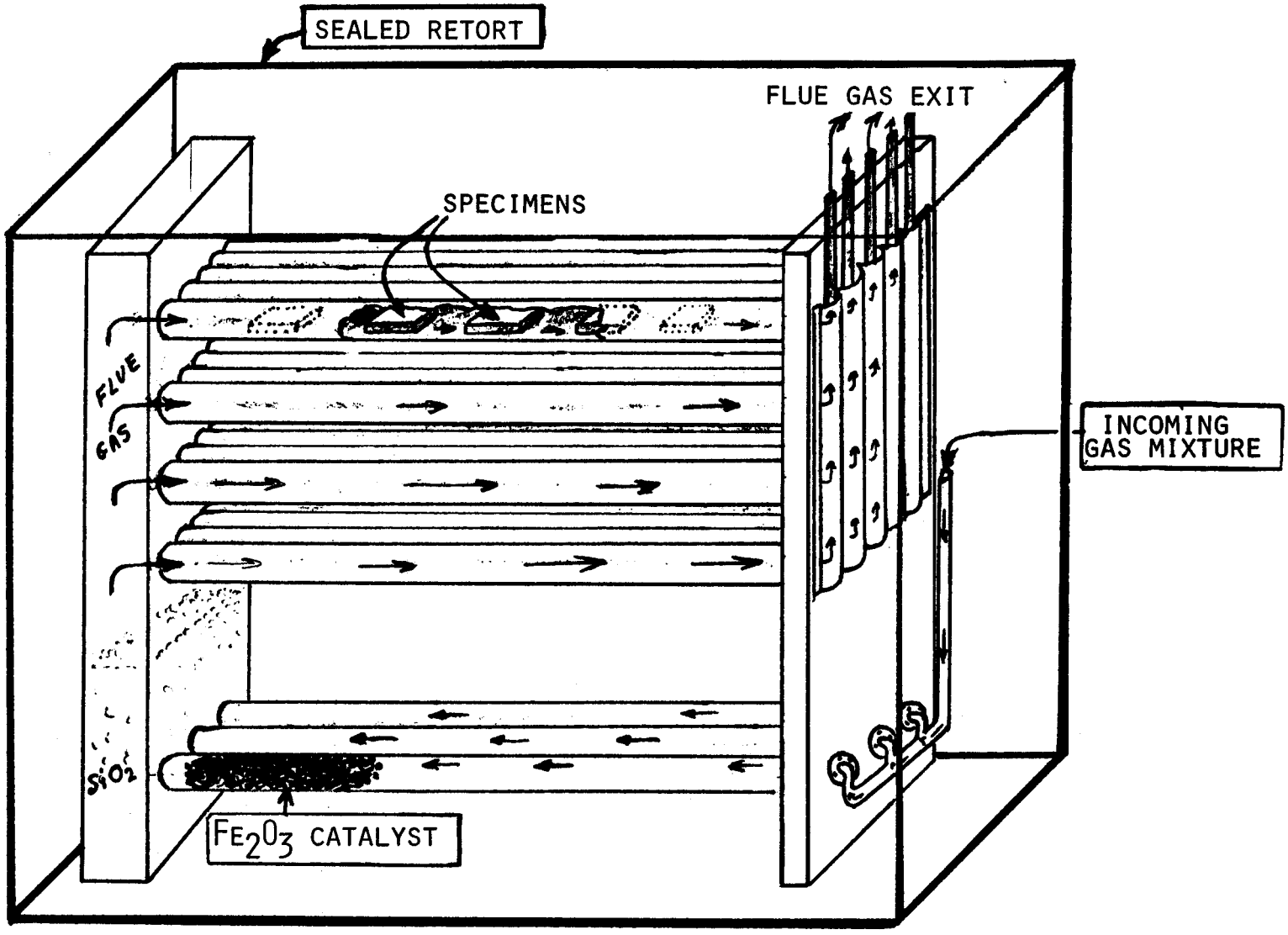

Figure C.1 Fireside Corrosion Retort

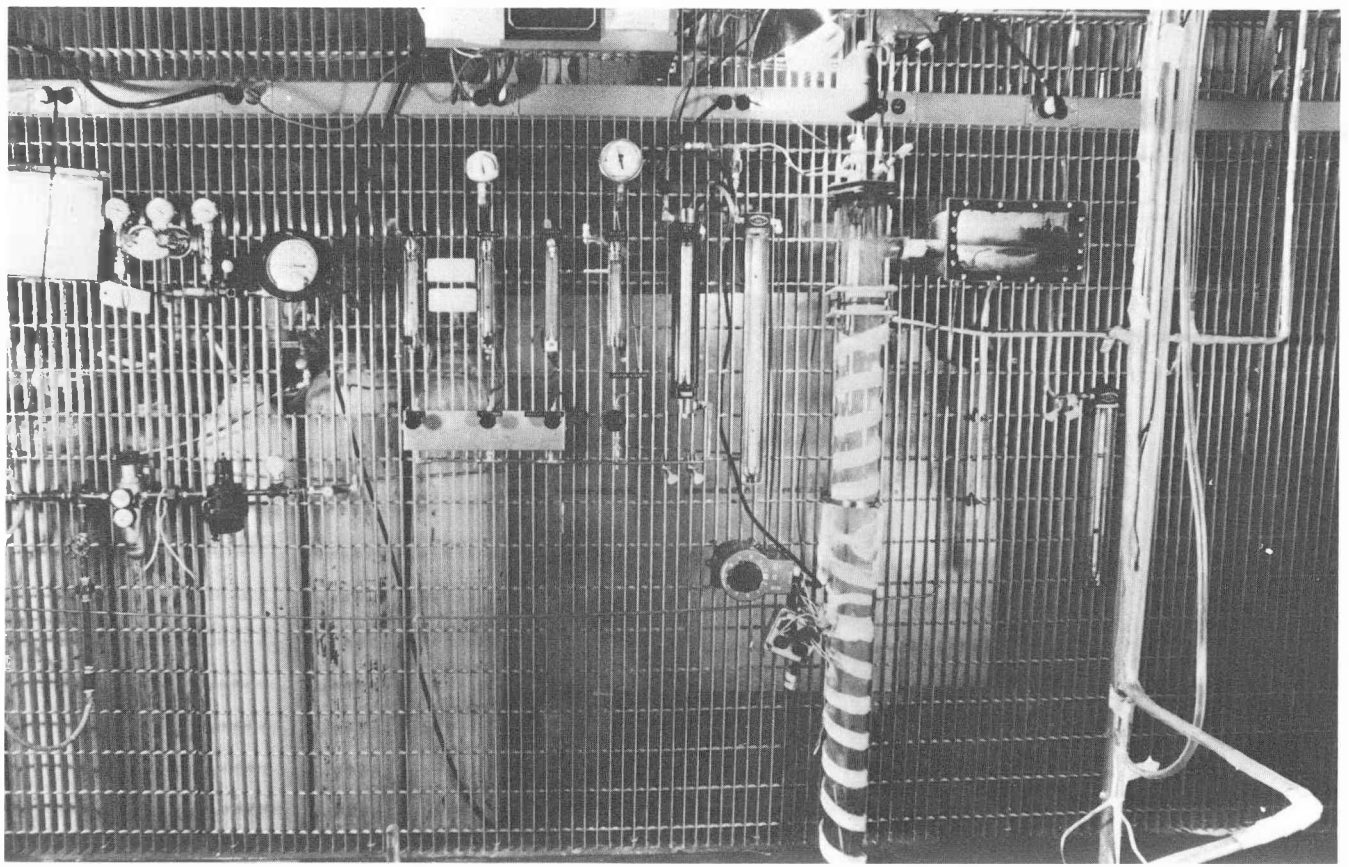

Figure C.2 Synthetic Flue Gas Blending and Control System Including the Water Bubbler Used to Add the Water Content (The major constituent, nitrogen, comes from a liquid nitrogen system which is not shown.)

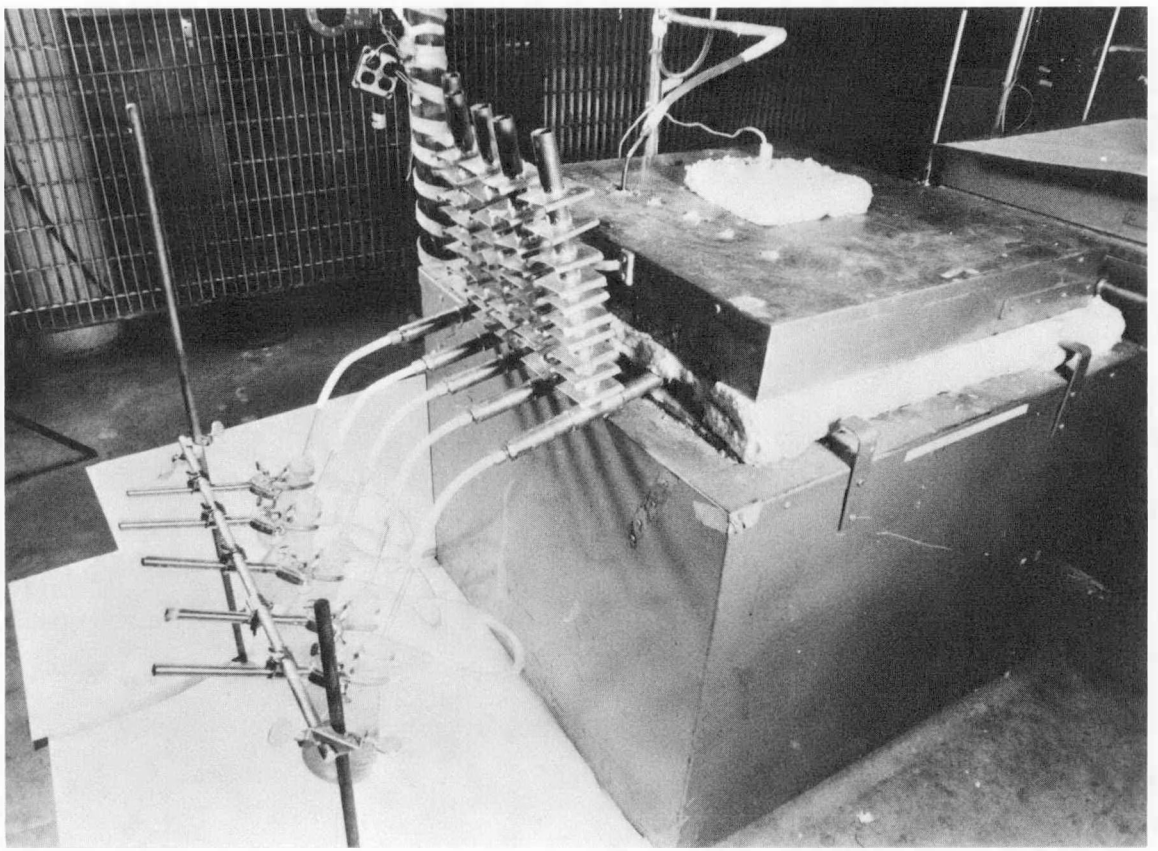

Figure C.3 Fireside Retort Installed in Furnace Showing the Five Gas Exit Tubes With Water-Cooled Teflon to Eliminate Acid Dewpoint Attack (The gas enters at the top through the heated tubing. The exit flow is indicated by bubbling through the glass flask and then passes through added traps and out the stack.)

APPENDIX D

REPRESENTATIVE DATA FROM PHASE 1 TESTS

INTRODUCTION

Included in Appendix D are the general results of all the specimens tested in the retorts, as well as representative data on all Phase 1 materials. Many repeated tests on the reference Phase 1 alloys have indicated that the results were reproducible within the range of the normal scatter for corrosion effects. Additional information on the scales formed, and on the surfaces of the corroded specimens, is included to make feasible a more detailed examination of the results. (Phase 2 results were fully evaluated in the 6th and 7th Quarterly Progress Reports.)

The appendix contains a table listing retort exposures for specimen alloys, a series of photomacrographs of descaled specimens, fireside corrosion effects for each Phase 1 alloy depicted in figures, data on metal loss and pitting, figures showing the analysis of corrosion deposits and scales, and photographs of fireside attack on Phase II alloys.

Table D.1 Summary of Exposures From Fireside Tests

RETORT #	EXPOSURE TIME HOURS	EXPOSURE TEMP. °F	GAS ATMOSPHERE	CORRODENT ASH	OBJECTIVE	COMMENT
1	250	1240	Flue Gas	None	Determine	Oxide Scale
2	500	1240	Flue Gas	None	Flue Gas	Oxide Scale
3	250	1440	Flue Gas	None	Oxidation Penetration	Oxide Scale and Some Alloys Sulfidation
4	250	1240	Flue Gas	Simulated Ash(2)	Fireside Attack by Trisulfate	Severe Attack and Pitting
5	500	1240	Flue Gas	Simulated Ash	Same Longer Time	No Increase over Retort #4
6	250	1440	Flue Gas	Simulated Ash	High Temperature Fireside Attack	Severe Pitting Less General Attack
7	100	1250	Flue Gas	Simulated Ash	Shorter Time Attack	Results Similar to Retort #4
8	24	1250	Flue Gas	a) Simulated Ash b) Synth.Trisulfate(3)	Determine Start-up of Attack	Attack Similar to 4, Reduced Pit Depth
9	50	1250	Air Only	a) Simulated Ash b) Synth.Trisulfate	Compare Trisulfate Attack with Gas-Solid Sulfate Oxidation	a) Simulated Ash No Sign Attack b) Trisulfate Attack in Air Was Similar to Retort #7
10	48	1250	Flue Gas	Simulated Ash Carbon Added	Effect of Carbon	Same as Retort #7

FOOTNOTES:

(1) Objective of Tests (using 18 base metal alloys, see Table 2) was not to duplicate all coal fired boiler conditions but to simulate the worst condition obtained in high alkali coals (such as Midwestern) which form liquid sodium-potassium iron trisulfate.

(2) The "Simulated Ash" was - 37.5% Na_2SO_4, 37.5%K_2SO_4, 25%Fe_2O_3 (Mole %) Blended and Dried.

(3) The synthetic $(Na,K)_3Fe(SO_4)_3$ was formulated, fused and ground in the lab.

Table D.2 Summary of Exposures From Fireside Tests (Retorts 11 through 18)

Retort No.	Time (h)	Temp. (°F)	Gas Atmosphere	Corrodent Ash	Objective	Alloys Tested	Comment
Phase 1 Materials Test:							
11	48	1250	Flue gas*	Simulated ash† + carbon	Effect of active free carbon in ash	Commercial alloys§	Very little effect caused by carbon.
12	48	1450	Flue gas*	Simulated ash† + carbon	High-temperature fireside attack	Commercial alloys§	Fused and pitted with carbon added. No pitting without carbon.
13	48	1250	Flue gas	Simulated ash	Evaluate pre-oxidized alloys	Commercial alloys	Reduced number but deeper pits.
14	48	1250	Flue gas	Simulated ash + 3%NaCl	Combined corrodent attack	Selected commercial alloys	Severe pitting by fused ash + NaCl.
15	48	1450	Flue gas	Simulated ash + 3%NaCl	High-temperature combined attack	Selected commercial alloys	Without NaCl no attack; some pitting with NaCl.
Phase 2 Materials Test:							
16	48	1250	Flue gas	Simulated ash†	Variation of fireside attack on high alloys	Special alloys¶	Benefit of silicon content verified.
17	48	1250	Flue gas	Simulated ash (3%NaCl on some)	Variation of fireside attack on high alloys	Special alloys¶	Synergistic effects and high Al effects noted.
18	48	1250	Flue gas	Simulated ash + 3%NaCl	Variation of fireside attack on high alloys	Special alloys¶	Verification of previous results.

*Simulated high sulfur gas was 72%N_2, 14%CO_2, 10%H_2O vapor, 3.6%O_2, 0.25%SO_2 + SO_3.
†"Simulated ash" was 37.5%Na_2SO_4, 37.5%K_2SO_4, 25%Fe_2O_3 (mol %) blended and dried.
§Commercial and Semicommercial alloys listed in "Fifth Quarterly Progress Report" (Appendix, Table 1A).
¶Special alloys prepared for this test (see Table 1).

Table D.3 Fireside Attack Using Carbon (Char) Added to Ash for 48-Hour Exposure at 1250°F (675°C)

Alloy	Retort 10--9%C*		Retort 11--15%C		Effects of Carbon
	General Attack (in.)	Pitting† (in.)	General Attack (in.)	Pitting† (in.)	
HT-9	0.005	0.010	0.006	0.010	None
304	0.005	0.010	0.005	0.010	None
310	0.003	0.008	0.004	0.008	None
314	0.002	0.006	0.0025	0.007	Slight
347	0.003	0.005	0.004	0.006	Slight
21-6-9	0.003	0.005	0.004	0.010	Slightly worse
IN-800H	0.006	0.012	0.006	0.013	None
IN-811	0.005	0.011	---	---	None
IN-671	0.001	0.004	---	---	None

*Results of Retort 10 were mentioned in Reference 3, p. 14. The details listed here support those remarks. See also Figures 9 and 10 in Reference 3.
†Maximum (total) penetration at pit as measured after descaling.

Table D.4 Fireside Tests at 1450°F (785°C) Showing Maximum Penetration or Pitting Caused by Adding Carbon or NaCl

Alloy	Retort 12		Retort 15	
	No Carbon (mil)	15%Carbon Added (mil)	No NaCl (mil)	3%NaCl Added (mil)
304	No attack*	18†	No attack*	8†
310	No attack	12	No attack	12§
347	No attack	Edge pitted	No attack	20§
21-6-9	No pits	10†	---	---
IN-800H	No attack	18†	No attack	21§
IN-811	No attack	21†	No attack	>10 (estimated)
IN-671	No attack	---	No attack	Edge attack about 8

*Ash not fused; molten alkali-iron trisulfate apparently not formed.
†Fused ash visible on all specimens showing attack, largely pitting.
§No general attack, excluding the thin oxide scale, but a few large pits were observed; ash fused.

Table D.5 Fireside Tests at 1250°F (675°C) for 48 Hours Showing Maximum Penetration Caused by Preoxidizing Surfaces and Adding NaCl to Ash

Alloy	Retort 13--Preoxidized Surfaces		Retort 14--3%NaCl Added to Ash	
	Polished (mil)	Preoxidized (mil)	No NaCl (mil)	3%NaCl Added (mil)
HT-9	14	13	12	15
304	12	12	8	10
347	8	8	6	11
314	10	16*	10	12
310	9	---	10	12
21-6-9	8	12	9	9
IN-800H	10	14†	12	12
IN-811	14	18†	11	15
IN-671	4	17†	None	8†

*Heat treatment for preoxidation apparently produced Si loss at the surface, and some Cr depletion was assumed.
†Few pits and much less attack elsewhere.

Table D.6 Pitting of Selected Commercial Alloys Exposed to Simulated Fireside Attack, Comparing Preoxidized and Unoxidized Specimens*

Alloy Specimen	Temperature of 24-Hour Air Oxidation Treatment (°F)	XRD Scale Identification	% of Surface Attacked (1 Section)	Pit Depth (mil)
800-34	---	---	50	5
800-32	1832	Cr_2O_3(m), Spinel(m)	100	11
811-26	---	---	100	12
811-21	2012	Spinel(m), Cr_2O_3(w) α-Al_2O_3(vw)	100	14
21-6-9	---	---	100	8
21-6-9	1652	$MnCr_2O_3$(s)	100	9
314-20	---	---	>95	8
314-17	2192†	Cr_2O_3(m), Spinel(mw)	100	10
671	---	---	<5	2§
671	2012	Cr_2O_3(s), Spinel(w)	1 pit	0.5§

*Measurements taken from low-magnification micrographs (one section); Retort 13

†In cracked NH_3 over NiO.

§View of specimen surface shows a low density of rather deep pits, up to 16 mil. These particular cross sections did not happen to intersect these large pits.

Table D.7 Performance of Phase 2 Alloys in Fireside Corrosion Tests [Specimens were exposed for 48 hours at 1250°F (675°C)]

	NOMINAL COMPOSITION				RETORT #16			RETORT #17			RETORT #18	
								STANDARD ASH			STANDARD ASH	ASH + 3%NaCl
ALLOY #	Ni	Cr	Al	Si	GENERAL ATTACK (mil)	MAXIMUM PENETRATION (mil)	TYPE OF PITS	GENERAL ATTACK	MAXIMUM PENETRATION	Ash + 3%NaCl MAXIMUM PENETRATION	MAXIMUM PENETRATION (mil)	MAXIMUM PENETRATION (mil)
1	25	20	-	-	*	15	L**	-	14	18	13	15
2	25	20	2	-	*	13	L	-	10	13	11	-†
3	25	20	-	2	4	8	S	3	5	-†	10	-
4	25	20	2	2	2.5	4.5	S	2	3	2	5	4
5	35	25	-	-	-	8.5	L	-	10	17	5	13
6	35	25	2	-	5	8	S	5	10	-	12	15
7	35	25	-	2	4	6	S	4	7	-	10	-
8	35	25	2	2	3	4	S	4	4	9	5	9
9	40	30	-	-	-	11	L	-	11	14	11	12
10	40	30	2	-	-	8	M	-	9	-	8	13
11	40	30	-	2	3	6	S	4	5	-	3	5
12	40	30	2	2	3	4	S	3	-	4	3.5	6
13	35	25	4	-	5	10	B	-	8	8	6	12
14	35	25	4	-	$\frac{Y}{0.1}$ 4	6	-	-	12	8	10	12
15	35	25	4	-	0.5 5	8	S	-	5	5	9	6
16	35	25	-	-	0.1 5	9.5	M	-	12	-	7	10
17	35	25	-	-	0.5 5	15	-	-	11(B)	-	10	7
18	20	25	-	-	0.6 4	8.5	-	-	8	-	9	5
19	20	23	-	-	$0.5Y_2O_3$	10	B	-	6	-	12	-

FOOTNOTES

* Pitted primarily but some areas unattacked

† Not Tested

** L = large pits S = small pits
M = moderate or shallow pits B = broad, shallow pits

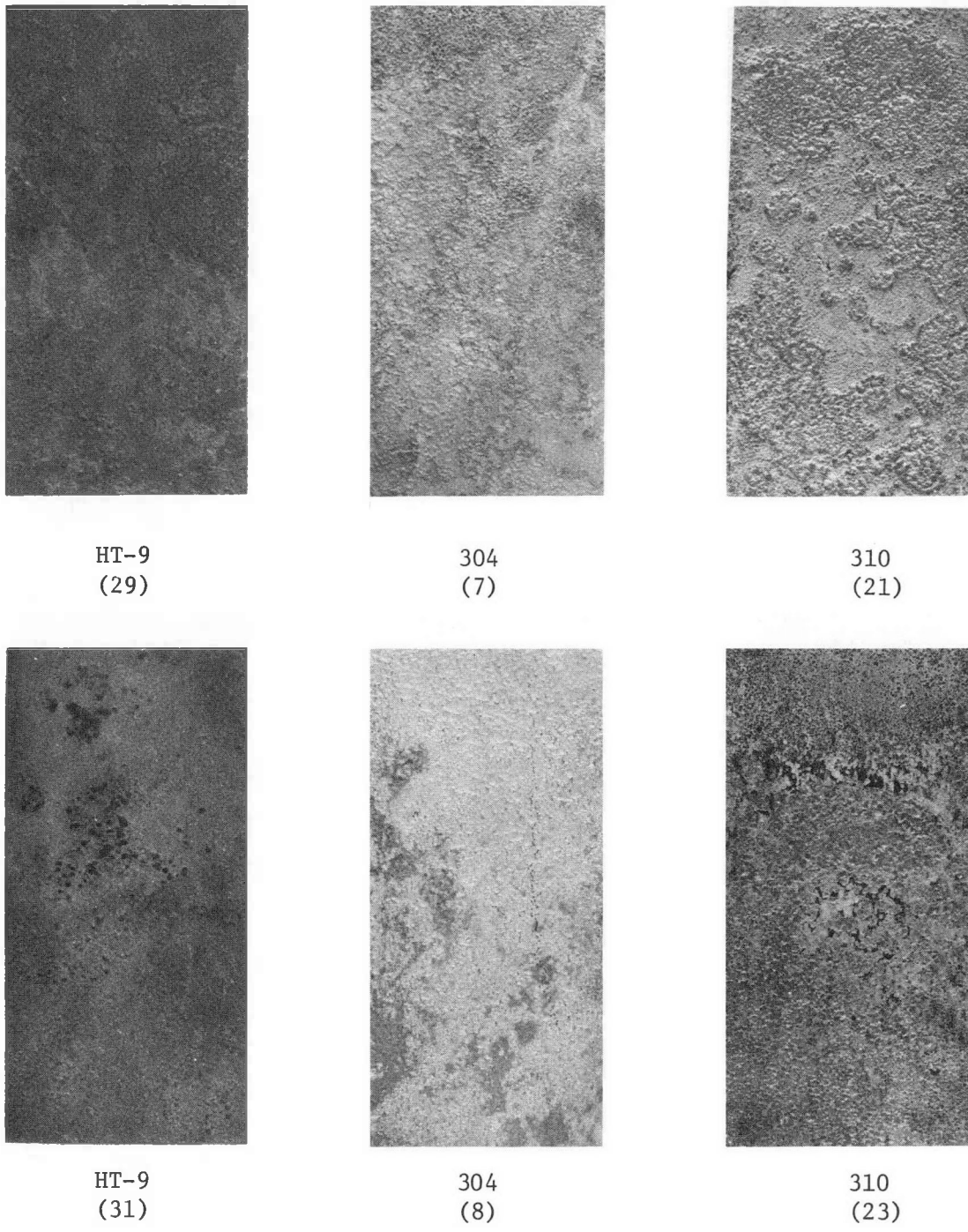

HT-9
(29)

304
(7)

310
(21)

HT-9
(31)

304
(8)

310
(23)

Figure D.1 Photomacrographs of Descaled Test Coupons--1.5X (Effects of Fireside attack on commercial steels using ash containing carbon showing no significant difference due to carbon.)

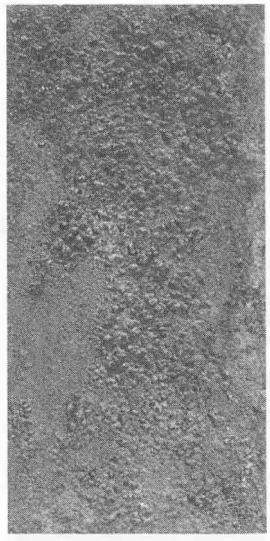

314
(15)

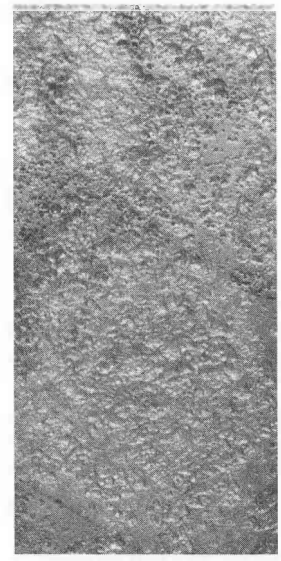

800
(2)

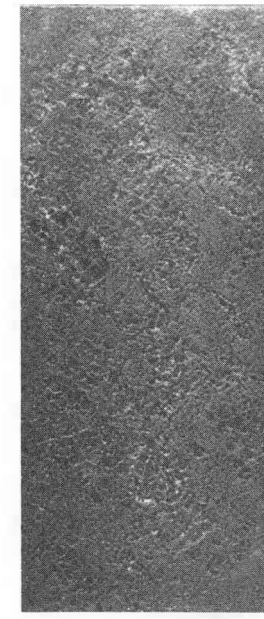

21-6-9
(26)

314
(18)

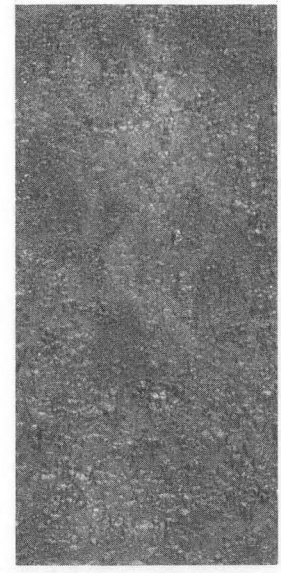

800
(3)

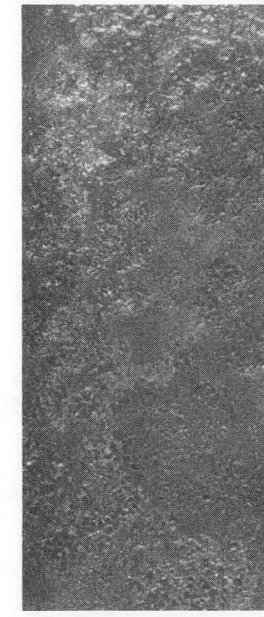

21-6-9
(28)

Figure D.2 Photomacrographs of Descaled Test Coupons from Retort 11--1.5X (Effects of carbon addition were slight which may be due to the rapid oxidation of the char.)

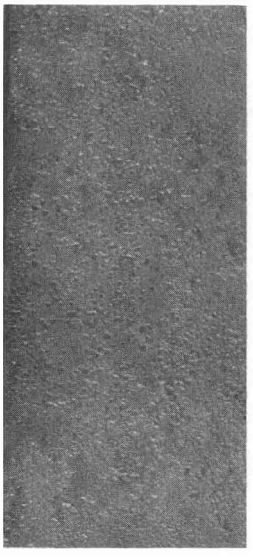

347
(31)

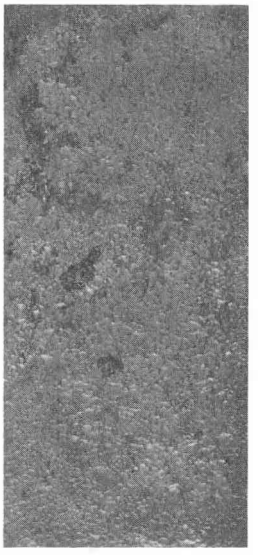

347
(32)

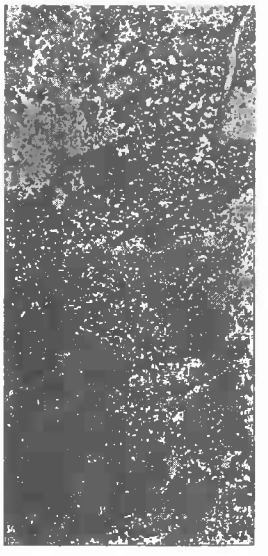

50-50 CB
(2)

347
(40)

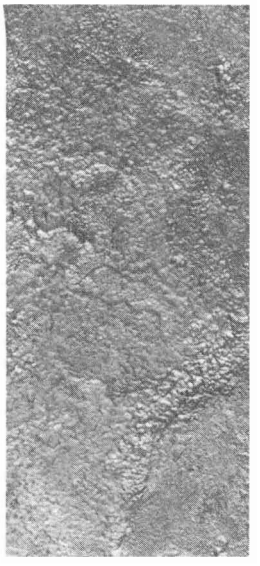

347
(41)

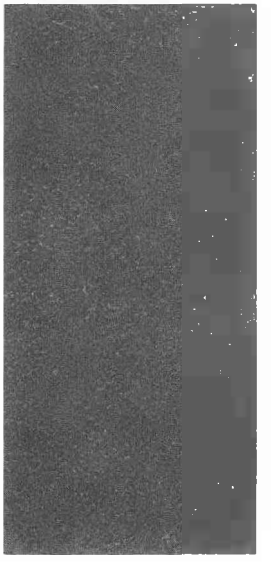

50-50 CB
(3)

Figure D.3 Photomacrograph of Descaled Test Coupons From Retort 11 (48-hour Fireside exposure)--1.5X

800
[31 (CS)]

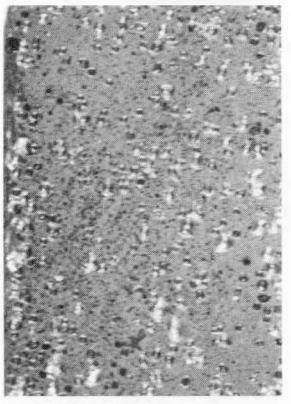

800
[20 (OX)]

800
[32 (OX)]

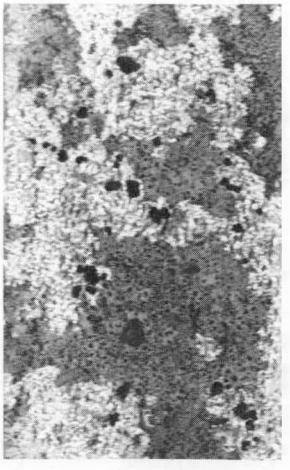

811
[21 (OX)]

Figure D.4 Photomacrographs of Preoxidized Descaled Specimens After Test--1.5X [After 1250°F (675°C) for 48 hours specimens from Retort 13 exhibited less general surface attack, but random, severe pitting.]

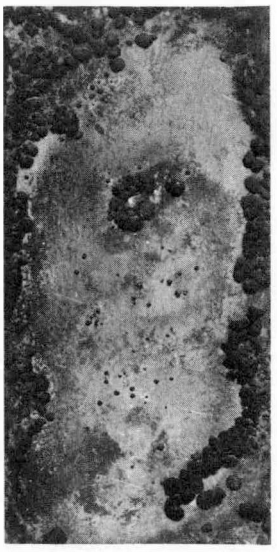

671
(24)

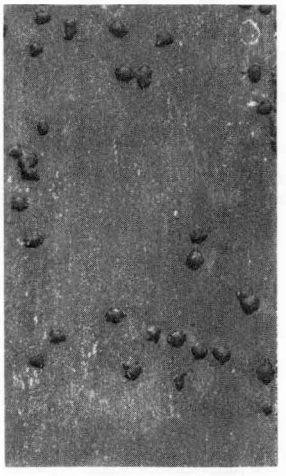

671
[4 (OX)]

671
(25)

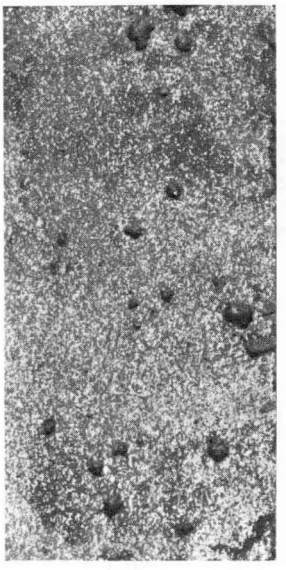

671
[22 (OX)]

Figure D.5 Photomacrographs of Descaled Specimens After Test--1.5X [After 1250°F (675°C) for 48 hours specimens on the right side were preoxidized and suffered fewer, but deeper, pits than the exposed as-polished coupons on the left.]

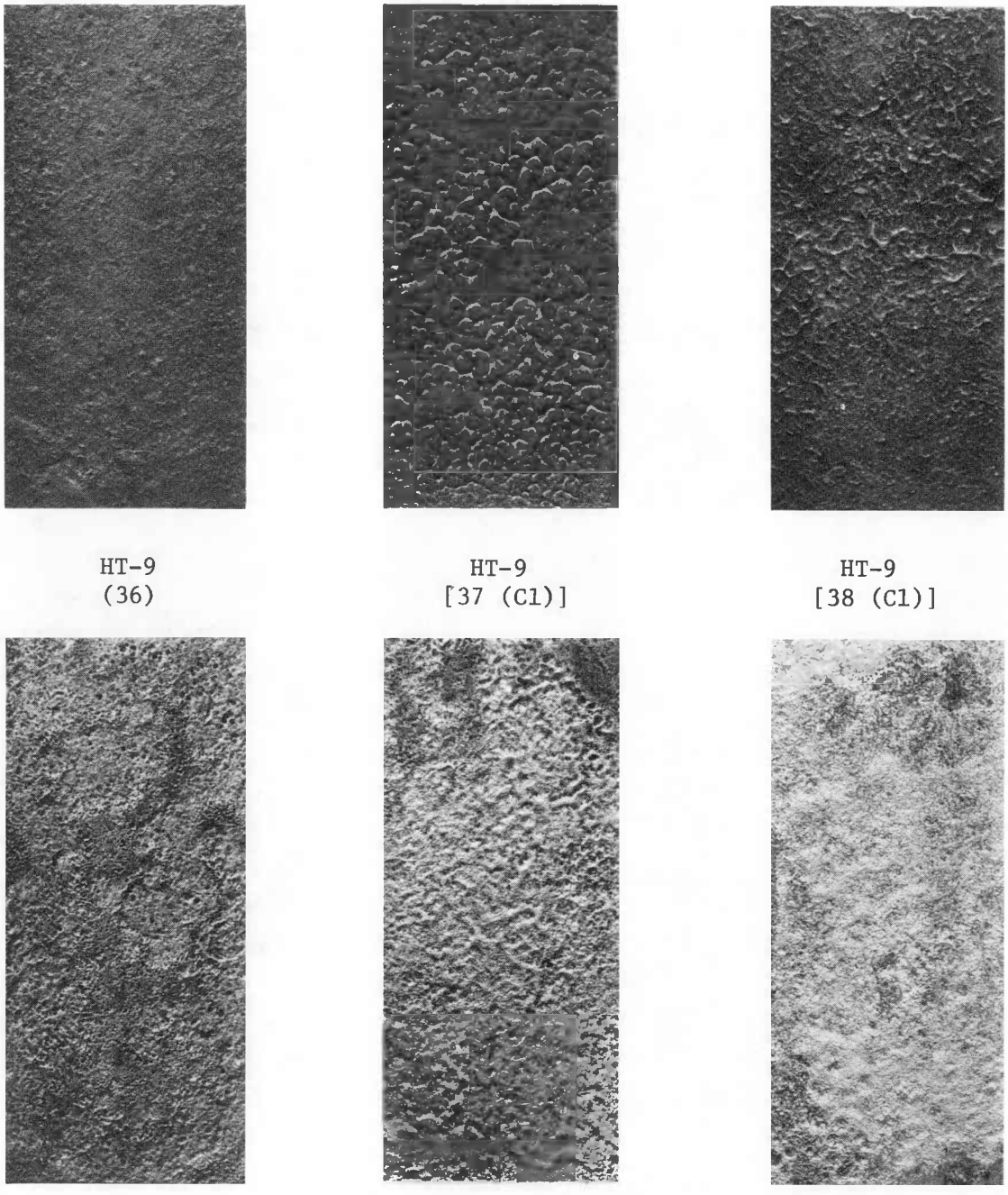

Figure D.6 Photomacrographs of Descaled Specimens After Test From Retort 14--1.5X [After 1250°F (675°C) for 48 hours the chloride addition appeared to increase general corrosion rather than pitting on iron-base alloys. Specimens on the left had no chloride added.]

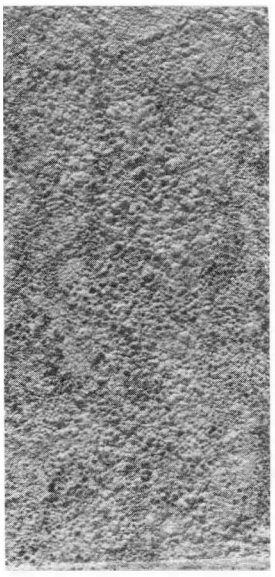

304
(41)

304
[42 (Cl)]

304
[43 (Cl)]

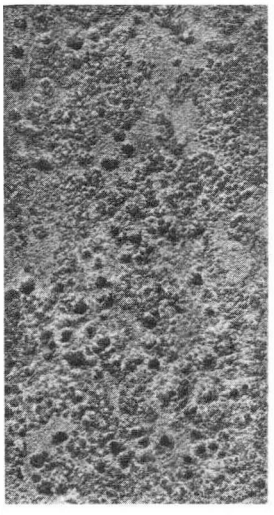

310
(27)

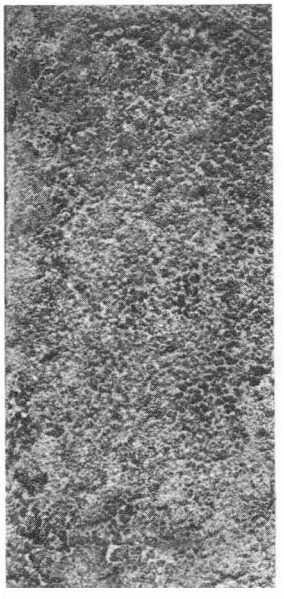

310
[28 (Cl)]

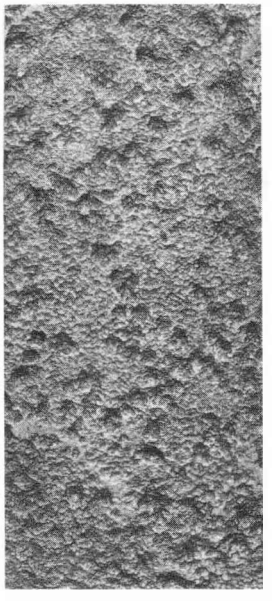

310
[29 (Cl)]

Figure D.7 Photomacrographs of Descaled Stainless Steel Specimens From Retort 14--1.5X [After 1250°F (675°C) for 48 hours the loss of metal attributed to chloride was less pronounced in the case of higher alloys. Specimens on the left had no chloride.]

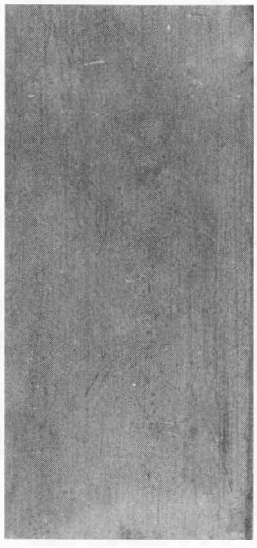

304
(50)

304
[52 (Cl)]

310
(31)

310
[33 (Cl)]

Figure D.8 Photomacrographs of Specimens Showing 1450°F (785°C) Chloride Effect From Retort 15--1.5X (The specimens on the right indicate the presence of chloride in the ash. A comparison of these specimens to the exposed and descaled specimens on the left reveals no significant loss of metal.)

800
(5)

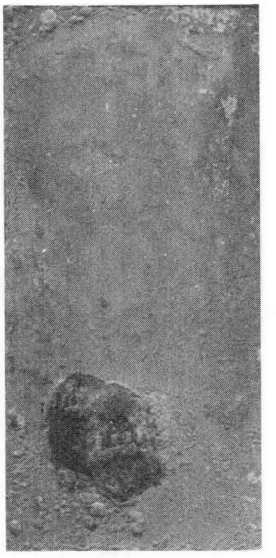

800
[31 (C1)]

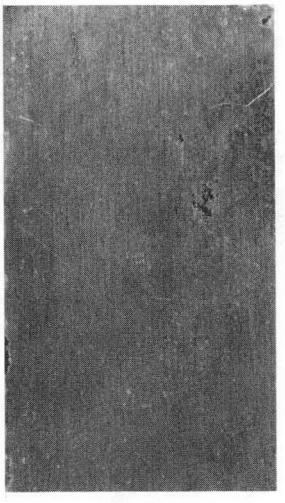

811
(30)

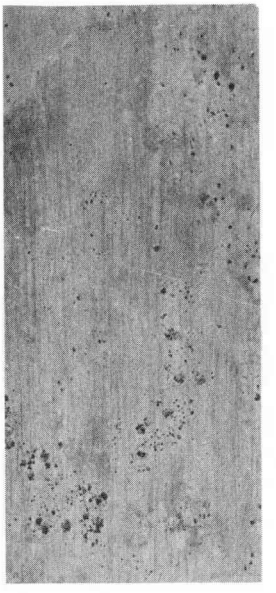

811
[31 (C1)]

Figure D.9 Photomacrographs of Specimens Showing Effects of Chloride at 1450°F (785°C) From Retort 15--1.5X (The general corrosion was not significant but pitting occurred in specimens with ash containing chloride. Note that the 811 alloy had fine pits while Incoloy 800 produced larger round pits.)

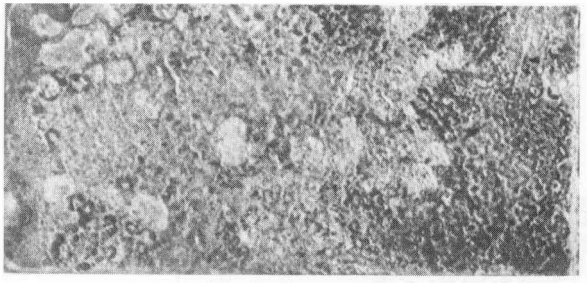

Descaled 1.5X

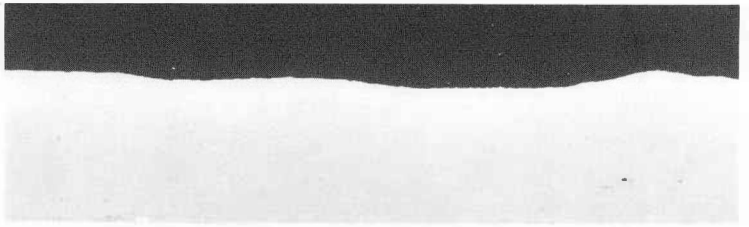

Unetched--Surface Exposed to Simulated Ash 20X

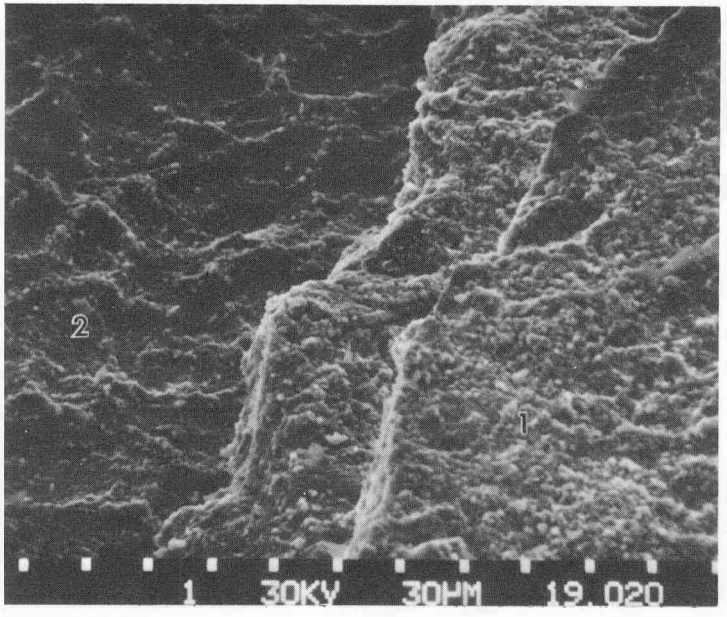

Tilted 300X

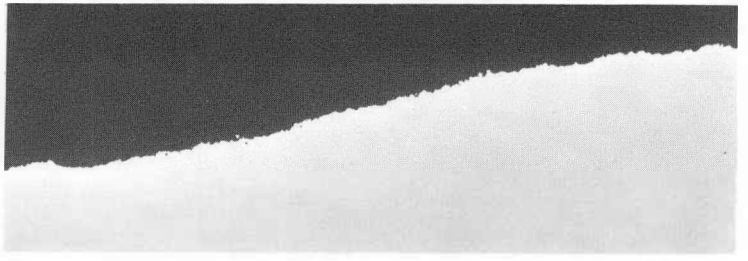

Surface Exposed to Simulated Ash 200X

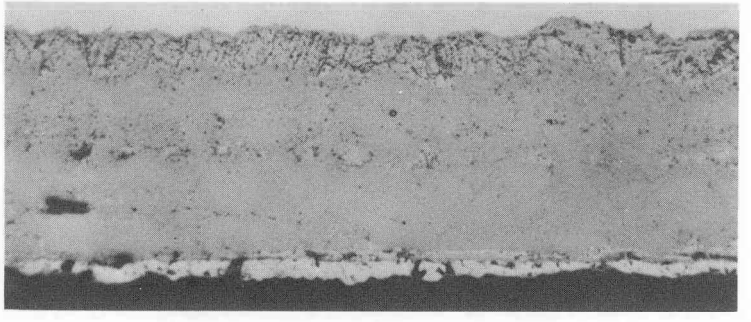

Bottom of Specimen - No Fuel Ash 200X

Figure D.10 Fireside Corrosion Effects on 2.25%Cr-1%Mo Steel [Figure shows descaled specimen (upper left) and nondescaled specimen after 250 hours exposure at 1240°F (670°C). Surfaces indicate that general corrosion attack by the fused ash predominated. The scale produced by the flue gas was more adherent (lower right), but the metal loss was only one-sixth that caused by the fused ash. The SEM view shows several scale layers on the top surface.]

Descaled 1.5X

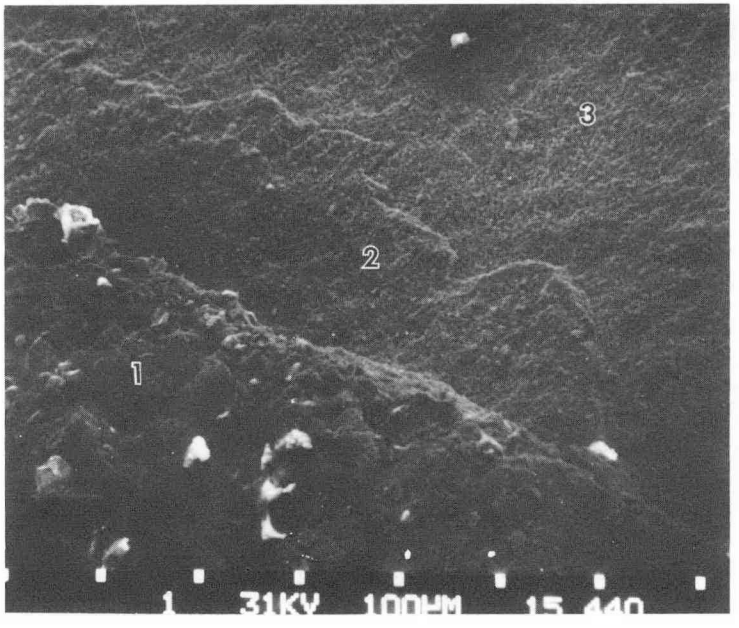

150X

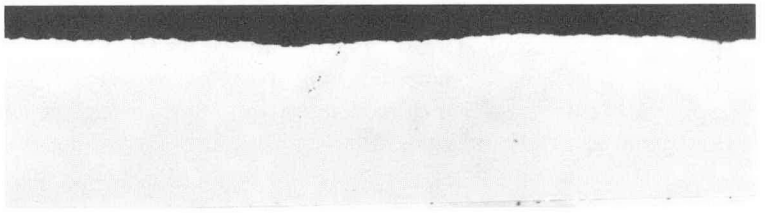

Surface Exposed to Simulated Ash 20X

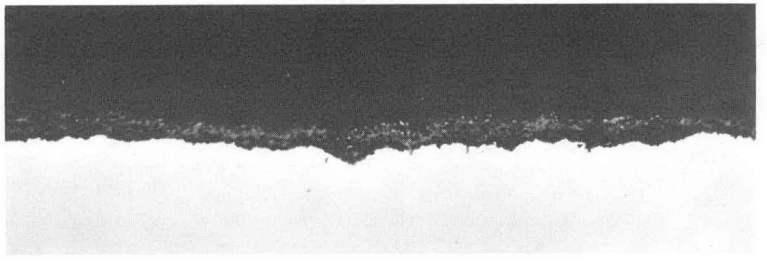

Unetched 200X

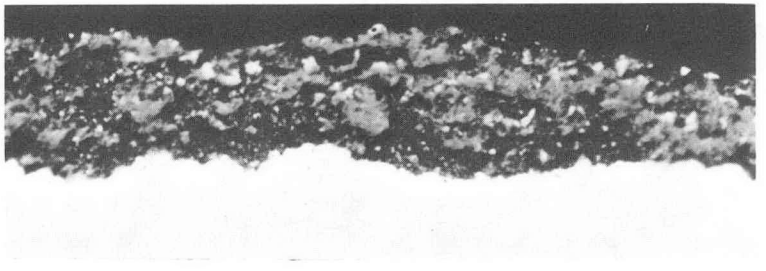

1000X

Figure D.11 Fireside Corrosion Effects on HT-9 [Figure shows descaled specimen (upper left), and nondescaled specimen after 250 hours exposure at 1240°F (670°C). The scale (lower right) produced below the simulated ash was adherent. The SEM view of the surface (lower left) shows part of the ash (1), the scale (2), which was partially exfoliated (3).]

Descaled 1.5X

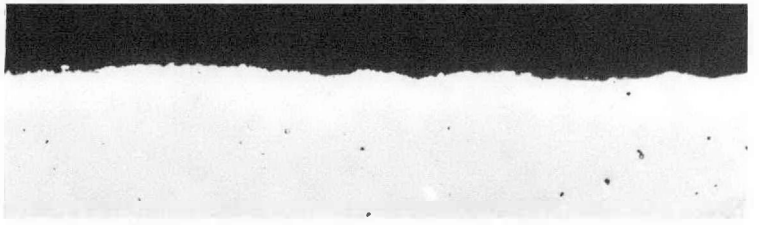

Surface Exposed to Simulated Ash 20X

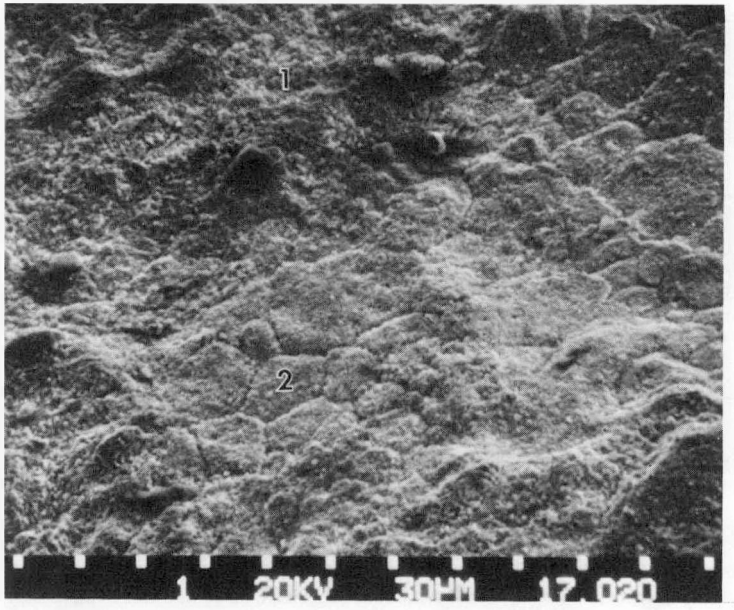

300X

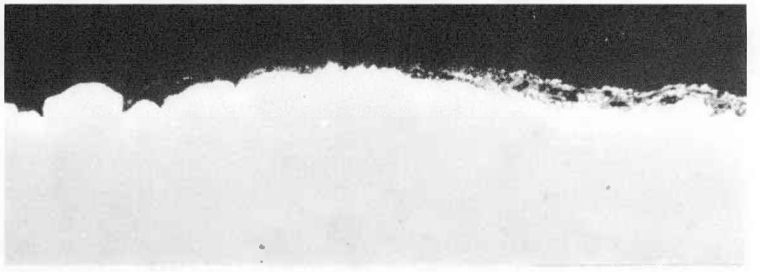

Unetched 200X

Figure D.12 Fireside Corrosion Effects on Type 304 Stainless Steel [Figure shows descaled specimen (upper left), and nondescaled specimen after 250 hours exposure at 1240°F (670°C). The scale (lower right) produced below the simulated ash was partially adherent. Note: The corrosion tended to attack grain boundaries, also shown in the SEM view of the surface (lower left), which was tilted (see location 2)].

Descaled 1.5X

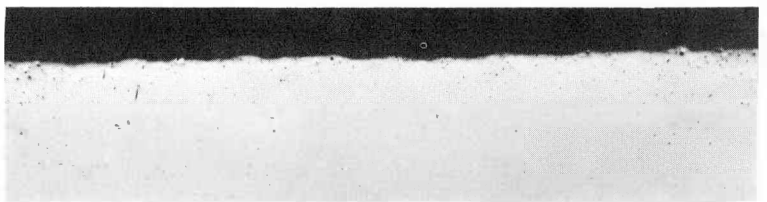

As-Exposed Surface 20X

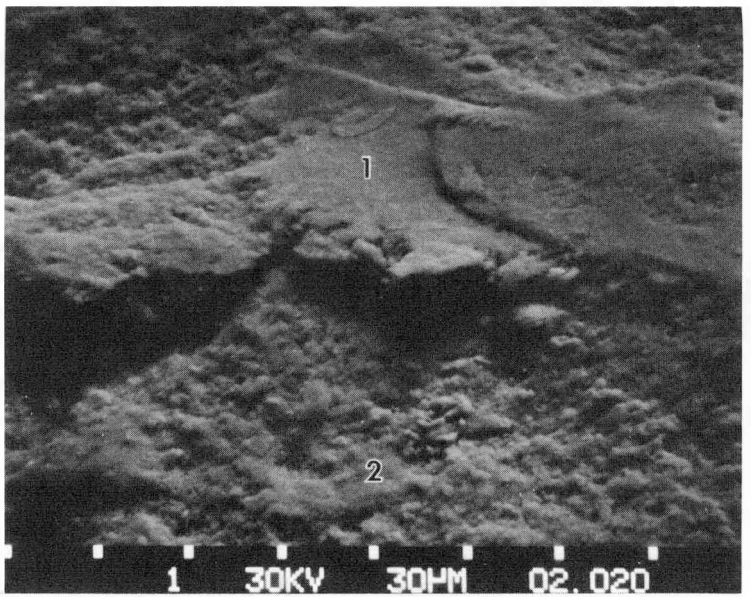

460X

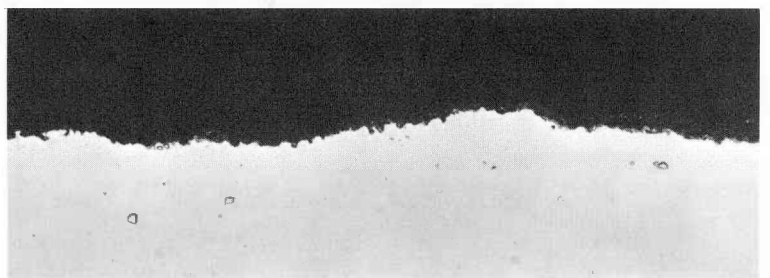

Unetched 200X

Figure D.13 Fireside Corrosion Effects on Type 347 Stainless Steel [Figure shows descaled specimen after 250 hours of exposure at 1240°F (670°C). The scale (lower right) formed below the trisulfate ash deposit was thin but adherent. SEM view (lower left) shows residual ash (1), and the scale surface (2). Note that the grain boundary attack was not in evidence in either the optical or the SEM examination.]

Descaled 1.5X

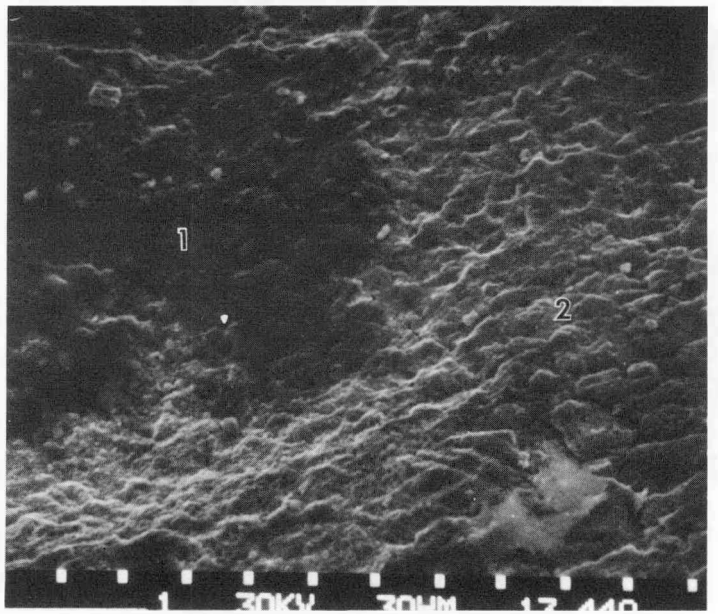

300X

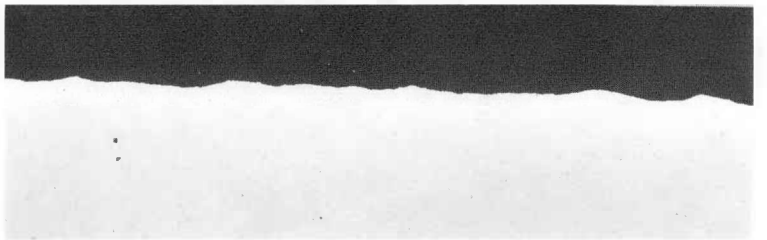

Exposed Surface 20X

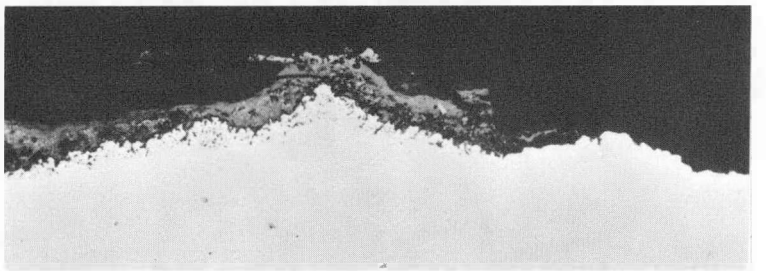

Unetched 200X

Figure D.14 Fireside Corrosion Effects on Types 310 Stainless Steel [Figure shows descaled specimen (upper left), and nondescaled specimen after 250 hours exposure at 1240°F (670°C). The unetched microsection (lower right) shows that general corrosion attack was accompanied by a subsurface attack. The slag deposits or residual ash is indicated by (1) in the SEM view, and the oxide scale indicated as (2). Some grain boundary attack was visible.]

Descaled 1.5X

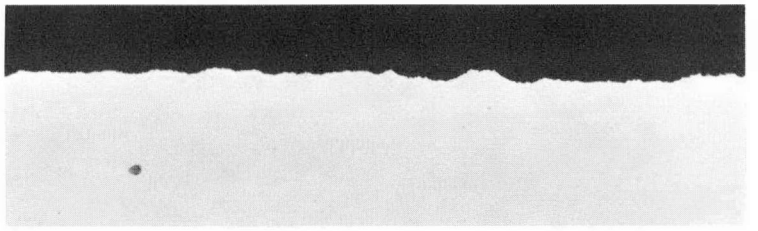

Exposed Surface 20X

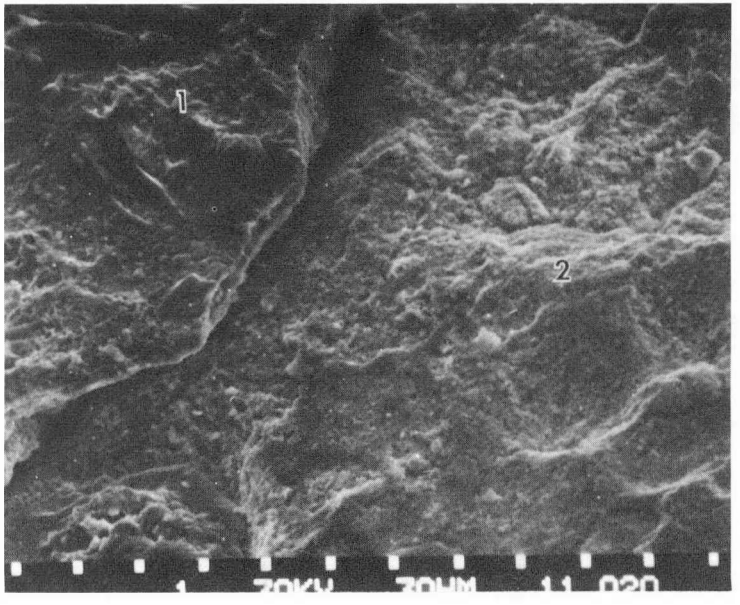

300X

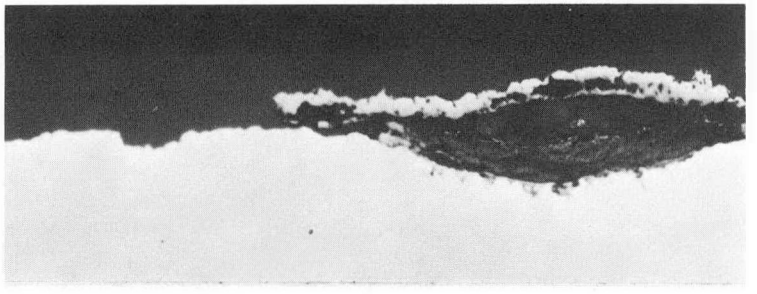

200X

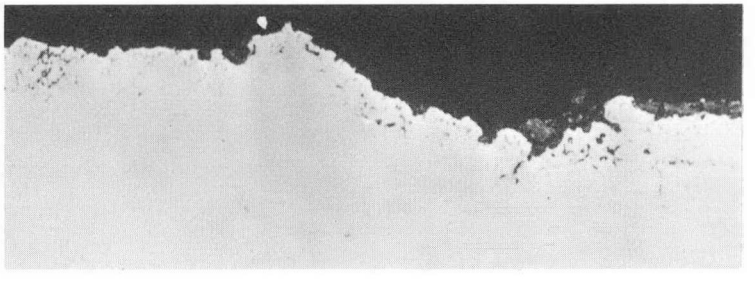

Unetched 500X

Figure D.15 Fireside Corrosion Effects on Type 314 Stainless Steel [Figure shows descaled specimen (upper left), and nondescaled specimen after 250 hours exposure at 1240°F (670°C). The unetched microsection (lower right) shows that general corrosion attack was accompanied by a subsurface attack, suggesting that the surface scale was not protective. Grain boundary attack was less pronounced than for Type 310.]

Descaled 1.5X

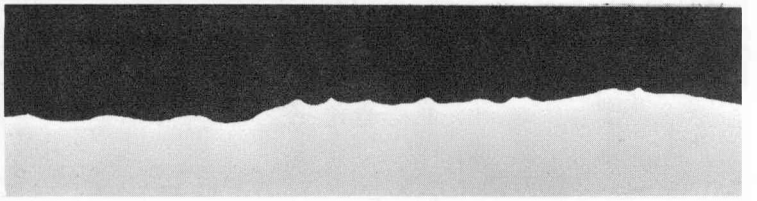

Surface Exposed to Simulated Ash 20X

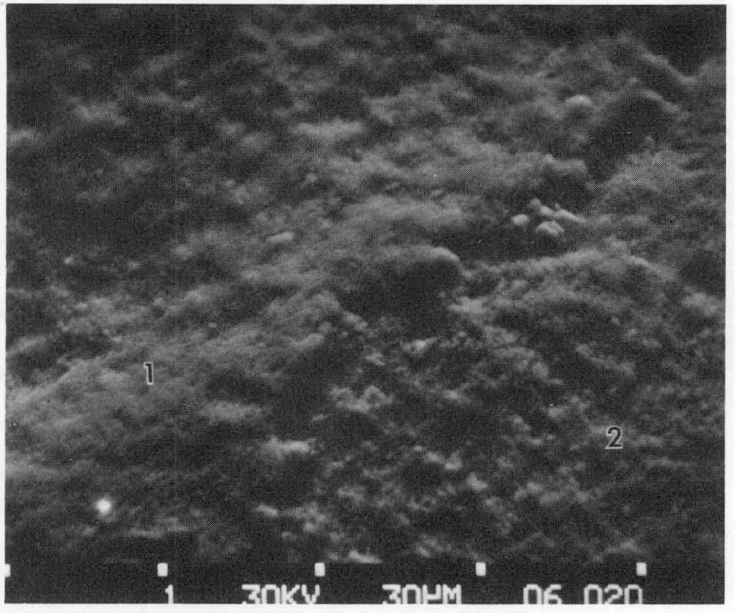

800X

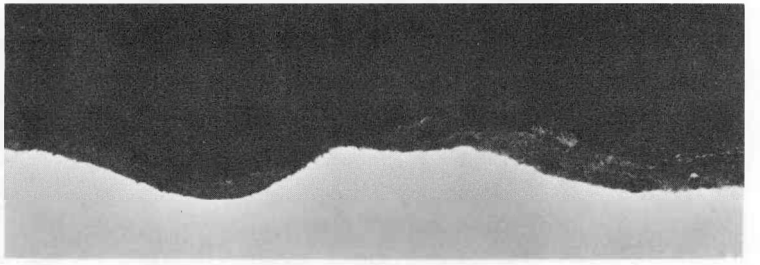

Unetched 200X

Figure D.16 Fireside Corrosion Effects on Incoloy 840 Surfaces [Figure shows descaled specimen (upper left), and nondescaled specimen after 250 hours exposure at 1240°F (670°C). The unetched microsection (lower right) at 200X shows that general corrosion attack was the predominant mode of attack. Grain boundary attack was not found, nor subsurface attack, as seen on Type 310.]

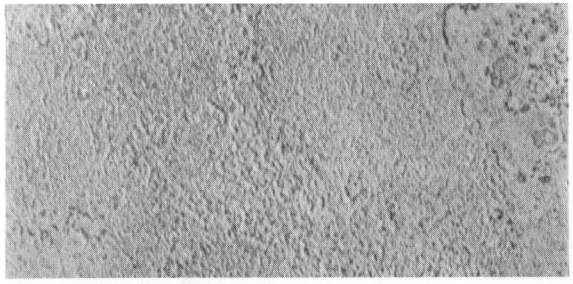

Descaled 1.5X

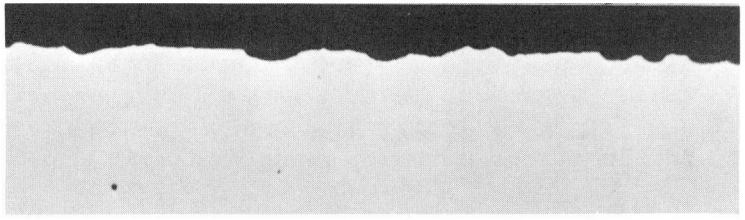

Exposed Surface 20X

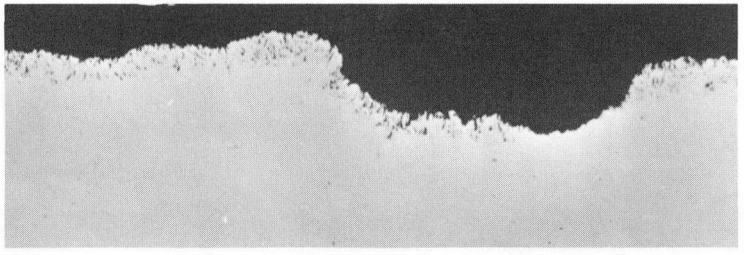

Unetched 200X

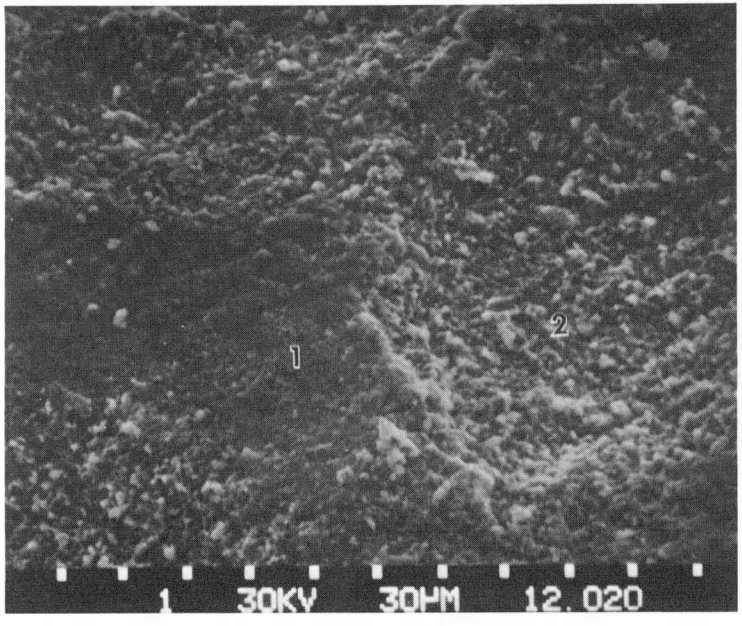

SEM 300X

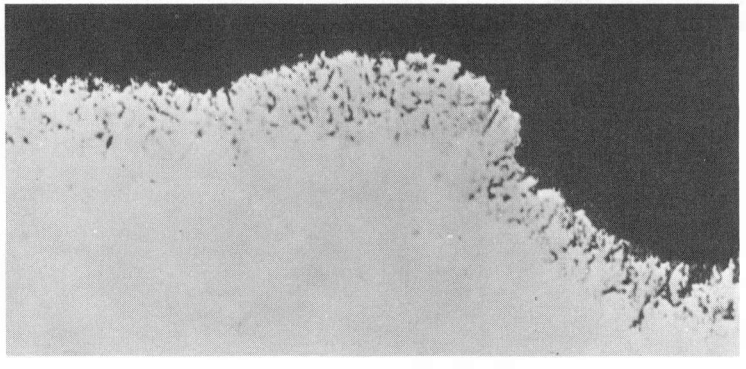

500X

Figure D.17 Fireside Corrosion Effects on Nitronic 40 (21-6-9) [Figure shows descaled specimen (upper left), and nondescaled specimen after 250 hours exposure at 1240°F (670°C). The unetched microsection at 200X shows that general corrosion attack was accompanied by a subsurface attack, and some grain boundary attack.]

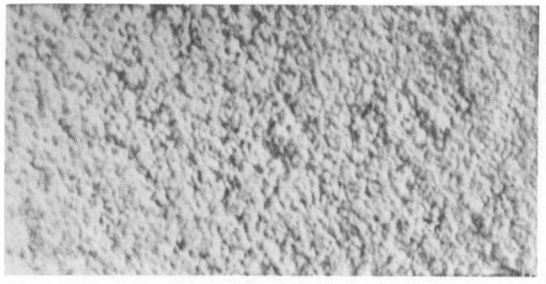

Descaled 1.5X

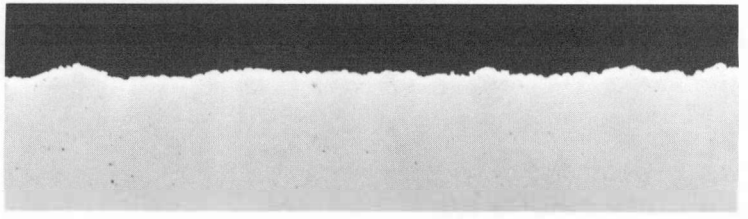

Surface Exposed to Simulated Ash 20X

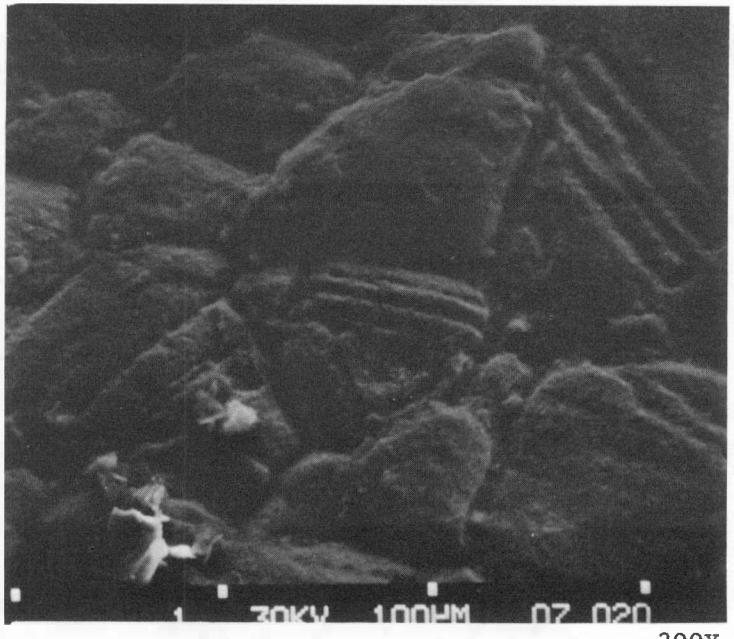

300X

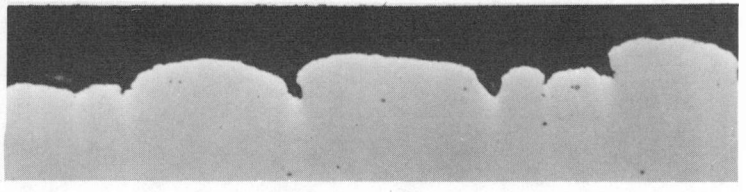

Unetched 200X

Figure D.18 Fireside Corrosion Effects on Incoloy 800H [Figure shows descaled specimen (upper left), and nondescaled specimen after 250 hours exposure at 1240°F (670°C). The unetched microsection (central right) at 200X shows the general corrosion attack and grain boundary attack. The SEM view shows that the scale replicated both the grain boundaries and twin boundaries.]

Descaled 1.5X

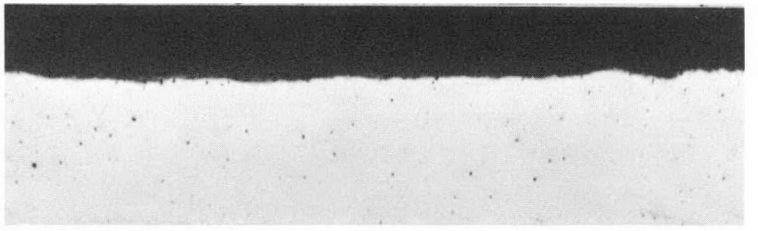

Exposed Surface 20X

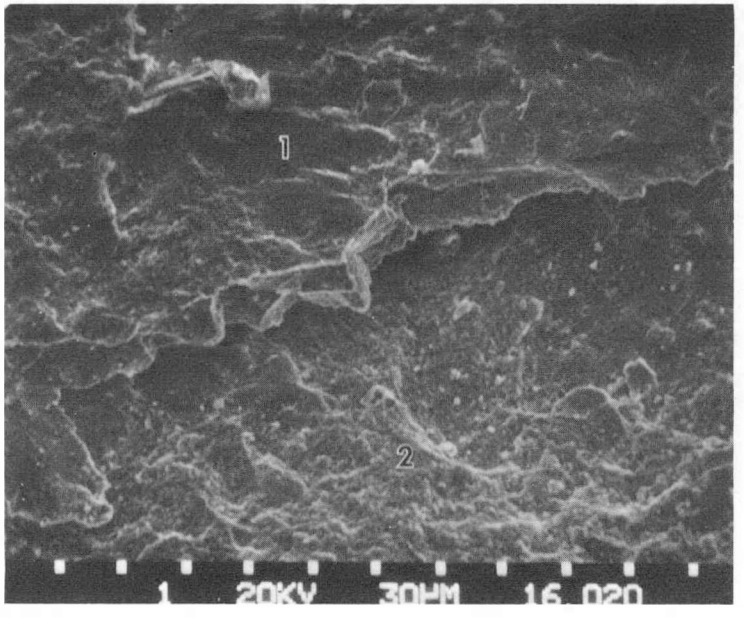

SEM

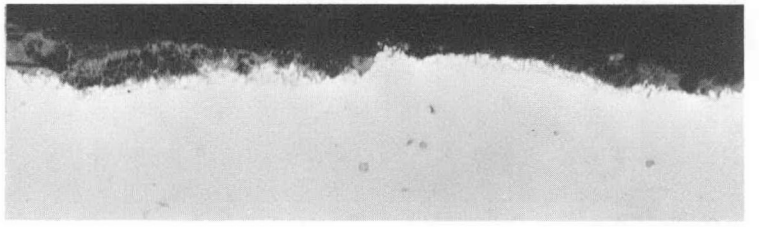

Unetched 200X

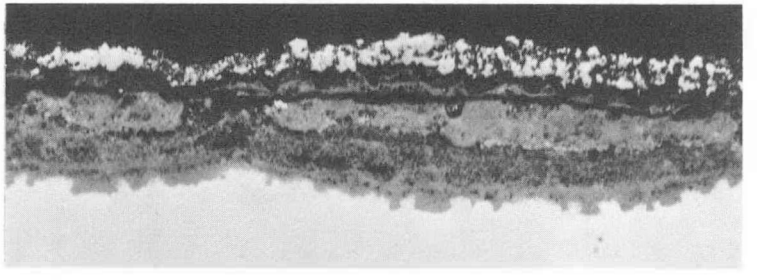

200X

Figure D.19 Fireside Corrosion Effects on A-286 [Figure shows descaled specimen (upper left), and nondescaled specimen after 250 hours exposure at 1240°F (670°C). The scale (lower right) was more complex but adherent. Note also (right, center) that general corrosion attack was accompanied by a subsurface penetration that was not the same as Type 304 for example. The SEM view shows the surface of the outer scale (1), and inner scale (2).]

Descaled 1.5X

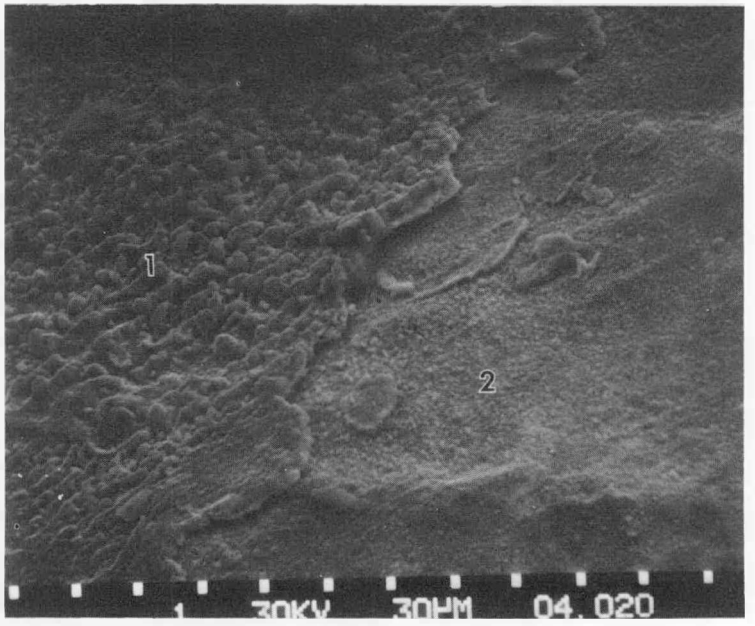

SEM 300X

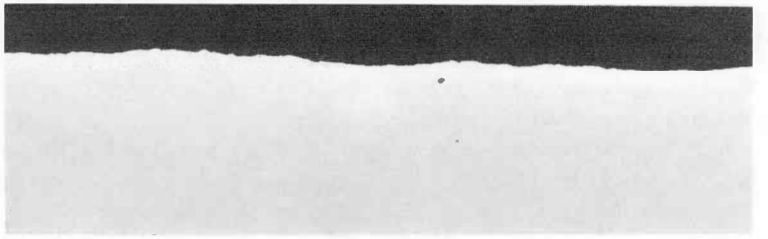

20X

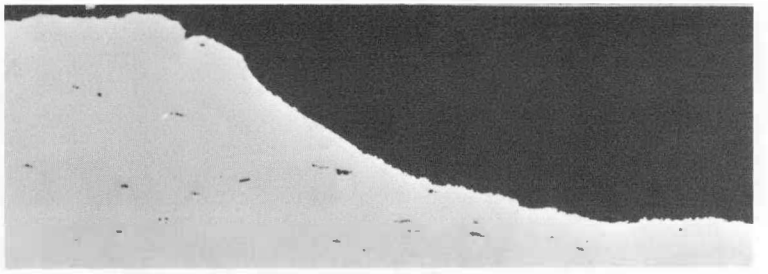

As-Exposed Surface 200X

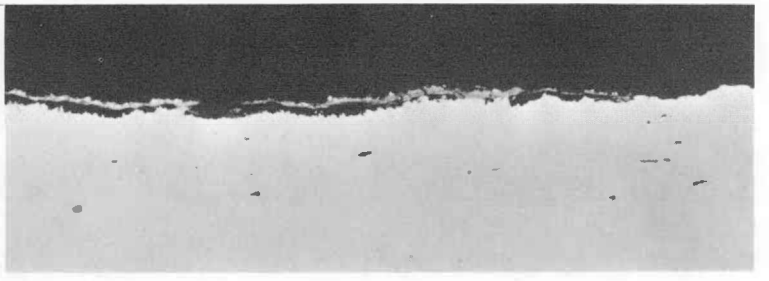

Unetched 200X

Figure D.20 Fireside Corrosion Effects on Al-6X [Figure shows descaled specimen (upper left), and nondescaled specimen after 250 hours at 1240°F (670°C). The scale (lower right) was very fragile and thin, but internal changes in the microstructure were not observed. The general corrosion rates were very high, possibly resulting from the high Mo content.]

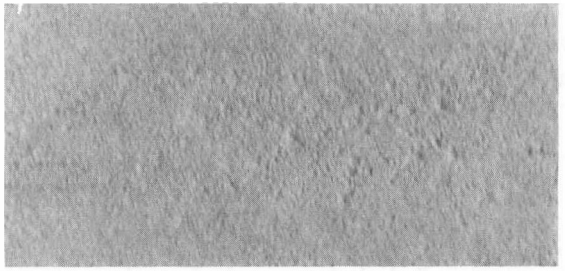

Descaled 1.5X

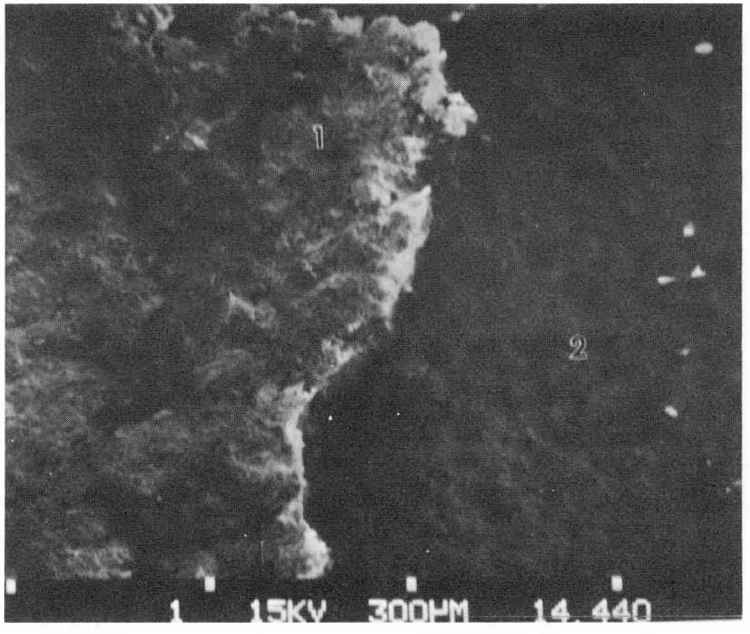

SEM 100X

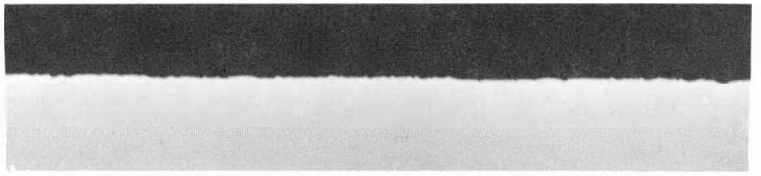

Unetched 20X

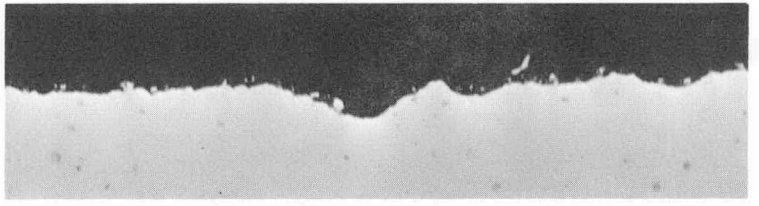

Exposed Surface 200X

Figure D.21 Fireside Corrosion Effects on Inconel 625 [Figure shows descaled specimen (upper left) and nondescaled specimen after 250 hours exposure at 1240°F (670°C). The scale (lower right) produced by the fused deposits was thin and adherent. The surface recession was low despite the high Mo content. The SEM view of the surface shows the residual ash (1), and the somewhat protective scale (2).]

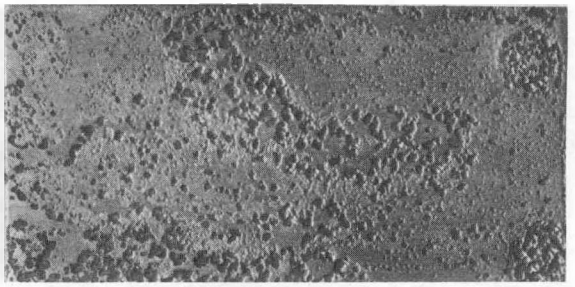

Descaled 1.5X

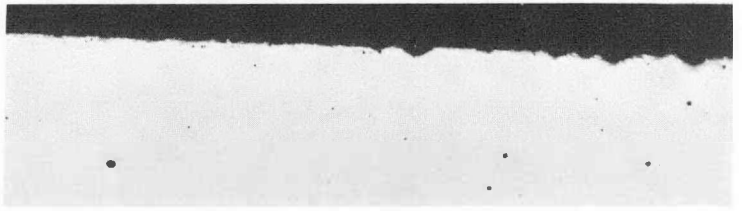

As-Exposed Surface 20X

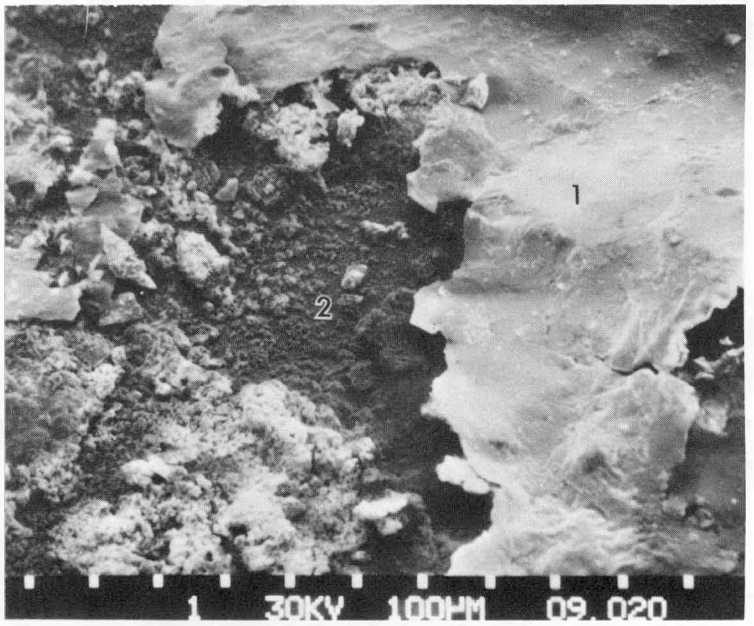

100X

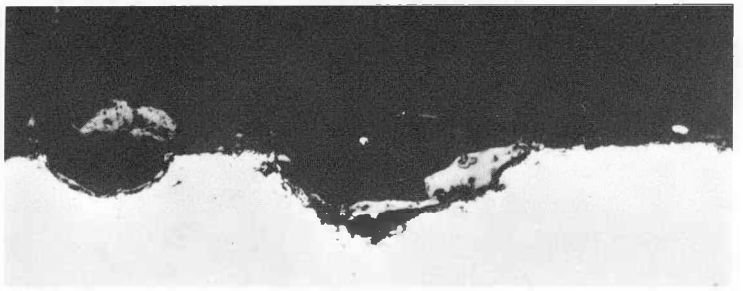

200X

Figure D.22 Fireside Corrosion Effects on Inconel 671 [Figure shows descaled specimen (upper left) and nondescaled specimen after 250 hours exposure at 1240°F (670°C). The unetched microsection (lower right) at 200X shows that attack by pitting predominated. The SEM view shows the surface of residual fused ash (1) and scales (2).]

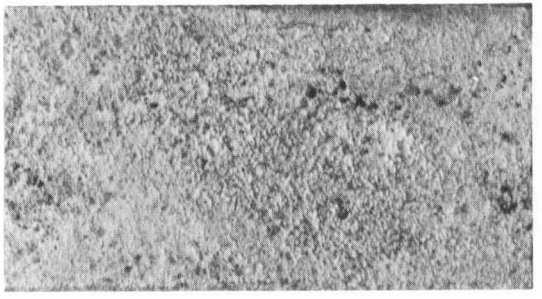

Descaled 1.5X

Surface Exposed to Simulated Ash 20X

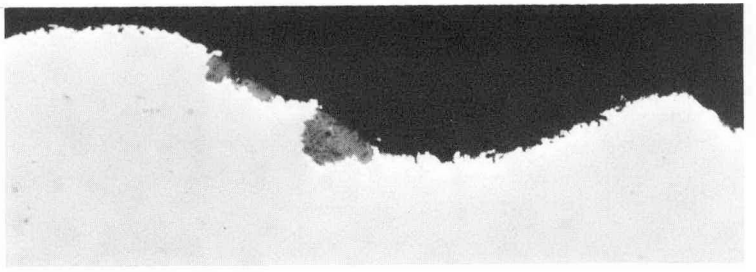

Unetched 200X

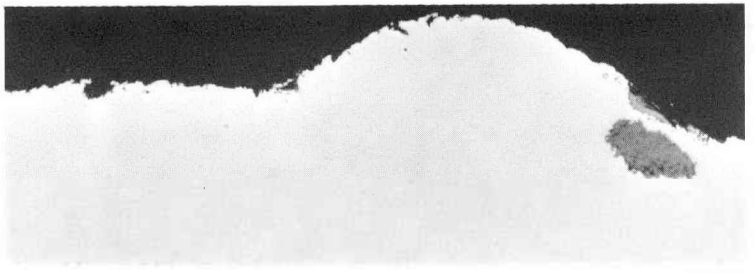

200X

Figure D.23 Fireside Corrosion Effects on In-737 [Figure shows descaled specimen (left), and non-descaled specimen after 250 hours exposure to simulated coal ash at 1240°F (670°C). Some areas of subsurface attack were observed, as well as small pits.]

Descaled 1.5X

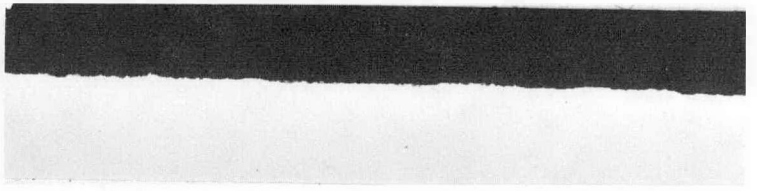

Unetched 20X

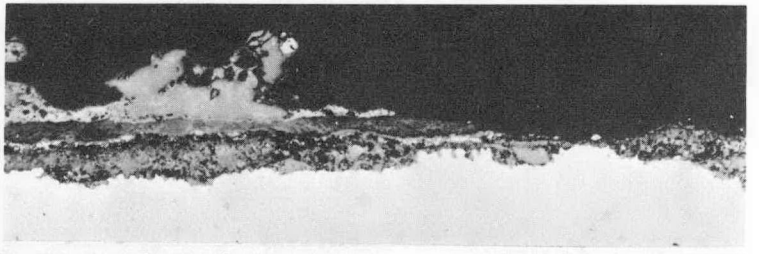

As-Exposed Surface 200X

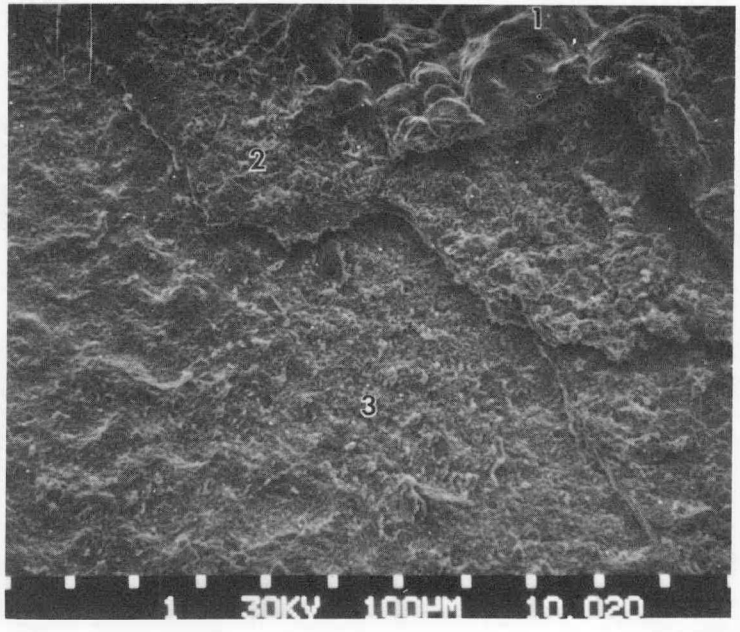

100X

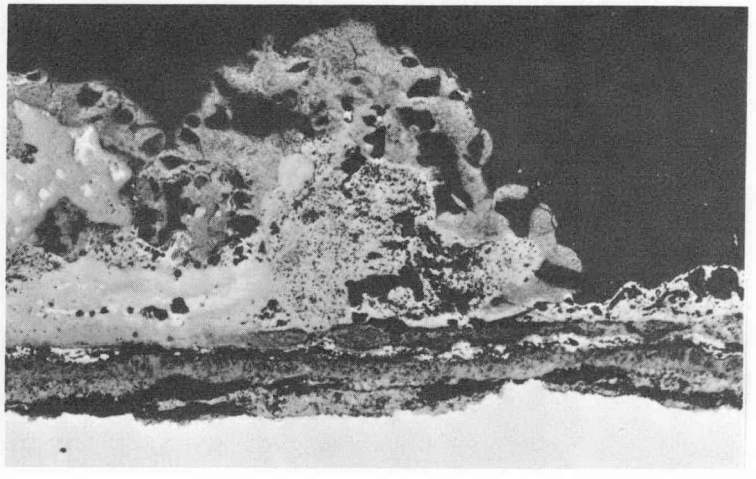

200X

Figure D.24 Fireside Corrosion Effects on IN-549 [Figure shows descaled specimen (upper left), and nondescaled specimen after 250 hours exposure at 1240°F (670°C). The scale (lower right) produced by the simulated ash attack was layered and mixed with slag as nodules at various locations. The SEM view shows several layers, the outer deposit (1), partially removed showing the more adherent scale below.]

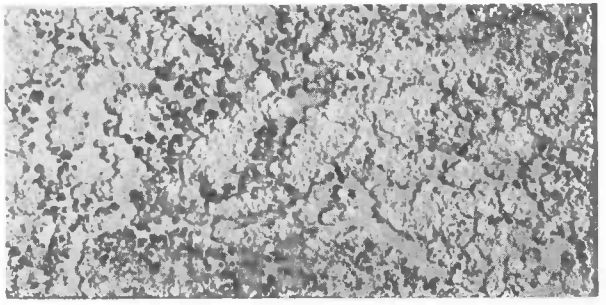

Descaled 1.5X

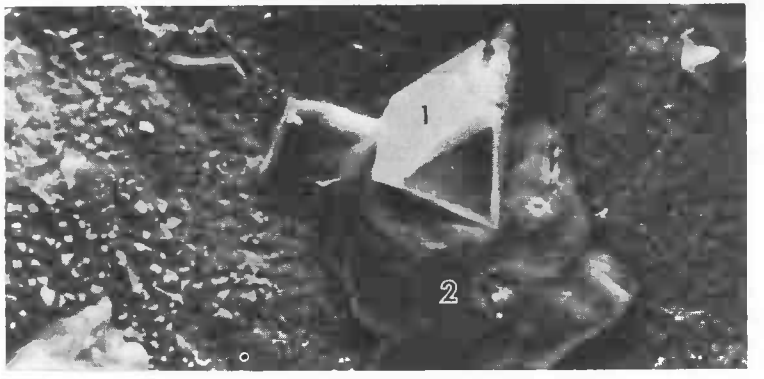

SEM Tilted 320X

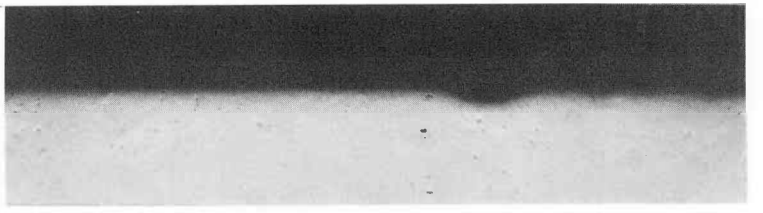

20X

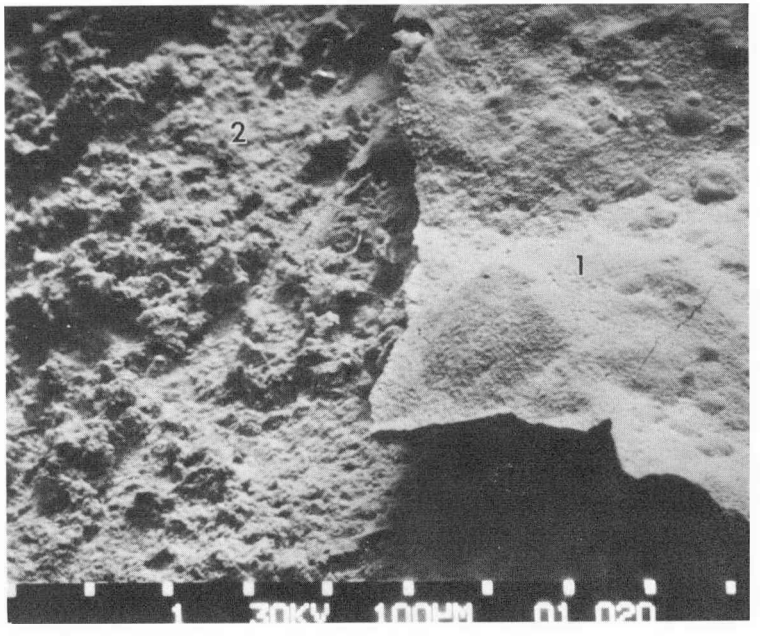

SEM

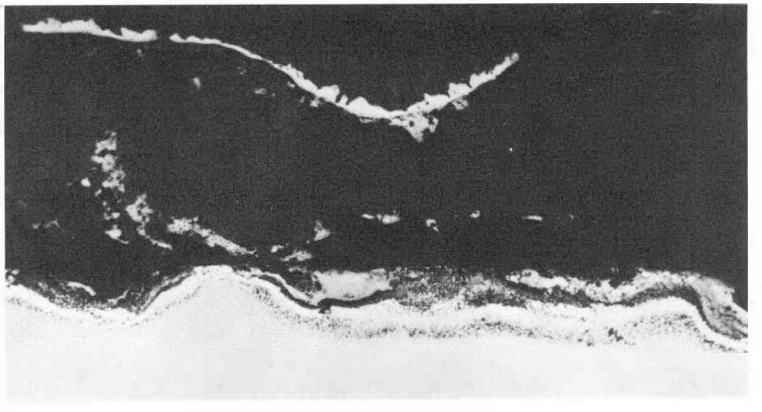

Unetched 200X

Figure D.25 Fireside Corrosion Effects on IN-809 [Figure shows descaled specimen and nondescaled specimen after 250 hours exposure at 1240°F (670°C). The scale (lower right) produced by the fused deposits was thin and adherent. The surface attack was accompanied by a thin layer of subsurface changes. The upper right SEM scan shows crystalline salts (1) and "slag" (2) on the scale surface. The lower left view shows the scale (2) below the residual ash or slag (1).]

Descaled 1.5X

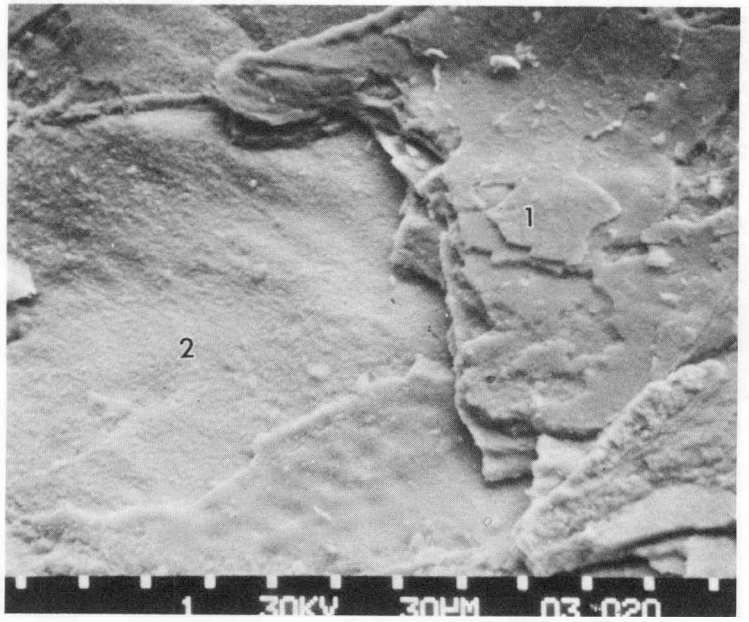

320X

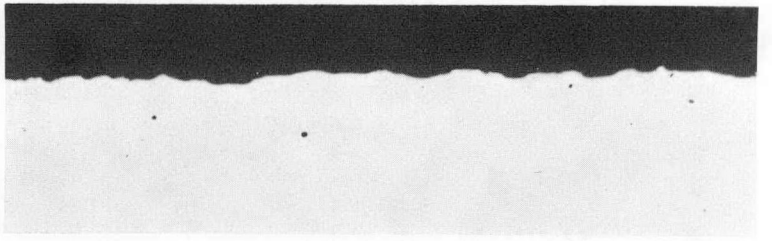

Surface Exposed to Simulated Ash 20X

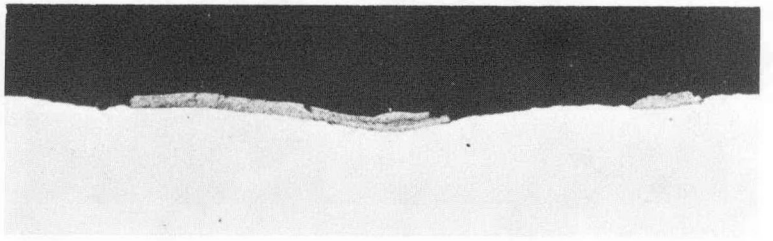

Unetched 200X

Figure D.26 Fireside Corrosion Effects on IN-811 [Figure shows descaled specimen (upper left) and nondescaled specimen after 250 hours exposure at 1240°F (670°C). The unetched microsection (lower right) at 200X shows that only the general surface attack was detected. The SEM view shows the surface of residual fused ash (1) and scale (2).]

Descaled 1.5X

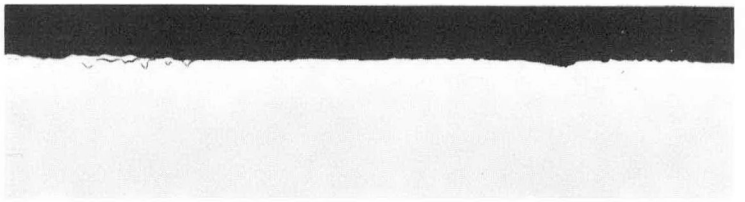

Surface Exposed to Simulated Ash 20X

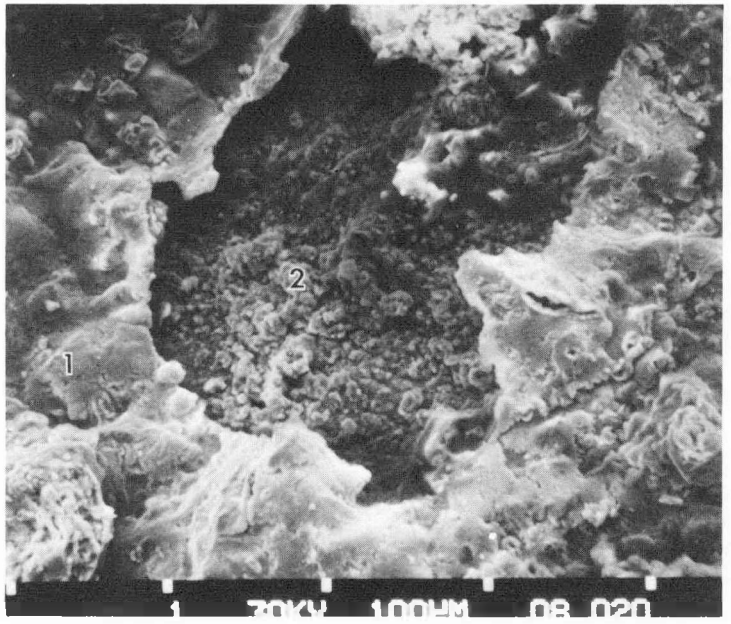

238X

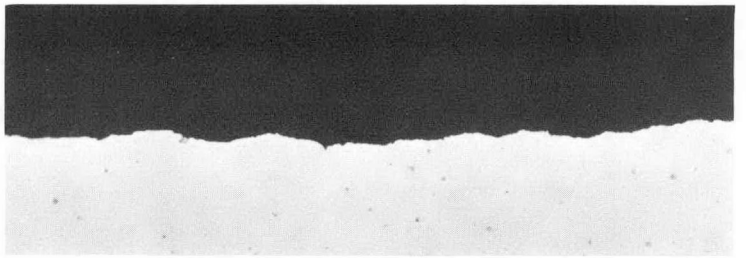

Unetched 200X

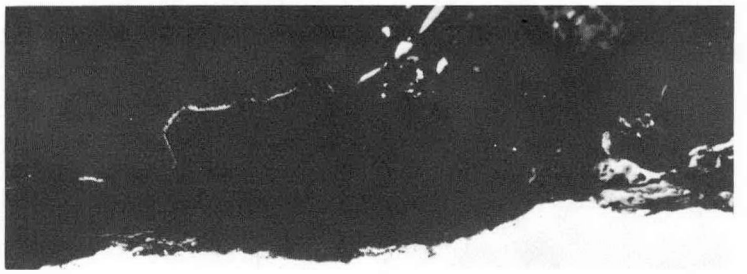

200X

Figure D.27 Fireside Corrosion Effects on IN-814 [Figure shows descaled specimen (upper left) and nondescaled specimen after 250 hours exposure at 1240°F (670°C). The scales (lower right) resulting from the simulated coal ash attack is the gray phase. The loose deposits (black) are also shown (1) in the SEM view.]

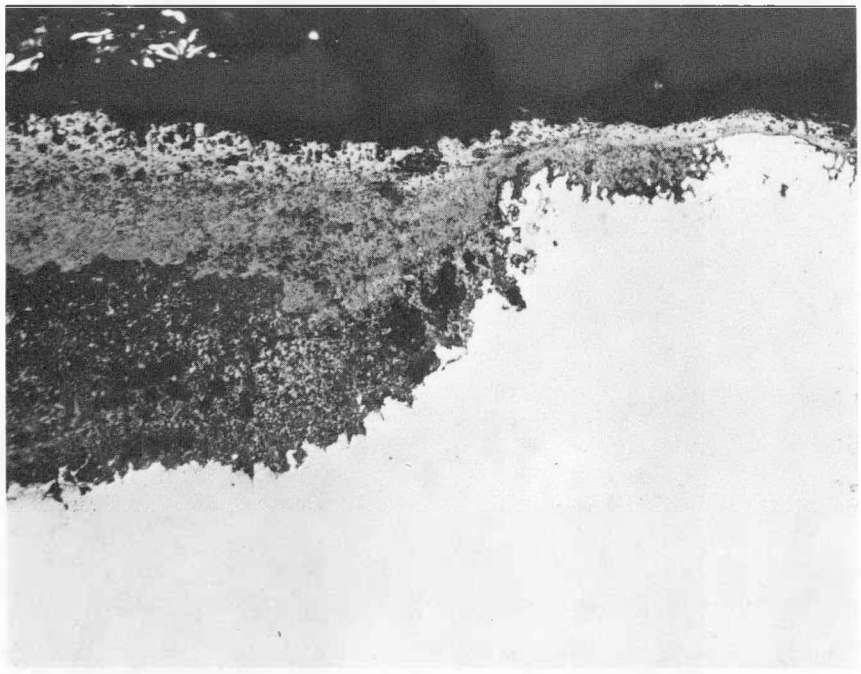

PN 61811 200X

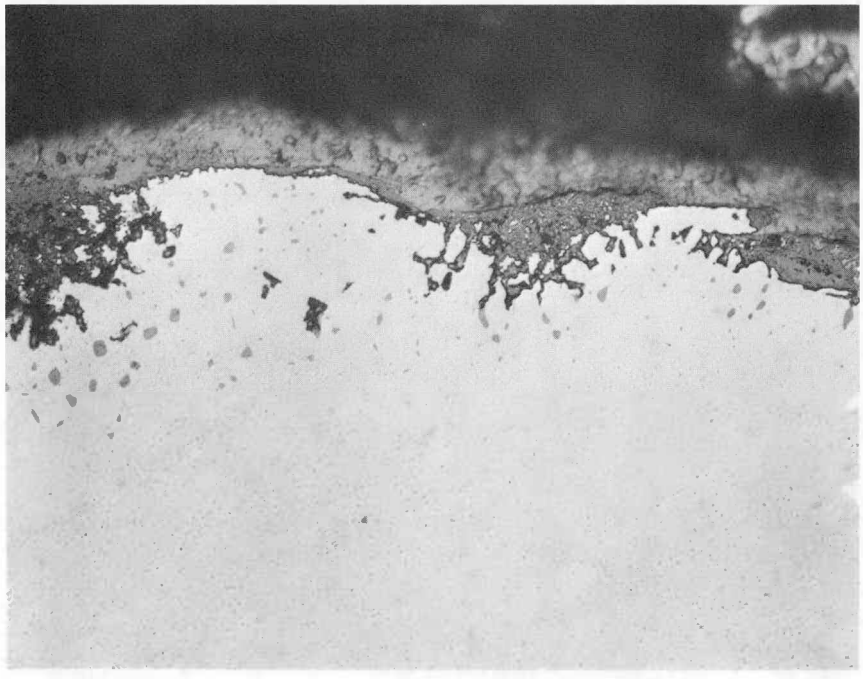

PN 61812 500X

Figure D.28 Fireside Corrosion Effects on HT-9--Unetched [Light micrographs show specimen from Retort 6, 1440°F (780°C) exposed for 250 hours.]

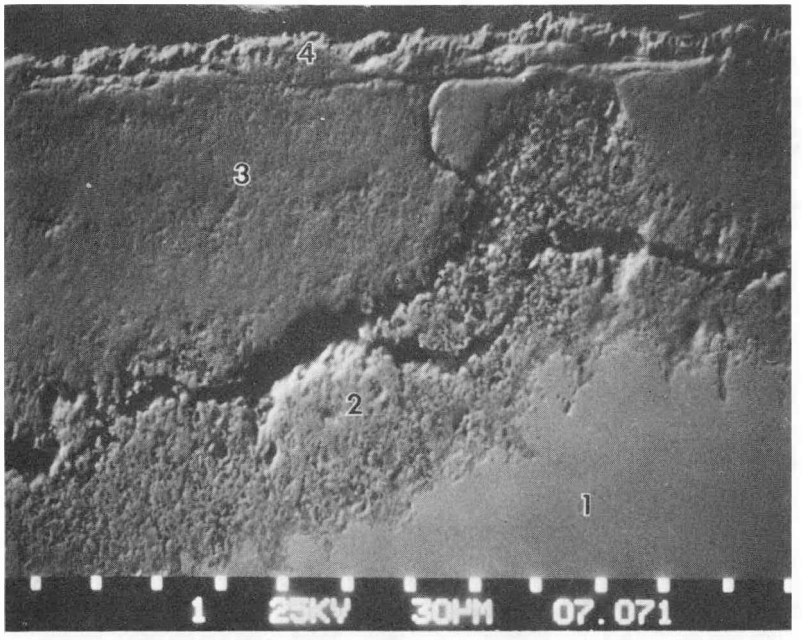

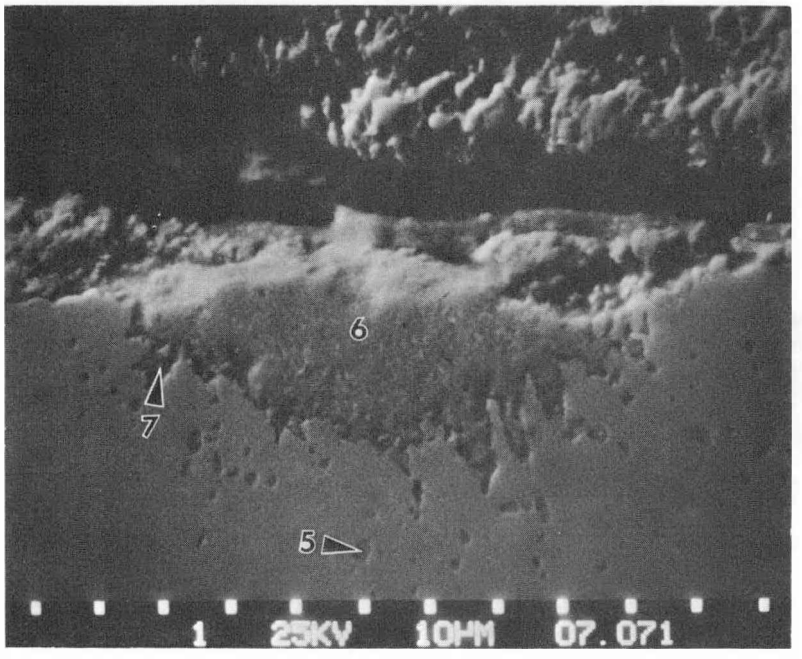

HT-9
(Fe-12%Cr-1%Mo-0.5%W)

1. Alloy
2. $Fe_{(1 - x)}S$
3. $(Cr,Fe)_2O_3$
4. Fe_3O_4
5. Mn,Cr,Fe sulfides
6. Cr sulfide
7. Fe,Cr,V,S

Figure D.29 Fireside Attack on HT-9--Not Descaled [Scanning electron micrographs of HT-9 show specimen from Retort 6 exposed at 1440°F (780°C) for 250 hours. Phases in the scale were identified from EDX information. The upper view is of a pit which was different at 1440°F (780°C) than at 1250°F (675°C) exposure.]

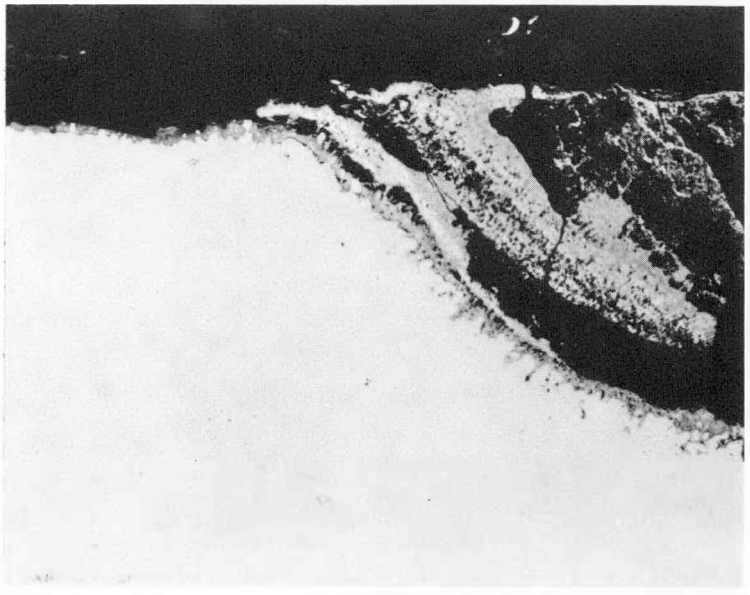

1440°F

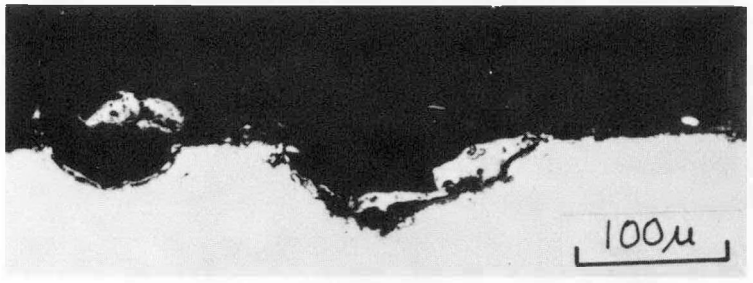

1240°F

Figure D.30 Fireside Attack on Type 347 Stainless Steel--200X Unetched [Light micrographs show Type 347 Stainless Steel (not descaled) specimen exposed at 1440°F (780°C) and at 1250°F (675°C) for 250 hours.

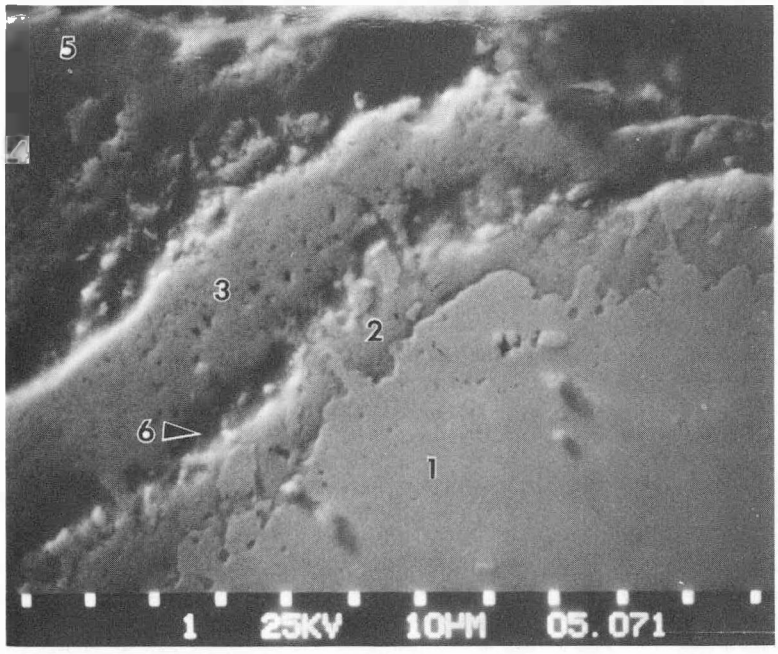

1440°F

1. Alloy

2,6. Cr,Fe sulfide

3. Fe sulfide

4. Cr sulfide

5. $(Cr,Fe)_2O_3$

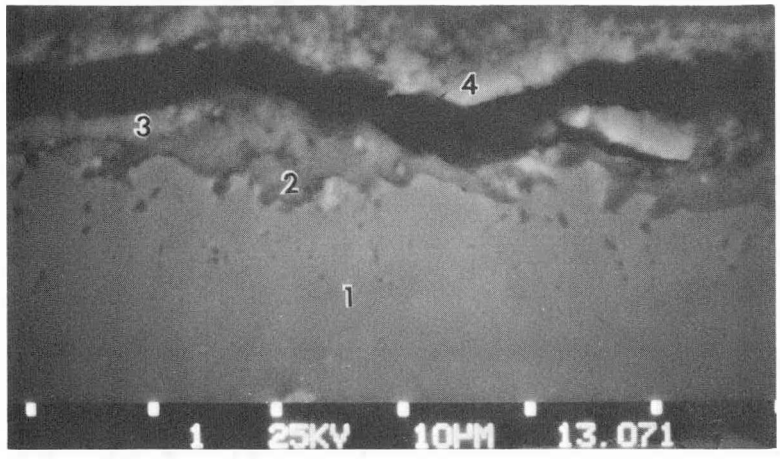

1250°F

1. Alloy

2,3,4. Fe,Cr sulfide

Figure D.31 Fireside Attack on Type 347 Stainless Steel [Scanning electron micrographs show Type 347 stainless steel specimens from Retorts 4 and 6 exposed at 1250 and 1440°F (675 and 780°C) for 250 hours. Phase identification was made from EDX information.]

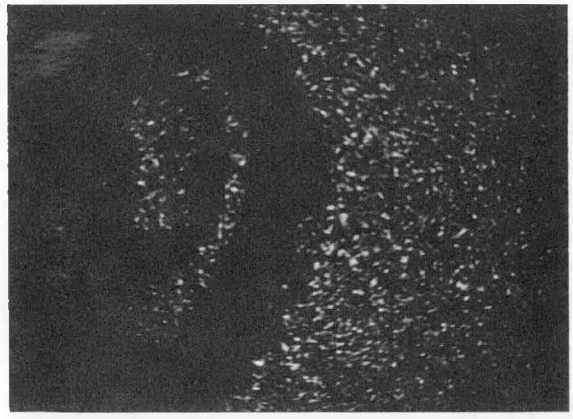

347-11 500X

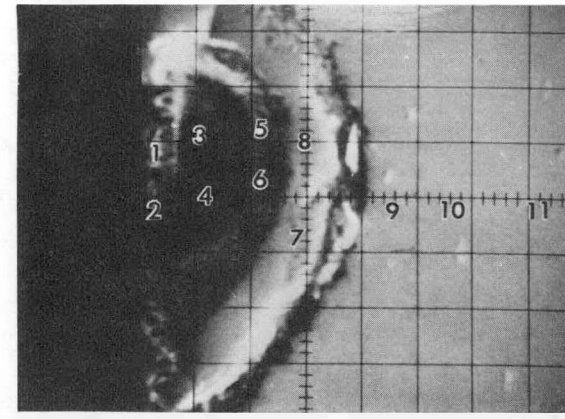

347-12 500X

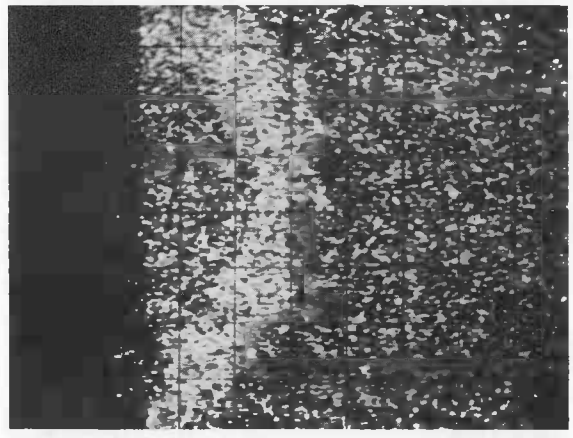

347-13 Cr 500X

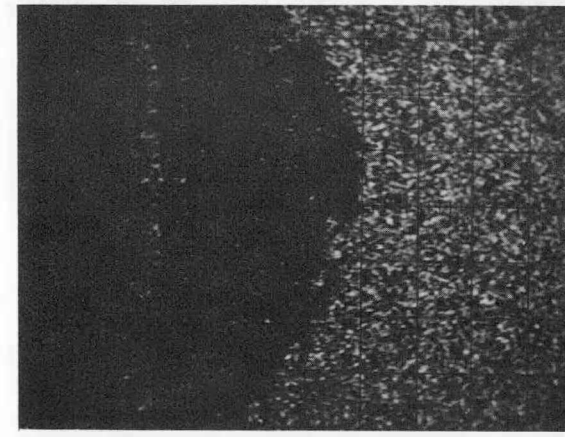

347-14 Fe 500X

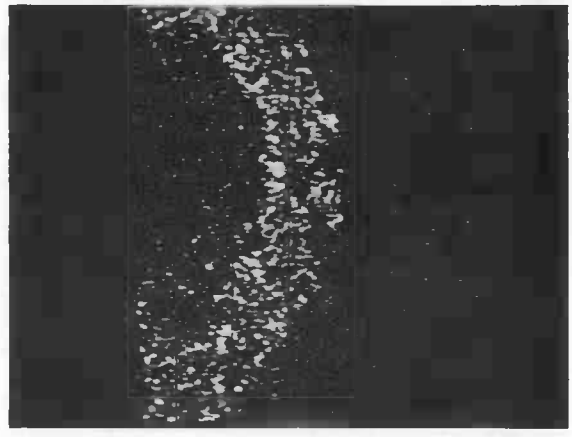

347-15 S 500X

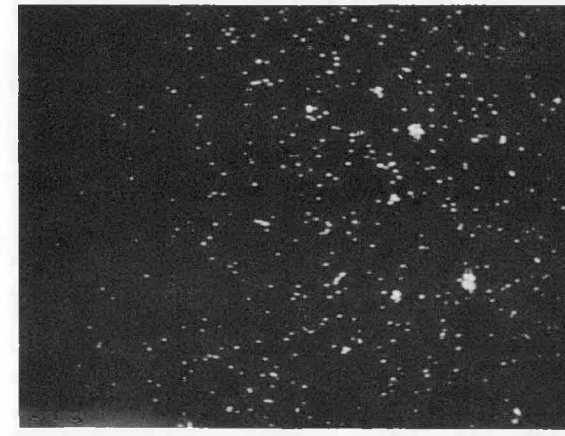

347-16 Nb 500X

Figure D.32 Fireside Deposit and Scale Analysis; Profiles on Stainless Steel--500X [Electron probe, SEM, and x-ray mapping show corrision in a pit on Type 347 stainless steel from Retort 4 exposed at 1250°F (675°C) for 250 hours.]

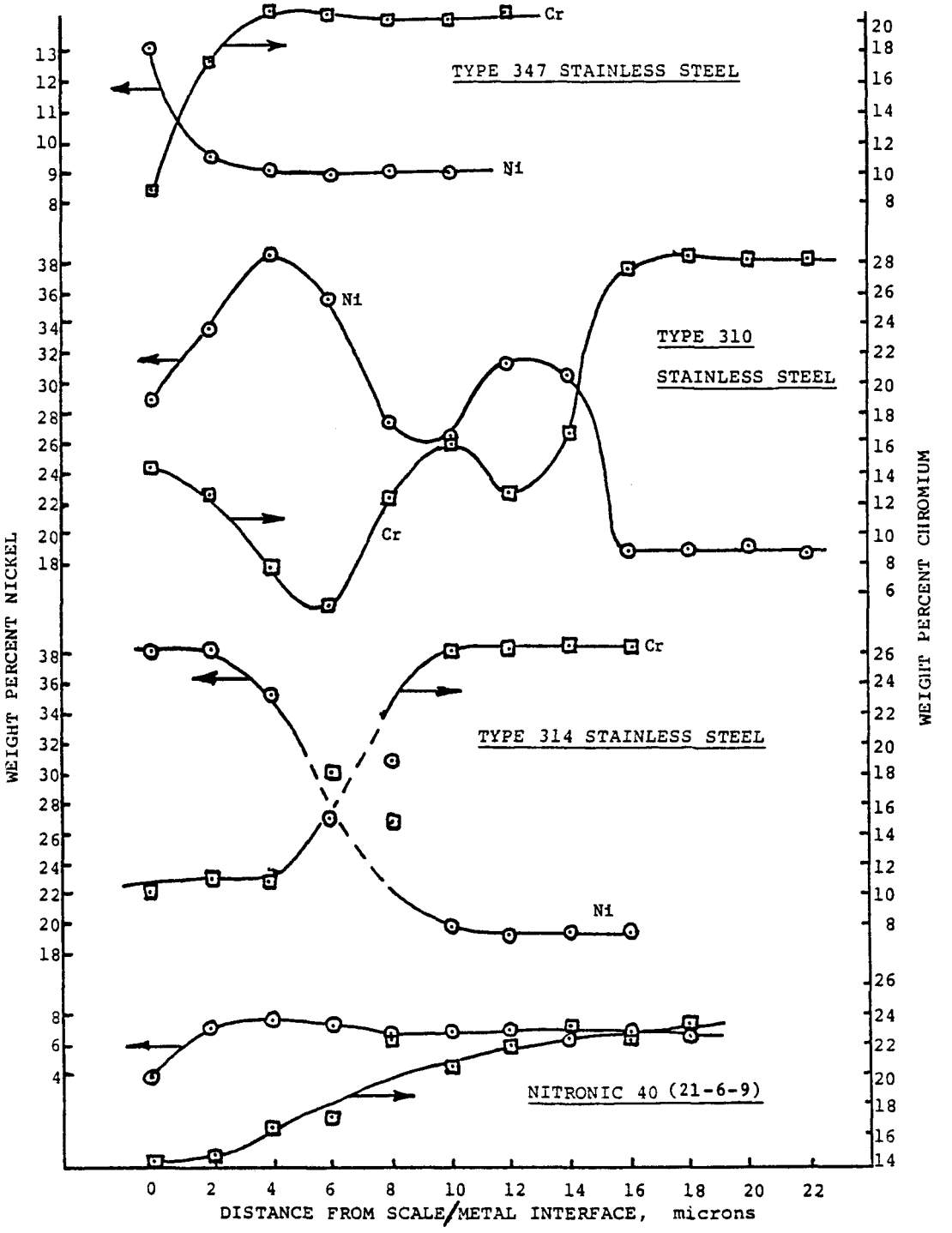

Figure D.33 Diffusion of Alloy Constituents Exposed at 1120°F (675°C) for 250 Hours (Figure shows concentration profiles for Ni and Cr Below the scale/metal interface for stainless steels exposed in Retort 4.)

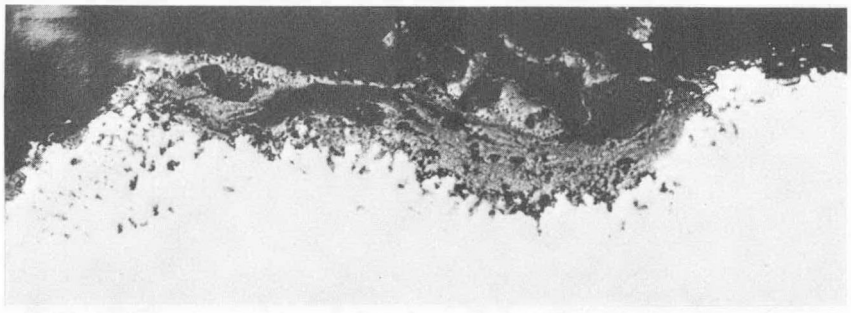

PN 63616 500 X

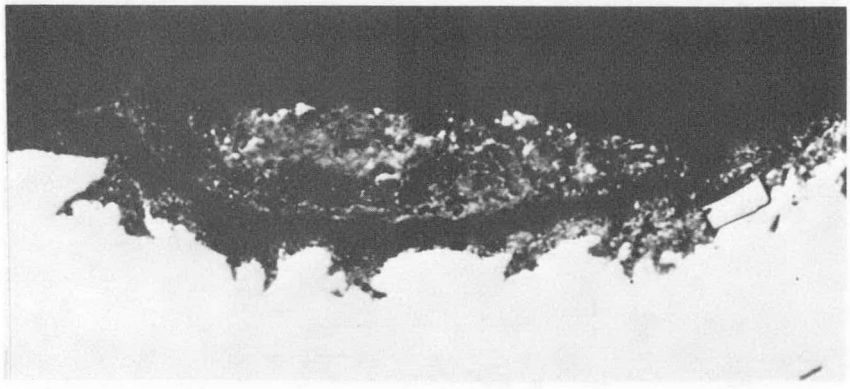

PN 63622 1000 X

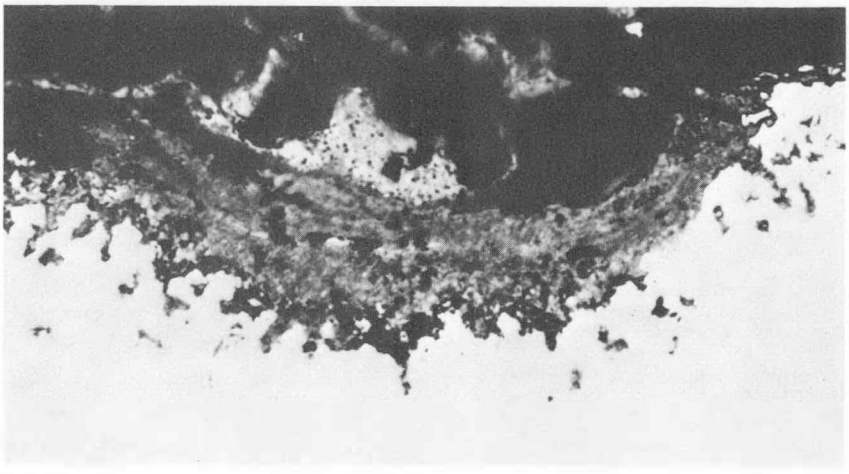

PN 63623 1000 X

Figure D.34 Fireside Corrosion of Type 310 Stainless Steel Exposed at 1250°F (675°C) for 250 Hours-Unetched [Light micrographs show Type 310 stainless steel (not descaled) from Retort 4.]

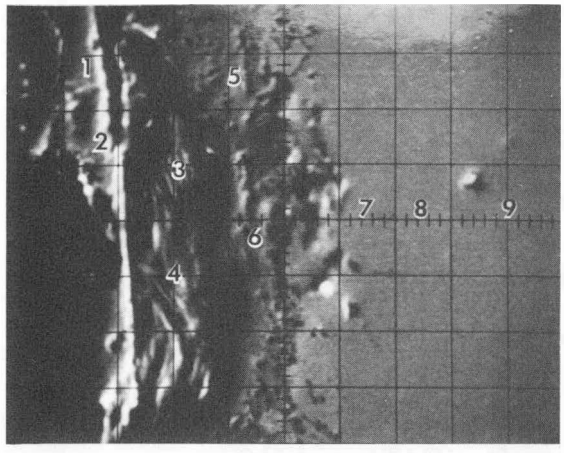

310-11 750x

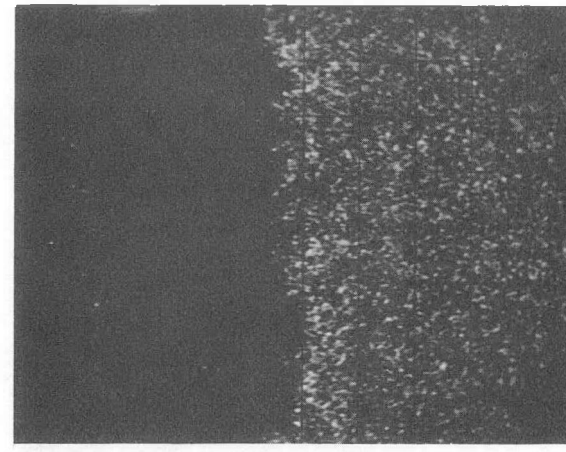

310-12 Ni 750X

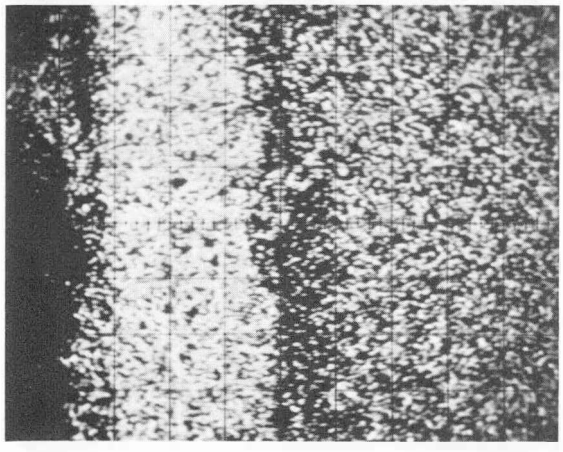

310-13 Cr 750X

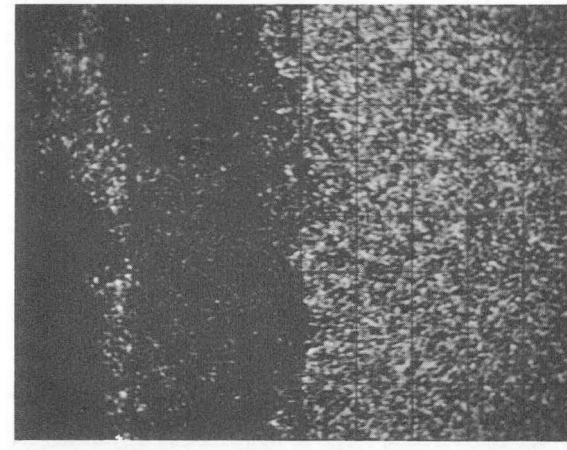

310-14 Fe 750X

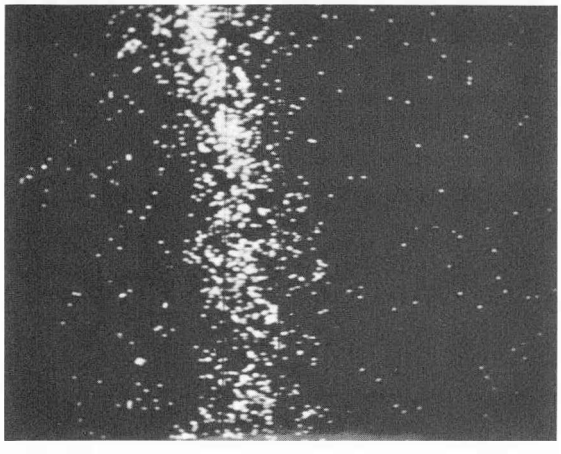

310-15 S 750X

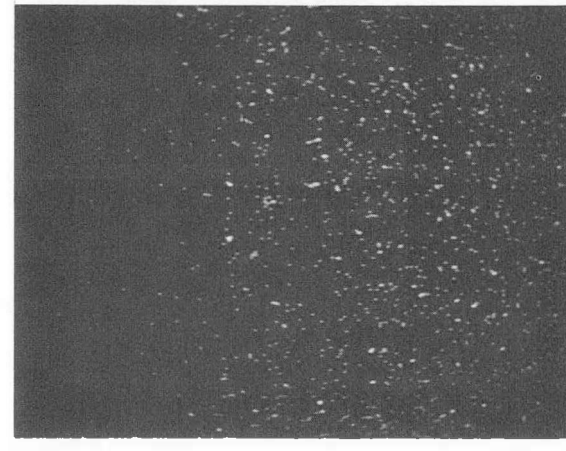

310-16 Mn 750X

Figure D.35 Fireside Deposit and Surface Analysis Profiles on Type 310 Stainless Steel [Electron probe, SEM, and x-ray mapping show corrosion product on this specimen from Retort 4 which was exposed at 1250°F (675°C) for 250 hours.]

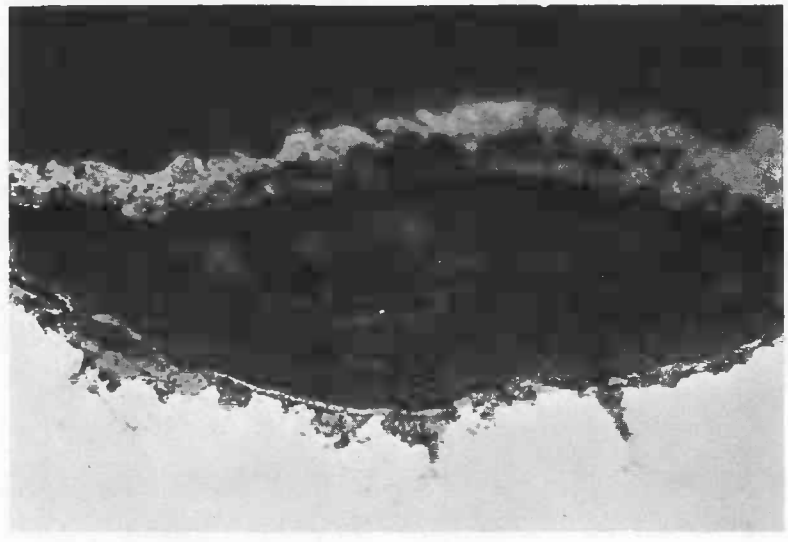

500X

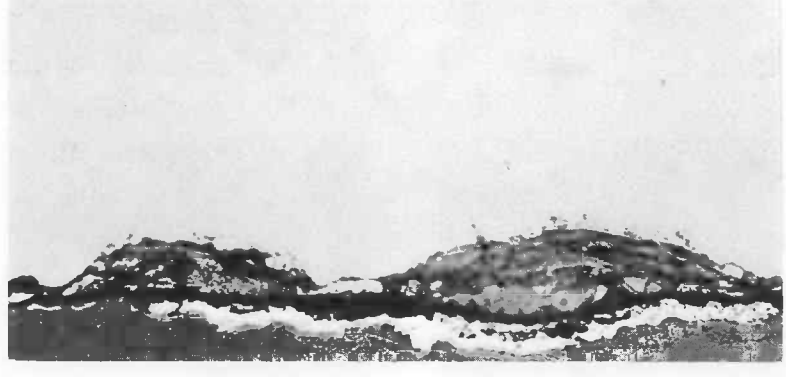

200X

Figure D.36 Fireside Attack of Type 314 Stainless Steel--Unetched [The specimen (not descaled) from Retort 4 was exposed at 1250°F (675°C) for 250 hours.]

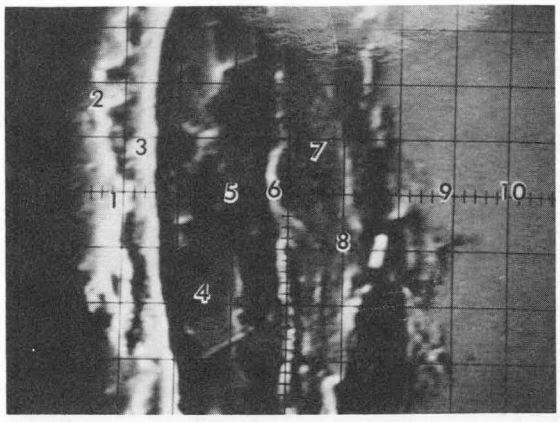

314-11

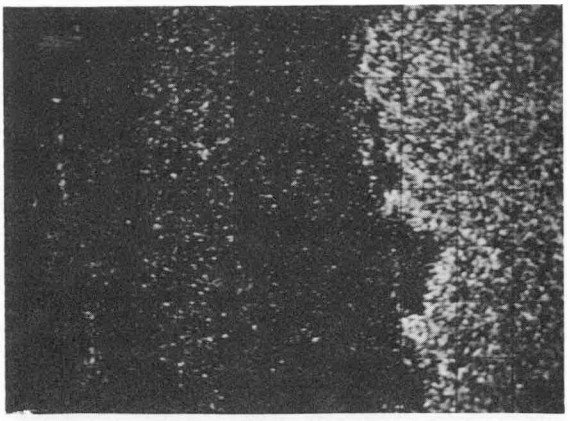

314-12 Ni

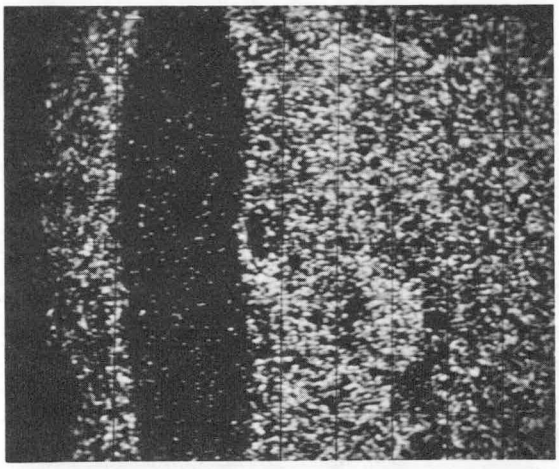

314-13 Cr

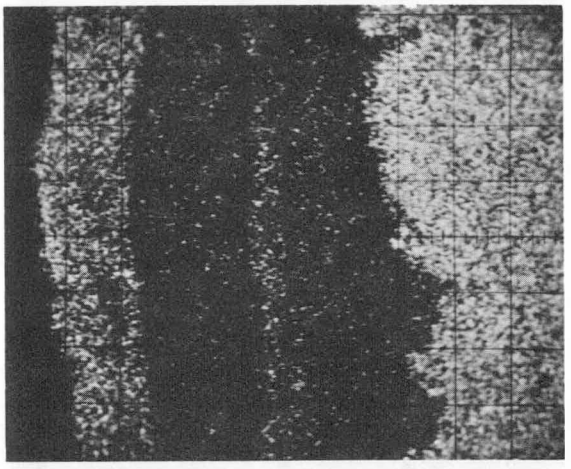

314-14 Fe

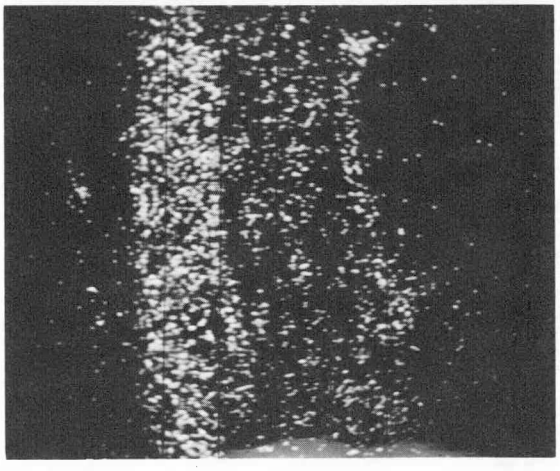

314-15 S

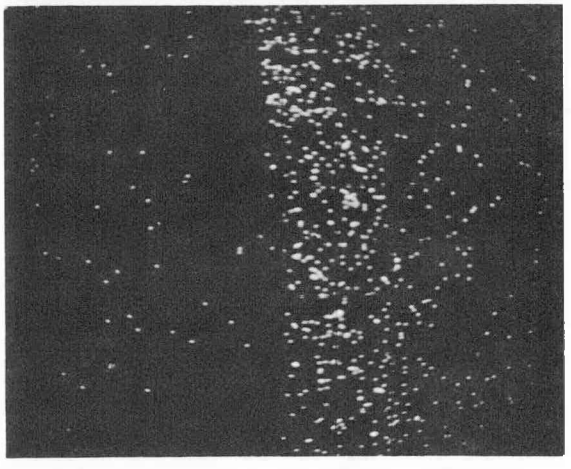

314-16

Figure D.37 Fireside Deposit and Surface Analysis Profiles of Type 314 Stainless Steel--750X [Electron probe, SEM and x-ray mapping show corrosion product on Type 314 stainless steel specimen from Retort 4 exposed at 1250°F (675°C) for 250 hours.]

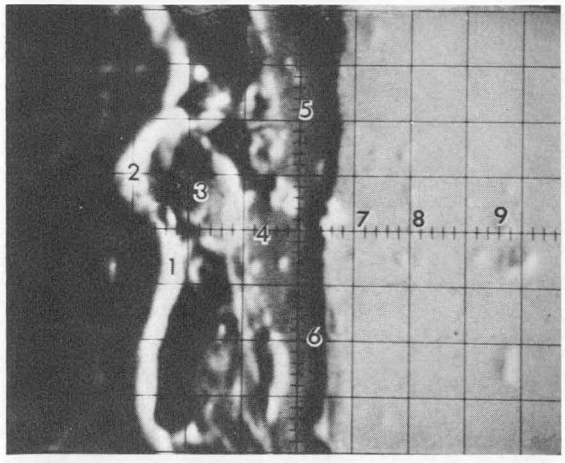

21-6-9-11

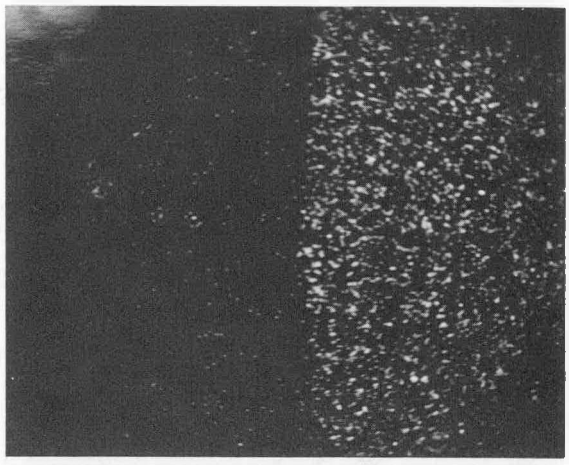

21-6-9-12

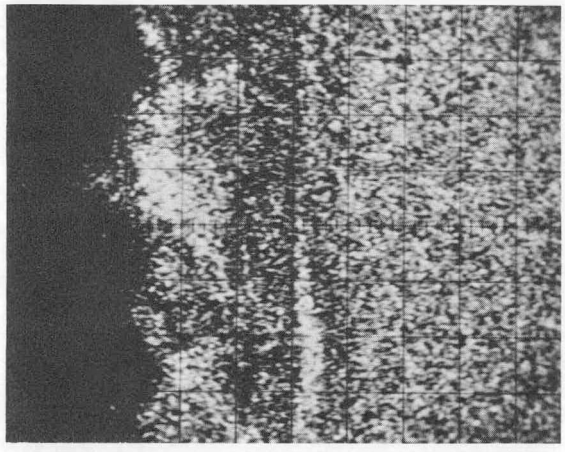

21-6-9-13 Cr

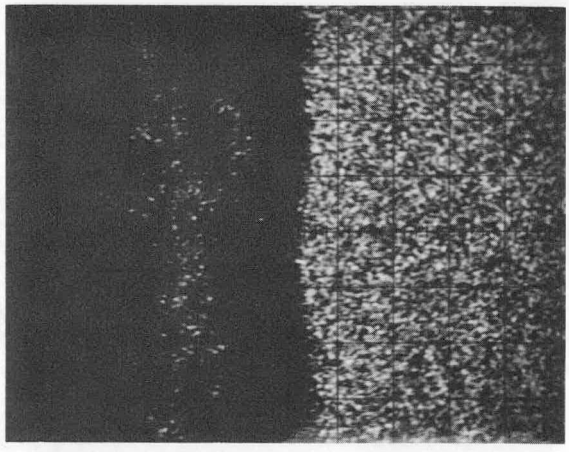

21-6-9-14 S

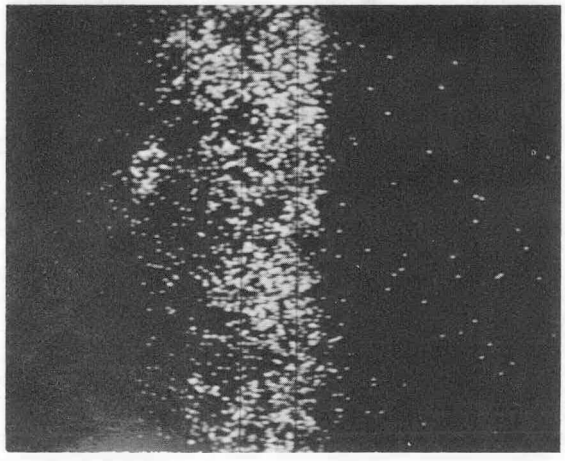

21-6-9-15 S

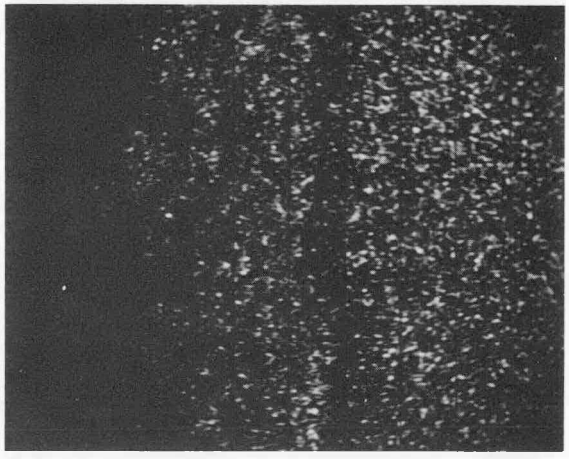

21-6-9-16 Mn

Figure D.38 Fireside Deposit and Surface Analysis Profiles of 21-6-9 (Nitronic 40) [Electron probe, SEM, and x-ray mapping show corrosion product on this specimen which was exposed at 1250°F (675°C) for 250 hours in Retort 4.]

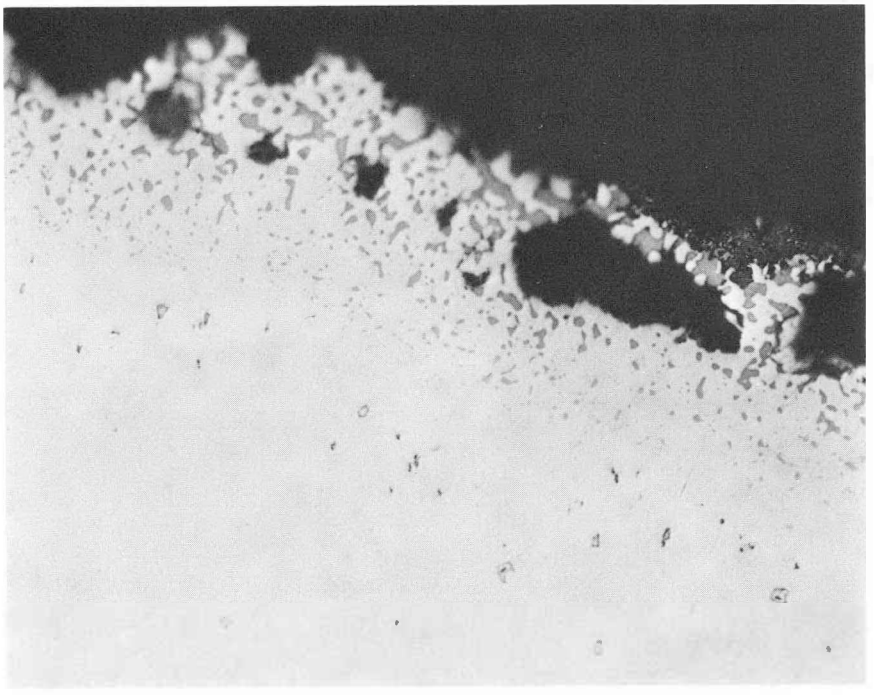

PN 61825

Figure D.39 Fireside Attack on Alloy A-286--500X Unetched [Light micrograph shows A-286 specimen (deposits removed mechanically) from Retort 6 exposed at 1440°F (780°C) for 250 hours.]

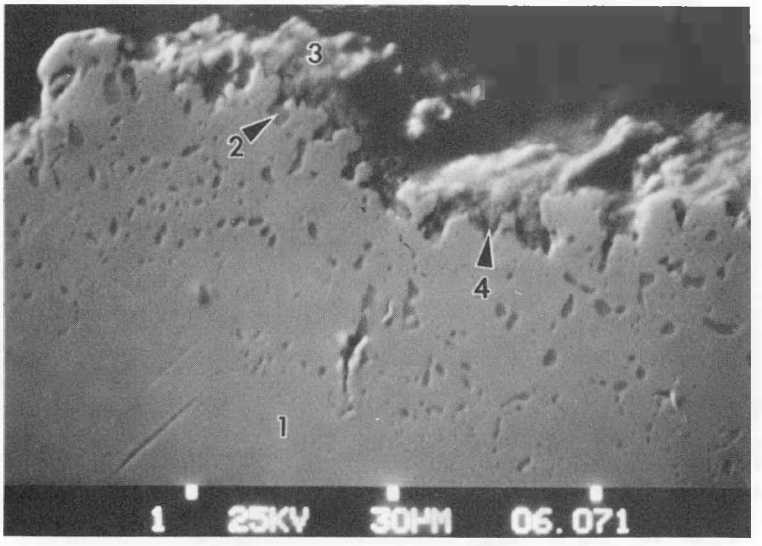

1. Alloy

2. Cr,Fe sulfide

3,4. Cr,Ti sulfide

1440°F

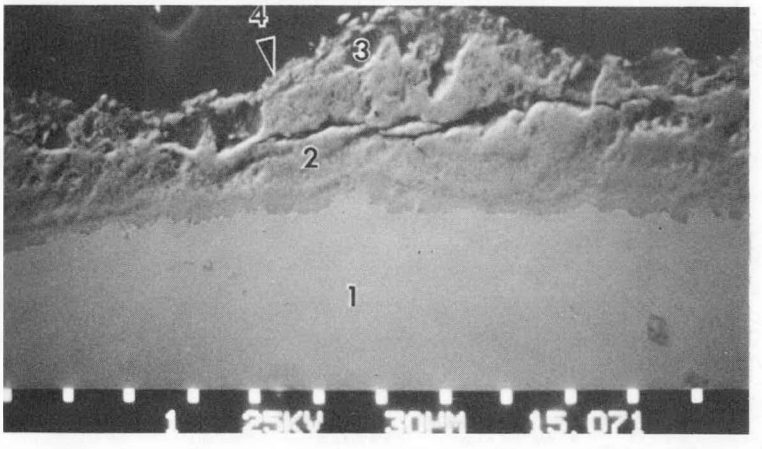

1. Alloy

2,3. Cr,Ti sulfide

4. Cr,Ti,K,S

1250°F

Figure D.40 Fireside Attack and Sulfide Penetration on Alloy A-286 [Scanning electron micrographs of Alloy A-286 show specimens from Retorts 4 and 6 exposed at 1250 and 1440°F (675 and 780°C) for 250 hours. Phase identification was made from EDX information.]

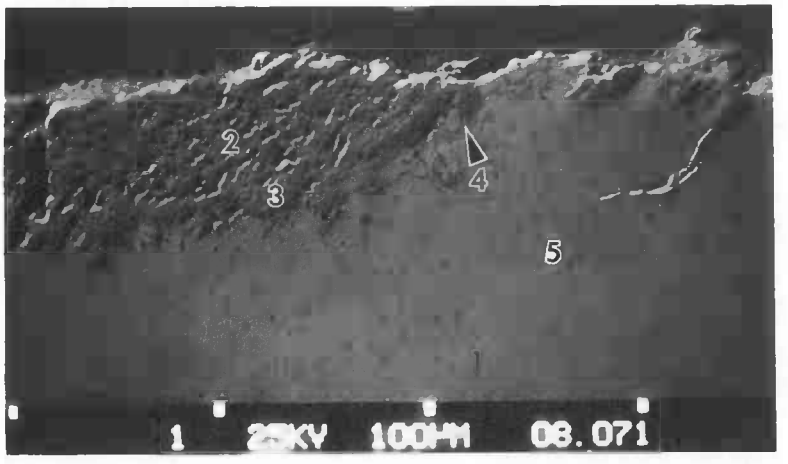

1. Alloy

2,3. Cr_2O_3

4,5. Cr sulfide

1440°F

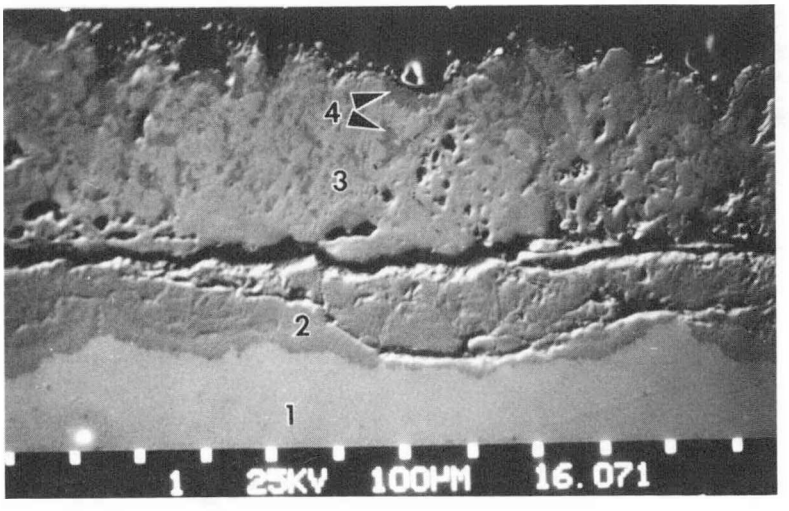

1. Alloy

2. Cr_2O_3

3. Fe,Cr,Ni spinel

4. Ni sulfide

1250°F

Figure D.41 Fireside Attack and Sulfide Penetration on Inconel 601 [Scanning electron micrographs of Inconel 601 show specimens from Retorts 4 and 6 exposed at 1250 and 1440°F (675 and 780°C) for 250 hours. Phase identification was made from EDX information.]

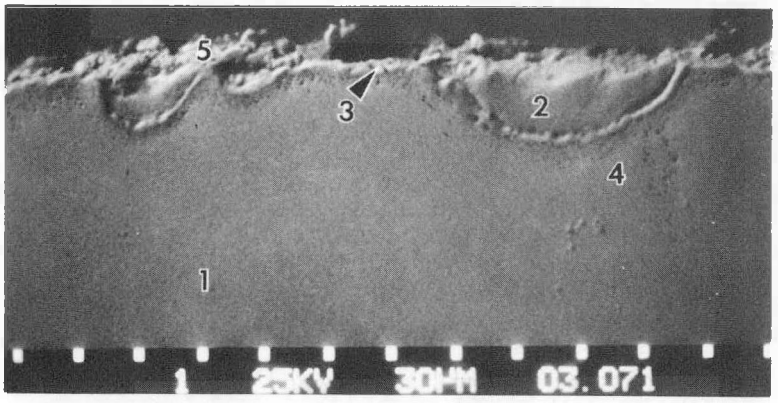

320X

1. Alloy

2,3. Cr_2O_3

4. Cr sulfide

5. Cr_2O_3 + spinel

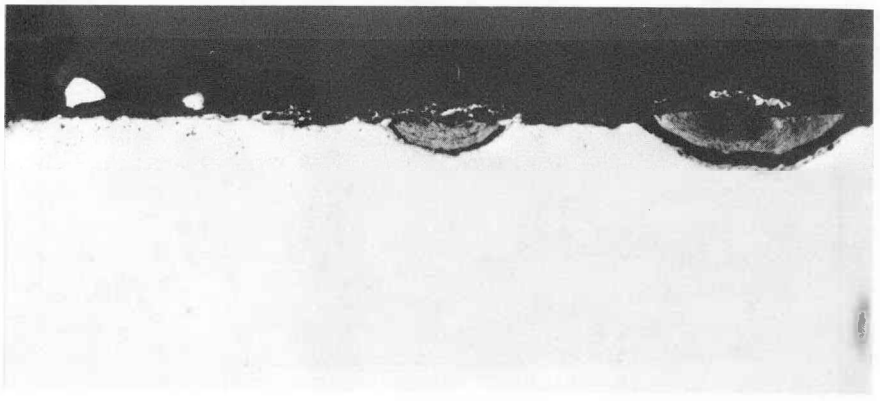

PN 61909

200X

Figure D.42 Fireside Attack on Alloy IN-809 [Light and scanning electron micrographs show IN-809 specimen from Retort 6 exposed at 1440°F (780°C) for 250 hours. Phase identification was made from EDX information.]

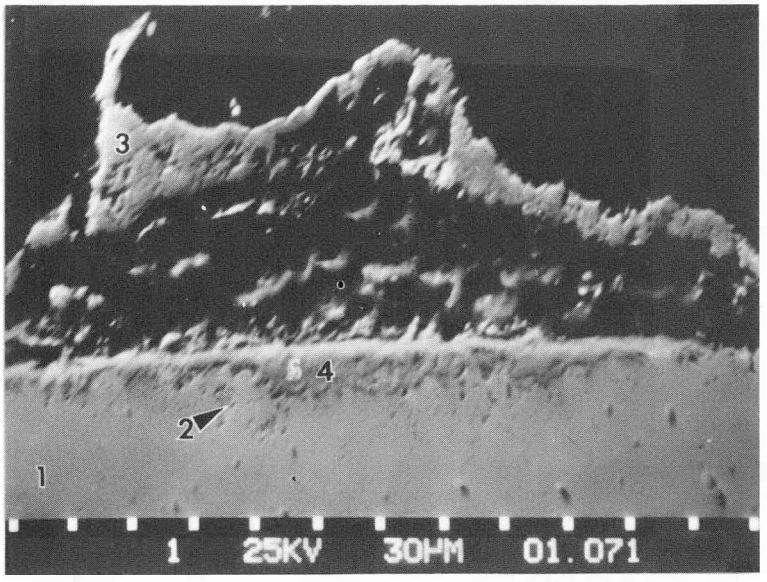

1. Alloy
2. Cr sulfide
3. Cr_2O_3 + spinel
4. Cr_2O_3

1440°F

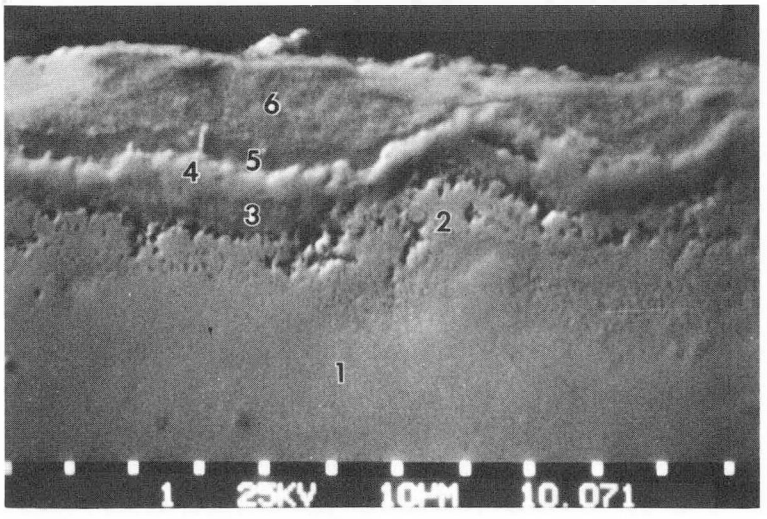

1. Alloy
2. Ni rich with Cr,Fe
3. Cr sulfide
4. Cr_2O_3
5,6. Cr,K,S

1250°F

Figure D.43 Fireside Attack on Alloy IN-814 [Scanning electron micrographs show IN-814 specimens from Retorts 4 and 6 exposed at 1250 and 1440°F (675 and 780°C) for 250 hours. Phase identification was made from EDX information.]

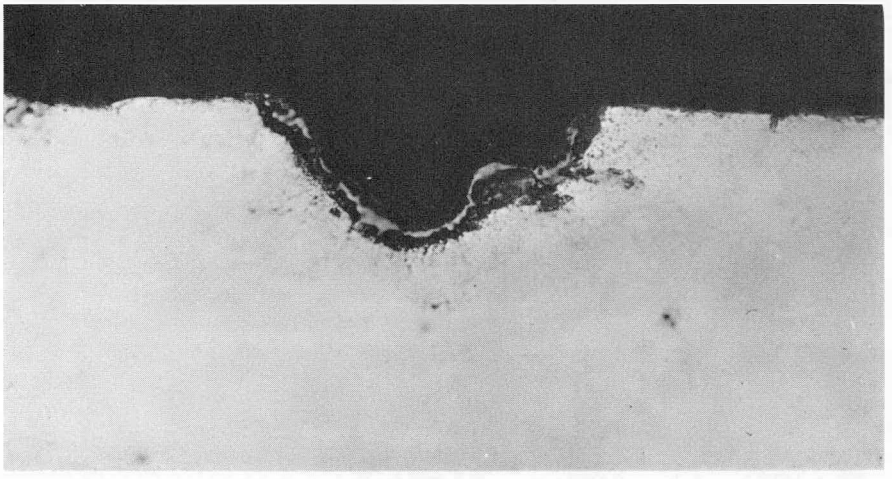

PN 63627

Figure D.44 Fireside Attack on Alloy IN-671--500X Unetched [Light micrograph shows Inconel 671 specimen from Retort 4 exposed at 1250°F (675°C) for 250 hours.]

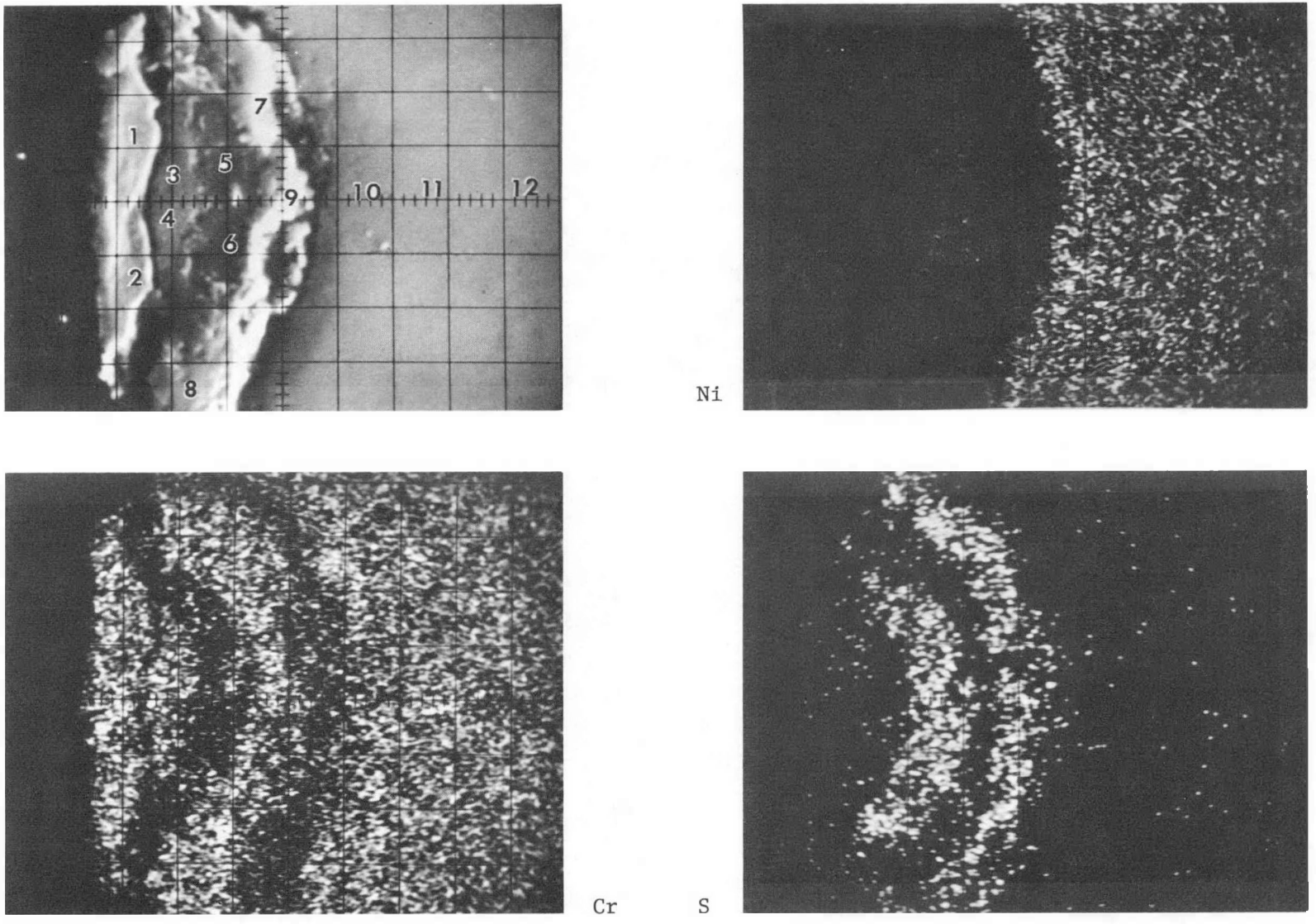

Figure D.45 Fireside Deposit and Surface Analysis Profiles on Alloy IN-671--500X [Electron probe, SEM, and x-ray mapping show corrosion product in a pit on Inconel 671 specimen from Retort 4 exposed at 1250°F (675°C) for 250 hours.]

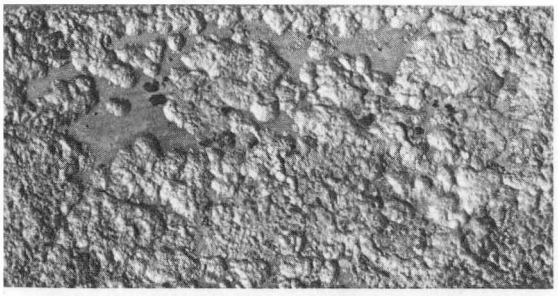

25%Ni-20%Cr-0.45%Si

Loss - largely pitting
0.015 in. (380 μm)

Alloy 1 (Serial 1)

25%Ni-20%Cr-2.3%Si

0.003 to 0.004 in. (76 to 101 μm) general attack plus 0.004 in. (101 μm) pits
0.007 to 0.008 in. (177 to 203 μm) maximum penetration

Alloy 3 (Serial 2)

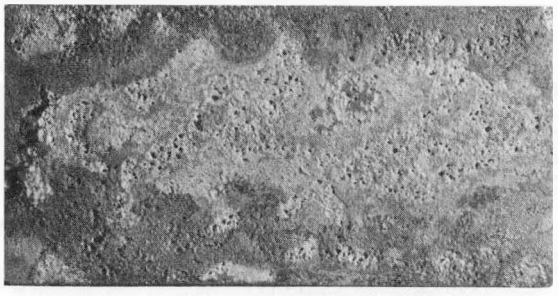

25%Ni-20%Cr-2%Al-2.4%Si

0.002 to 0.003 in. (50 to 76 μm) general attack plus 0.002 in. (50 μm) pits
0.004 to 0.005 in. (101 to 127 μm) maximum penetration

Alloy 4 (Serial 1)

21%Ni-24%Cr-2%Si (shot peened)

Total penetration 0.002 to 0.0025 in. (50 to 63 μm)

Alloy 314 (Serial 16)

Figure D.46 Photomacrographs of Fireside Attack--Phase II

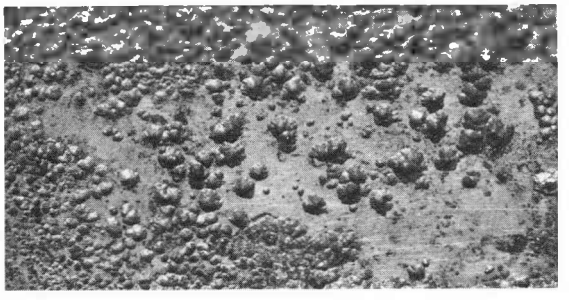

35%Ni-25%Cr-0.4%Si

Chloride added (shown)
0.017 in. (431 μm) pitting
0.008 in. (203 μm) without chloride

Alloy 5 (Serial 3)

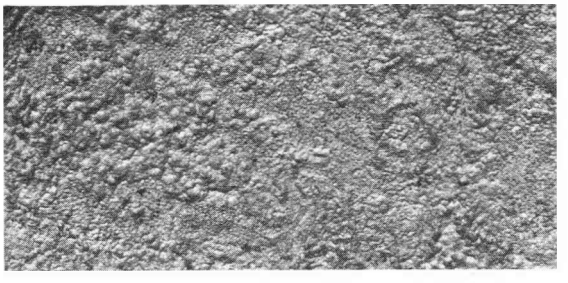

35%Ni-25%Cr-2%Al-0.4%Si

General attack plus pitting
0.010 in. (254 μm)
(no chloride)

Alloy 6 (Serial 4)

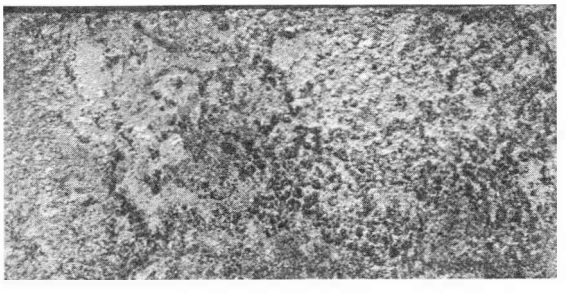

35%Ni-25%Cr-2.3%Si

General attack plus pitting
0.007 in. (177 μm)

Alloy 7 (Serial 4)

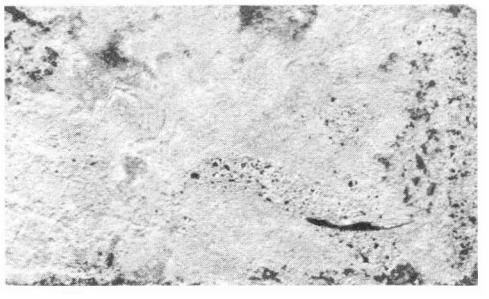

35%Ni-25%Cr-2%Al-1.29%Si*

General attack 0.005 in. (127 μm)

Alloy 8 (Serial 4)

*Surface depletion suspected from preparation of specimen.

Figure D.47 Photomacrographs of Fireside Attack--Phase II

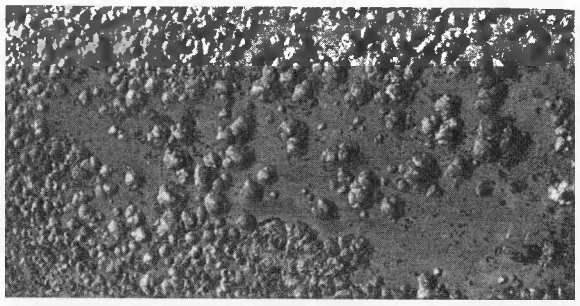

35%Ni-25%Cr

Maximum penetration 0.010 in. (254 μm)

Alloy 5 (Serial 4)

35%Ni-25%C4-2%Al

Maximum penetration 0.010 in. (254 μm)

Alloy 6 (Serial 4)

35%Ni-25%Cr-4%Al

Maximum penetration 0.008 in. (203 μm)

Alloy 13 (Serial 4)

35%Ni-25%Cr-4%Al-0.5%Y

Maximum penetration 0.005 in. (127 μm)

Alloy 15 (Serial 102)

Figure D.48 Photomacrographs of Fireside Attack--Phase II

APPENDIX E

EXAMINATION OF SCALES AND DEPOSIT

INTRODUCTION

The data contained in this appendix will be useful to those who have a special interest in the composition of scales and deposits. Examinations of scales and deposits were performed on specimens subjected to fireside attack in an effort to discover more about the mechanism of attack and the weakness of the passive film formation. (Further data were reported in the 3rd, 4th, and 5th Quarterly Progress Report.)

This appendix contains measurements of the x-ray diffraction of scales formed by flue gas exposure. Tables are provided which collate information on scales formed in simulated fireside exposure and which detail the results of electron probe analysis of the corrosion product in representative alloys.

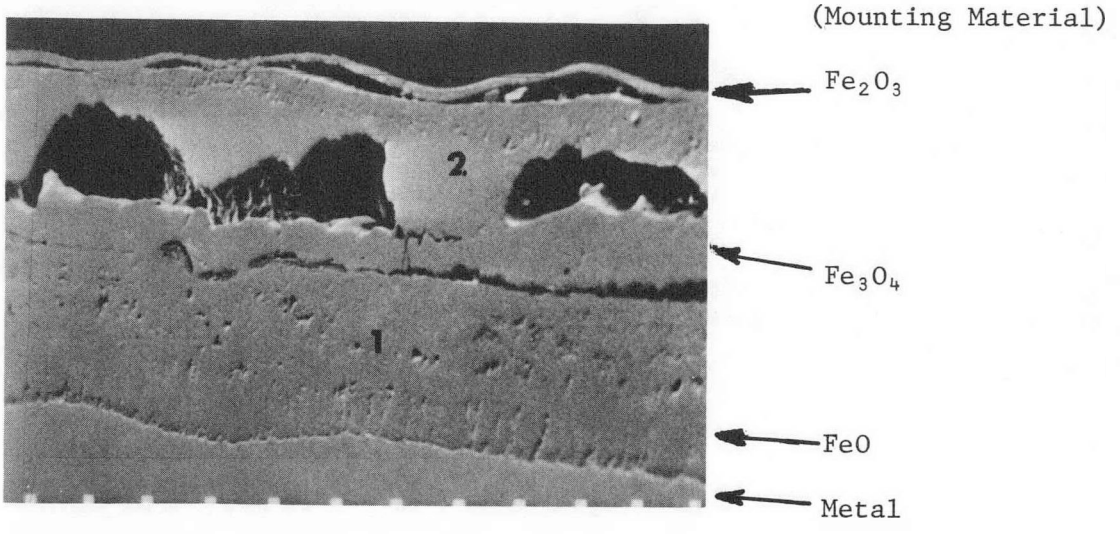

Figure E.1 Scanning Electron Micrograph of 2-1/4%Cr-1%Mo Steel Exposed to Synthetic Flue Gas at 1440°F (780°C) for 250 Hours--30X (The distance between each white mark below the figure equals 300 μm.)

Table E.1 X-Ray Diffraction Analysis of Scales on Base Materials Exposed to Flue Gas for 250 Hours at 1440°F (780°C)

	Oxide				
Material	Cr_2O_3	Spinel or Fe_3O_4	α-Fe_2O_3	NiO	Other Lines
2-1/4Cr-1Mo		vs	m		FeO(m)
HT-9	s	vs			
304	m	m			α-Fe(vs)
347	w	m			α-Fe(vs)
310	m	s			
314	m	w			
840	s	vs			
21-6-9		vs			Mn_2O_3(s),α-Fe
800H	ms	s			
A-286	s	s		w	TiO_2(w)
AL-6X	mw	vs		w	
601	vs				
625	s	vw			Ni_3Mo(m)
671	vs				
IN-737	s	vw			
IN-549	m	vw			
IN-809	vs				
IN-811	w	m			
IN-814	vw				

Table E.2 Electron Probe Step-Scan Across Scale-Metal Interface in 2 μm Increments [The 2-1/4%Cr-1%Mo steel was exposed to flue gas at 1440°F (780°C) for 250 Hours.]

Step No.	Composition, Wt.%				
	Fe	Cr	Mn	Si	Mo
1	27.8	34.0	0.3	0.3	1.5
2	44.8	20.2	0.1	0.2	0.8
3	44.1	14.2	0.1	0.4	0.7
4	38.5	31.9	0.3	0.1	0.01
5	90.0	3.6	1.1	0.5	0.5
6	94.1	1.0	0.04	0.3	0.3
7	95.4	0.9	0.1	0.2	0.2
8	96.8	0.6	0.1	0.1	0.5
9	96.5	0.6	0.1	0.2	0.4
10	95.6	1.0	0.1	0.2	0.2
11	96.5	0.7	0.2	0.2	0.5
12	96.1	1.5	0.4	0.2	0.4
13	95.8	2.0	0.3	0.3	0.7
14	94.1	2.2	0.3	0.2	0.6
15	95.2	2.2	0.3	0.2	0.5
16	94.9	2.1	0.5	0.2	0.5
17	95.6	2.2	0.4	0.2	0.4
18	94.5	2.3	0.5	0.2	0.3

Table E.3 X-Ray Diffraction Analysis of Outer Layer of Scale on Base Materials Exposed to Simulated Coal-Ash and Flue Gas [Specimens were from Retort 6 and were exposed for 250 hours at 1440°F (780°C)]

	Cr_2O_3	Spinel or Fe_3O_4	NiO	α Al_2O_3	γ Al_2O_3	$KNaSO_4$
Ferritic Alloys						
2-1/4Cr-1Mo	ms	mw				
HT-9	s	vw				vw
Austenitic S/S						
304	m	mw				w
347	s	mw				
310	vs	ms				w
314	m	vs	mw			
IN-840	m	w				m
High Manganese						
21-6-9	m	m				
High Fe Superalloys						
IN-737	w	ms			vw	
INCOLOY 800H	m	m				m
A-286	s	ms				mw
AL-6X	mw	vs	w			
IN-793						
Ni-Base Superalloys						
IN-601	m	vs				w
INCONEL 625	m	m	ms	mw		
IN-671	ms					vs
Semicommercial Alloys						
IN-549	mw	vs				m
IN-809	s	m				vs
IN-811	m	s				mw
IN-814	mw	vs				m

Table E.4 X-Ray Diffraction Analysis of Layer Adjacent to Metal Surface on Base Material Exposed to Simulated Coal Ash and Flue Gas [Specimens were from Retort 6 and were exposed for 250 hours at 1440°F (780°C)]

	Cr_2O_3	Spinel or Fe_3O_4	$KNaSO_4$	Other
Ferritic Alloys				
2-1/4Cr-1Mo	w	ms		
HT-9				$Fe_{(1-x)}S$ (Pyrrhotite) S, M(BCC) S
Austenitic S/S				
304	m			
347				
310	mw	mw		
314		vw		
IN-840	w	w		Ni vs. oriented
High Manganese				
21-6-9	w			
High Fe Superalloys				
IN-737	vs			K_2SO_4 or $K_2(SO_4)_{0.67}(CrO_4)_{1.33}$
INCOLOY 800H				
A-286	mw			
AL-6X				
IN-793				
Ni-Base Superalloys				
IN-601	m	ms		
INCONEL 625				
IN-671	w		ms	$K_{(1-x)}Na_{(1+x)}SO_4$, m
Semicommercial Alloys				
IN-549	mw	ms	mw	
IN-809	s	m	ms	
IN-811	ms		mw	
IN-814	mw	m		

Table E.5 X-Ray Diffraction Analyses of Outer Loose Deposits and the Scale Near the Surface of 19 Alloys Exposed to Simulated Coal Ash and Flue Gas [Coupons were exposed in Retort 17 for 48 hours at 1250°F (675°C) and cycled.]

Alloy No.	Nominal Composition* Ni	Cr	Al	Si	Y	Deposit** or Scale	Scale Component (XRD) γ-Fe_2O_3	α-Fe_2O_3	Cr_2O_3	Fe_2SiO_4	$Fe(AlCr)_2O_4$	FeS	$KNaSO_4$
1	25	20	-	-	-	SS	← none →						
						Dep	s†		vw†			vw	m†
2	25	20	2	-	-	SS	← none →						
						Dep	s		vw			w	m
3	25	20	-	2	-	SS	s		w			w	
						Dep	s	m	vw			m	w
4	25	20	2	2	-	SS	m	m					
						Dep	s					m	w
5	35	25	-	-	-	SS	w						
						Dep	s		m			m	m
6	35	25	2	-	-	SS	vw						
						Dep	s		w			m	w
7	35	25	-	2	-	SS	w		w				
						Dep	s	m	m			m	
8	35	25	2	2	-	SS	w		s				
						Dep	m		m			w	w
9	40	30	-	-	-	SS	s		w				
						Dep	s	m	m			w	w
10	40	30	2	-	-	SS	m						
						Dep	s		w			m	w
11	40	30	-	2	-	SS	m		m			w	
						Dep	w	s	w			w	w
12	40	30	2	2	-	SS	w		s	s			
						Dep	m		m	m			w
13	35	25	4	-	-	SS			w				
						Dep	s	m	w			w	w
14	35	25	4	-	0.1	SS	s		s				w
						Dep	s		w			w	w
15	35	25	4	-	0.5	SS	s		w		m	w	
						Dep	s	w	w		m	w	
16	35	25	-	-	0.1	SS	m						
						Dep	s		m			m	m
17	35	25	-	-	0.5	SS	m		m				
						Dep	s	w	m			w	m
18	20	25	-	-	0.6	SS	m		m				
						Dep	s		s			w	m
19	20	23	-	-	0.5 Y_2O_3	SS	← none →						
						Dep	s	m	m			w	w
310	20	25	-	-	-	SS	s						
						Dep	← none →						

Footnote:

† nomenclature: s = strong m = medium w = weak vw = very weak

* Bal-Fe

** SS: Scale retained on the metal surface
Dep: Outer loose deposit or scale/deposit mixture

Table E.6 Electron Probe Analysis of Several Locations in the Corrosion Product in a Pit on Type 347 Stainless Steel (This specimen was exposed in Retort 4.)

POINT	ELEMENT	WEIGHT PERCENT	ATOMIC PERCENT
1.			
	NI KA	0.79	0.38
	CR KA	6.92	3.77
	FE KA	53.31	27.04
	S KA	0.11	0.09
	MN KA	0.06	0.03
	SI KA	0.05	0.05
	O *	38.76	68.63
2.			
	NI KA	0.26	0.13
	CR KA	5.85	3.34
	FE KA	58.35	30.95
	S KA	0.18	0.16
	MN KA	0.02	0.00
	SI KA	0.06	0.07
	O *	35.28	65.34
3.			
	NI KA	4.30	1.90
	CR KA	33.20	16.61
	FE KA	15.42	7.18
	S KA	0.47	0.38
	MN KA	0.35	0.16
	SI KA	2.11	1.96
	O *	44.16	71.80
4.			
	NI KA	4.75	2.04
	CR KA	31.29	15.19
	FE KA	14.25	6.45
	S KA	0.51	0.40
	MN KA	0.38	0.18
	SI KA	1.93	1.74
	O *	46.91	74.02
5.			
	NI KA	1.92	0.85
	CR KA	39.17	19.57
	FE KA	11.42	5.31
	S KA	2.04	1.65
	MN KA	0.32	0.15
	SI KA	1.21	1.12
	O *	43.92	71.33
6.			
	NI KA	5.96	2.79
	CR KA	37.22	19.66
	FE KA	14.41	7.09
	S KA	0.80	0.68
	MN KA	0.47	0.23
	SI KA	1.44	1.41
	O *	39.70	68.14
7.			
	NI KA	0.64	0.35
	CR KA	45.11	27.72
	FE KA	13.71	7.84
	S KA	12.32	12.28
	MN KA	2.20	1.28
	SI KA	1.63	1.85
	O *	24.38	48.68
8.			
	NI KA	0.00	0.00
	CR KA	45.63	28.70
	FE KA	13.41	7.86
	S KA	14.95	15.25
	MN KA	2.59	1.54
	SI KA	1.41	1.64
	O *	22.01	45.01

Table E.7 Electron Probe Analysis of Several Locations in the Corrosion Product Scale on Type 310 Stainless Steel (This specimen was exposed in Retort 4.)

POINT	ELEMENT	WEIGHT %	ATOMIC %
1.			
	NI KA	0.25	0.11
	CR KA	25.68	14.08
	FE KA	36.30	18.53
	MN KA	0.00	0.00
	S KA	0.07	0.06
	O *	37.72	67.21
2.			
	NI KA	1.90	0.93
	CR KA	22.97	12.67
	FE KA	37.41	19.21
	MN KA	0.00	0.00
	S KA	0.47	0.42
	O *	37.24	66.76
3.			
	NI KA	0.36	0.17
	CR KA	51.78	27.72
	FE KA	8.43	4.20
	MN KA	0.02	0.01
	S KA	0.78	0.68
	O *	38.63	67.22
4.			
	NI KA	0.37	0.17
	CR KA	50.60	26.81
	FE KA	8.38	4.13
	MN KA	0.14	0.07
	S KA	1.07	0.92
	O *	39.43	67.89
5.			
	NI KA	0.12	0.07
	CR KA	50.77	32.69
	FE KA	5.67	3.40
	MN KA	1.01	0.62
	S KA	24.38	25.46
	O *	18.04	37.76
6.			
	NI KA	0.19	0.10
	CR KA	53.56	34.00
	FE KA	7.13	4.21
	MN KA	1.24	0.74
	S KA	16.65	17.14
	O *	21.23	43.80

Table E.8 Electron Probe Analysis of Several Locations in the Corrosion Product Scale on Type 314 Stainless Steel (This specimen was exposed in Retort 4.)

POINT	ELEMENT	WEIGHT PERCENT	ATOMIC PERCENT
1.			
	NI KA	3.40	1.66
	CR KA	21.19	11.73
	FE KA	38.01	19.59
	MN KA	0.00	0.00
	S KA	0.24	0.22
	SI KA	0.02	0.02
	O *	37.13	66.78
2.			
	NI KA	0.67	0.34
	CR KA	30.66	17.76
	FE KA	35.11	18.94
	MN KA	0.00	0.00
	S KA	0.26	0.24
	SI KA	0.00	0.00
	O *	33.30	62.71
3.			
	NI KA	0.37	0.18
	CR KA	30.18	16.44
	FE KA	31.15	15.80
	MN KA	0.00	0.00
	S KA	0.19	0.17
	SI KA	0.06	0.07
	O *	38.03	67.33
4.			
	NI KA	7.64	2.70
	CR KA	5.11	2.04
	FE KA	6.56	2.44
	MN KA	0.80	0.30
	S KA	17.00	10.99
	SI KA	0.00	0.00
	O *	62.89	81.53
5.			
	NI KA	6.62	2.33
	CR KA	5.51	2.19
	FE KA	7.22	2.68
	MN KA	0.75	0.28
	S KA	16.65	10.74
	SI KA	0.00	0.00
	O *	63.25	81.78
6.			
	NI KA	0.91	0.39
	CR KA	32.16	15.55
	FE KA	16.60	7.47
	MN KA	0.08	0.04
	S KA	2.50	1.96
	SI KA	0.63	0.57
	O *	47.11	74.03
7.			
	NI KA	1.97	0.7
	CR KA	28.27	11.9
	FE KA	0.06	0.0
	MN KA	0.73	0.2
	S KA	7.60	5.2
	SI KA	4.59	3.6
	O *	56.78	78.1
8.			
	NI KA	1.59	0.6
	CR KA	27.27	12.1
	FE KA	8.69	3.6
	MN KA	0.23	0.0
	S KA	4.58	3.3
	SI KA	5.66	4.6
	O *	51.98	75.4

* Determined by difference

Table E.9 Electron Probe Analysis of Several Locations in the Corrosion Product Scale on Specimen 21-6-9 (Nitronic 40) (This specimen was exposed in Retort 4.)

POINT	ELEMENT	WEIGHT PERCENT	ATOMIC PERCENT
1	NI KA	0.00	0.00
	CR KA	3.57	1.24
	FE KA	5.68	1.84
	MN KA	5.01	1.65
	S KA	3.25	1.84
	O *	82.49	93.43
2			
	NI KA	9.50	3.74
	CR KA	14.77	6.57
	FE KA	14.55	6.02
	MN KA	3.19	1.34
	S KA	2.06	1.49
	O *	55.93	80.84
3			
	NI KA	0.68	0.33
	CR KA	41.77	22.97
	FE KA	14.44	7.39
	MN KA	4.36	2.27
	S KA	2.46	2.20
	O *	36.28	64.84
4			
	NI KA	0.00	0.00
	CR KA	13.44	5.79
	FE KA	3.06	1.23
	MN KA	10.72	4.37
	S KA	18.84	13.15
	O *	53.94	75.47
5			
	NI KA	0.03	0.01
	CR KA	14.94	6.38
	FE KA	0.72	0.28
	MN KA	10.07	4.07
	S KA	19.80	13.71
	O *	54.44	75.54
6			
	NI KA	0.00	0.00
	CR KA	43.30	25.88
	FE KA	5.13	2.85
	MN KA	16.73	9.46
	S KA	6.72	5.83
	O *	28.82	55.97

Table E.10 Electron Probe Analysis of Several Locations in the Corrosion Product Scale on Inconel 671 (This specimen was exposed in Retort 4.)

POINT	ELEMENT	WEIGHT PERCENT	ATOMIC PERCENT
1.	NI KA	2.18	1.00
	CR KA	51.94	26.97
	FE KA	0.24	0.12
	S KA	6.06	5.10
	O *	39.59	66.81
2.	NI KA	1.57	0.73
	CR KA	56.63	29.85
	FE KA	0.45	0.22
	S KA	1.90	1.63
	O *	39.44	67.57
3.	NI KA	1.10	0.52
	CR KA	59.07	31.77
	FE KA	0.31	0.15
	S KA	1.75	1.53
	O *	37.78	66.03
4.	NI KA	1.35	0.63
	CR KA	56.45	29.60
	FE KA	0.40	0.19
	S KA	1.95	1.66
	O *	39.86	67.93
5.	NI KA	5.06	2.17
	CR KA	38.68	18.72
	FE KA	0.85	0.37
	S KA	10.73	8.42
	O *	44.71	70.32
6.	NI KA	9.05	3.24
	CR KA	11.09	4.48
	FE KA	0.00	0.00
	S KA	19.08	12.50
	O *	60.78	79.78
7.	NI KA	0.75	0.32
	CR KA	49.50	23.73
	FE KA	0.00	0.00
	S KA	1.99	1.55
	O *	47.76	74.41
8.	NI KA	0.71	0.36
	CR KA	62.39	35.51
	FE KA	0.00	0.00
	S KA	4.45	4.11
	O *	32.45	60.03